

STRUCTURAL STUDIES OF ANTICANCER DRUG MITOXANTRONE AND ITS COMPLEX WITH DNA

A THESIS

*Submitted in fulfilment of the
requirements for the award of the degree
of
DOCTOR OF PHILOSOPHY
in
BIOTECHNOLOGY*

By

MANPREET KAUR NARANG



DEPARTMENT OF BIOTECHNOLOGY
INDIAN INSTITUTE OF TECHNOLOGY ROORKEE
ROORKEE-247 667 (INDIA)

JUNE, 2006



INDIAN INSTITUTE OF TECHNOLOGY

ROORKEE

CANDIDATE'S DECLARATION

I hereby certify that the work which is being presented in the thesis entitled, "STRUCTURAL STUDIES OF ANTICANCER DRUG MITOXANTRONE AND ITS COMPLEX WITH DNA" in fulfilment for requirements for the award of the Degree of Doctor of Philosophy and submitted in the Department of Biotechnology of the Institute is an authentic record of my own work carried out during a period from January 2001 to June 2006 under the supervision of Prof. Ritu Barthwal, Department of Biotechnology and Assoc. Prof. Sudhir Barthwal, Department of Physics at Indian Institute of Technology Roorkee, Roorkee.

The matter presented in this thesis has not been submitted by me for the award of any other degree of this or any other University / Institute.

Dated: 21.6.2006

Manpreet Kaur Narang
(Manpreet Kaur Narang)

This is to certify that the above statement made by the candidate is correct to the best of our knowledge.

Dated: 21.6.06

Sudhir Barthwal

(Sudhir Barthwal)
Associate Professor
Department of Physics,
Indian Institute of Technology
Roorkee, (IITR)
Roorkee – 247 667 (India)

Ritu Barthwal

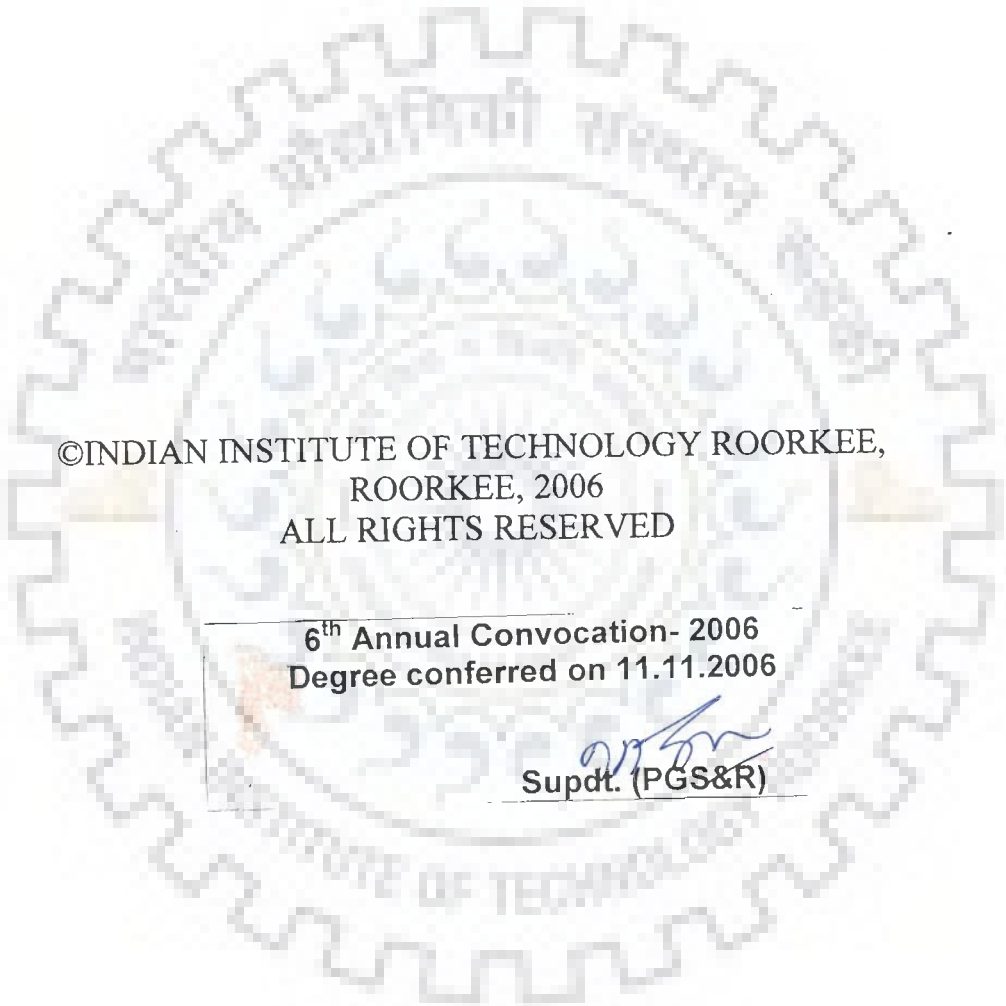
(Ritu Barthwal)
Professor
Department of Biotechnology,
Indian Institute of Technology
Roorkee, (IITR)
Roorkee – 247 667 (India)

The Ph.D. Viva-Voce Examination of *Manpreet Kaur Narang*, Research Scholar has been held on 27-10-06

Ritu Barthwal
Signature of Supervisor (s)


S. Barthwal
Signature of H.O.D.

M. Majumdar
Signature of External Examiner



©INDIAN INSTITUTE OF TECHNOLOGY ROORKEE,
ROORKEE, 2006
ALL RIGHTS RESERVED

6th Annual Convocation- 2006
Degree conferred on 11.11.2006


Supdt. (PGS&R)

CONTENTS

CANDIDATES'S DECLARATION

ABSTRACT

ACKNOWLEDGEMENTS

LIST OF PUBLICATIONS

	Page No.
CHAPTER 1	
INTRODUCTION	1-58
1.1 General	1
1.2 Mode of Action of Anticancer Drugs	2
1.3 Mitoxantrone	9
1.4 Intercalation General Phenomenon	12
1.5 Forces Between Intercalators and DNA	13
1.6 Nucleic Acid Structure and Function	15
1.7 Helicoidal Parameters of DNA	26
1.8 Literature Review	29
1.9 Scope of Thesis	56
CHAPTER 2	
MATERIALS AND METHODS	59-100
2.1 Materials	59
2.2 Sample Preparation for UV studies	59
2.3 Sample Preparation for NMR Studies	60
2.4 NMR Theory	63
2.5 Experimental Parameters	82
2.6 Determination of Three Dimensional Structure	84
2.7 Restrained Molecular Dynamics and Simulated Annealing	94
2.8 Strategy used for Molecular Modelling	99
CHAPTER 3	
STUDY OF MITOXANTRONE IN WATER BY NMR AND ABSORPTION SPECTROSCOPY	101-130
3.1 Introduction	101
3.2 Results and Discussions	101
3.2.1 NMR Assignments	101
3.2.2 Absorption and Fluorescence Studies	122
3.2.3 Molecular Modelling Studies	126
CHAPTER 4	
STUDY OF MITOXANTRONE IN DMSO BY NMR AND ABSORPTION SPECTROSCOPY	131-169
4.1 Introduction	131
4.2 Results and Discussions	131
4.2.1 NMR Assignments	131
4.2.2 Absorption studies	142

	4.2.3	Molecular Modelling Studies	162
	4.2.4	Solvent Effect	166
CHAPTER 5		PHOSPHORUS-31 NMR STUDIES ON BINDING OF MITOXANTRONE WITH d-(CGATCG)₂	170-199
	5.1	Introduction	170
	5.2	Results and Discussions	170
CHAPTER 6		PROTON NMR STUDIES ON BINDING OF MITOXANTRONE WITH d-(CGATCG)₂	200-290
	6.1	Introduction	200
	6.2	Results and Discussions	200
	6.2.1	Titration Studies	200
	6.2.2	Absorption Studies	278
	6.2.3	Conformational features of DNA and drug in Complex	279
	6.2.4	Structure of Complex	286
CHAPTER 7		STRUCTURE OF d-(CGATCG)₂ COMPLEXED WITH MITOXANTRONE BY RESTRAINED MOLECULAR DYNAMICS	291-310
	7.1	Introduction	291
	7.2	Results and Discussions	291
	7.2.1	Conformational features of rMD Structure	292
	7.2.2	Helicoidal Parameters	292
	7.2.3	Groove Width	296
		APPENDIX A	304
CHAPTER 8		CONCLUSIONS	311
REFERENCES			312-326

ABSTRACT

Nature has evolved a diverse set of antibiotics that bind to DNA in a variety of ways, but with the common ability to act as potent inhibitors of DNA transcription and replication. As a consequence, these natural products have been of considerable interest as potential anti cancer agents. Many synthetic compounds have been added to this list in the search for more potent drugs for use in chemotherapy. While it is appreciated that DNA is a primary target for many potent antitumor agents, data that pinpoint the exact mechanism of action are generally unavailable. A substantial body of research has been directed towards understanding the molecular basis for DNA sequence specificity for binding, by identifying the preferred binding sequences of many key drugs with DNA. Structural tools such as X-ray crystallography and NMR spectroscopy, coupled with molecular modeling techniques have had considerable impact in advancing our understanding of the microscopic structural homogeneity of DNA and the molecular basis for drug-DNA interactions. The purpose of present study understands the molecular basis of action of these drugs enabled by solution studies using nuclear magnetic resonance spectroscopy.

Here, we have studied mechanism of anticancer drug mitoxantrone with DNA which has been developed as an alternative to existing drugs namely daunomycin, adriamycin etc. owing to their lethal effects such as cardiotoxicity. Mitoxantrone has shown comparable activity and less cardiotoxic effect. Various analogues of the drugs have also been studied through computer modeling techniques.

Chapter 1 contains brief introduction of the subject as well as an overview the work carried out in literature. Chapter 2 deals with the materials and methods being used. Chapters 3 and 4 deals with the study of the mitoxantrone by Nuclear Magnetic

Resonance techniques in three different solvents namely D₂O, H₂O and DMSO. Various homonuclear 2D experiments DQF COSY, 2D ROESY and ¹H – ¹³C (proton – carbon) heteronuclear experiments namely HSQC and HMBC have been carried for complete, unambiguous assignment and determination of structure of drug.

Structural refinement of has been carried out using NOE distance constraints by restrained Molecular Dynamics (rMD) with different starting structures, potential functions and rMD protocols for all three solvents. Chapters 5 and 6 deal with Phosphorus-31 and proton NMR investigations on binding of mitoxantrone with DNA hexamer sequence d-(CGATCG)₂. Titrations of drug with DNA have been carried out by adding increasing amounts of drug to a fixed concentration of DNA and recording one dimensional NMR spectra at 278 K, 2D ³¹P exchange NOESY spectra and 2D proton NOESY spectra have been recorded for 1:1, 1.5: 1 and 1.75:1 and 2:1 drug to DNA stoichiometric ratios at 278 K. New resonance peaks corresponding to bound drug / DNA in the complex are found be in slow exchange with the corresponding resonances in free drug / DNA. The intramolecular and intermolecular distances have been used to analyze the conformational aspects of drug / DNA in complex. Chapter 7 describes the structure of complex obtained by restrained energy minimized and molecular dynamics simulations. The helicoidal parameters and backbone torsional angles have been obtained using curves software. Chapter 8 summarizes results obtained and their implications in understanding molecular basis of drug action.

ACKNOWLEDGEMENTS

It gives me great pleasure in expressing my sincere gratitude and immense veneration towards my supervisor, *Prof. Ritu Barthwal* and co-supervisor *Assoc. Prof. Sudhir Barthwal* and for their meticulous guidance discreet support and keen interest through out the course. Under their esteem guidance, I have strengthened my skills in research methodology and also developed a never ending quest for knowledge. I really thank them to provide me the opportunity to work under their guidance.

I am most thankful to all the members of FT-NMR National Facility at Tata Institute of Fundamental Research, (TIFR, Mumbai) and Centre for Biomedical Resonance (CBMR, Lucknow) for extending their cooperation and providing friendly atmosphere of work. I am especially grateful to the faculty of the department comprising famous NMR experts *Prof. G. Govil*, *Prof. R. V. Hosur* (TIFR), *Prof. C. L. Khetrpal* and *Prof. G. A. N. Gowda* (CBMR), for help and valuable discussions during my stay.

At this moment in time I would like to make particular mention of valued friend *Dr. Monica*, with whom I have spent even and odds of this memorable journey. She shared all my doubts and provided me strength and courage in moments of despair. Her cherished, appropriate and responsive advice had always pushed me forward. I wish her a bright prospective and joyful life.

I also remember another dear friend *Tripta* for her invariable support. Her positive approach had always been great succor. I wish her a successful and happy living.

I am also obliged to my labmates *Prashansa*, *Durai*, *Santosh*, *Amit*, *Lata*, and *Kushuma* and *Asif* for their sincere efforts, amiable attitude and cooperation while working in lab especially during compilation of this thesis.

Suitable help and suggestions of *Dr. Soma, Dr. Arshi and Dr. Tarun* will always be remembered.

I am also thankful to the staff of the department for their support, especially Mr. V. Saini, for all the technical support throughout the period of this work.

I also remember, *Nupur, Ruchi, Pulkita, Anju, Garima and Indira* with whom the stay at hostel had been enjoyable.

And last but not the least I am eternally appreciative to my loving parents and grand parents I am in dearth of words to express my heart-felt reverence to them. Apart from providing the best available education and poignantly bearing my long absence from home, my parents have always encouraged me in all my endeavors and felt proud of my every achievement. Their prudence and morals paved the way for an honored education and unreserved support at every turn of this journey.

I am also thankful to my two bubbly younger sisters *Kawal and Simran* for providing humorous and lighter moments in difficult phase and forever motivating me in this venture.

Finally, I am obliged to Council of Scientific and Industrial Research, (CSIR), Govt. of India for awarding Junior Research Fellowship (JRF) and Indian Council of Medical Research, (ICMR), Govt. of India for awarding Senior Research Fellowship (SRF) for financial assistance.

I am also grateful to Department of Biotechnology (DBT) and Centre for Development of Advance Computing (CDAC) for providing funding during the period I was working on adhoc basis.

Manpreet Kaur Narang

LIST OF PUBLICATIONS

1. Ritu Barthwal, Uma Sharma, Nandana Srivastava, Monica, Pamita Awasthi, **Manpreet Kaur**, Sudhir Kumar Barthwal and Girjesh Govil (2006)
Structure of daunomycin complexed to d-TGATCA by two-dimensional Nuclear Magnetic Resonance Spectroscopy. European Journal of Medicinal Chemistry, Vol. 41, pp. 27–39.
2. Ritu Barthwal, Pamita Awasthi, Monica, **Manpreet Kaur**, Nandana Srivastava, S. K. Barthwal and Girjesh Govil. (2004)
Structure of DNA sequence d-TGATCA by two-dimensional Nuclear Magnetic Resonance Spectroscopy and Restrained Molecular Dynamics. Journal of Structural Biology, Vol. 148, pp. 34–50.
3. Ritu Barthwal, Monica, Pamita Awasthi, Nandana Srivastava, Uma Sharma, **Manpreet Kaur** and Girjesh Govil. (2003)
Structure of DNA hexamer sequence d-CGATCG by two-dimensional Nuclear Magnetic Resonance Spectroscopy and Restrained Molecular Dynamics. Journal of Biomolecular Structure and Dynamics, Vol. 21, pp 817 – 839.
4. Ritu Barthwal, Nandana Srivastava, Uma Sharma, Monica, Pamita Awasthi, **Manpreet Kaur**, Sudhir Kumar Barthwal and Girjesh Govil (2006)
Structure of adriamycin complexed to d-CGATCG by two-dimensional Nuclear Magnetic Resonance Spectroscopy. To be communicated
5. **Manpreet Kaur Narang**, Pamita Awasthi, Monica, Sudhir Kumar Barthwal, Ritu Barthwal and Girjesh Govil (2006)
Conformational Analysis of the antitumour drug Mitoxantrone by NMR and Absorption Spectroscopy. To be communicated.
6. Ritu Barthwal, **Manpreet Kaur Narang** and Sudhir Kumar Barthwal (2006)
³¹P NMR Studies on Binding of Anticancer Drug Mitoxantrone with d- (CGATCG)₂. To be communicated.
7. Ritu Barthwal, **Manpreet Kaur Narang** and Sudhir Kumar Barthwal (2006)
¹H NMR Studies on Binding of Anticancer Drug Mitoxantrone with d- (CGATCG)₂. To be communicated.

Chapter 1

Introduction

1.1 GENERAL

DNA, as carrier of genetic information is a major target for drug interaction because of the ability to interfere with transcription (gene expression and protein synthesis) and DNA replication, a major step in cell growth and division. The latter is central for tumor genesis and pathogenesis.

Cancer is defined as the uncontrolled growth of cells, with loss of differentiation and commonly, with metastasis, spread of the cancer to other tissues and organs. For most cancers, the most important mechanisms of drug resistance are not known. In particular, it remains unclear which of the molecular and cellular drug resistance mechanisms identified by basic research are relevant to the clinic. Although there are many new ideas and treatments being studied every day, chemotherapy and radiation are still the most widely used treatments for the majority of cancers. In an effort of better understanding for drug resistance focus has been made on resistance to new and promising anticancer drugs that are being applied to treating common, recalcitrant tumors, including breast cancer, prostate cancer and melanoma.

Anticancer, or anti-neoplastic drugs are used to treat malignancies and cancerous growths. There are many types of naturally occurring and synthetic chemical agents employed in treatment of cancer. The three principally different ways of drug binding to DNA are: first, through control of transcription factors and polymerases. Here, the drugs interact with the proteins that bind to DNA. Secondly, RNA binding to DNA double helices to form nucleic acid triple helical structures or RNA hybridization (sequence specific binding) to exposed DNA single strand regions forming DNA-RNA hybrids that may interfere with transcriptional activity. Third, small aromatic ligand molecules that bind to DNA double helical structures by (i) intercalating between stacked base pairs thereby distorting the DNA backbone conformation and interfering with DNA-ligand interaction or

(ii) the minor groove binders. The latter cause little distortion of the DNA backbone. Both work through non-covalent interactions.

To understand the fundamental biophysical aspects, sequence-specific recognition, spectroscopic, molecular modeling, and isothermal calorimetric titration methods coupled with high-resolution structural data obtained by NMR spectroscopy using deoxy-oligonucleotides of defined lengths and sequence offer correlation between energetics and sequence-recognition thus provides key role in rational drug design.

1.2 MODE OF ACTION OF ANTICANCER DRUGS

In a broad sense, DNA and DNA topoisomerases are primary targets for numerous anti-tumor drugs. Drug can directly damage DNA by binding covalently or non-covalently. They can alkylate the DNA or intercalate between the base pairs as well as bind to the major or minor groove of DNA. The inhibitors may exert their effect at three levels and can be divided into three groups accordingly. First group of drugs act by alkylation of DNA and thereby forming reactive intermediates which crosslink the DNA or intercalate or binds to groove non-covalently. Second group comprises of many small molecules that mimic or block enzymatic process of DNA offer potential therapeutic agents. Third class of drugs may inhibit the DNA proliferation at the chromatin level itself.

1.2.1 COVALENT DNA BINDING DRUGS

1.2.1.1 Polyfunctional alkylating agents

Drugs that interfere with DNA function by chemically modifying specific nucleotides.

These drugs damage DNA. There are two types of alkylating agents: mono-functional (one reactive group) which cause single-strand breaks in DNA or damage bases and bi-functional (two reactive groups) which form cross-links. A large number of first generations of anti-cancer drugs were designed to combine a simple alkylating function. Their common feature is

that they form an initial physical complex with DNA before covalently bonding to it. The vital purpose is to kill bacteria by disrupting the synthesis of DNA and RNA. Many of them have also shown selective anti-tumor activity, which must arise from selected toxicity. This can be attributed to DNA binding specificity or to preferential metabolic activation by tumour cells. The mechanism of action of these anticancer agents is by alkyl group transfer and they cause alkylation of DNA at N7 or N2 position of guanine (other sites as well) and interaction may involve single strands or both strands. Anthramycin is an anti-tumor antibiotic that binds covalently to N-2 of guanine located in the minor groove of DNA. Anthramycin has a preference of purine-G-purine sequences with bonding to the middle G. Cisplatin is a transition metal complex *cis-diamine-dichloro-platinum* and clinically used as anticancer drug. The effect of the drug is due to the ability to platinate the N-7 of guanine on the major groove site of DNA double helix. This chemical modification of platinum atom, cross-links two adjacent guanines on the same DNA strands, interferes with the mobility of DNA polymerases. Other interactions involve the reaction of these drugs with amino, hydroxyl and phosphate groups of other cellular constituents. These drugs usually form a reactive intermediate ethyleneimmonium ion.

Poly-functional alkylating drugs offer resistance against cancer by increased ability to repair DNA defects, decreased cellular permeability to the drug, increased glutathione synthesis, which inactivates alkylating agents through conjugation reactions. Mitomycin C is a well characterized anti-tumor antibiotic which forms a covalent interaction with DNA after enzymatic reductive activation of its quinone to alkylate DNA. The activated antibiotic forms a cross-linking structure between guanine bases on adjacent strands of DNA thereby inhibiting single strand formation which is essential for m-RNA transcription and DNA replication.

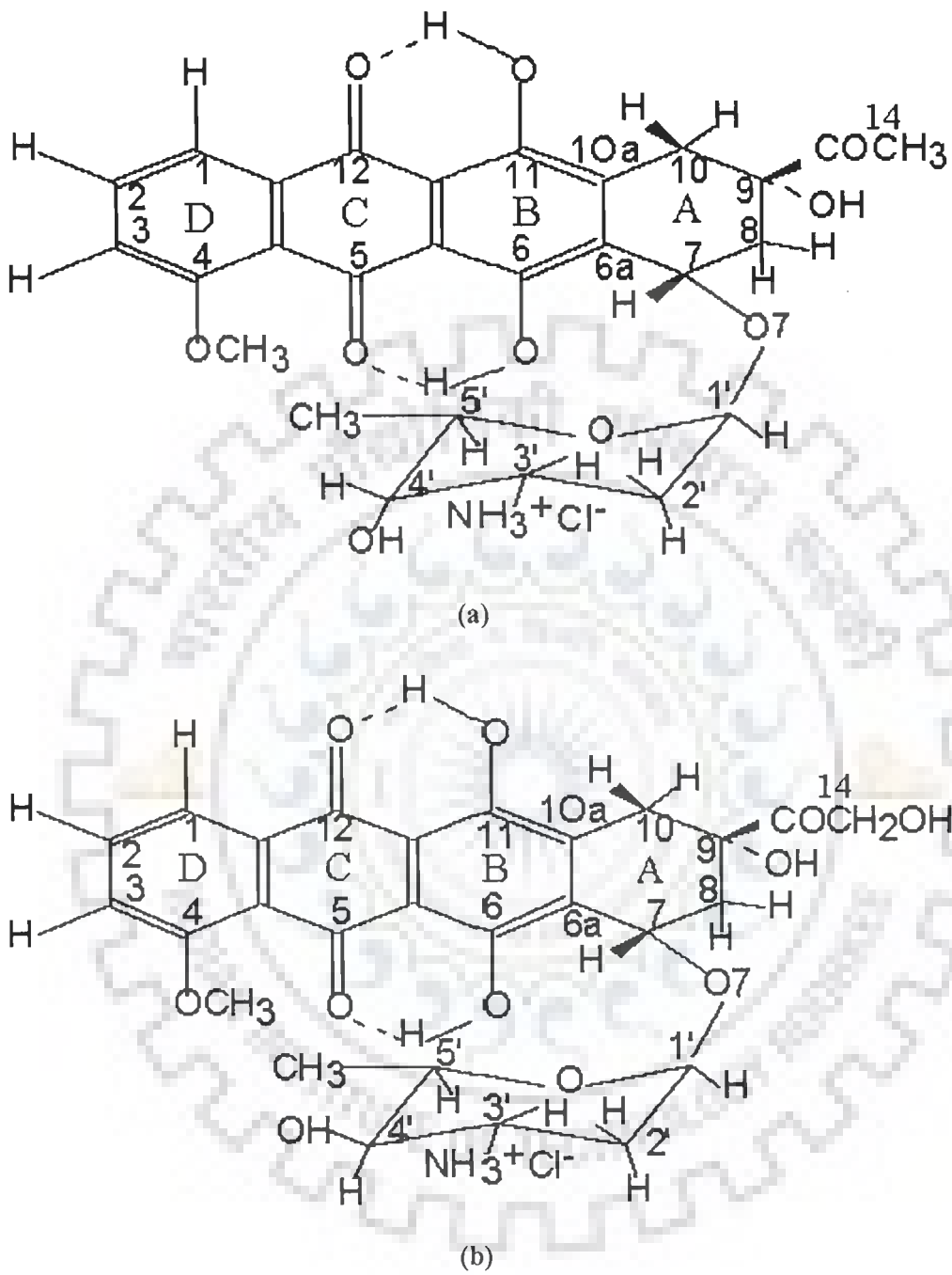


Fig. 1.1 Molecular structure of intercalator drugs (a) Daunomycin (b) Adriamycin

1.2.2 NONCOVALENT DNA BINDING DRUGS

1.2.2.1 Intercalators

Intercalators are the most important group of compounds that interact reversibly with the DNA double helix. These are clinically useful anticancer antibiotics, which are primarily derived from *Streptomyces peucetius*. Some of them are valuable anticancer drugs currently used for the treatment of ovarian and breast cancers and acute leukemia, while many others are in different phases of clinical trials. Intercalating agents share common structural features such as the presence of planar polyaromatic systems, which bind by insertion between DNA base-pairs, termed as intercalation, [71]. Nowadays it is well accepted that the anti-tumor activity of intercalators is closely related to the ability of these compounds to stabilize the DNA–intercalator–topoisomerase II ternary complex. Some of the classical intercalators are shown in Fig. 1.1(a–b). Majority of these drugs have shown marked preference for 5'-pyrimidine–purine–3' steps. The chromophores are linked to basic chains that might also play an important role in the affinity and selectivity shown by these compounds. Bis–intercalators have two potential intercalating ring systems connected by linkers, which can vary in length and rigidity. They also alter membrane fluidity and ion transport. One potential mechanism is based on the ability of these agents to participate in electron–transfer processes, with the subsequent generation of free radicals. The property results from the presence of two very different types of redox–active groups, namely the quinone and hydroquinone moieties on daunomycin, adriamycin and on mitoxantrone Fig. 1.1(a-b). Quinone moiety of daunomycin undergo one–electron reduction to a semiquinone radical, which in the presence of oxygen gives rise to superoxide and other reactive oxygen species (ROS). The first crystal structure with a mono–intercalator and oligonucleotide was obtained by Wang and co–workers [114] for a complex of antibiotic daunomycin and d–(CGTACG)₂.

1.2.2.2 Groove binding molecules

The major and minor groove differs significantly in electrostatic potential, hydrogen bonding characteristics, steric effects and hydration. Typically minor groove binding molecules have several simple aromatic rings connected by bond with torsional freedom. This creates compounds, which with the appropriate twist, can fit into the helical curve of the minor groove with displacement of water from the groove and forming Van der Waal's contacts with the helical chains which define the walls of the groove. Additional specificity in the binding comes from contacts between the bound molecule and the edges of the base pairs on the 'floor' of the groove. Thus, the aromatic rings of many groove binding molecules form close contact with AH2 protons in the minor grooves of DNA. Pullman and coworkers have shown that the negative electrostatic potential is greater in the A.T minor groove than G.C rich regions, and this provides an additional important source for A.T specific minor groove binding of cations. Examples of minor groove binding drugs are netropsin and distamycin.

1.2.3 ANTIMETABOLITES

1.2.3.1 Nucleic Acid synthesis inhibition

Purine antagonists like mercaptopurine (purinethol) act by hypoxanthine-guanine phosphoribosyl transferase (HGPRT) to form 6-thioinosinic acid, which inhibits enzymes involved in purine metabolism. Thioguanine which acts as inhibitor of purine nucleotide pathway is an enzyme which decreases intracellular concentration of guanine nucleotides and inhibit glycoprotein synthesis, finally blocking DNA / RNA synthesis.

1.2.4 INHIBITION OF CHROMATIN FUNCTION

1.2.4.1 Topoisomerase targeting drugs

Chromosomal DNA is extensively twisted and topoisomerases permit selected regions of DNA to untangle so as to allow transcription and replication. These enzymes temporarily

break DNA, allowing for topological changes, and then reseal the breaks. Topoisomerase targeting drugs like etoposide (VP-16) stabilizes the topoisomerase II–DNA complex preventing it from making a topological change. This results in an irreversible double strand break, which is lethal to cells in S and G2 phases. Six anti-neoplastic drugs targeting topoisomerase II, i.e., doxorubicin, daunorubicin, idarubicin, mitoxantrone, etoposide and teniposide are currently approved for clinical use in the United States.

DNA topoisomerase II is a ubiquitous enzyme that is essential for the survival of all eukaryotic organisms and plays critical roles in virtually every aspect of DNA metabolism. The enzyme unknots and untangles DNA by passing an intact helix through a transient double-stranded break that it generates in a separate helix. Beyond its physiological functions, topoisomerase II is the target for some of the most active and widely prescribed anticancer drugs currently utilized for the treatment of human cancers.

These antibiotics act by intercalating between base pairs of DNA causing lengthening of the double helix and a decrease in the helical twist on unwinding, inducing mediated strand scission. These drugs act in an insidious fashion and kill cells by increasing levels of covalent topoisomerase II–cleaved DNA complexes that are normally fleeting intermediates in the catalytic cycle of the enzyme. The anti-tumor topoisomerase II inhibitors presently used in the clinic poison the enzyme by stabilizing cleavable complexes, presumably by inhibiting decreasing the rate of backward reaction i.e. slow rate of religation of cleaved DNA (Fig 1.2). Thus synthesis of DNA and RNA is blocked. DNA religation and preventing enzyme catalytic activity thereby making the ternary complex stable either by increasing the rate of forwards reaction i.e. more rate of DNA cleavage or by decreasing the rate of backward reaction i.e. slow rate of religation of cleaved DNA. Thus synthesis of DNA and RNA is blocked.

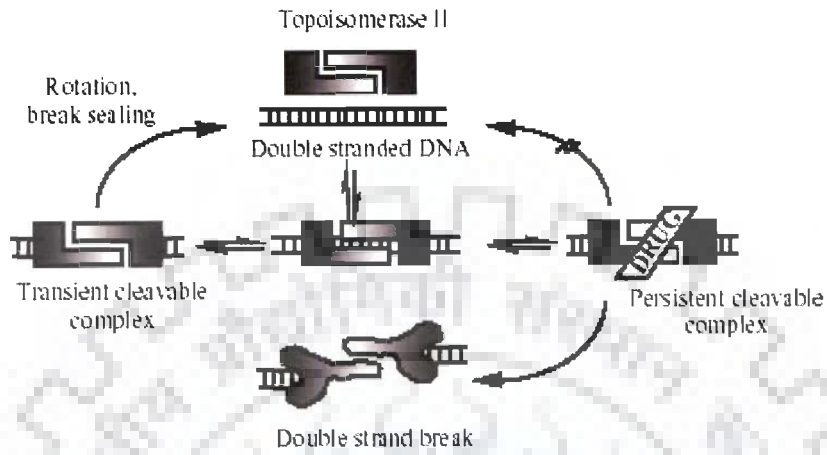


Fig. 1.2 DNA damage induced by inhibition of Topoisomerase II

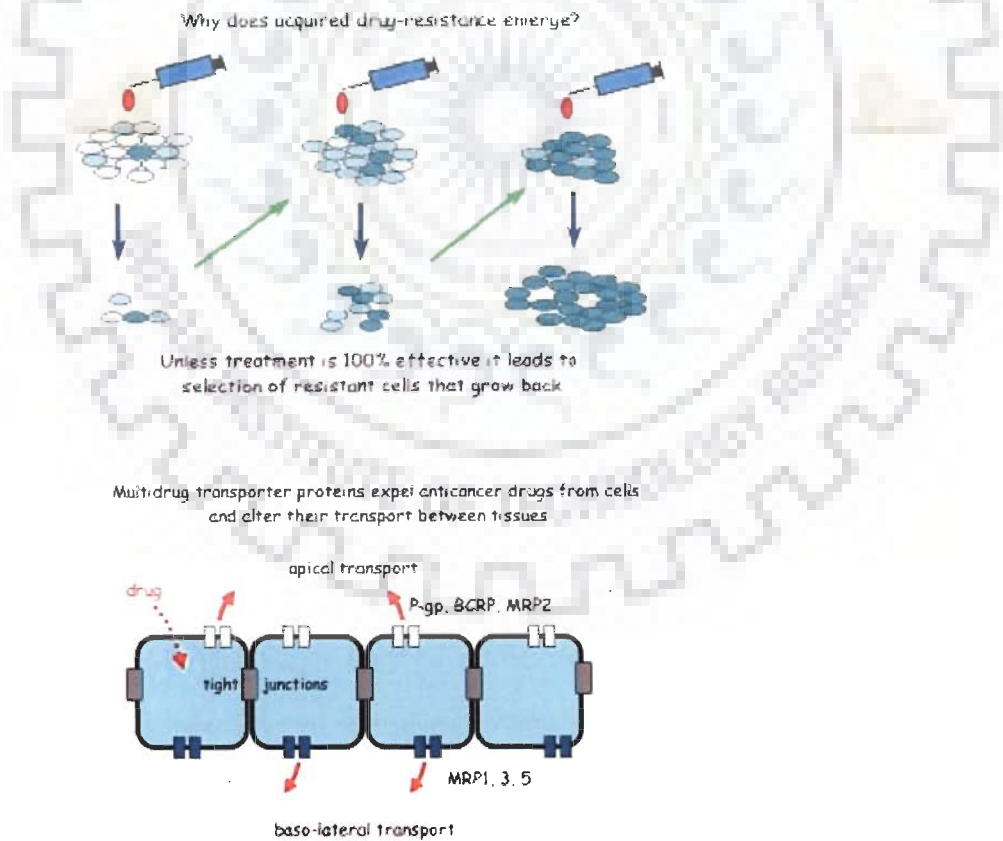


Fig. 1.3 Acquired multiple drug resistance and its Mechanism

(Adopted from internet)

1.2.4.2 Microtubule Inhibitors

Microtubules are protein polymers involved in cellular movement and morphology. Microtubules occur in equilibrium between polymerized and free tubulin dimers. Inhibitor drugs disrupt this equilibrium. Vinca alkaloids (vinblastine, vincristine) are examples of this type of drugs.

1.3 MITOXANTRONE

Structure–activity relationships do exist between cytotoxicity and strength of intercalative binding; these correlations are not general but they are confined to the series of structurally related analogs in which biological activity is manifested. Thus, there is need for continuing search for novel compounds of potential clinical utility with a true selectivity towards tumor cells, reduced toxicity and lesser resistance towards cell lines particularly in view of reports on multi–drug resistance, MDR depicted in Fig. 1.3. The structures of the clinically used anthracyclines are shown in Fig. 1.1(a–b). The anthracyclines are a fermentation product of *Streptomyces peucetius* var. *caesius* and were originally described as antitumour antibiotics. Mitoxantrone, (MTX), namely, 1, 4–dihydroxy–5,8–bis[[2–[2–hydroxyethyl) amino]amino]–9, 10–anthracenedione (Fig. 1.4a) is synthetic analogue of the anthracycline antibiotic first synthesized by independent group of workers [83, 122] . It was found to have anti neoplastic activity both in animals and in–vitro test systems. Structurally similar to anthracyclines, MTX was developed as replacement for doxorubicin (adriamycin) (Fig. 1.1b) to circumvent the cardiotoxic effects (irreversible damage to heart muscles) after extended use of chemotherapy by anthracyclines. The benefit of mitoxantrone is that not only is its antitumor activity more efficient than adriamycin, doxorubicin and daunomycin, but more importantly, it shows considerably reduced dose – related cardiotoxic effects over the other anthracycline [18, 106].

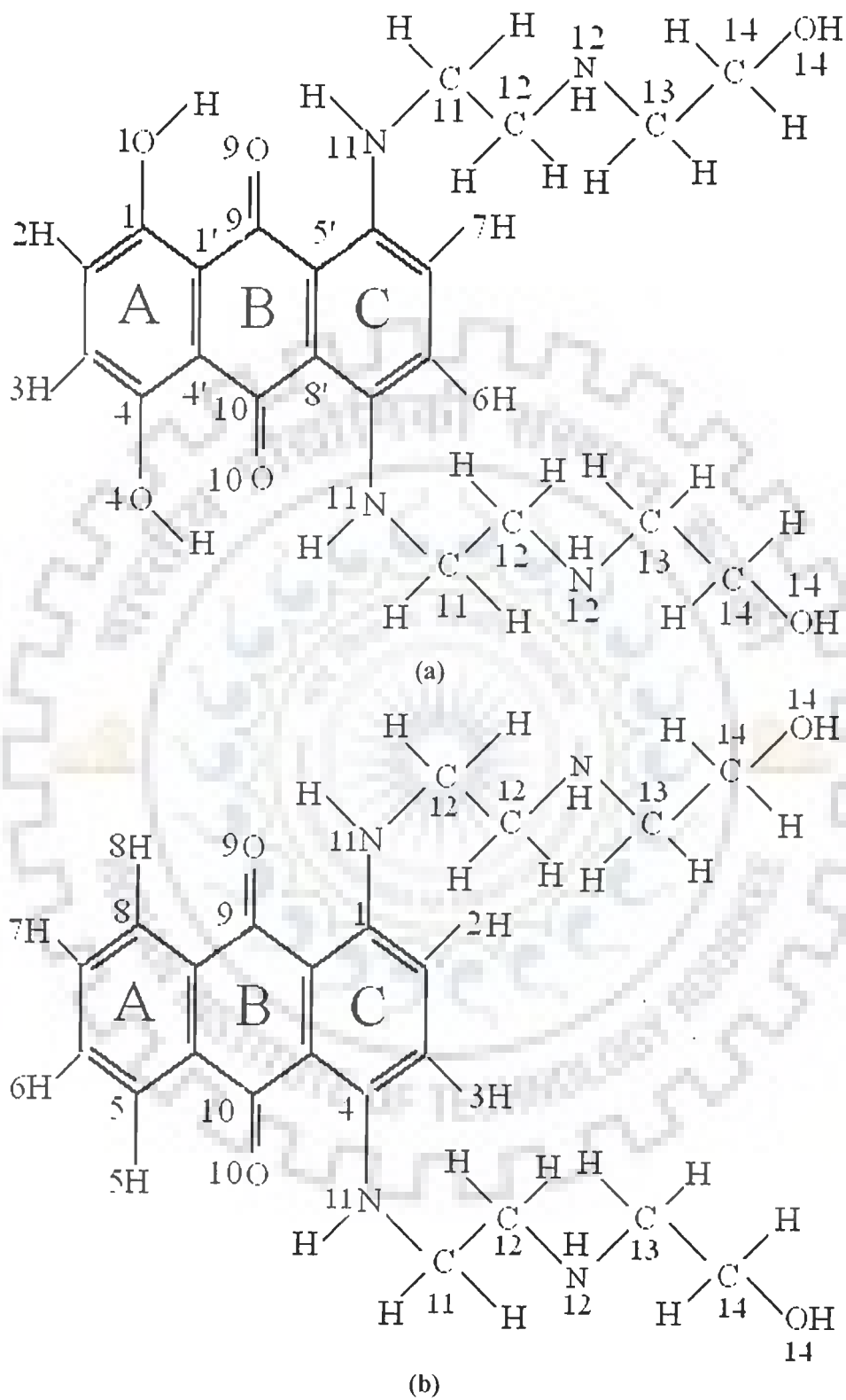


Fig. 1.4 Molecular structure (a) Mitoxantrone (b) Ametantrone

1.3.1 STRUCTURE ACTIVITY RELATIONSHIPS

MTX possesses quinone moieties on adjacent rings that allow it to participate in electron transfer reactions and generate oxygen free radicals. Chemical substituents present on its ring as are also known to offer the therapeutic properties. Structure activity relationship studies showed the crucial role of diaminoalkyl group in side chains of anthracenediones for the biological activity of the compound. Good efficacy and potency in MTX has been imparted due to ethyldiamine substituents at both 5 and 8 positions and further 1, 4 dihydroxylation of the aromatic nucleus substantially increases its activity [10, 83]. It is known in absence of 1OH / 4OH substituents (Fig. 1.4b) ametantrone (AME) does not show any anticancerous activity. MTX has also shown to exhibit DNA topoisomerase II activity at least in some cellular systems [107].

1.3.2 BIOLOGICAL ACTIVITY

Mitoxantrone, (MTX) is effective against wide spectrum of tumors; it is being used for the treatment of advanced breast cancer, non-small cell lung cancer, non-Hodgkin's lymphoma, non-lymphocytic leukemia. Clinically, MTX is applied either as a single agent or as a component of combination treatment regimens. Against P-388 leukemia, its efficacy and therapeutic index equaled or surpassed those of adriamycin, daunomycin, methotexate, or 5-fluorouracil.

1.3.3 MECHANISM OF ACTION

The anthracycline based drugs are highly reactive in solution and create panoply of effects on biological systems. A major component of their cytotoxicity is due to poisoning of topoisomerase II. Anthracycline also intercalate into double-stranded DNA and produce structural changes that interfere with DNA and RNA synthesis. Before the effect of the anthracyclines on topoisomerase II were fully appreciated, it was their ability to participate in

oxidation–reduction reactions that was believed to produce cytotoxicity. The photo–physical properties of the mitoxantrone [3–5] and also the efficiency with which it generates singlet oxygen are very sensitive to the state of its aggregation.

1.4 INTERCALATION GENERAL PHENOMENON

1.4.1 CHANGES INDUCED BY INTERCALATION

Intercalation changes the physical properties of a double helix of DNA because base pairs must separate vertically to allow the drug entry, the sugar phosphate bone is distorted and the regular helical structure is destroyed. According to such a model, the DNA must lengthen with increasing amount of added drug. This is indeed observed by enhanced viscosity and the diminution of the sedimentation coefficient, effects which also suggest overall stiffening of the DNA duplex [39] A two stage containing, anti–cooperative process was established from non–linear scatchard plot and from the kinetics, which is the characteristic of intercalating agents.

1.4.2 NEAREST–NEIGHBOUR EXCLUSION PRINCIPLE

This principle states that intercalators can at most bind at alternate possible base pair sites on DNA, giving a maximum one intercalator between every second site. The exclusion principle states that when an intercalator binds at one particular site, binding of another intercalator at adjacent site is inhibited probably because nucleotides flanking the intercalator are geometrically distorted. All spaces between base pairs are potential binding sites for a non–specific intercalator.

1.4.3 DNA UNWINDING

The separation of base pairs makes room for the intercalator. This can be visualized as a combination of pulling along the B–DNA double helix axis and left handed unwinding in order to prevent breakage of sugar–phosphate backbone. Intercalation into the pyrimidine 3’–

5' purine sequence is 7–13 Kcal / mole more favorable than purine 3'–5' pyrimidine intercalation because base overlap is more pronounced in former than latter. The intermolecular interaction is supported by intra-molecular electrostatic forces rendering pyrimidine 3'–5' purine sequences more prone to intercalation.

1.5 FORCES BETWEEN INTERCALATORS AND DNA

1.5.1 HYDROGEN BONDING

The phosphate group, sugar, bases in nucleic acids and hydrophilic groups in anthracycline drug participate in hydrogen bonding with water. Since all linear hydrogen bonds have similar free energies, they make little net contribution to the favorable free energy change when drug and nucleic acid interact in solution. By contrast, formation of poorly aligned hydrogen bonds, or absence of some of them on the complex formation, carries a free energy penalty of about 4 KJ mol⁻¹. Thus hydrogen bonds are one of the most important means of making sequence specific interaction of nucleic acid with drug.

1.5.2 ELECTROSTATIC FORCES: SALT BRIDGES

Salt bridges are electrostatic interactions between groups of opposite charge. They typically provide about 40 KJ mol⁻¹ of stabilization per salt bridge. In drug–DNA complexes, strength of salt bridges decreases with the increase in concentration of the salt. They are much stronger when there are no water molecules between the ionized groups because water has a high dielectric constant. These are relatively long-range forces.

1.5.3 ENTROPIC FORCES: THE HYDROPHOBIC EFFECT

The hydrophobic effect is due to the behavior of water at an interface. Any molecule in water creates a sharply curved interface and so orders a layer of water molecules around itself. When molecules aggregate, the ordered water molecules at the interface are released

Polar surfaces, where the enthalpy loss tends to offset the entropy gain or desolvation are less likely to aggregate than non-polar ones. Molecules of water left at the interface between the drug and the nucleic acid obviously decrease the entropy of the system.

Therefore the surface of the non-planar aromatic chromophore of drug tends to be exactly complementarily so that no unnecessary water molecules remain when the complex forms.

1.5.4 BASE STACKING: DISPERSION FORCES

Base stacking is caused by two kinds of interaction: the hydrophobic effect mentioned above and dispersion forces. Molecules with no net dipole moment can attract each other by a transient dipole-induced dipole interaction. Such dispersion forces decreases with the inverse sixth power of the distance separating the two dipoles, and so are very sensitive to the thermal motion of the molecules involved. Despite their extreme distance dependence, dispersion forces are clearly important in maintaining the structure of double stranded nucleic acids because they help to cause base stacking. Besides they allow aromatic ring of the drug to intercalate between bases and stabilize it by base stacking.

1.6 NUCLEIC ACID STRUCTURE AND FUNCTION

Nucleic acid (DNA) and ribonucleic acid (RNA) are the informational molecules of all living organisms. Besides storing and transmitting information, RNA forms structural and functional parts of units such as the ribosome and in some system has a catalytic function as ribozymes. Both DNA and RNA (Fig. 1.5a) are long polymers assembled of repeating subunits, the nucleotides. The sequence of nucleotide information in nucleic acids molecules (mainly DNA) makes up a code that stores and transmits the direction required for assembling all types of proteins. In addition to providing the building blocks of nucleic acids, carry out a variety of biological functions. Many nucleotides are molecules, built on nucleotides that transport chemical energy in the form of phosphate groups or electrons from

one reaction system to another. Others carry metabolites such as acetyl groups between reactions. Still other nucleotides in cyclic form are important in cell regulation.

1.6.1 NUCLEOTIDE BASES

1.6.1.1 Purines: Adenine and Guanine

Two different heterocyclic aromatic bases with a purine ring (composed of carbon and nitrogen) are found in DNA (Fig 1.5b). Adenine has an amino group ($-\text{NH}_2$) on the C6 position of the purine ring. Guanine has an amino group at the C2 position and a carbonyl group at the C6 position. Besides these, minor bases like inosine, 7-methyl guanosine, etc. are also found as components of nucleic acids.

1.6.1.2 Pyrimidines: Thymine, Cytosine and Uracil

Thymine contains a methyl group at the C5 position with the carbonyl group at C4 and C2 positions. Cytosine contains a hydrogen atom at the C5 position and an amino group at C4 (Fig 1.5 a). In RNA thymine is replaced by uracil.

1.6.2 SUGAR RING

Ribose sugar is found in all RNA molecules while a slightly different sugar, β -D-2-deoxyribose is found in DNA. This is a derivative of β -D-ribose in which the hydroxyl ($-$) the 2' position is replaced by hydrogen ($-\text{OH}$) (Fig. 1.6a). The sugar moiety of DNA is one of the more flexible and dynamic parts of the molecule. The sugar base combination is called nucleoside unit. A nucleotide is a nucleoside phosphorylated at one of the free sugar hydroxyls.

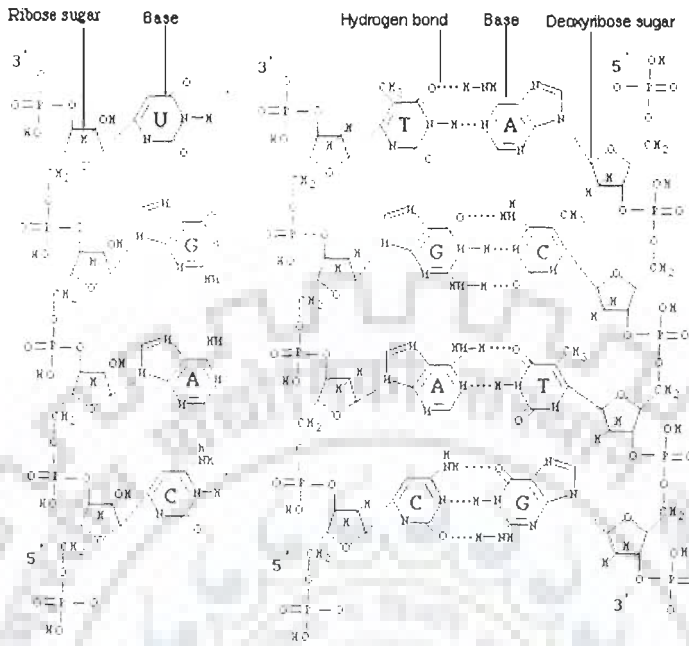
1.6.3 SUGAR PUCKER

Usually all complexes have purine sugar at the 5' position in C3'-endo pucker. In most of them, the pyrimidine sugar at the 3' end is C2'-endo with only few cases of C3'-endo are found (Fig. 1.6b). Upon intercalation both χ and β increase by over 50° , χ being

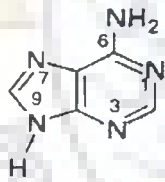
RNA and DNA

RNA (single stranded)

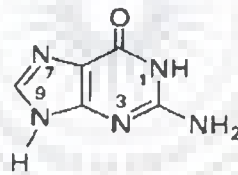
DNA (double stranded)



(a)

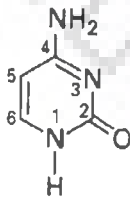


adenine

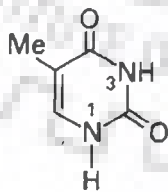


guanine

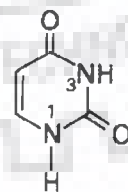
Purines



cytosine



thymine



uracil

Pyrimidines

(b)

Fig. 1.5 (a) Structure of RNA and DNA (b) Structure of purines and pyrimidines.

pushed into high anti range. Model building studies suggested that the unwinding angle is dependent on a combination of small variations in the backbone torsion angles and base-pair geometry expressed as bend and twist, and not just on sugar pucker. It is clear that a correlation exists between unwinding angle and shape of intercalator agent.

1.6.3 SUGAR PUCKER

Usually all complexes have purine sugar at the 5' position in C3'-endo pucker. In most of them, the pyrimidine sugar at the 3' end is C2'-endo with only few cases of C3'-endo are found (Fig. 1.6b). Upon intercalation both χ and β increase by over 50°, χ being pushed into high anti range. Model building studies suggested that the unwinding angle is dependent on a combination of small variations in the backbone torsion angles and base-pair geometry expressed as bend and twist, and not just on sugar pucker. It is clear that a correlation exists between unwinding angle and shape of intercalator agent.

1.6.4 ENDOCYCLIC TORSIONAL ANGLES: FURANOSE SUGAR RING

The sugar ring occupies a pivotal position in the nucleotide unit because it is part of both the backbone and the side chain. In order to provide a complete description of the ring conformation, it is necessary to specify the endocyclic torsion angles for the ring as well as the bond lengths and bond angles. The five endocyclic torsion angles (Fig. 1.7a) for the bonds $O4' \rightarrow C1'$, $C1' \rightarrow C2'$, $C2' \rightarrow C3'$, $C3' \rightarrow C4'$ and $C4' \rightarrow O4'$ are denoted by the symbols, ν_0 , ν_1 , ν_2 , ν_3 and ν_4 respectively.

1.6.5 THE PHOSPHODIESTER BOND

In DNA and RNA the individual nucleotides are joined by a 3'-5' phosphodiester bond. The nucleotides are joined from the 3' sugar carbon of one nucleotide, through the phosphate to the 5' sugar carbon of adjacent nucleotide. This is termed as 3'-5' phosphodiester bond (Fig. 1.7b). The primary sequence of nucleic acids is determined by the

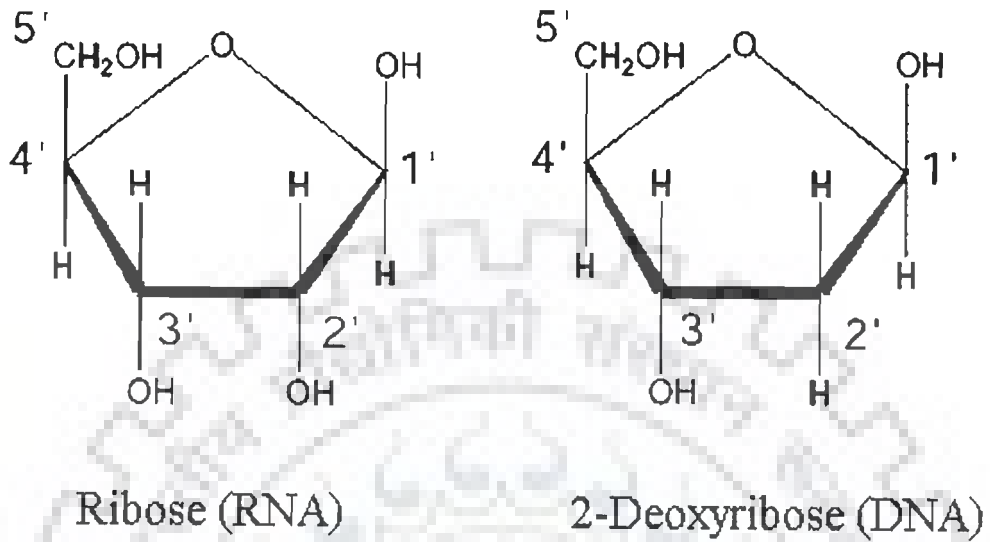


Fig. 1.6(a) Five membered furanose ring of deoxyribose and ribose sugar

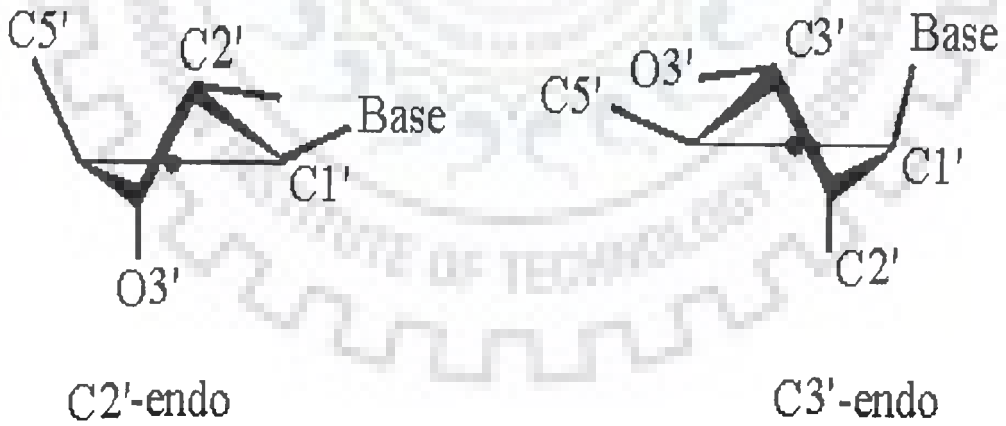


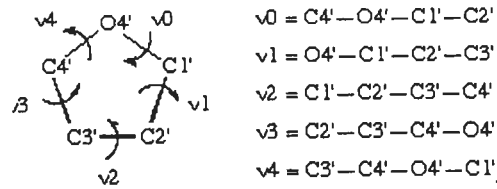
Fig. 1.6(b) Preferred conformations C2'-endo and C3'-endo of sugar pucker

sequence of bases along the nucleotide chain and the function of acids namely replication, transcription and translation are governed by this sequence. The three-dimensional backbone conformation of nucleic acids is governed by a number of torsion. The sequential numbering of atoms $(n-1)P \rightarrow O5' \rightarrow C5' \rightarrow C4' \rightarrow C3' \rightarrow O3' \rightarrow P \rightarrow O5'_{(n+1)}$ is defined by torsion angles α , β , γ , δ , ϵ and ζ as shown in (Fig. 1.7b).

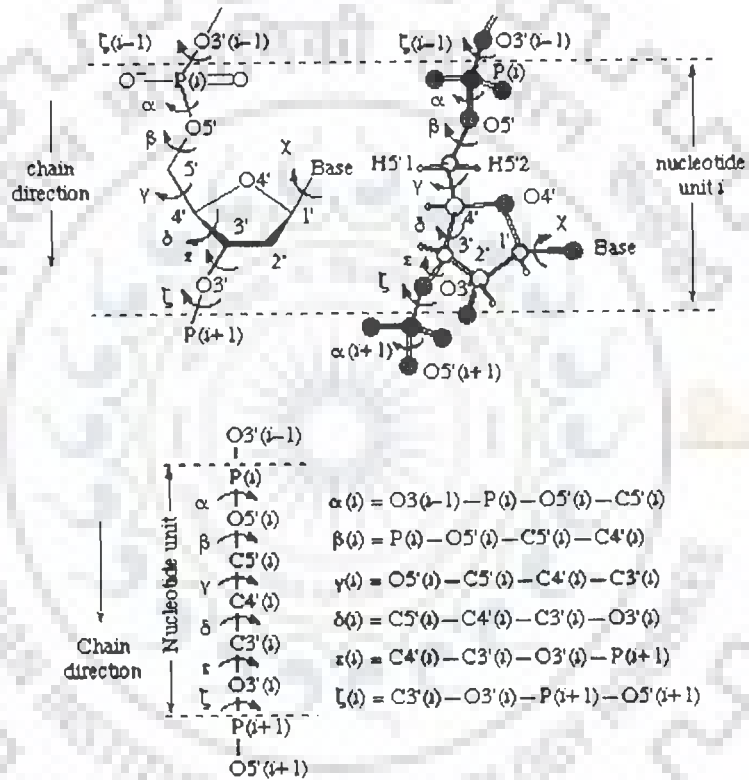
Duplex DNA is a right-handed helix formed by two individual DNA strands aligned in anti-parallel fashion. The two strands are held together by hydrogen bonds between individual bases as shown in (Fig. 1.5a). The bases are stacked near the center of the cylindrical helix. The hydrophobic interactions provide stability to the helix. A common feature of all the double helices is base stacking. Although the geometry of adjacent base pair varies, in each case the distance between neighbouring base pair plane is about 3.4 Å. This is equal to Van der Waal's radius of planar aromatic compound. It was shown that purines cause large upfield chemical shift due to stacking as compared to pyrimidines. The sugar and phosphate groups are at the outer side of the helix and forms a backbone of the helix. In a double helix, complementary base pairing connects the two-polynucleotide chains. Adenine always forms base pair with thymine and cytosine forms base pair with guanine according to Watson and Crick base pairing scheme (Fig. 1.5a). Although right handed DNA is presumed to be the predominant conformation in vivo but under different conditions of salt and humidity DNA shows structural polymorphism i.e. it exists in alternative conformations like A and Z DNA. The main features of A, B and Z-DNA are listed in Table 1.1. The structure of DNA can be described by number of helicoidal parameters like rise, pitch, tilt, roll, twist, no of bases per turn, etc. These different types of DNA differ from each other in their helicoidal parameters, like rise, pitch, tilt, roll, twist, no of bases per turn, etc. These different types of DNA differ

Table 1.1 Structural characteristics of A, B and Z type of double helices

Characteristics	A	B	Z
Helix sense	Right handed	Right-handed	Left handed
Repeating unit	1 bp	1bp	2 bp
Rotation/bp	33.6°	35.9°	60°/ 2
Mean bp/turn	10.7	10.0	12
Inclination of bp to axis	+19°	-1.2°	-9°
Rise/bp along axis	2.3Å	3.32Å	3.8Å
Pitch/turn of helix	24.6Å	33.2Å	45.6Å
Mean propeller twist	+18°	+16°	0°
Glycosyl angle	Anti	anti	C: anti, G: syn
Sugar pucker	C3'-endo	C2'-endo	C: C2'-endo, G: C2'-exo
Diameter	26Å	20Å	18Å



(a)



(b)

Fig 1.7 (a) A ribose unit showing atomic numbering and definition of torsion angles, v_0 , v_1 , v_2 , v_3 and v_4 b) Section of a polynucleotide backbone showing the atom numbering and the notation for torsion angles α , β , γ , δ , ϵ , and ζ

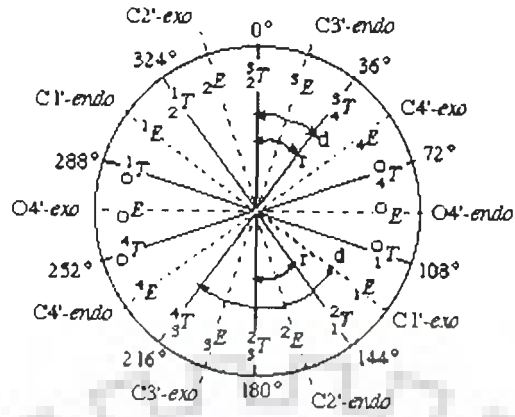


Fig 1.8 Pseudorotation cycle of furanose ring in nucleosides (Altona, and Sundarlingam, [2])

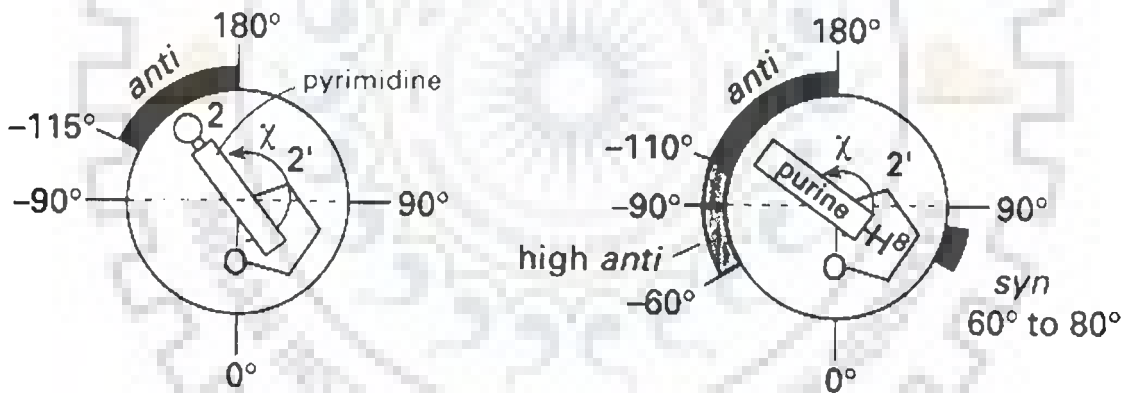


Fig 1.9 Anti high, anti and syn orientations about the glycosidic bond in pyrimidine and purines

from each other in their helicoidal parameters, which define the helix of DNA. At high temperature, the secondary structure of DNA is lost and random coils are generated. Each conformation of the furanose ring can be unequivocally described by two pseudorotational parameters: the phase angle of pseudorotation, P , and the degree of pucker, ψ_{\max} .

Each conformation of the furanose ring can be unequivocally described by two pseudorotational parameters: the phase angle of pseudorotation, P , and the degree of pucker, ψ_{\max} .

In nucleotides, the pseudorotation phase angle P is calculated from the endocyclic sugar torsion angles Fig. 1.8 [2]

$$\tan P = \frac{(v_4 + v_1) - (v_3 + v_0)}{2 \cdot v_2 (\sin 36^\circ + \sin 72^\circ)}$$

Given the phase angle P , the five torsional angles are related by

$$v_j = v_{\max} \cdot \cos (P + j \cdot \psi)$$

where $j = 0$ to 4 and $\psi = 720^\circ / 5 = 144^\circ$. The maximum torsion angle, v_{\max} is derived by setting $j = 0$

$$v_{\max} = v_0 / \cos P$$

At every phase angle P , the sum of the positive torsional angles is equal to the sum of the negative torsional angles, i.e. the sum of the five angles is zero.

$$v_0 + v_1 + v_2 + v_3 + v_4 = 0$$

Standard conformation ($P=0^\circ$) is defined with a maximally positive $C1'-C2'-C3'-C4'$ torsion angle [i.e. the symmetrical 3T_2 form], and P has value $0-360^\circ$. Conformations in the upper or northern half of the circle ($P = 0-90^\circ$) are denoted N and those in the southern half of the circle ($P = 180 / 90^\circ$) are denoted S conformation. The relationship between P and the *endo* / *exo* and T / E notations is illustrated in. It may be seen that the symmetrical twist (T)

conformations arise at even multiples of 18° of P and the symmetrical envelope (E) conformations arise at odd multiples of 18° of P .

The symbols 'r' and 'd' represent the usual range of P values for N and S conformations of ribo-(r) and 2'-deoxyribo-(d) furanose rings of $-D$ -nucleosides and nucleotides. In B-DNA two ranges of pseudorotation phase angles are preferred C3' endo at $0^\circ \leq P \leq 36^\circ$ (N conformer) and C2' endo at $144^\circ \leq P \leq 180^\circ$ (S -conformer).

1.6.6 GLYCOSYL TORSION ANGLE (χ)

The glycosyl torsion (χ) angle define the orientation of the purine and pyrimidine bases relative to sugar ring. For pyrimidine nucleoside, χ is defined as torsion angle $O4'-C1'-N1-C2$ and for purines χ is $O4'-C1'-N9-C4$. Relative to the sugar moiety the base can adopt two main orientations about the glycosyl $C1'-N$ link, called *syn* and *anti* (Fig 1.9). Rotamers with *chi* values between -90° and $+90^\circ$ are called *syn* whereas *anti* refers to *chi* values from $+90^\circ$ to $+270^\circ$. In Watson-Crick double helices both bases of base pairs are in *anti* conformation. Bases in *syn* conformation indicate a distortion of the double helix due to base pair opening or mismatched base pairs. The *syn* conformation is also found with guanines in left-handed Z-DNA (zig-zag helix). In *anti*, the bulk of heterocyclic atoms i.e., the six-membered pyrimidine ring in purines and O_2 in pyrimidines is pointing away from the sugar, and in *syn*, pyrimidine is over and toward the sugar. An *anti* conformation is located near $\chi = 0^\circ$, whereas in *syn* domain is around 210° . There is also a high *anti* which denotes a torsion angle lower than *anti*.

1.6.7 MAJOR AND MINOR GROOVE

As a result of the double helical nature of DNA, the molecule has two asymmetric grooves. One groove is smaller than the other. This asymmetry is a result of the geometrical configuration of the bonds between the phosphates, sugar, and base groups that forces the

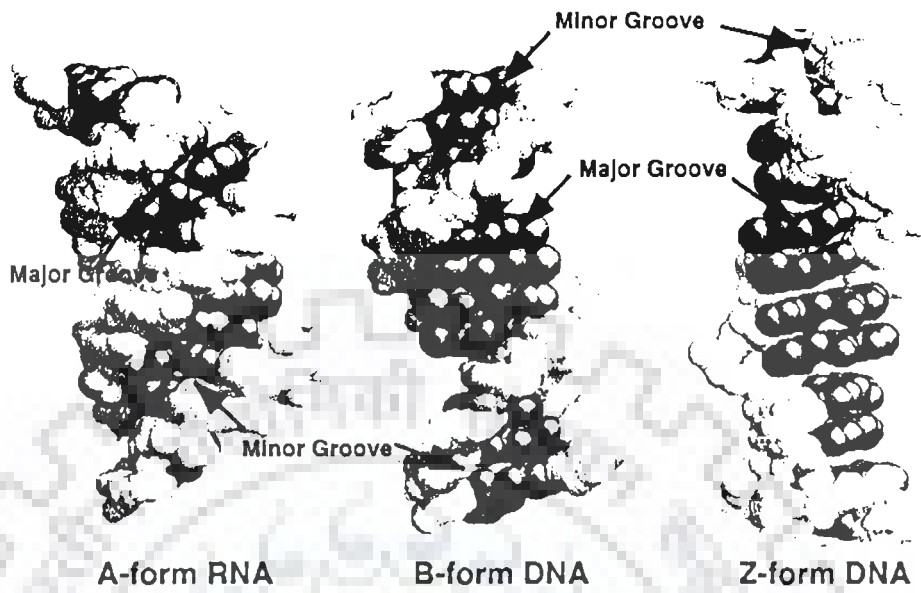


Fig 1.10 Major and Minor grooves in A-, B- and Z-forms of DNA.

base groups to attach at 120° angles instead of 180° degrees. The larger groove is called the *major groove* while the smaller one is called the *minor groove* Fig 1.10

1.7 HELICOIDAL PARAMETERS OF DNA

1.7.1 DEFINITION

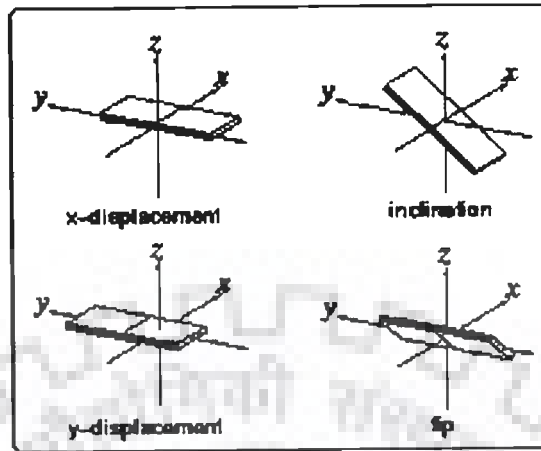
The structure of DNA can be described by a number of parameters (Fig. 1.11) that define the helix [31]. Polynucleotides in helical arrangement display order can be expressed in terms of “helical or helicoidal” parameters. Helical parameters can be analyzed from output of CURVES program developed by Richard Lavery [65–68]. The helicoidal parameters are grouped into three categories:

- i. global base pair–axis parameters
- ii. intra–base pair or global base–base parameters
- iii. inter–base pair or base pair–step parameters

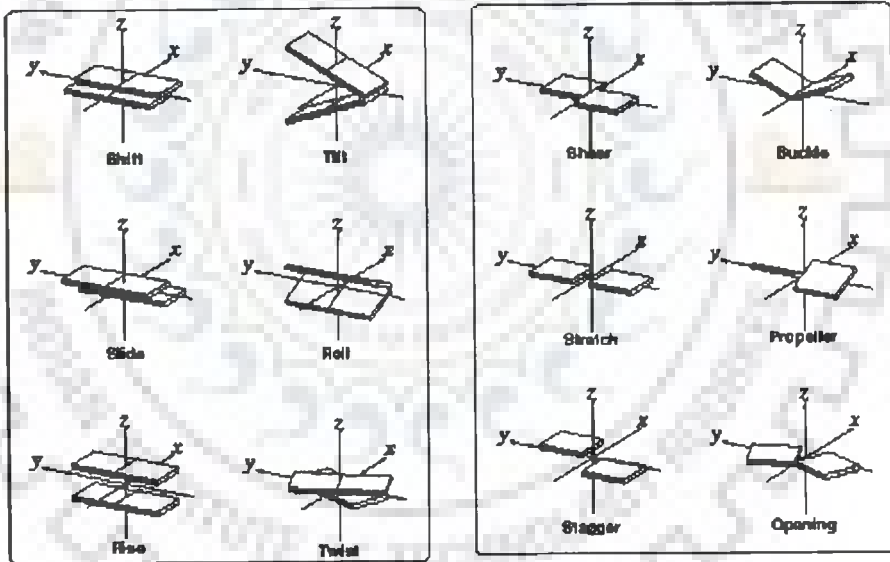
These parameters include “global helical parameters” defined relative to a global helix axis and “local helical parameters” defined relative to local helix axis at each base pair.

1.7.2 GLOBAL BASE PAIR AXIS PARAMETERS

The terms “global” and “local” are used with two different meanings in the field of nucleic acid structure analysis. A global property of a molecular structure depends on all the atoms in the structure, while a local property arises if only a subset of neighboring atoms is used to analyze that quantity. The global axis parameters as well as the local inter base pair parameters are related to particular base pair steps. These parameters are vector quantities,



(a)



(b)

(c)

Fig. 1.11 Helicoidal parameters of DNA (a) Global base–base parameters (b) Interbase parameters (c) Intrabase pair parameters

which have a defined location in 3-dimensional space and with respect to the nucleic acid sequence. They characterize properties of the whole structure. Local parameters are related to parts of a structure while global parameters are valid for the whole structure. In this sense the global helical parameters from CURVES are also local. Among global base pair-axis parameters, x- and y-displacement refers to the shift of bases in positive or negative x and y direction with respect to each other.

1.7.3 INTERBASE PARAMETERS (BASE PAIR STEP PARAMETERS)

In contrast, the average inter base pair parameters are scalar values that are not related to any part of the structure. The helical parameters are derived from the spatial location of the bases, while the sugar phosphate backbone is not taken into account. The six inter base pairs parameters (rise, twist, shift, roll, tilt, slide) describe the local conformation of a double helix at every base pair step. In a regular helix such planar elements are stacked on each other. Each step from one plate to the next can be described as a combination of a translational and a rotational movement. The translational and the rotational displacements are 3-dimensional vectors, which can be split into three orthogonal components. The three translational components are rise, shift and slide. Rise is a translation in the direction of the helical axis (z-axis), and shift is orthogonal to the helical axis and directs to the major groove side. If the bases in base pairs were coplanar and the base pairs exactly perpendicular to the helix axis, the axial rise per nucleotide should correspond to the van der waal's distance, 3.4 Å. Twist, roll and tilt are the three rotational components. Twist is a rotation about the helical axis (z-axis). A positive roll indicates that there is a cleft between two stacked base pairs which opens towards the minor groove. A negative roll is related to an opening towards the major

groove. Base pair tilt refers to the angle of the planer bases with respect to the helical axis. In the B-form DNA the bases are tilted by only -6° . In the A-form DNA the base pairs are significantly tilted at an angle of 20° . The sense of the base-pair tilt is associated with sugar puckering. In double helical polynucleotides, the normals to the base pair are not exactly parallel to the helix axis but inclined to it by up to 20° . The sense of tilt is positive in A-type and negative in B-type of helices, and hence is correlated with sugar puckering. Base tilt angle is correlated with rise per residue.

1.7.4 INTRABASE PAIR STEP PARAMETERS (BASE PAIR PARAMETERS)

These are six parameters describing the translational and rotational displacement between the two bases of a base pair. Again, the translational and rotational displacement is divided into orthogonal components. The translational components are stagger, stretch and shear and the rotational components are propeller-twist, buckle, opening.

The base pairs in nucleic acid structures are not really planar. For example, the propeller twist of AT base pairs in B-DNA is usually in the range of -15° to -20° . If the base pairs are not planar, the six inter base pair parameters will give only a rough model of the helix. A more detailed picture is obtained if the intra base pair parameters are also taken into account. The Cambridge convention defines six base pair parameters which describe the deviation from planarity within a base pair as shown in Fig. 1.11.

1.8 LITERATURE REVIEW

1.8.1 SYNTHESIS OF ANTICANCER DRUG MITOXANTRONE AND ITS ANALOGUES.

Series of 1, 4-bis- [(amioalkyl) amino]-9,10-anthracenediones were synthesized [83] from condensation of alkyldiamines with quinizarin or with 2, 3-dihydro-1, 4, 5, 8-tetrahydroxy-9,10-anthracenedione. It was found these compounds and their 5, 8-hydroxyl derivatives were marked active against both leukemia and solid tumors in mice. Activity was found to be maximal for 5, 8-dihydroxylation and 1,4-bis[(2-aminoethyl)amino]substituted compounds, in which the terminal nitrogen atoms were either unsubstituted or carried 2-hydroxyethyl groups (MTX), indicating the importance of the hydrophilicity. It was found that MTX has better efficacy and potency as compared to adriamycin.

1.8.2 SPECTROSCOPIC STUDIES

1.8.2.1 NMR Spectroscopic Studies:

(a) Uncomplexed drug

¹H NMR of MTX [75] indicated symmetrical nature of the drug. They reported that all the methylene protons; namely, 11CH₂, 12CH₂, 13CH₂ and 14CH₂ lies in the region (3–4 ppm) where as the 6H / 7H and 2H / 3H protons are observed around 6–7 ppm. They assigned 2H / 3H downfield with respect to the 6H / 7H protons which was contradicted by the studies carried out later [28, 15].

Concentration dependent NMR experiments [15] revealed a down field shift of the proton resonances upon dilution, attributable to the self-association due to π - π^* transitions. 1D NOE experiments indicated proximity between 2H / 3H and 6H / 7H indicatives of the head to tail dimer formations. The 6H / 7H protons of MTX showed strong cross peaks with 11CH₂ and 12CH₂ hence confirming their assignment. [28] reported that since the MTX has plane of symmetry and so chemical equivalence is found for resonances of 2H / 3H and 6H / 7H and the protons of the two amino alkyl side chains. The 2D ROESY spectrum of the MTX solution at initial drug concentration 1.01 mM exhibits an intermolecular contact between 2H

/ 3H and 11CH₂ of the antibiotic, provided the unambiguous evidence of the inverse (head to tail) orientation of the antibiotic chromophore in the aggregate. The self association constant of MTX (K_a) was found to be higher than found substantially [26, 113]. The concentration dependent experiment showed the shift of proton chemical shifts to lower frequencies at higher concentrations, which result from intermolecular stacked complexes in solution in common with intermolecular stacked complexes in common with the aromatic drug molecule [26, 77] the structure of MTX monomer obtained theoretically by energy minimization showed that planes showed significant overlap of the chromophore and amino alkyl side chains also H-bond may be formed between the side chains secondary amino 11NH and hydroxyl groups (1OH / 4OH) of the antibiotic chromophore. Indirect conformation of the assumption of intermolecular hydrogen bonding were shown by optical investigation of AME (lacking 1OH / 4OH) was characterized by five times smaller dimerization constant as compared to MTX. They also proposed that MTX dimer in solution by excitation model [69], is unlikely to be correct, resembles the head to tail orientation but the orientation of the planes of the chromophore is much higher (~ 0.62 nm) because at such large separation between the chromophores the magnetic shielding of the drug protons in the aggregate, as well as changes of proton chemical shifts with concentration and temperature should be negligible. [41].

They also proposed relatively high negative value of enthalpy of self-association of MTX is determined by dispersive interaction between the aromatic chromophore and possible formation of intermolecular H-bonds in the antibiotic aggregated.

(b) Binding studies of drug with DNA

Complete assignment of the stoichiometric 1: 1 complex of mitoxantrone with d-(CGCG)₂ tetranucleotide sequence [75] was made by 2D-COSY, 1D NOE and 2D-HH-INADEQUATE techniques.

Upfield shifts of 0.22 ppm and 0.19 ppm for C1H5 and C3H5 protons respectively, substantial line broadening for G2H8 and C3H5 suggested their closeness to the binding site and hence the observed shifts. Sugar protons of the tetramer, H1', H2' H2'' and H4' showed large shifts, indicating that they lie with in the immediate vicinity of the ring current due to the aromatic chromophore of mitoxantrone while the H3' showed intermediate change in the chemical shift whereas H5' and H5'' showed negligible shifts suggesting they are remote from the binding site. These results were in accord with the intercalated chromophore [73] rather than one externally bound to duplex [38, 58] since the H3', H5' and H5'' protons for links to the sugar phosphate backbone on the outside edges of the miniature double helix. On intercalation largest upfield shift was observed for the 11NH followed by the aromatic protons, namely 2H / 3H and 6H / 7H respectively with in the drug molecule. The effect diminishes along the side chain to terminal 14OH group.

Several intermolecular NOEs (Nuclear Overhauser effect) connectivities between the drug and DNA i.e, 14OH-C1H6, 14OH-C3H6, and 11CH₂-G4H8 (weak NOEs) were observed. Intramolecular NOEs with in the drug (d_i) were also observed between 11CH₂-12CH₂ and 11CH₂-13CH₂. This indicated that 14OH, 11NH and 12NH bind to the neighbouring base pairs from the intercalation site and in major groove and also to the central phosphate backbone as was also evident from the ³¹P studies.

The ¹³C and ³¹P NMR signals showed that neither the tetramer nor the 1:1 complex showed doubling of signals signifying no loss of symmetry on complexation, thus compatible with intercalation of the mitoxantrone is in the center of the tetramer i.e. between G2 and C3 i.e.

G2pC3 base pair step. ^{31}P studies suggested that terminal 14OH of the side chains binds to central phosphates such that the methylene groups are proximate to the C1H6, C3H6 and G4H8 all in the major groove, suggesting that side chain bind at the intercalation site from the major groove. This was in accordance with the GC preference for binding from spectroscopic and electron microscopic data [74] ^1H and ^{31}P NMR studies of the hexanucleotide d-(CGATCG)₂ and mitoxantrone [63] was carried out in H₂O solvent with particular in attention to the imino protons and ^{31}P assignments of the oligonucleotide. The detection of only three signals for imino protons was consistent with the anticipated two-fold symmetry of the duplex. ^{31}P - ^1H shift correlation contours were implied in ^{31}P assignments and confirming ^1H assignments of the duplex.

Further, titrimetric addition of mitoxantrone (MTX) resulted in selective and progressive chemical shifts with critical changes at stoichiometric of 1:1 and 2:1 drug / DNA (D / N) ratios as evident from the fact that the addition did not cause the hexanucleotide ^1H and ^{31}P to drift continuously, instead it gives rise to new set of broad signals at the expense of the intensity of the originals one. Consequently, the complex formation formed was regarded as the non-labile one with respect to the NMR time scale and point towards "slow exchange". The finite stoichiometry and the non-liability of the complex imply binding site-selectivity at the hexanucleotide duplex. Since, there was only one set of new signals observed in both proton and phosphorus studies it lead to the possibilities either the binding process is (a) fully co-operative at both binding sites or (b) the binding is symmetrical and remote from each other such that at one site will not influence binding at other site. Assumption (a) was ruled out as it would lead to combine ring effect of the two drug molecule resulting in upfield shift ~1ppm of imino protons as well as that of thymine and methyl protons which was not observed. The results were thus simply interpreted as that that drug preferably binds

at CG base pairs at the both end of the duplex. Same conclusion that binding was CG base pair selective was lead by other assumption. Kinetic study of the SDS (sodium dodecyl sulphate) driven dissociation of MTX from DNA, poly d(G-C)₂ and poly d(A-T)₂ [64] reported two rate components differing by factor of four which was consistent with assumption (a), though the MTX has much slower dissociation rate from poly d(G-C)₂ than poly d(A-T)₂. Independent electron microscopic studies [73] and equilibrium binding studies of MTX to natural and synthetic studies revealed GC base pair specificity. The results were in accord with the previous studies that MTX intercalates into DNA preferentially at CG sites [37, 74–75]. Best fit model for the drug at the intercalation site with the chromophore approximately perpendicular to the base pair axis and with the side chain extending into the major groove [54] was obtained by computer graphics.

The interaction of (2S)-2-morpholinodoxorubicin and morpholinodoxorubicin with hexanucleotides d-(CGATCG)₂ and d-(CGTACG)₂ by ¹H and ³¹P NMR spectroscopy was investigated [95]. In all the complexes the aglycon was shown to be located in the middle of the double helix, orthogonally oriented with respect to the base pairs, with ring D out of helix, extending out of the helix on the major groove and ring A, with ⁹H₈ conformation, between guanine G2 and G12. The variation of ³¹P chemical shifts was interpreted in terms of the conformational equilibrium leading to different populations of conformers. Alpha (α) and zeta (ζ) torsional angles monitored during the molecular dynamics simulations indicate a relevant population of terms of ζ and also α angles for C5pG6 and G2pT3 (G2pA3) units while the other phosphates exist in α ζ gauche gauche conformation. The assignments for phosphate groups of the oligomers were done at low drug / DNA ratio. They reported intensity of the C5pG6 signal in bound state as a function of ratio R = (drug / DNA) gave a stoichiometry ratio of two drugs per molecule. The second molecule of the drug intercalates

at the symmetrically located C5pG6 site of opposite strand. The decrease of K_{off} of (2S)-2-morpholinodoxorubicin corresponding to 10 fold increase of the residential time of the drug in the intercalation site, was in line with the higher activity found for this component.

1D and 2D homonuclear NMR spectroscopy [33] was combined with simulated annealing / rMD to characterize the interaction of 2-(pyrido[1,2-e]-purin-4-yl) with d-(CGATCG)₂. Intercalation occurs at the C1pG2 step. Pyridopurine derivative rings were not exactly perpendicular to the helix. C1 was not involved in the intercalation process and does not stack with its upper base G2. There was a weak, stacking interaction between the intercalated ligand and the DNA bases; however the drug / DNA affinity was enhanced by a hydrogen bond between the hydroxyl group at the end of the intercalator (drug) side chain and amide group of G6. The structure of the intercalated complex enabled insight into the structure activity relationship.

Interaction of (2S)-2-methoxymorpholino doxorubicin and morpholino doxorubicin with hexanucleotide d(CGATCG)₂ and d(CGTACG)₂ by 2D ¹H NMR and ³¹P NMR coupled with molecular dynamics techniques [80]. The results of above study were compared with doxorubicin and daunorubicin. On intercalation of drug, deformation was noticed in DNA as torsional angle α and ξ changes from value of gauche gauche (as found in B-DNA) to gauche trans values. The change is associated with downfield shift of phosphorus. Different nucleotide sequences do not affect the dissociation rate constants of the drug from the DNA. As a consequence it appeared that structural modifications at a level of ring A and amino sugar in the anthracycline molecule are important and the methoxymorpholino moiety plays a significant role in stabilizing the complex.

(c) Heteroassociation of drug other than DNA

Inclusion of the MTX [15] in cyclomaltooligosachharides was studied by ^1H NMR investigations. The presence of the cross peak between 2H / 3H of MTX and H-3 of sugar indicates the presence of the inclusion complexes. Cross peak was not observed between the 2H / 3H of the drug and H5 of the cyclomaltooctaoase (sugar) implying that the guest molecule enters into the sugar from the large hole. Factors affecting the stability of the inclusion complexes were explained by formation of hydrogen bonding between guest's polar and primary and secondary hydroxyl groups of cyclomaltooligosaccharides. Studies of MTX with sugar counterparts possessing no hydroxyl groups indicated the absence of the inclusion complexes indicating no inclusion took place in encapsulated in both cyclomaltooligosaccharides and thus could be used for adjusting release rate, and also enhancing the solubility of other analogues.

Hetero-association of MTX [25] with caeffine (CAF) was reported and comparison of the concentration dependence chemical shifts of MTX with and without CAF in solutions showed that presence of CAF in solution shifts proton resonances of MTX to higher frequencies (low field) due to hetero-association between MTX and CAF molecules. This was explained by smaller shielding effects by CAF molecules on the protons of MTX molecules in the hetero-complexes compared with that of the MTX in self-association aggregates.

Association constant obtained for complexation of CAF with MTX was intermediate between values of self-association constants of self-association constants of the interacting aromatic drug molecules, as found for systems studied previously [26].

Equilibrium constant of hetero-association is consistent is somewhat higher than other drug-CAF systems. Hydrophobic interactions between methyl group and alkyl side chains of MTX impart stabilization to the complex. The calculated 1:1 hetero-association

proposed that planes of chromophores of NOV and CAF in 1:1 are parallel to each other at distance of 0.34 Å. The structure of the NOV–CAF complex was consistent with that obtained using molecular modeling from which it was concluded that “rotation of caffeine by 180°” relative to the DNA intercalation ring system does not significantly alter the relative binding.

Solution study of the complex between 4'6-diamidino-2-phenylindole (DAPI) and DNA oligomer d-(CGATCG)₂ at 2:1 drug / duplex was studied [112]. Structure perturbations, and resonance shifts induced by binding provide evidence that DAPI interacts with DNA hexamer by two different binding mechanisms, in fast exchange on the NMR time scale, without any significant distortion of the B-type conformation of DNA hexamer. The results indicate that the ligand binds to into the dimer groove of central 5'–ATC–3' region of the hexamer and on the oligomer by $\pi - \pi$ stacking interaction with the terminal C1: G6 base pairs. A model for both binding mechanisms that accounts for all experimental data was generated by molecular mechanics and dynamics calculations based on experimental noes. IN the minor groove binding, N2 amino group of G2 precludes a deep insertion of phenyl ring of DAPI into the groove. Position and orientation of the drug in the external stacking interaction resemble those suggested for intercalation of DAPI between C:G base pairs.

(d) X-ray studies

The binding of macrocyclic bisacridine and ametantrone to CGATCG was studied [118]. Only one acridine of the bisacridine drugs binds at C5pG6 step of DNA, with the other acridine plus both linkers completely disordered. Surprisingly both terminal G.C base pairs are unreveted. The C1 nucleotide is disordered and the G2 base is bridged to its own phosphate through a hydrate Co⁺ ion, G2 swing towards the minor groove with its base stacked over the backbone. The C7 nucleotide is flipped away from the duplex part and base

paired to a two-fold symmetry related to G6. The central four base pairs adopt the B-DNA conformation. An unusual intercalator platform is formed by bridging four complexes together such that the intercalator cavity is flanked by two sets of G.C base pairs (i.e., C5G8 and G6C7) on each side, joined together by G6.G8 tertiary base pair interaction. In the bisacridine–CGATCG complex, only one ametantrone is bound. NMR titration of the bisacridine to AACGATCGTT suggests that the bisacridine prefers to bridge more than one DNA duplex by intercalating each acridine to different duplexes. The result may be relevant in understanding binding of certain intercalators to DNA structure associated with the quadruplet helix and holiday junction.

Structure of 9–Amino–N–[2–(4–morpholinyl)ethyl]–4–acridinecarboxamide bound to d–(CGATCG)₂ has been resolved at 1.8 Å [1]. The complex has been resolved at the space group P6₄ and the final structure has an overall R factor of 21.9%. The drug molecule intercalate between each of the CpG dinucleotide steps with the side chain lying in the major groove, and is protonated morpholino nitrogen partially occupying positions close to N1 and O6 atoms of guanine G2. The morpholino group is disordered, the major conformer adopting a twist boat conformation that makes Van der Waals contact with O4 oxygen of Thymine T3. A water molecule forms bridging hydrogen bonds between the 4–carboximide NH and the phosphate group of guanine G2. Sugar rings are found in alternating C3′–exo and C2′–endo conformations except for cytosine C1 which is C3′–endo. Intercalation perturbs the helix winding throughout the hexanucleotide compared with B–DNA with CpG and GpT steps being unwound by 10° and 8° degrees, respectively while the central TpA step is overwound by 11°. An additional drug molecule lies at the end of each DNA helix linking it to next duplex to form continuous stacked structure. The protonated morpholino nitrogen of this “end stacked” drug hydrogen, bonds to the N7 atom of guanine O6 oxygen. In both drug molecules

the 4-carboximide group is internally hydrogen bound to the protonated N10 atom of the acridine ring.

1.8.2.2 UV-Visible, Fluorescence and Vibrational Spectroscopy, Circular Dichroism studies

(a) Uncomplexed MTX and analogues

For the uncomplexed MTX [58] four distinct peaks $\lambda_A = 242$; $\lambda_B = 276$; $\lambda_C = 610$ and $\lambda_D = 662$ peaks were observed in the UV region. The amplitude of these peaks varied on drug concentration and pH, and to lesser extent on ionic strength. The molar absorption of D peak was particularly sensitive to drug concentration. Beer-Lambert law was obeyed between the concentrations between 1 μ M to 50 μ M at isobestic point of 682 nm. Also, [96] reported that mitoxantrone (MTX) has three absorption bands in the U.V. region one around 200 nm and the others around 243 and 279 nm with extinction coefficient of the later two being 26,700 and 11,000 $\text{cm}^{-1} \text{M}^{-1}$ respectively.

UV-Vis absorption studies [69] of the uncomplexed drug (MTX) in different solvents namely, acetone, water, methanol and chloroform respectively. Four absorption bands at 225 nm, 243 nm, 240 nm and 380 nm were observed in the aqueous media (H_2O) and these bands were assigned readily to the band characterized by four $\pi-\pi^*$ transition in UV region. The fifth band in the visible region was characterized by electron donating substituents on the anthraquinone ring by amino and hydroxyl groups and several interpretations for this group was postulated for this band such as interchange in position of bands of anthraquinones due to H-bonding and charge transfer from the substituent to the carbonyl group to the ring or the intramolecularly H-bonded carbonyl chelate ring. It had also been assigned due to imino 11NH and 12NH to ring charge transfer transition with red shift and conjugation due the phenolic groups as compared to the $-\text{NH}_2$ substituents. This band was shifted to lower frequencies, presumably due to increased electron donating ability.

Major influence of the solvent was found to be dominant as solvents appear to be shifting of the absorption peaks at the higher wavelengths as the solvent polarity decreases and the energy transitions were found to occur at 660, 680, 677 and 665 nm in H₂O, CH₃OH, CH₃COCH₃ and CHCl₃ respectively. It was further supported by observed red shift with decreasing solvent polarity is contrast to generally observed blue shifts in the emission spectra. As mirror image relationship was absent, it showed difference in the geometry of the ground and excited states. The opposite trend of MTX indicated that the ground electrostatic state of the solute is stabilized by bonding of the phenolic-OH (1OH / 4OH) groups with polar solvent molecules.

Fluorescence excitation (λ_{ex}) to be 610 nm and 660 nm and fluorescence excitation (λ_{em}) was found to be 685 nm [13] Fluorescence of MTX was found to be sensitive to pH and exhibited decrease in intensity at pH levels above 7.8 reflecting the ionization state of the hydroxyl groups. The extinction coefficient of the 608 nm bands was determined to be 14,000 cm⁻¹ M⁻¹ in the SSC buffer. They also reported the peaks at 608 nm and 657 nm in the visible spectra.

(b) Binding studies of MTX and its analogues with DNA

Absorption studies [75] indicated shift of λ_{max} values of MTX of 612 nm and 660 nm to 660 and 674 nm, respectively, on binding with d- (CGCG)₂ compared with those resulting from intercalation of ethidium from 492 to 528 nm [117] Thus it was proposed that the intercalation mechanism exist for MTX on binding with DNA as red shift was observed.

Preliminary studies of ct-DNA-MTX complex [13] showed that on increase in amount of DNA indicated increase in fluorescence polarization at maximum value at 25 μ g / ml DNA. Fluorescence polarization increased due to the binding of mitoxantrone with DNA due to restricted mobility of drug. Further addition showed decrease in polarization due to

aggregation of the resultant complex, which leaves only those molecules free in solution detected by the instruments optics. They reported that shifts in the excitation and emission spectra within the molecule were suggestive of the intercalative mechanism. On binding with DNA the absorption studies showed red shift suggestive of the fact these substituents are unable to form H-bond with the solvent water molecule. Both absorption and emission spectra were found to be dependent on the concentration of the drug.

Kapunsciski, J., et al [58] reported that both A-DNA and B-DNA structures form intercalation complexes with mitoxantrone (MTX) although electrostatic interaction also plays part in the binding. Interaction with the polymers containing A-T base pairs were somewhat weaker than with other polymers, and alternating polymers exhibited stronger affinity than did homopolymers pairs.

Interaction with natural nucleic acids showed large red shift in the C and D band ($\lambda_C = 610$ and $\lambda_D = 662$ nm peaks) as well as increase in relative absorption of D and C band i.e. ϵ_D / ϵ_C . The titration with calf thymus-DNA showed that absorption at 682 nm was found to be proportional to the concentration of DNA-MTX complex. The intrinsic constant of the drug (K_i) was found to be $1.8 \times 10^6 \text{ M}^{-1}$, binding site size (n) = 5 and the unwinding angle (ϕ) was 26.5° .

Interaction of MTX with synthetic nuclei duplexes indicated the shift in the D band replicates the red shift characteristic of drug intercalation, unwinding of the closed, circular, double stranded DNA by MTX. All earlier studies had suggested intercalative mode of binding of DNA as evident by the characteristics of C and D bands. However, it was also postulated that long chains at 1, 4-position could hinder intercalation. The value for unwinding angle (ϕ) of MTX was found to be 21.5° .

Interaction of mitoxantrone (MTX) and ametantrone (AME) with natural and synthetic DNA [57] by spectroscopic method was studied in order to establish the monomeric and dimeric form of ligands (uncomplexed drug) and their complex with DNA at low drug / phosphate ratios (D / P) or drug / nucleotide ratio (D / N). The spectra of the complexes were red shifted and had lower amplitude compared with spectra of the free ligands monomer. This observation was consistent with the already well-established intercalative mode of drug-nucleic acid interaction.

At higher D / N ratio, a secondary mode of binding was detected by both spectroscopic and light microscopy. Homo-polymers pairs containing the dI and dC were especially susceptible to the secondary type of binding. It was reported that both MTX and AME are strong intercalators [56] and their intercalative modes of binding are most plausible explanation for their pharmacological activity. No significant differences were explained on the basis of their intercalative properties, but the ability to condense nucleic acid is twice as much for MTX than AME. The condensation was found to be base and sugar-specific and the long purine sequences of single stranded RNA were found to be most sensitive.

Sodium sulphate driven dissociation of mitoxantrone, daunomycin and ametantrone and related compounds with calf thymus DNA, poly[(G-C)].poly[(G-C)] and poly[(A-T)].poly[(A-T)] was studied by stopped flow kinetics methods [64] and found that all the four compounds exhibit biphasic dissociation reactions. Daunomycin exhibited similarity with mitoxantrone in similar dissociation rate constant, effect of temperature and ionic strength. Rate constant of these two drugs were suggestive that both of the drugs involve formation of the initial outside complex followed by intercalation where as dissociation in ametantrone follows single-phase kinetics.

Mitoxantrone followed biphasic kinetics for both poly [(G-C)].poly [(G-C)], poly[(A-T)].poly[(A-T)] but rate constant for poly[(G-C)].poly[(G-C)] are approximately 10 times lower than poly[(A-T)].poly[(A-T)]. This behavior, which is unique to the mitoxantrone, was suggestive of the selective binding and dissociation from the alternating polymer intercalation sites / and or dual mode of binding, modes of intercalation with both the side chains in the same groove or one side in each groove.

It was reported [96] that CD spectra of the poly [d (G-C)] had a maximum at ($[\theta]_{275} = 6,500 \text{ deg cm}^2 \text{ d mol}^{-1}$ of nucleotide) with distinct shoulder at 285 nm and negative band at 250 nm ($[\theta]_{250} = -16,600 \text{ deg cm}^2 \text{ d mol}^{-1}$). On increasing the concentration of MTX the intensity of the long wavelength increased steeply, the 285 nm shoulder lost its identity increased steeply and resulting band was centered on 278 nm. At drug / nucleotide (D / N) ratio of 0.2 a saturation in the ellipticity was observed. With limiting value of ($[\theta]_{278} = 37,100 \text{ deg cm}^2 \text{ d mol}^{-1}$) i.e. approximately six fold rise. Reversal of the 250 nm band to positive 251 nm band had ellipticity value of $28,300 \text{ deg mol}^{-1} \text{ cm}^{-1}$, was not reported for daunomycin, actinomycin etc. The indication of the CD in the visible region showed that band decreased in the two stages at maxima centered at 688 nm one below the D / N ratio of 0.11 and other above this ratio. At the D / N < 0.11 enhancement in ellipticity was slow but at D / N > 0.11 sharp and apparently cooperative growth in the ellipticity reaching $[\theta]_{688} = 48,000$ at D/N = 0.22.

Ellipticity changes at 251 nm and 278 nm to revealed that interaction of the drug occurs at D / N = 0.12 and other above this value. The induction of the intense circular dichorism in the 250 and 278 nm regions, apart from that in the visible region for MTX–poly [(d(C-G))] system suggested that mode of intercalation is different from that of ethidium and acridine orange.

As the drug has two symmetrical side chains it prevents the classical type of intercalation with the long axis of the molecule tangential to the helix and as suggested in an NMR study [75] instead they proposed that the drug might then intercalate with its short axis tangential to the base pair axis.

Babayan, Y., et al [9] reported increase in DNA concentration at constant mitoxantrone resulted in hypochroism red shift and absence of isobestic point at 676 nm. At low concentration, it was observed that DNA concentration in the solution changes such that interaction of mitoxantrone with double stranded nucleic acids depends upon the solution's ionic strength. With increase in MTX concentration (at constant DNA concentration) the CD spectra changes and the isobestic point at 265 nm was observed. Thermal denaturation studies of the poly [d(A-T)]-poly[d(A-T)] at high ionic strength (0.11) showed that the shape of the melting curves does not change with increase in temperature, but range of melting temperature remains the same, whereas at the ionic strength of (0.011) the curve becomes biphasic. The same pattern was observable between MTX and double stranded helical polynucleotides. On the basis of the absorption and CD spectra it was concluded that when the negative charged phosphate groups are fully screened and MTX binds through intercalation at high ionic strength of 0.11 [96].

MTX also showed specificity for different nucleotide pair and dissociation constant (K) is of almost an order of magnitude higher for binding to DNA than RNA. The values of dissociation constant (K) and binding constant (n) agreed well [74]. The value of ΔH was found to be negative for binding with mitoxantrone with M. lysodiklius DNA and poly (G). Poly(C) and ΔS are positive for both. ΔH is positive for compounds, which do not intercalate into DNA. This anomalous behaviour for MTX was explained as besides intercalation interaction of the side-chains in the major groove contributing towards ΔH . The value for

number of binding sites (n) reported for mitoxantrone complexes with DNA [63] agreed well, i.e. two mitoxantrone molecules per duplex to one mitoxantrone molecule per three base pairs, that mitoxantrone binds to G–C base pairs.

Babayan et al, 1998, [9] studied the interaction of mitoxantrone and ametantrone with DNA as determined from the changes in the circular dichroism spectra. Their study was performed into the effect of the ionic strength and temperature of the medium on the changes in the various nucleotide compositions. The change in the circular dichroism spectra indicated transformation of the DNA helix geometry upon the interaction with geometry. The relative change in the dichroic absorption at maximum was integrated as function of the relative concentrations of C_o and C_p where C_o is the concentration of the mitoxantrone (MTX) and ametantrone (AME) and C_p is the concentration of DNA and dependence were deduced at maximum and minimum in the circular dichroism spectra of the complex of mitoxantrone and ametantrone with poly [d (G–C)] poly – [d (G–C)]. They found that the increase in per base pair raises the $\Delta E^{(M)}_{273} / \Delta E^{(o)}_{273}$ ratio. The slope of the curve is far larger for complexes of MTX; which exhibits deviation from linearity even at low C_o / C_p , and change in the helix geometry less pronounced. Similar pattern was observed for the relative change in dichroic absorption at the maximum.

On interaction with mitoxantrone with DNA the linearity of dependence with MTX, the linearity of dependence of DNA with MTX, the linearity of dependence of $\Delta E^{(M)} / \Delta E^{(o)}$ is retained till $C_o / C_p = 0.15$ where as in DNA–AME complex formation the linearity is violated when the $C_o / C_p = 0.05$.

The effect of temperature on change in the $\Delta E^{(M)}_{273} / \Delta E^{(o)}_{273}$ upon complex formation was also monitored. It was observed that changes at 30° were more pronounced than changes at 50° i.e. helix geometry is altered more strongly at low temperatures.

Raising the C_o / C_p increases $\Delta E^{(M)}_{273} / \Delta E^{(o)}_{273}$ and this increase is much higher than increase upon binding that proceeds only through intercalation mode. At fairly high C_o / C_p ΔE tend to saturation. The change base pair geometry upon intercalation followed the order CG, AT and IC at 0.11 ionic strength. They concluded that upon interaction of mitoxantrone and ametantrone with DNA from the changes in the CD spectra one could determine the mechanism of binding of mitoxantrone and ametantrone to DNA to study the possible conformational changes in DNA upon binding.

1.8.3 FOOTPRINTING STUDIES

SEQUENCE SPECIFICITY OF MITOXANTRONE

Transcriptional essay [84] determined the sequence specificity of binding of mitoxantrone. Transcriptional blockages were observed dominantly prior to 5'-CpA sequences (64%) occurrence and to lesser extent 5'-CpG sequences (29%). Overall 93% of the blockages were prior to the pyrimidine (3'-5') purine sequences. An effect of flanking sequence was evident since the blockage sites contained A / T base pair prior to the consensus of the CpA and CpG intercalation sites. The location of transcriptional base pair prior to the intercalation site was consistent with [20, 74– 75] manifesting that mitoxantrone intercalates perpendicular to the base pair axis with both side chains in the major groove and extending approximately to one base-pair 5' to the intercalation site, it was expected that progression of the polymerase will be halted one base prior to the intercalation site.

Though it was not clear how 5'(A / T)GC and 5'(A / T)CG sequences specifically relate to drug action, it was possible that the drug is localized preferentially in the specific control regions of the genome such as transcriptional promoter enhancer regions where it could result in critical effect on the regulation of the transcriptional process.

Mitoxantrone can be activated by formaldehyde to form adduct in DNA [87–89], *in vitro* and the result revealed that formaldehyde activated mitoxantrone blocked the progression about *E. coli* RNA polymerase and λ exonuclease in a sequence dependent manner. The major transcription blockages were described at CpG and CpA sites on the non-template strand of DNA. Exonuclease studies revealed that the formaldehyde activated mitoxantrone blockage were specified at CpG sites and suggested that the adducts at CpG sequences may distort the DNA helix to produce a lesion which can block the progression of exonuclease, whereas the CpA lesion does not.

The proposed structure of the mitoxantrone–DNA adduct implied the likelihood of hydrogen bonding to the second DNA strand. The hydrogen bonding at CpA / TpG sequences may therefore be weaker due to absence of the guanine residue on the second strand. Although the sequence specificity occupancy of MTX suggested no significant effect of flanking sequence on adduct formation and frequency most stable adducts were detected with ACGC sequence. They also proposed if compared with adriamycin, formaldehyde activated mitoxantrone might be covalently bound to only one strand of DNA at most likely the N2 amino group of guanine residues at CpG and CpA i.e. TpG dinucleotide. They are likely to contain an interstrand (virtual) crosslink with covalent attachment to guanine on one DNA strand. It is possible that the CA sites contain the same site of lesion that occur at the CG sites, but with difference in hydrogen bonding to the second strand due to lack of guanine (on the non covalently bound strand), resulting in reduced stabilities. The activity of mitoxantrone against myeloid and solid tumors was also consistent with the proposed mechanism of activation of MTX by formaldehyde, associated with higher levels of formaldehyde in these tumors.

Bailly, C. et al, [10] studied closely related derivatives of mitoxantrone and found that both of the derivatives were capable of intercalating into DNA as evident by their unwinding angles comparable to that of the mitoxantrone and structurally related anthraquinones. The two drugs bind preferentially to alternating purine–pyrimidine sequence containing both A–T and G–C base pairs. For the dihydroxy derivative every region is protected from DNAase I cleavage (a presumptive drug binding site). Tri nucleotide ACG or 5'(A/T) CA which is equivalent to 5'–TG (A / T), triplets are the consensus sequences as reported for mitoxantrone hence indicating that the hydroxyethyl terminal groups which distinguishes mitoxantrone from this compound are not responsible for sequence selective recognition process.

However, there was rather poor correspondence between the drug–protected site and ACG but good correlation with sites containing CCA, TCA and TGT. Therefore, the results suggested the binding to 5'–(A/T) CG site is dependent on the presence of the 5, 8 hydroxyl groups on the anthracenedione where the binding to 5'–(A / T) CA sites proceed to a large extent by presence or absence of hydroxyl groups.

The regions of the reduced nuclease cleavage in the presence of the compounds A and B match quite well, though not exclusively with CG –or (TG) containing sites.

The most of the foot printing studies at X–CG are observed for bis hydroxylated than non–hydroxylated analogue, whereas as found to be identical with footprints of CA or TG are almost identical.

Both compounds were found to footprint on the natural DNA as well as natural DNA as much as in the same way as try T–DNA finding that the sequence recognition does not depends upon interaction with 2–amino group of guanine located in the minor groove, but is

consistent with the alkyl amine chains in the major groove as found for mitoxantrone [84–86].

1.8.4 METAL COMPLEXES OF MITOXANTRONE WITH DNA

Studies were done on the interaction of mitoxantrone, ametantrone Pd (II) complexes with DNA by means of ultraviolet and circular dichroism spectroscopy [62]. These complexes behaved like complexes of other antitumor drugs like daunomycin, carminomycin, which bind strongly with Fe (III) and Pd (II). These complexes also exhibited higher cytotoxicity as well as cardiotoxicity towards P-388 leukemia as compared to that of free drug. MTX and AME were found to be less susceptible to enzymatic reduction therefore appeared to be less toxic than Adriamycin and daunorubicin. However, on complexation they exhibited different biological properties in comparison to free which was explained on the basis that drugs owing to change in polarity, modifies its interaction with cell components such as membrane and nucleic acids.

Both drugs formed 2:2 stoichiometry with Pd (II), i.e. the complex is formed with two molecules of drug (D1 and D2). One Pd (II) is bound to the nitrogen's of the side chains on C-5 of the molecule D1 and other to two side chains of the side chain of the C-5 of molecule D2 whereas second Pd (II) is bound to the to the nitrogen's of the side chains on C-8 of molecule D1 and D2.

This complex formation prevents the intercalation of the drug between the base pair of DNA but preserves the ability of the drug to condense DNA. Nitrogen atoms have been proposed for most suitable candidates for complex formation to both ametantrone and mitoxantrone. Both yielded similar results, which would have been different if the 1, 4 groups had been candidates for complexation giving rise to very stable five membered chelate on release of two protons per molecule. It was further found that both drugs exhibited decrease in

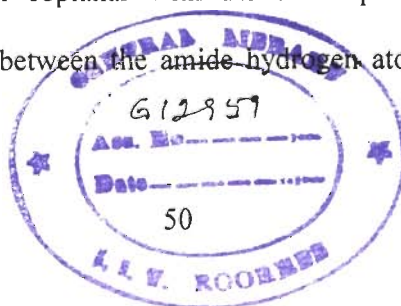
intensity of absorption in the visible region, decrease in pH indicating the release of protons simultaneously with complex formation.

Mitoxantrone (MTX) and its Cu (II) complexes [119] were studied by the methods of electrochemistry and fluorescence spectroscopy. On complexation it was observed that fluorescence emission was quenched completely at Cu (II) / MTX= 2:1 whereas the absorption spectra did not change. At Cu (II) / MTX= 2:1 indicated that one molecule of the drug can bind with two molecules of the Cu (II) ions. Cu (II) ions complex with nitrogen's of the side chains of mitoxantrone as similarity reported for Pd (II) complexes [62]. Taking into steric hindrance Cu (II) complexes are usually tetra coordinate. Cu (II)-MTX complex showed stronger inhibiting ability on the DNA synthesis and hence better anti-tumor agent. Cu (II) / MTX = 1:1 is more potent than Cu (II) / MTX = 2:1.

In CD study when MTX bound to calf thymus DNA the positive band at 275 nm of DNA increase greatly, and the negative band at 245 decreases rapidly indicating MTX leads to the conformational change of DNA from B to A. The transition metal ions interacted preferentially with GC by the chelation of N-7 of guanine and to phosphate residue. Thus it was assumed that Cu (II)-MTX (side chain)-DNA is formed to cause denaturation of DNA which may be plausible action mechanism of the complex.

1.8.5 THEORETICAL STUDIES

Series of 1 and 1, 4 di-substituted anthraquinones [24] were examined in relation to their cytotoxic and anti-tumor properties as compared with Mitoxantrone. The representative structure, N-(9,10)-dihydro-9,10-dioxo-1-anthracenyl)-3-[4-3-(hydroxypropyl)-piperazine-1-yl] propanamide hydrochloride was taken from X-ray crystallography. Thus compound possessed hydrogen coplanar with the anthraquinone ring and there is an intermolecular hydrogen bond between the amide hydrogen atom and the quinoid oxygen



atom on the ring (NH1 --- O9) distance of 1.84 Å. For molecular modeling studies both AT and CG sites were examined with these models. For the mono-substituted compounds the intercalation was found to occur in the both the wide major groove and narrower minor groove. The major groove was suggested to be preferred over minor groove for side chains on account of the more favorable electrostatic interactions between the phosphate groups of the di-nucleotide backbone and side chain protonated amino groups of the drugs, whereas for the di-substituted compounds the low energy intercalated geometries were produced with the side chain lying in the major groove, or in spear mode with side chains lying in each groove.

The models studied indicated that the amide groups even though they are coplanar with the anthraquinone chromophores, do not take part in the intercalative stacking interaction and thus suggesting that primary role of these groups is to diminish the flexibility of the side chain compared to their amido analogues. In mitoxantrone (MTX) two carbon chain separates the nitrogen atoms immediately attached to the anthraquinone and the base side chain nitrogen atom, this short chain has unconstrained conformational flexibility and allows the terminal chain of the atoms to form favorable short range interactions with the bases specially with the nitrogen bases [11, 54] and such arrangement are not present in amido anthraquinones studies on account of their less flexible side chains.

It was also apparent that changes in the nature and dimensions of the $-(CH_2)_2$ group present between amide and basic groups would be deleterious in the formation of electrostatic interactions. The predictions for the major grooves for the side chains of the di-substituted compounds on purely steric grounds was in accord with the NMR [63] and kinetic studies [64] studies on the di-substituted compounds.

The in vivo and in vitro activities of compounds has been done and found that a marked divergence of behaviour for the mono-substituted compared to the di-substituted

compounds. The former ones showed little or no activity against tumour models (L120 cell lines) whereas later showed marginal to moderate activity. The clearance rate of these compounds was in marked contrast to the mitoxantrone. Thus it was found that amidoanthraquinones as a class are probably less metabolic active than amino anthraquinones as a result of liability of amide linkage.

Solutions studies on (amino alkyl) amino substituted anthraquinones, differing in the substituted pattern, namely, 1- (diethylamino)ethylamino] and 1,4; 1,5; and 1, 8-bis[(diethylamino)ethylamino] anthraquinones [54] were reported. The study has been correlated with the computer graphics modeling of their fit into a DNA intercalation site. Degree of unwinding with ccc-DNA was 10.6° for monosubstituted compounds and $14.2^\circ - 14.3^\circ$ for di- substituted compounds. Spectrometric titrations of drug with DNA showed order of DNA affinity as $1, 5 > 1, 4 > 1, 8 > 1$ -compounds.

Intercalative mode of binding of the antitumor drug MTX and AME was studied [78] with dodecamer duplex (CGCGAGCTCGCG)₂ with drug molecule intercalated in the GC base pairs. Molecular simulations were carried out in water by applying GROMOS force field.

Four different starting orientations namely, (S, N, E and W) for the intercalation of the drug in relation to the axis of inter-base pair 9 G6-C19) hydrogen bonds were examined by short presimulations and most favorable orientation was chosen.

In the S-orientation (perpendicular mode, with side chains lying in the minor groove) was found to be preferred over N (perpendicular mode, with side chains of the drug in the major groove), E and W orientations (with parallel orientation and side chains in minor and major groove each.).

S-orientation was more favored in terms of high electrostatic energy ($-2580 + 30$ kJ / mol), and hydrogen bond formation between the 14OH group as well as the aliphatic amino

groups with the DNA base pairs. It was found that the hydrogen atoms are formed between the side chains of the drugs and oxygen atoms and sugar as well as between the side chain and base moieties of DNA up to four base pairs with side chains stretched along the groove. No hydrogen bonds were observed between the 1OH / 4OH groups with DNA. Thus two conformations were supposed to exist (i) either they form hydrogen bond with adjacent quinone moieties (9CO / 10CO) or (ii) they are interacted with water in the major groove.

Both MTX and AME complex exhibited similar intermolecular interactions but intermolecular topologies were significantly higher in case of the MTX complex. In MTX–complex MTX molecule observed was coplanar with the base pair axis. They suggested that the 1OH / 4OH group being at para–position enhances the width of the aromatic ring and decreases the inclination and hence better intercalation whereas AME intercalate at an angle of 13° with respect to DNA base pairs though both possess identical side chains. This leads to better electrostatic interaction between MTX–DNA complexes as compared to AME–DNA complex.

1.8.6 CLINICAL STUDIES

The anticancer agent MTX was found to be readily oxidized by human haem enzyme myeloperoxidase and hydrogen peroxide [84]. Intercalation of mitoxantrone with DNA inhibited oxidation of the drug myeloperoxidase but at physiological strength the significant oxidation was evident. 1:1 (H₂O₂: MTX) mitoxantrone was oxidized to product which binds reversibly with DNA whereas at higher 5:1 (H₂O₂: MTX) further two products were formed none of which binds reversibly with DNA as indicated by absence of spectral change in the presence of DNA, indicating that further oxidation of the product at 1:1 H₂O₂:MTX by myeloperoxidase occurs probably at the hydroquinone ring. Since, mitoxantrone has been shown to intercalate into DNA with chromophore perpendicular to the base pair axis, it was

proposed that the oxidation of the chromophore may affect the binding of this highly oxidized form of DNA.

The binding of mitoxantrone to DNA has been found to inhibit direct oxidation of myeloperoxidase in a DNA dependent manner. Hence, when mitoxantrone is intercalated into DNA the drug cannot gain access to the active site of the myeloperoxidase to enable subsequent oxidation to drug, that would therefore facilitate the access of myeloperoxidase to the drug, and enable the oxidation to occur. Thus, it was therefore likely that significant oxidation would occur both within the cytoplasm and the nucleoplasm. Thus myeloperoxidase catalysed oxidation of mitoxantrone to products capable of interacting covalently and non-covalently with nucleic acids that may represent an important mode of action of mitoxantrone against acute leukemia since these cells (including neutrophils, monocytes and their precursors) contains certain levels of myeloperoxidase.

The cytotoxic activity of mitoxantrone and related anthracenediones (2-aza-2aza-oxideanthracenedione) has been ascribed to the ability of these compounds to interfere with DNA top-II function resulting in DNA cleavage stimulation [53]. Their results indicated that the substitution of the pyridine ring for the deoxyphenylene ring in the planar chromophore caused a marked reduction in the cytotoxicity and of the ability to stimulate top-II mediated DNA cleavage in the intact cell. Though all the derivatives were shown to intercalate into DNA their binding affinities were lower than that of mitoxantrone. The behaviour of 2-aza derivatives closely resembled that of the ametantrone suggesting that the potency of these agents is influenced by hydroxyl group rather than by phenylene ring. The observation that dramatic reduction of the stability of the aza derivatives to stimulate DNA cleavage was associated with marked reduction of cytotoxic potency supported a primary role of top II in the mechanism of action of this class.

Compounds containing 9, 10 anthracenediones with one or two peptide chains at 1, 4 positions with the introduction of glycine (Gly), Lysine (Lys) and Tryptophan (Tryp) with the derivatives of the latter two in both L- and D-conformation [40] were studied.

Formation of the DNA-anthraquinone complex caused the total almost total quenching of the fluorescence signal for all the compounds. All the compounds exhibit remarkable affinity for DNA (K in the range of 10^5 M^{-1}) close that of ametantrone but clearly lower than that of mitoxantrone. On increasing the basicity of the compounds i.e. in doubly charged amino side chains increased the efficiency of interaction with DNA. The L-isomers were found to compare well with the mitoxantrone while the D-isomers were even more effective than that of reference compound i.e. mitoxantrone. 1-(glyclamino)-4-aminanthracene-9, 10-dione (AG10) and 1, 4 bis(glyclamino) anthracene-9, 10 dione (AG-11) showed changes of fluorescence with formation of sparingly soluble material. Mono-di-triglyceral derivatives showed a distinct preference for CG-rich sequences as many anthraquinones do the most specific being the 1, 4-bis[glycyl-glycl-glycyl amino] anthracene, 9, 10 dione (AG₃-11) and 1, 4 bis [glycyl-glycl amino] anthracene, 9, 10 dione (AG₂-11) comparing well with the ametantrone and mitoxantrone exhibiting the clear preference for the CG steps in polynucleotide chain. Less specific proved to be lysyl derivatives. Geometry of the intercalation of the peptidyl anthraquinones was similar to that of ametantrone and mitoxantrone and the induced rotational strength was negative. However, different values of induced molar ellipticity pointed to slightly different peptidyl arrangements when inserted between the base pair. Cell toxicity correlated with the nature of the amino acids in the side chains than to presence of one or two of them at positions at 1 and /or 4 of the anthraquinone ring. AG_n and 1, 4 Bis [D-tryptophnyl-glycyl-amino] anthracene-9,10-dione [(AG_w-11)] are less effective in top II mediated cleavage show reduced cardiotoxicity than stimulate top

II functions, which suggests competition between the drug and the enzyme in DNA template occupancy. Accordingly, they were found devoid of cell killing properties, which indirectly points to the importance of top II mediated mechanisms in anticancer activity. This finding was consistent with the reduced activity shown by number of mitoxantrone congeners bearing bulky substituents and additional bulky charges in the side chains [22].

The physiological, cytotoxic and pharmacological properties of 2, 3 diazaanthracene diones [53] were studied by spectroscopic and voltametric measurements. In comparison with mitoxantrone and ametantrone they were characterized by less negative reduction potential, lower affinity for DNA and modified geometry of intercalation. The biological effects of the new compounds were not affected by the biosteric N or C replacement. Stimulation of Topoisomerase II mediated DNA cleavage was not observed, whereas the other mechanism of cell cytotoxicity, possibly involving oxidative DNA damage, appeared to be operative. The inability to generate the protein associated DNA breaks was explained by unfavorable orientation of the drug in the intercalation complex rather than reduced binding to DNA. DNA damaging pathway of 2, 3 diaza substituted derivatives which could produce radical species to a remarkably greater extent than carbocyclic parent drug.

1.9 SCOPE OF THESIS

Interactions of small molecules with DNA have been studied for several decades in the hope of learning design principles for the targeting of specific DNA sequences in order to control gene expression. Many small molecules that bind to DNA are clinically proven therapeutic agents although their exact mode of action remains incompletely defined. There is a renewed focus on the use of small molecules as therapeutic agents in the biotechnology industry. This renewed interest arises, in part, as a result of several advantages of small molecules as potential drugs, including the economics of their synthesis and their effective

delivery to cells. The results of these studies are correlated with biological (antitumor) efficiency of the compounds tested with the aim to exploit these data for design of new cytostatics with better therapeutic properties as compared to the drugs already used in the clinic. Therefore, these studies are aimed in particular at the development of new anticancer drugs whose antitumor efficacy is associated with their interactions with DNA, i.e. for which DNA is the main target inside tumor cells. Understanding structure-function directed macromolecule-target interactions of anticancer drugs, and further rational design of improved anticancer agents are the long-term research goals of any laboratory.

This thesis deals with the study of detailed study of anticancer drug Mitoxantrone in different solvents namely D₂O, H₂O and DMSO by NMR to obtain the 3D conformation of the drug. Some of the results are supported by the UV and Fluorescence method.

Structure elucidation of the Mitoxantrone with particular hexanucleotide sequence (CGATCG)₂ has been studied in particular detail by NMR. Preferential accumulation of mitoxantrone in nucleoli, binding to chromatin and cytoplasmic RNA, its affinity for DNA in solution has been demonstrated. The drug stabilizes DNA against thermal denaturation and inhibits thymidine and uridine incorporation [37]. Intercalative mode of binding is proposed but there is much evidence for the same. The consensus sequence for preferred intercalation sites [84] are 5' (A / T) CA and 5' (A / T) CG. Since the drug has two long chains symmetrically located to opposite side of anthraquinone ring it remains to be elucidated how the three ring anthraquinone inserts itself between base pairs. Does it intercalate with its long axis parallel or perpendicular to the DNA? In the parallel mode the long side chains would be forced to thread through the base pairs and to be located in the opposite groove. In the perpendicular mode both side chains would reside in the same groove. The down field shift in the resonances binding to d-CGCG [75] has been observed to be insignificant as compared to

that in typical intercalators in which base pairs open to accommodate aromatic chromophore. The proximity of mitoxantrone protons to DNA protons has been shown [63, 75]. The only structure of similar drug–DNA complex has so far been an X-ray crystallographic analysis of ametantrone complexed to d–CGATCG [118]. We have therefore undertaken the study on solution structure of mitoxantrone and its complex with d–CGATCG. The model DNA hexamer sequence sequence has been selected as the mitoxantrone sequence has been shown to bind to 5' (A / T) CG [84] sites. Also the selected DNA hexamer sequence has two binding sites expected in duplex. It is self complementary so that complexity of NMR spectra is reduced.

The Ph.D thesis work has been reported in the form of eight chapters. Chapter 1 contains introduction as of the subject as well as review of literature. Chapter 2 deals with the materials and Methods used. In Chapter 3, we have discussed the NMR results of the uncomplexed drug mitoxantrone in D₂O and H₂O along with that by UV and Fluorescence methods. In Chapter 4, studies of uncomplexed drug in DMSO solvent are reported. Chapter 5 deals with the ³¹P studies of (CGATCG)₂ – MTX complex. 1D and 2D – ³¹P exchange studies have been carried out for the complex at 278 K. Chapter 6 describes the proton NMR results on binding of mitoxantrone with d–(CGATCG)₂ by carrying out titration at 278 K. The structural analysis has been carried out in detail by using 2D NOESY distance restraints in complex having 1:1, 1.5:1, 1.75:1 and 2:1 drug to DNA stoichiometric ratios. In Chapter 7, the conformation of DNA in the structure of complex is obtained by restrained molecular minimization and molecular dynamics simulations have been discussed. Chapter 8 summarizes the result obtained.

Chapter 2

Materials and Methods

2.1 MATERIALS

The deoxyribonucleic sequence d-(CGATCG)₂ was purchased from Microsynth, Switzerland and further purification was done by dialysis using Benzoylated dialysis tubing (Sigma Chemicals Co. U.S.A.). Further the d-(CGATCG)₂ was synthesized on Applied Biosystems DNA synthesizer (model 392 A), 10µm scale using cyanoethyl phosphoramidite approach for routine 1D NMR and absorption studies.

Mitoxantrone Hydrochloride was obtained from Sigma Chemicals Co. and Calbiochem Ltd. Deuterium Oxide (D₂O) with isotopic purity 99.9% and dimethyl sulphoxide (DMSO-d₆) with isotopic purity 99.96% were obtained from Sigma Chemicals Co. U.S.A. Sodium 2, 2-dimethyl-2-silapentane-5-sulphonate (DSS), an internal NMR reference for proton NMR were purchased from Merck Ltd. Methylene diphosphonic acid was used as external NMR reference for phosphorus NMR had been procured from Sigma-Aldrich. All other chemicals like Na₂HPO₄ and NaHPO₄ etc. used for buffer preparation were from Sigma Chemicals Pvt. Ltd. HPLC grade solvents and reagents water, triethyl amine, acetonitrile, glacial acetic acid etc were purchased from Qualigens, Ltd.

2.2 SAMPLE PREPARATION FOR UV STUDIES

A computer aided Perkin Elmer spectrophotometer equipped with a thermoelectric control unit (peltier unit) was used for the UV-VIS absorption studies.

2.2.1 Preparation of Buffer Solution

All experiments were performed in the standard buffer containing 50mM NaCl, 20mM phosphate buffer, pH= 7.0 at 25°C. The buffer was filtered through 0.45µm pore Millex Millipore filters.

2.2.2 Preparation of Sample.

The concentration of Mitoxantrone in buffer solution was determined spectrophotometrically at the isobestic point at 682 nm ($\epsilon_i = 8300 \text{ M}^{-1}\text{cm}^{-1}$). The λ_{max} is observed at 600 nm and 660 nm. The titrations were monitored from 200 nm to 700 nm.

The concentration of d-(CGATCG)₂ was prepared in 50 mM NaCl, 20mM phosphate buffer and determined by using the standard value of the molar extinction coefficients i.e. 51,400 $\text{M}^{-1}\text{cm}^{-1}$ by the UV-VIS Spectrophotometer

2.2.3 Titration of d-(CGATCG)₂ with Mitoxantrone

The 1ml aliquot containing Mitoxantrone of 20 μM concentration dissolved in buffer solution was placed in a quartz cuvette in the thermostatic holder of the spectrophotometer. The d-(CGATCG)₂ of 40 μM were added in small amount of 10 μM to the aliquot containing Mitoxantrone for the titration. The concentration calculations are done based on the Beer's Lambert's equation:

$$\text{O.D.} = \log I_0/I = \epsilon c l$$

where ϵ is the molar extinction coefficient, c is the concentration, l is the path length of the cuvette in cm and O.D. is the optical density or absorbance.

2.3 SAMPLE PREPARATION FOR NMR STUDIES

2.3.1 DNA Synthesis

The starting material is a solid support derivatized with a nucleoside, which will become the 3'-hydroxyl end of the oligonucleotide. The 5' hydroxyl end is blocked with a

dimethoxytrityl (DMT) group. The steps of the DNA synthesis cycle are as follows:

- i. The treatment of derivatized solid support with acid removes the DMT group and thus frees the 5'-hydroxyl for the coupling reaction. An activated intermediate is created simultaneously adding the monomer and tetrazole, a weak acid, to the reaction column. The intermediate is so reactive that addition is complete within 30 seconds.
- ii. The next step, capping, terminates any chains which did not undergo addition. Capping is done with acetic anhydride and 1-methylimidazole. Capping minimizes the length of the impurities and thus facilitates their separation from the final product.
- iii. During the last step of oxidation, the internucleotide linkage is converted from the phosphite to the more stable phosphotriester. Iodine is used as an oxidizing agent and water as oxygen donor. The reactions complete in less than 30 seconds.
- iv. After oxidation, the DMT group is removed with trichloroacetic acid. The cycle is repeated until chain elongation is complete. Treatment with concentrated ammonium for 1 hour with ammonium hydroxide removes β -cyanoethyl protecting groups and also cleaves the oligonucleotide from the support.
- v. The benzoyl and isobutyryl base protecting groups are removed by heating at room temperature in ammonia for 8–15 hours.

2.3.2 DNA Purification

Purification is carried out using RPLC and ion-exchange chromatography. RPLC is performed on Shimadzu HPLC instrument with acetonitrile and triethyl ammonium acetate (0.01 M) buffer system (pH 7.0.) Desalting is carried out after purification by dialysis. Benzoylated dialysis tubing was cut into pieces of convenient length (1 cm for 100 μ l volume), boiled for 10 minutes in a large volume of 2 % w / v NaHCO_3 and 1mM EDTA (pH= 8.0) for activation

followed by rinsing thoroughly with distilled water. It was again boiled for 10 minutes in 1mM EDTA (pH 8.0). The sample was then put into the tubing, sealed with holders and dialysed against 4 M NaCl for 12 hours followed by dialysis against distilled water for 12 hours twice. Sample was then taken out, lyophilized and dissolved in phosphate buffer (pH = 7.0). The purified oligonucleotide was annealed by heating upto 80°C at the rate of 1°C per minute with hold time of 10 minutes and then slowly cooled to get oligonucleotide in the duplex state. Thus a duplex of d-(CGATCG)₂ is prepared.

2.3.3 Preparation of DNA solution

Solution of purified deoxynucleotide, d-(CGATCG)₂ (1.64 mM duplex concentration) was prepared by dissolving known quantity of sample in 0.5 ml phosphate buffer (20 mM) pH 7.0 having 50mM Na⁺ salt and its concentration is determined by absorbance measurements at 260 nm using Cary 100 spectrophotometer (Varian Inc., USA). The extinction coefficient (ϵ) used was 51,400 M⁻¹cm⁻¹.

2.3.4 Preparation of drug solution

Solution of Mitoxantrone (10.0mM) is prepared by dissolving the known quantity of sample in D₂O. In the similar manner the sample was prepared in H₂O and DMSO. The DSS signal and DMSO signals were used as internal NMR reference for recording spectra in these solvents.

2.3.5 Preparation of complex

The DNA-Drug complex was prepared by titrating mitoxantrone against d-(CGATCG)₂. 45 μ l of mM mitoxantrone is added in steps to of 1.64 mM of d-(CGATCG)₂ during titration in order to make 1.75 : 1 complex of drug: DNA. The concentration of hexamer (N₁) in total volume of 0.501 is determined as follows:

$$N_1V_1 = N_2V_2$$

$$N_1 \times 0.501 = 1.64 \times 0.5$$

$$N_1 = 1.63 \text{ mM}$$

The concentration of drug in this solution is determined as follows:

$$N_3V_3 = N_4V_4$$

$$N_3 \times 0.501 = 37.4 \times 0.001$$

$$N_3 = 0.07 \text{ mM}$$

Like wise other different Drug / Nucleotide (D / N) ratios were prepared. The concentration of mitoxantrone (D), d-(CGATCG)₂ (N) and D / N ratio are shown in Table 2.1.

2.4 NMR THEORY

2.4.1 Phenomenon

NMR is a type of phenomenon, which is dependent on the property of the spin, possessed by the nuclei e.g. isotopes such as ¹H, ¹³C, ¹⁵N and ³¹P present in nucleic acids. These nuclei behave like small magnets when placed in static magnetic field. These spins are capable of interacting with beam electromagnetic radiations. When the frequency of the beam is same as that of precessing spin, then absorption of energy takes place which causes them to “flip” from a lower energy state to higher energy state by a process termed resonance Fig.(2.1a-c). Hence the technique is known as “Nuclear Magnetic Resonance Spectroscopy”.

The fundamental NMR equation that correlated frequency of radiation (ν) with magnetic field strength (B_0) is

$$\nu = \gamma B_0 / 2\pi \quad (1)$$

Table 2.1: Various concentration ratios for the complex formed between mitoxantrone and d-(CGATCG)₂

Drug (D) Concentration (mM)	Nucleotide (N) Concentration (mM)	D / N
0.00	1.64	0
0.07	1.63	0.040
0.19	1.63	0.116
0.37	1.62	0.230
0.54	1.61	0.340
0.61	1.61	0.384
0.73	1.60	0.456
1.08	1.58	0.684
1.43	1.51	0.95 (1)
1.79	1.43	1.25
2.05	1.36	1.50
2.1	1.20	1.75
2.20	1.10	2.0

The fundamental NMR equation that correlated frequency of radiation (ν) with magnetic field strength (B_0) is

$$\nu = \gamma B_0 / 2\pi \quad (2)$$

The energy levels correspond to the spin states where spins align along or against the applied magnetic field B_0 (Fig. 2.1a). These spins do not align perfectly along the B_0 and this gives rise to permanent torque. The nucleus has property of angular momentum because of its spin and thus as a result the nucleus precesses, where the frequency of precession is given (Fig. 2.1(b-c)).

$$\omega_0 = \gamma B_0 \quad (3)$$

where, ω_0 is the resonant frequency or Larmor frequency in radians seconds and B_0 is the magnitude of the applied static magnetic field.

But,

$$\nu = \gamma B_0 / 2\pi \quad \text{so that } \omega_0 = 2\pi\nu \quad (4)$$

On interaction with magnetic field, nuclei with spin $I > \frac{1}{2}$ distribute themselves among $(2I + 1)$ energy levels with the separation given by (5)

$$\Delta E = h\nu = h / 2\pi\gamma B_0 \quad (5)$$

The magnetic quantum number m_I , characteristic of each energy level depends upon spin quantum number. Thus, the nucleus of spin $I = \frac{1}{2}$ has two allowed energy levels corresponding to the m_I values of $+\frac{1}{2}$ and $-\frac{1}{2}$, respectively, where m_I is the quantum number characterizing Z-component of I.

2.4.2 NMR signal

If the α and β states would be populated equally, no net change in energy could be observed. The signal intensity is proportional to the population difference of the two states:

$$N^\alpha / N^\beta = e^{(E_\beta - E_\alpha) / kT} \quad (6)$$

where T being the temperature and k the Boltzmann constant. $E^\beta - E^\alpha$ is the energy difference between the α and the β -state.

2.4.3 Chemical Shift

The resonance frequency depends on the strength of the applied static field and on the gyromagnetic ratio of the nucleus

$$\omega_0 = \gamma B_0 \quad (7)$$

However, the field strength to be considered is not exactly the strength of the applied magnetic field, B_0 , *in vacuo* but is locally modified by the electronic environment of the nucleus. What is really important is the *effective* field strength at the nucleus site. Many different mechanisms are known.

$$\sigma = \sigma_{\text{dia}}(\text{local}) + \sigma_{\text{para}}(\text{local}) + \sigma_{\text{m}} + \sigma_{\text{rc}} + \sigma_{\text{ref}} + \sigma_{\text{solv}} \quad (8)$$

where σ is the shielding constant usually has a positive sign.

σ_{dia} the diamagnetic contribution; σ_{para} the paramagnetic contribution; σ_{m} the neighbor anisotropy effect; σ_{rc} the ring-current contribution; σ_{ref} the electric field effect; σ_{solv} the solvent effect thus the effective field strength is given by (9)

$$B_{\text{eff}} = B_0 (1 - \sigma) \quad (9)$$

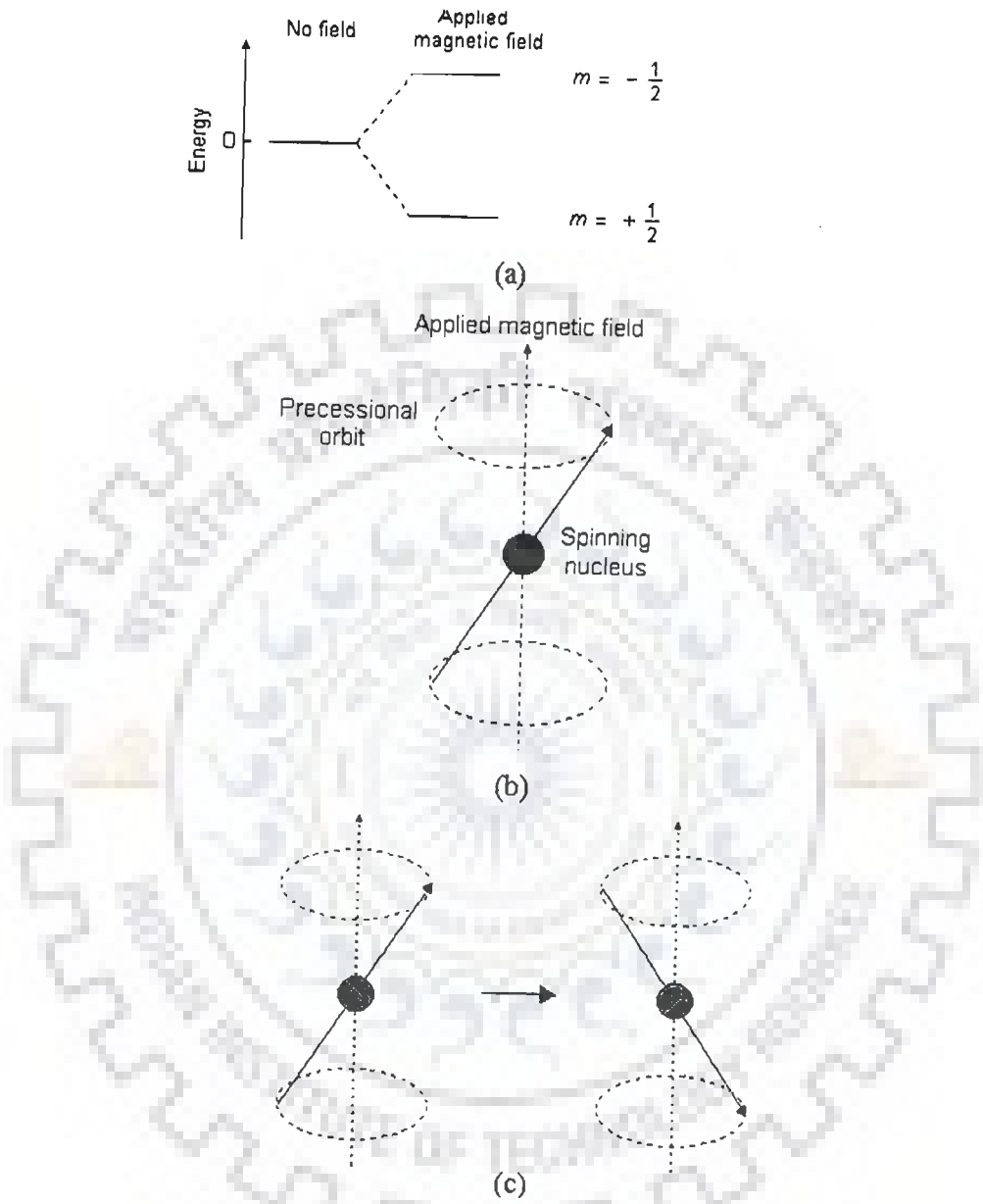


Figure 2.1: (a) Energy levels for a nucleus with spin quantum number $m = +\frac{1}{2}$ and $m = -\frac{1}{2}$ (b) Precessional motion by the nucleus spinning on its axis in presence of the external magnetic field. (c) Flipping of the magnetic moment on absorption of the radiations.

Different nuclei experience different fields, depending on their intermediate chemical environment and hence the observed shifts known as chemical shift. It is expressed (10) in parts per million (ppm) given as:

$$\delta = 10^6 \times \left(\frac{\delta_{\text{ref}} - \delta_{\text{obs}}}{\delta_{\text{ref}}} \right) \quad (10)$$

2.4.4 Spin-spin coupling constant

It is an important phenomena occurring between the magnetically and chemically non-equivalent nuclei, which are directly coupled through bonds. The strength of the coupling is called spin-spin coupling constant (nJ) where n indicates the number of intervening bonds. This phenomenon causes splitting of the resonance signals, expressed in Hz.

In order to be able to detect scalar spin-spin couplings it is necessary that the two protons are not isochronous, meaning that they don't have the same chemical shift. The one-bond coupling constant usually has a positive sign.

(a) Geminal Couplings (2J)

In order to be able to detect scalar spin-spin couplings it is necessary that the two protons are not isochronous, meaning that they don't have the same chemical shift. The one-bond coupling constant usually has a positive sign.

(b) Vicinal Couplings (3J)

The most important parameter in deducing the three dimensional conformation of biological macromolecule is vicinal or three bond coupling constant (3J) between H^a and H^b in $H^a-C-C-H^b$ fragment. It is related to the dihedral angle θ (Fig. 2.2a) between planes $H^a-C^a-C^b$ and $C^a-C^b-H^b$ by Karplus relationship. For ${}^1H-{}^1H$ couplings, following has been suggested by Karplus [59-60] and depicted in Karplus Curve (Fig. 2.2b).

$${}^3J = 8.5 \cos^2\theta - 0.28 \quad 0^\circ < \theta < 90^\circ$$

$${}^3J = 9.5 \cos^2\theta - 0.28 \quad 90^\circ < \theta < 180^\circ$$

2.3.5 Relaxation time

The magnetization does not precess infinitely in the transverse plane but turns back to the equilibrium state. This process is called relaxation. Two different time-constants describe this behaviour:

a) T1 relaxation time (Spin lattice / longitudinal relaxation time)

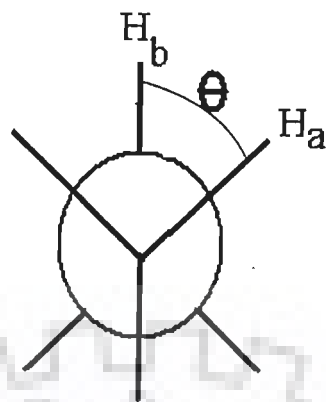
It is a measure of the recovery of Z-component after perturbation, re-establishing of the equilibrium α / β state distribution. The rate at which a Boltzman population is set up among the energy level is $1 / T_1$. The term spin lattice is used because the process involves an exchange of energy between nuclear spin and their molecular framework. Spin-lattice relaxation depends on several factors: dipole-dipole interaction, spin-spin rotation, scalar coupling etc. T_1 spin-lattice relaxation rate is then measured by plotting magnetization (M) as a function of τ :

$$M(\tau) = M_0 (1 - 2\exp^{-(\tau/T_1)}) \quad (11)$$

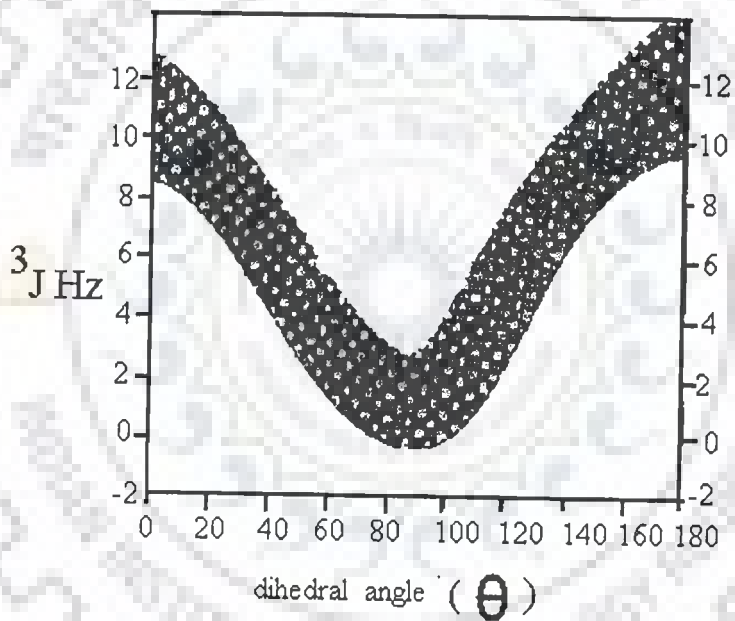
b) T2 relaxation time (Spin-Spin/ transverse relaxation time)

The T2 constant characterizes the exponential decay of the signal in the receiver coil. The precessing spins slowly return to the z-axis. Instead of moving circularly in the transverse plane they slowly follow a spiral trajectory until reached their initial position aligned with the + / - z-axis. X, Y and Z components of the magnetization.

A mechanical equivalent is a spring oscillating in time. The oscillation occurs periodically so that the displacement from the equilibrium position follows a cosine time-dependence. Due to



(a)



(b)

Fig. 2.2 (a) Definition of dihedral angle (b) Karplus Curve showing the relationship between vicinal couplings (3J) and dihedral angle θ .

frictional energy loss the oscillation is damped so that after some time the spring is not oscillating anymore. It characterizes the time it takes so that the signal has decayed to $1/e$ of its original magnitude. The damping time-constant is called T_2 or transverse relaxation time. It characterizes the time it takes so that the signal has decayed to $1/e$ of its original magnitude.

The transverse relaxation constant T_2 is related to the line-width of the signals. The width of the signal at half height is given by:

$$(\Delta\omega)_{1/2} = 1 / \pi T_2 \quad (12)$$

The transverse relaxation constant T_2 of spin $I = 1/2$ nuclei is mainly governed by the homogeneity of the magnetic field (the "shim"), the strength of the dipolar interaction with other $I = 1/2$ nuclei, depending on the number and the distance of neighboring nuclei and the overall tumbling time of the molecule which is related to its size.

2.4.6 2D NMR spectroscopy

The introduction of two-dimensional NMR spectroscopy has largely increased the potential power of NMR as a tool for structure elucidation of larger molecules. Its main advantages are dispersion of signals into two orthogonal dimensions and identification of correlations. The 2-dimensional NMR experiment is characterized by the introduction of a second frequency axis which allows correlating frequencies.

The 2D data matrix is recorded by performing a set of 1D spectrum, in which a delay called the evolution time is systematically incremented. The signal of the spin B, which is detected, varies in amplitude from experiment to experiment, and the modulation frequency of the signal intensity corresponds to the chemical shift of the spin A. The 2D spectrum is yielded from a two-dimensional Fourier transformation. The two frequency domains are called the direct

(F2) and the indirect (F1) frequency domains. Frequencies of signals in the direct dimension have been directly detected in the receiver coil; those of the indirect dimension were derived from the second Fourier transform of the amplitude modulated signals.

Each pulse–sequence for a 2D experiment contains the four basic elements

i. Preparation period

In principle, the preparation period serves to create transverse coherences. In a proton, proton correlation experiment like the COSY, (Fig. 2.3a) it is a simple 90° pulse for excitation. Some experiments that correlate carbon (or nitrogen) with proton frequencies use an initial INEPT polarization transfer from proton to carbon to increase sensitivity (dramatically). These experiments are the so–called inverse–detection experiments

ii. Evolution period (t_1)

The evolution period is the pulse sequence element that enables frequency labeling in the indirect dimension. Usually, the corresponding time is called t_1 in constant to t_2 in the direct detection dimension. Fourier transform of the t_1 –domain data yields the frequency dimension F1 and t_2 corresponds to F2. In order to understand how frequency labeling in the indirect dimension is achieved, it is useful to recall how the frequencies in the direct dimension are sampled. The signal is sampled in discontinuous mode. Consecutive data points are separated by a dwell time. The length of the dwell time (dw) is related to the spectral width (SW, the width of the spectrum in Hz). The resolution depends on the number of data points sampled and the spectral width (neglecting relaxation effects). Frequency labeling in the indirect dimension is done analogously. However,

$$dw = 1 / SW \quad (13)$$

However, data points are taken in separate 1D experiment. During a 2D experiment a series of 1D spectra is recorded which differ by the fact that the evolution time has been systematically incremented from experiment to experiment. The signal precesses during t_1 . Depending on the length of the evolution period more or less of the magnetization will be turned onto the z-axis thereby modulating the intensity of the remaining signal. Since the evolution time is incremented systematically in successive FIDs the frequency in the indirect dimension is sampled analogously to the one of the direct dimension.

iii. The mixing time (τ_m)

The many 2D experiments differ in the way they transfer magnetization from spin A to spin B, which means in the construction of the mixing process. Possible transfer-sequences may rely on scalar couplings (i.e. COSY, TOCSY), dipolar couplings (i.e. NOESY / ROESY) and chemical exchanges (EXSY type experiments).

iv. The detection period (t_2)

The detection period simply comprises acquisition of the FID with or without heteronuclear decoupling.

2.4.7 Two-dimensional NMR Methods

(a) Homonuclear 2D experiments

i. COSY (COrrrelation SpectroscopY)

The COSY experiment is used in determining which atoms are connected through bonds. The basis of COSY experiment whose pulse sequence is shown in Fig. 2.3 is the classical Jeener sequence [55]. In the COSY experiment, the first 90° pulse creates magnetization in the transverse plane. During the evolution period t_1 , the delay is incremented systematically to

sample the spectra in the other dimension also. The second 90° pulse mixes the magnetization between the spins coupled to each other. The data is saved as an array that is Fourier transformed, first in one dimension and then the second. This gives a 2D spectrum where the diagonal looks like the normal one-dimensional spectrum and the off-diagonal peaks (cross peaks), (Fig. 2.3b) give information on the nuclei that are coupled to each other through a chemical bond. Some spins do not exchange magnetization and give rise to peaks along the diagonal in the 2D COSY spectrum. Both diagonal and off-diagonal cross peaks have multiplet characteristic of the spins from which they originate. The COSY spectra is acquired with phase cycling to remove axial peaks and set of mirror image in which the diagonal runs in opposite direction. Special phase cycling and data processing also be done in a COSY experiment to change line shape into pure 2D absorption mode allowing the use of the phase sensitive display.

There are two different methods in use, the first requires the result of two complete COSY experiments with different phase cycling [108]. to be added and second known as TPPI (Time Proportional Phase Incrementation) method uses a single experiment with phase cycling with changes with t_1 increments. [16, 61, 76, 97]. The active coupling between pair of protons which give rise to cross peaks has antiphase multiplet structure. Extra splittings present in multiplet but which do not give rise to cross peaks are called passive couplings and appear in phase. Thus, the advantage of phase-sensitive COSY is that the phase relation between peaks can be used for accurate assignments and calculation of coupling constants.

i. ***DQF-COSY (Double Quantum Filtered COSY)***

Double quantum filtered COSY is a phase sensitive technique. The experiment uses a pulse sequence $90_\phi-t_1-90_\phi-90_\zeta-t_2$ where ϕ , φ and ζ are the appropriate phase cycles [94]. In double

quantum filter COSY experiment, (Fig. 2.3a) the resonance from a COSY experiment is passed through a double quantum filter, thereby removing methyl and other singlets from the final spectrum. This pulse sequence converts the dispersive diagonal peak into antiphase absorption which eliminates problems encountered in COSY spectra because multiplet resonance of interest is sometimes buried beneath its noise and spinning sidebands from the singlets as observed for ^1H NMR spectra, methyl singlets are very intense and split due to spin-spin coupling.

INADEQUATE sequence specifically excludes singlets from the spectrum by creating multiple quantum coherence and forcing the phase cycling to follow the latter than the single quantum coherence. Combining these ideas gives a sequence in which the responses from the COSY spectrum are passed through a double filter, thereby removing methyl and other singlets from the final spectrum. Another advantage of DQF-COSY is that it converts the phase of COSY diagonal signals from dispersive antiphase to absorptive antiphase. Thus, there is less interference of these signals with cross peaks lying close to the diagonal are more clearly discernible than in corresponding COSY spectra. Twice as much transients are needed in this experiments to achieve same signal to noise as in conventional COSY.

iii. Total Correlated Spectroscopy (TOCSY)

During this pulse sequence, after the evolution period t_1 , the magnetization is spin-locked during this mixing time the magnetization exchange through scalar coupling. During this spin-lock period, the magnetization behaves as a strongly coupled spin system and evolves under the influence of a "collective spin-mode" (Fig. 2.3a). In that collective mode, coherence transfer is possible between all coupled nuclei in a spin system, (even if they are not directly coupled). This essentially gives the same information as that of COSY, except that COSY gives information only on the directly coupled spins, whereas TOCSY gives the complete spin-coupling network

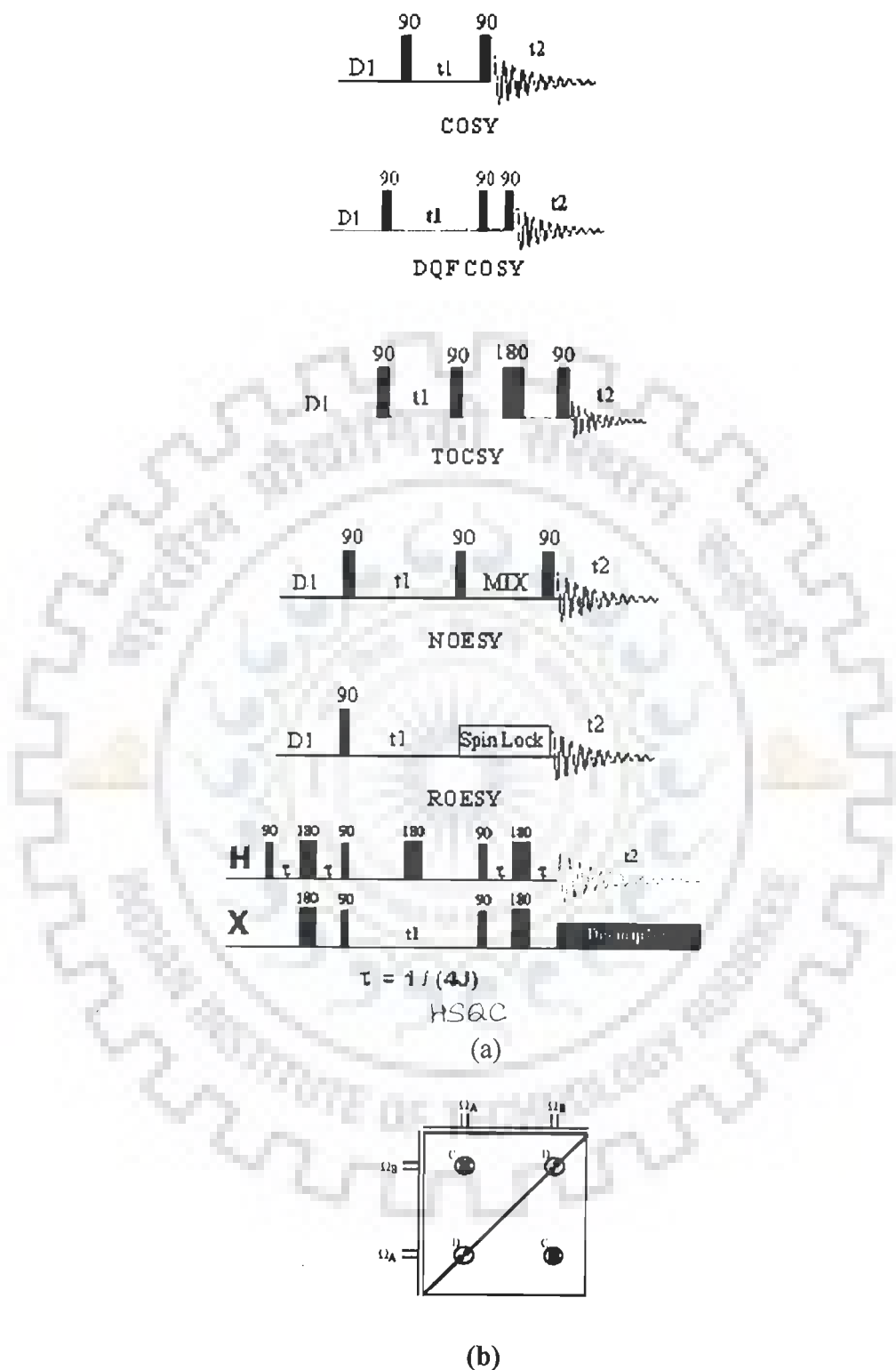


Fig. 2.3 (a) Pulse sequences for 2D experiments (b) Schematic representation of homonuclear COSY spectrum with crosspeaks (C) and diagonal peaks (D)

iv. Total Correlated Spectroscopy (TOCSY)

During this pulse sequence, after the evolution period t_1 , the magnetization is spin-locked during this mixing time the magnetization exchange through scalar coupling. During this spin-lock period, the magnetization behaves as a strongly coupled spin system and evolves under the influence of a "collective spin-mode". In that collective mode, coherence transfer is possible between all coupled nuclei in a spin system, (even if they are not directly coupled). This essentially gives the same information as that of COSY, except that COSY gives information only on the directly coupled spins, whereas TOCSY gives the complete spin-coupling network

v. Nuclear Overhauser Enhancement Spectroscopy (NOESY)

Nuclear Overhauser Enhancement Spectroscopy is one of the most useful techniques as it allows correlating nuclei through space (distance smaller than 5\AA). By measuring cross peak intensity, distance information can be extracted. The exact three-dimensional conformation of the molecule can be deduced by 2D Nuclear Overhauser Enhancement Spectroscopy. It gives us information about cross relaxation occurring between a pair of protons through dipole-dipole interaction and it gives us an idea about pairs of protons present in close proximity to each other in space.

The pulse sequence starts as usual with a 90° pulse followed by an evolution time t_1 (Fig 2.3a). This delay is varied systematically as usual to provide chemical shift information in the F1 domain. Then a 90° pulse transmit some of the magnetization to the Z-axis and during the following mixing period, the non-equilibria Z-component will exchange magnetization through relaxation (dipole-dipole mechanism). This exchange of magnetization is known as NOE

(Nuclear Overhauser Effect). After some time (shorter than the relaxation time T_1), the transverse magnetization is restored and detected. If relaxation exchange (or chemical exchange) has taken place during the mixing time, τ_m , cross peaks will be observed in the spectra during t_2 which has modulation frequencies different from their precessing frequencies during t_1 . The complete set of data $S(t_1, t_2)$ after Fourier transformation with respect to both t_1 and t_2 yields a 2D spectrum.

The magnetization components which have the same frequency in time domains t_1 and t_2 lie along the diagonal of the NOESY spectrum, while those along magnetization components which have crossed over during the mixing time, τ_m , owing to NOE, lie on both sides of the diagonal and are called cross peaks.

The phase cycling ensures proper detection of NOESY signal. In small / medium size molecules, the mixing time can be selected to be about 80% of the relaxation time. For larger molecules, shorter mixing time should be used to avoid "spin-diffusion" problems.

In NOESY experiment, the distinction between cross peaks originating from NOE effect and those originating from chemical or conformational exchange is not easy. In small molecules, having long correlation time, $\omega\tau_c \gg 1$, (where ω is the angular frequency $\omega = \gamma B$ and τ_c is the effective correlation time) and the phase of the peak can be used as evidence i.e., Diagonal signal phased "up"; NOE cross peak is phased "down"; Chemical Exchange cross peak is phased "up"

For large molecule, having short correlation time, the phase of the diagonal, the NOE cross peak and the exchange cross peak is the same. A large number of cross peaks are observed, each indicating a NOE or exchange between nuclei of interest of the corresponding diagonal. Exchange also gives rise to cross peaks identical to negative NOE (same sign of the diagonal)

and can only be distinguished from NOE by the use of the rotating frame NOE method (ROESY). The data in the NOE experiment is analyzed by measuring the peak volume of a cross peak in a series of 2D experiment with different mixing times, τ_m . The initial rate of growth of the NOE is directly proportional to $1 / r^6$ to calculate the proportionality constant; the rate is compared with some known distance.

vi. Rotating-frame Overhauser Effect Spectroscopy (ROESY)

ROESY is an experiment in which homonuclear NOE effects are measured under spin-locked conditions. ROESY (Fig. 2.3a) is especially suited for molecules with motional correlation times (τ_c) such that $\omega\tau_c \approx 1$, where ω is the angular frequency $\omega = \gamma B$. In such cases the laboratory-frame NOE is nearly zero, but the rotating-frame NOE (or ROE) is always positive and increases monotonically for increasing values of τ_c . In ROESY the mixing time is the spin-lock period. During this time spin exchange occurs among spin-locked magnetization components of different nuclei (recall that spin exchange in NOESY occurs while magnetization is aligned along the z axis). Contrary to NOE that can be positive (for small molecule), negative (for large molecule) or null (if the correlation time happen to cancel the NOE), the ROE (NOE in the rotating frame) is always positive. Alternation in sign of the ROE effect allows distinguishing the "three-spin effect" from true small ROE). Different spectral density functions are relevant for ROESY than for NOESY and these causes the ROE's to be positive for all values of τ_c .

ROESY spectra can be obtained in 2D absorption mode. This is also useful for the identification of certain artifacts. Spurious cross peaks, both COSY-type and TOCSY-type, can be observed due to coherence transfer between scalar coupled spins. COSY-type artifacts (anti-phase) arise when the mixing pulse transfers antiphase magnetization from one spin to another (the long

spin-lock pulse acts like the mixing pulse in COSY). TOCSY-type artifacts (which have the same phase as the diagonal peaks, while ROESY cross peaks have the opposite phase) arise when the Hartmann-Hahn condition is met (e.g., when spins A and B have opposite but equal offsets from the transmitter frequency or when they have nearly identical chemical shifts). In general, to minimize these artifacts, it is suggested to limit the strength of the spin-locking field.

The peak phase behavior from the ROESY experiment is as follows:

If Diagonal peaks are phased "up" or positive; ROE cross peaks will be phased "down" or negative; HOHAHA peaks will be phased "up" or positive; Exchange peaks will be phased "up" or positive.

(b) Heteronuclear 2D Experiments

i. HSQC (Heteronuclear Single Quantum Correlation)

The HSQC experiment is in fact a double INEPT experiment. This experiment correlates protons with their directly attached heteronuclei. Proton magnetization is detected (during t_2 -detection time) while the low-gamma nuclei evolve during the evolution time (t_1). Because of the detection of the high frequency nuclei, this sequence is very sensitive. The enhancement in sensitivity this experiment permits is much greater than the enhancement obtained by simple NOE (Nuclear Overhauser Effect). This is why this experiment has been referred to as the "OverBodenhausen" experiment. The HSQC experiment starts with proton magnetization.

Therefore the recycle time is based on proton relaxation time ($1.26 * T_1$). The first INEPT step is used to create proton antiphase magnetization (2τ delay) which is then transferred to the directly attached heteronuclei (Carbon, Nitrogen). This X nuclei magnetization is left to evolve with its chemical shift (during t_1 -evolution time). The effect of proton coupling and

chemical shift is removed by the use of a 180° proton pulse applied at mid evolution time. The double 90° pulse applied to both nuclei (in the beginning of the last INEPT step) transfers the magnetization back to proton as an anti-phased magnetization, which will then refocus during the last (2τ delay). The proton in-phase magnetization can then be detected in the presence of the X-nuclei decoupler.

ii. *HMBC (Heteronuclear Multiple Bond Correlation)*

The HMBC experiment detects long range coupling between proton and carbon (two or three bonds away) with great sensitivity. The length of the τ (tau) delay can be adjusted to detect relatively large coupling constants (4–10 Hz) τ (tau) = 0.06 s or smaller couplings (2–7 Hz) τ = 0.1 s. In this sequence, the first 90° pulse on Carbon-13 serves as a low-pass filter that suppresses one-bond correlation and passes the smaller coupling. This pulse creates multiple quantum coherence for the one-bond coupling, which is removed from the spectra by alternating the phase of the Carbon-13 pulse. The second 90° pulse on C-13 creates multiple quantum coherence for the long-range couplings. After the evolution time t_1 , the magnetization is converted back into detectable single quantum proton magnetization. The carbon decoupler is never used in this sequence: therefore the protons displays homonuclear as well as heteronuclear couplings. This technique is very valuable to detect indirectly quaternary carbons coupled to protons— especially useful if direct Carbon-13 is impossible to obtain due to low amount of material available.

This very useful sequence provides information about the skeleton of a molecule. It could be an alternative to the 2D-INADEQUATE experiment (which is so insensitive). It is also very useful in carbohydrate area as a sequence analysis tool that provides unique information

concerning connectivities across glycosidic linkages.

2.5 EXPERIMENTAL PARAMETERS

NMR experiments were carried on Bruker AMX 500 FT-NMR spectrometer equipped with aspect X32 computer and Varian Unity + 600 MHz FT-NMR spectrometer with SPARK station LX computer located at National NMR Facility, Tata Institute of Fundamental research (TIFR), Mumbai, 400 MHz Bruker spectrometer available at Centre for Biomedical Resonance (CBMR), Lucknow and 500 MHz Bruker AVANCE spectrometer available at and Indian Institute of Technology Roorkee (IITR).

2.5.1 Study of drug Mitoxantrone

Uncomplexed mitoxantrone has been studied in detail in three different solvents, namely D₂O and H₂O (Chapter 3) and DMSO-d₆ (Chapter 4).

1D ¹H NMR temperature dependent studies have also been carried out in D₂O (278 K–353 K), H₂O (278–353 K) and DMSO-d₆ (298 K–353 K). Concentration dependent studies have also been carried out in water and DMSO-d₆ at 298 K.

¹H NMR experiments were acquired with 32 / 64 K data points; number of scans = 64–128 and digital resolution = 0.25–0.5 Hz / point. ¹³C 1D NMR were acquired with number of data points = 32 K / 64 K, no. of scans = 2048 and digital resolution= 0.7335 Hz / point.

(a) Homonuclear (¹H–¹H) 2D experiments

Acquisition parameters for the experiments are as follows

i. DQF-COSY experiment 2048 data points along t₂ dimension; 512 induction decays in t₁ dimension; no. of scans = 40 and digital resolution 3.73037 Hz / point in t₁ dimension and relaxation delay of 2.0 secs.

ii. 2D ROESY experiment 2048 / 4096 data points along t_2 dimension; 512 induction decays in t_1 dimension; no. of scans = 40 and digital resolution 3.73037 Hz / point in t_1 dimension and relaxation delay of 2.0 secs and mixing time (τ_m) = 300 ms.

iii. 2D TOCSY experiment 2048 data points along t_2 dimension; 512 induction decays in t_1 dimension; no. of scans = 40 digital resolution 3.73037 Hz / point in t_1 dimension and relaxation delay of 2.0 secs; FnMode = TPPI and mixing time (τ_m) = 70 ms.

(b) Heteronuclear (^{13}C - ^1H) 2D experiments

The acquisition parameters are

i. HSQC experiment: 2048 data points along t_2 dimension; 400 induction decays in t_1 dimension; no. of scans = 48; digital resolution 3.09 Hz / point in t_1 dimension and relaxation delay of 2.0 secs.

ii. HMBC experiment: 2048 data points along t_2 dimension; 400 induction decays in t_1 dimension; no. of scans = 48 digital resolution 3.09 Hz / point in t_1 dimension and relaxation delay of 2.0 secs. τ value was optimized for 8Hz coupling constants.

2.5.2 Study of Mitoxantrone-*d*-(CGATCG) Complex

^{31}P (Chapter 5) and ^1H (Chapter 6) NMR experiments were recorded for *d*-(CGATCG)₂ and its complex formation with mitoxantrone on successive addition of drug (Table 2.1) at 278 K in H₂O solvents. Complex formation at D / N = 1, 1.5, 1.75 and 2.0 was studied particularly in detail. At these D / N ratios the temperature dependent ^1H and ^{31}P experiments were also performed in the range of 278– 353 K.

The parameters were as follows:

^1H 1D NMR experiments were acquired with 32 / 64 K data points; number of scans = 64–128 and digital resolution = 0.25–0.5 Hz / point. Receiver gain was optimized in each instance to obtain the best signal to noise ratio.

^{31}P 1D NMR experiments were acquired with 64 K data points, number of scan = 128 –196 and digital resolution 1.495 Hz / point.

2D NOESY ($^1\text{H} - ^1\text{H}$ experiment) were recorded with variable mixing times (τ_m) 200, 300 and 350ms at 278 K. Number of data points = 2048 / 4096 data points along t_2 dimension; 256–512 induction decays in t_1 dimension; no. of scans = 40–48 digital resolution 1.495 Hz / point in t_1 dimension and relaxation delay of 2.0 secs. Mixing time (τ_m) = 200 and 300 ms were used for D / N = 1, 1.5, 1.75 and 2.0 complex. Additionally, for D / N = 1.75 complex the 2D NOESY spectra was recorded at (τ_m) = 350 ms.

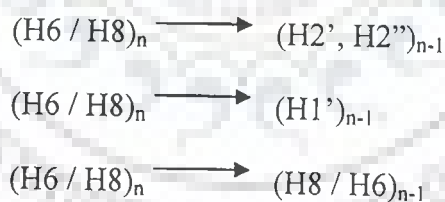
$^{31}\text{P} - ^{31}\text{P}$ 2D NOESY experiments for D / N = 1, 1.5 and 1.75 at 278 K were recorded with mixing time of 150 ms; 4096 data points along t_2 dimension; 300 free-induction decays in t_1 dimension; no. of scans = 120; digital resolution 1.495 Hz / point in t_1 dimension and relaxation delay of 2.0 secs.

2.6 DETERMINATION OF THREE-DIMENSIONAL STRUCTURE

2.6.1 Resonance assignments in nucleic acids

Resonance assignment is the first endeavour in the structural determination of DNA. From the NMR point of view, the protons can be grouped into four categories; (i) exchangeable OH, NH and NH_2 protons of the bases and nonexchangeable base protons between 7–15 ppm (ii) nonexchangeable sugar protons between 2–6.5 ppm (iii) methyl protons of thymine between 0.5–2 ppm. In order to observe OH, NH and NH_2 protons, experiments have been carried out in

water whereas the other protons were observed in D₂O solution. The strategy for resonance assignment consists of two steps. In the first stage, the J correlated spectra are used to identify network of coupled spins. In the second stage, the spin systems so identified are assigned to particular nucleotides along the sequence of the molecule by making use of the NOESY spectrum as described below. The sugar protons H1', H2', H2'', H3', H4', H5' and H5'' form a complex J correlated network (Fig. 2.4). The various cross peaks observed in the 2D J-correlated between these protons was used in identification of spin system within individual nucleotide units. The H1' proton shows a cross peak with H2', H2'' sugar protons. The H2' and H2'' protons are further coupled to H3' proton. We have used phase sensitive DQF-COSY spectra to identify the various J-coupled cross peaks. In the second phase sequential assignment is carried out using NOESY spectrum. Short internucleotide distances between adjacent nucleotide units are used as shown in Fig. 2.4. In right handed DNA with sugars in C3'-endo / C2'-endo/O1'-endo pucker and glycosidic angle in anti domain, a convenient strategy for sequential assignment is



Where, n stands for nth residue in 5'-3' oligonucleotide sequence. In case of Z-DNA, where the repeating unit is a dinucleotide. The internucleotide pathway is Base (2n-1) H5' (2n-1) Base (2n) H1' (2n) H2' (2n) and H2'' (2n) Base (2n+1).

2.6.2 Pseudorotation

Because of the r^{-6} dependence of the pre-steady state NOE, the relative magnitude of the NOEs provide a sensitive probe which can be used to obtain a qualitative view of the solution structures of short oligonucleotides. The glycosidic and sugar pucker conformations can be assessed qualitatively on the basis of the relative magnitudes of the intranucleotide sugar-base NOEs. The flexible five-membered sugar ring plays a pivotal role in nucleic acid structure and dynamic behaviour. In B-DNA family sugar responds to its surroundings (e.g. base stacking pattern) by an appropriate adaptation of its geometry. X-ray studies have now shown that P values usually occur in two distinct ranges. In a conformational wheel (Chapter 1, Fig. 1.8) one range of form occupies the “Northern” half of the circle (N-type, $P_N 0^\circ \pm 90^\circ$); the second range occupies the “Southern” hemisphere (S-type, $P_S 180 \pm 90^\circ$). To a good approximation (0.4–0.7°) the torsion angles can be reproduced by a two-parameter pseudorotation equation:

$$\nu_j = \phi_m \cos [P + 0.8\pi (j-2)] \quad (14)$$

for j equals 0–4 and ϕ_m is amplitude of pucker. In crystal structures of nucleotides usually a single pure N- or S- type conformer is found, but not necessarily the one that is predominant in aqueous solution. In some cases both N and S forms reside side by side in the same unit cell. Statistical analyses of X-ray data make it clear that details of sugar geometry of monomers are influenced by anisotropic crystal packing forces.

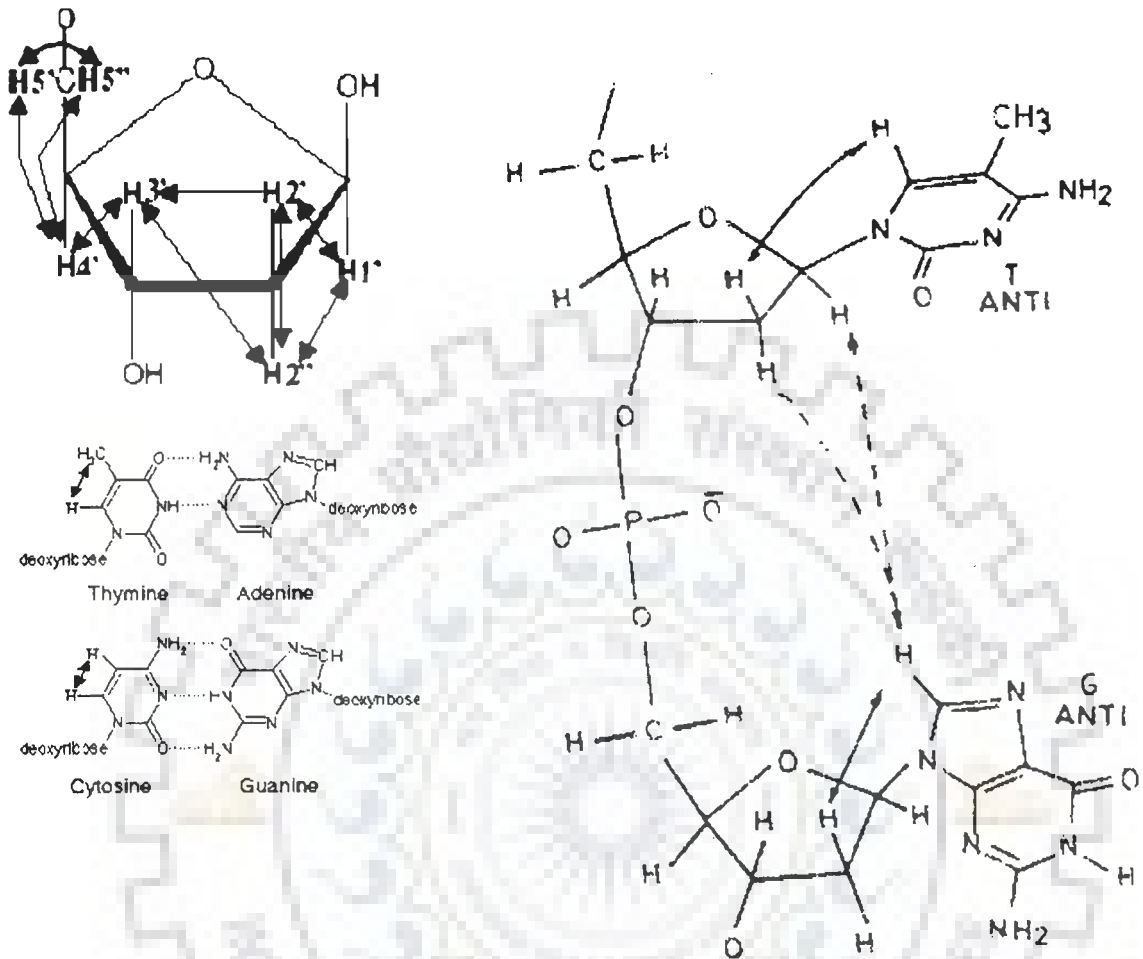


Figure 2.4 Schematic representation of through bond J connectivities (\longleftrightarrow) and short interproton distances between adjacent nucleotides units in right handed DNA bases

The situation appears to be different in the helical oligomers, where stacking forces may play a more predominant role. NMR investigations in solution have demonstrated that N (C3'–endo) and S (C2'–endo) type conformations are in rapid equilibrium. If the interconversion rate between conformers is sufficiently rapid then observed couplings represent weighted average of couplings in individual conformers. Generally, in deoxyribose sugar, a trend to a larger proportions of C2'–endo pucker sugar is observed. A phase sensitive DQF–COSY spectrum allows J–coupling patterns to be delineated from the well–resolved crosspeaks. In general, the relation between 3J and φ takes the form of the semiempirical Karplus equation:

$${}^3J = A \cos^2(\varphi) + B \cos(\varphi) + C \quad (15)$$

The constants A, B and C have to be determined from 3J values measured for compounds for which the value of φ , in solution, is known. There are five 3J values in deoxyribose sugar, H1'–H2', H1'–H2'', H2'–H3', H2''–H3' and H3'–H4', which are related to the relevant H–C–C–H dihedral angle, φ , according to the relation:

$$J = 10.2 \cos^2\varphi - 0.8 \cos \varphi \quad (16)$$

The above dihedral angles are inter–dependent and their values can be calculated in terms of the two pseudorotation parameters, P and φ_m . φ_m is a constant for deoxyribose and thus various geometries can be expressed in terms of P. Fig. 2.6 [51] shows the plots of five coupling constants in a deoxyribose ring as a function of P, ($T_m = 38^\circ$). It is clear from the curves that the value of coupling constants 3J (H1'–H2'') and 3J (H2'–H3') vary within a narrow range of 6–10 Hz and are comparatively insensitive to the sugar geometry. Values of 3J (H2''–H3'), 3J (H3'–H4') and 3J (H1'–H2') coupling constants varying in the range 0–10 Hz and can be utilized with greater advantage in fixing the domains of sugar geometry. 2J (H2'–H2'') is a geminal coupling

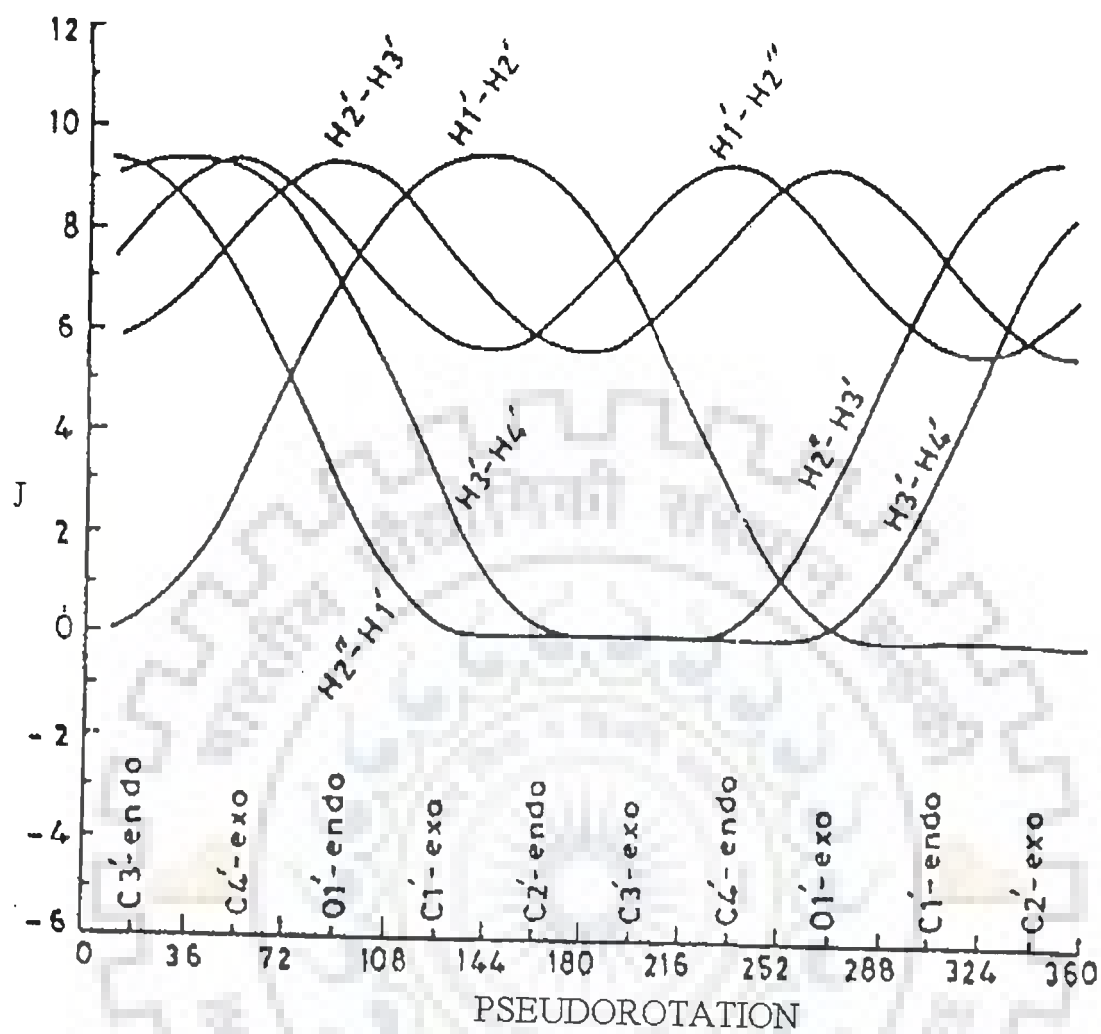


Figure 2.5 Variation of the vicinal coupling constants in the deoxyribose ring as a function of the ring geometry

which does not show significant conformational dependent variation. Rest five i.e. 3J (H1'–H2'), 3J (H1'–H2''), 3J (H2'–H3'), 3J (H2''–H3') and 3J (H3'–H4') are vicinal coupling which show a strong dependence on the conformation of the deoxyribose ring [51]. The approach used for determination of sugar geometry is based on interpretation of intrasugar proton–proton distances. The approach used for determination of sugar geometry is based on interpretation of intrasugar proton–proton distances.

2.6.3 Conformation about the glycosidic bond

A large body of crystallographic data for nucleotides and nucleotides clearly establishes that the torsional angle, χ_{CN} , defining the orientation of base ring falls into two relatively narrow ranges designated as syn and anti conformation as defined by Sundaraligham [109].

$$\chi \begin{cases} \text{O4'-C1'-N9-C4 (Purines)} \\ \text{O4'-C1'-N1-C2 (Pyrimidines)} \end{cases}$$

- i. The relative magnitudes of the intranucleotide and internucleotide (H8 / H6)–H1' and (H8 / H6)–(H2', H2'') cross peaks in NOESY spectra at different mixing times can be used to establish the domains of glycosidic dihedral angles of individual nucleotide unit [51]. Below the spin diffusion limit, the intensity patterns of the cross peak look similar at all mixing times although the absolute intensity may vary with the mixing time. The expected intensity patterns for the above mentioned cross peaks for different glycosidic dihedral angles are given below.

- a. For the syn conformation, a strong NOE between base H8 / H6 and H1' protons should be observed. At the same time, the NOEs from base to H2' and H2'' protons will be relatively weak and will have different intensities.
- b. In the high anti conformation, the (H8 / H6)–H2' and (H8 / H6)–H2'' NOEs will have similar intensities for C2'–endo geometry. The (H8 / H6)–H1' distance depends only on χ while, other distances depend on both P and χ . Iso-distance contours have been calculated by Wuthrich [117] in (P, χ) space for H8 / H6–H2', H2'', H3', H4' and H5' distances.

2.6.4 Estimation of Interproton Distances

If one resonance A is irradiated, an increase (positive NOE) or decrease (negative NOE) of signal intensity of other resonances such as resonance C is observed when spin C is close in space to spin A. This phenomenon is called Nuclear Overhauser Effect or NOE. The NOE effect is the method for elucidation of 3D structural features and stereochemistry using NMR together with information from scalar spin–spin couplings. The most important quantity derived from NOE cross peaks is the cross-relaxation rate between protons i and j . The cross relaxation rate σ_{ij} between two spins i and j is related to the distance between protons i and j in the following way:

$$\sigma_{ij} = \langle d_{ij}^{-6} \rangle f(\tau_{ij}) \quad (17)$$

$\langle d_{ij}^{-6} \rangle$ denotes an ensemble average of molecular structures interconverting in thermal equilibrium where $f(\tau_{ij})$ is a function of correlation time τ_{ij} for the vector connecting the two spins. This function accounts for the influence of motional averaging processes on the NOE. The

cross relaxation rates can be measured from buildup rates of cross peaks in 2D NOE spectra at several mixing times. According to equation (1), the measured cross relaxation rates are a function of the ensemble average properties, which are dependent on the configurational space accessible to the molecular system at the temperature and time scale. If the interconversion between conformational equilibria in the oligonucleotide is fast on NMR time scale, NOEs from several equilibrium conformations will be observed simultaneously. This means the derived set of distance constraints does not necessarily represent the average structure, and there may be no single conformation that is consistent with the data set. Initially the intensity of the cross peak in equation (1) varies linearly with mixing time, and therefore this condition is referred to as “linear regime”, but on higher mixing times, this condition does not exist due to multispin relaxation. Interproton distances can be estimated by measuring the intensities of cross peaks in the “linear regime”. Two-spin approximation is used in NOE distance measurements in which only the rate of dipolar magnetization transfer between proximal spins i and j is monitored and all other spins are ignored. For two spin approximation, the intensity I_{ij} can be written as:

$$I_{ij} = \frac{\gamma^4 \hbar^2 \tau_c \tau_m}{10r_{ij}^{-6}} \quad \text{when } \omega \tau_c \gg 1 \quad (18)$$

where γ is gyromagnetic ratio and \hbar , is planck's constant divided by 2π . In order to determine the accurate value of τ_m for estimation of interproton distances, NOE build up curves should be obtained as a function of τ_m for several cross peaks, since spin diffusion can be different for different protons. Correlation times, τ_c , can be obtained from T_2 and T_1 measurements, according to the equation:

$$\tau_c = 2\omega^{-1}(3T_2/T_1)^{-1/2} \quad (19)$$

which holds good for $\omega\tau_c \gg 1$

If protons i, j, k, l have similar τ_c values and if r_{ij} is a known distance, then the unknown distance r_{kl} can be calculated by comparing the intensities I_{ij} and I_{kl} in a single spectrum.

$$\frac{I_{ij}}{I_{kl}} = \frac{r_{kl}^6}{r_{ij}^6} \quad (20)$$

The choice of known distance is important in the light of the mobility associated with different atoms in the nucleic acid. Gronenborn et al [23, 47] have expressed the opinion of using different yardsticks for NOEs involving different group of protons. The CH5–CH6 and H2'–H2'' distances have different effective correlation times and can be used as reference depending on the cross peak being compared.

The thymidine (H6–CH₃) distance of 3.0 Å can be used as reference for all NOEs involving CH₃ protons, the sugar H2'–H2'' protons and for the rest, cytidine H5–H6 distance of 2.45 Å can be used. Reid et al [98] examined H2'–H2'' and H5–H6 cross relaxation at 15, 30, 60, 90 and 100 ms in dodecamer DNA duplexes. Results indicate that sugars and bases have the same correlation times, therefore all proton–proton distances in short DNA duplexes can be determined by scaling the initial NOE build up rate to the slope of cytosine H5–H6 cross peak, as H2'–H2'' NOE cross peak are close to diagonal and are usually unresolved. The characteristics of NMR data can be summarized as below

- i. NOEs cannot be translated into the precise distances. In practice this means that NOEs give only a number of approximate upper limits (e.g., 3 Å, 4 Å and 5 Å for strong,

medium and weak NOEs). Sometimes it is not possible to make this division and only one single upper limit is used. For some proton pairs, corrections have to be applied to the upper limit value. This may arise due to stereospecific assignments (e.g., methyl group of thymine) or because of dynamic effects such as rotation of hydrogens in a methyl group and flipping of the aromatic rings.

- ii. Translating NOEs into reliable lower limit constraints is difficult, and it is preferable to take the sum of vander waals radii as a lower limit to the distance. The absence of NOEs between two assigned protons may be translated into a minimum distance of proton pair.
- iii. NMR data contain contributions from different molecular conformations. Not all distance constraints need to be consistent with the single conformation. NOE information is limited to short distance relative to the size of the drug–DNA complex. For some part of the molecule none or only a few NOEs are observed.

2.7 RESTRAINED MOLECULAR DYNAMICS AND SIMULATED ANNEALING

When restrained energy minimization methods are used, inevitable local energy minima are encountered which can lead to inaccurate structures. To circumvent this, restrained molecular dynamics (rMD) are usually employed. This involves including NMR restraints in one of the many molecular dynamics simulation programs. Molecular dynamics solve Newton's equation of motion,

$$F_i = m_i a_i \quad (21)$$

where F_i is the force, m_i is the mass and a_i is the acceleration of atom i . The force on atom i can be computed directly from the derivative of the potential energy V with respect to the coordinates r_i . The energy can be expressed in an explicitly differentiable form:

$$Dv/dr_i = m_i d^2 r_i/d t^2 \quad (22)$$

Therefore, with an adequate expression for the potential energy and the known masses, this differential equation can be solved for future positions in time t_i . In general, this can be solved only approximately, since V is usually a complex function of the coordinates of all (or many) of the atoms (i.e. $V = V(r_1, r_2, r_3, \dots, r_N)$). The temperature can be calculated from the atomic velocities

$$3N/2 k_B T = \sum_{i=1}^N 1/2 m_i v_i^2 \quad (23)$$

where, k_B is Boltzmann's constant, m_i and v_i are the mass and velocity of atom i , and N is the number of atoms (and $3N$ is the number of degrees of freedom). For a simulation at constant energy, the temperature fluctuates due to the interconversion of kinetic and potential energy. If the temperature is held constant then the atomic velocities can be adjusted accordingly. If the pressure is held constant, the volume is allowed to fluctuate by rescaling the interatomic distances.

The total potential energy V_{total} is usually defined as the sum of a number of terms:

$$V_{\text{total}} = V_{\text{bond}} + V_{\text{angle}} + V_{\text{dihedr}} + V_{\text{vdw}} + V_{\text{coulomb}} + V_{\text{NMR}} \quad (24)$$

where, V_{bond} , V_{angle} and V_{dihedr} keep bond lengths, angles, and dihedral angles at their equilibrium values. The first five terms are empirical energy terms describing the physical

interactions between the atoms, whereas the last term is a means of including the NMR information, but does not correspond to any real physical force. They can be summarized as follows:

$$V_{\text{bond}} = \sum_{\text{bond}} 1/2 K_b (b - b_0)^2 \quad (25)$$

$$V_{\text{angle}} = \sum_{\text{angles}} 1/2 K_\theta (\theta - \theta_0)^2 \quad (26)$$

$$V_{\text{dihedr}} = \sum_{\text{dihedr}} K_\phi (1 + \cos(n\phi - \delta)) \quad (27)$$

These are pseudo-harmonic potentials that constrain bond lengths (b), bond angles (θ), and the rotamer angles (ϕ , δ) for staggered and eclipsed conformations, and K is a constant. The Van der Waals and electrostatic interactions are described by V_{vdw} and V_{coulomb} as (28) and (29)

$$V_{\text{vdw}} = \sum_{\text{pairs}(ij)} [C_{12}/r_{ij} - C_6/r_{ij}] \quad (28)$$

$$V_{\text{coulomb}} = \sum_{\text{pairs}(ij)} q_i q_j / 4\pi\epsilon_0\epsilon_r r_{ij} \quad (29)$$

where equation (28) is the Lennard-Jones potential, containing repulsive and attractive terms (C is a constant), and equation (29) describes the coulombic interactions between two charged particles (i , j) with partial charges q that are a distance r_{ij} apart in a dielectric medium described by $\epsilon_0\epsilon_r$ term. The potential V_{NMR} contains the NMR restraints, and has the effect of pulling the protons that show an NOE interaction closer to the measured distance r_{ij} . Similarly, these potentials are also pseudo-harmonic functions of similar forms to equations (25-27). Distance

constraints which can be reasonably accurately determined may therefore be defined as follows:

$$V_{\text{NOE}} = \begin{cases} K_1 (r_{ij} - r_{ij}^0)^2 & \text{if } r_{ij} > r_{ij}^0 \\ K_2 (r_{ij} - r_{ij}^0)^2 & \text{if } r_{ij} < r_{ij}^0 \end{cases} \quad (30)$$

where, r_{ij} and r_{ij}^0 are the calculated and experimental interproton distances, respectively, and K_1 and K_2 are force constants given by:

$$K_1 = k_B TS / [2(\Delta_{ij}^+)^2] \quad \text{and} \quad K_2 = k_B TS / [2(\Delta_{ij}^-)^2] \quad (31)$$

where k_B is Boltzmann's constant, T , absolute temperature of the simulation, S a scale factor, and Δ_{ij}^+ and Δ_{ij}^- are the positive and negative error estimates, respectively, of r_{ij} . If, however, only ranges of distances can be specified, then the distance restraints are incorporated into a pseudosquare-well potential of the form:

$$V_{\text{NOE}} = \begin{cases} K_{\text{NOE}} (r_{ij} - r_{ij}^u)^2 & \text{if } r_{ij} > r_{ij}^u \\ 0 & \text{if } r_{ij} \leq r_{ij}^u \\ K_{\text{NOE}} (r_{ij} - r_{ij}^l)^2 & \text{if } r_{ij} < r_{ij}^l \end{cases} \quad (32)$$

where r_{ij}^u and r_{ij}^l are the upper and lower limits, respectively, of the target distances obtained from the experimental, and K_{NOE} is the force constant, which is typically chosen to be the order of $1000 \text{ kJ mol}^{-1} \text{ nm}^{-1}$.

To ensure that the experimental restraints are the dominating factor in determining the

conformation of the molecule, it is very important that the force constants for the restraints are set sufficiently high that the experimental data are satisfied within the precision of the measurements. At the same time, the contribution from the empirical energy function should be such that any individual RMD structure, the deviations from ideal geometry are small, and the non-bonded interactions are good (i.e. the Lennard–Jones potential is negative). Thus convergence on the structure is guided by the requirement to minimize NOE or other restraint violations. The number of distance restraint violations N_{viol} is counted when, for example, $r_{ij} \geq r_{ij}^0 + 1$, which would be for 1 Å fluctuations. Other parameters which can be minimized in addition to N_{viol} are the sum of the distances in excess of the constraints $\sum \Delta r_{\text{viol}}$, which is defined as:

$$\sum \Delta r_{\text{viol}} = \sum_{K=1}^{N_{\text{viol}}} (r_{ij})_K - [(r_{ij}^0)_K + 1] \quad (33)$$

where the sum runs over all those interproton (or pseudoatom) distances for which N_{viol} is defined. Although an arbitrary structure may be used for restrained molecular dynamics calculation, in practice a starting structure obtained from distance geometry and energy minimization is often used. The rMD approach requires a relatively large amount of computation time compared to distance geometry methods. This problem can be overcome by using a simplified potential energy function, where all non-bonded contact interactions are described by a single Van der Waals repulsion term. Also by using a cut off distance, in which non-bonded interactions for pairs of atoms that are separated by a distance greater than some reasonable value (e.g. 5–10 Å) are excluded, the number of non-bonded interactions is decreased considerably. Simulated annealing involves raising temperature of the system followed by slow cooling in order to overcome local minima and locate the global minimum region of the target

function. It is computationally more efficient than rMD and yield structures of similar quality. The potentials are very similar to rMD and again Newton's laws of motion are solved as a function of time. However, in implementations found in commercial programs, the non-bonded interaction potential is modified so that there is a simple Van der Waals repulsion term with a variable force constant K_{rep} :

$$V_{\text{repel}} = \begin{cases} 0 & \text{if } r \geq s \cdot r_{\text{min}} \\ K_{\text{rep}} \left(\frac{2}{s \cdot r_{\text{min}} - r} \right)^2 & \text{if } r < s \cdot r_{\text{min}} \end{cases} \quad (34)$$

The values of r_{min} are given by the sum of the standard values of the Van der Waals radii between two atoms as represented by the Lennard-Jones potential.

2.8 STRATEGY FOR MOLECULAR MODELLING

2.8.1 RESTRAINED MOLECULAR DYNAMICS (rMD) OF UNCOMPLEXED DRUG

The structure of mitoxantrone (MTX) dimer was made by using builder module in MOE (Molecular Operating Environment software) module. Pseudoatoms were defined for the equivalent set of protons. $^{13}\text{CH}_2$ - $^{14}\text{CH}_2$ peak of MTX was used as the reference using a distance = 2.40 Å. The NOEs were categorized as very strong, strong, medium, weak and very weak within the corresponding distances in the range 1.8–2.5 Å, 2.5–3.0 Å, 3.0–3.5 Å, 3.5–4.0 Å and 4.0–5.0 Å set for the respective protons. The total number of distance restraints used in the calculations was 16 and 34 derived from H_2O (Chapter 3) and DMSO (Chapter 4) respectively. The initial model of the MTX duplex was subjected to 100, 1000 and 200 steps of Steepest Descent, Conjugate Gradient and Newton Raphson minimization to remove any bad contacts

using MMF (Molecular Mechanics Forcefield). Restrained Molecular dynamics was carried out for 100ps Dielectric constant was fixed as $1.0 \cdot r$ ($r = \text{distance}$) for calculation of electrostatic interactions. At the end of dynamics structures were minimized by 1000 steps of Steepest Descent until a predefined convergence limit of root mean square derivative of $< 0.001 \text{ Kcal mole}^{-1} \text{ \AA}^{-1}$ was reached. The minimum energy structure obtained was examined in detail

2.8.2 rMD OF MITOXANTRONE COMPLEXED WITH d-(CGATCG)₂

In Chapter 7 we have discussed the conformational features of the structure of with d-(CGATCG)₂ complexed with mitoxantrone obtained after rMD simulations. Starting structure of 2:1 complex of mitoxantrone-d(CGATCG)₂ was made using builder module in MOE (Molecular Operating Environment software) module. The molecule was subjected to 10,000 steps each of Steepest Descent, Conjugate Gradient and Newton Raphson methods of minimization to remove any to short contacts in starting structure using MMF force field. CH5-CH6 peak of cytosine was used as the reference using a distance = 2.45 Å. A total of 99 distance restraints used in the structure calculations using restrained molecular dynamics. A distance dependent dielectric constant of $1.0 \cdot r$ ($r = \text{distance}$) was used during simulations in vacuum for restrained molecular dynamics (rMD) calculations to mimic the presence of a high dielectric solvent. Pseudo atom corrections were used for methyl and other equivalent protons. A cut off value of 9.0 Å was chosen to calculate all non-bonded interactions in the system. A typical rMD run consisted of 100 ps simulations with time step of 1 fs. Structural information was collected after every 1 ps i.e. in total 100 structures were saved. At the end of dynamics all the structures were minimized by 1000 steps of Steepest Descent until a predefined convergence limit of root mean square derivative of $< 0.001 \text{ Kcal mole}^{-1} \text{ \AA}^{-1}$ was reached. To gain more insight into structural details the resulting rMD structure was thoroughly analyzed with program CURVES, version 5.1.

Chapter 3

Self association of Mitoxantrone in water by NMR and Absorption Spectroscopy

3.1 INTRODUCTION

In this chapter, results on complete assignment of mitoxantrone drug and self association in water are reported. The proton 1D NMR, DQF COSY, HSQC (^1H - ^{13}C), HMBC (^1H - ^{13}C) and ROESY spectra have been used to get the assignment of all protons (11NH, 6H / 7H, 2H / 3H, 11CH₂, 12CH₂, 13CH₂ and 14CH₂) and carbon resonances and spin-spin coupling constants. 12NH, 1OH / 4OH and 14OH protons are not observed presumably due to exchange with solvent. Inter proton distances from ROESY spectra, chemical shift as a function of concentration and temperature and restrained molecular dynamics simulations yield structure of self associated dimer. These are also correlated with results on absorption and fluorescence spectroscopy data obtained as a function of concentration of mitoxantrone.

3.2 RESULTS AND DISCUSSION

3.2.1 NMR ASSIGNMENTS

The one-dimensional proton NMR spectra of mitoxantrone in water and DQF COSY spectra of mitoxantrone in D₂O and H₂O are shown in Figs. 3.1 and 3.2, respectively. The two singlets resonating in the region 6.8–7.0 ppm are due to aromatic ring protons, 2H / 3H and 6H / 7H. Four triplets resonating in the region 3.3–4.0 ppm in the spectra taken in D₂O (Fig. 3.1a) are attributed to four sets of methylene protons. The triplet resonating at 3.64 ppm (Fig. 3.1a) appears as a quartet at 3.64 ppm in spectra taken in water (Fig. 3.1b) and is assigned to 11CH₂ protons. Among the spin-spin coupled pairs of methylene protons, 14CH₂-13CH₂ and 11CH₂-12CH₂ (Fig. 3.3a), the 14CH₂ and 11CH₂ protons are expected to be downfield shifted, being attached to 14OH and 11NH protons, respectively; hence all methylene protons are assigned accordingly. The imino proton coupled to 11CH₂ protons is assigned to 11NH (Fig. 3.1b and 3.2b).

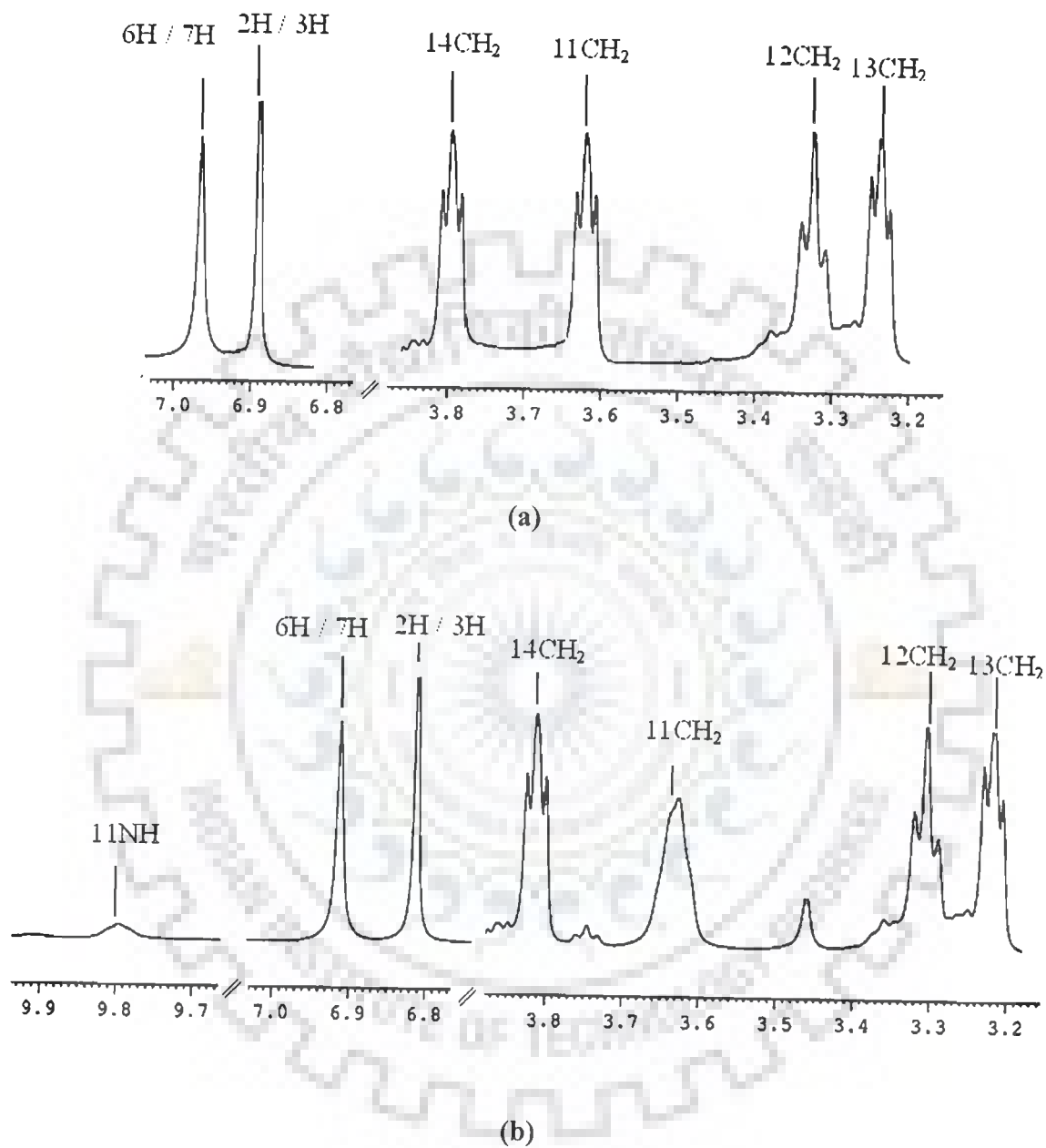
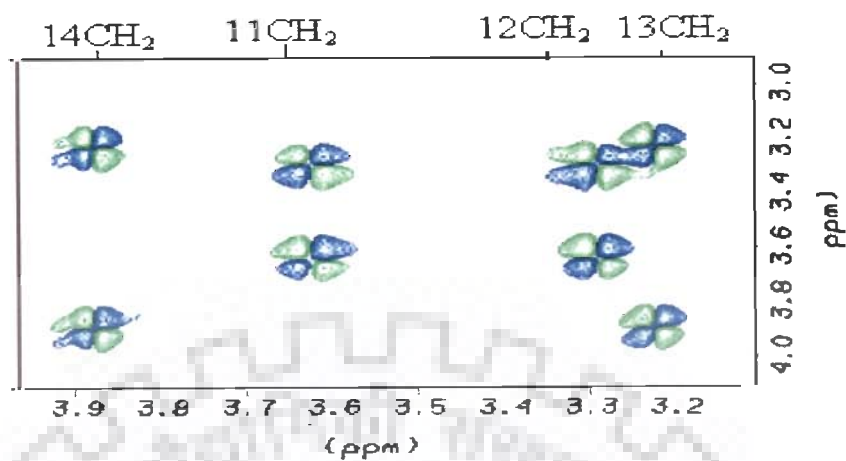
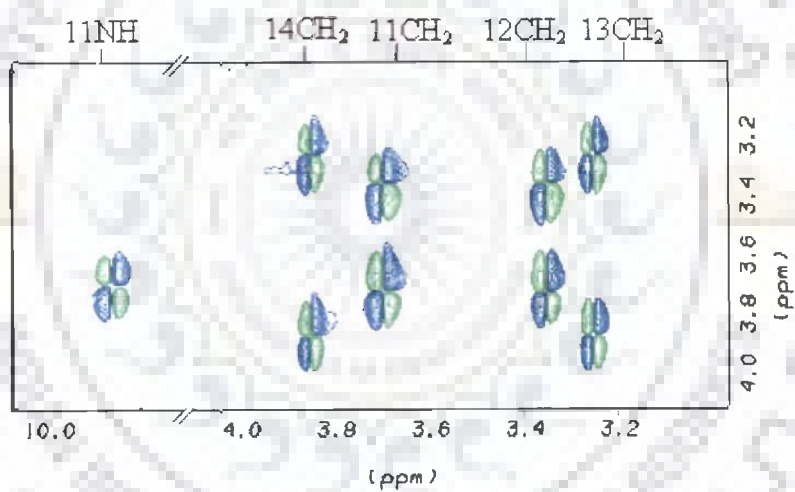


Fig. 3.1 Proton NMR spectra of 10 mM mitoxantrone in (a) D_2O (b) H_2O at 298K at 500 MHz.

In the ^1H - ^{13}C hetero single quantum coherence (HSQC) spectra (Fig. 3.3), the four carbon resonances in the aliphatic region 40–60 ppm are assigned to 11C, 12C, 13C and 14C being directly coupled to their respective bonded protons, that is, 11CH₂, 12CH₂, 13CH₂ and 14CH₂. The other carbons which are not directly bonded to protons have been assigned on the basis of hetero multiple bond correlation (HMBC) spectra (Fig. 3.4a–b). Fig. 3.4a shows splitting of 11CH₂ protons by 11C as well as coupling of 11C with protons of neighbouring carbon atom, that is, 12CH₂. Similarly, 12C, 13C, and 14C split the 12CH₂ and 14CH₂ peaks, respectively. Besides 12C, 13C, and 14C show cross peak with protons of neighbouring / next to neighbour carbons which are ultimately 2 or 3 bonds away, that is, 11CH₂ / 13CH₂, 12CH₂ / 14CH₂, and 13CH₂, respectively. The carbonyl carbons 9C / 10C resonate at 187 ppm while the four aromatic carbons 1'C / 4' C, 1C / 4C, 5'C / 8'C and 5C / 8C resonate in the region 110–160 ppm (Fig. 3.4b). The coupling of 11NH with 5'C / 8'C and 11CH₂ with 5C / 8C (Fig. 3.4b) are observed. The cross peak of 11NH with carbon peak at 126.93 ppm, which splits the proton resonance at 6.93 ppm, establishes the assignment of proton resonance at 6.93 to 6H / 7H. Thus the other singlet at 6.82 ppm gets assigned to 2H / 3H protons. This is further corroborated by bond correlation between 1OH / 4OH protons with 1'C / 4'C (and 5'C / 8'C) and 1C / 4C observed in separate HMBC experiments carried out in DMSO solvent (data in Chapter 4). The assignment of each proton and carbon to a specific single resonance is thus unambiguously made on the basis of ^1H DQF COSY, ^1H - ^{13}C HSQC and ^1H - ^{13}C HMBC spectra and is given in Table 3.1. The spin–spin couplings obtained are shown in Table 3.2. The assignment of 6H / 7H and 2H / 3H protons in the NMR data of mitoxantrone complexed with d-(CGCG)₂ [75] and d-(CGATCG)₂ [12], published earlier in literature, are interchanged. The present proton assignments however are in agreement with that published by Davies and coworkers [28, 25,



(a)



(b)

Fig. 3.2 DQF COSY spectra of 10 mM mitoxantrone in (a) D_2O
(b) H_2O at 298K at 500 MHz

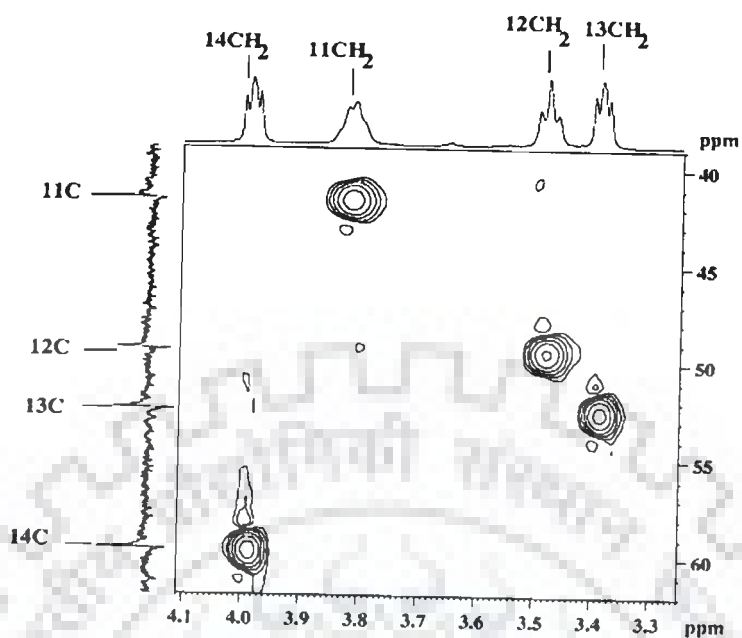


Fig. 3.3(a)

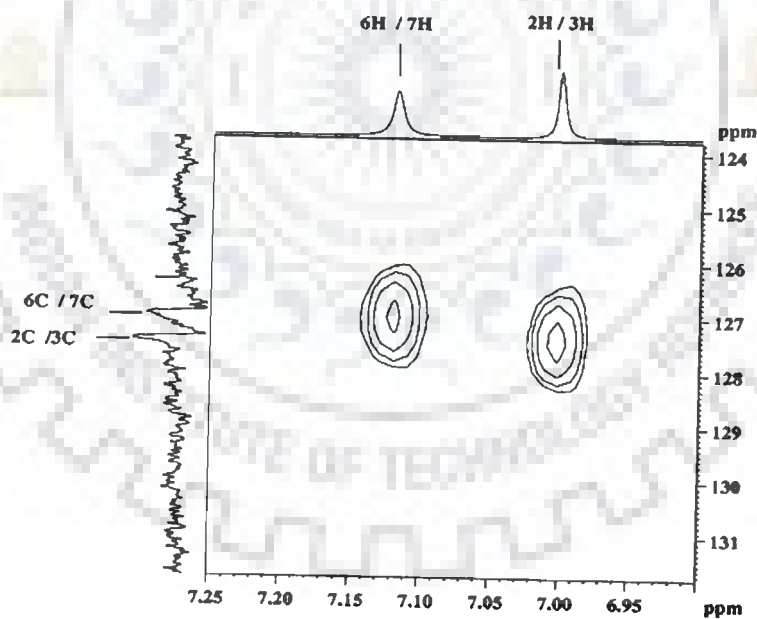


Fig. 3.3(b)

Fig.3.3(a–b) Expansions of specific regions of HSQC spectra of 10 mM mitoxantrone in H₂O at 298 K at 400 MHz showing ¹H–¹³C correlations. The one dimensional ¹³C and ¹H NMR spectra are shown along ω₁ and ω₂ axis, respectively.

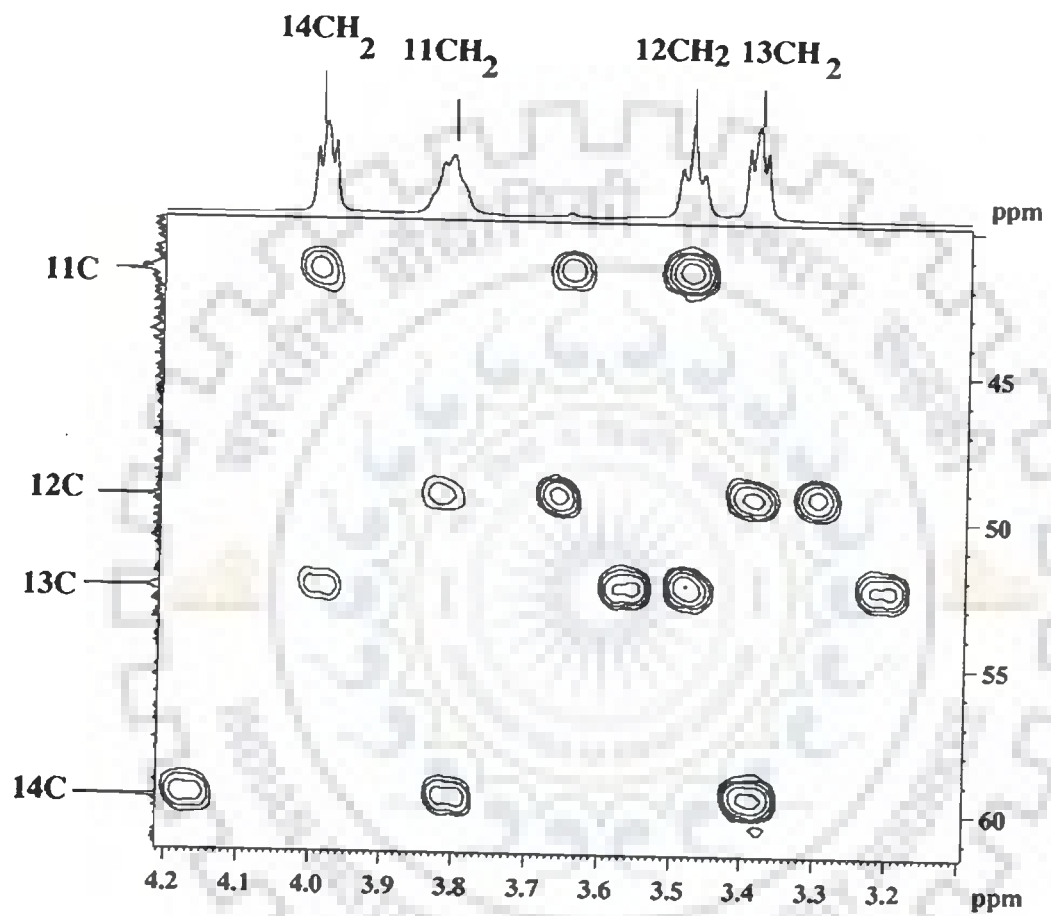


Fig. 3.4(a)

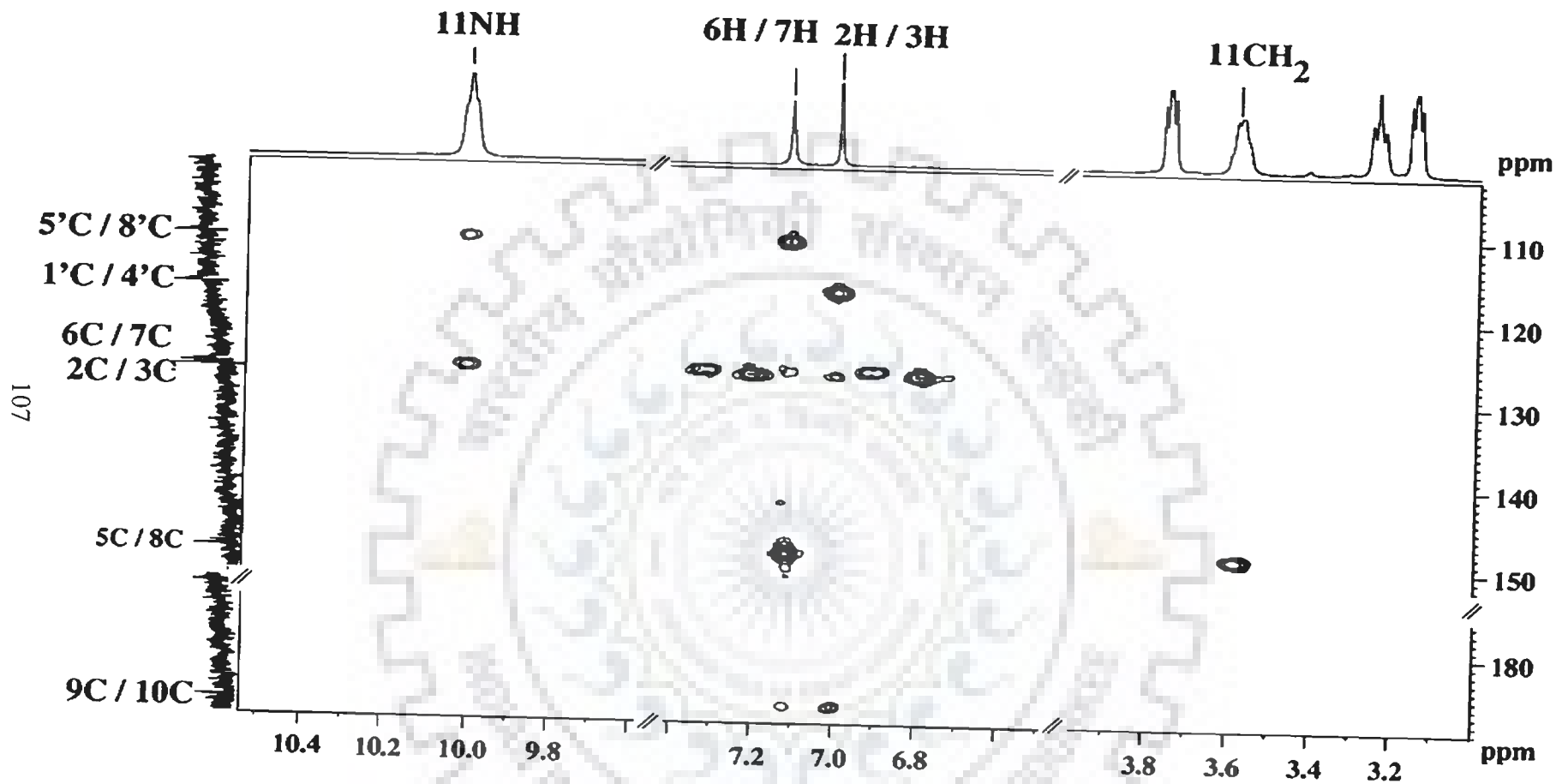


Fig. 3.4(b)

Fig.3.4(a-b) Expansions of specific regions of HMBC spectra of 10 mM mitoxantrone in H_2O at 298 K at 400 MHz showing multiple bond ^1H - ^{13}C correlations.

Table 3.1 Proton and carbon assignments of 10 mM mitoxantrone at 298 K

Proton	Chemical shift δ (ppm)		Carbon	Chemical shift
	D ₂ O	H ₂ O		H ₂ O δ (ppm)
6H / 7H	6.96	6.93	1C / 4C	156.86
2H / 3H	6.89	6.82	2C / 3C	127.36
14 CH ₂	3.88	3.81	5C / 8C	149.0
11CH ₂	3.64	3.64	6C / 7C	126.93
12 CH ₂	3.30	3.32	9C / 10 C	186.97
13CH ₂	3.23	3.30	11 C	41.64
11NH	–	9.80	12 C	49.34
			13 C	52.4
			14 C	59.6
			5'C / 8'C	111.0
			1'C / 4' C	116.8

Table 3.2 Observed average values of spin-spin coupling constant J (Hz).

Connectivity	J (Hz)	
	D ₂ O	H ₂ O
11CH ₂ –12 CH ₂	5.80	6.20
13CH ₂ –14 CH ₂	4.70	4.98
11NH–11CH ₂	–	4.80

113] and in the complex of mitoxantrone with cyclomaltooligosaccharide [15]. Thus we report here a complete set of assignment for all protons and carbons as well as the spin–spin coupling constants for the first time in literature.

2D ROESY spectrum of mitoxantrone obtained at concentration of 10 mM in D₂O solvent (Fig. 3.5a) exhibits several inter–proton contacts (Table 3.3). The expected contacts among methylene protons and their proximity to 6H / 7H protons of aromatic rings (ring C) are observed. In addition, contact of 2H / 3H protons with all methylene protons is observed. Intensity of ROE cross peak decreases as 11CH₂ > 12 CH₂ > 13CH₂ > 14CH₂ and therefore cannot be attributed to folding of side arm towards ring A. Besides a weak contact between 6H / 7H and 2H / 3H is observed, which is possible only if two aromatic rings of two different molecules stack over each other in an inverse orientation (head to tail) of the antibiotic chromophores in the aggregate. Thus, the five intermolecular ROE contacts establish self–association of molecules by stacking. This is an agreement with the result reported by Davies et al [26] in which only strongest out of this five cross peaks, that is, 11CH₂ with 2H / 3H protons was observed. The ROESY spectra in H₂O (Fig. 3.5b) showed similar results. However, an additional weak intermolecular contact of 11NH with 2H / 3H proton is observed. Thus, the existences of six intermolecular cross–peaks are sure proof of self–association stabilized by stacking of aromatic rings. In absence of internal standard for distance measurements, the average distance between 13CH₂–14CH₂ protons is taken as 2.4 Å, and all the other distances were calculated (Table 3.3) accordingly.

It may be noted that a similar conclusion about the mutual arrangement of mitoxantrone chromophores in the dimer aggregate was made previously on the basis of the 1D NMR [15].

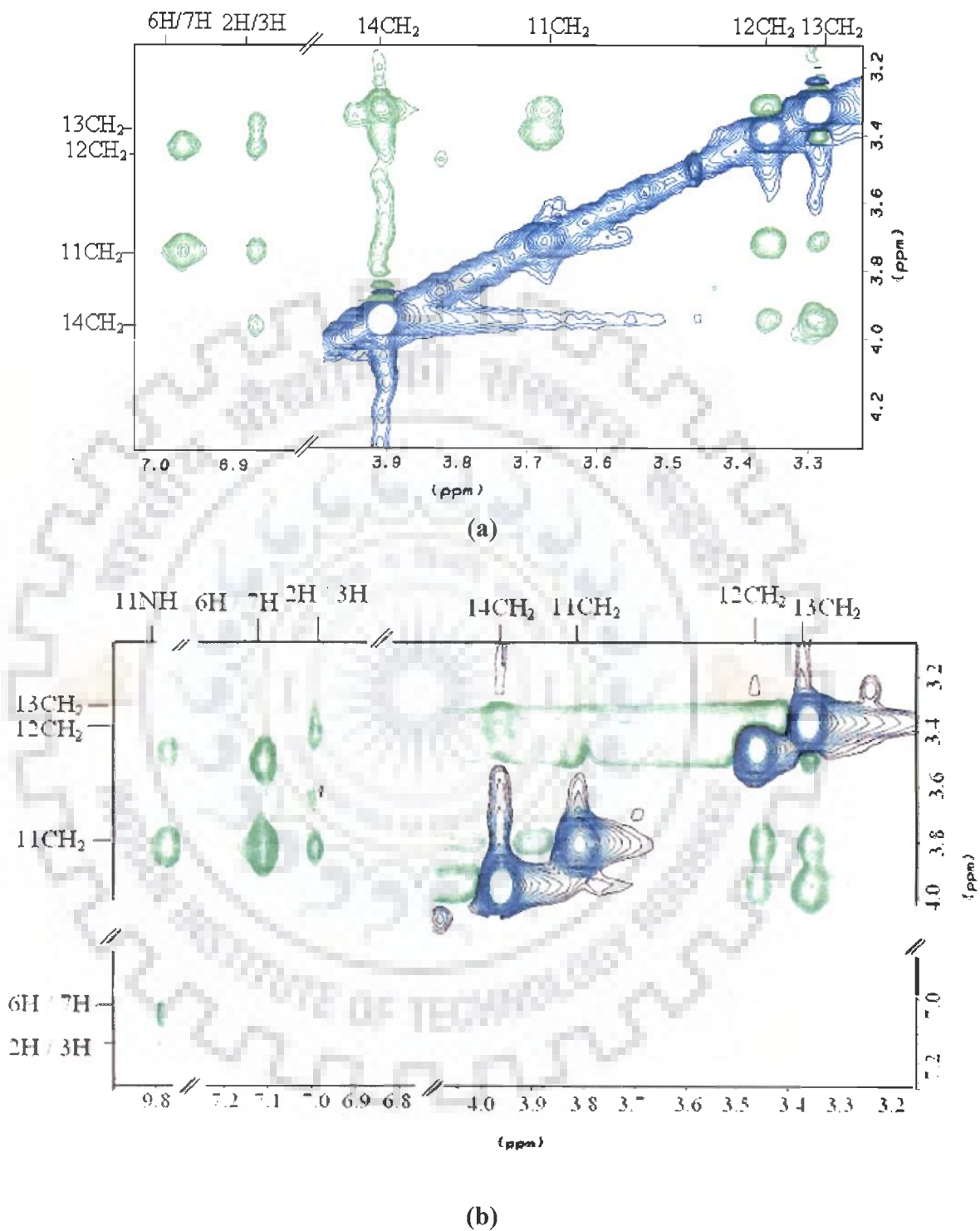


Fig. 3.5 ROESY spectra of 10 mM mitoxantrone in (a) D_2O (b) H_2O at 298K at 500 MHz.

The figure shows expansions of specific regions to highlight connectivities.

Table 3.3 The relative intensities of cross peaks and interproton distances (Å) from ROESY spectra of 10 mM mitoxantrone in D₂O and H₂O recorded at 300 ms at 298K

S.No.	Connectivity	D ₂ O		H ₂ O	
		Intensity	Distance (Å)	Intensity	Distance (Å)
1.	13CH ₂ – 14 CH ₂ ^{ref}	5.50	2.40	0.54	2.40
2.	11CH ₂ – 12 CH ₂	1.60	2.95	0.20	2.83
3.	12CH ₂ – 14CH ₂	0.49	3.59	0.13	3.04
4.	11CH ₂ – 13 CH ₂	0.32	3.89	0.12	3.08
5.	12CH ₂ – 13 CH ₂	1.2	3.28	0.05 (o)	2.9 – 3.6
6.	11CH ₂ – 6H / 7H	2.5	2.73	1.03	2.15
7.	12CH ₂ – 6H / 7H	1.01	3.18	0.37	2.55
8.	11NH – 11CH ₂	–	–	0.27	2.69
9.	11NH – 12CH ₂	–	–	0.08	3.32
10	11NH – 6H / 7H	–	–	0.01	3.6 – 4.7
11	11CH ₂ – 2H / 3H*	0.42	3.68	0.07	3.38
12	12CH ₂ – 2H / 3H*	0.38	3.98	0.04	3.64
13	13CH ₂ – 2H / 3H*	0.23	4.32	0.004 (o)	5.43
14	14 CH ₂ – 2H / 3H*	0.22	4.35	–	–
15	11NH – 2H / 3H*	–	–	0.02	5.5 – 6.1
16.	6H / 7H– 2H / 3H*	0.10	4.70	–	–

^{ref} Reference for distance calculations

* Intermolecular peaks

Table 3.4a Chemical shift of 10 mM mitoxantrone in D₂O as a function of temperature. $\Delta\delta = \delta_{353}$ K- δ_{278} K indicates change in chemical shift due to temperature

Temp (K)	6H / 7H	2H / 3H	11CH ₂	12 CH ₂	13CH ₂	14CH ₂
278	6.89	6.84	3.60	3.29	3.21	3.88
283	6.90	6.85	3.61	3.29	3.22	3.88
288	6.92	6.85	3.62	3.29	3.23	3.88
293	6.94	6.87	3.63	3.30	3.23	3.88
298	6.96	6.89	3.64	3.30	3.23	3.88
303	7.00	6.92	3.65	3.30	3.23	3.88
308	7.00	6.92	3.66	3.30	3.23	3.88
313	7.01	6.93	3.66	3.30	3.23	3.88
318	7.03	6.95	3.67	3.31	3.23	3.88
323	7.05	6.96	3.68	3.31	3.23	3.88
328	7.06	6.96	3.68	3.31	3.23	3.88
333	7.07	6.97	3.68	3.31	3.23	3.88
338	7.09	6.99	3.69	3.32	3.23	3.88
343	7.11	7.00	3.70	3.32	3.23	3.88
348	7.13	7.01	3.71	3.33	3.24	3.88
353	7.15	7.03	3.72	3.34	3.24	3.88
$\Delta\delta$	+0.26	+0.19	+0.12	+0.05	+0.03	0.00

Table 3.4b Chemical shift of 10 mM mitoxantrone in H₂O as a function of temperature $\Delta\delta = \delta_{353K} - \delta_{298K}$

indicates total change in chemical shift due to temperature.

Temp (K)	6H / 7H	2H / 3H	11CH ₂	12CH ₂	13CH ₂	14CH ₂	11NH
278	7.07	6.97	3.75	3.39	3.29	3.90	10.00
283	7.07	6.97	3.75	3.39	3.29	3.90	10.00
288	7.11	6.99	3.77	3.40	3.29	3.90	10.00
293	7.11	6.99	3.77	3.40	3.29	3.90	10.00
298	7.11	6.99	3.77	3.40	3.29	3.90	10.00
303	7.11	7.00	3.78	3.40	3.29	3.90	10.00
308	7.13	7.01	3.78	3.40	3.29	3.90	10.01
313	7.15	7.03	3.79	3.41	3.29	3.90	10.02
318	7.17	7.05	3.80	3.42	3.29	3.90	10.03
323	7.19	7.06	3.80	3.42	3.30	3.90	10.04
328	7.21	7.07	3.80	3.42	3.30	3.90	10.05
333	7.23	7.09	3.81	3.43	3.30	3.90	10.06
338	7.25	7.10	3.82	3.43	3.30	3.90	10.06
343	7.27	7.12	3.83	3.43	3.30	3.90	10.06
348	7.29	7.13	3.84	3.43	3.30	3.90	10.06
353	7.32	7.14	3.85	3.45	3.30	3.90	10.06
$\Delta\delta$	+0.25	+0.17	+0.10	+0.06	+0.01	0.00	+0.06

-ve $\Delta\delta$ indicates upfield shift+ve $\Delta\delta$ indicates downfield shift.

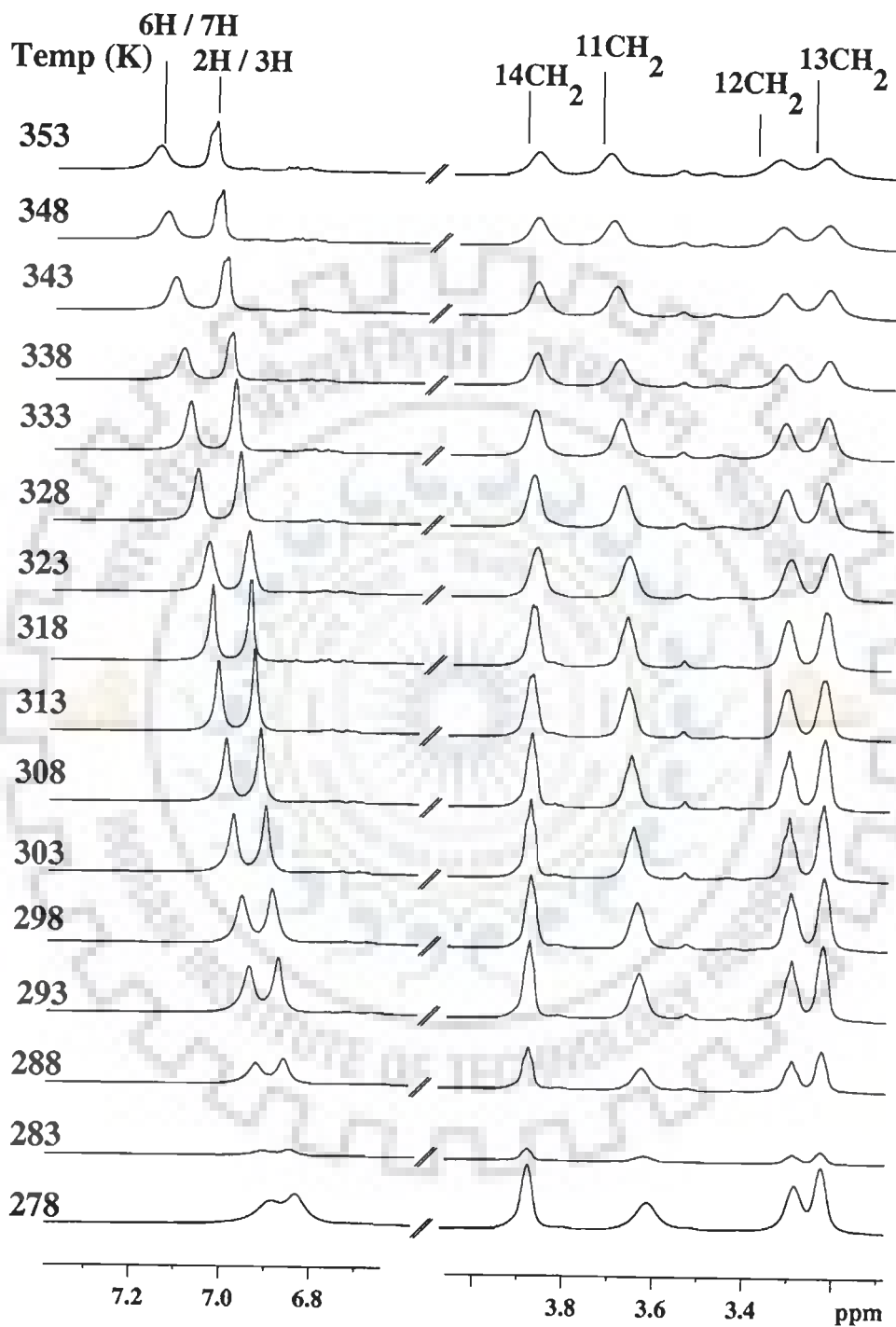


Fig. 3.6(a) One dimensional proton NMR spectra of mitoxantrone in D₂O as a function of temperature at 500 MHz.

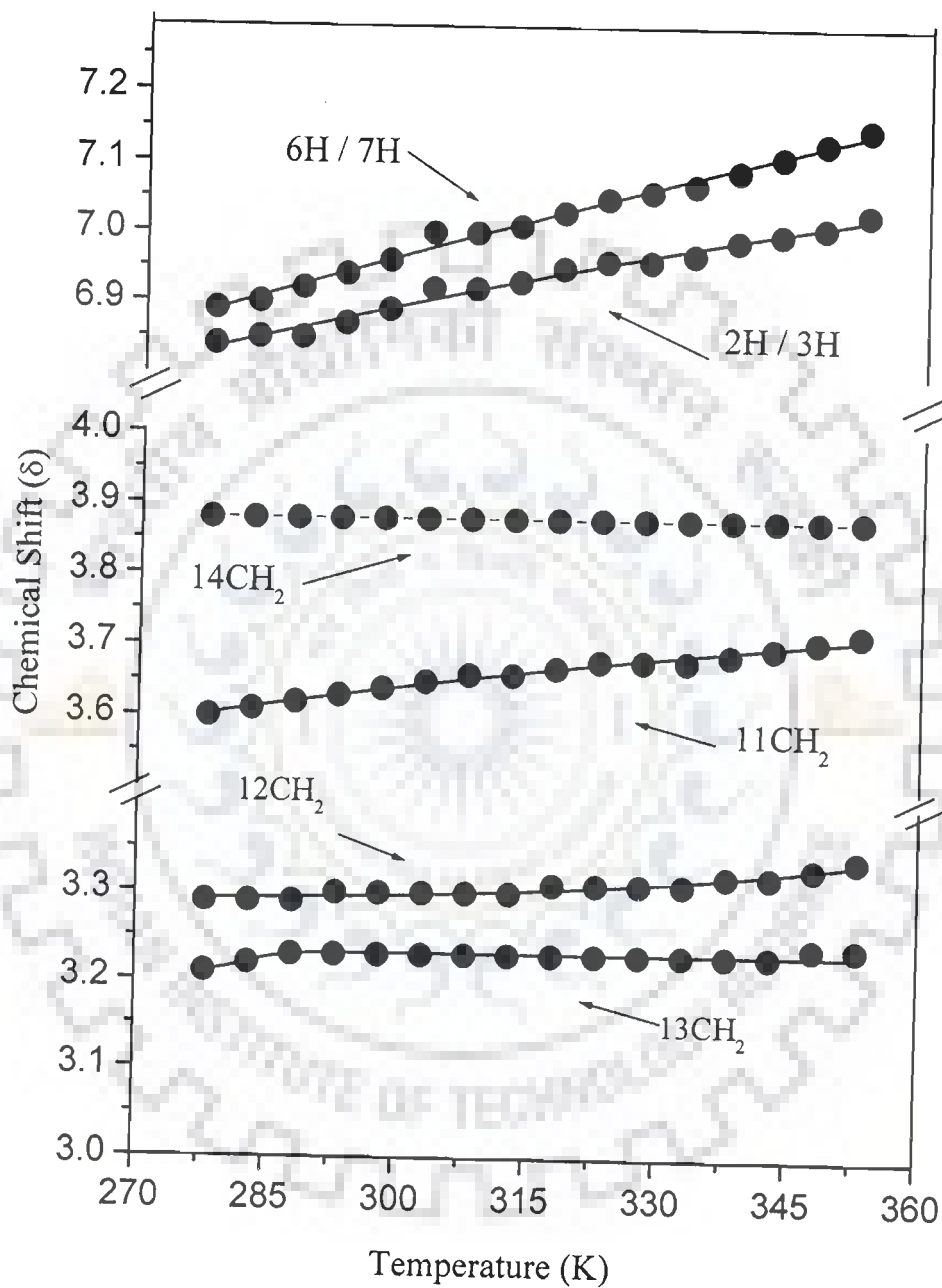


Fig. 3.6(b) Chemical shift of 10 mM mitoxantrone in D₂O as a function of temperature at 500 MHz.

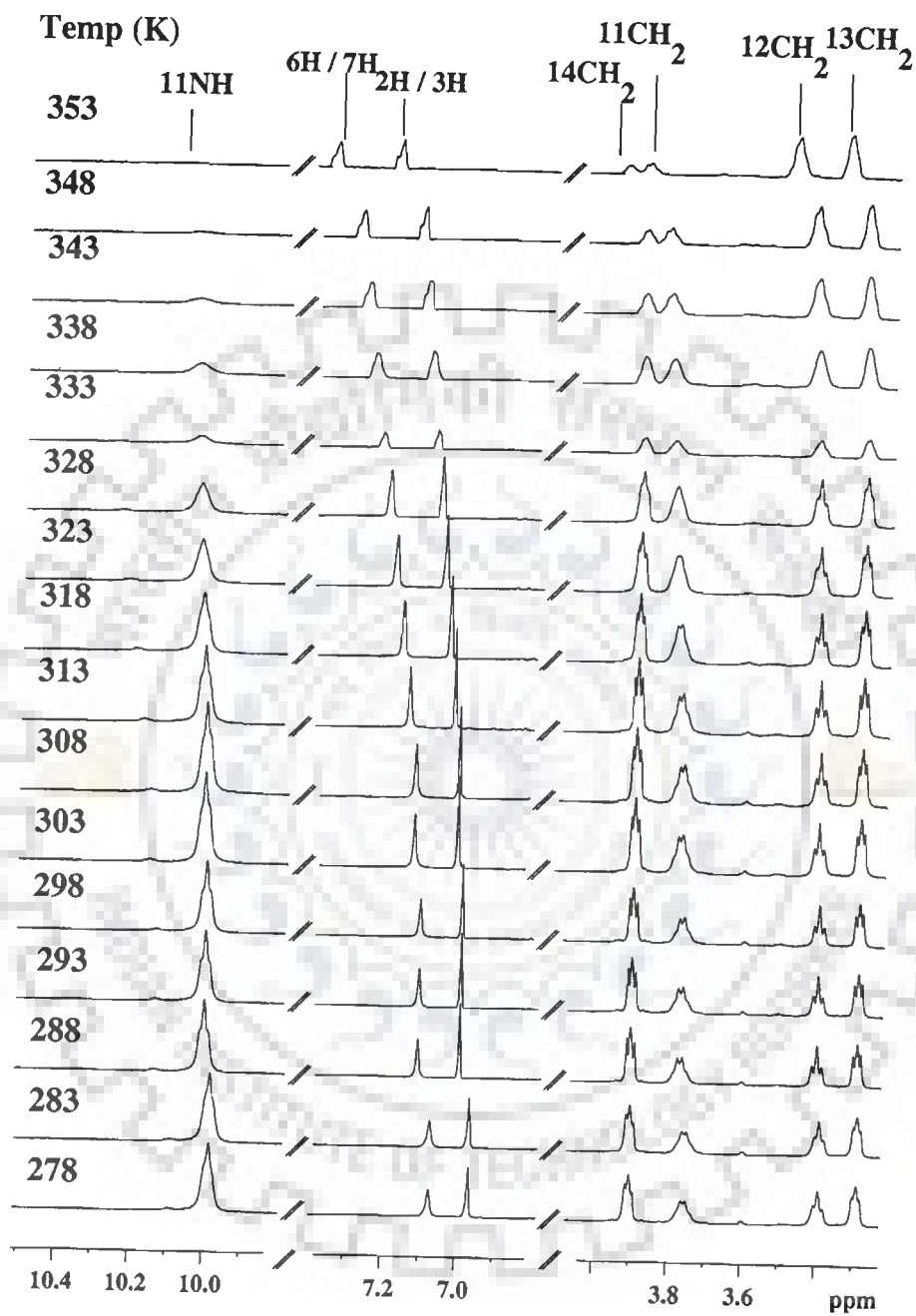


Fig.3.7(a) One dimensional proton NMR spectra of 10mM mitoxantrone in H₂O as a function of temperature at 500 MHz.

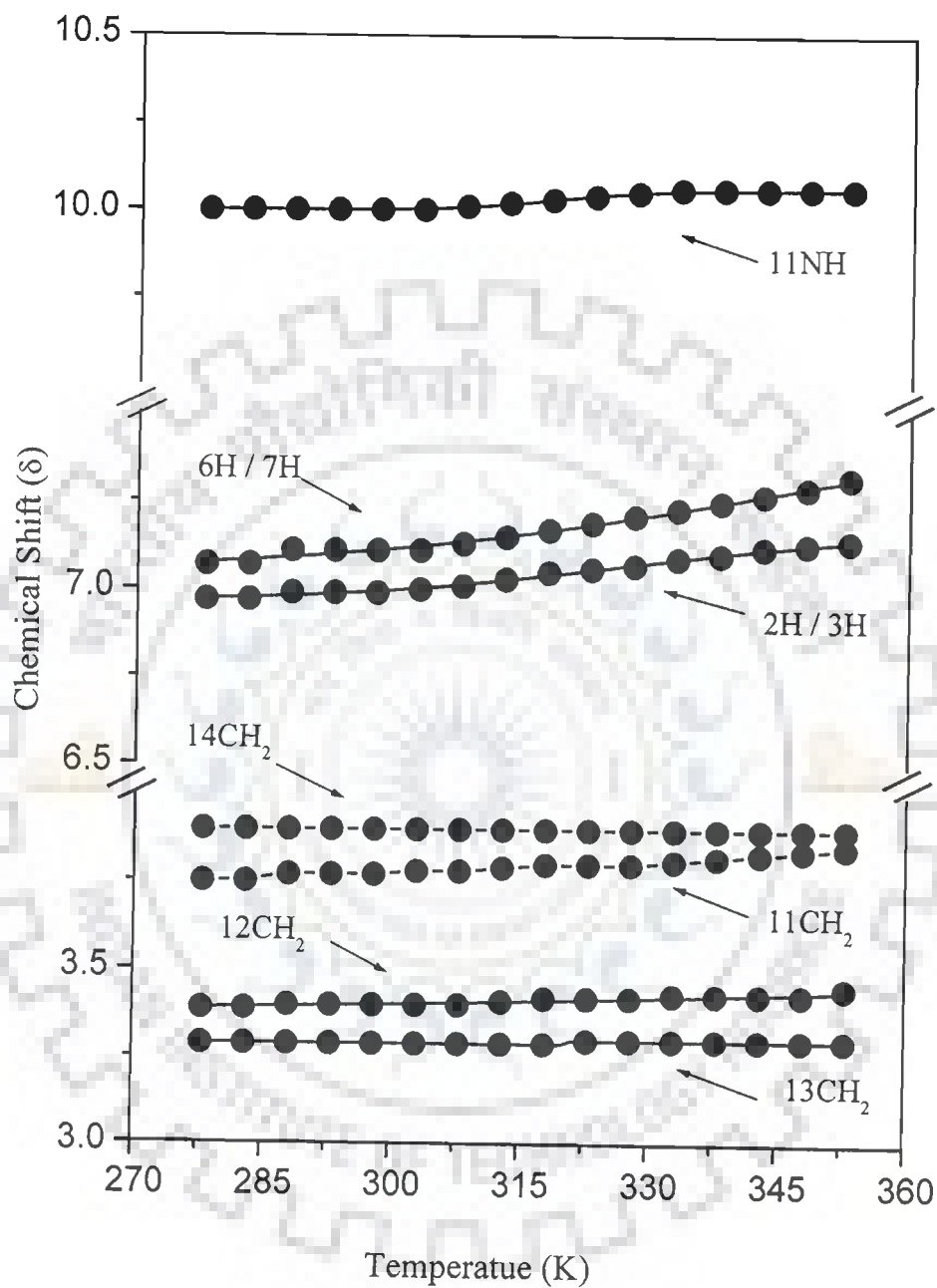


Fig. 3.7(b) Chemical shift of 10 mM mitoxantrone in H₂O as a function of temperature at 500 MHz.

Table 3.4c Chemical shift of mitoxantrone in H₂O as a function of concentration at 298 K.

$\Delta\delta = \delta_{1.82 \text{ mM}} - \delta_{0.01 \text{ mM}}$ indicates total change in chemical shift due to self association.

Concentration (mM)	6H / 7H	2H / 3H	11CH ₂	12CH ₂	13CH ₂	14CH ₂	11NH
0.01	7.39	7.13	3.75	3.29	3.10	–	10.24
0.04	7.23	7.10	3.75	3.29	3.13	–	10.12
0.08	7.18	7.02	3.75	3.29	3.13	–	10.09
0.392	7.11	6.99	3.71	3.29	3.14	3.76	10.04
0.796	7.09	6.97	3.71	3.29	3.15	3.76	10.02
1.13	7.06	6.94	3.69	3.28	3.15	3.76	9.99
1.15	7.04	6.93	3.68	3.28	3.15	3.76	9.98
1.82	7.04	6.95	3.40	3.36	3.18	3.78	9.95
$\Delta\delta$	-0.35	-0.18	-0.35	+0.07	+0.08	+0.02	-0.29

Table 3.4d Change in chemical shift ($\Delta\delta$) of various drug protons with temperature and concentration, in D₂O and H₂O solvents. For comparison result obtained by Davies et al [28] in literature are also shown

Protons					Total change in chemical shifts ($\Delta\delta$)			
	$\delta_{353 \text{ K}}$	$\delta_{278 \text{ K}}$	$\delta_{353 \text{ K}}$	$\delta_{278 \text{ K}}$	Present work			Davies et al [28]
					Drug vs. Temp. $\Delta\delta = \delta_{353 \text{ K}} - \delta_{278 \text{ K}}$ (10mM)	Drug vs. Conc(at Temp. 298 K) $\Delta\delta = \delta_{1.82 \text{ mM}} - \delta_{0.01 \text{ mM}}$		
	D ₂ O		H ₂ O		D ₂ O	H ₂ O	H ₂ O	
2H / 3H	6.89	7.15	7.32	7.07	-0.26	-0.25	0.18	0.40
6H / 7H	6.84	7.03	7.14	6.97	-0.17	-0.17	0.35	0.50
11 CH ₂	3.60	3.72	3.85	3.75	-0.12	-0.10	0.03	-
12 CH ₂	3.29	3.34	3.45	3.39	-0.05	-0.06	0.03	-
13 CH ₂	3.21	3.24	3.30	3.29	-0.02	-0.01	-0.03	-
14 CH ₂	3.88	3.88	3.90	3.90	0.00	0.00	0.00	-
11 NH	–	–	10.06	10.00	-	-0.06	0.29	0.27

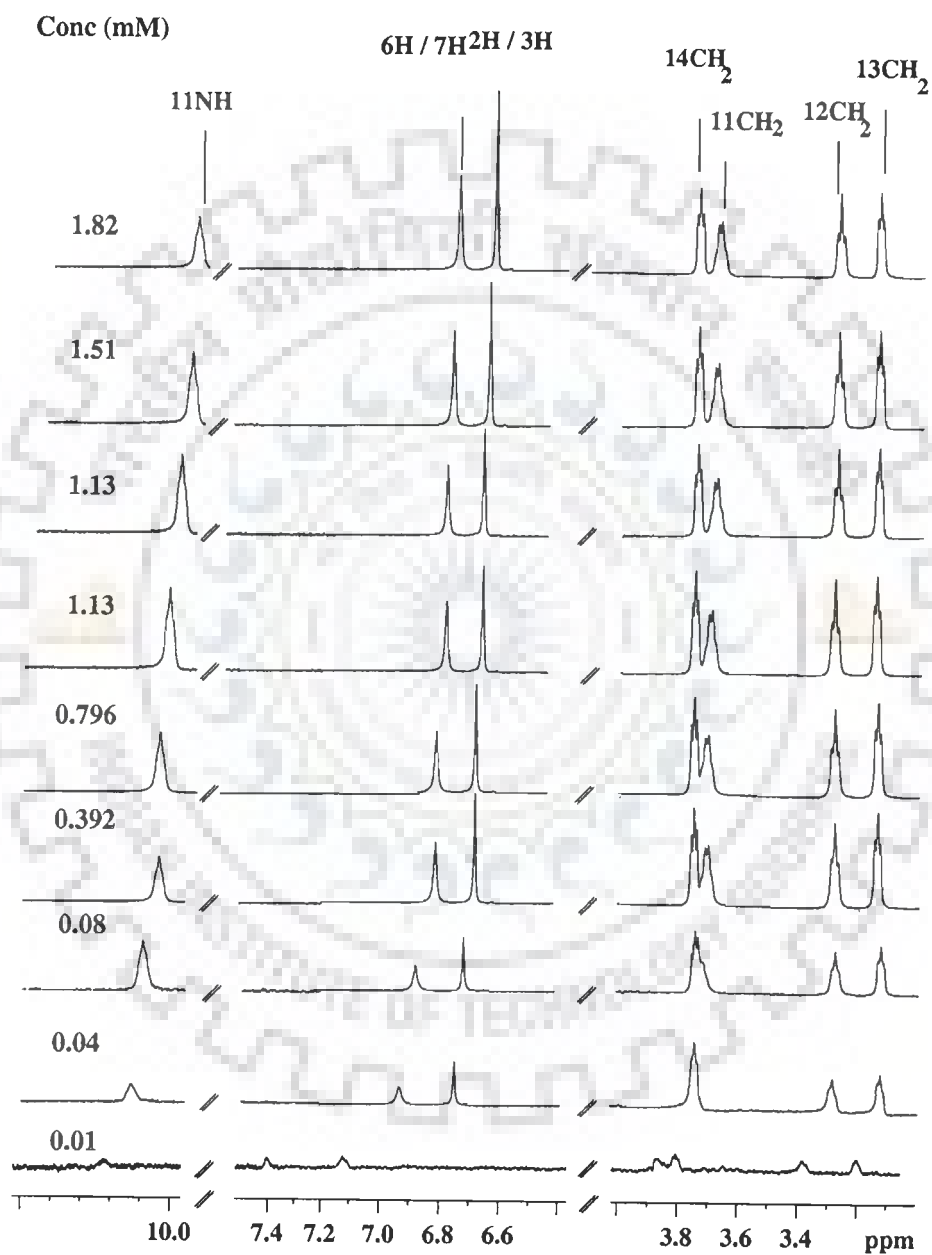


Fig. 3.8(a) One dimensional proton NMR spectra of mitoxantrone as a function of concentration at 298 K.

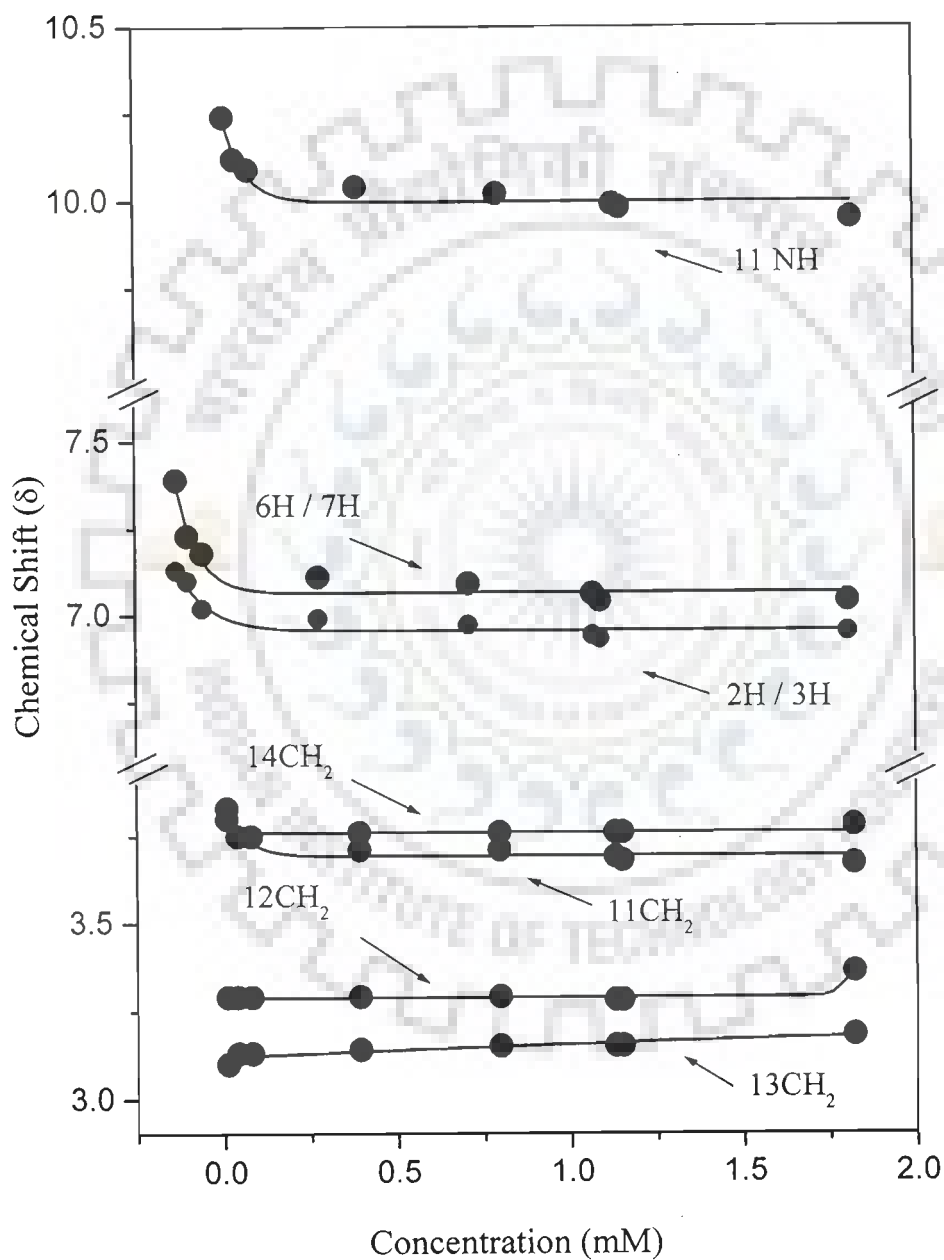


Fig. 3.8(b) Chemical shift of mitoxantrone in H₂O as a function of concentration at 298 K.

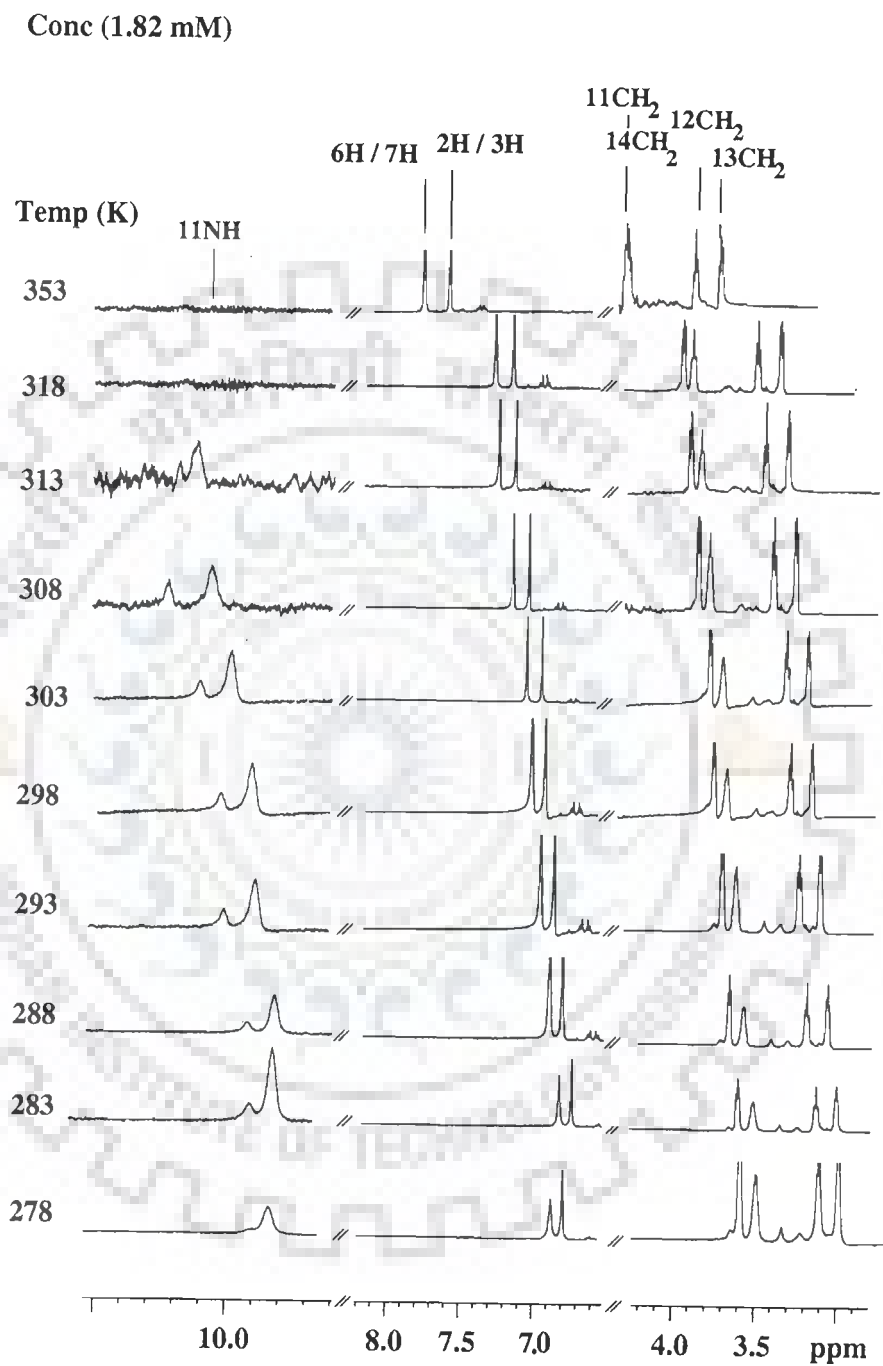


Fig.3.9a One dimensional proton NMR spectra of 1.82mM mitoxantrone in H₂O as a function of temperature at 500 MHz.

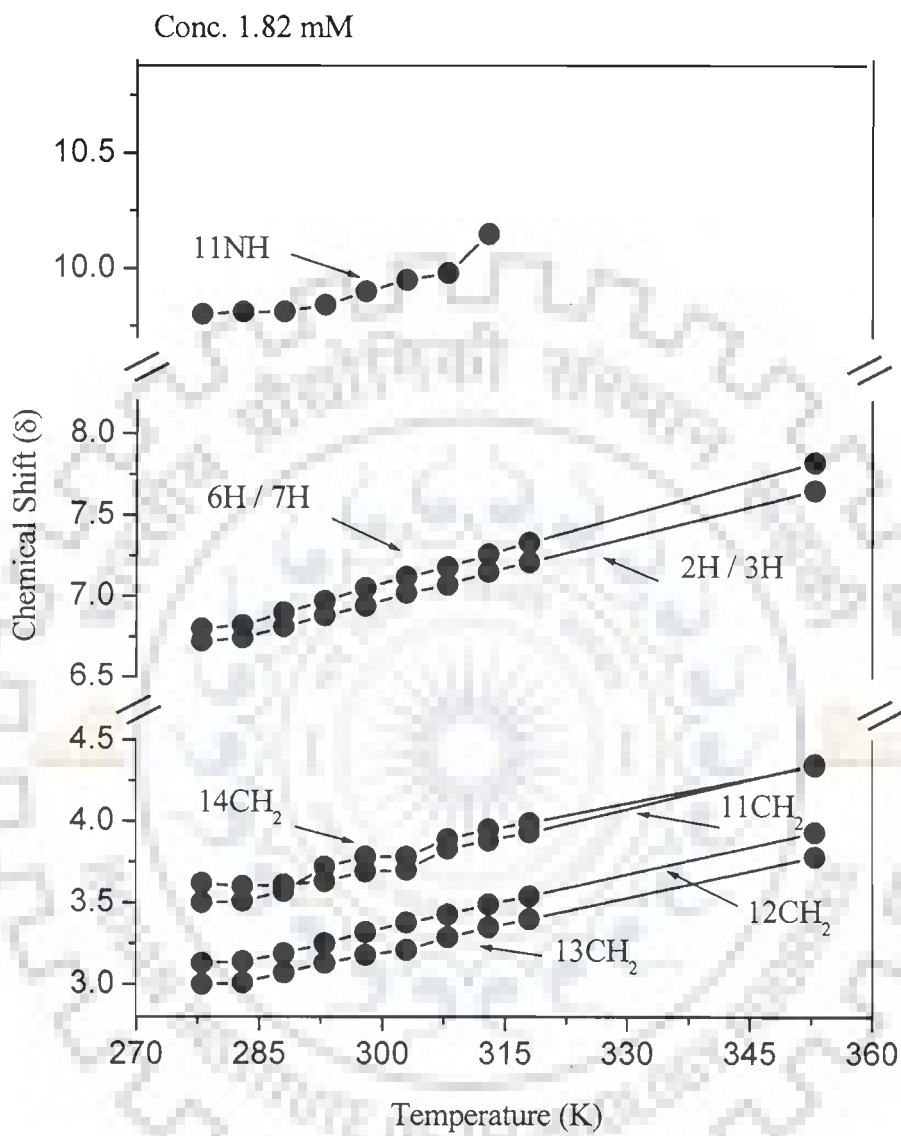


Fig. 3.9b Chemical shift of 1.82 mM mitoxantrone in H₂O as a function of temperature at 500 MHz.

and 1D NOE [75] experiments. The 1D NMR spectra and changes in chemical shift with temperature and concentration are presented in Figs. 3.6– 3.9. The aromatic ring proton 6H / 7H, 2H / 3H and 11NH protons shift upto 0.35 ppm with concentration which result from intermolecular (Table 3.4a–d) stacked complexes in solution in common with other aromatic drug molecule 19, 26–27]. The observed chemical shift δ of the drug proton at a given temperature T can be written as

$$\delta (T) = f_m (T) \delta_m + f_s (T) \delta_s$$

where f_m and f_s are the equilibrium molar fractions of the drug at temperature T in the monomer (m) and the stacked aggregate (s) state, respectively. As shown earlier for different aromatic drugs [26], δ_m and δ_s do not vary with temperature in the temperature range studied. The change in chemical shift with temperature (Figs. 3.6–3.7) results from changes in the mole fractions, f_m and f_s , which are simply related to the equilibrium association constant K at a given temperature. It may be noted that the equilibrium shifts towards the monomer formation (destacking) with the temperature and hence the total $\Delta\delta = \delta_{353K} - \delta_{278K} = \delta_s - \delta_m$ is comparable to $\Delta\delta$ with decrease in concentration except that for the 11NH proton (Table 3.4a–d).

3.2.2 ABSORPTION AND FLUROESCENCE STUDIES

We have also observed the absorption (Fig. 3.10) and emission spectra (Fig. 3.11) of mitoxantrone at different concentrations to study self–association. The absorption spectra show the presence of four distinct peaks at λ_{max} values of 240, 274, 609 and 660 nm. The molar absorption at 660 nm is found to decrease with concentration suggesting self–association at higher concentration [57, 69] and the isobestic point is observed at 682 nm*. The emission spectra shows that even though concentration is increased 100 fold, the emission intensity at 685 nm ($\lambda_{exc} = 610$ nm) increases only by a factor of ten. At higher concentrations, the increasing

* From literature

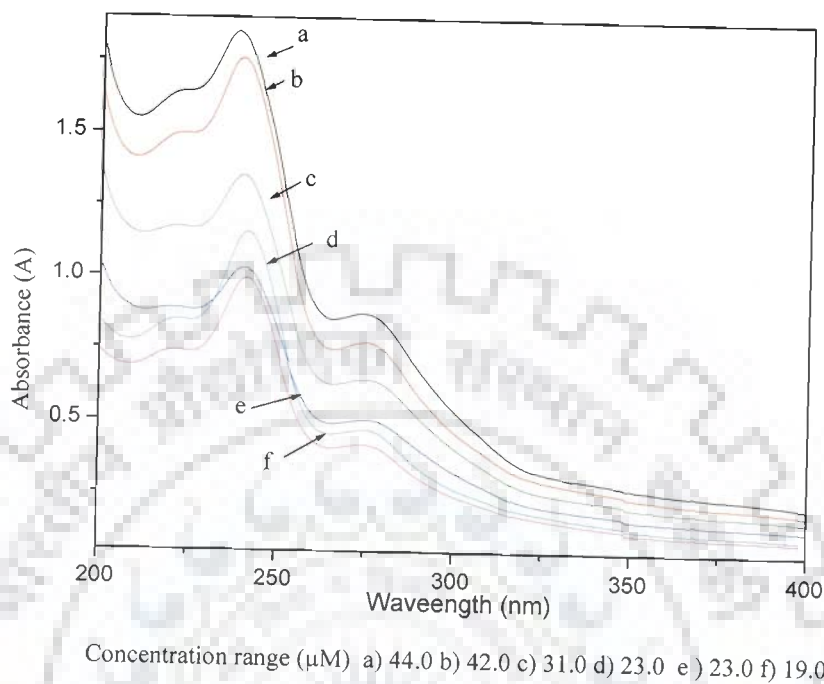


Fig. 3.10a

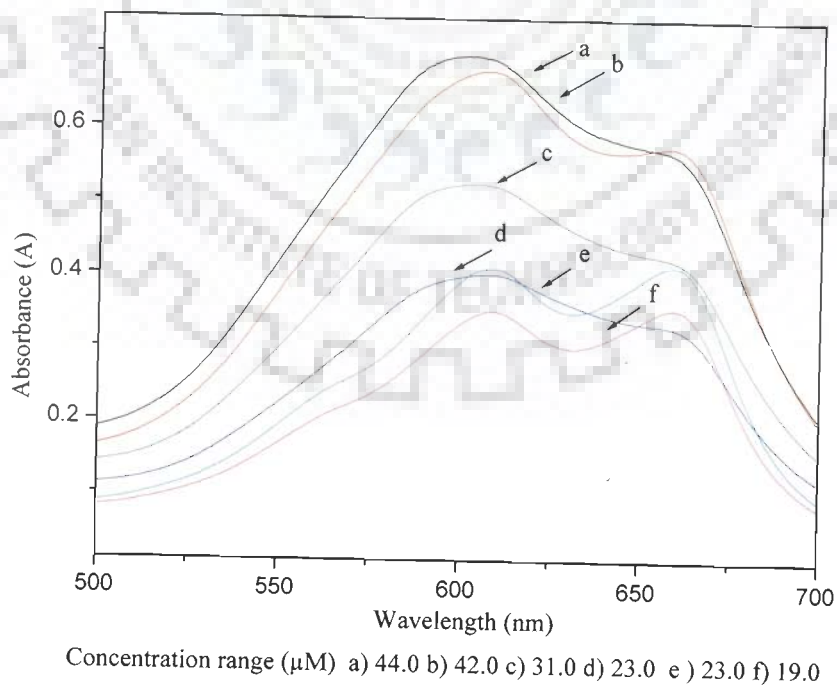


Fig. 310b

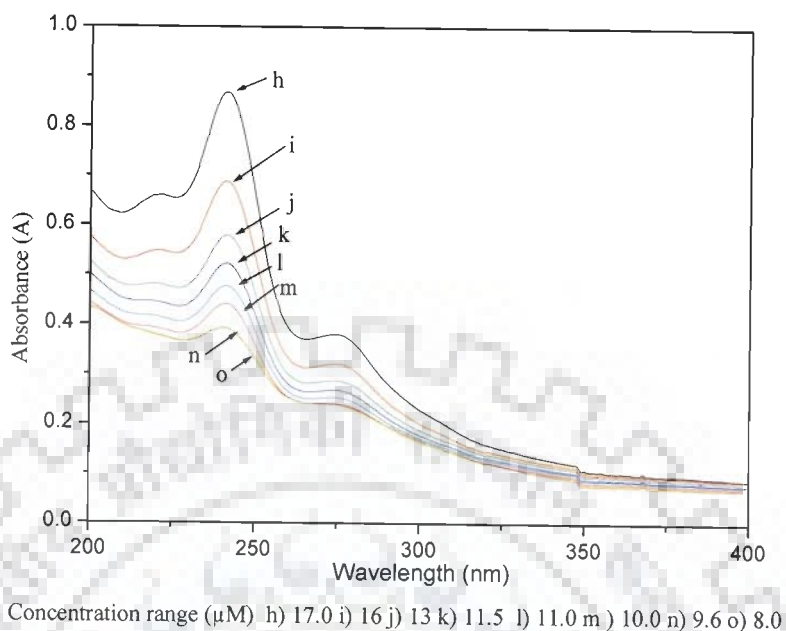


Fig. 3.10c

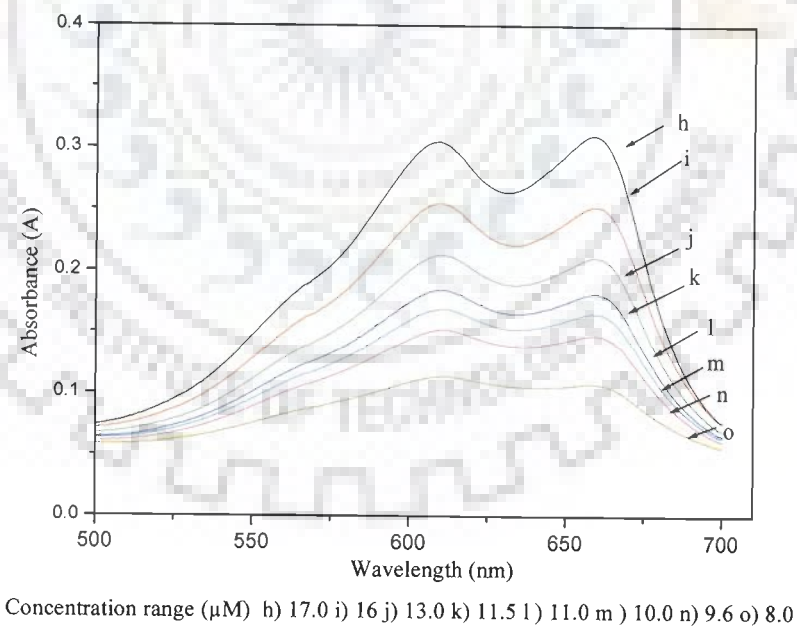
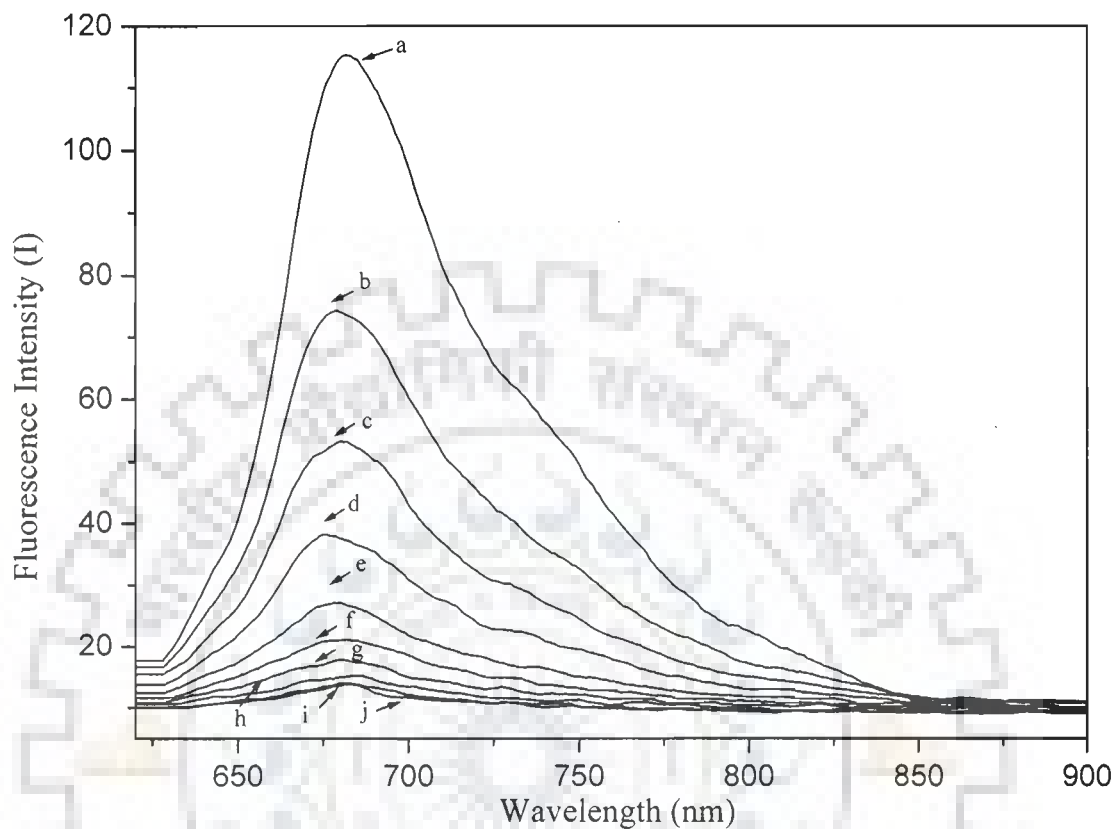


Fig. 3.10d

Fig. 3.10(a-d) Absorption Spectra of the mitoxantrone solution in water as a function of concentration at 298 K.



Concentration Range (μM) a) 12.72 b) 6.66 c) 3.71 d) 2.09 e) 1.18 f) 0.707 g) 0.412 h) 0.216 i) 0.12 h) 0.09

Fig. 3.11 Emission spectra of mitoxantrone solution in water as a function of concentration at 298 K. The excitation wavelength is 610 nm.

fractions of drug are present as aggregates. Since the fluorescent intensity is a direct measure of the concentration of the monomer, the relative fluorescence (per mole) decreases with concentration [69].

It has been observed that the [13, 69] 660 nm peak is due to the charge transfer from 5, 8 amino substituent group, the 11NH, lone pair transfer to aromatic ring itself, modified by 1OH / 4OH, which alters with solvent. The peak at 660 nm shows red shift on changing the solvent from polar to non-polar one, presumably due to the stabilization of ground state by hydrogen bonding with polar solvent. Similar is the case with 685 nm emission band [69]. Our results show that 660 nm absorption band and fluorescence emission are affected severely by increase in concentration and hence self-association; therefore suggesting that 11NH and 1OH / 4OH groups are involved in structure of dimer formation.

3.3.3 MOLECULAR MODELLING STUDIES

We have attempted to make a molecular model of the self-associated molecule using experimental results. The mutual orientation of two chromophores of drug in the dimer is roughly dictated by the $\Delta\delta$ values (Table 3.4) and their theoretical values from quantum mechanical calculations of iso-shielding curves for aromatic molecules [41]. The stacked structure is based on anti-parallel orientation of the planes of chromophores with a separation of 0.34 nm to be consistent with the 2D ROESY data. The NMR distance restraints are used and energy minimization followed (Table 3.5) by restrained molecular dynamics is carried out. The structure (Fig. 3.12) shows that there is significant overlap of the aromatic rings and the side arms containing alkyl chains are well separated. The observed distances in the model are shown in Table 3.5. The large extent of overlapping of aromatic chromophore is consistent with observed upfield shifts in 6H / 7H, 2H / 3H and 11NH protons upto 0.35 ppm due to magnetic

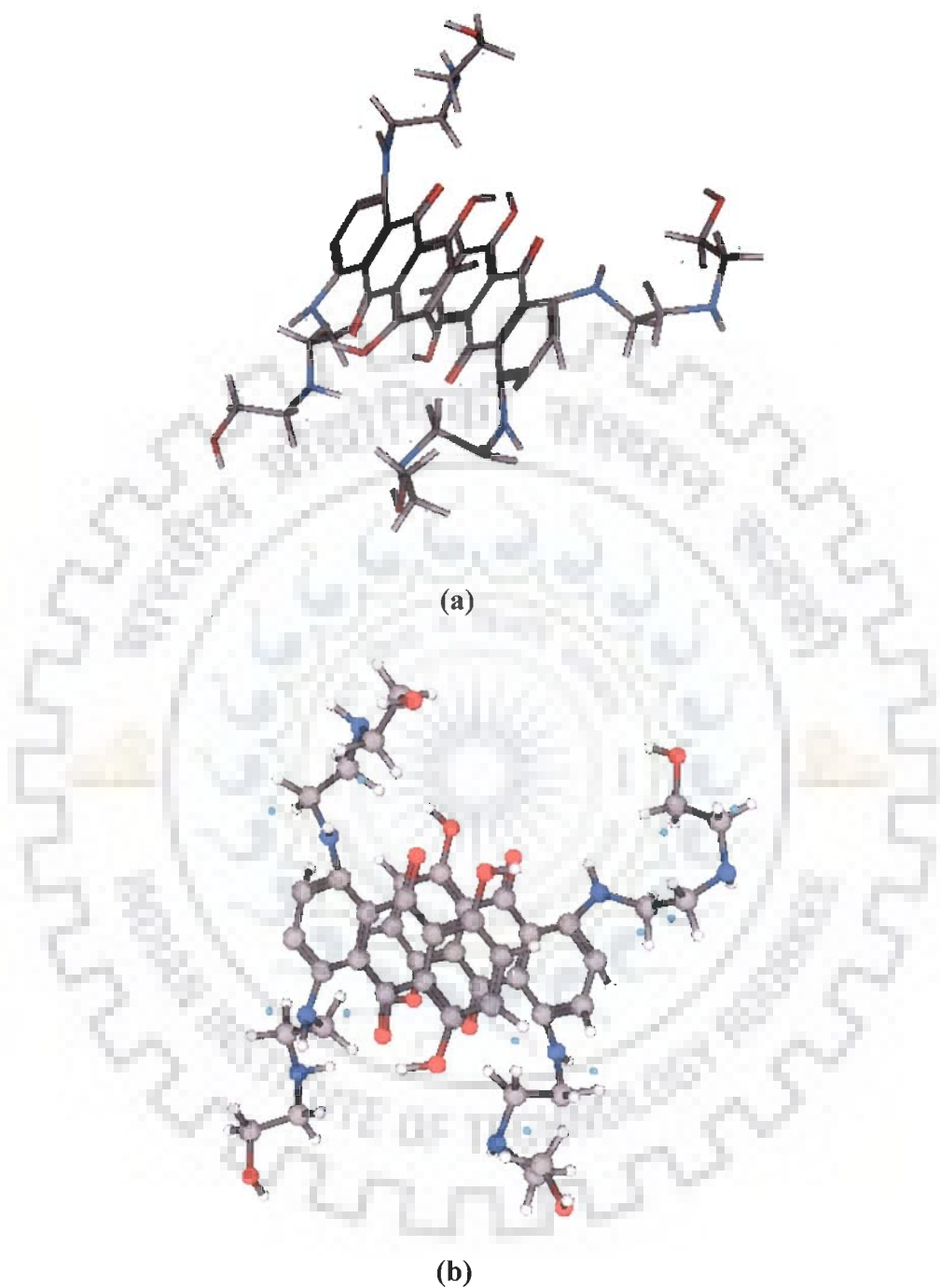


Fig. 3.12 Structure of self associated dimer of mitoxantrone based on restrained molecular dynamics simulations using experimental distance restraints from ROESY spectra (a) side view (b) view, looking perpendicular to the plane of chromophore.

Table 3.5: Comparisons of the interproton distances (Å) obtained from NMR data with that observed in model of dimer obtained by restrained molecular dynamics simulations.

S. No.		Experimental Distances (Å)	Distances in model of dimer (Å)			
			M _I -Chain _I	M _I -Chain _{II}	M _{II} -Chain _I	M _{II} -Chain _{II}
	Intramolecular Connectivities					
1.	13CH ₂ -14CH ₂	2.40	2.46	2.47	3.27	2.48
2.	11CH ₂ -12CH ₂	2.83	2.61	2.55	2.68	2.39
3.	12CH ₂ -14CH ₂	3.04	3.10	3.25	3.18	3.18
4.	11CH ₂ -13CH ₂	3.08	3.43	3.22	4.65	2.92
5.	12CH ₂ -13CH ₂	2.90-3.60	3.28	2.72	4.61	3.76
6.	11CH ₂ -6H / 7H	2.15	2.51	2.31	2.45	1.22
7.	12CH ₂ -6H / 7H	2.55	2.41	2.92	2.72	2.32
8.	11NH-11CH ₂	2.69	2.43	2.59	2.53	3.00
9.	11NH-12CH ₂	3.32	3.45	3.24	3.31	2.96
10.	11NH-6H / 7H	3.6-4.7	3.46	3.50	3.64	3.61
	Intermolecular Connectivities		M _I Chain _I - M _{II}	M _I Chain _{II} - M _{II}	M _{II} Chain _I - M _I	M _{II} Chain _{II} - M _I
11.	11CH ₂ - 2H / 3H	3.38	3.21	4.62	6.20	3.68
12.	12CH ₂ - 2H / 3H	3.64	3.80	3.44	4.80	3.34
13.	13CH ₂ - 2H / 3H	5.43	5.48	5.50	7.65	3.09
14.	14CH ₂ - 2H / 3H		6.20	6.40	6.46	5.94
15.	11NH- 2H / 3H	5.5 - 6.1	5.44	5.42	5.46	6.00
16.	6H / 7H- 2H / 3H	4.70	4.55		4.57	

shielding arising from ring currents of π electrons. A separation of 0.62 nm proposed by Lee and Dutta [69] is unlikely to exist. It is also noted that the alkyl chains tend to be well separated but their orientation is somewhat different from the corresponding structure obtained by Davies et al [26]. In the monomeric state, the hydrogens of the 1OH of ring A and 11NH of ring C close to 8 carbon atom point towards the 9CO of ring B forming two intramolecular hydrogen bonds; the distances being 1OH–9CO–11N = 4.23 Å, 4OH–10CO–11N = 4.08 Å, 1OH–9CO–11N = 5.75 Å, 4OH–10CO–11N = 4.23 Å. In the dimeric state, with two molecules (M_I and M_{II}) stacked with head to tail or anti-parallel arrangement of ABC rings, 11NH close to 8C atoms of one molecule M_I is close to 1OH of other molecule M_{II} . Similarly, the 11NH close to the 5C atom of one molecule M_I is close to 4OH of other molecule M_{II} . The observed distances are 1OH (M_I)–CO (M_I)–11N(M_{II}) = 4.22 Å; 4OH (M_I)–9CO(M_I)–11N(M_{II}) = 3.87 Å; 1OH(M_{II})–9CO (M_{II})–11N(M_I)= 4.65 Å; and 1OH(M_{II})–9CO(M_{II})–11N(M_I) = 4.28 Å. These short distances between 11NH and 1OH / 4OH suggest the possibility of intermolecular hydrogen bonded network. Lack of this kind of intermolecular hydrogen bonding due to substitution of 1OH / 4OH groups by H atoms in pharmacologically less active ametantrone molecule may be responsible for significantly lower dimerization constant [57] in ametantrone. Further, on heating from 278 K to 353 K, 11NH protons shifts downfield by 0.06 ppm (Table 3.4b) due to unstacking of aromatic rings whereas the downfield shift due to unstacking on decreasing concentration from 1.8mM to 10 μ M (Table 3.4c) is 0.29 ppm. This may largely be due to the fact that both intramolecular and intermolecular H₂ bonds are broken on increase of temperature to 353 K and 11NH becomes broad leads to upfield shift in 11NH which is being compensated by downfield shift on unstacking consequently, the observed $\Delta\delta \sim 0.06$ ppm with temperature. On the other hand unstacking due to transition from self associated to monomeric form on decreasing the

concentration leaves intramolecular H₂ bonds (1OH–9CO–11NH at 8C atom and 4OH–10CO–11NH at 5C atom) intact and hence shows $\Delta\delta \sim 0.29$ ppm. This indirectly proves that intermolecular hydrogen bonds exist in aggregate form. This is also consistent with absorption and fluorescence spectroscopy data which implicate 11NH protons in self association.

Thus we conclude that mitoxantrone is self-associated at high concentration. There is considerable overlapping of aromatic rings placed in anti-parallel orientation, which is, stabilized by stacking interactions. This accounts for large upfield shifts in 6H / 7H, 2H / 3H, 11NH protons with increased concentration and decrease in temperature. A decrease in molar concentration of 660 nm absorption band and 685 nm emission bands indicate involvement of 1OH / 4OH and 11NH in self association which is supported by six direct short contacts involving ring protons 6H / 7H, 2H / 3H and 11NH protons.

Chapter 4

Study of Mitoxantrone in DMSO-d₆ by NMR and Absorption Spectroscopy

4.1 INTRODUCTION

In this chapter, results on complete assignment of mitoxantrone drug and self – association in DMSO-d₆ are reported. The 1D NMR, DQF COSY, HSQC (¹H – ¹³ C), HMBC (¹H – ¹³ C) and ROESY spectra have been used to get assignment of all protons (11NH, 1OH / 4OH, 14OH, 6H / 7H, 2H / 3H, 11CH₂, 12CH₂, 13CH₂ and carbon resonances and spin–spin coupling constants. In DMSO-d₆ solvent 12NH, 1OH / 4OH and 14OH proton resonances, which were not observed in spectra taken in water, are also observed. 1D proton NMR as a function of concentration and temperature and absorption spectra as a function of concentration are reported. Inter proton distance constraints obtained from ROESY spectra are used to get structure of self associated mitoxantrone in DMSO-d₆ solvent.

4.2 RESULTS AND DISCUSSIONS

4.2.1 NMR ASSIGNMENTS

The one–dimensional proton NMR spectra of mitoxantrone and DQF COSY spectra in DMSO-d₆ are shown in Figs. 4.1 and 4.2 respectively. The two singlets resonating at 7.68 and 7.22 ppm are assigned due to 6H / 7H and 2H / 3H, respectively. Four triplets resonating in 3.0–4.0 ppm respectively, are attributed to four sets of methylene protons. Among the spin–spin coupled pairs of methylene protons 13CH₂–14CH₂ and 11CH₂–12CH₂ (Fig. 4.2), the 11CH₂ protons is shifted downfield with respect to 14CH₂ proton contrary to the results observed in H₂O solvent (data in Chapter3). Hence all methylene protons are assigned accordingly. The downfield shift of the 11CH₂ with respect to 14CH₂ is explained in terms of solvent effect described later. The imino proton coupled to 11CH₂ protons is assigned to 11NH (Fig. 4.2). Some extra

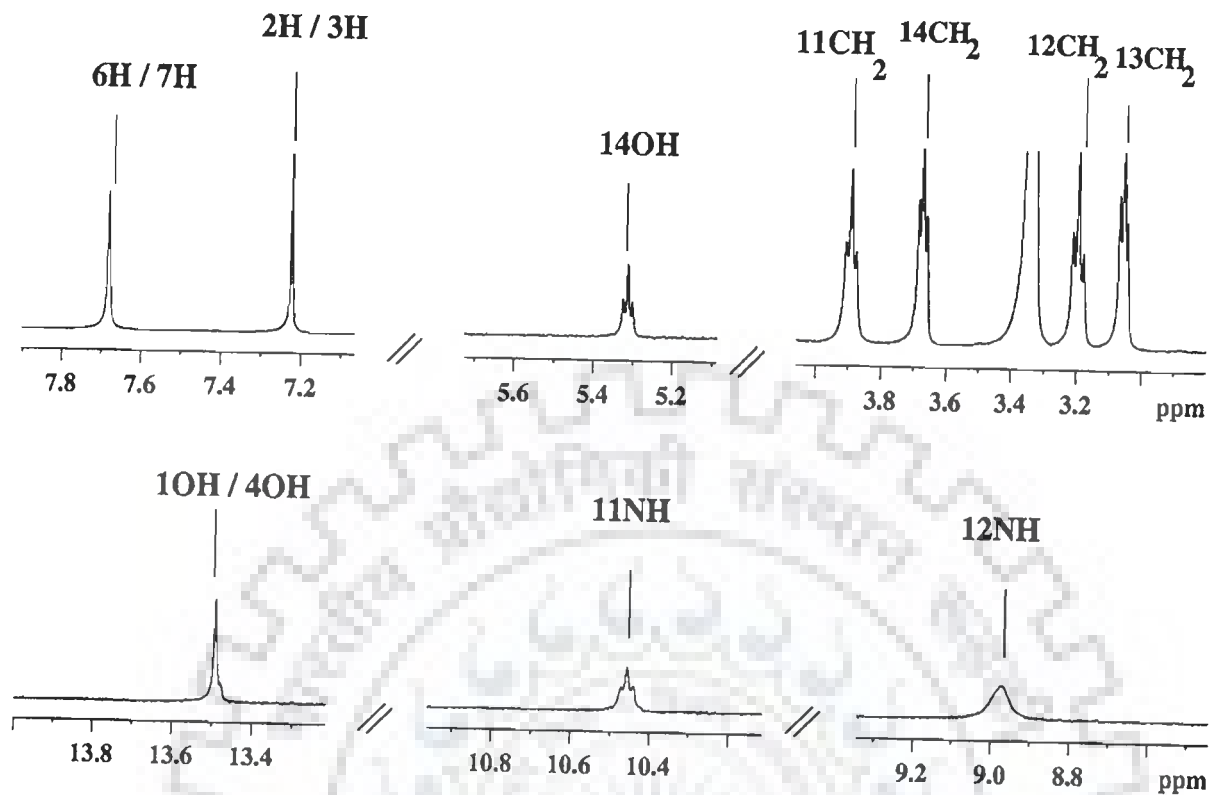


Fig. 4.1 1D NMR spectra of 10 mM mitoxantrone in DMSO- d_6 at 298 K at 400 MHz

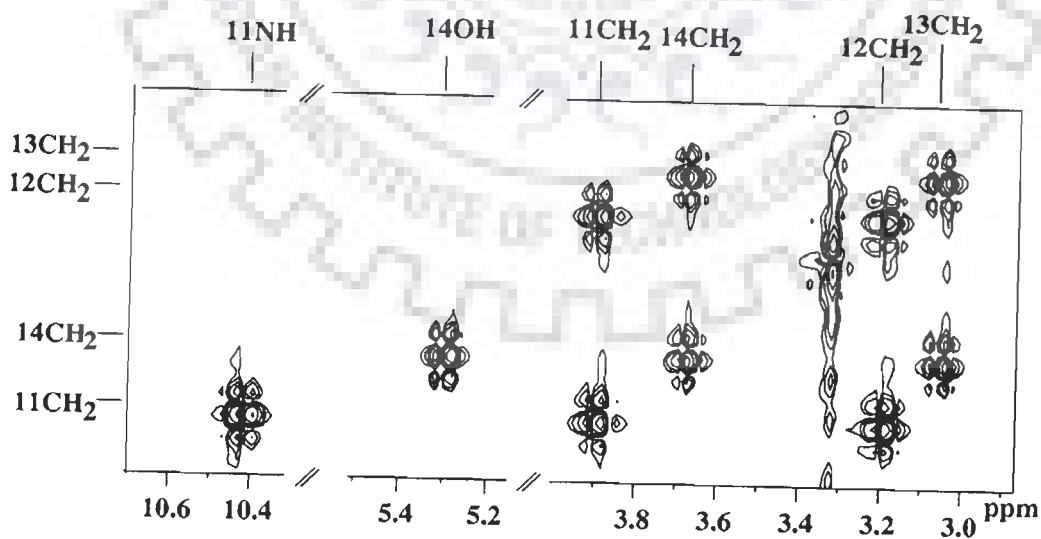


Fig. 4.2 DQF COSY spectra of 10mM mitoxantrone in DMSO- d_6 at 298 K.

resonances for mitoxantrone in DMSO-d₆ have also been observed which were earlier not observed for in the H₂O solvent (Chapter 3). The triplet resonating at 5.31 ppm coupled to 14CH₂ proton is assigned to 14OH (Fig. 4.2). In the homonuclear 2D Total Correlation Spectroscopy (TOCSY) it also shows relay peaks with 13CH₂ protons which further confirms its position (Fig. 4.3). TOCSY spectra also shows that broad resonances at 8.97 ppm gives relay peaks with 11CH₂, 12CH₂, 13CH₂ and 14CH₂ and hence is assigned to 12NH protons. A multiplet resonating at 13.49 ppm has been assigned to 1 OH / 4OH being the maximum downfield shifted protons. In the ¹H -¹³C hetero single quantum coherence (HSQC) spectra (Fig.4.4) the four carbon resonances in the aliphatic region 40–60 ppm are assigned to 11C, 12C, 13C and 14C being directly coupled to their respective protons, that is, 11CH₂, 12CH₂, 13CH₂ and 14CH₂ appreciably similar chemical shift has been observed for the carbon resonances mitoxantrone in DMSO-d₆ solvent as observed for the H₂O solvent (Chapter 3). The other carbons have been on basis of hetero multiple bond correlation (HMBC) spectra (Fig. 4.5).

The assignment of 11C, 12C, 13C, 14C, 9C / 10C and 5C / 8C is essentially the same that has been observed for water solvent. The coupling of 1OH / 4OH with 1'C / 4'C, 2C / 3C and 1C / 4C (110–160 ppm) have been observed in the HMBC spectra (Fig.4.5b) which further confirms its assignment. The cross peak of 11NH with carbon resonance at around 126 ppm splits the proton resonance at 7.22 ppm (similar to water solvent) established the protons resonance at 7.22 ppm 6H / 7H. The other singlet gets assigned to 2H / 3H which shows cross peak with 1'C / 4'C, 1C / 4 C and 2C / 3C (Fig. 4.5b–c). The unambiguous assignments for both ¹H and ¹³C resonances are made on the basis of ¹H DQF COSY, ¹H-¹³C HSQC and HMBC spectra is given in Table 4.1. The spin-spin coupling protons are shown in Table 4.2. The 2D

Table 4.1 Proton and carbon assignment of 10 mM mitoxantrone in DMSO-d₆ at 298 K.

Protons	Chemical shift (δ)	Carbon	Chemical shift (δ)
2H / 3H	7.22	1C / 4C	155.31
6H / 7H	7.68	2C / 3C	130.37
14 CH ₂	3.67	5C / 8C	1496.85
11CH ₂	3.89	6C / 7C	125.63
12 CH ₂	3.20	9C / 10C	184.98
13CH ₂	3.06	11C	38.80
11NH	10.46	12C	46.32
12NH	8.97	13C	49.50
14OH	5.31	14C	56.63
1OH / 4OH	13.49	5'C / 8'C	109.01
		1'C / 4'C	115.09

Table 4.2 Observed average values of spin-spin coupling constant, J (Hz).

Connectivity	J (Hz)
11CH ₂ -12 CH ₂	6.4
13CH ₂ -14 CH ₂	3.84
11NH-11CH ₂	4.60
12NH-12CH ₂	12 NH broad
12NH-13CH ₂	12 NH broad
14 CH ₂ - 14OH	7.00

Table 4.3 Relative intensities of cross peaks and interproton distances (Å) from ROESY spectra of 10 mM mitoxantrone in DMSO-d₆ recorded at 300 ms at 298 K.

	Connectivity	Intensity	Distances (Å)
1.	13CH ₂ – 14 CH ₂ ^{ref}	1.3	2.4
2.	11CH ₂ – 12CH ₂	0.72	2.65
3.	12CH ₂ – 14CH ₂	0.18	3.34
4.	11CH ₂ – 13CH ₂	0.20	3.28
5.	12CH ₂ – 3CH ₂	0.52	2.79
6.	11CH ₂ – 14CH ₂	0.051	4.11
7.	11CH ₂ – 6H / 7H	1.8	2.27
8.	12CH ₂ – 6H / 7H	0.67	2.60
9.	13CH ₂ – 6H / 7H	0.024	4.66
10.	14CH ₂ – 6H / 7H	0.013	5.17
11.	11CH ₂ – 2H / 3H*	0.005	6.06
12.	12CH ₂ – 2H / 3H*	0.003	6.6
13.	13CH ₂ – 2H / 3H*	0.003	6.9
14.	11NH – 11CH ₂	0.23	3.20
15.	11NH – 12CH ₂	0.16	3.40
16.	11NH – 13 CH ₂	0.01	5.40
17.	11NH – 6H / 7H	0.043	4.23
18.	11NH – 2H / 3H	0.009	5.68
19.	12NH – 11CH ₂	0.008	5.60
20.	12NH – 12CH ₂	0.015	5.30
21.	12NH – 13CH ₂	0.28	3.13
22.	12NH – 14CH ₂	0.004	6.67
23.	12NH – 6H / 7H	0.01	5.40
24.	12NH – 2H / 3H*	0.004	6.0 – 7.0
25.	14OH – 12CH ₂	(o)	–
26.	14OH – 13CH ₂	(o)	–
27.	14OH – 14CH ₂	0.016	5.38
28.	1OH / 4OH – 11CH ₂ *	0.016	5.38
29.	1OH / 4OH – 12CH ₂ *	(o)	–
30.	1OH / 4OH – 13CH ₂ *	0.054	4.07
31.	1OH / 4OH – 14CH ₂ *	0.013	5.17
32.	1OH / 4OH – 11NH*	0.01	5.37
33.	1OH / 4OH – 12NH*	0.01	3.30
34.	1OH / 4OH – 2H / 3H	0.19	4.49
35.	1OH / 4OH – 6H / 7H*	0.03	4.23
36.	6H / 7H – 2H / 3H	0.015	4.73

^{ref} Reference for distance calculations

* Intermolecular peaks

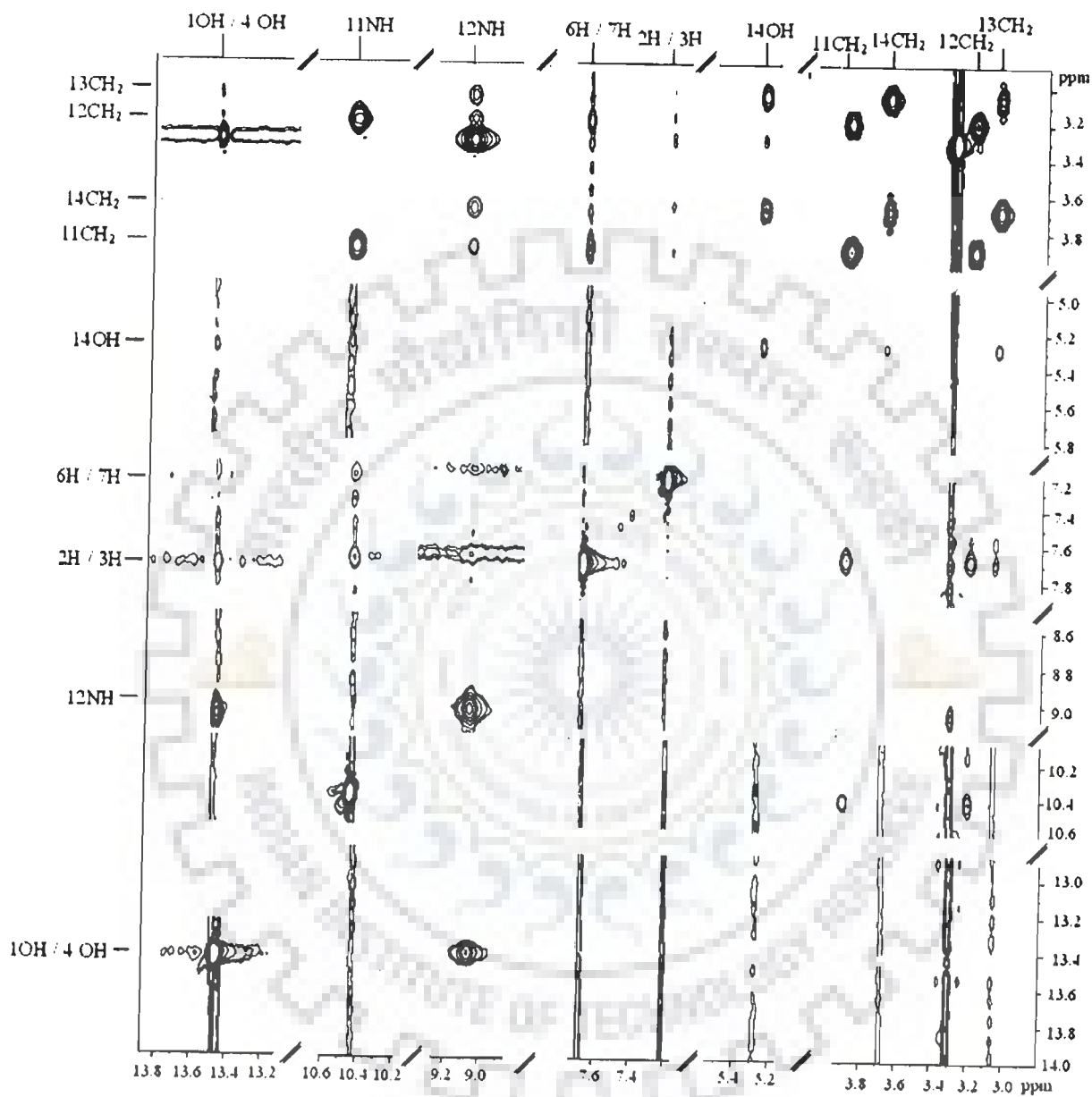


Fig. 4.3 TOCSY spectra of 10 mM mitoxantrone in DMSO-d₆ at 298 K.

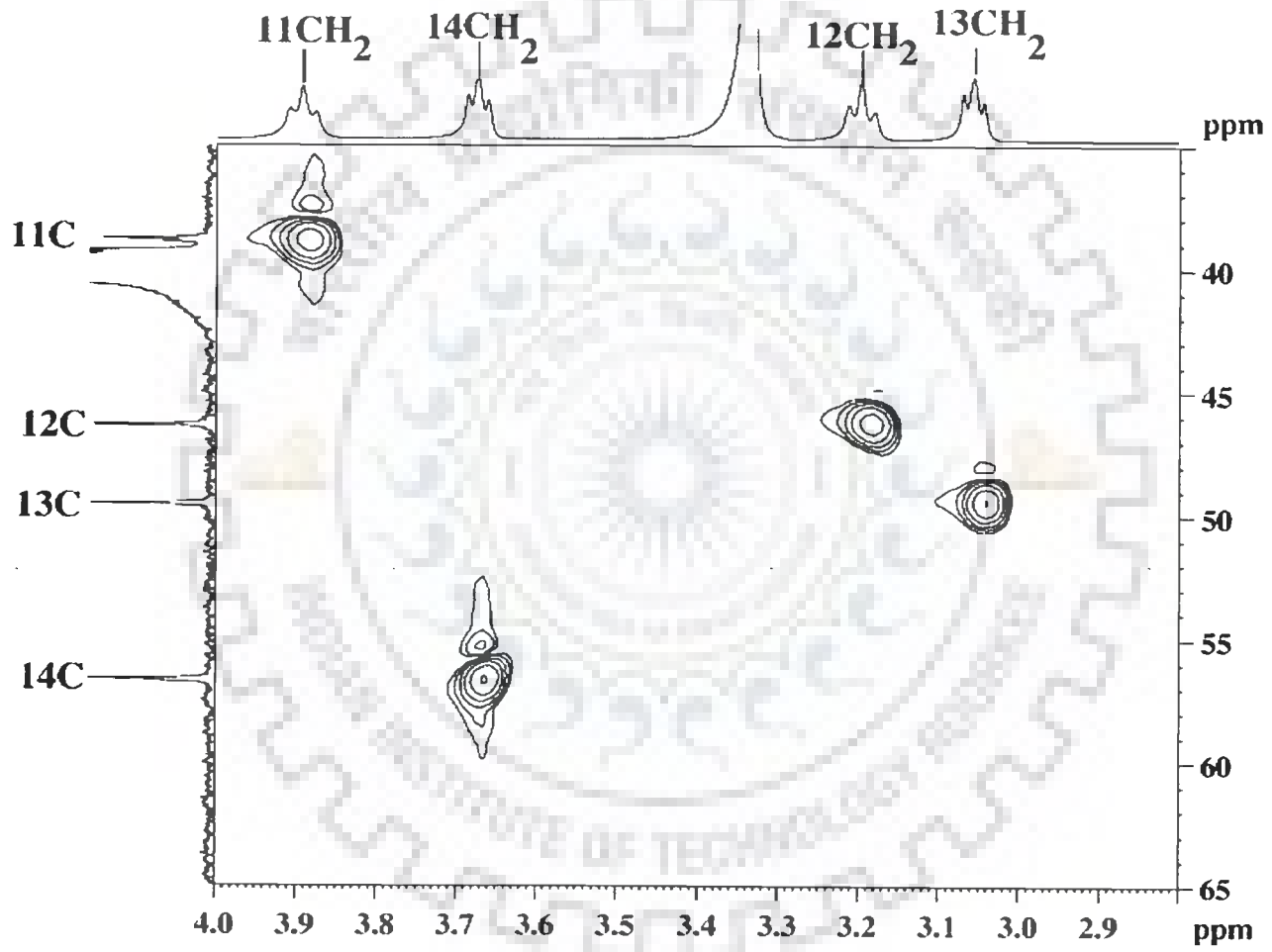


Fig.4.4(a)

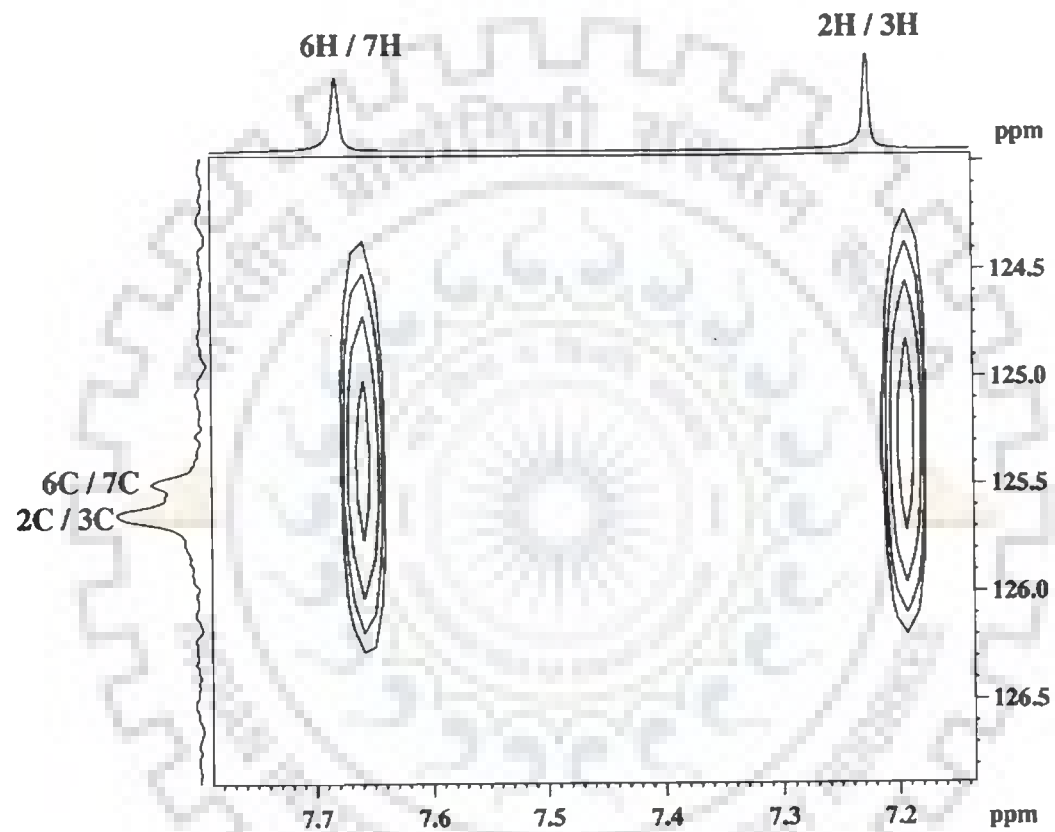


Fig.4.4(b)

Fig. 4.4(a-b) Expansion of specific regions of HSQC spectra of 10mM mitoxantrone in DMSO-d_6 at 298 K showing ^1H - ^{13}C correlations. The one dimensional ^{13}C and ^1H spectra are shown along w1 and w2 axis, respectively.

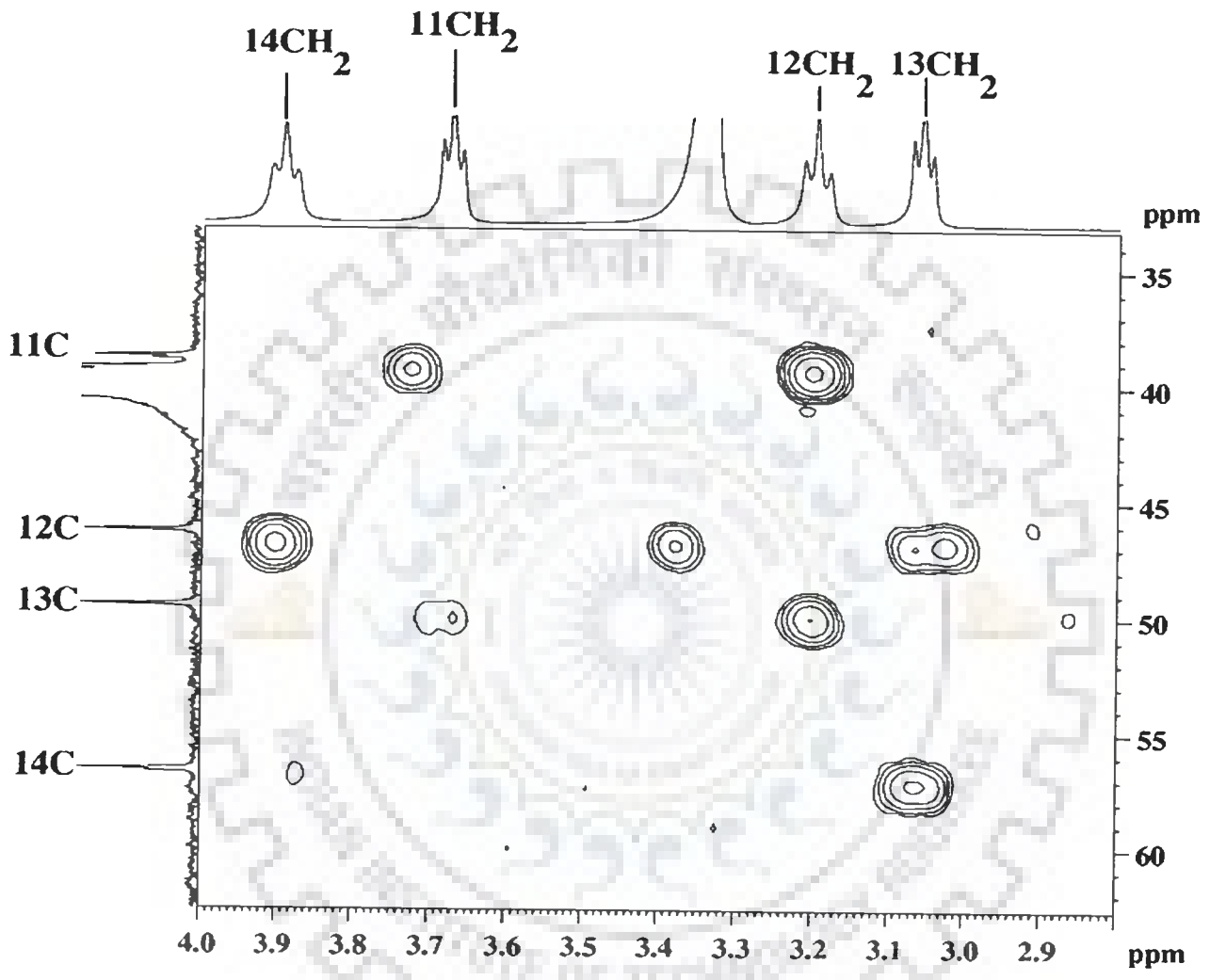


Fig. 4.5(a)

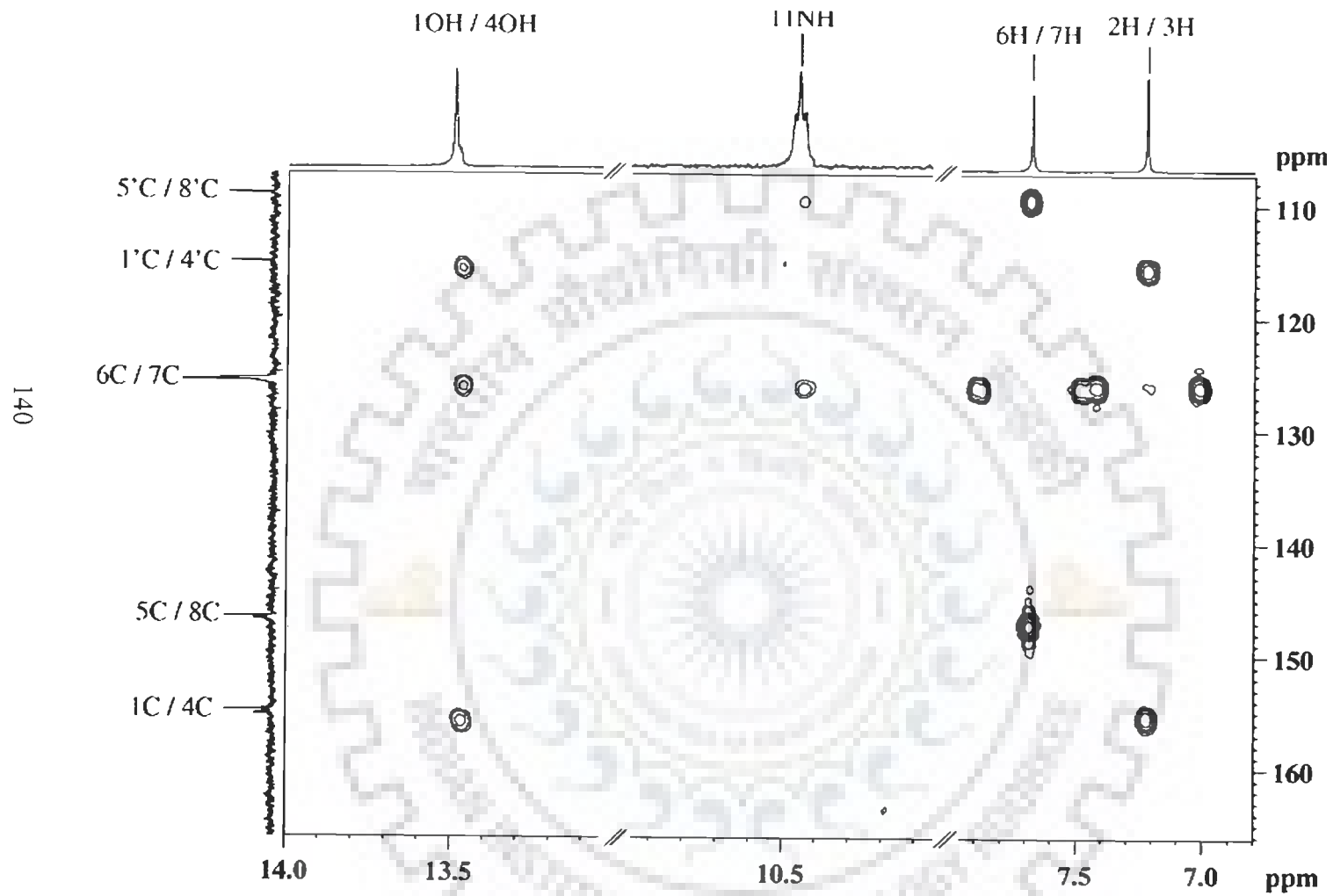


Fig. 4.5(b)

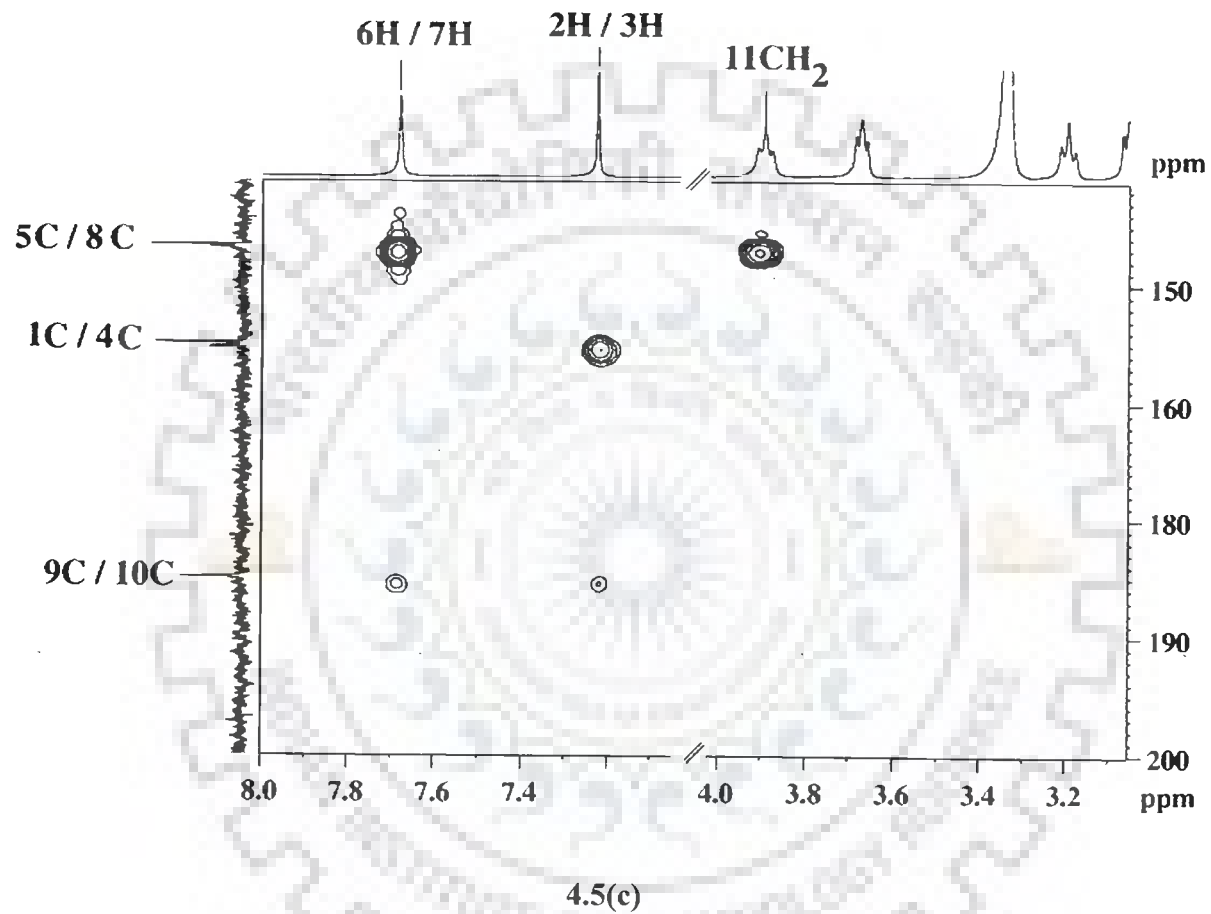


Fig. 4.5(a-c) Expansions of specific regions of HMBC spectra of 10mM mitoxantrone in DMSO-d₆ at 298K showing multiple bond ¹H-¹³C.

ROESY spectrum of mitoxantrone in DMSO- d_6 exhibits several intermolecular cross peaks (Table 4.3). The expected contacts among methylene protons with 6H / 7H (Fig. 4.6a) have been observed. Very intense cross peaks between 6H / 7H-11CH₂ and 6H / 7H-12CH₂ protons and weak contacts have been observed between 6H / 7H-13CH₂ and 6H / 7H-14CH₂ protons, that is the intensity decreases in the order of 11CH₂ > 12CH₂ > 13CH₂ > 14CH₂ similar to the observed seen in the H₂O solvent (Chapter 3) which can be attributed to the inverse-orientation (head to tail) of the antibiotic chromophore.

Other proof of stacking interaction of the chromophore ring can also be seen by the ROE contacts observed for 1OH / 4OH protons with 6H / 7H protons. Thus the presence of these intermolecular peaks confirms the inverse orientation of the stacked chromophore in DMSO- d_6 solvent.

Several exchange peaks have also been observed for the non-exchangeable protons, namely 12NH, 14OH and 1OH / 4OH protons as can be seen in the 2D TOCSY (Fig. 4.3) and 2D ROESY (Fig. 4.6) spectra. The NMR and changes in chemical shift with concentration and temperature are presented in Figs. 4.7-4.8. Table 4.6 gives comparison of the ROESY connectivities observed for self associated mitoxantrone in D₂O, H₂O and DMSO solvents.

4.2.2 ABSORPTION STUDIES

The λ_{\max} maximum in absorption spectra (Fig. 4.9) of DMSO is 687 nm (at 3 μ M) concentration as compared to that of 660 nm in water. Since the ground state is stabilized by hydrogen bonding with protic solvents the absorption peak is red shifted in comparatively less polar solvents such as DMSO. This is consistent with the results reported in literature [69]. It is observed that 682 nm shifts to 685 nm with concentration, that is, an aggregation of

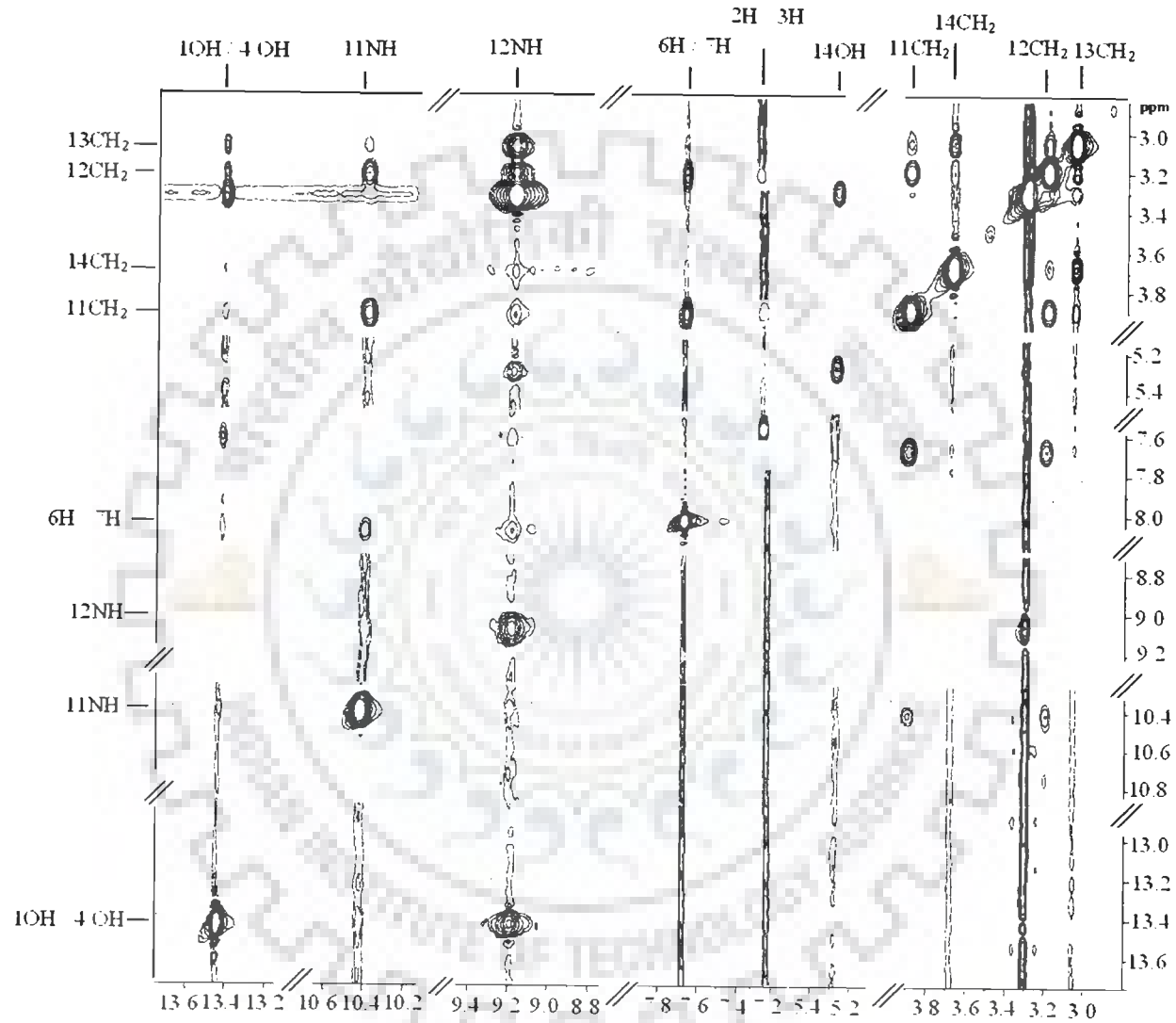


Fig. 4.6 ROESY spectra of 10 mM mitoxantrone in DMSO-d₆ at 298 K. Expansions of specific regions are shown to highlight connectivities.

Table 4.4a Chemical shift of 10 mM mitoxantrone in DMSO- d_6 as a function of temperature $\Delta\delta = \delta_{353\text{ K}} - \delta_{298\text{ K}}$ indicates change in chemical shift due to temperature

Temp (K)	1 OH / 4OH	11NH	12NH	6H / 7H	2H / 3H	11CH ₂	12 CH ₂	13CH ₂	14 CH ₂	14OH
298	13.48	10.46	8.97	7.68	7.22	3.82	3.13	3.06	3.68	5.31
303	13.48	10.48	8.99	7.67	7.24	3.88	3.16	3.09	3.70	5.32
308	13.48	10.48	8.00	7.71	7.26	3.84	3.14	3.11	3.70	5.33
313	13.51	10.51	9.04	7.74	7.28	3.86	3.05	3.13	3.75	5.33
318	13.51	10.52	9.06	7.76	7.30	3.91	3.22	3.15	3.78	5.31
323	13.53	10.52	9.08	7.77	7.32	3.94	3.24	3.17	3.81	5.30
328	13.56	10.56	9.12	7.80	7.34	3.98	3.30	3.21	3.84	5.31
333	13.56	10.57	9.12	7.82	7.36	3.99	3.30	3.21	3.84	5.32
338	13.56	10.57	9.14	7.84	7.38	3.99	3.36	3.24	3.86	broad
343	13.56	10.59	9.15	7.86	7.40	4.04	3.352	3.28	3.90	–
348	13.56	10.59	9.15	7.88	7.41	3.99	3.36	3.29	3.91	–
353	13.57	10.61	9.20	7.89	7.44	4.06	3.38	3.30	3.93	–
$\Delta\delta$	+0.09	+0.15	+0.23	+0.21	+0.22	+0.24	+0.25	+0.24	+0.25	+0.01

-ve $\Delta\delta$ indicates upfield shift

+ve $\Delta\delta$ indicates downfield shift.

Table 4.4b Chemical shift of 0.05 mM mitoxantrone in DMSO as a function of temperature $\Delta\delta = \delta_{353\text{ K}} - \delta_{298\text{ K}}$ indicates change in chemical shift due to temperature

Temp (K)	1 OH / 4OH	11NH	12NH	6H / 7H	2H / 3H	11CH ₂	12CH ₂	13CH ₂	14CH ₂	14OH
298	13.51	10.47	8.77	7.66	7.25	3.87	3.21	3.07	3.68	5.31
318	13.43	10.42	8.74	7.64	7.22	3.88	-	3.07	3.68	5.21
328	13.39	10.39	8.73	7.63	7.22	3.88	3.22	3.07	3.68	5.17
353	13.31	10.34	8.70	7.62	7.20	3.88	3.24	-	3.70	5.05
$\Delta\delta$	+0.20	-0.13	-0.07	-0.04	-0.05	-0.01	+0.03	0.00	+0.02	-0.26

Table 4.4c Chemical shift of 1 mM mitoxantrone in DMSO as a function of temperature. $\Delta\delta = \delta_{353\text{ K}} - \delta_{298\text{ K}}$ indicates change in chemical shift due to temperature

Temp (K)	1 OH / 4OH	11NH	12NH	6H / 7H	2H / 3H	11CH ₂	12 CH ₂	13CH ₂	14 CH ₂	14OH
298	13.52	10.48	8.57	7.61	7.24	3.86	-	3.07	3.66	5.32
318	13.45	10.45	8.58	7.60	7.24	3.86	3.22	3.08	3.68	5.22
328	13.42	10.43	8.56	7.60	7.23	3.87	3.22	3.08	3.68	5.16
353	13.35	10.38	8.53	7.58	7.23	3.85	3.22	3.08	3.69	5.06
$\Delta\delta$	-0.17	-0.10	-0.04	-0.03	-0.01	-0.01	0.00	+0.01	+0.03	-0.26

-ve $\Delta\delta$ indicates upfield shift

+ve $\Delta\delta$ indicates downfield shift.

Table 4.4d: Chemical shift of mitoxantrone in DMSO as a function of concentration at 298 K. $\Delta\delta = \delta_{1.00 \text{ mM}} - \delta_{0.01 \text{ mM}}$

indicates total change in chemical shift due to self association.

Conc(mM)	1 OH / 4OH	11NH	12NH	6H / 7H	2H / 3H	11CH ₂	12 CH ₂	13CH ₂	14 CH ₂	14OH
0.01	13.53	10.51	8.56	7.61	7.23	3.85	-	-	3.65	-
0.02	13.52	10.48	8.57	7.61	7.24	3.85	-	3.07	3.66	5.32
0.05	13.52	10.48	8.59	7.62	7.24	3.86	-	3.08	3.66	5.32
0.1	13.51	10.48	8.61	7.62	7.24	3.87	3.22	3.07	3.67	5.31
0.2	13.51	10.48	8.64	7.63	7.24	3.87	3.22	3.07	3.67	5.31
0.4	13.51	10.47	8.69	7.64	7.24	3.88	3.22	3.07	3.68	5.31
0.8	13.51	10.47	8.73	7.64	7.25	3.88	3.22	3.07	3.68	5.31
1.0	13.51	10.47	8.77	7.66	7.25	3.87	3.21	3.07	3.68	5.31
$\Delta\delta$	-0.02	-0.04	+0.21	+0.05	+0.02	+0.02	-0.01	0.00	+0.03	-0.01

-ve $\Delta\delta$ indicates upfield shift

+ve $\Delta\delta$ indicates downfield shift.

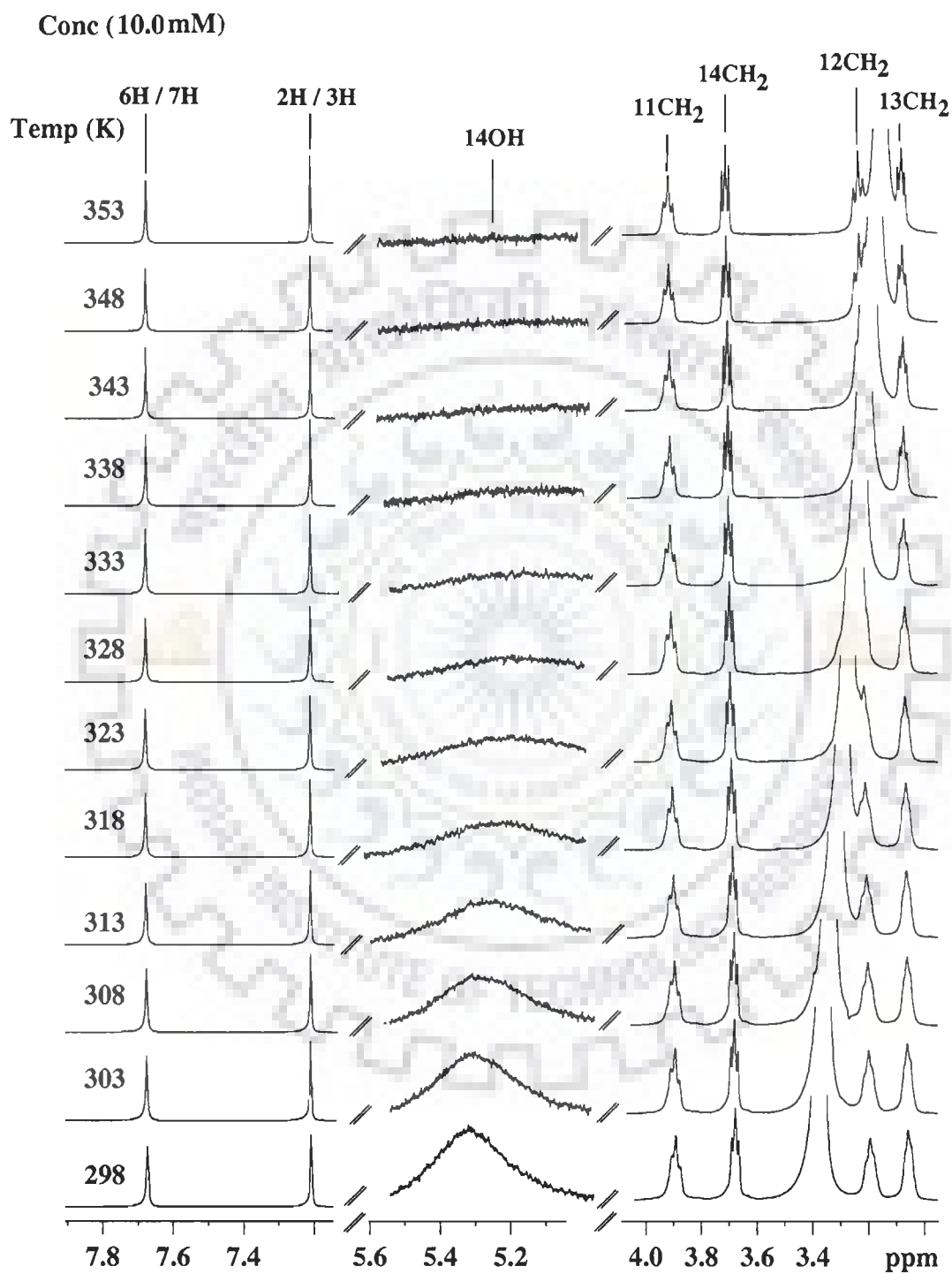


Fig. 4.7a(i)

Conc (10.0mM)

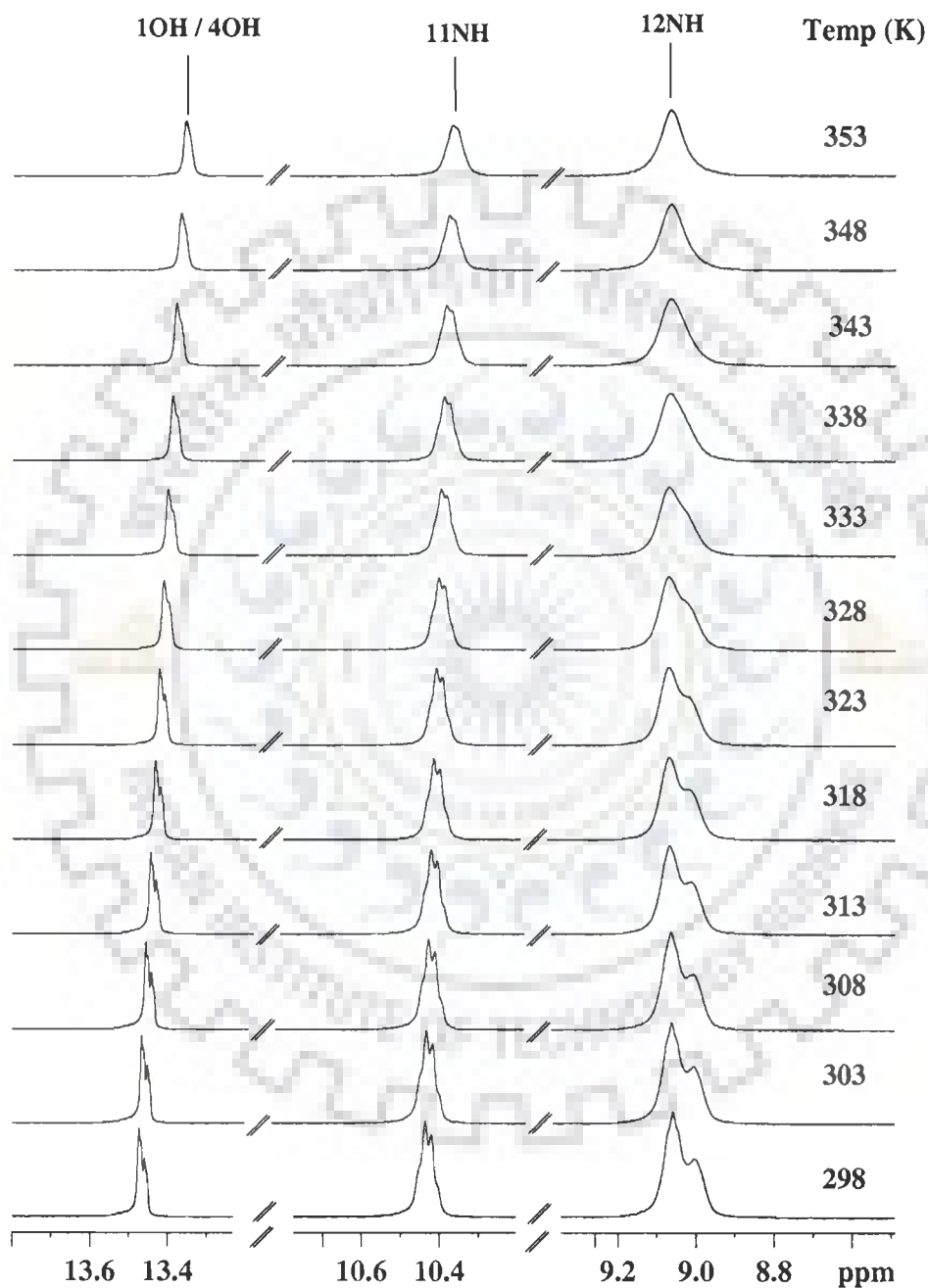


Fig. 4.7a(ii)

Fig. 4.7a One dimensional spectra of 10 mM mitoxantrone in DMSO-d₆ as a function of temperature i) 3-8 ppm ii) 8-14 ppm

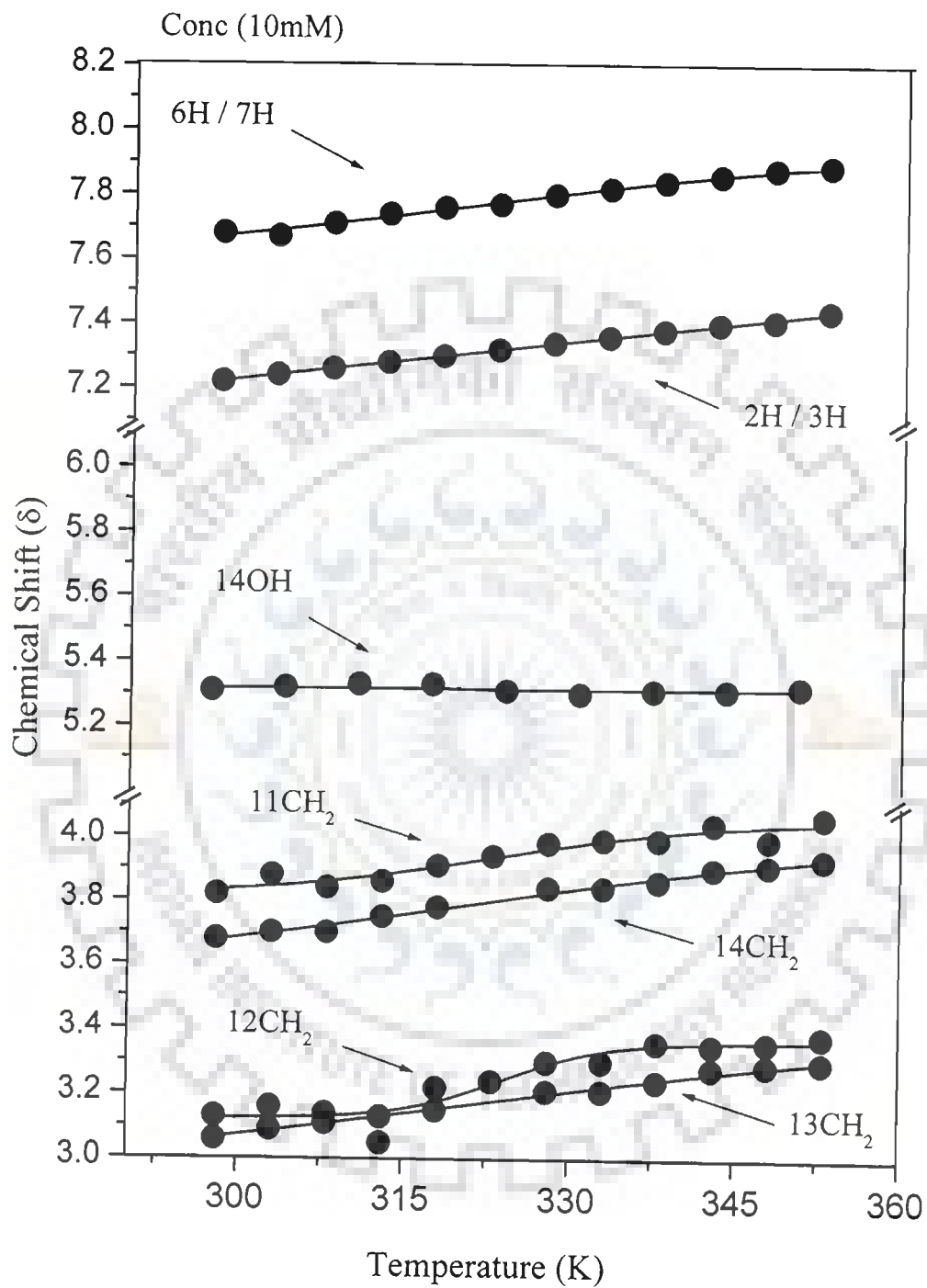


Fig. 4.7b(i)

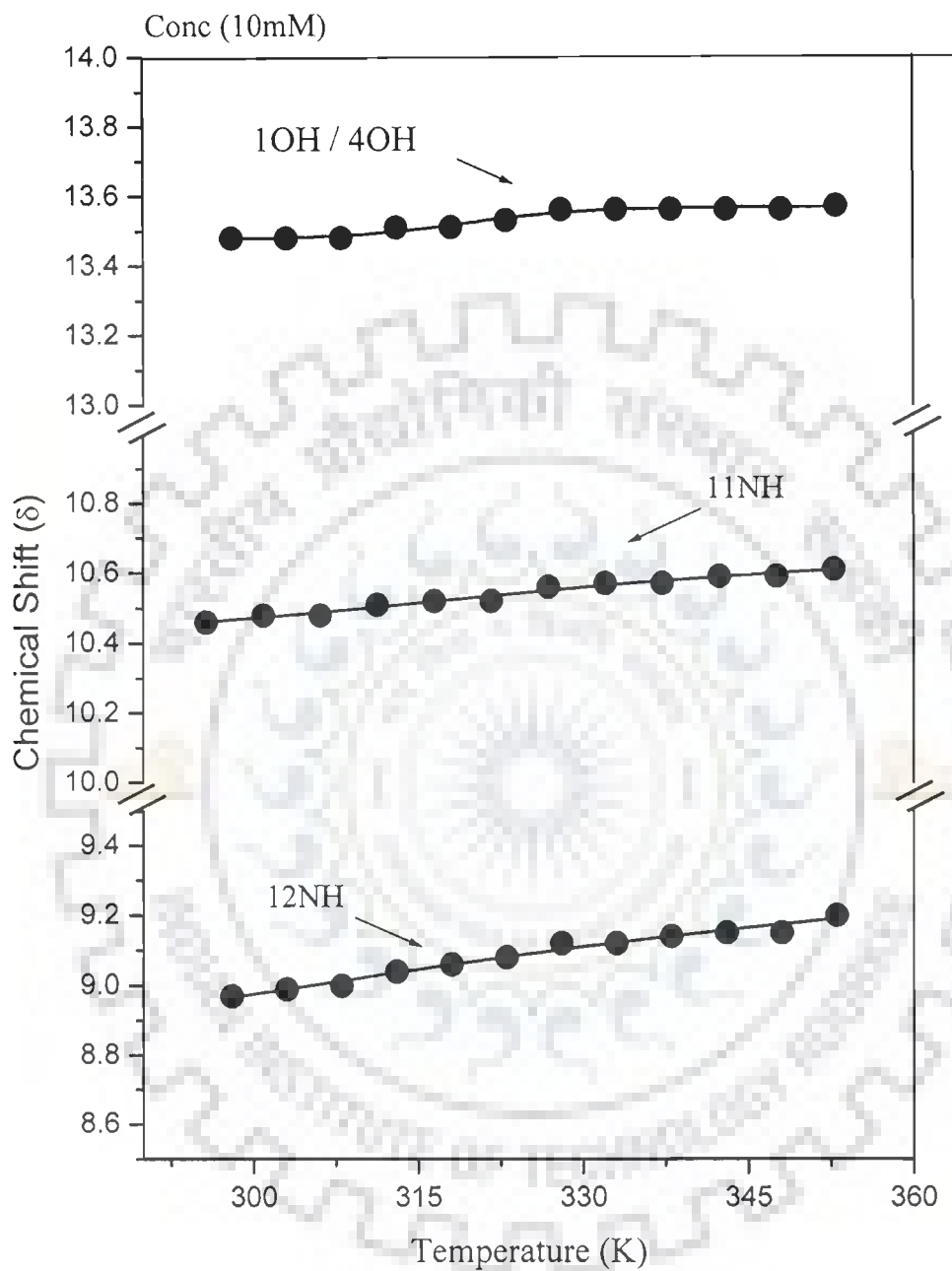


Fig. 4.7b(ii)

Fig. 4.7b Chemical shift of 10 mM mitoxantrone in DMSO- d_6 as a function of temperature in the range 298K -353K. i) 3-8ppm ii) 8-14 ppm

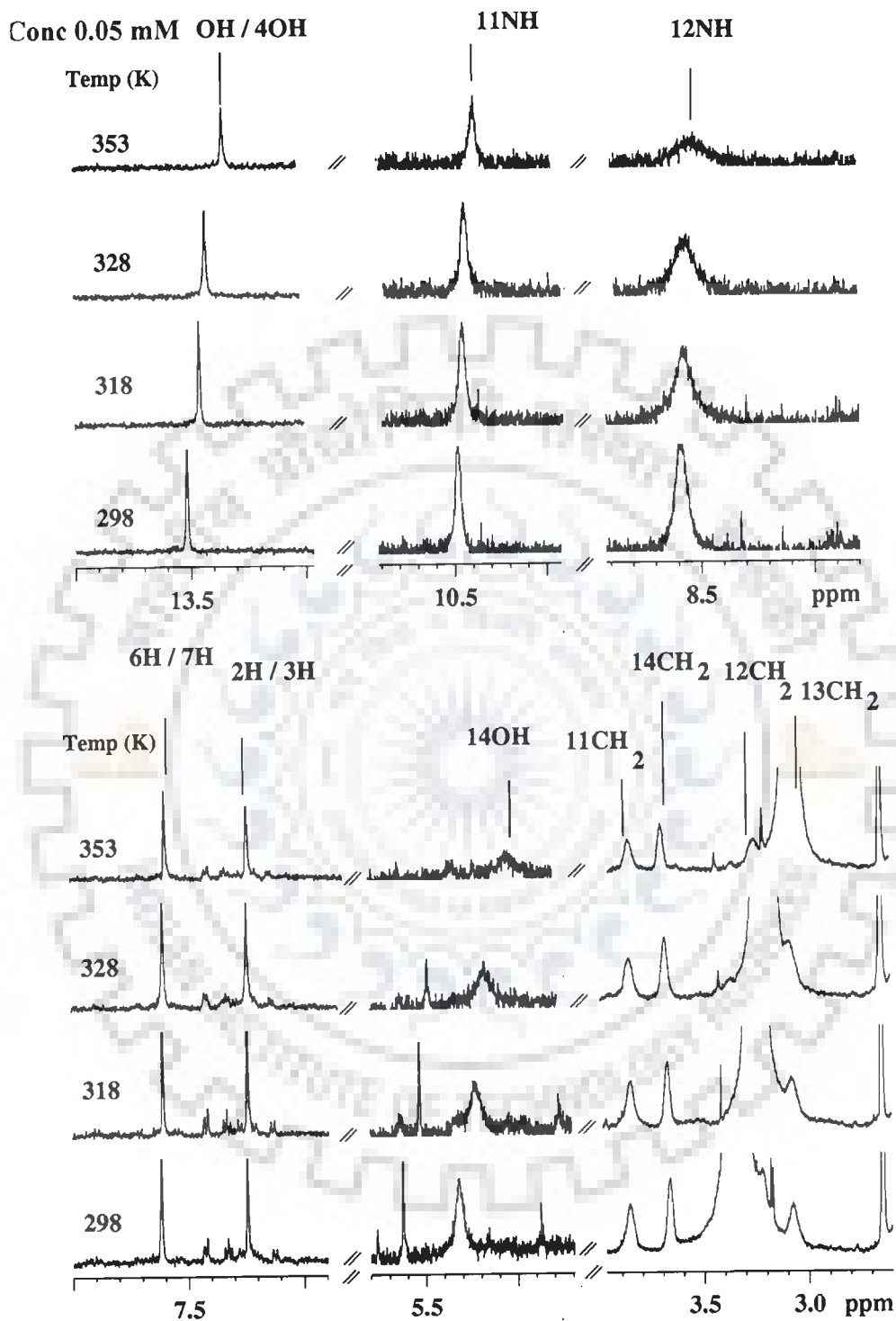


Fig. 4.7c

Fig. 4.7c One dimensional spectra of 0.05 mM mitoxantrone in DMSO-d₆ as a function of temperature.

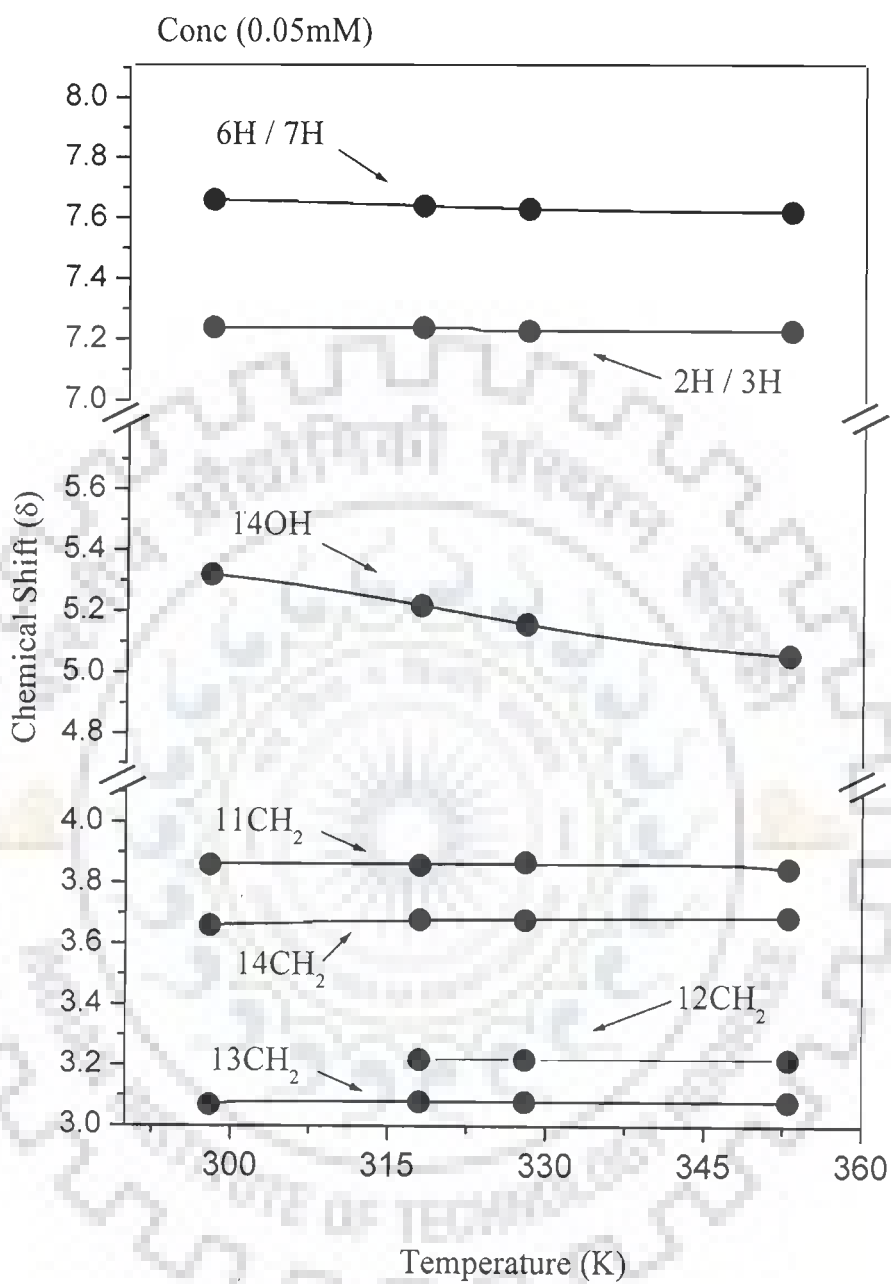


Fig. 4.7d(i)

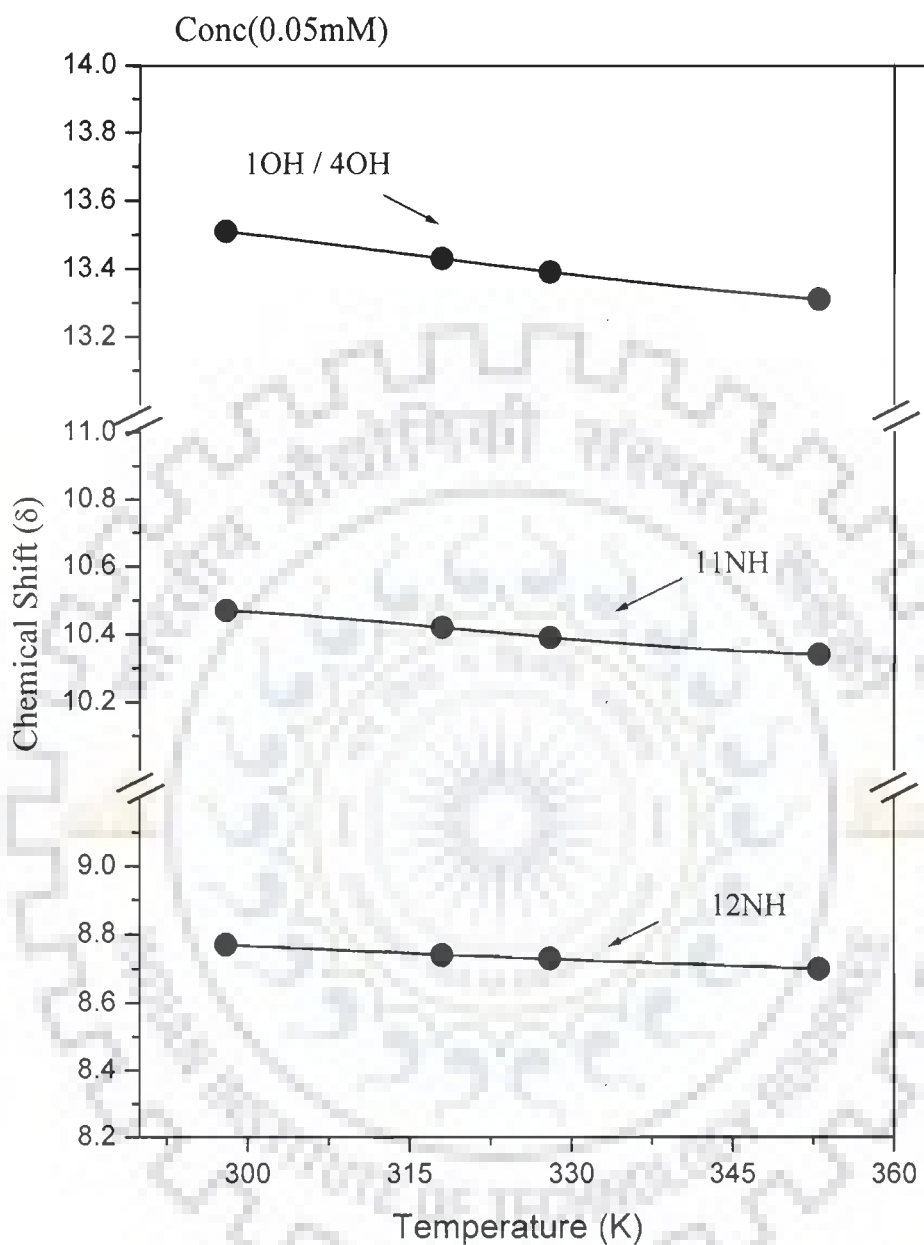


Fig. 4.7d (ii)

Fig. 4.7d Chemical shift of 0.05 mM mitoxantrone in DMSO-d₆ as a function of temperature in the range 298K -353K. (i) 3-8 ppm (ii) 8-14 ppm

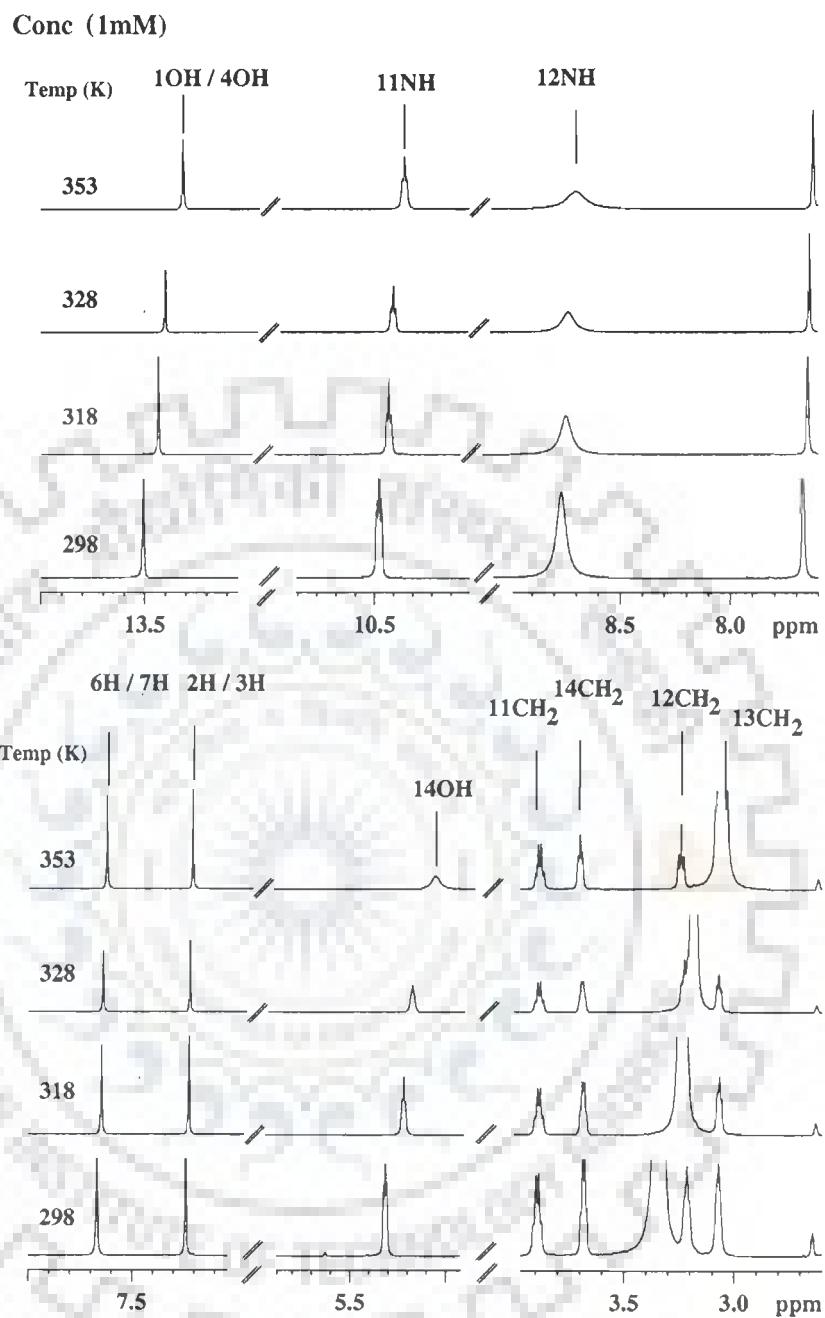


Fig. 4.7e

Fig. 4.7e One dimensional spectra of 1mM mitoxantrone in DMSO-d₆ as a function of temperature.

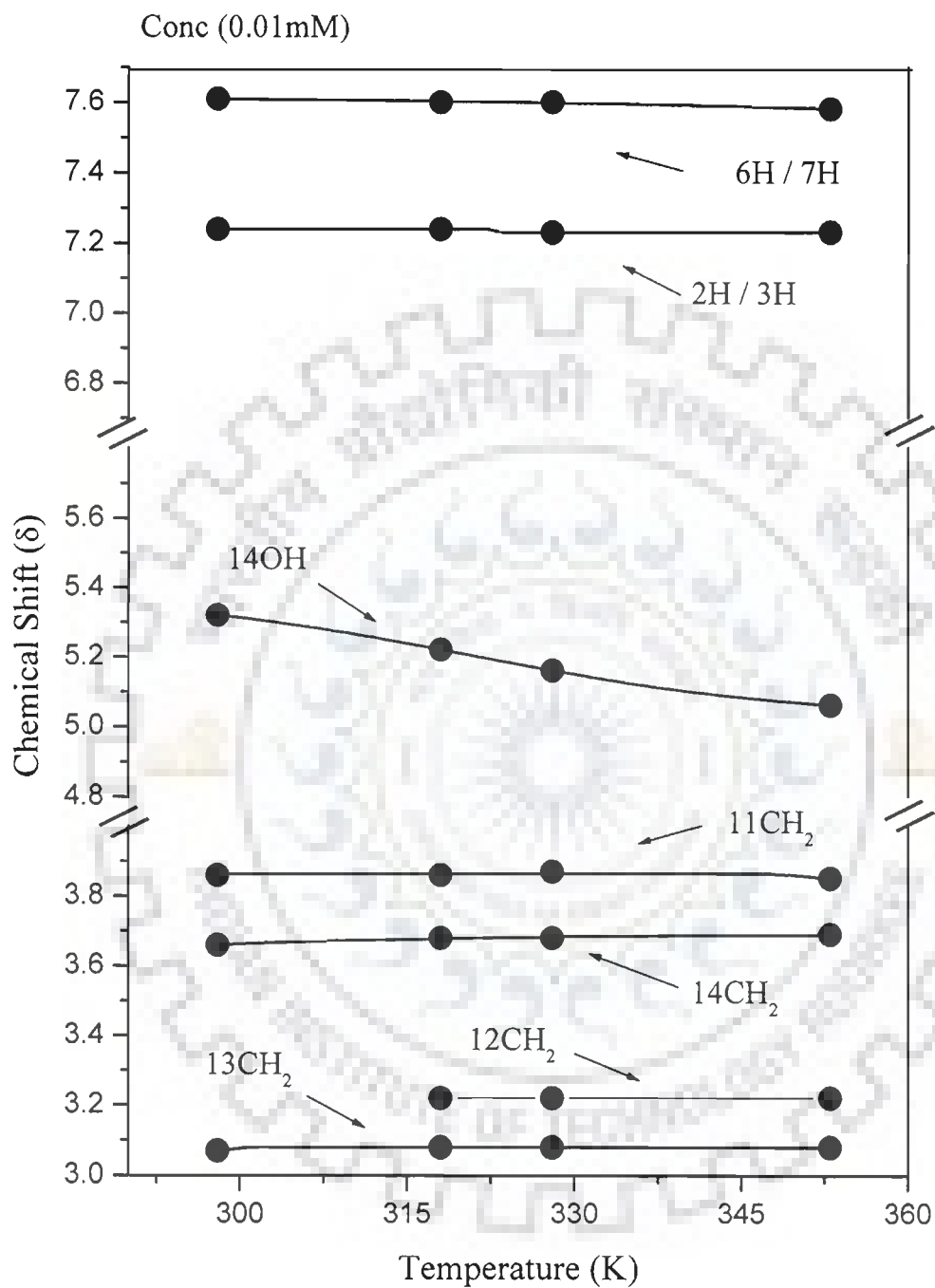


Fig. 4.7f(i)

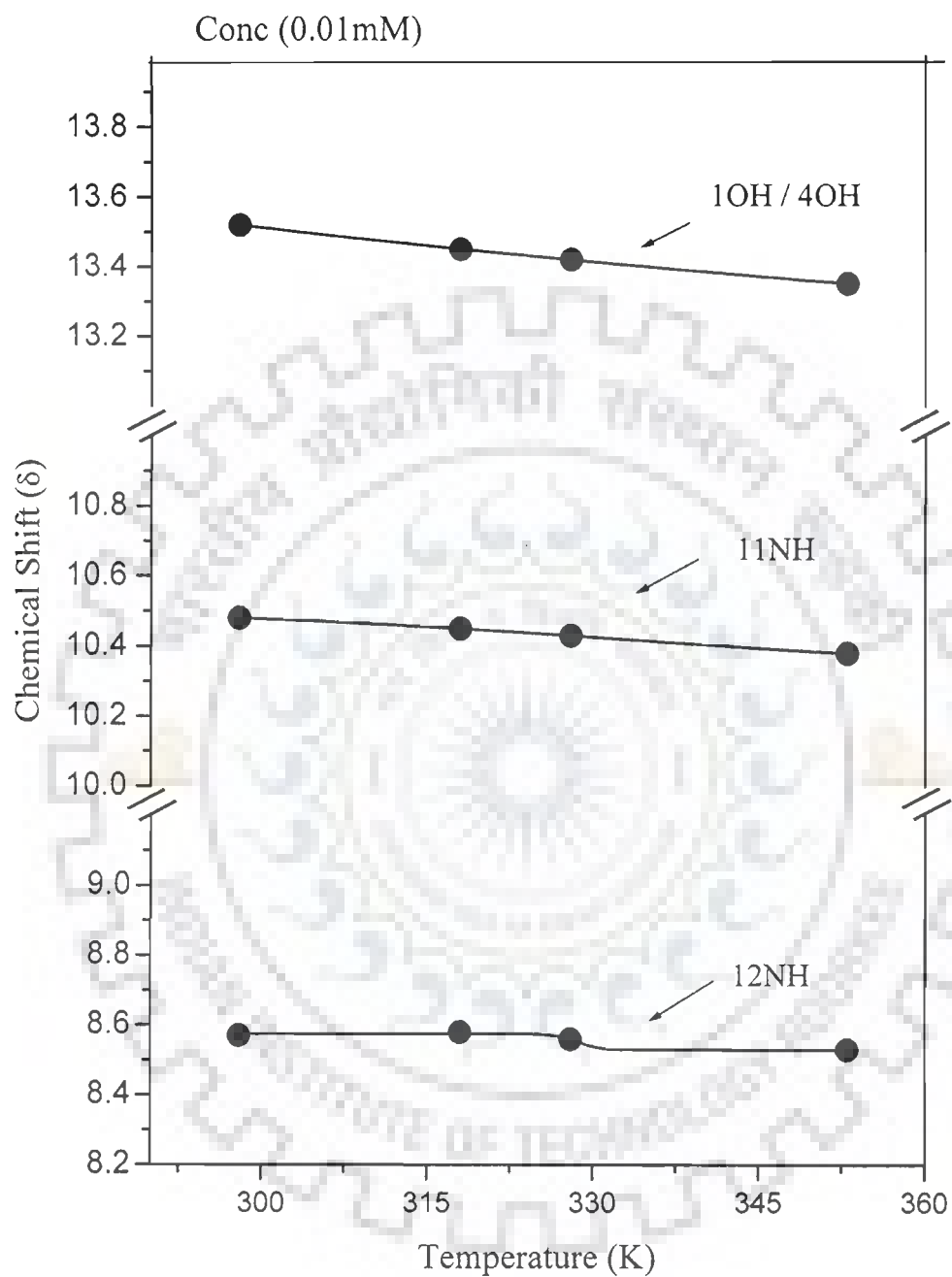


Fig. 4.7f (ii)

Fig. 4.7f Chemical shift of 0.01 mM mitoxantrone in DMSO- d_6 as a function of temperature in the range 298K -353K. i) 3-8 ppm ii) 8-14 ppm

Temp 298 K

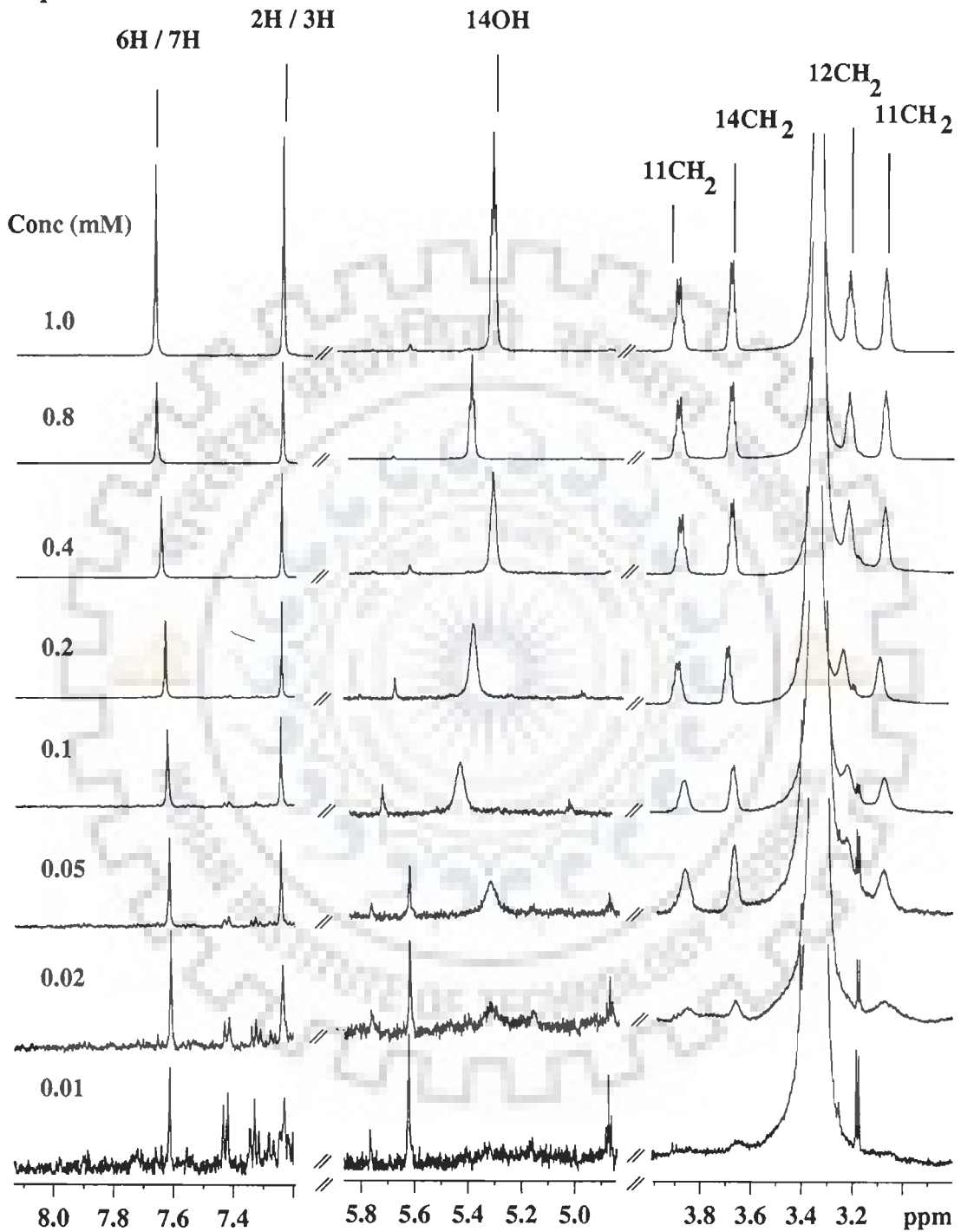


Fig. 4.8a(i)

Temp 298 K

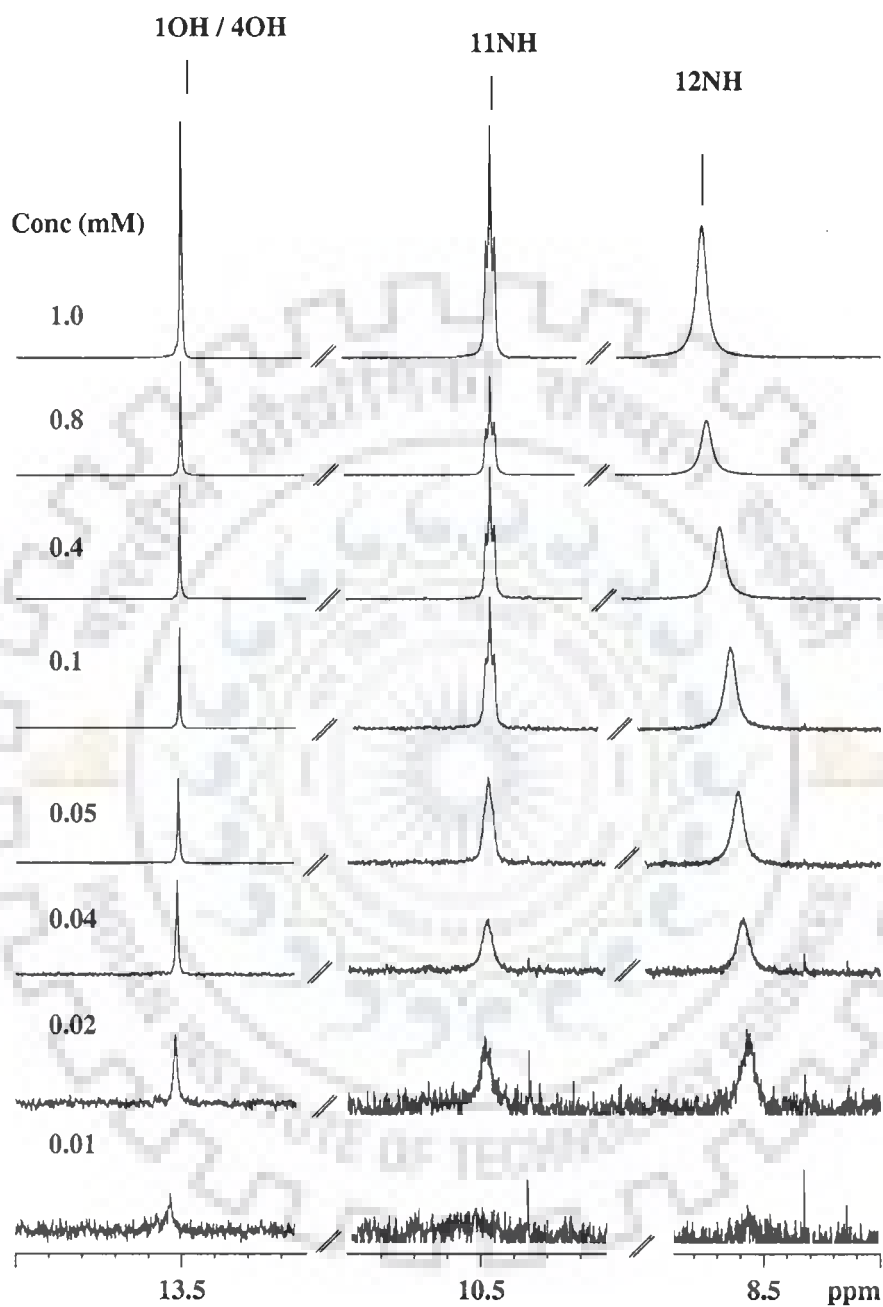


Fig. 4.8a(ii)

Fig. 4.8a One dimensional proton NMR spectra of mitoxantrone in DMSO-d₆ as a function of concentration at 298 K. i) 3–8 ppm ii) 8–14 ppm

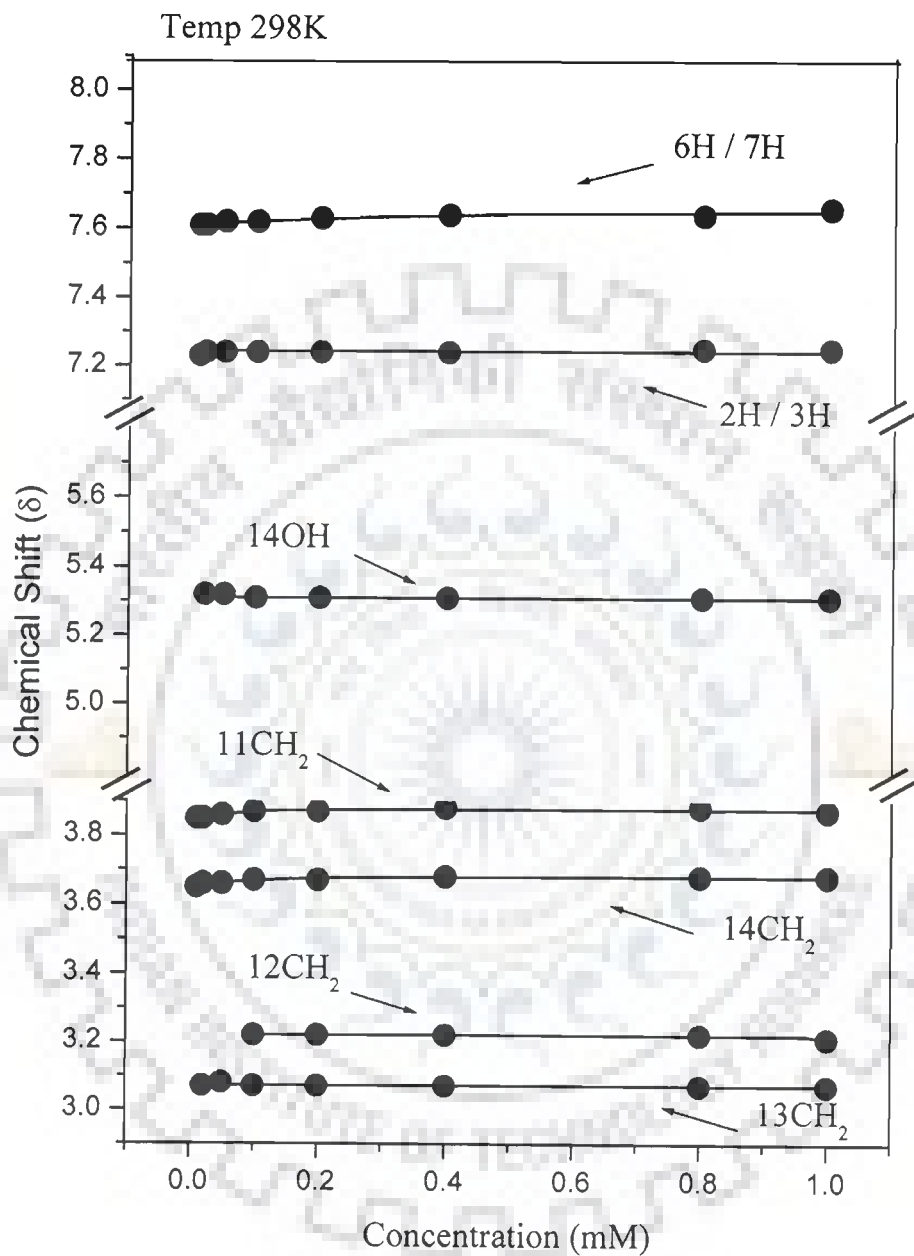


Fig. 4.8b(i)

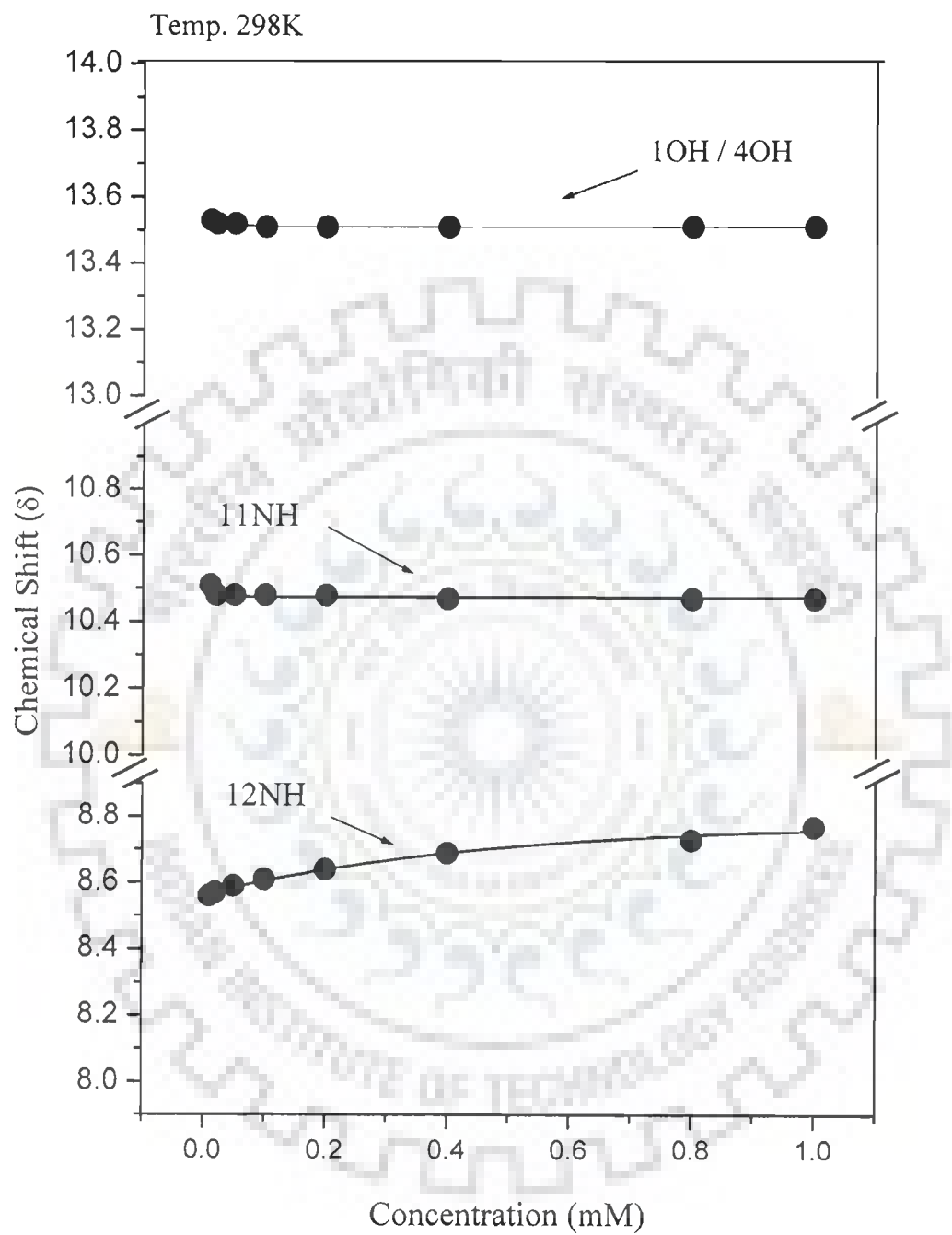


Fig. 4.8b(ii)

Fig. 4.8b Chemical shift of mitoxantrone in DMSO- d_6 as a function of concentration at 298

K. i) 3–8 ppm ii) 8–14 ppm

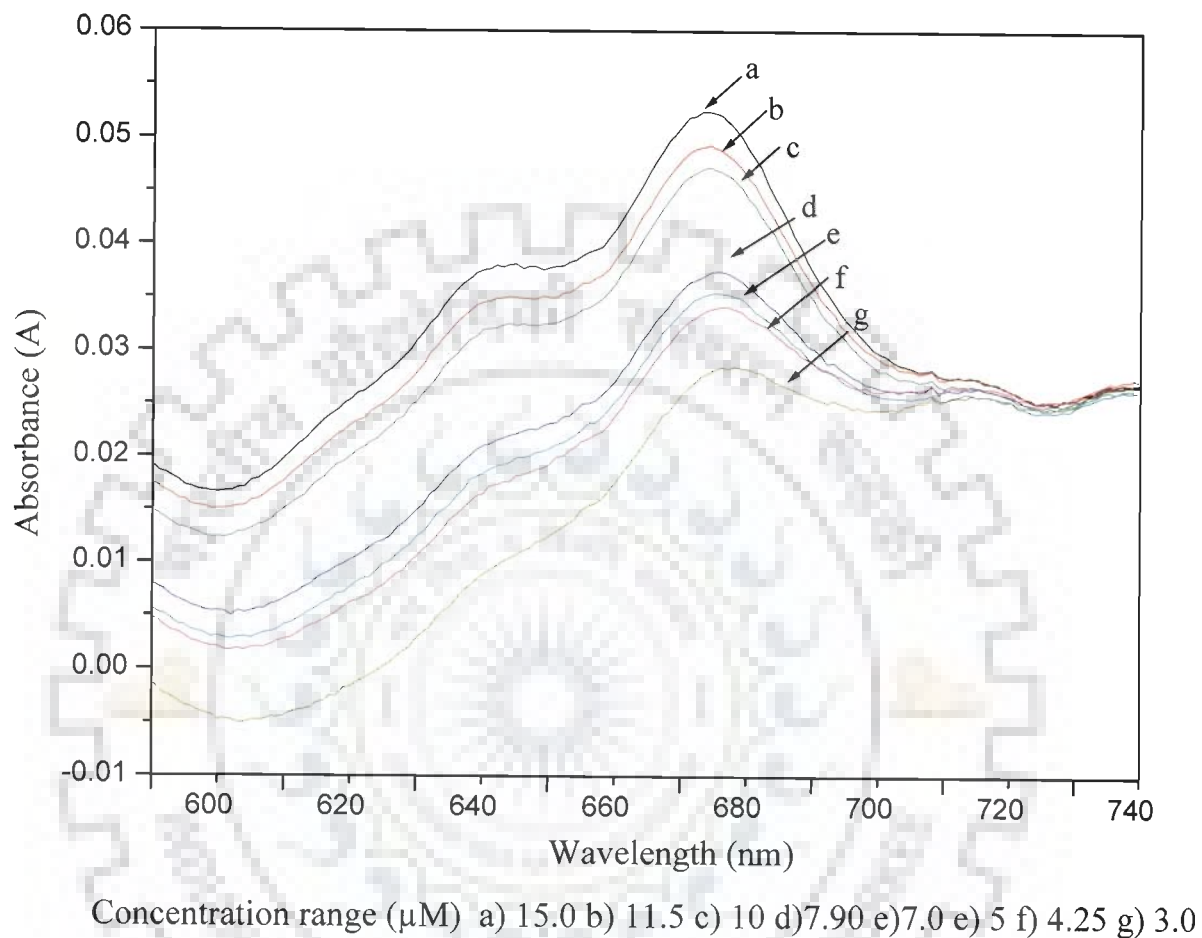


Fig. 4.9 Absorption spectra of mitoxantrone in DMSO as a function of concentration in the range 3 -15 μM at 298 K.

mitoxantrone. The molar absorption decreases significantly as a five fold increase in concentration increases O.D. by approximately 2 fold only. This indicates a change in disposition of the 11NH moiety and 1 OH / 4OH groups attached to aromatic ring and hence the charge transfer from base pair of electrons to aromatic ring.

The ROESY spectra in DMSO showed that 2H / 3H are close to 11CH₂, 12CH₂ and 13CH₂ protons, as in the case with corresponding spectra of mitoxantrone in water. This indicates that the self associated stacked dimer has two mitoxantrone molecules in head to tail or inverse orientation such that ring ABC of say M_I stacks over ring CBA of M_{II} molecule. There are three additional distinct inter proton contacts observed in DMSO solvent as compared to that of water. These are 1 OH / 4OH – 11NH; 1OH / 4OH–11CH₂; and 12NH–2H / 3H of which the first one can be either due to the intermolecular hydrogen bonding or else due to intermolecular hydrogen bonding on stacking of M_I over M_{II} in inverse orientation. However, 1 OH / 4OH – 11CH₂ and 12 NH – 2H / 3H connectivities clearly show stacking of M_I over M_{II}.

4.2.4 MOLECULAR MODELING STUDIES

We have attempted to make a molecular model of the self associated molecule (Fig. 4.10) on the basis of the inter proton distance constraints. The stacked structure is based on anti parallel orientation of the plane of chromophore with a separation of 0.34 nm to be consistent with the 2D ROESY also. The energy minimized followed by restrained molecular dynamics is carried out. The structure shows that there is significant overlap of the aromatic rings and the side arms containing alkyl chains are well separated. The orientations of the side arms are however different from that in water (Fig 3.12 Chapter 3). Although there is overlapping of molecule M_I and M_{II}, the observed upfield shift in 11NH protons, ~ 0.04 ppm, may be a balance

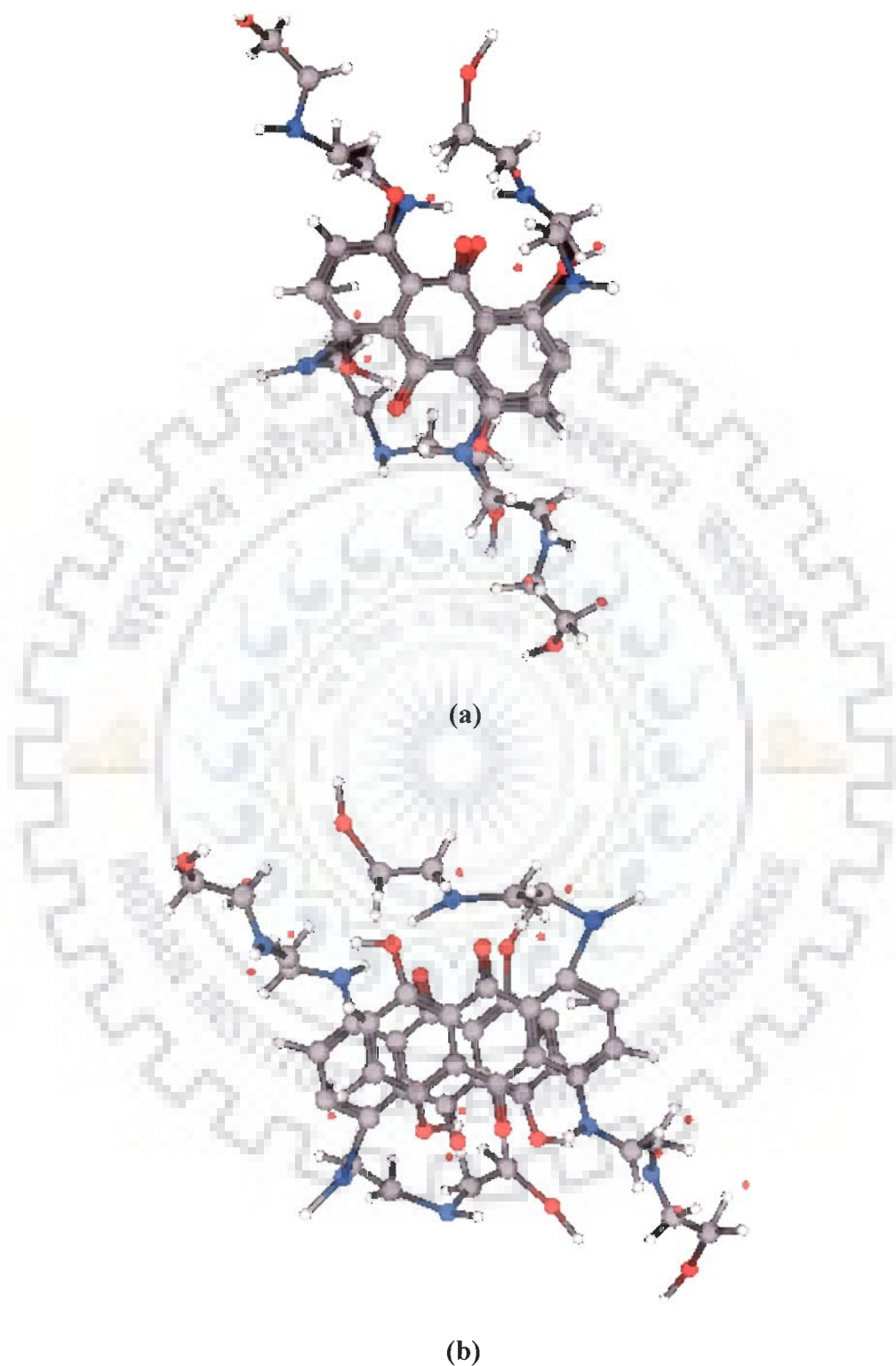


Fig. 4.10 Structure of self-associated dimer of mitoxantrone based on restrained molecular dynamics simulations using experimental interproton distances a) side view b) view, looking perpendicular to the plane of chromophore.

Table 4.5 Comparison of the interproton distances (Å) obtained from ROESY spectra with that observed in model of dimer obtained by restrained molecular dynamics simulations.

S.No.	Intramolecular Connectivities	NMR Distances (Å)	Mitoxantrone (Dimer Model) after minimization with restraints Distances(Å)			
			M _I -Chain _I	M _I -Chain _{II}	M _{II} -Chain _I	M _{II} -Chain _{II}
1.	13CH ₂ -14CH ₂	2.4	2.15	2.63	1.81	1.96
2.	11CH ₂ -12CH ₂	2.65	1.49	2.58	1.71	1.96
3.	12CH ₂ -14CH ₂	3.34	3.54	5.17	3.64	3.64
4.	11CH ₂ -13CH ₂	3.28	3.18	3.13	3.69	3.64
5.	12CH ₂ -13CH ₂	2.79	3.15	3.31	2.93	2.37
6.	11CH ₂ -14CH ₂	4.11	4.36	4.17	4.26	3.97
7.	11 CH ₂ -6H /7H	2.27	2.91	2.70	1.55	2.54
8.	12CH ₂ -6H/7H	2.60	2.04	3.19	1.71	3.05
9.	13CH ₂ -6H /7H	4.66	4.62	4.80	3.69	4.71
10.	14CH ₂ -6H /7H	5.17	5.00	6.22	4.26	5.05
11.	11NH-11CH ₂	3.2	3.83	2.91	3.48	3.40
12.	11NH-12CH ₂	3.4	2.72	2.76	3.71	3.07
13.	11NH-13CH ₂	5.4	5.26	5.26	5.17	5.35
14.	11NH-6H / 7H	4.23	3.89	3.82	3.89	3.94
15.	12NH-11CH ₂	5.60	5.49	4.98	5.39	6.06
16.	12NH-12CH ₂	5.30	5.01	5.44	4.99	4.98
17.	12NH-13CH ₂	3.13	2.96	3.07	3.10	3.98
18.	12NH-14CH ₂	6.67	3.37	2.93	4.74	4.17
19.	12NH - 6H / 7H	5.40	5.52	5.56	5.64	5.30
20.	14OH-13CH ₂	o	4.70	4.51	4.55	5.25
21.	14OH-14CH ₂	5.38	5.11	5.11	5.12	5.11
22.	1OH / 4OH -12CH ₂	o	6.49	6.70	6.57	7.21
23.	1OH / 4OH -13CH ₂	4.07	6.87	4.21	8.68	8.91
24.	1OH / 4OH -14CH ₂	5.17	8.66	2.30	3.96	10.70
25.	1OH / 4OH -12NH	3.30	7.28	2.93	3.61	10.57

contd

	Intermolecular Connectivities*	NMR Distances (Å)	Mitoxantrone (Dimer Model) after minimization with restraints Distances (Å)			
			M _I ChainI - M _{II}	M _I ChainII - M _{II}	M _{II} ChainI - M _I	M _{II} ChainII - M _I
26.	11CH ₂ -2H / 3H	6.06	6.00	5.86	6.06	6.11
27.	12CH ₂ -2H / 3H	6.6	5.50	6.86	7.35	4.92
28.	13CH ₂ -2H / 3H	6.9	5.35	6.82	7.54	5.22
29.	11NH - 2H / 3H	5.68	5.63	7.55	5.35	6.34
30.	1OH / 4OH -6H /7H	4.49	4.35	4.61	4.12	4.58
31.	1OH / 4OH -11NH	5.37	5.23	5.62	5.23	5.6
32.	1OH / 4OH -11CH ₂	5.20	5.18	5.28	3.30	4.90
33.	12NH- 2H / 3H	6.0-7.0	3.72	5.56	6.57	4.64
34.	6H / 7H-2H / 3H	4.70	4.07		4.20	

of the shielding arising from ring currents of π electrons (upfield shift) and stacking intermolecular hydrogen bonded network e.g. 1OH (M_I) – 9CO (M_I) – 11NH (M_{II}) promoted in DMSO solvent. The intermolecular hydrogen bond distances in the molecular model are – 1OH–9CO–11NH = 3.79; 4OH–10CO–11N = 4.50 ; 1OH – 9CO – 11N = 4.65 ; 4OH –10CO–11N = 4.50; in the dimeric state the observed distances of 11NH of one molecule with 1OH / 4OH–9CO / 10CO of the other molecule are : 1OH (M_I) – CO (M_I)–11N (M_{II}) = 5.28 ; 1OH (M_{II}) – 9CO (M_{II})–11N(M_I) = 5.03. These short distances confirm the existence of intermolecular H_2 bond. Thus we conclude that mitoxantrone is self-associated at high concentration in DMSO solvent as demonstrated by interproton contacts 11CH₂, 12CH₂, 13CH₂ with 2H / 3H; 1OH / 4OH with 11CH₂ and 12NH with 2H / 3H. Upfield shifts in 11NH perhaps much less due to strong H_2 bond formation as well as stacking interactions. The 6H / 7H and 2H / 3H may not be well stacked as compared to that in water. Absorption spectra corroborate involvement of 11NH and 1OH / 4OH in self – associated stacked dimer formation.

4.2.4 SOLVENT EFFECT

All the exchangeable protons which were not observed in proton spectra recorded in H₂O solvent (Chapter 3), that is, 12NH, 14OH and 1OH / 4OH protons are observed in the DMSO solvent in addition to the other protons. This can be explained in terms of solvent effect as follows, the exchange rates in the presence of 90 % D₂O and 95 % H₂O exhibits characteristic acid and base catalyzed reactions which is suppressed as much as four orders in 95 % DMSO. Thus in DMSO (a basic aprotic solvent base catalysed exchange rates can be attributed to the large pK_a values of the NH group whereas solvent effect of pK_w seems less important [123].

We have observe that 11CH₂ protons in DMSO is shifted downfield with respect to the 14CH₂ contrary to the observation made in D₂O and H₂O solvent (Chapter 3), the assignment for

which has been made in accordance with the DQF COSY (Fig. 4.2) 2D ROESY (Fig. 4.3) and 2D TOCSY (Fig. 4.4) and HSQC (Fig.4.5) spectra. The observed shifts can be explained in terms of its highly solubilizing nature such that organic compounds which are difficult to dissolve are readily soluble in DMSO. Plausible mechanism thus can be explained in terms of the capability of either of NHs or OHs, (11NH / 12 NH or 1OH / 4OH or 14OH) to protonate the DMSO solvent owing to its basicity and lack of protons. Out of these four possibilities to proton, 11NH will result in better resonance stabilized anion as compared to others. Thus, the 11CH₂ now in turn carries a partial double bond character where as such effect is absent at 14OH end hence to the observe shifts for the 11CH₂ and 14CH₂ protons in DMSO solvent. No such effect was observed in water, which behaves as proton donor solvent and its capability to donate protons to oxygen atom is more than the nitrogen atom due to its high electronegativity, it has high tendency to better accommodate the protons. Thus, it can be said that while in water the inductive effect predominates the resonance stabilization effects precedes in the DMSO solvent and hence the 14CH₂ protons are shifted downfield with respect to the 11CH₂ protons in H₂O solvent.

Table 4.6 Presence (+) and absence (-) of ROESY connectivities indicating intramolecular and intermolecular contacts as well as inter proton distances (Å) in self associated mitoxantrone in D₂O, H₂O and DMSO solvents.

S. No.	Connectivity	D ₂ O		H ₂ O		DMSO	
			Distance (Å)		Distance (Å)		Distance (Å)
1.	13CH ₂ – 14CH ₂ ^{ref}	+	2.40	+	2.40	+	2.40
2.	11CH ₂ – 12CH ₂	+	2.95	+	2.83	+	2.65
3.	12CH ₂ – 14CH ₂	+	3.59	+	3.04	+	3.34
4.	11CH ₂ – 13 CH ₂	+	3.89	+	3.08	+	3.28
5.	12CH ₂ – 13 CH ₂	+	3.28	+	2.9 – 3.6	+	2.79
6.	11CH ₂ – 14 CH ₂	-	-	-	-	+	4.11
7.	11CH ₂ – 6H / 7H	+	2.73	+	2.15	+	2.27
8.	12CH ₂ – 6H / 7H	+	3.18	+	2.55	+	2.60
9.	13CH ₂ – 6H / 7H	-	-	-	-	+	4.66
10.	14CH ₂ – 6H / 7H	-	-	-	-	+	5.17
11.	11CH ₂ – 2H / 3H*	+	3.68	+	3.38	+	6.06
12.	12CH ₂ – 2H / 3H*	+	3.98	+	3.64	+	6.6
13.	13CH ₂ – 2H / 3H*	+	4.32	+	5.43	+	6.9
14.	14 CH ₂ – 2H / 3H*	+	4.35	-	-	-	-
15.	11NH – 11CH ₂	-	-	+	2.69	+	3.2
16.	11NH – 12CH ₂	-	-	+	3.32	+	3.4
17.	11NH – 13CH ₂	-	-	-	-	+	5.4

contd.

S. No.	Connectivity	D ₂ O		H ₂ O		DMSO	
			Distance (Å)		Distance (Å)		Distance (Å)
18.	11NH – 6H / 7H	–	–	+	3.6–4.7	+	4.23
19.	11NH – 2H / 3H*	–	–	+	5.5– 6.1	+	5.68
20.	12NH – 11CH ₂	–	–	+	–	+	5.60
21.	12NH – 12CH ₂	–	–	–	–	+	5.30
22.	12NH – 13CH ₂	–	–	–	–	+	3.13
23.	12NH – 14CH ₂	–	–	–	–	+	6.67
24.	12NH – 6H / 7H	–	–	–	–	o	5.40
25.	12NH – 2H / 3H*	–	–	–	–	+	6.0–7.0
26.	14 OH – 12CH ₂	–	–	–	–	o	–
27.	14OH – 13CH ₂	–	–	–	–	o	–
28.	14OH – 14CH ₂	–	–	–	–	+	5.38
29.	1OH / 4OH – 11CH ₂ *	–	–	–	–	+	5.38
30.	1OH / 4OH – 12CH ₂ *	–	–	–	–	o	–
31.	1OH / 4OH – 13CH ₂ *	–	–	–	–	+	4.07
32.	1OH / 4OH – 14CH ₂ *	–	–	–	–	+	5.17
33.	1OH / 4OH – 11NH*	–	–	–	–	+	5.37
34.	1OH / 4 OH – 12NH*	–	–	–	–	+	3.30
35.	1OH/ 4OH – 2H / 3H	–	–	–	–	+	4.49
36.	1OH / 4OH – 6H / 7H*	–	–	–	–	+	4.23
37.	6H / 7H – 2H / 3H*	+	4.70	–	–	+	4.73

^{ref} Reference for distance calculations

+ / – Presence / Absence of peaks, o – overlap of peaks

I *Intermolecular peaks

Phosphorus-31 NMR Studies on binding of Mitoxantrone with d-(CGATCG)₂

5.1 INTRODUCTION

The phosphorus-31 NMR spectra of deoxyhexanucleotide d-(CGATCG)₂ is taken at an interval of 5°C in the temperature range 278–353K and two dimensional ³¹P / ¹H shift correlation spectra is taken at 298 K for assignment of ³¹P resonances in the hexamer. The binding of mitoxantrone drug to d-(CGATCG)₂ is investigated by proton and phosphorus-31 NMR techniques by titrating the drug with hexamer sequence. A known concentration of mitoxantrone is added successively to a fixed concentration of 1.64 mM (duplex concentration) oligomer to arrive at drug to DNA (D / N) stoichiometric ratios of 0.04, 0.116, 0.23, 0.34, 0.384, 0.456, 0.684, 0.95, 1.25, 1.50, 1.75 and 2.0. One dimensional ¹H and ³¹P NMR are recorded at 5° C (278 K) for each complex. For the complex having D / N of 1 (exact ratio being 0.95), 1.5 1.75 and 2.0 one dimensional ¹H and ³¹P NMR as a function of temperature (278 K–353 K), two dimensional ¹H nuclear overhauser effect spectra (NOESY) at 278 K at mixing times of 200 ms and 300 ms and ³¹P NOESY exchange spectra at 278 K are also recorded. In this chapter, the ³¹P NMR spectra and their analysis are discussed.

5.2 RESULTS AND DISCUSSIONS

Fig. 5.1 gives one dimensional phosphorus-31 NMR spectra of d-(CGATCG)₂ in the temperature range 278K–353K. The assignment of ³¹P nuclei is done by using ³¹P / ¹H hetero multiple bond correlation (HMBC) method (Fig. 5.2). Three bond scalar coupling of ³¹P with (H3')_n and (H5'/H5'')_{n+1} protons as well as (H4')_n and (H4')_{n+1} protons are manifested as cross peaks in the 2D ³¹P–¹H correlation map (Fig. 5.2). Since the proton assignments have earlier been done [12] identification of ³¹P nucleotide resonances was straightforward: A3pT4

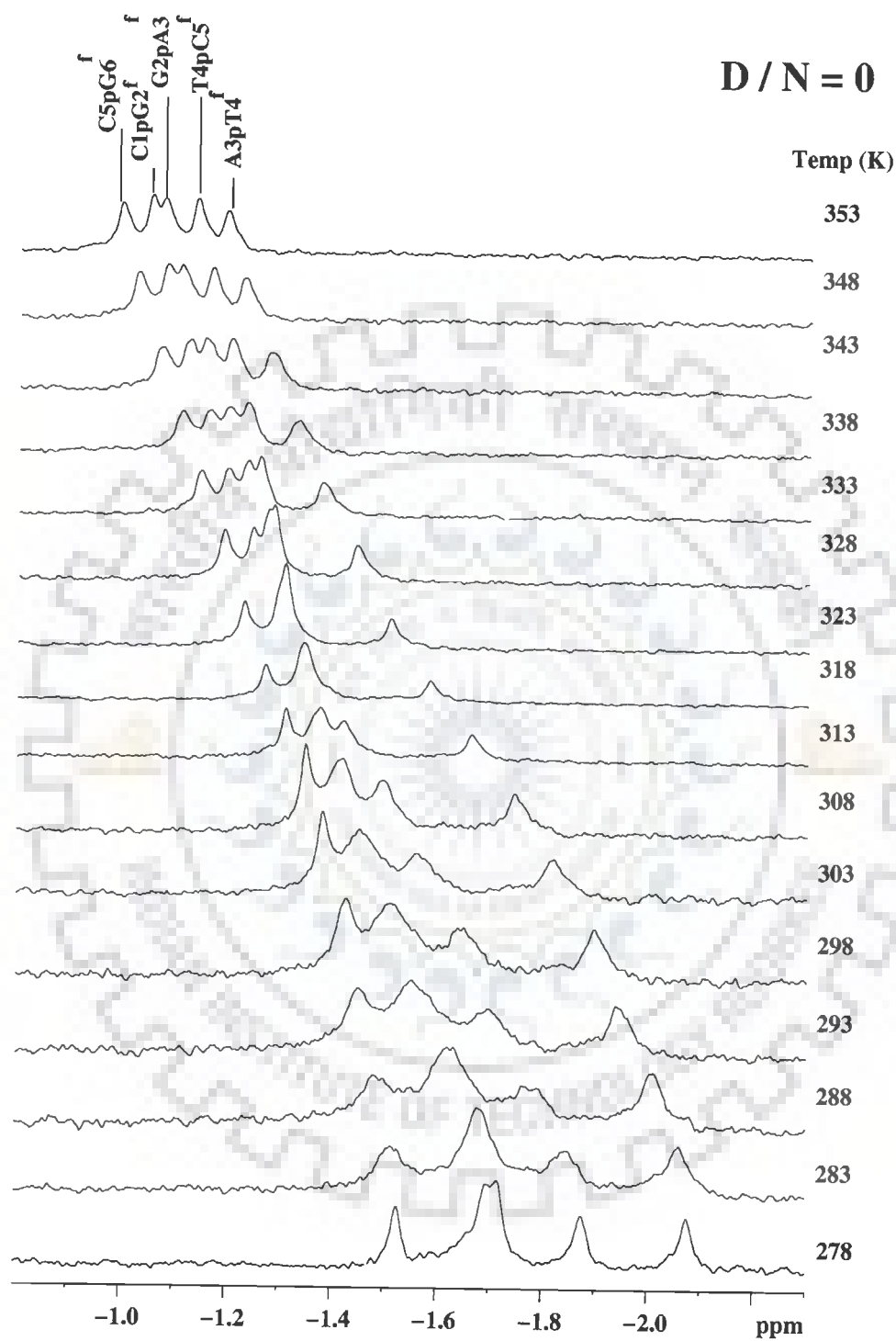


Fig.5.1 ^{31}P NMR spectra of 2.00 mM pure $d\text{-(CGATCG)}_2$ as a function of temperature.

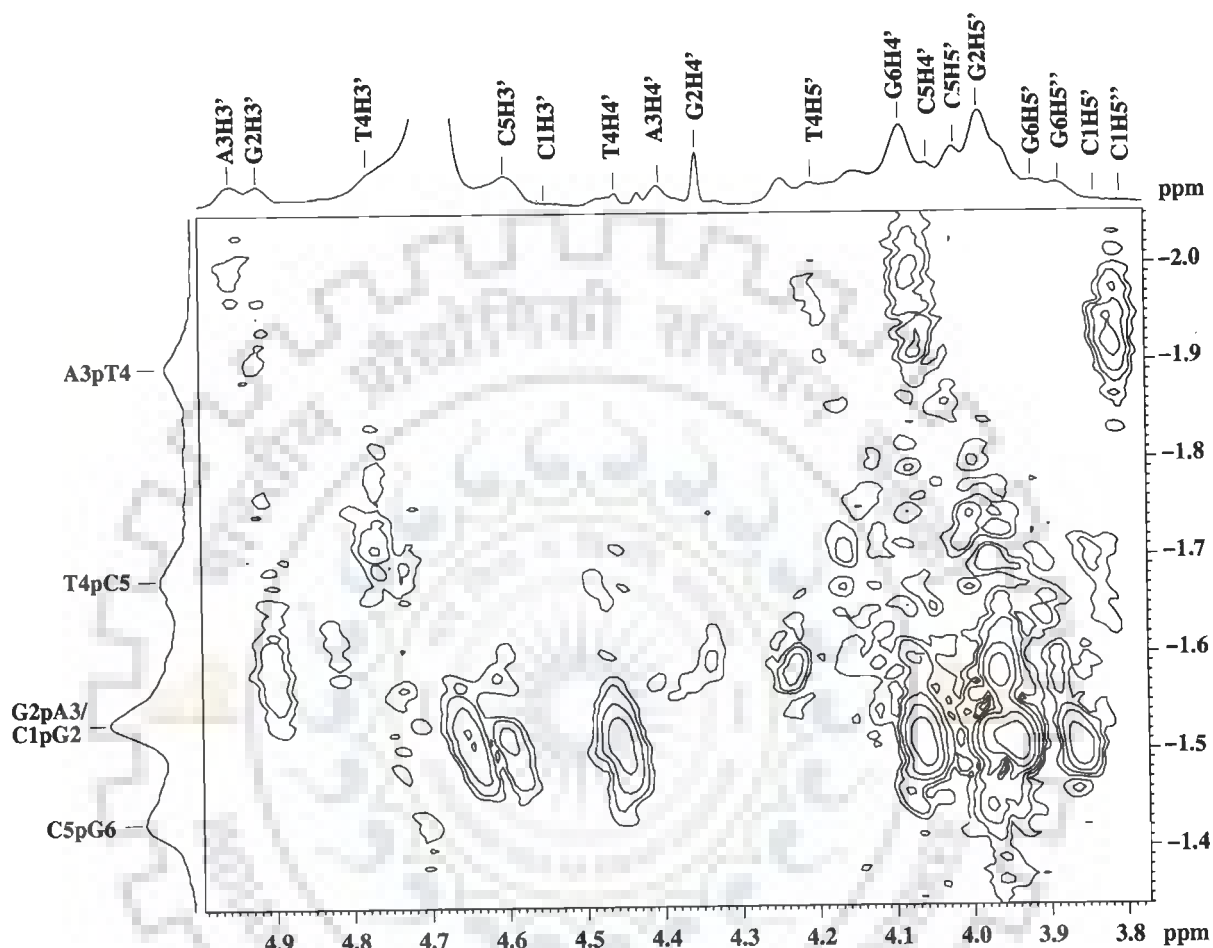


Fig.5.2 Two dimensional $^{31}\text{P} - ^1\text{H}$ heteromultiple bond correlation (HMBC) spectra 2.00-mM d-(CGATCG)₂ at 298K. The horizontal projection shown on the top of figure corresponds to H3', H4', H5'/ H5'' protons and the vertical projection corresponds to 5-phosphorus resonances.

phosphorus signal gives correlation with A3H3'; T4pC5 with T4H3'; C1pG2 with C1H3'; G2pA3 with G2H3'; and so on. Spectral assignments thus obtained are listed in Table 5.1.

Fig. 5.3 shows 1D NMR spectra as the drug is progressively added to the hexanucleotide. It is noted that apart from 4 resonance peaks at -1.58, -1.73 (having intensity corresponding to 2 resonance), -1.96 and -2.18 corresponding to C5pG6, G2pA3 & C1pG2, T4pC5 and A3pT4 phosphorus resonances, respectively, additional broad resonances started appearing. The three new peaks at -1.37, -1.19 and -2.22 ppm, present outside the range -1.6 to -2.1 ppm (in which five ^{31}P signal of uncomplexed d-CGATCG appear), are clearly evident in spectra of D / N ratio of 1.0 and higher values. The resonances for other complexes at other D / N ratios also get assigned and are given in Table 5.3.

Fig. 5.4(a-c) show 2D ^{31}P NMR exchange spectrum of the complex of mitoxantrone with d-(CGATCG)₂ at drug to DNA (D / N) ratios of 1, 1.5, 1.75 and 2.0 at 278 K. The ^{31}P spectra are shown at the top of each NOESY spectra. It is observed each of the 5 phosphorus signals seen in uncomplexed DNA give cross peak due to chemical exchange with a specific broad peak, which gets assigned to the corresponding phosphate group in the bound DNA. Since there are only two sets of resonances present at the same chemical shift position in all complexes, there exist only two species in solution, free hexamer and a hexamer bound to drug. These spectra are a direct proof of the fact that the drug is bound to the DNA. The resonance peaks of the bound species are significantly broadened. The chemical shift position of each of the free and bound phosphorus nuclei, thus obtained is shown in Table 5.2.

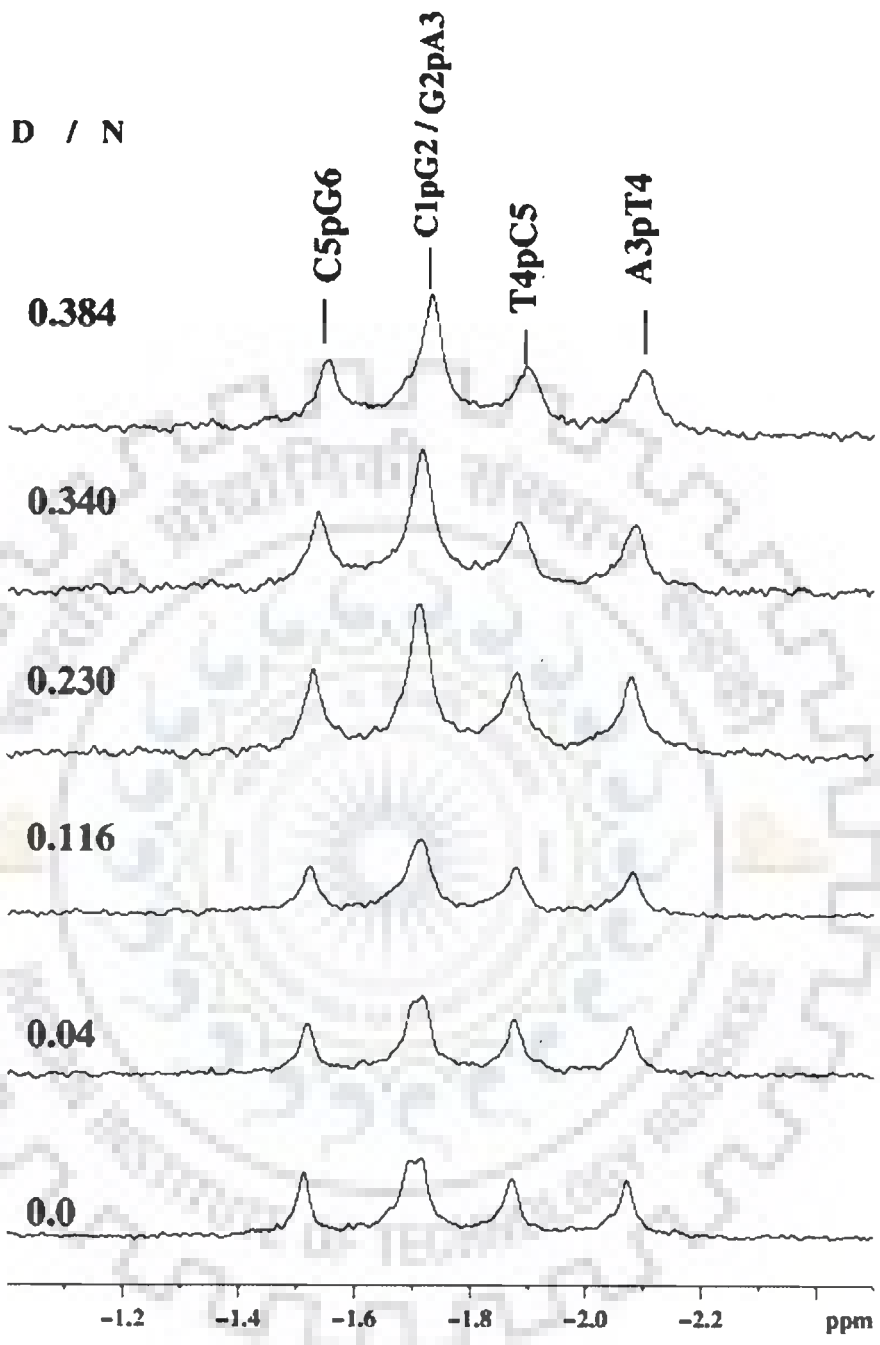


Fig. 5.3(a)

D / N

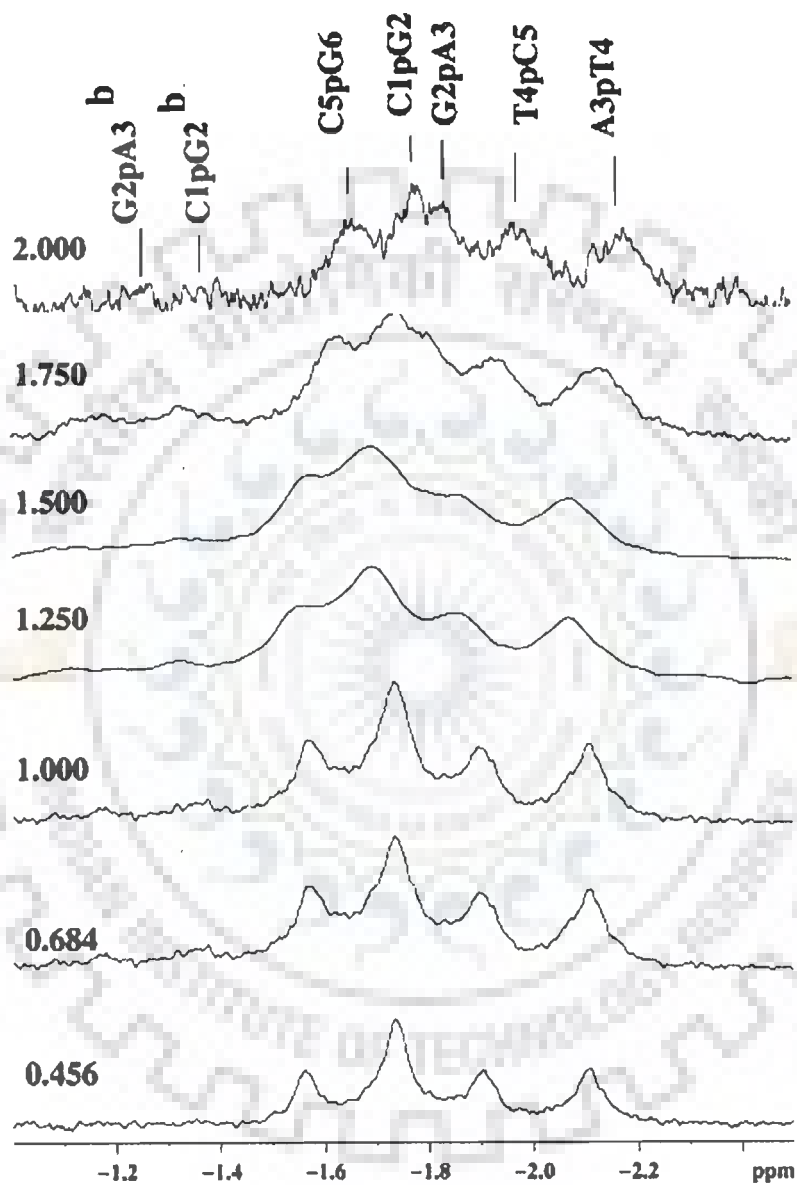


Fig. 5.3(b)

Fig. 5.3(a–b) Proton decoupled ^{31}P NMR spectra of 1.64 mM $d\text{-(CGATCG)}_2$ in uncomplexed state and complexed with mitoxantrone with increasing drug (D) to nucleic acid duplex (N) ratios, D / N, at 278K.

D / N = 1.0

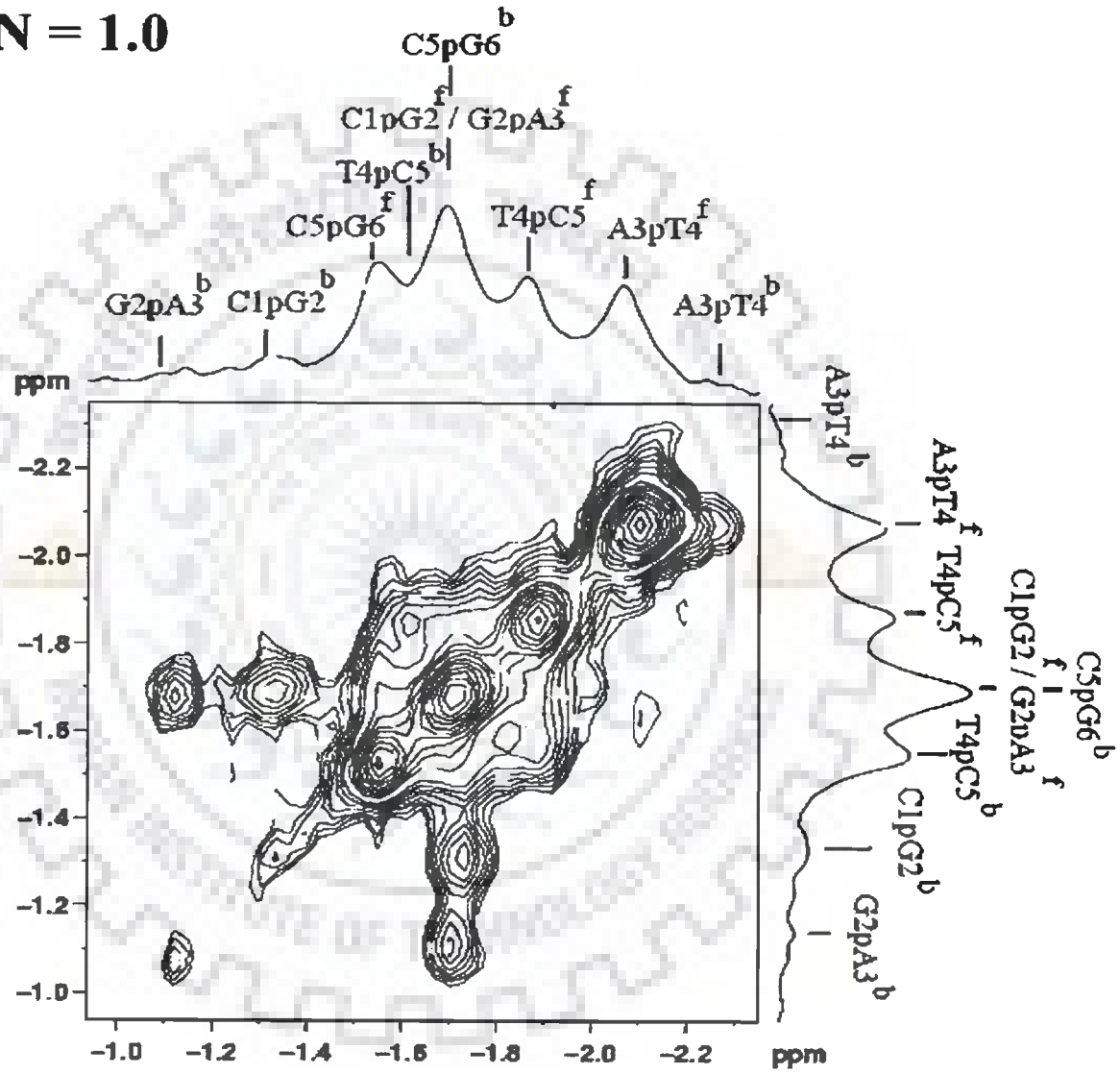


Fig. 5.4a

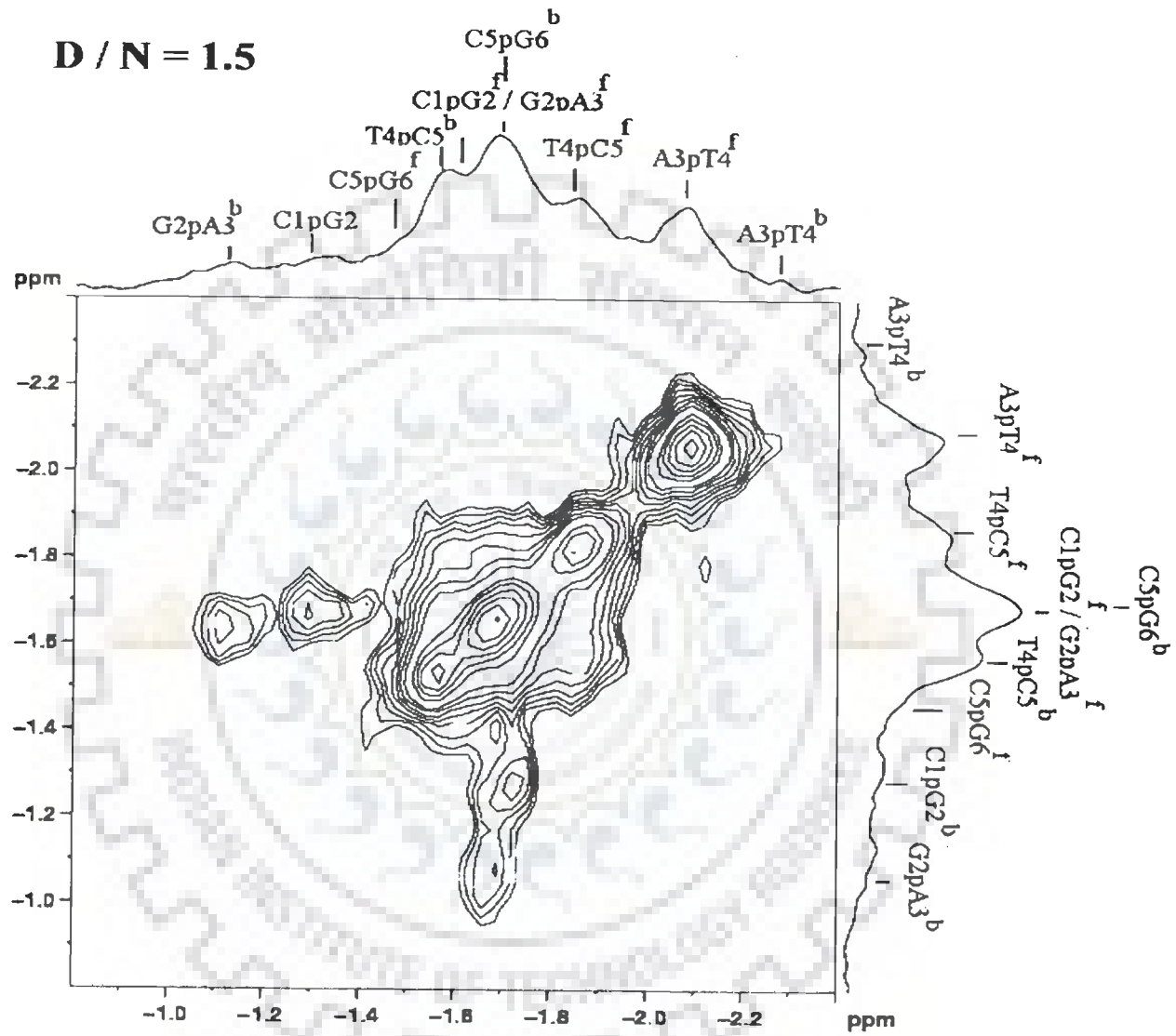


Fig. 5.4b

177

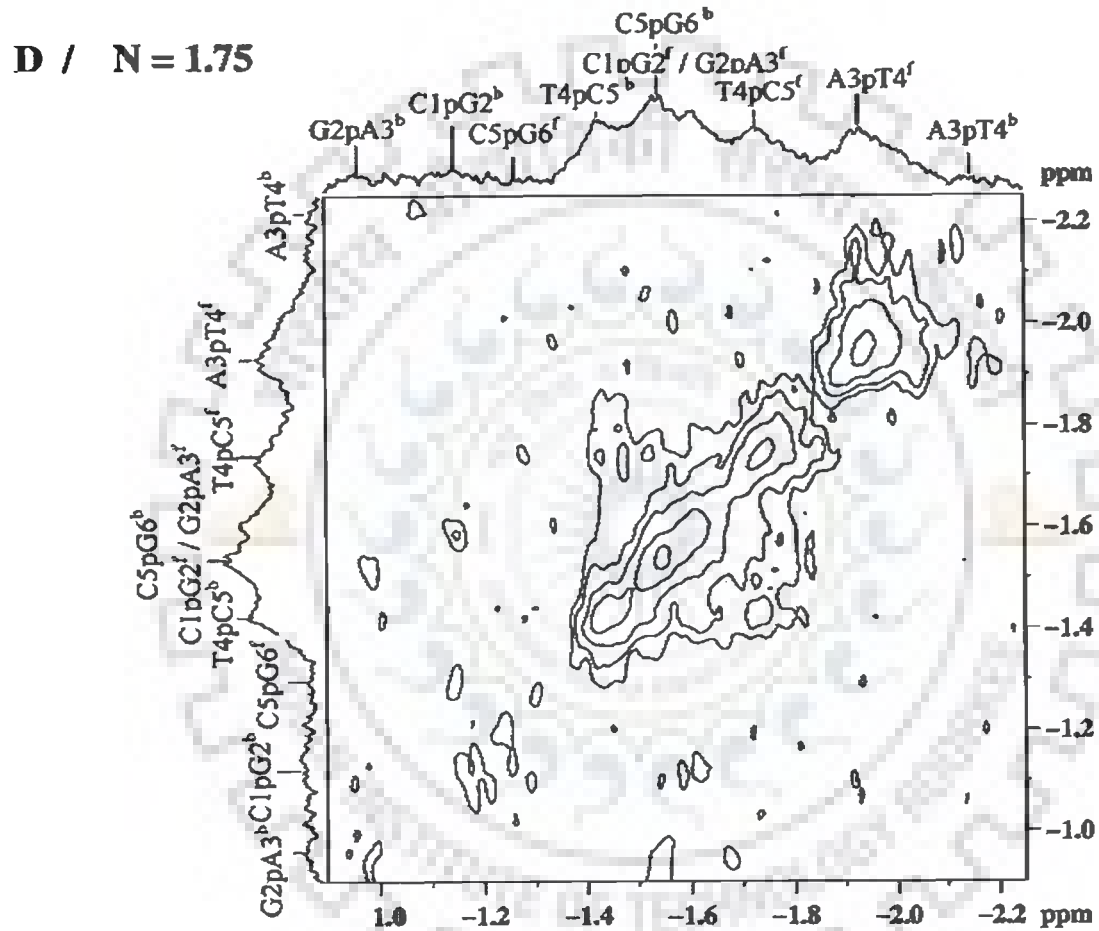


Fig. 5.4c

Fig. 5.4 ³¹P NMR exchange spectrum of the complex of mitoxantrone with d-(CGATCG)₂ at drug (D) to nucleic acid duplex (N) ratios, D / N of (a) 1 (b) 1.5 and (c) 1.75 at 278K. The 1D spectrum is shown at the top.

Table 5.1 ³¹P chemical shift assignments (δ) of d-(CGATCG)₂ in the free duplex at different temperatures. The total change in chemical shift with temperature, $\Delta\delta = \delta_{353K} - \delta_{278K}$ is also shown.

Temp(K)	Phosphate Group				
	C1pG2 ^f	G2pA3 ^f	A3pT4 ^f	T4pC5 ^f	C5pG6 ^f
278	-1.691	-1.721	-2.074	-1.875	-1.576
283	-1.682	-1.682	-2.064	-1.849	-1.518
288	-1.625	-1.628	-2.009	-1.760	-1.478
293	-1.550	-1.550	-1.937	-1.695	-1.449
298	-1.508	-1.508	-1.895	-1.648	-1.425
303	-1.449	-1.449	-1.818	-1.557	-1.380
308	-1.409	-1.4109	-1.735	-1.486	-1.338
313	-1.373	-1.373	-1.661	-1.418	-1.308
318	-1.342	-1.342	-1.581	-1.342	-1.229
323	-1.306	-1.306	-1.507	-1.306	-1.223
328	-1.278	-1.284	-1.441	-1.244	-1.190
333	-1.196	-1.234	-1.376	-1.257	-1.146
338	-1.162	-1.198	-1.330	-1.232	-1.110
343	-1.124	-1.152	-1.276	-1.202	-1.077
348	-1.108	-1.106	-1.227	-1.165	-1.025
353	-1.050	-1.074	-1.192	-1.136	-0.993
$\Delta\delta$	+0.586	+0.647	+0.882	+0.739	+0.583

Table 5.2 ³¹P chemical shift assignments of free (δ^f) and bound (δ^b) phosphate groups in the mitoxantrone – d-(CGATCG)₂ complex at drug (D) to nucleic acid duplex (N) ratios, D / N = 1, 1.5 and 1.75. The change in chemical shift, $\Delta\delta = \delta^b - \delta^f$, due to binding is also indicated for the three complexes.

Phosphate Group	D/N = 1			D/N = 1.5			D/N = 1.75		
	δ^f	δ^b	$\Delta\delta$	δ^f	δ^b	$\Delta\delta$	δ^f	δ^b	$\Delta\delta$
C1pG2	-1.69	-1.33	+0.36	-1.69	-1.32	+0.37	-1.69	-1.30	+0.39
G2pA3	-1.69	-1.17	+0.52	-1.69	-1.17	+0.52	-1.69	-1.13	+0.56
A3pT4	-2.07	-2.18	-0.11	-2.07	-2.18	-0.11	-2.07	-2.16	-0.09
T4pC5	-1.86	-1.62	+0.24	-1.86	-1.62	+0.24	-1.86	-1.62	+0.24
C5pG6	-1.54	-1.70	-0.16	-1.54	-1.70	-0.16	-1.54	-1.70	-0.16

+ve $\Delta\delta$ indicates downfield shift

-ve $\Delta\delta$ indicates up field shift

Table 5.3 Chemical shift of ^{31}P resonances of the phosphate groups of DNA oligomer, present in free and bound state, in the complex of mitoxantrone with $d\text{-(CGATCG)}_2$ at 278 K at different drug (D) to nucleic acid duplex (N) ratios (D / N). The total change in chemical shift with increasing D / N ratio, $\Delta\delta = \delta_{(D/N=2.00)} - \delta_{(D/N=0)}$ is also shown.

D / N	C1pG2 ^f	G2pA3 ^f	A3pT4 ^f	T4pC5 ^f	C5pG6 ^f	C1pG2 ^b	G2pA3 ^b
0	-1.690	-1.717	-2.072	-1.873	-1.513	–	–
0.04	-1.717	-1.717	-2.077	-1.875	-1.519	–	–
0.116	-1.717	-1.717	-2.081	-1.879	-1.524	–	–
0.23	-1.708	-1.708	-2.075	-1.878	-1.524	–	–
0.34	-1.715	-1.715	-2.075	-1.882	-1.534	–	–
0.384	-1.732	-1.732	-2.10	-1.89	-1.550	–	–
0.456	-1.733	-1.733	-2.107	-1.903	-1.560	–	–
0.684	-1.733	-1.733	-2.107	-1.893	-1.565	–	–
1	-1.691	-1.691	-2.074	-1.875	-1.576	-1.330	-1.170
1.50	-1.694	-1.694	-2.074	-1.859	-1.578	-1.320	-1.170
1.75	-1.685	-1.685	-2.073	-1.865	-1.573	-1.300	-1.130
2.00	-1.680	-1.680	-2.000	-1.793	-1.473	–	–
$\Delta\delta$	-0.010	-0.037	-0.072	-0.080	-0.040	-0.030	-0.040

+ $\Delta\delta$ indicates downfield shift

-ve $\Delta\delta$ indicates up field shift

Table 5.4a Chemical shift of free (δ^f), bound (δ^b), and the change in chemical shift due to binding, $\Delta\delta = \delta^b - \delta^f$ in phosphate resonances of some of the drug–DNA complexes taken from literature. +ve $\Delta\delta$ indicates downfield shift.

Phosphate Group	Lown et al [75] d-(CGCG) ₂ + mitoxantrone			Kotovych et al [63] d-(CGATCG) ₂ + mitoxantrone			Favier et al [33] d-(CGATCG) ₂ + pyridopurine			Mazinni et al [79] d-(AAGAATTCTT) ₂ + berberine				
	δ^f	δ^b	$\Delta\delta$	Phosphate Group	δ^f	δ^b	$\Delta\delta$	δ^f	δ^b	$\Delta\delta$	Phosphate Group	δ^f	δ^b	$\Delta\delta$
C1pG2	-3.46	-3.31	+0.15	C1pG2	-1.71	-1.70	+ 0.01	1.2	1.1	-0.1	A1pA2	-1.31	-1.19	+0.12
G2pA3	-3.30	-3.40	-0.10	G2pA3	-1.71	-1.70	+ 0.01	1.1	1.1	0.0	A2pG3	-1.00	-0.98	+0.02
C3pG4	-3.46	-3.31	+0.15	A3pT4	-2.19	-2.21	-0.02	0.7	0.8	-0.1	G3pA4	-1.14	-1.12	+0.02
				T4pC5	-1.95	-1.97	-0.02	0.4	0.5	-0.1	A4pA5	-1.40	-1.23	+0.17
				C5pG6	-1.59	-1.25	+0.34	1.2	1.2	0.0	A5pT6	-1.37	-1.40	+0.03
											T6pT7	-1.18	-1.10	+0.08
											T7pC8	-1.11	-1.07	+0.04
											C8pT9	-1.14	-1.10	+0.04
											T9pT10	-1.04	-1.07	+0.03

Table 5.4b Chemical shift of free (δ^f), bound (δ^b), and change in chemical shift due to binding, $\Delta\delta = \delta^b - \delta^f$ in phosphate groups of some of the drug–DNA complexes taken from literature. +ve $\Delta\delta$ indicates downfield shift.

Phosphate Group	Mazzini et al [80] d-(CGATCG) ₂ + Adriamycin			Mazzini et al [80] d-(CGTACG) ₂ + Adriamycin			Searle et al [102] d-(GCATGC) ₂ + Nogalamycin		
	δ^f	δ^b	$\Delta\delta$	δ^f	δ^b	$\Delta\delta$	δ^f	δ^{b*}	$\Delta\delta$
C1pG2/ G1pC2	-0.91	-0.48	+0.43	-1.03	-0.58	+0.45	-3.30	-2.90	+0.20
G2pA3/ C2pA~	-0.86	0.67	+1.53	-1.40	-0.56	+0.84	-3.00	-2.50	+0.50
A3pT4/ T3pA4	-1.26	-1.28	≤-0.2	-1.12	-1.26	-0.14	-3.40	-3.20	+0.20
T4pC5/ T4pG6	-1.06	-1.12	-0.06	-1.20	-1.34	-0.14	-3.10	-1.60	+1.50
C5pG6/ G5pC6	-0.73	0.84	+1.57	-0.90	+0.63	+1.53	-3.00	-3.00	+0.00

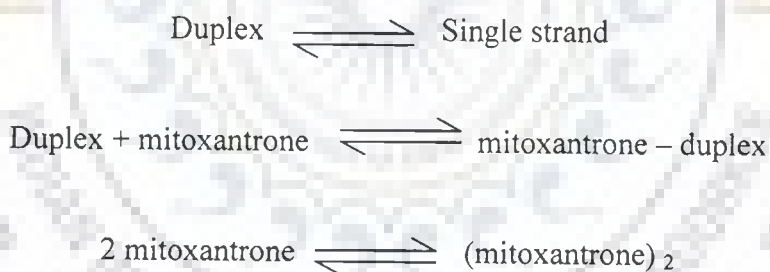
*Tentative assignment

It is observed that the C1pG2, G2pA3 and T4pC5 resonances shift downfield by 0.36–0.39, 0.52–0.58 and 0.22–0.29 ppm, respectively while the A3pT4 and C5pG6 resonance shift upfield to a lesser extent by 0.04–0.18 and 0.16–0.17 ppm, respectively in all the three complexes. These may be compared with that obtained in literature (Table 5.4a–b) for binding of mitoxantrone with d-(CGCG)₂ [75], 2-pyrido with d-(CGATCG)₂ [33], berberine with d-(AAGAATTCTT)₂ [79], nogalamycin with d-(GCATGC)₂ [102], adriamycin and methoxy –morpholinodoxorubicin with d-(CGATCG)₂, [80]. In case of mitoxantrone downfield field shift of 0.5 ppm has been reported [75], while in pyridopurine [33] and berberine [79], downfield shift in the range 0–0.17 ppm have been reported.

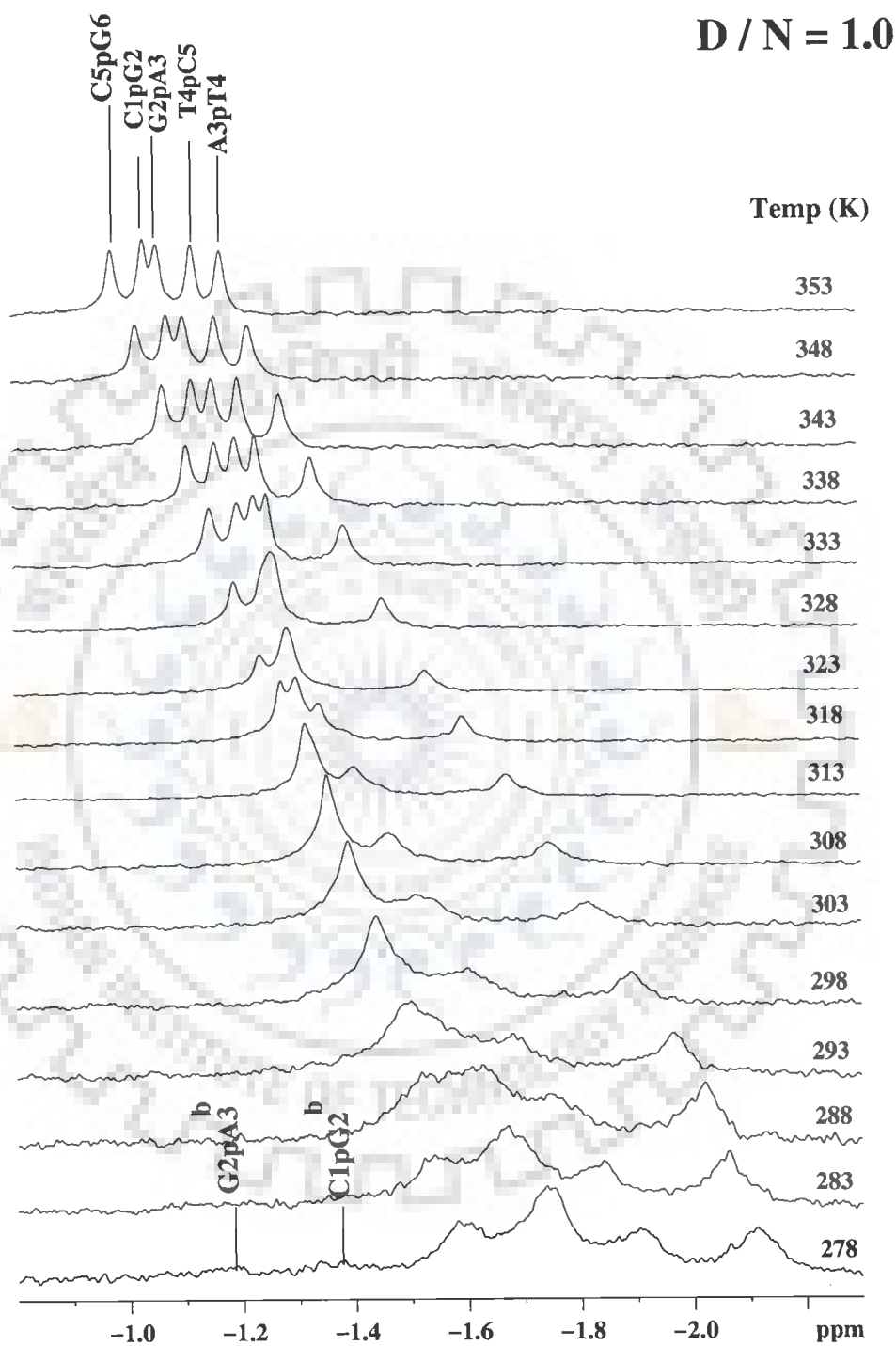
On the other hand adriamycin, nogalamycin and morpholinylodoxorubicin, which intercalate between two base pairs of DNA oligomer, lead to downfield shifts upto 1.25 ppm of phosphorus resonances at the intercalation site or at site adjacent to it. ³¹P chemical shift variations in nucleotides is the conformation of the phosphodiester groups at the level of the P–O5' and O3'–P bonds i.e. the values of torsional angles $\alpha = \text{O3}'\text{--P--O5}'\text{--C5}'$ and $\xi = \text{C3}'\text{--O3}'\text{--P--O5}'$. For a nucleotide in a B–DNA type conformation, the phosphate groups are normally found in gauche, gauche (g, g) conformation with α and ξ angles of -60° and -90° , respectively whereas the gauche, trans (g, t) conformation ($\alpha = -60^\circ$, $\xi = 180^\circ$) is generally associated with a deshielding of 1.5 ppm. Such transition from g, g to g, t on intercalation of drug chromophore by opening of adjacent base pairs at intercalation site from a distance of 3.4 to 6.8 Å have been reported in X–ray crystallographic structure of adriamycin and daunomycin to d–CGATCG, d–TGATCA, d–CGTACG sequences [38] as well in similar NMR structures [80]. The pyridopurine and berberine, which do show such large shifts in phosphorus resonances on binding to DNA, have

been shown to bind externally in the restrained molecular dynamics structures obtained by using experimental intermolecular interproton distances from NOESY spectra. Thus it may be inferred that binding of mitoxantrone to d-(CGATCG)₂ in present case may not lead to opening of base pairs, which is generally associated with down field shift of ³¹P resonance by ~1.25 ppm. The proton NMR results, discussed in next chapter however give a more explicit idea of the drug-DNA complex.

We have also examined the variation of ³¹P NMR spectra of d-(CGATCG)₂ and its 4 complexes with temperature. Figs. 5.5 and 5.6 show the NMR spectra and the variation of chemical shift. Table 5.5(a-d) lists the resonance positions at various temperatures. The signals are found to shift with temperature which may be due to shift in the following equilibrium reactions:



These reactions correspond to single strand transition, drug-DNA complexation and self association of mitoxantrone to form dimer molecules. It is observed that shift in ³¹P resonances in d-(CGATCG)₂ in the range 5°C–80°C are very gradual and not abrupt. This is consistent with the earlier observations [90] on change in δ with temperature due to helix to coil transition. The shift in base protons with temperature monitor stacking while the ³¹P shifts monitor change in backbone conformation, that is ester bond C4'–C3'–O3'–P and C3'–O3'–P–O5 which change from g⁻, g⁻ (ξ α) conformation seen in well stacked DNA duplex (typically B_I conformation) to t,



T:
in

Table 5.5a ³¹P chemical shift CGATCG - MTX complex (D / N = 1) as a function of temperature in the range 278–353 K.

Temp(K)	C1pG2 ^f	G2pA3 ^f	A3pT4 ^f	T4pC5 ^f	C5pG6 ^f
278	-1.696	-1.710	-2.071	-1.862	-1.540
283	-1.656	-1.668	-2.071	-1.837	-1.538
288	-1.602	-1.620	-2.015	-1.737	-1.513
293	-1.519	-1.555	-1.924	-1.640	-1.460
298	-1.448	-1.448	-1.893	-1.610	-1.448
303	-1.384	-1.384	-1.809	-1.503	-1.384
308	-1.394	-1.458	-1.741	-1.502	-1.394
313	-1.394	-1.394	-1.667	-1.431	-1.301
318	-1.346	-1.346	-1.591	-1.367	-1.257
323	-1.327	-1.327	-1.519	-1.307	-1.058
328	-1.307	-1.307	-1.451	-1.272	-1.160
333	-1.209	-1.272	-1.384	-1.261	-1.125
338	-1.175	-1.238	-1.326	-1.247	-1.111
343	-1.163	-1.211	-1.272	-1.244	-1.065
348	-1.143	-1.198	-1.216	-1.228	-1.088
353	-1.153	-1.172	-1.168	-1.238	-1.096
Δδ	+0.543	+0.534	+0.782	+0.624	+0.444

+ve Δδ indicates downfield shift

-ve Δδ indicates up field shift

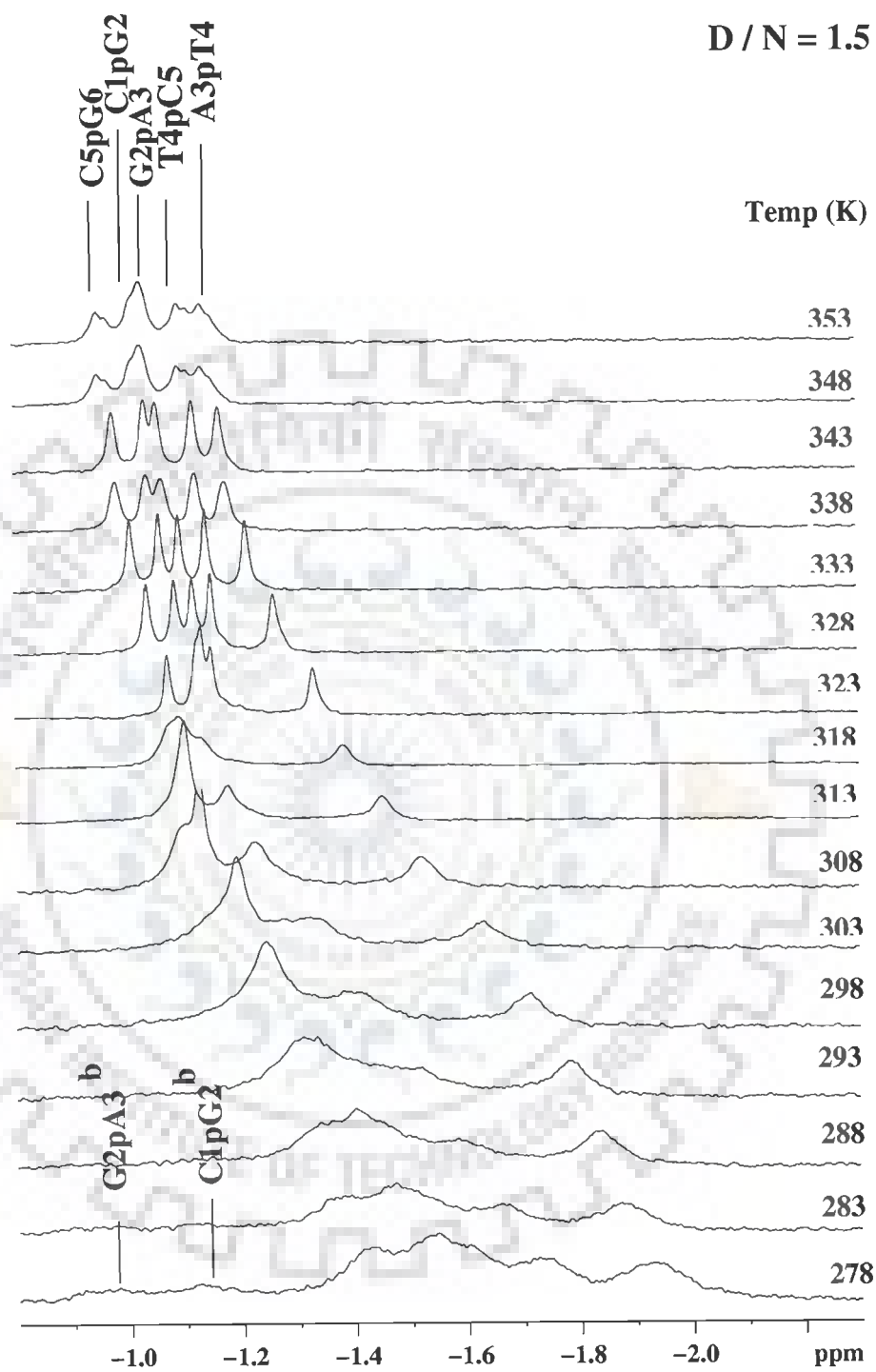


Table 5.5b ³¹P chemical shift CGATCG - MTX complex (D / N = 1.5) a function of temperature in the range 278–353 K.

Temp(K)	C1pG2	G2pA3	A3pT4	T4pC5	C5pG6
278	-1.694	-1.694	-2.074	-1.859	-1.578
283	-1.652	-1.652	-2.062	-1.818	-1.520
288	-1.575	-1.575	-2.010	-1.736	-1.508
293	-1.370	-1.370	-1.834	-1.508	-1.370
298	-1.338	-1.338	-1.796	-1.475	-1.338
303	-1.270	-1.270	-1.710	-1.373	-1.270
308	-1.231	-1.231	-1.642	-1.328	-1.231
313	-1.192	-1.192	-1.580	-1.280	-1.192
318	-1.152	-1.225	-1.512	-1.225	-1.152
323	-1.126	-1.126	-1.450	-1.190	-1.130
328	-1.140	-1.140	-1.417	-1.199	-1.140
333	-1.117	-1.117	-1.339	-1.117	-1.077
338	-1.091	-1.091	-1.272	-1.091	-1.029
343	-1.058	-1.087	-1.231	-1.115	-1.000
348	-1.513	-1.082	-1.209	-1.124	-1.0000
353	-1.065	-1.093	-1.211	-1.145	-1.012
$\Delta\delta$	+0.689	+0.534	+0.62	+0.714	+0.566

+ve $\Delta\delta$ indicates downfield shift

-ve $\Delta\delta$ indicates up field shift

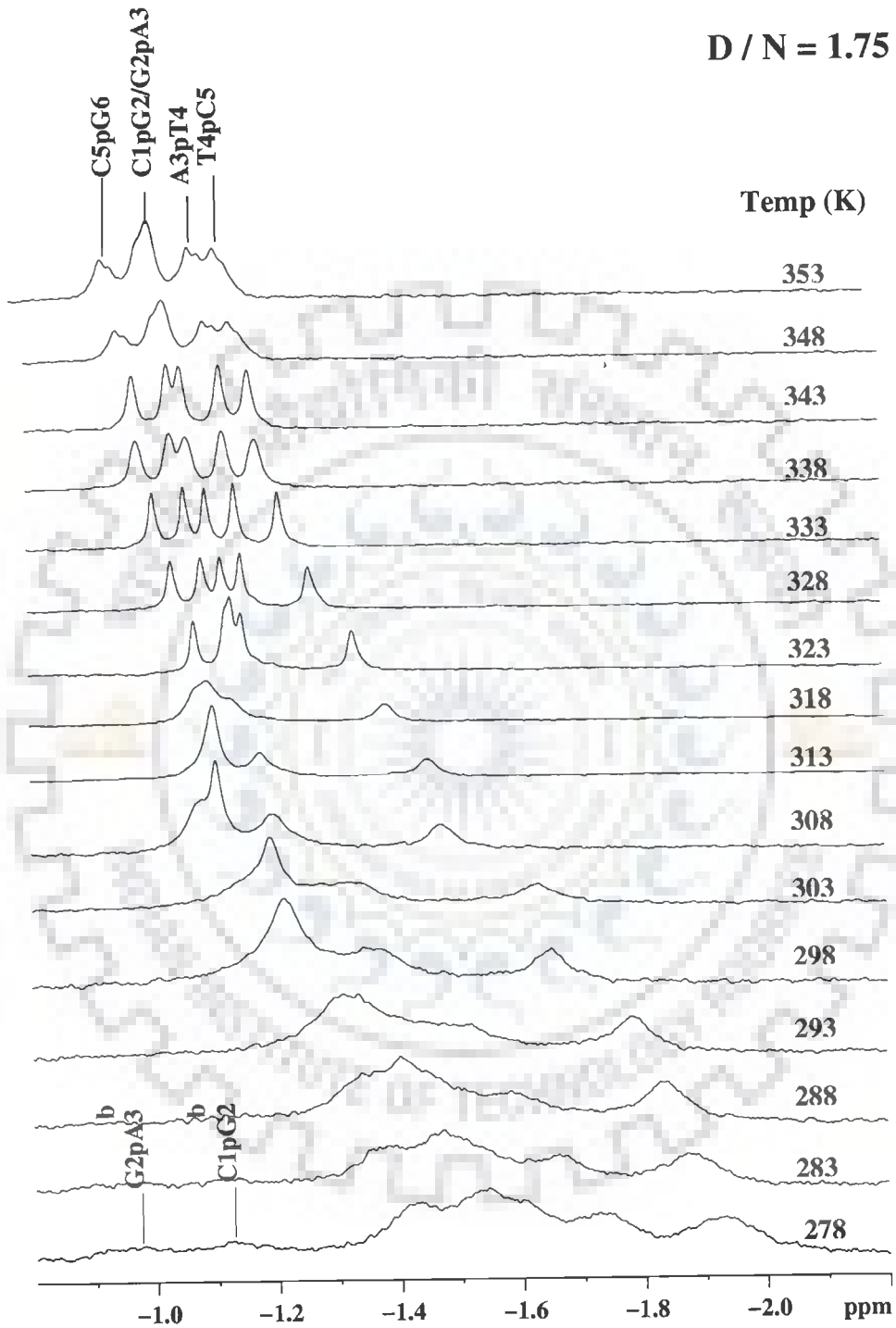


Fig 5.5(c)

T
u

Table 5.5c ³¹P chemical shift CGATCG - MTX complex (D / N = ~~2.70~~^{1.75}) as a function of temperature in the range 278–353K

Temp(K)	C1pG2	G2pA3	A3pT4	T4pC5	C5pG6
278	-1.685	-1.685	-2.073	-1.865	-1.573
283	-1.663	-1.663	-2.063	-1.851	-1.577
288	-1.577	-1.577	-2.012	-1.757	-1.510
293	-1.287	-1.310	-1.760	-1.491	-1.287
298	-1.252	-1.252	-1.721	-1.390	-1.252
303	-1.189	-1.189	-1.628	-1.319	-1.189
308	-1.167	-1.167	-1.560	-1.267	-1.128
313	-1.137	-1.137	-1.489	-1.214	-1.137
318	-1.120	-1.120	-1.412	-1.163	-1.091
323	-1.126	-1.134	-1.334	-1.152	-1.075
328	-1.099	-1.130	-1.260	-1.149	-1.034
333	-1.071	-1.106	-1.225	-1.153	-1.020
338	-1.053	-1.082	-1.174	-1.141	-0.981
343	-1.074	-1.094	-1.164	-1.160	-0.976
348	-1.076	-1.095	-1.134	-1.093	-0.950
353	-1.062	-1.080	-1.106	-1.086	-0.930
$\Delta\delta$	+0.623	+0.605	+0.886	+0.719	+0.570

+ve $\Delta\delta$ indicates downfield shift

-ve $\Delta\delta$ indicates up field shift

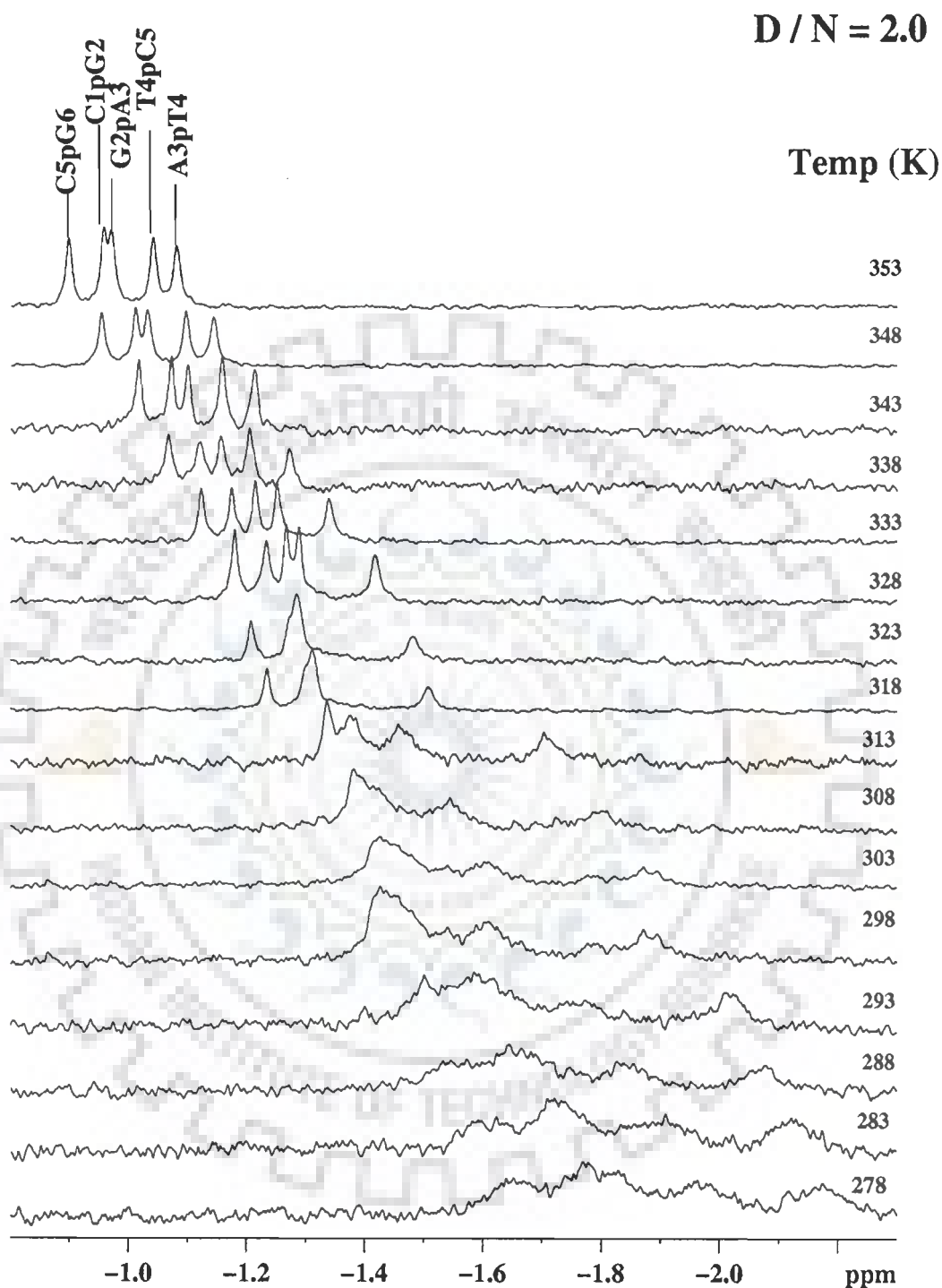


Fig 5.5(d)

Fig. 5.5 Proton decoupled ^{31}P NMR spectra $d\text{-(CGATCG)}_2$ complexed with mitoxantrone various D / N ratios (a) 1 (b) 1.5 (c) 1.75 (d) 2.0 as function of temperature.

Table 5.5d ³¹P chemical shift CGATCG–MTX complex (D / N = 2 .00) as a function of temperature in the range 278–353K

Temp(K)	C1pG2	G2pA3	A3pT4	T4pC5	C5pG6
278	-1.77	-1.77	-2.17	-1.963	-1.643
283	-1.721	-1.721	-2.12	-1.903	-1.59
288	-1.572	-1.572	-2.07	-1.74	-1.433
293	-1.500	-1.500	-2.01	-1.64	-1.400
298	-1.426	-1.426	-1.871	-1.603	-1.426
303	-1.426	-1.426	-1.871	-1.603	-1.426
308	-1.412	-1.422	-1.809	-1.540	-1.382
313	-1.374	-1.383	-1.7028	-1.456	-1.336
318	-1.299	-1.31	-1.509	-1.311	-1.234
323	-1.298	-1.312	-1.510	-1.312	-1.234
328	-1.233	-1.266	-1.418	-1.288	-1.179
333	-1.173	-1.213	-1.338	-1.250	-1.1216
338	-1.120	-1.150	-1.271	-1.204	-1.067
343	-1.190	-1.110	-1.220	-1.180	-1.040
348	-0.954	-0.101	-1.143	-1.096	-0.954
353	-0.957	-0.970	-1.080	-1.040	-0.898
$\Delta\delta$	+0.813	+1.613	+1.09	+0.923	+0.745

+ve $\Delta\delta$ indicates downfield shift

-ve $\Delta\delta$ indicates up field shift

resonances in the bound complex are also gradual but the total change, $\Delta\delta$, is somewhat higher in all the 4 complexes (Table 5a–d) as compared to that in free DNA. In 2:1 complex, the $\Delta\delta_{353K-278K}$ is comparatively large.

We have also looked into the chemical shift variation as a function of the drug to DNA duplex (D / N) ratio at various temperatures (Fig.5.6a–e) (278K) the ^{31}P signals from the bound DNA are in slow exchange with the corresponding signals in free DNA (Fig. 5.4). But at 45°C or above (318–353K) the signals are in fast exchange regime and are sufficiently narrow to be followed individually through the titration. The chemical shift at 45°C is an average position of that in free and bound state due to chemical exchange. The experimental results show that at 45°C the free d-(CGATCG)₂ is about 70% double helix. When bound to mitoxantrone, the DNA hexamer is more stabilized and may exist in duplex state to a comparatively higher extent; the binding acting as a stabilizing factor. The ^{31}P chemical shift, δ , as a function of D / N ratio at 45°C (Fig. 5.7b) shows that the variation in δ saturates as D / N tends towards 2. This is an indication of the fact that 2 drug molecules may be binding to one molecule of DNA complex. The results on proton NMR experiments, discussed in Chapter 6, provide a further insight into the drug–DNA interactions in the complex.

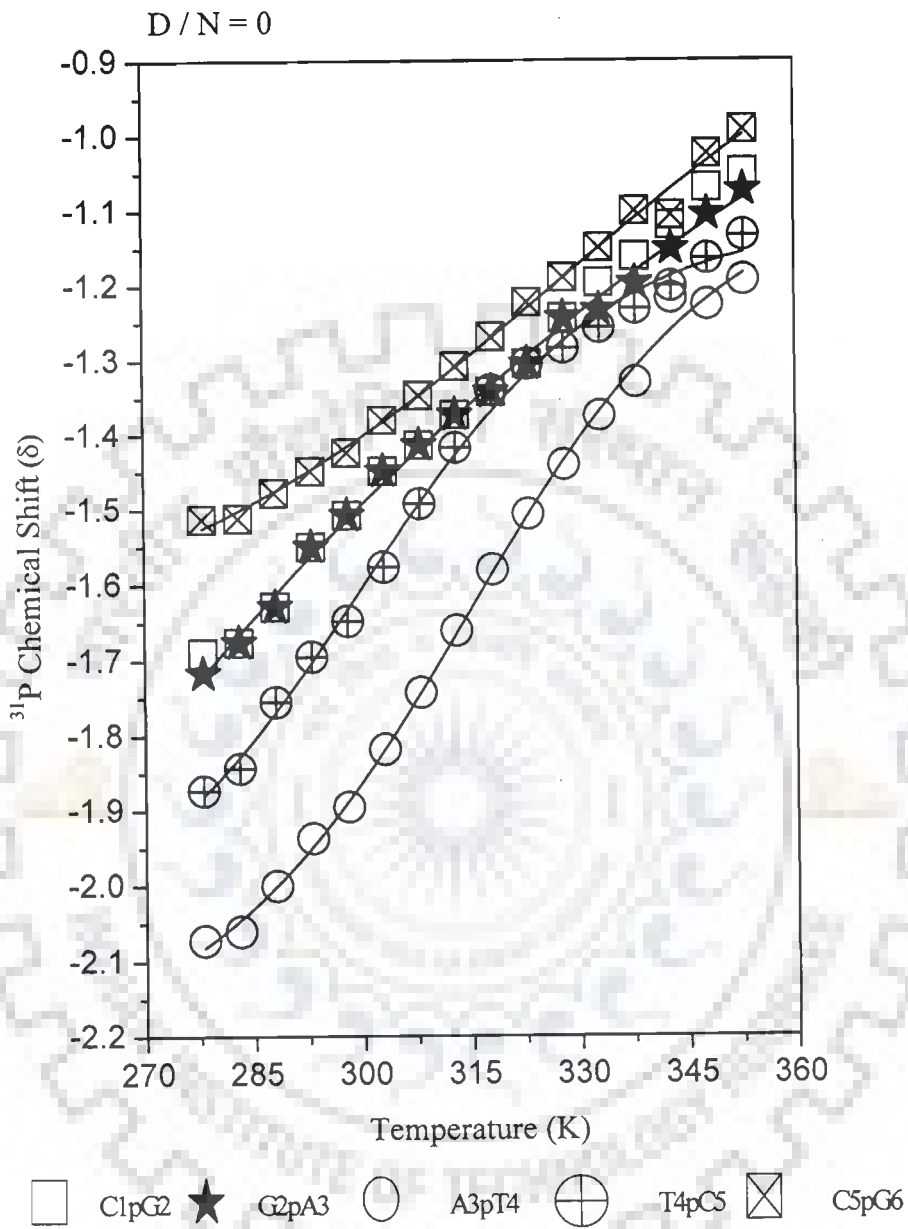


Fig. 5.6a

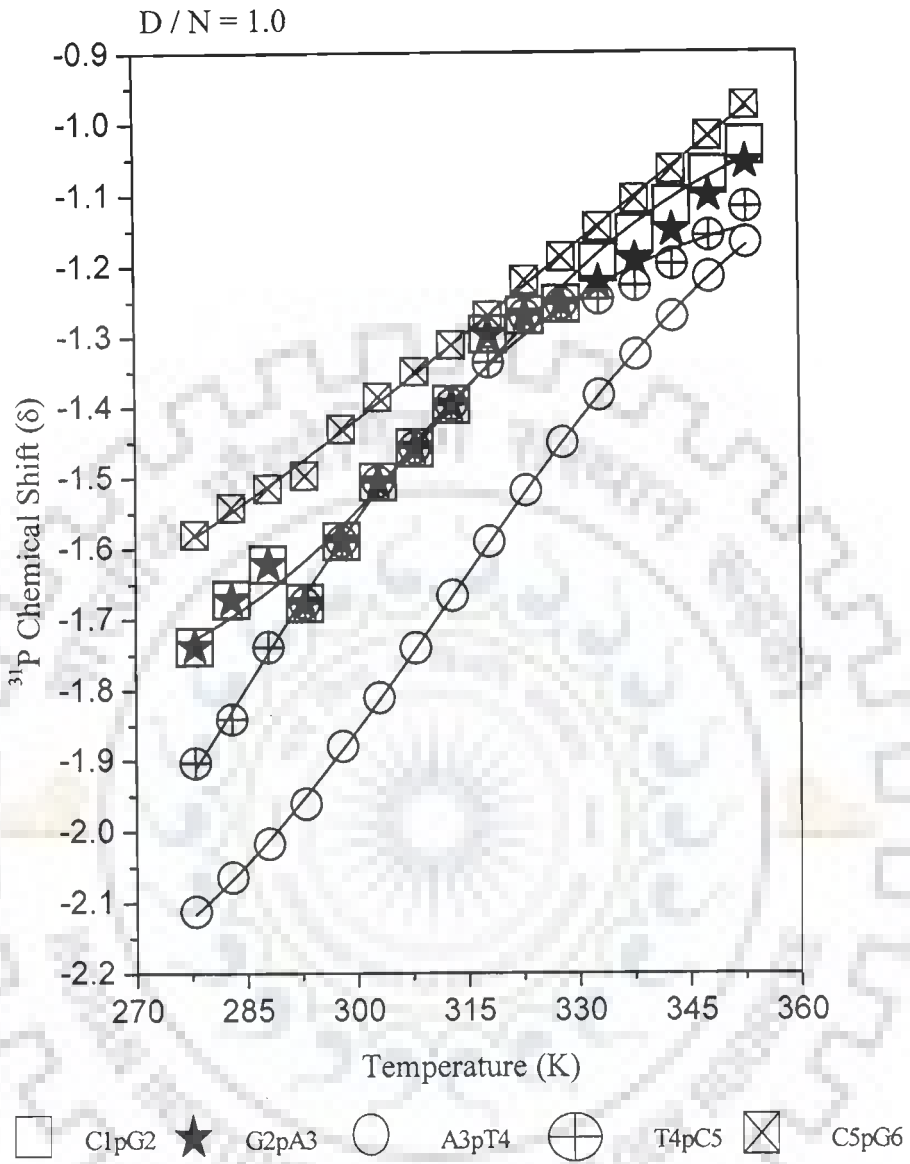


Fig. 5.6b

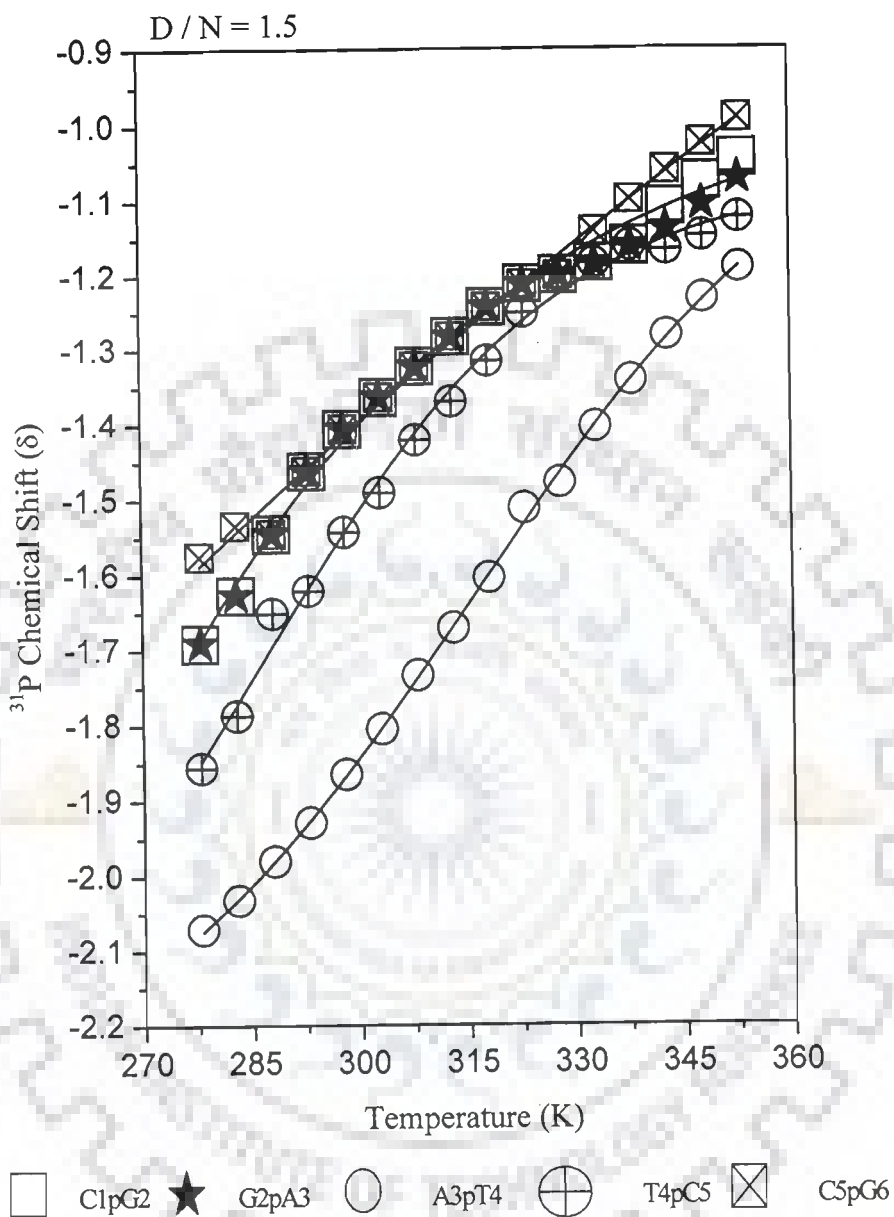


Fig. 5.6c

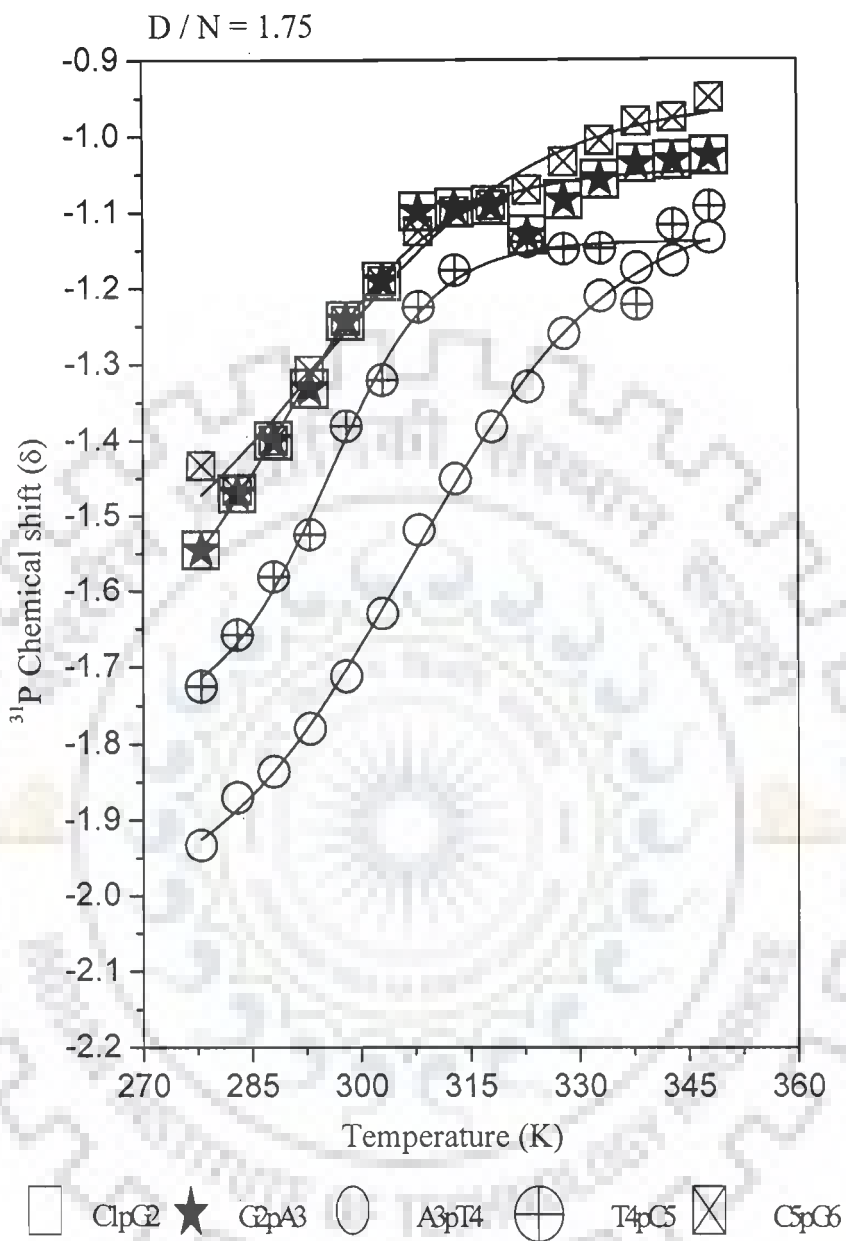


Fig. 5.6d

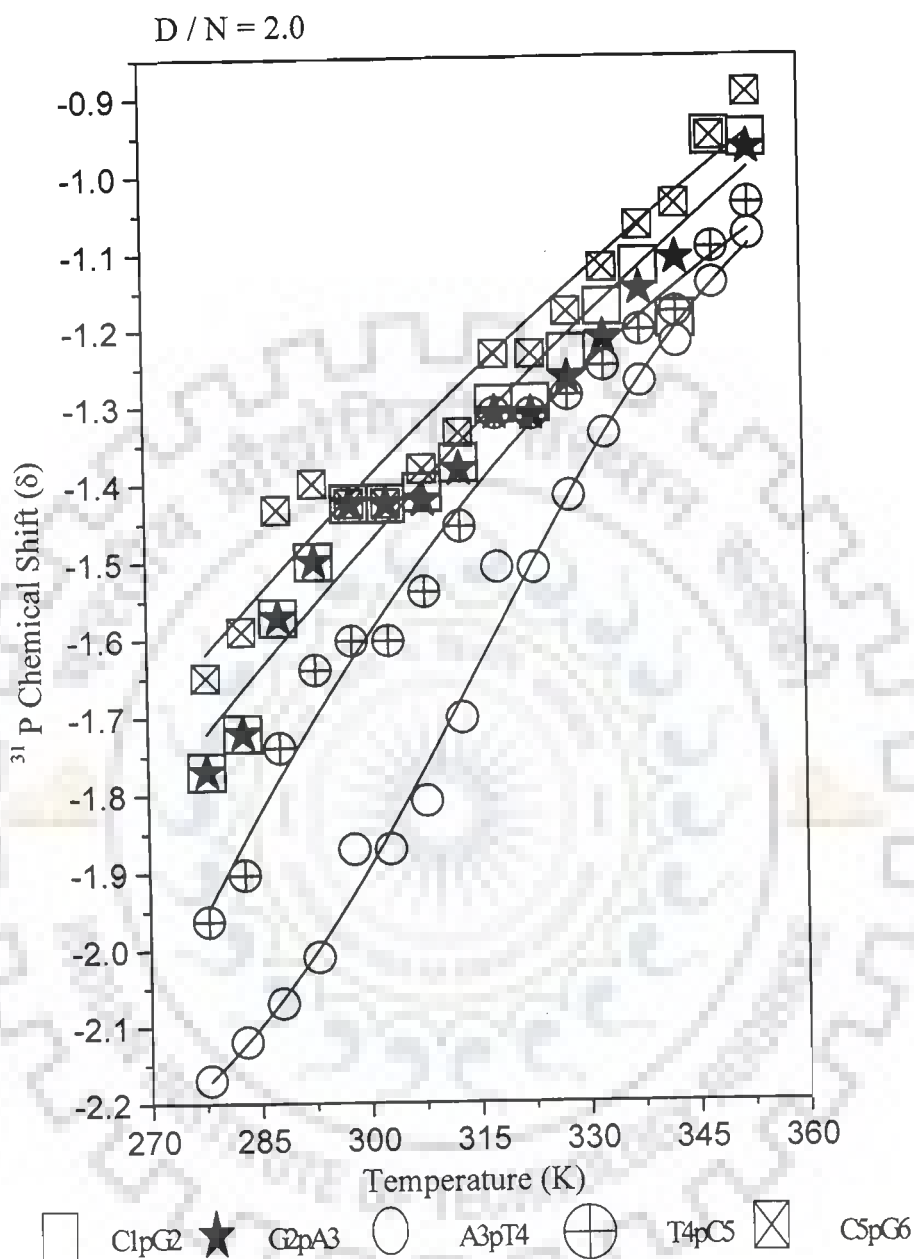


Fig. 5.6e

Fig. 5.6 ³¹P Chemical shift d-(CGATCG)₂ uncomplexed (a) and complexed with mitoxantrone at D / N ratios (b) 1 (c) 1.5 (d) 1.75 (e) 2.0 temperature in the range 278K-353K. At 278 K the ³¹P resonances from bound complex are in slow exchange with that of free DNA whereas at 318 K and above gives average position of these resonance due to fast exchange.

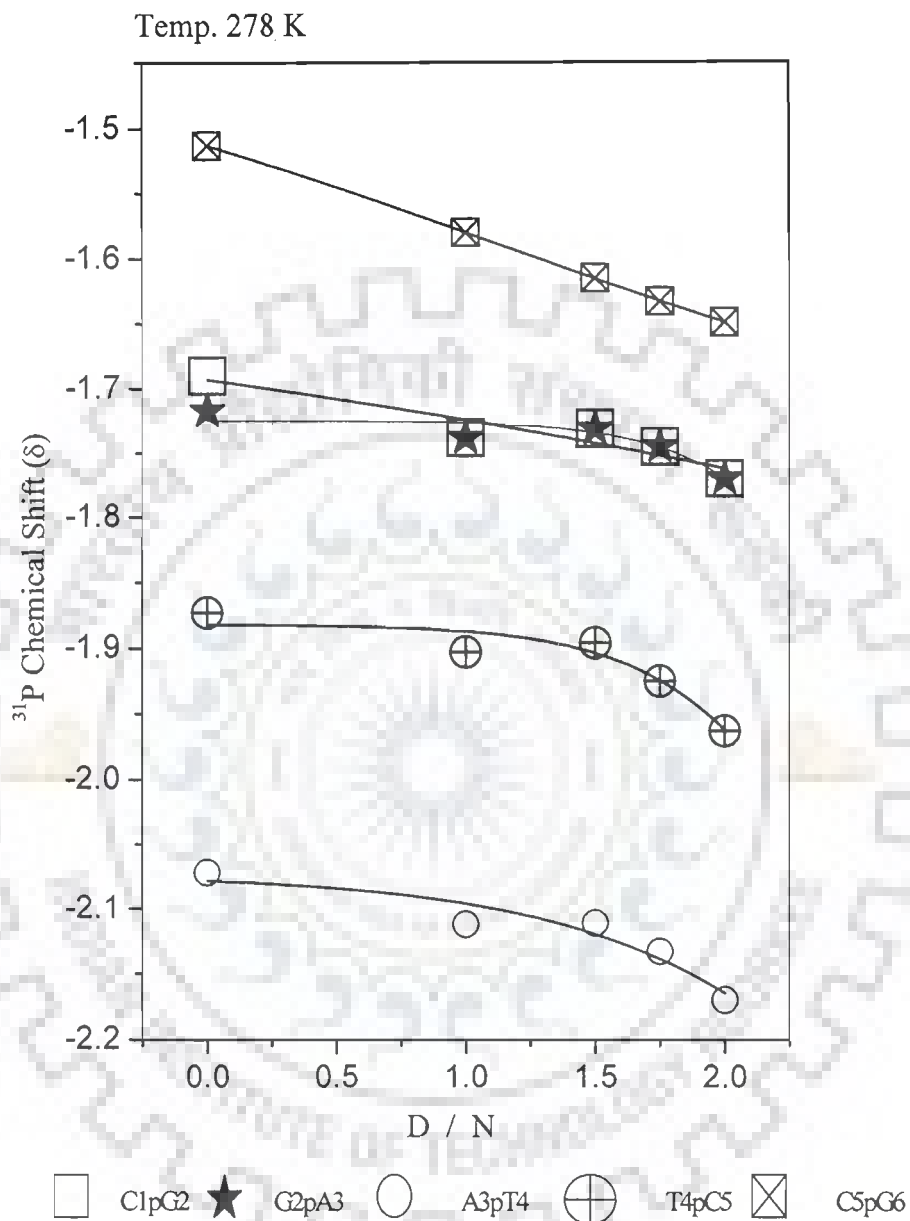


Fig 5.7a

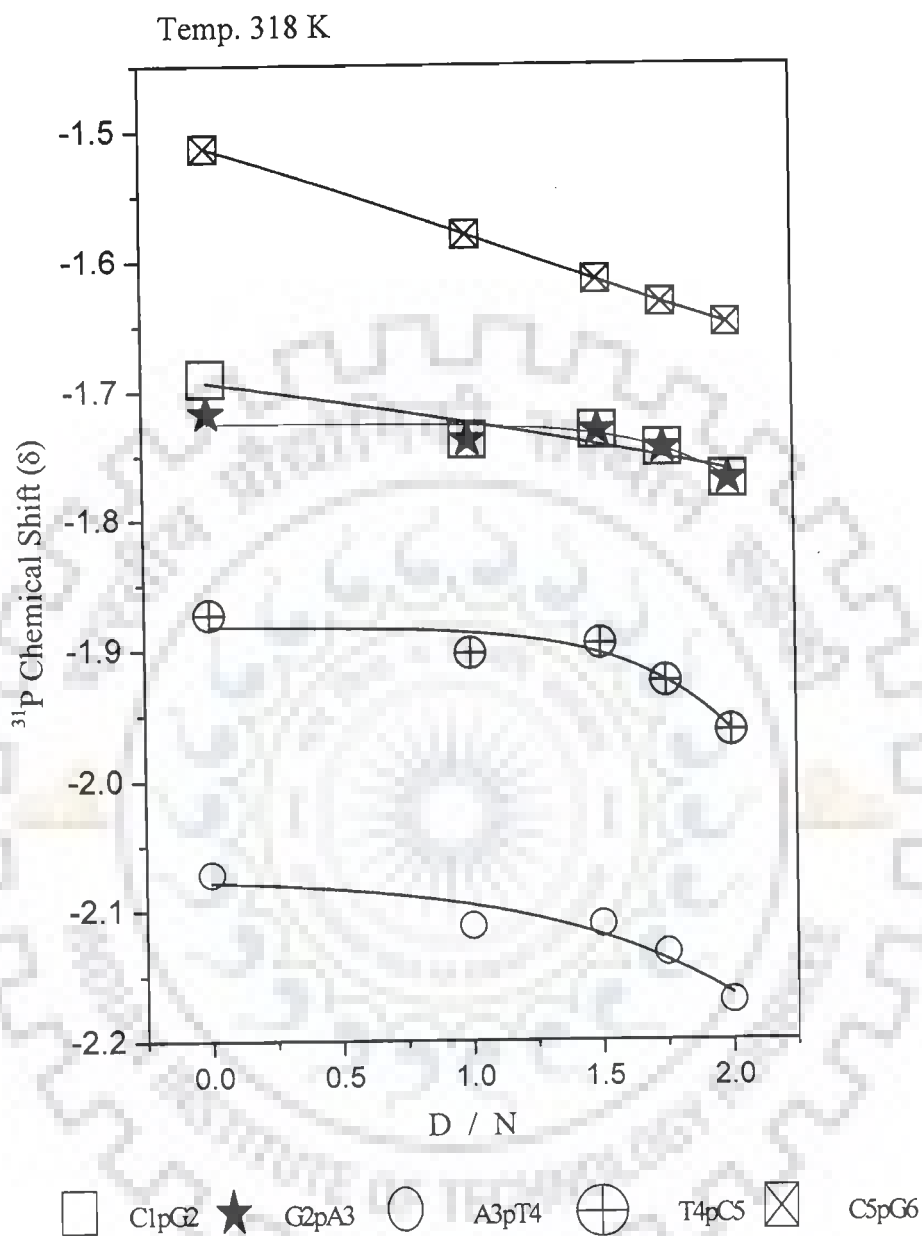


Fig. 5.7b

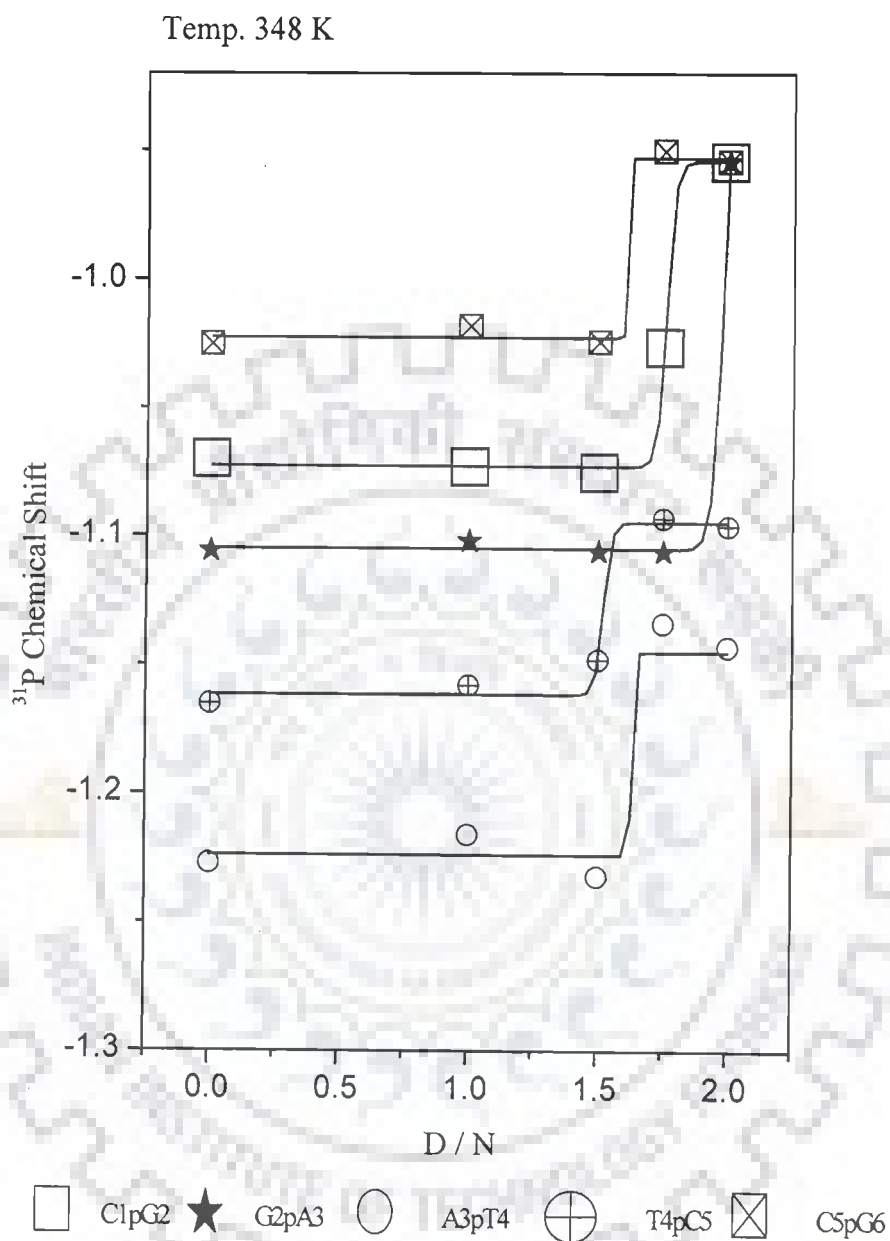


Fig. 5.7c

Fig. 5.7 ^{31}P chemical shift of $d\text{-(CGATCG)}_2$ complexed with mitoxantrone at various D / N ratios at (a) 278 K (b) 318 K (c) 348 K

Chapter 6

Proton NMR studies on binding of mitoxantrone with d-(CGATCG)₂

6.1 INTRODUCTION

The binding of mitoxantrone drug to deoxyhexanucleotide d-(CGATCG)₂ has been investigated by proton and phosphorus-31 NMR techniques by titrating the drug with oligomer. A known concentration of mitoxantrone is added successively to a fixed concentration of 1.64 mM (duplex concentration) oligomer to arrive at drug to DNA complex (D / N) stoichiometric ratios of 0.04, 0.10, 0.23, 0.34, 0.384, 0.456, 0.684, 0.95, 1.25, 1.50, 1.75 and 2.0. One dimensional ¹H and ³¹P NMR spectra are recorded at 5° C (278 K) for each complex. For the complex having D / N of 1 (exact ratio being 0.95), 1.5 and 1.75 and 2.0 one dimensional ¹H and ³¹P NMR as a function of temperature (278 K–353 K), two dimensional ¹H nuclear Overhauser effect spectra (NOESY) at 278 K at mixing times of 200 ms, 300 ms and 350 ms and ³¹P NOESY exchange spectrum at 278 K are also recorded. In this chapter, the ¹H NMR results of titrations of drug with DNA followed by change in chemical shift, analysis of NOE data, structural features of drug and DNA hexamer in the complex, and finally the drug–DNA contacts in mitoxantrone d-(CGATCG)₂ complex are described.

6.2 RESULTS AND DISCUSSION

6.2.1 TITRATION STUDIES

Fig. 6.1a–c shows the proton NMR spectra at 278 K on successive addition of drug to DNA. Fig. 6.1d shows a plot of area for d-(CGATCG)₂ and its complex at D / N ratio of 1. Most of the NMR experiments are carried out at 278 K as imino protons are sharpened and intensified at this temperature. Besides, DNA is expected to be present completely in duplex state at 278 K.

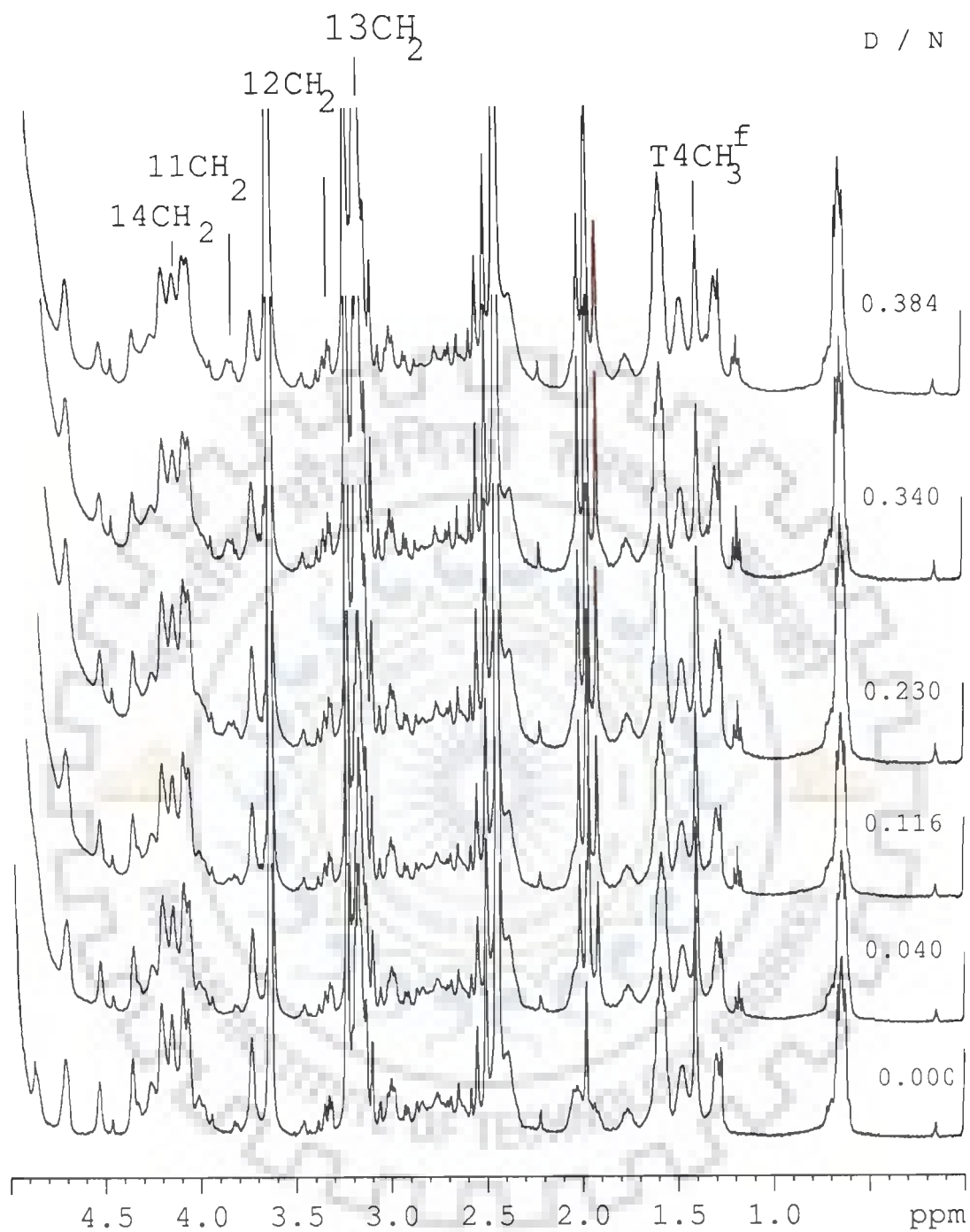


Fig. 6.1 a(i)

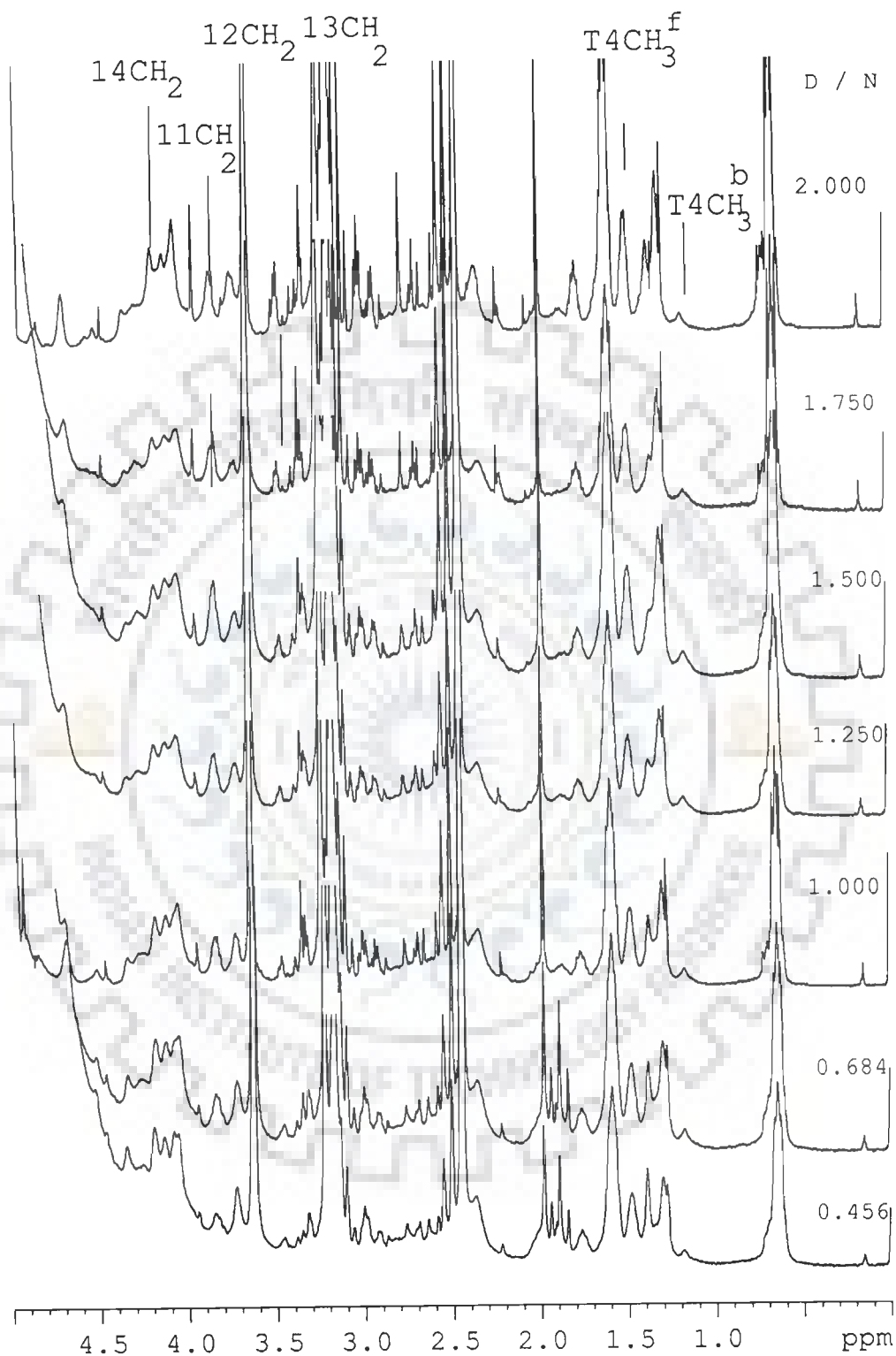


Fig. 6.1 a(ii)

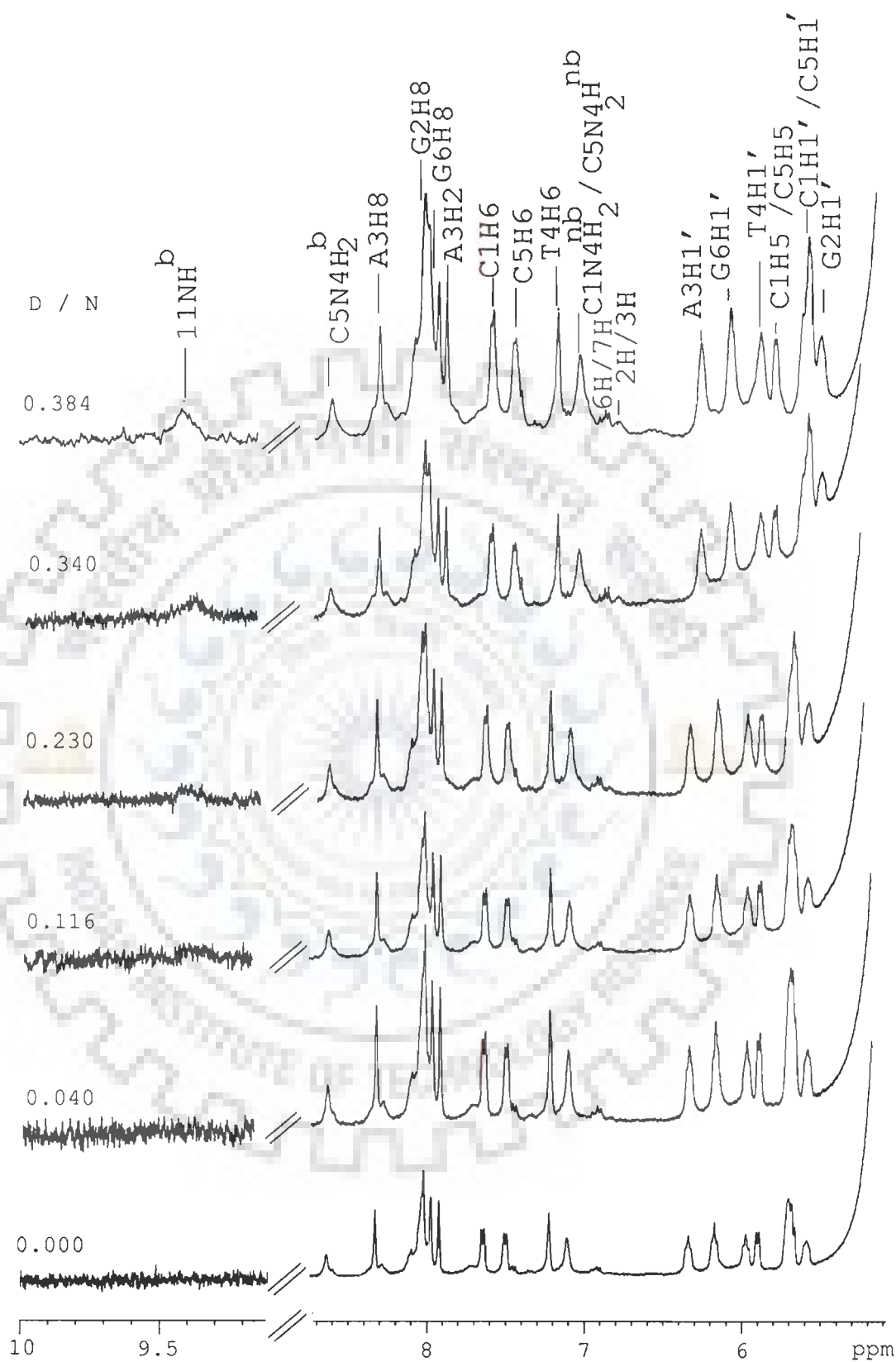


Fig. 6.1 b(i)

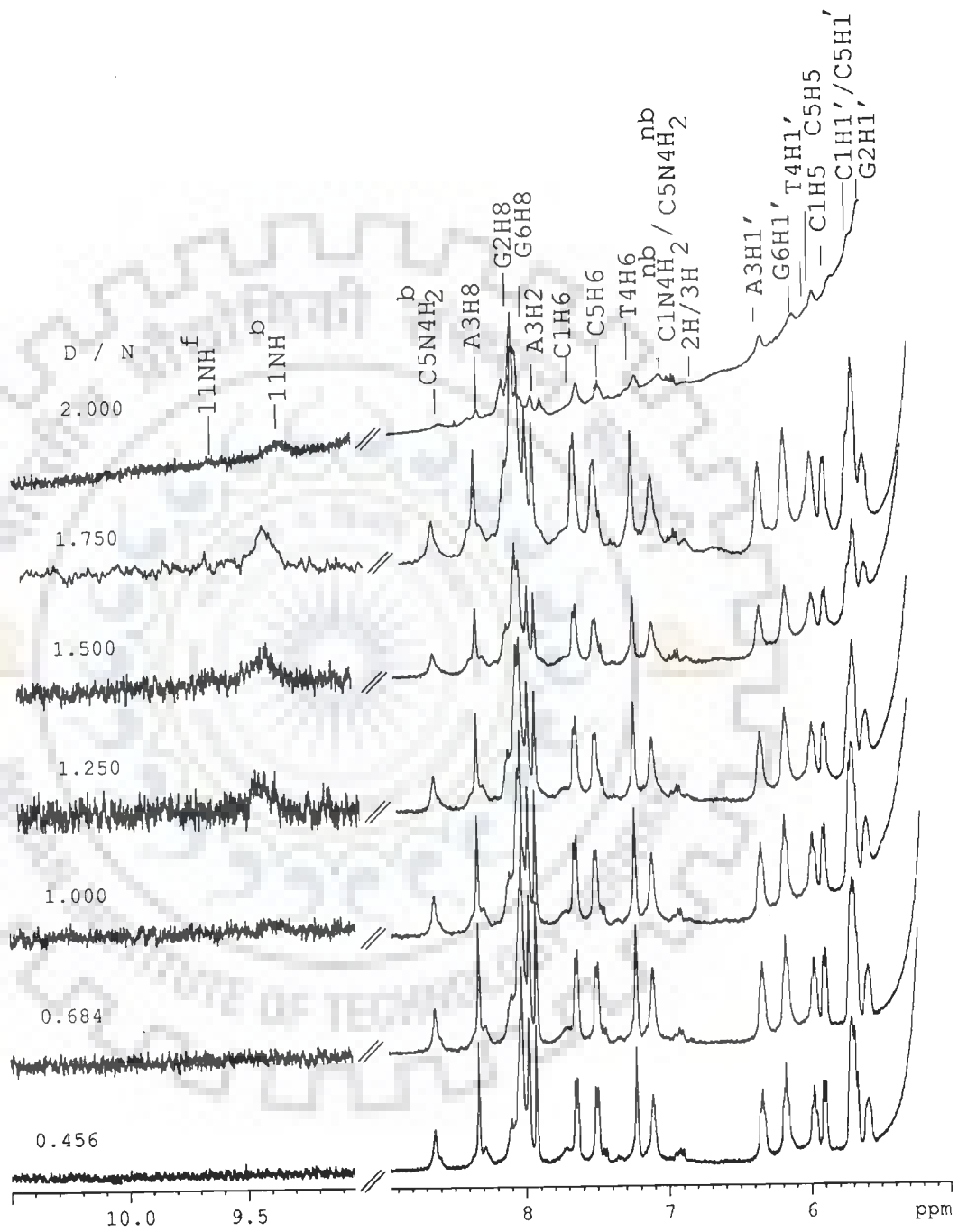


Fig. 6.1 b(ii)

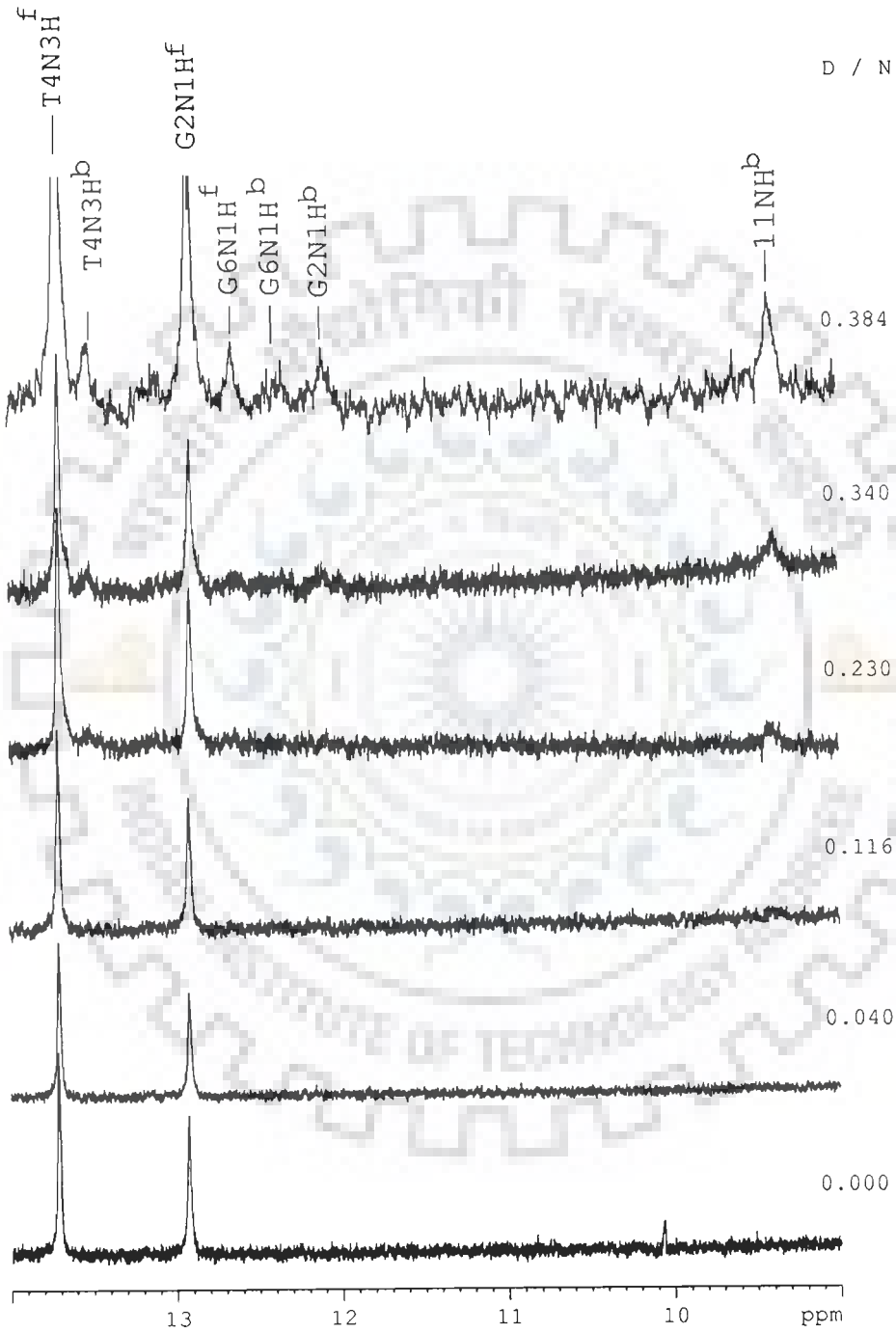


Fig. 6.1 c(i)

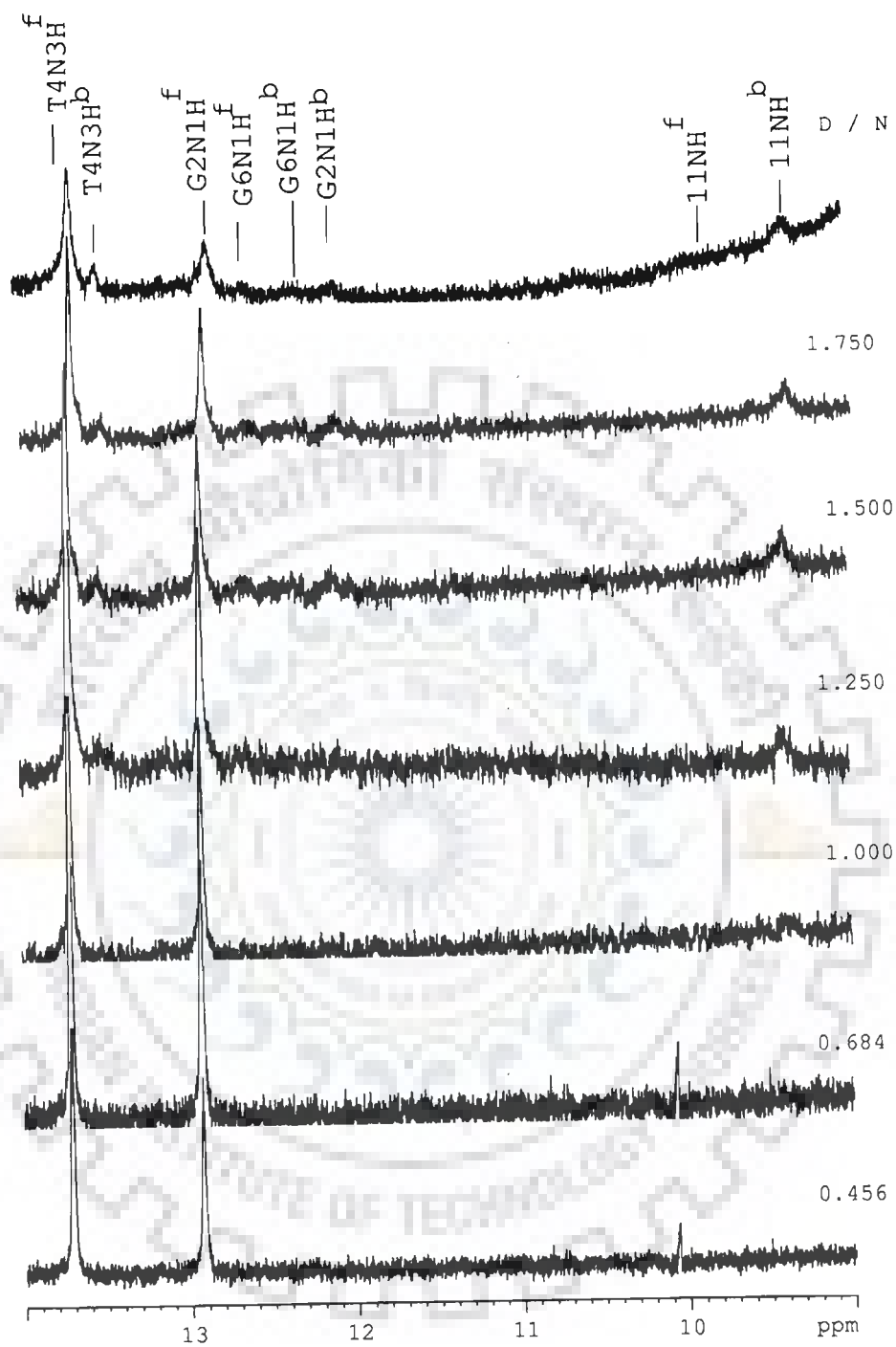


Fig. 6.1 c(ii)

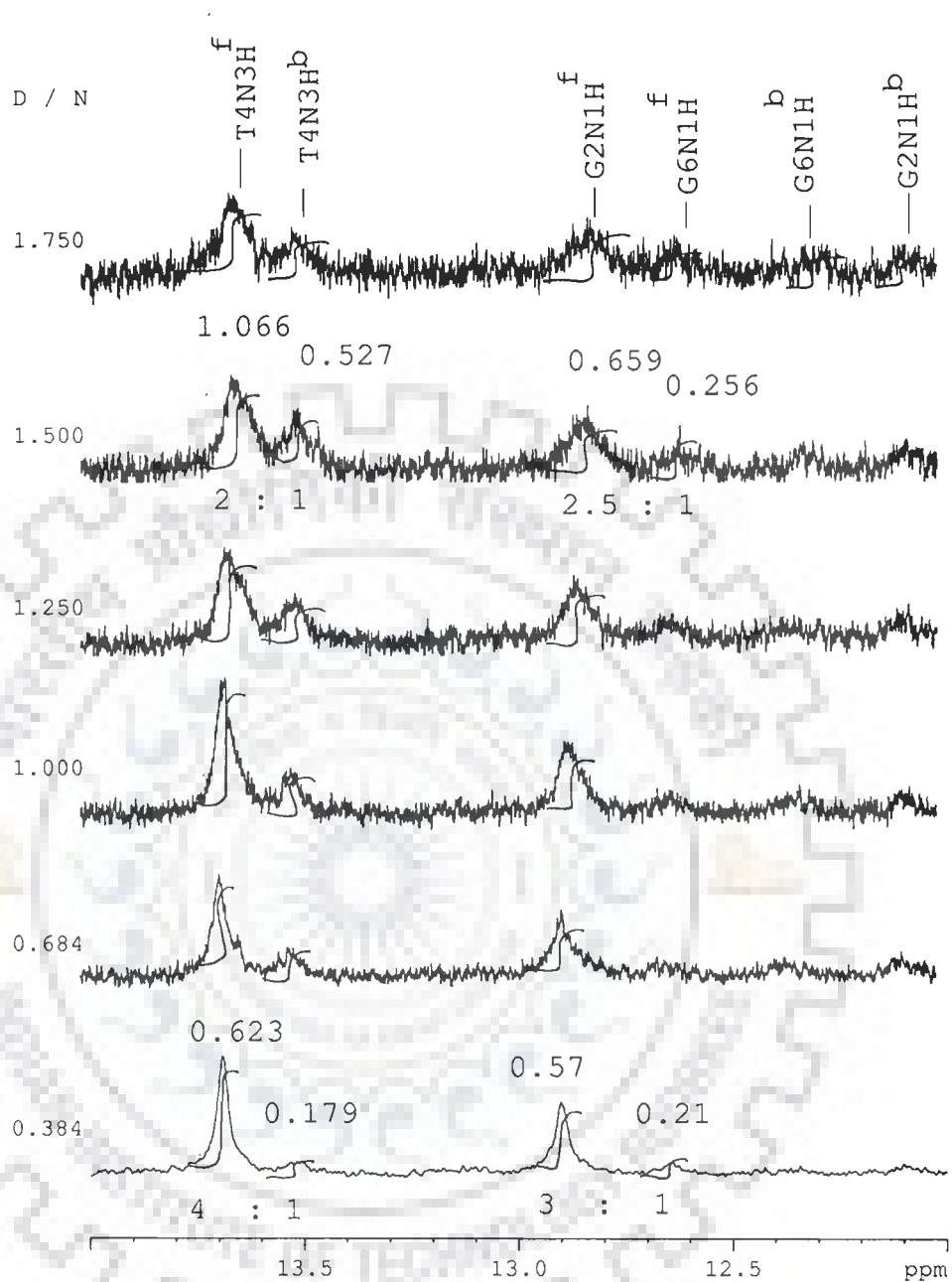


Fig. 6.1d

Fig.6.1 Expansions of the specific regions of the proton NMR spectra of complex of mitoxantrone with $d\text{-(CGATCG)}_2$ at various D / N ratios (a) 0–5 ppm (b) 5–9 ppm (c) 9–14 ppm (d) Area plot.

The assignment of spectral lines to specific proton of drug have been made by following strategies used for assignments in NMR spectra of uncomplexed drug described in Chapter 3. The assignments of nucleotide protons has been carried out by following strategies adopted for standard B-DNA structures that is, sequential NOEs (base H8/H6)_n-sugar (H1')_{n-1}, (base H8/H6)_n-sugar(H2'')_{n-1}, (base H8/H6)_n-sugar(H2')_{n-1}; expected NOEs due to several short intranucleotide distances [117] as well as our NMR data of uncomplexed d-(CGATCG)₂ published earlier [12]. The observation of the shifts on cumulative additions of drug to DNA, plot of area, Fig. 6.1d, further helped to resolve the overlapping resonance peaks and hence permitted unambiguous assignments.

The chemical shift of nucleotide base and sugar H1' protons as a function of D / N, is at shown in Table 6.1a and plotted in Fig. 6.2a. The same for drug protons are given in Table 6.1b and Fig. 6.2b. 2D NOESY experiments are carried out at 278 K for 1:1 complex and it was possible to ascertain the position of each and every proton resonance of drug as well as oligomer. The chemical shift positions of uncomplexed drug monomer / DNA, complexed 1:1 drug-DNA complex and the change in chemical shift due to binding are given in Tables 6.2a-b. It may be noted that the data of 10 μ M mitoxantrone has been taken to be that due to monomer (δ_{monomer}), as the drug is self-associated at higher concentrations δ^f , as discussed in previous chapters (although a lower concentration eg. 1 μ M would be ideally in monomeric state). NMR spectra of 4 drug-DNA complexes at different temperatures are shown in Fig. 6.3a-d. The chemical shift of base, H1' and drug protons for complexes with D / N ratio of 1, 1.5, 1.75, and 2.0 as a function of temperature are given in Tables 6.3-6.4 and Figs. 6.4-6.5. Sequence specific assignments are shown in Fig. 6.6(i-vii). Fig. 6.6a-b, Fig. 6.7a-d, Fig. 6.8a-c shows 2D NOESY spectra of mitoxantrone complexed to d-(CGATCG)₂ in the stoichiometric ratio of 1, 1.5, 1.75 respectively. At D / N = 2.0 considerable broadening has occurred.

The spectra of d-(CGATCG)₂ are well resolved. On addition of drug to DNA, new resonance peaks pertaining to drug protons start appearing which increase in intensity as D / N ratio increases. Sharp resonance peaks are observed up to D / N ~ 0.46. The spectral lines start broadening uniformly at D / N ~ 0.684 and higher ratios indicative of binding of DNA to drug. In uncomplexed or free d-(CGATCG)₂, NH peaks appear at 13.72 and 12.92 ppm, respectively while the G6NH resonance is not seen. This may be attributed to increased fraying at the end of DNA which leads to a significant exchange of NH proton with that of water solvent. On successive addition of mitoxantrone to DNA, four additional resonance peaks are observed in this region at 13.52, 12.62, 12.32, 12.12 ppm at D / N = 1.75 besides the 11 NH peak at about 9.39 ppm. The 2D NOESY spectra (Fig. 6.6a) showed that pairs of protons resonating at 12.12, 12.92; 13.52, 13.72; and 12.32, 12.62; shows cross peaks with each other. Since T4NH and G2NH appear at 13.72 and 12.92 ppm in uncomplexed / free d-(CGATCG)₂, the peaks at 13.52 and 12.12 ppm get assigned to T4NH and G2NH in the d-(CGATCG)₂ complexed to drug at D / N = 1.0 (designated as T4NH^b and G2NH^b). The remaining pair (12.62, 12.32 ppm), by elimination gets assigned to G6NH present in free (G6NH^f at 12.62 ppm) and bound state (G6NH^b at 12.32 ppm). The area under the NH peaks, (Fig. 6.1d), confirmed that the T4NH / G2NH / G6NH indeed splits in to two sets of peaks. The ratio of area of uncomplexed to complexed T4NH decreased from 4:1 (approximately) for D / N ratio of 0.384 to 2:1 for D / N ratio of 1.5 that is, on addition of increased amount of drug to DNA, as expected. It is noted that the intensity of G6NH peaks is significantly lesser than that of G2NH and T4NH. Also the NOE cross peaks of G6NH^f (12.62 ppm) and G2NH^f (12.92 ppm) resonance corresponding to a distance of 3.7 Å in standard B-DNA structures, is considerably weaker in intensity than the NOE cross peak of T4NH^f (13.72 ppm) and G6NH^f (12.62 ppm) which correspond to a distance of 3.72 Å. This indicates that G6NH proton which completely exchanges with water in free d-

(CGATCG)₂, is immobilized in the drug–DNA complex although it still is fraying to some extent being the terminal base pair of DNA. For the same reason, the line width of G6NH is also greater than that of G2NH and T4NH.

It is observed that the sharp T4CH₃ peak appearing at 1.38 ppm in d-(CGATCG)₂ decreases in intensity as D / N ratio increase and a new, relatively broad, peak appearing at 1.17 ppm starts growing in intensity with D / N (Fig.6.1a); the same is also manifested in the area plots Fig. 6.1b shows that these two peaks exchange with each other and hence the peak at 1.17 ppm gets assigned to T4CH₃ of DNA bound to the drug molecule (designated hereafter as T4CH₃^b). It is noted that T4CH₃^b shows all expected interproton NOE connectivities, that is, to A3H2', A3H2'' (Fig. 6.6b), C5H6, A3H8, T4H6, C5NH₂^{nb}, A3H1' (Fig. 6.6c), but are weaker in intensity than the corresponding NOEs of T4CH₃^f protons resonating at 1.38 ppm.

The 11 NH resonant peak of the drug appearing at 9.39 ppm increases in intensity with D / N ratio. However in addition, another peak starts appearing at 9.73 ppm which is somewhat clear at D / N = 1.75 (Fig. 6.1b). These two resonances shows chemical exchange in 2D NOESY spectra (Fig. 6.8b) and both the resonances shows NOE cross peak with 12CH₂ and 13CH₂ protons (Table 6.6). Since most of the drug is in bound state in complex having lowest D / N ratio, the resonance peak at 9.39 ppm is assigned to 11NH proton in the bound species, designated as 11NH^b, while that at 9.72 ppm is the corresponding proton in free state, that is 11NH^f as D / N increases more and more drug exist in free state and the intensity of 9.72 ppm peak increases. This is further corroborated by the fact that the resonance at 9.39 ppm (11NH^b) shows intermolecular NOE crosspeaks with specific nucleic acid protons (Table 6.7, Fig. 6.8b.) that at 9.72 ppm (11NH^f) does not give any such intermolecular connectivity.

The existence of two sets of T4NH, G2NH, G6NH, T4CH₃ and 11NH (drug) clearly demonstrates that the drug thus indeed binds to the DNA hexamer and there is a slow exchange of free and bound DNA on NMR time scale at 278 K.

The palindromic symmetry of the system implies that two intercalative sites are available for the drug. The change in chemical shift ($\Delta\delta$) of base and H1' protons with D / N ratio are gradual (Fig. 6.2a) and small in magnitude. The $\Delta\delta$ increases with D / N ratio as more and more DNA oligomer binds to the drug a maximum of 0.12 to 0.14 ppm upfield shift is observed for C1H5, C1H1' and G6H1' protons. All the bound imino protons on the DNA oligomer are upfield shifted with respect to the corresponding imino protons in free state (Table 6.2a, Fig. 6.6a); the shift being 0.80, 0.20 and 0.30 ppm for G2NH; T4NH and G6NH, respectively. Such changes may be attributed to stacking or structural changes in complexation which may be compensatory in nature.

The shift in drug protons on binding is expected to be maximum at low D / N ratio when maximum amount of drug is present in the bound state we do not observe any significant variation of δ with D / N ratio. The ring protons, 6H / 7H and 2H / 3H, shift upfield substantially up to 0.45 ppm with respect to the chemical shift position of drug monomer (that is that at 10 μ M or lower concentration) in 1:1 drug to DNA complex at 278 K (Table 6.2b). The 11NH proton shifts upfield by 0.86 ppm. The shift in the 11CH₂, 12CH₂, 13CH₂ and 14CH₂ protons is not significant, it being up to \sim 0.2 ppm at 278 K. Large upfield shifts in 11NH, 6H / 7H and 2H / 3H protons on binding demonstrate that aromatic chromophore of mitoxantrone is well stacked with base pairs of DNA. Some of the drug is in free state at D / N = 1, the concentration of which is likely to be in mM range and hence expected to be in self-associated form (Chapter 3).

Difference in chemical shift, $\Delta\delta = \delta^b - \delta^f$, is 0.33 ppm (upfield) for 11NH proton (Table 6.2b) while it is 0.17–0.19 ppm downfield for 6H / 7H and 2H / 3H protons. Apparently the 6H / 7H and 2H / 3H protons are better stacked in self-associated mitoxantrone dimer as compared to that in drug–DNA complex. It is not noteworthy that 14 OH proton which exchanges with water and does not show up in the spectra of uncomplexed mitoxantrone in water, appears at 6.6 ppm in the spectra of drug–DNA complex. It gives strong intramolecular cross peaks with 6H / 7H protons (Fig. 6. 6e). Apparently 14OH participates in binding and gets immobilized. We also followed the ^1H resonance signals on addition of increasing amount of drug at D / N ratio of 1, 1.5, 1.75 and 2.0 in the temperature range 278 K–353 K at steps of 5 K. These NMR spectra are shown in Fig. 6.3a–d. At temperature of 318 K and above, the signals are in fast exchange regime and are sufficiently narrow to be followed individually through the titration. It is observed that the variation of chemical shift with temperature (Fig. 6.4–6.5) is not significant for both nucleic acid and drug protons and the change is practically negligible in the range 278–303 K (Table 6.3a–d and 6.4a–d). This indicates that structurally only one complex is being formed and the chemical shift at any one temperature is average of bound and unbound DNA / drug instead of being average of several structures, the equilibrium of which is likely to shift with temperature. In case T4NH, G2NH, G6NH, T4CH₃ and 11NH there is slow chemical exchange of signals belonging to bound species (shifted upfield) with those of same protons in the free State; however only one bound species observed as also confirmed by area plots. The gradual and low net change with temperature (Fig. 6.4) may be due to several reasons such as destacking / decreased intercalation, duplex to single strand transition, etc. At 318 K for instance, the free DNA may only be 65% (average) duplex but when bound to an intercalator drug, such as mitoxantrone (since it has 3 conjugated planar aromatic rings), it may entirely exist as duplex, with intercalation / stacking acting as a stabilizing factor. Among drug protons, the change in

chemical shifts with temperature is observed to the maximum for ^{11}NH protons, which are presumably close to oligomer due to stacking of mitoxantrone chromophore with base pair of DNA. These changes in chemical shift presumably due to structural alterations in drug–DNA complex cannot be correlated directly to a specific structural parameter and hence not a sufficient marker of interaction. Therefore one needs to look at the structure of the specific complex by alternate ways, such as interproton contacts.



Table 6.1a Chemical shift (ppm) of nucleotide protons as a function of drug (D) to nucleic acid duplex (N) ratio, D/N, at 278 K. Also shown here is the change in chemical shift on binding, that is, $\Delta\delta = \delta_{(D/N=2.00)} - \delta_{(D/N=0.00)} = \delta_{total} = \delta^b_{(D/N=2.00)} - \delta^f$.

D/N	C1H6	G2H8	A3H8	T4H6	C5H6	G6H8	C1H5	A3H2	C5H5
0.000	7.64	8.02	8.33	7.22	7.50	7.98	5.90	7.92	5.70
0.040	7.64	8.02	8.32	7.22	7.50	7.97	5.90	7.92	5.69
0.116	7.63	8.02	8.32	7.22	7.50	7.96	5.88	7.92	5.70
0.230	7.63	8.01	8.31	7.21	7.48	7.95	5.88	7.90	5.70
0.340	7.62	8.00	8.31	7.21	7.47	7.95	5.87	7.90	5.69
0.384	7.61	8.03	8.31	7.21	7.47	7.95	5.87	7.90	5.69
0.456	7.60	8.00	8.31	7.20	7.46	7.94	5.86	7.89	5.69
0.684	7.60	8.00	8.30	7.20	7.46	7.93	5.84	7.88	5.69
1.000	7.60	7.99	8.29	7.20	7.45	7.92	5.83	7.88	5.68
1.250	7.59	7.99	8.28	7.19	7.44	7.91	5.80	7.85	5.68
1.500	7.57	7.99	8.28	7.17	7.43	7.90	5.78	7.84	5.67
1.750	7.57	7.99	8.28	7.17	7.43	7.90	5.76	7.84	5.67
2.000	7.58	8.00	8.28	7.17	7.43	7.87	5.81	7.84	5.67
$\Delta\delta$	-0.06	-0.02	-0.05	-0.05	-0.07	-0.11	-0.09	-0.08	-0.03

D/N	C1H1'	G2H1'	A3H1'	T4H1'	C5H1'	G6H1'	T4CH ₃ ^f	T4CH ₃ ^b
0.000	5.68	5.59	6.34	5.97	5.66	6.17	1.40	-
0.040	5.68	5.58	6.34	5.97	5.66	6.17	1.40	-
0.116	5.68	5.59	6.34	5.97	5.68	6.17	1.40	-
0.230	5.67	5.58	6.33	5.96	5.65	6.15	1.39	-
0.340	5.66	5.58	6.32	5.95	5.66	6.15	1.39	1.18
0.384	5.66	5.58	6.32	5.96	5.64	6.14	1.39	1.18
0.456	5.64	5.56	6.32	5.95	5.64	6.13	1.39	1.18
0.684	5.62	5.56	6.31	5.94	5.62	6.12	1.38	1.18
1.000	5.60	5.56	6.31	5.94	5.60	6.11	1.38	1.17
1.250	5.60	5.54	6.30	5.93	5.60	6.09	1.37	1.17
1.500	5.57	5.51	6.28	5.92	5.57	6.06	1.36	1.16
1.75	5.56	5.50	6.28	5.92	5.56	6.05	1.35	1.17
2.00	5.57	5.51	6.29	5.93	5.6	6.06	1.35	1.17
$\Delta\delta$	-0.11	-0.08	-0.05	-0.04	-0.06	-0.11	-0.05	-0.01

-ve $\Delta\delta$ indicates upfield shift

+ve $\Delta\delta$ indicates downfield shift.

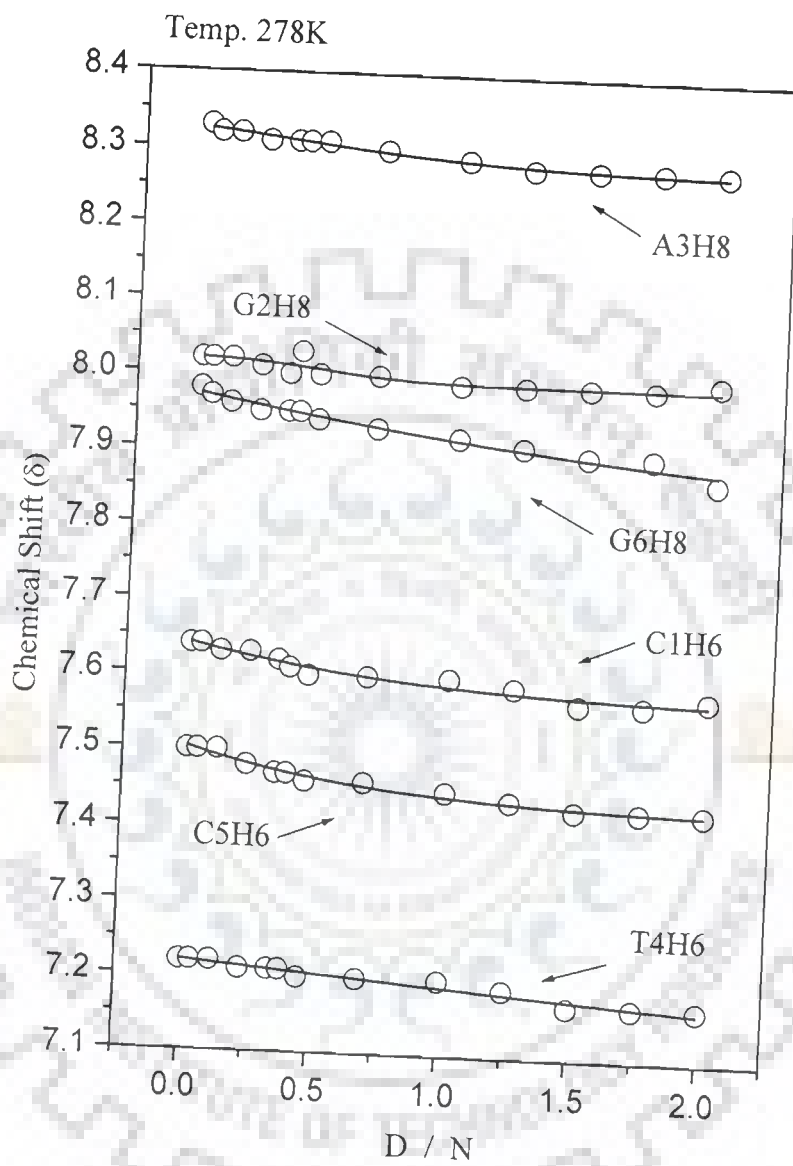


Fig. 6.2 a(i)

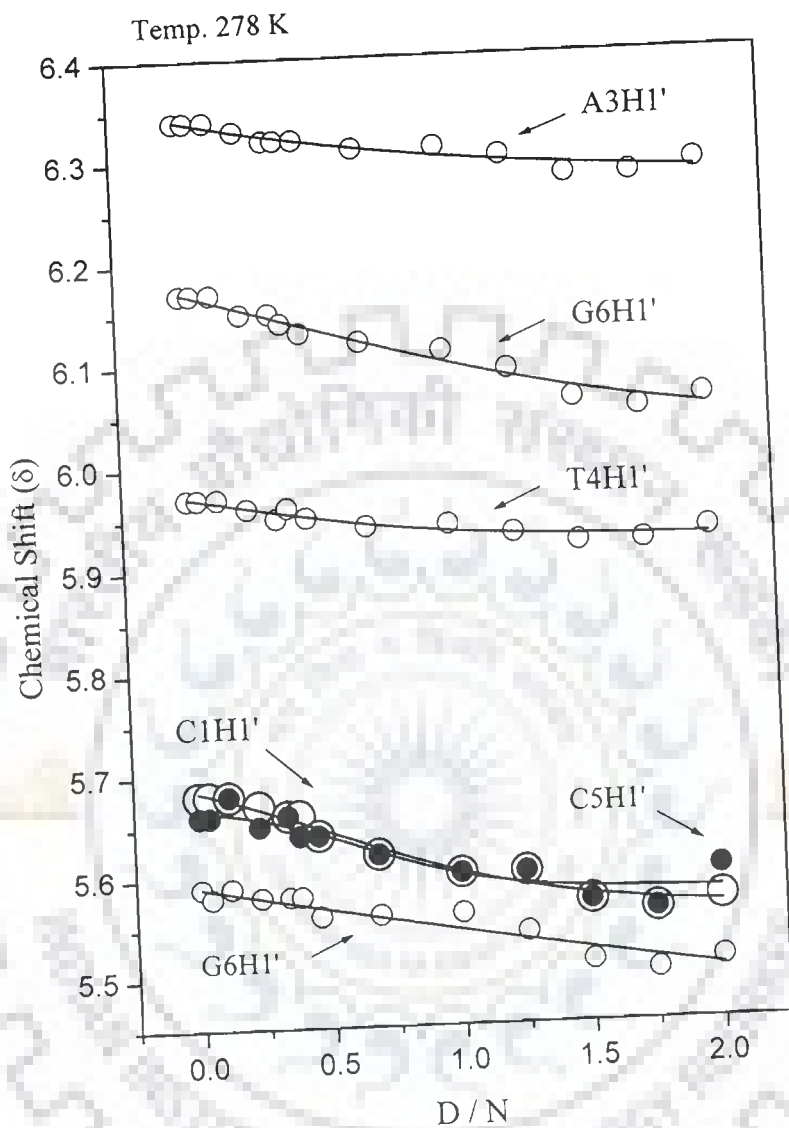


Fig. 6.2 a(ii)

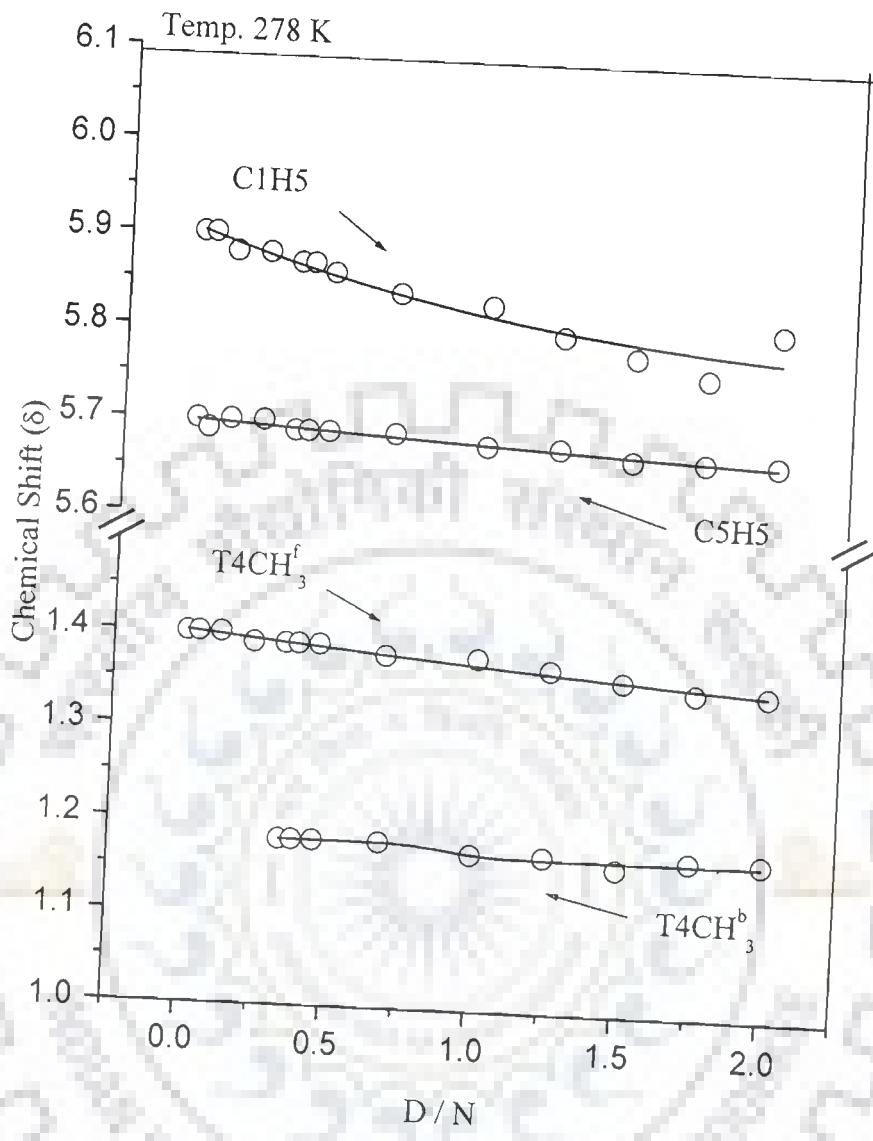


Fig. 6.2a(iii)

Fig 6.2a ¹H chemical shift of mitoxantrone complexed with d-(CGATCG)₂ at various D /N ratios at 278 K showing DNA protons. (i) Base region (ii) H1' region (iii) CH5 / TCH₃

Table 6.1b Chemical shift (ppm) of drug protons as a function of drug (D) to nucleic acid duplex (N) ratio, D / N, at 278 K. Also shown here is the maximum change in chemical shift due to binding, with respect to drug in free self associated form, δ^f , (1–10 mM, 278 K) as well as the drug in monomeric form, δ_{monomer} , of the bound form for D / N = 0.23.

D / N	6H / 7H	2H / 3H	11NH
δ_{monomer}	7.39	7.13	10.25
δ^f	6.75	6.67	9.71
0.04	-	6.83(broad)	-
0.116	-	6.83(broad)	9.40
0.23	6.93	6.85	9.40
0.384	6.93	6.84	9.38
0.456	6.94	6.84	9.38
0.684	6.94	6.83	9.38
1.0	6.94	6.84	9.39
1.25	6.94	6.84	9.38
1.50	6.94	6.80	9.38
1.75	6.93	6.80	9.38
2.00	6.93	6.81	9.38
$\Delta\delta' = \delta^b - \delta^f = \delta^{(D/N=0.23)} - \delta^f$ 1–10 mM, 278 K	+0.18	+0.18	-0.31
$\Delta\delta = \delta^b - \delta_{\text{monomer}} = \delta^{(D/N=0.23)} - \delta_{\text{monomer}}$	-0.46	-0.28	-0.85

-ve $\Delta\delta$ indicates upfield shift

+ve $\Delta\delta$ indicates downfield shift.

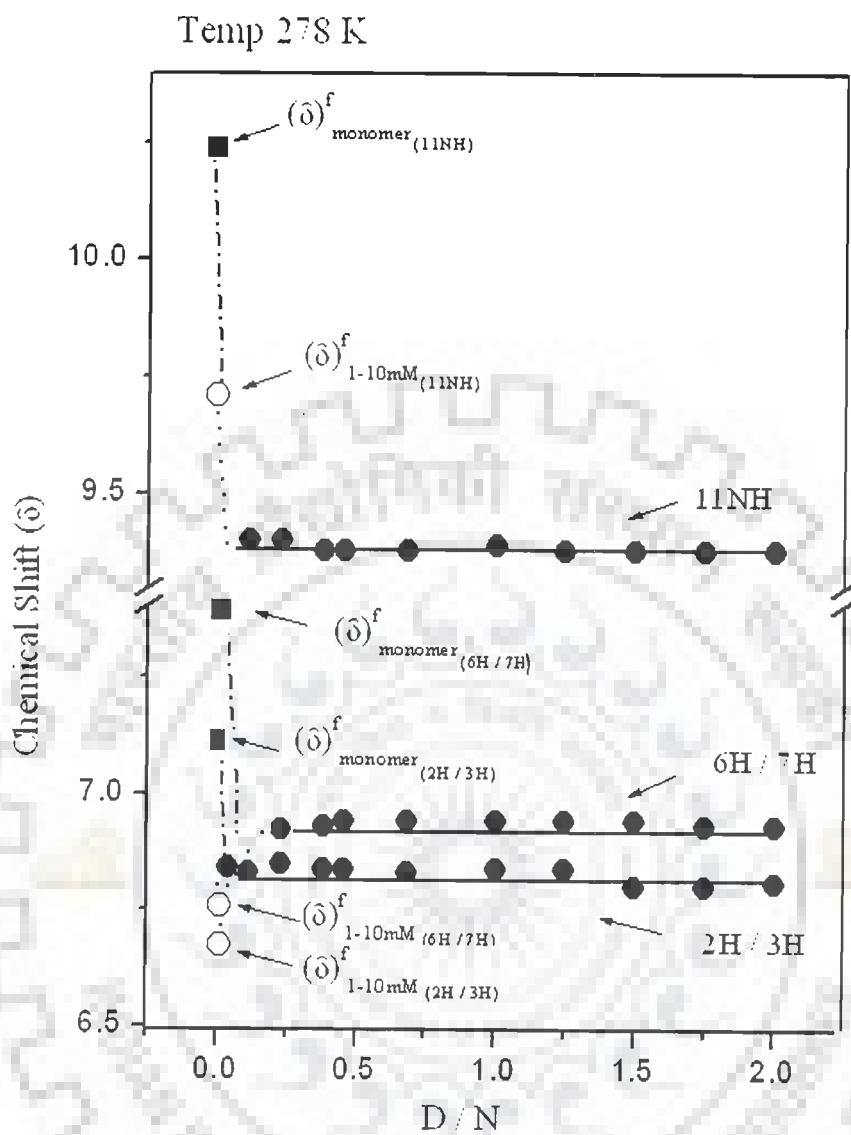


Fig .6.2b

Fig .6.2b ^1H chemical Shift of mitoxantrone complexed with $d\text{-(CGATCG)}_2$ at various D / N ratios showing drug protons at 278 K.

Table 6.2a: Chemical shift (ppm) of nucleic acid protons in free state (δ^f) and that bound to drug (δ^b) at drug (D) to nucleic acid duplex (N) ratio D/N = 1 at 278 K. Change in chemical shift on binding, that is, $\Delta\delta = \delta^b_{(D/N=1.0)} - \delta^f$ is also shown.

Protons	C1			G2			A3			T4			C5			G6		
	δ^b	δ^f	$\Delta\delta$	δ^b	δ^f	$\Delta\delta$	δ^b	δ^f	$\Delta\delta$	δ^b	δ^f	$\Delta\delta$	δ^b	δ^f	$\Delta\delta$	δ^b	δ^f	$\Delta\delta$
H8/H6	7.60	7.64	-0.04	7.99	8.02	-0.03	8.28	8.32	-0.04	7.19	7.22	-0.03	7.47	7.50	-0.03	7.92	7.98	-0.06
H1'	5.60	5.68	-0.08	5.56	5.59	-0.03	6.31	6.34	-0.03	5.94	5.97	-0.03	5.60	5.66	-0.06	6.11	6.17	-0.06
H2'	1.99	2.02	-0.03	2.81	2.80	+0.01	2.74	2.75	-0.01	2.08	2.08	0.00	2.00	2.02	-0.02	2.63	2.66	-0.03
H2''	2.37	2.43	-0.06	2.72	2.74	-0.02	2.99	3.02	-0.03	2.46	2.48	-0.02	2.36	2.42	-0.06	2.35	2.41	-0.06
H3'	4.69	4.73	-0.04	2.81	2.86	-0.05	5.05	5.09	-0.04	4.86	4.88	-0.02	4.85	4.88	-0.03	4.68	4.73	-0.05
H4'	4.14	4.10	-0.04	5.03	5.04	-0.01	4.54	4.55	-0.01	4.33	4.34	-0.01	4.18	4.17	+0.01	4.20	4.20	0.00
H5'	3.75	3.73	+0.02	4.32	4.31	-0.01	4.33	4.29	-0.04	4.19	4.21	-0.02	4.13	4.15	-0.02	4.15	4.19	-0.04
H5''	3.72	3.75	-0.03	4.18	4.21	-0.03	4.28	4.29	-0.01	4.17	4.27	-0.10	4.10	4.20	-0.10	4.09	4.10	-0.01
H2/H5/ CH ₃ ^f	5.83	5.90	-0.07	4.13	4.18	-0.04	7.85	7.91	-0.06	1.38	1.43	-0.05	5.60	5.70	-0.10	--	--	--
CH ₃ ^b	--	--	--	--	--	--	--	--	--	1.17	--	--	--	--	--	--	--	--
NH ₂ ^b	8.28	8.30	-0.02	7.02	--	--	7.67	7.72	-0.05	--	--	--	8.58	8.63	-0.05	7.06	--	--
NH ₂ ^{nb}	7.02	7.10	-0.08	5.60	--	--	6.14	6.15	-0.01	--	--	--	7.06	7.11	-0.05	5.90	--	--
NH	--	--	--	12.12	12.92	-0.80	--	--	--	13.52	13.72	-0.20	--	--	--	12.32	12.62	-0.30

-ve $\Delta\delta$ indicates upfield shift on binding

+ve $\Delta\delta$ indicates downfield shift on binding

Table 6.2b: Chemical shift (ppm), δ^b , of drug protons bound to nucleic acid duplex at drug (D) to nucleic acid (N) ratio D/N = 1; that in free state, δ^f (concentration 10 mM); and that in monomeric form, δ^{monomer} (concentration 10 μM) at 278 K. Change in chemical shift, due to binding, that is, $\Delta\delta = \delta^b - \delta^f$ with respect to free drug as well as $\Delta\delta' = \delta^b - \delta^{\text{monomer}}$ with respect to the drug in monomeric state are also shown.

Protons	$\delta^b_{(D/N=1)}$	δ^f	$\Delta\delta = \delta^b_{(D/N=1)} - \delta^f$	δ^{monomer}	$\Delta\delta' = \delta^b_{(D/N=1)} - \delta^{\text{monomer}}$
6H/7H	7.12	6.93	+0.19	7.39	-0.45
2H/3H	6.84	6.97	-0.13	7.13	-0.29
11CH ₂	3.83	3.60	+0.23	3.75°	+0.07
12CH ₂	3.53	3.32	+0.21	3.29	+0.14
13CH ₂	3.28	3.23	+0.05	3.15	+0.13
14CH ₂	4.14	3.81	+0.33	3.75°	+0.39
11NH	9.39	10.00*	-0.61	10.24	-0.85
14OH	6.60	–	–	–	–

* observed at D/N = 2.0

-ve $\Delta\delta$ indicates upfield shift on binding

+ve $\Delta\delta$ indicates downfield shift on binding

Table 6.3a Chemical shift (ppm) of nucleic acid protons in drug – DNA complex having D / N = 1 as a function of temperature. Also shown here is the net change in chemical shift with temperature,

that is, $\Delta\delta = \delta_{(353\text{ K})} - \delta_{(278\text{ K})}$

Temp. (K)	C1H6	G2H8	A3H8	T4H6	C5H6	G6H8	C1H5	A3H2	C5H5
278	7.60	7.99	8.29	7.20	7.45	7.92	5.83	7.88	5.68
283	7.60	7.99	8.30	7.20	7.45	7.93	5.83	7.88	5.65
288	7.60	7.99	8.30	7.18	7.46	7.88	5.85	7.88	5.65
293	7.60	7.99	8.29	7.17	7.46	7.88	5.85	7.87	5.61
298	7.60	7.93	8.27	7.16	7.45	7.88	5.84	7.82	5.64
303	7.60	7.93	8.26	7.16	7.45	7.88	5.84	7.82	5.66
308	7.59	7.93	8.25	7.18	7.47	7.88	5.83	7.79	5.68
313	7.59	7.93	8.25	7.20	7.49	7.88	5.84	7.76	5.71
318	7.58	7.93	8.24	7.22	7.52	7.90	5.91	7.73	5.76
323	7.57	7.90	8.24	7.26	7.52	7.91	5.94	7.74	5.81
328	7.57	7.92	8.25	7.27	7.55	7.90	5.97	7.74	5.85
333	7.60	7.95	8.27	7.34	7.55	7.92	5.99	7.82	5.89
338	7.64	7.98	8.27	7.39	7.55	7.92	6.01	7.82	5.90
343	7.64	7.98	8.27	7.39	7.59	7.92	6.03	7.81	5.93
348	7.68	8.02	8.28	7.44	7.56	7.92	6.09	7.81	5.93
353	7.70	8.03	8.28	7.45	7.56	7.92	6.10	7.81	5.93
$\Delta\delta$	+0.10	+0.04	-0.01	+0.25	+0.11	0.00	+0.27	-0.07	+0.25

Temp. (K)	C1H1'	G2H1'	A3H1'	T4H1'	C5H1'	G6H1'	T4CH ₃ ^f	T4CH ₃ ^b
278	5.60	5.56	6.31	5.94	5.60	6.11	1.38	1.17
283	5.63	5.57	6.31	5.94	5.63	6.11	1.38	1.18
288	5.64	5.57	6.30	5.94	5.64	6.11	1.38	1.20
293	5.68	5.57	6.29	5.94	5.64	6.11	1.38	1.20
298	5.64	5.54	6.29	5.95	5.64	6.11	1.38	–
303	5.66	5.54	6.29	5.96	5.64	6.11	1.38	–
308	5.69	5.55	6.28	5.96	5.69	6.12	1.38	–
313	5.72	5.56	6.27	5.98	5.72	6.12	1.39	–
318	5.76	5.59	6.27	6.00	5.76	6.13	1.38	–
323	5.80	5.62	6.27	6.03	5.80	6.13	1.38	–
328	5.86	5.67	6.28	6.05	5.88	6.14	1.38	–
333	5.89	5.70	6.29	6.07	5.89	6.15	1.38	–
338	5.92	5.74	6.29	6.10	5.92	6.15	1.38	–
343	5.94	5.78	6.30	6.14	5.93	6.160	1.37	–
348	5.98	5.81	6.31	6.17	5.93	6.16	1.37	–
353	5.99	5.83	6.31	6.18	5.94	6.18	1.37	–
$\Delta\delta$	+0.39	+0.27	0.00	+0.24	+0.34	+0.07	-0.01	+0.03

-ve $\Delta\delta$ indicates upfield shift

+ve $\Delta\delta$ indicates downfield shift.

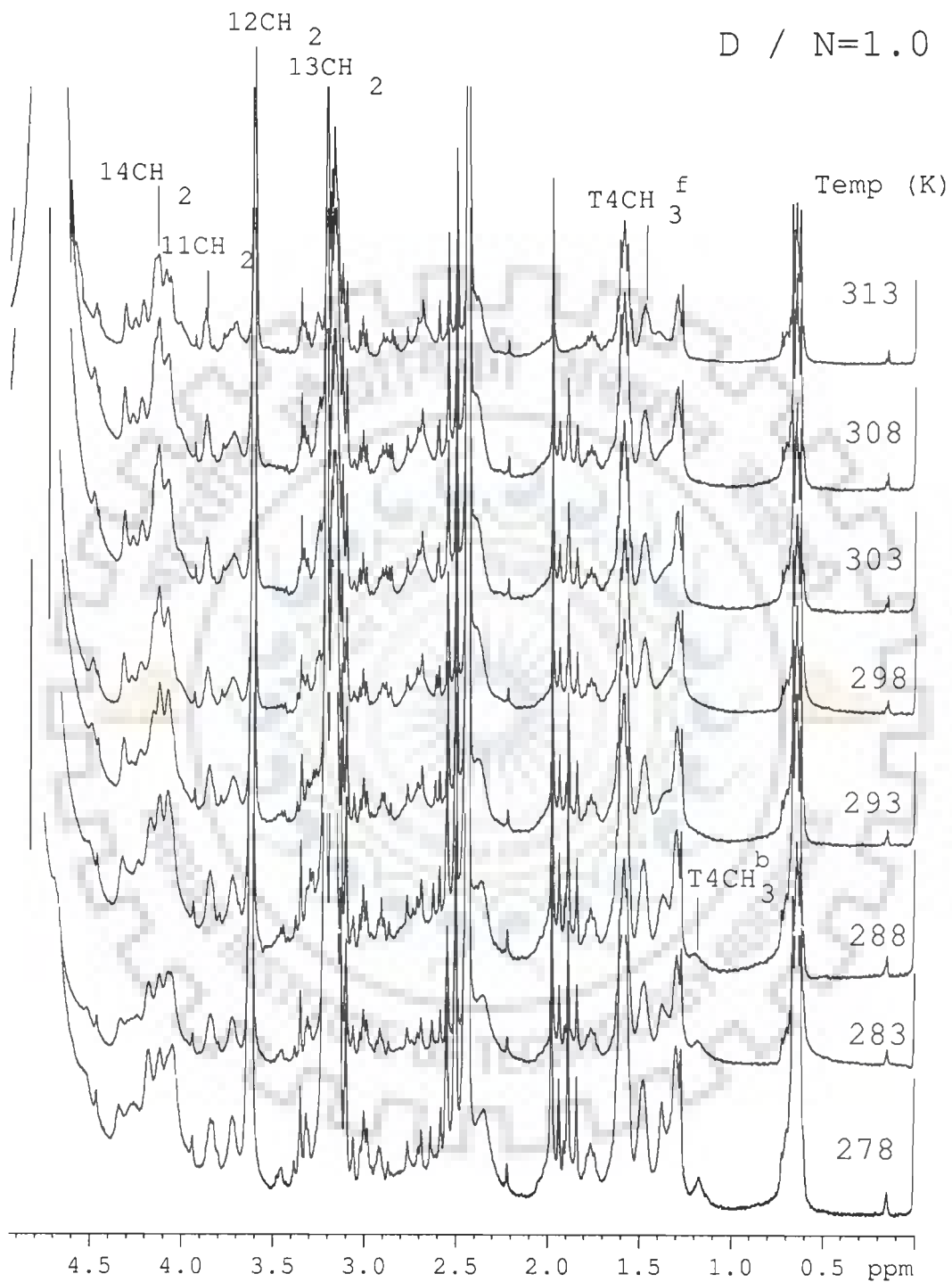


Fig. 6.3a(i)

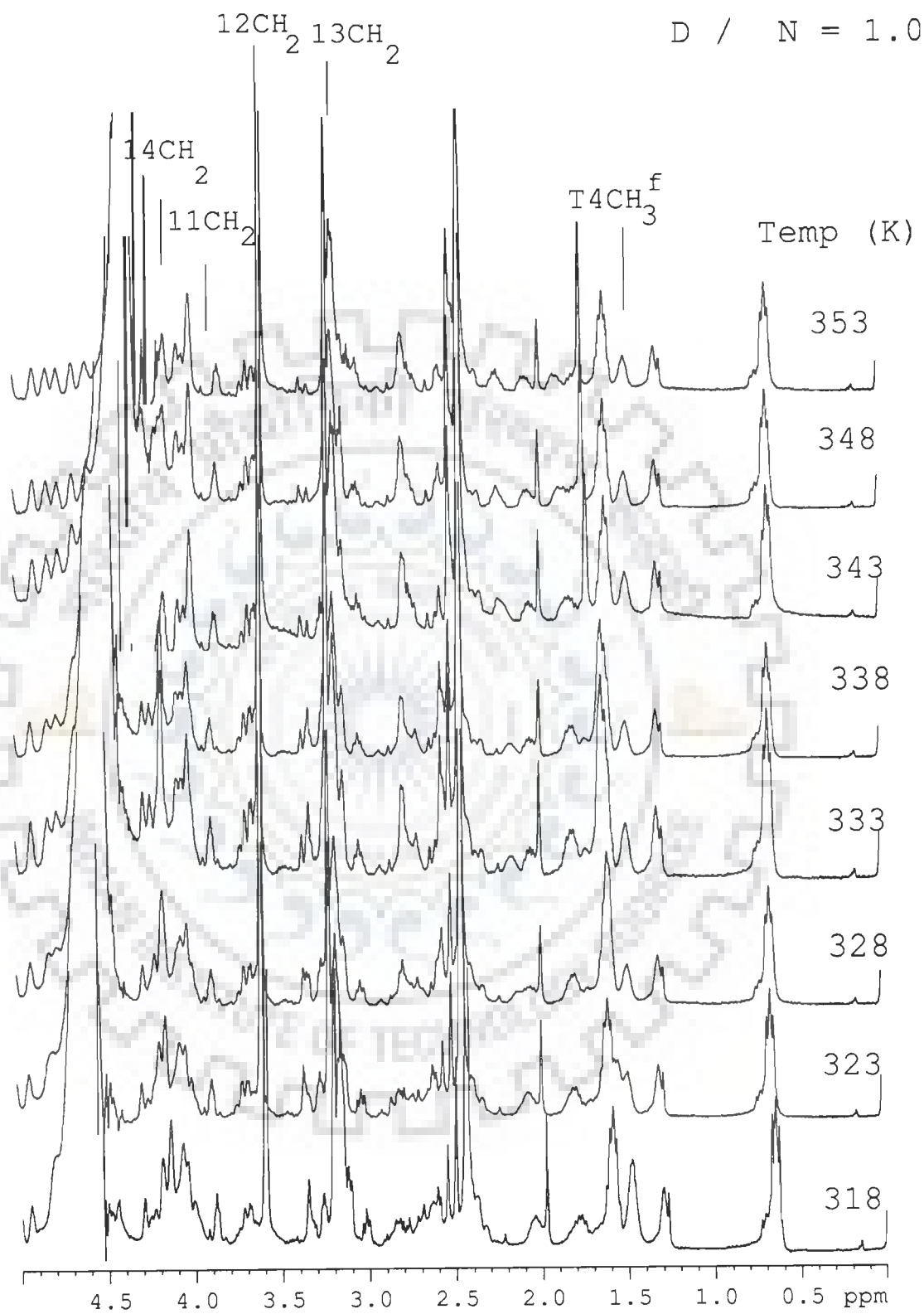


Fig. 6.3a(ii)

D / N = 1.0

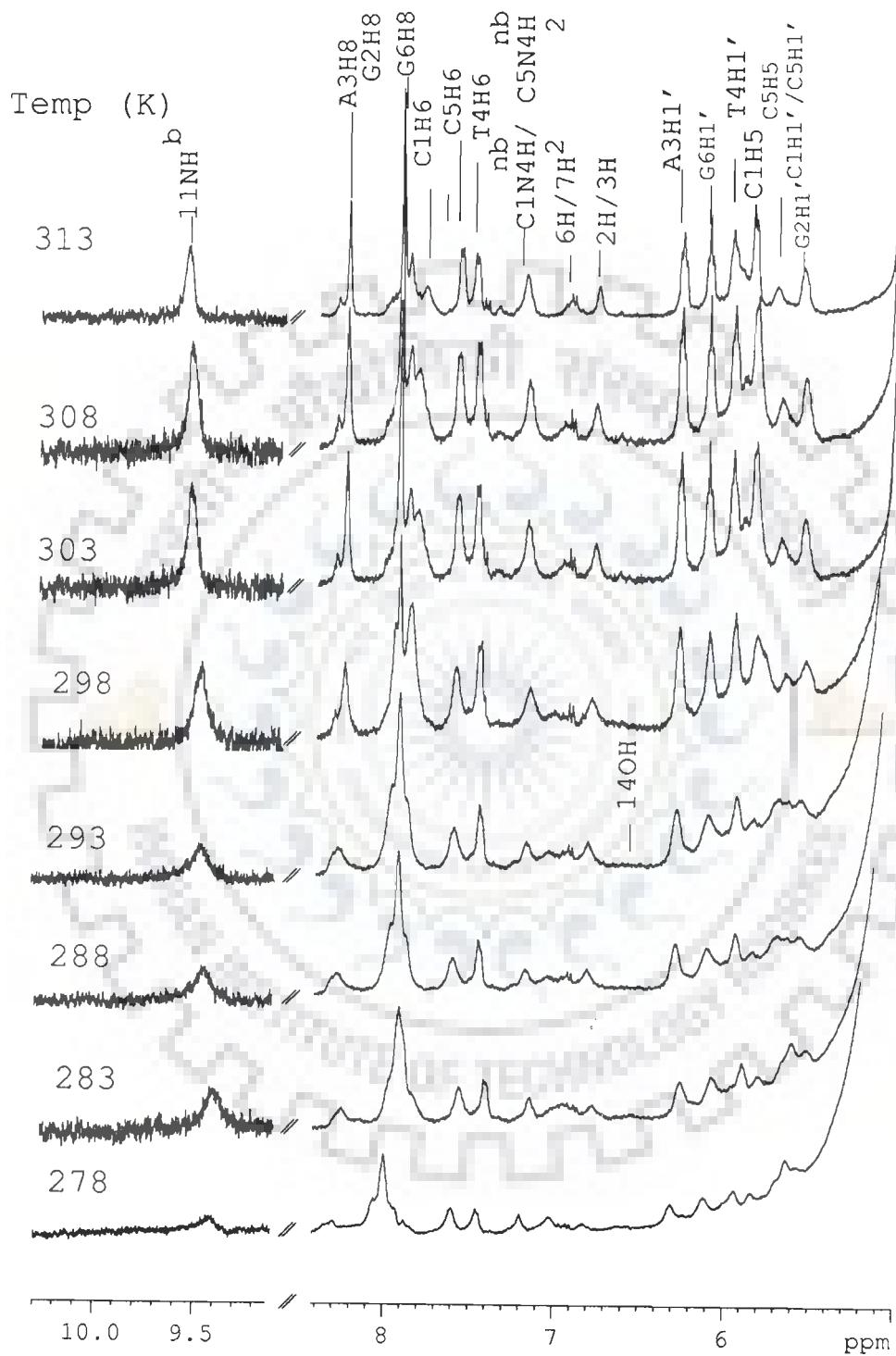


Fig. 6.3a(iii)

D / N = 1.0

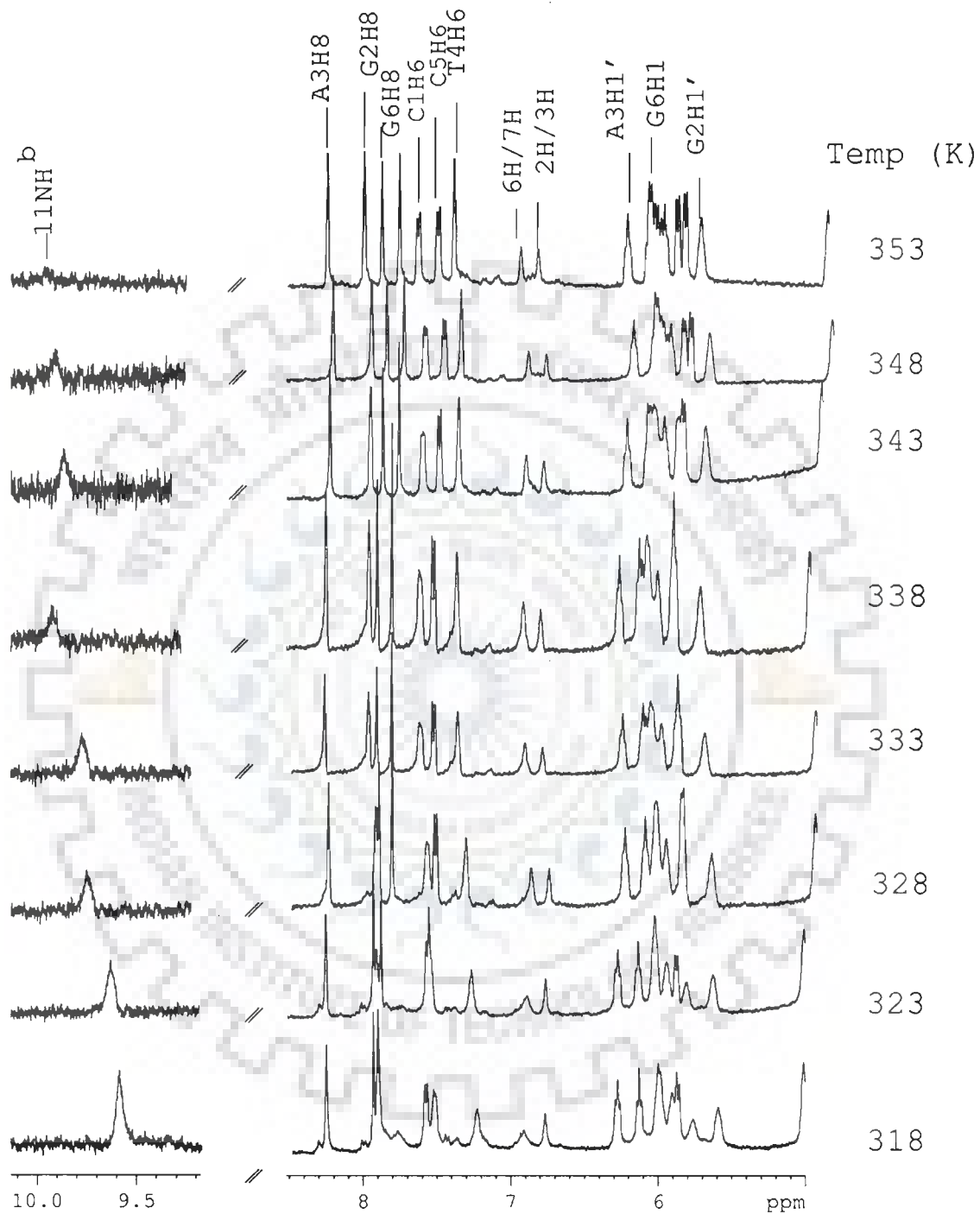


Fig. 6.3a(iv)

Fig 6.3a ¹H NMR spectra of mitoxantrone complexed with d-(CGATCG)₂ at D / N =1.0 function of temperature 278 K – 353K.

Table 6.3b Chemical shift (ppm) of nucleic acid protons in drug – DNA complex having D / N = 1.5 as a function of temperature. Also shown here is the net change in chemical shift with temperature, that is, $\Delta\delta = \delta_{(353\text{ K})} - \delta_{(278\text{ K})}$

Temp. (K)	C1H6	G2H8	A3H8	T4H6	C5H6	G6H8	C1H5	A3H2	C5H5
278	7.57	7.99	8.28	7.17	7.43	7.90	5.78	7.84	5.67
283	7.59	7.99	8.28	7.18	7.43	7.90	5.81	7.83	5.67
288	7.58	7.95	8.28	7.18	7.43	7.91	5.80	7.84	5.70
293	7.60	7.95	8.31	7.18	7.43	7.92	5.80	7.84	5.75
298	7.60	7.95	8.31	7.18	7.45	7.89	5.80	7.84	5.80
303	7.59	7.92	8.31	7.17	7.45	7.85	5.80	7.86	5.79
308	7.59	7.92	8.30	7.13	7.45	7.84	5.80	7.84	5.80
313	7.59	7.92	8.30	7.16	7.46	7.85	5.82	7.79	5.82
318	7.57	7.92	8.29	7.18	7.46	7.85	5.84	7.77	5.84
323	7.57	7.92	8.29	7.25	7.50	7.87	5.94	7.75	5.96
328	7.56	7.92	8.29	7.29	7.54	7.85	5.97	7.71	5.98
333	7.60	7.90	8.29	7.33	7.54	7.83	5.97	–	5.97
338	7.63	7.91	8.26	7.38	7.56	7.85	6.02	–	6.02
343	7.64	7.91	8.26	7.39	7.56	7.82	5.98	–	5.98
348	7.67	7.91	8.27	7.41	7.56	7.81	5.98	–	5.98
353	7.68	7.91	8.27	7.44	7.56	7.82	5.98	–	5.93
$\Delta\delta$	+0.11	-0.08	-0.01	+0.27	+0.13	-0.08	+0.20	-0.13	+0.26

Temp. (K)	C1H1'	G2H1'	A3H1'	T4H1'	C5H1'	G6H1'	T4CH ₃ ^f	T4CH ₃ ^b
278	5.57	5.51	6.28	5.92	5.57	6.06	1.36	1.17
283	5.60	5.54	6.29	5.92	5.60	6.07	1.36	1.17
288	5.62	5.54	6.29	5.92	5.60	6.08	1.36	1.18
293	5.60	5.54	6.28	5.94	5.60	6.09	1.34	1.19
298	5.60	5.51	6.27	5.93	5.60	6.07	1.34	–
303	5.61	5.51	6.27	5.94	5.61	6.08	1.34	–
308	5.64	5.52	6.26	5.95	5.64	6.08	1.34	–
313	5.67	5.54	6.26	5.96	5.67	6.09	1.38	–
318	5.71	5.56	6.26	5.97	5.71	6.10	1.32	–
323	5.80	5.62	6.26	6.02	5.80	6.12	1.35	–
328	5.84	5.65	6.26	6.04	5.84	6.13	1.30	–
333	5.88	5.66	6.27	6.05	5.86	6.13	1.30	–
338	5.90	5.69	6.27	6.05	5.90	6.15	1.30	–
343	5.92	5.74	6.29	6.05	5.90	6.16	1.30	–
348	5.96	5.77	6.29	6.05	5.92	6.16	1.30	–
353	5.97	5.80	6.31	6.06	5.93	6.16	1.30	–
$\Delta\delta$	+0.40	+0.29	+0.03	+0.14	+0.36	+0.10	-0.06	+0.02

-ve $\Delta\delta$ indicates upfield shift

+ve $\Delta\delta$ indicates downfield shift

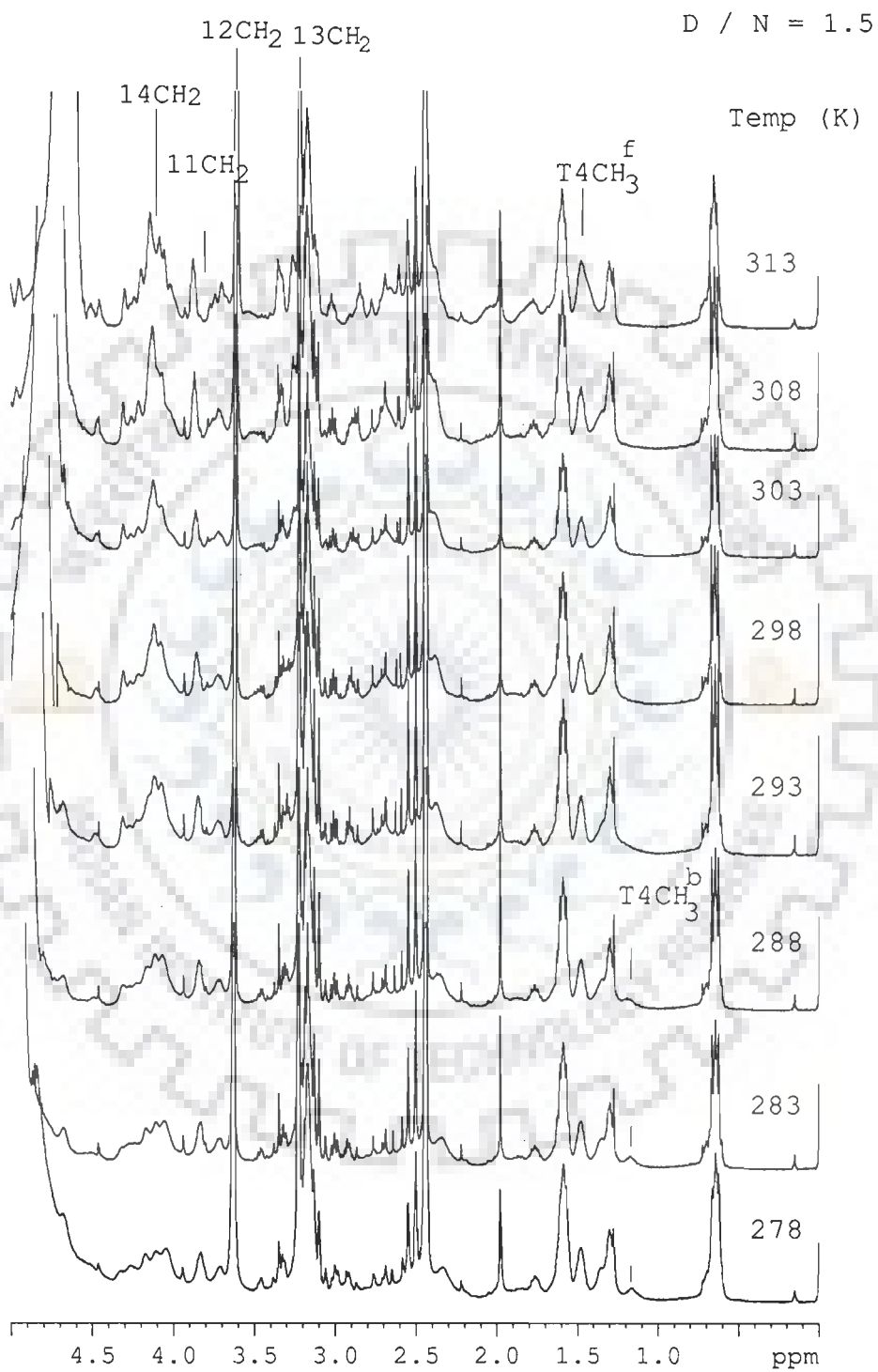


Fig. 6.3b(i)

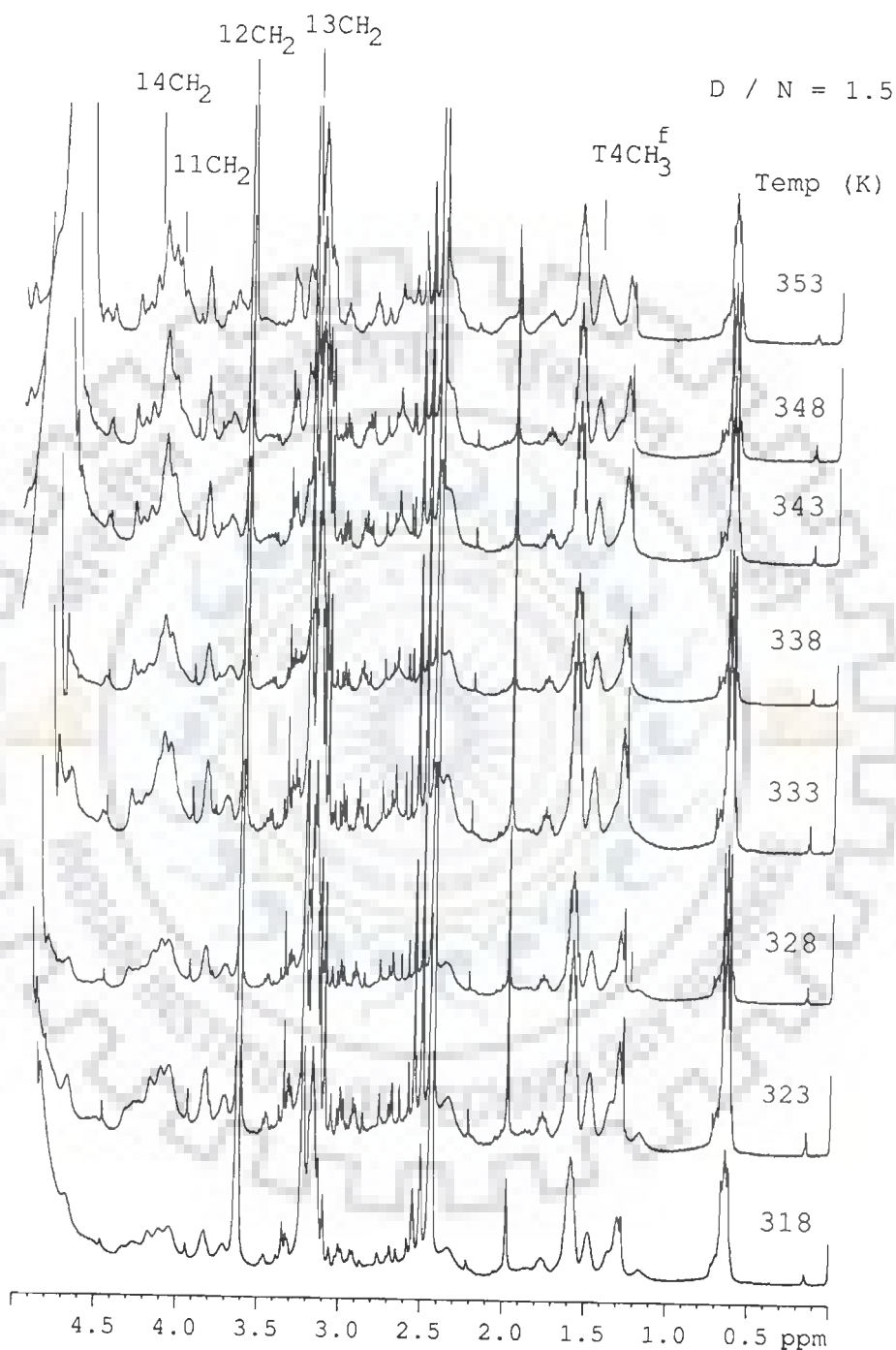


Fig. 6.3b(ii)

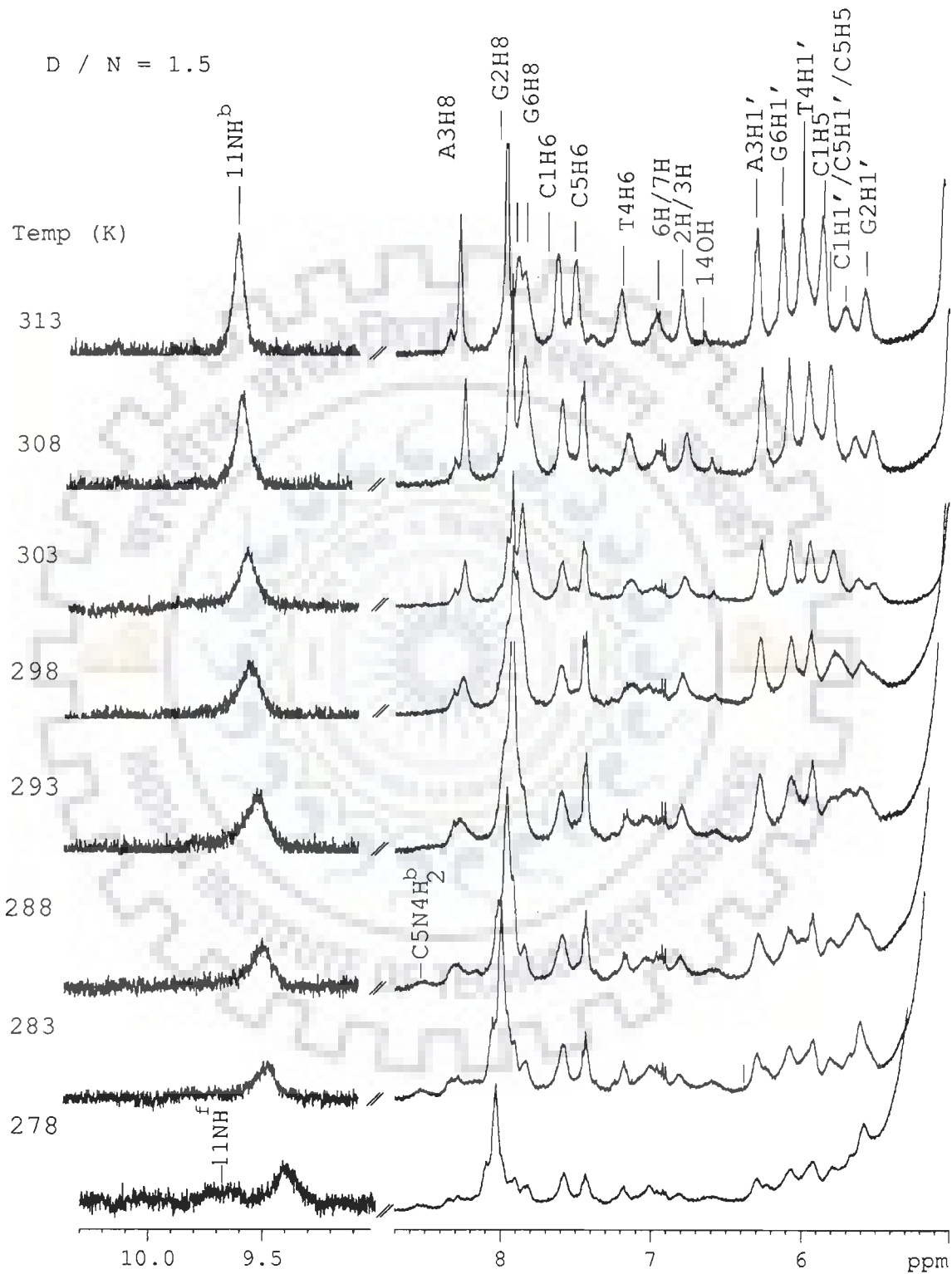


Fig. 6.3b(iii)

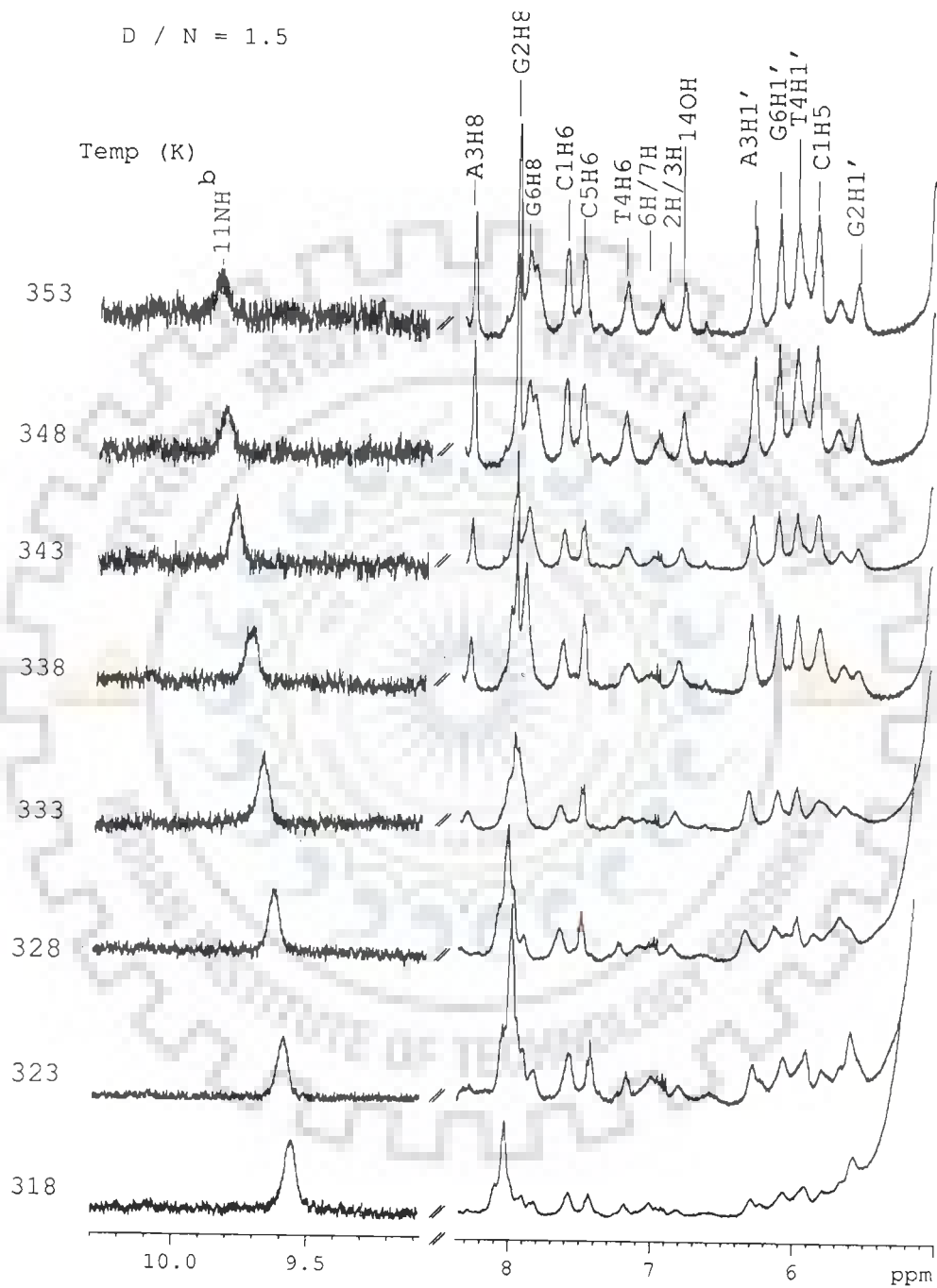


Fig. 6.3b(iv)

Fig 6.3b ^1H NMR spectra of mitoxantrone complexed with $d\text{-(CGATCG)}_2$ at $D/N = 1.5$ function of temperature 278 K – 353K.

Table 6.3c Chemical shift (ppm) of nucleic acid protons in drug – DNA complex having D / N = 1.75 as a function of temperature. Also shown here is the net change in chemical shift with temperature, that is, $\Delta\delta = \delta_{(353\text{ K})} - \delta_{(278\text{ K})}$

Temp. (K)	C1H6	G2H8	A3H8	T4H6	C5H6	G6H8	C1H5	A3H2	C5H5
278	7.57	8.06	8.27	7.17	7.43	7.90	5.76	7.82	5.67
283	7.57	8.01	8.27	7.18	7.44	7.89	5.80	7.84	5.68
288	7.57	7.97	8.27	7.16	7.44	7.92	5.79	7.83	5.67
293	7.58	7.92	8.27	7.16	7.43	7.92	5.79	7.84	5.70
298	7.58	7.90	8.23	7.16	7.43	7.92	5.79	7.84	5.73
303	7.58	7.91	8.23	7.14	7.43	7.91	5.77	7.84	5.68
308	7.57	7.91	8.23	7.16	7.48	7.84	5.78	7.79	5.64
313	7.57	7.91	8.23	7.21	7.50	7.90	5.88	7.85	5.83
318	7.57	7.91	8.24	7.27	7.55	7.89	5.94	7.86	5.85
323	7.59	7.92	8.25	7.33	7.55	7.91	5.99	7.84	5.88
328	7.63	7.92	8.26	7.39	7.54	7.91	6.03	7.82	5.92
333	7.66	7.92	8.27	7.43	7.56	7.92	5.98	7.80	5.93
338	7.69	7.92	8.28	7.45	7.56	7.92	5.99	7.81	5.94
343	7.69	7.92	8.28	7.46	7.56	7.92	5.99	7.81	5.96
348	7.71	7.92	8.28	7.47	7.57	7.92	5.99	7.81	5.96
353	7.71	7.93	8.28	7.47	7.57	7.92	6.00	7.81	5.97
$\Delta\delta$	+0.14	-0.13	+0.01	+0.30	+0.14	+0.02	+0.24	-0.01	+0.30

Temp. (K)	C1H1'	G2H1'	A3H1'	T4H1'	C5H1'	G6H1'	T4CH ₃ ^f	T4CH ₃ ^b
278	5.56	5.40	6.28	5.92	5.56	6.05	1.35	1.16
283	5.59	5.42	6.28	5.90	5.57	6.06	1.35	1.17
288	5.60	5.43	6.28	5.91	5.58	6.06	1.35	1.18
293	5.60	5.47	6.27	5.96	5.60	6.05	1.36	1.20
298	5.58	5.49	6.26	5.92	5.58	6.05	1.35	–
303	5.60	5.49	6.26	5.94	5.64	6.06	1.36	–
308	5.64	5.53	6.25	5.96	5.68	6.08	1.35	–
313	5.73	5.57	6.26	5.98	5.73	6.09	1.34	–
318	5.80	5.62	6.26	6.02	5.73	6.11	1.34	–
323	5.88	5.68	6.27	6.07	5.88	6.12	1.39	–
328	5.92	5.74	6.29	6.09	5.92	6.14	1.35	–
333	5.93	5.79	6.30	6.10	5.93	6.17	1.35	–
338	5.94	5.83	6.31	6.12	5.94	6.17	1.35	–
343	5.94	5.86	6.32	6.15	5.94	6.17	1.34	–
348	6.00	5.88	6.33	6.17	6.00	6.17	1.35	–
353	6.00	5.88	6.33	6.17	6.00	6.17	1.35	–
$\Delta\delta$	+0.44	+0.48	+0.05	+0.25	+0.44	+0.12	0.00	+0.04

-ve $\Delta\delta$ indicates upfield shift

+ve $\Delta\delta$ indicates downfield shift

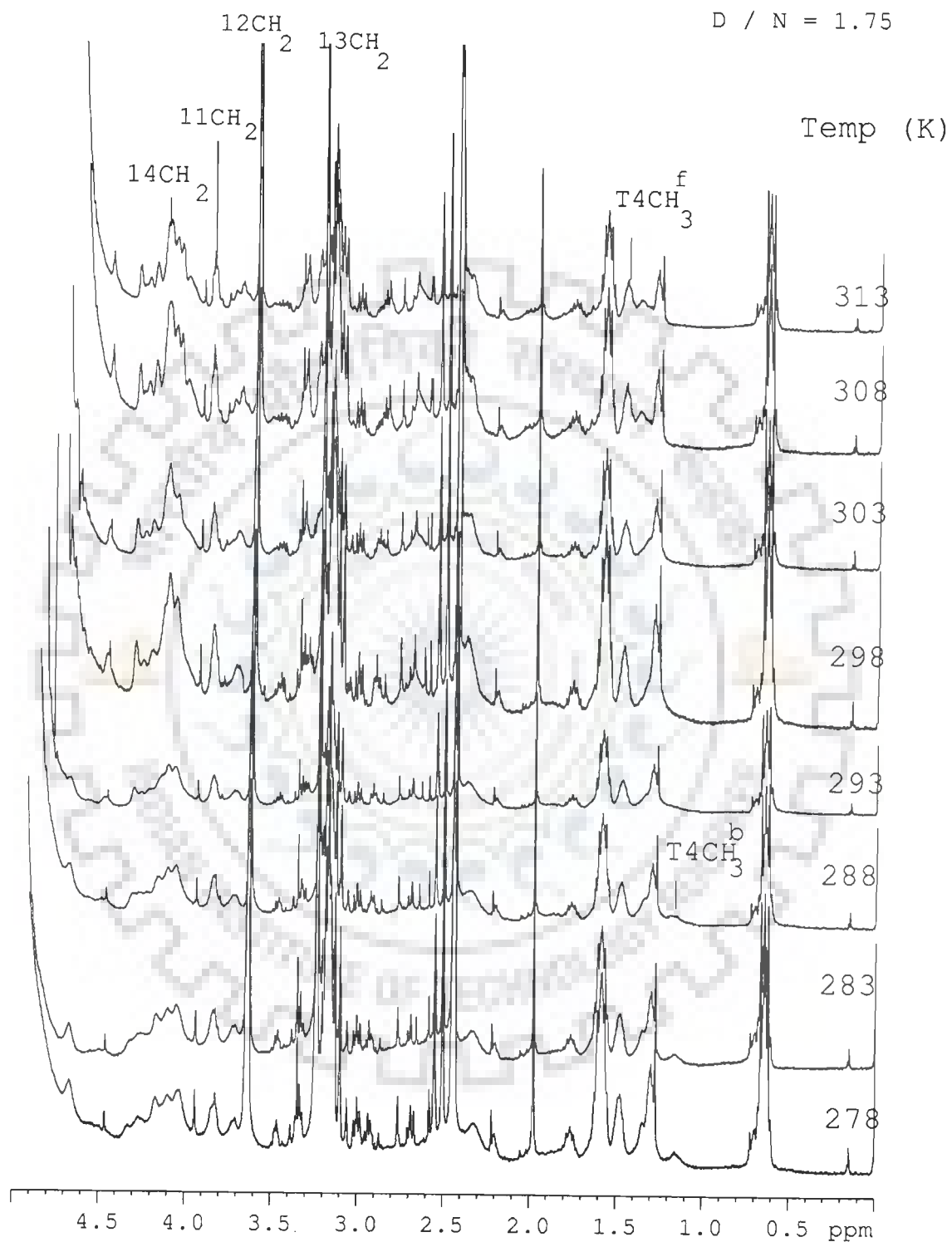


Fig. 6.3c(i)

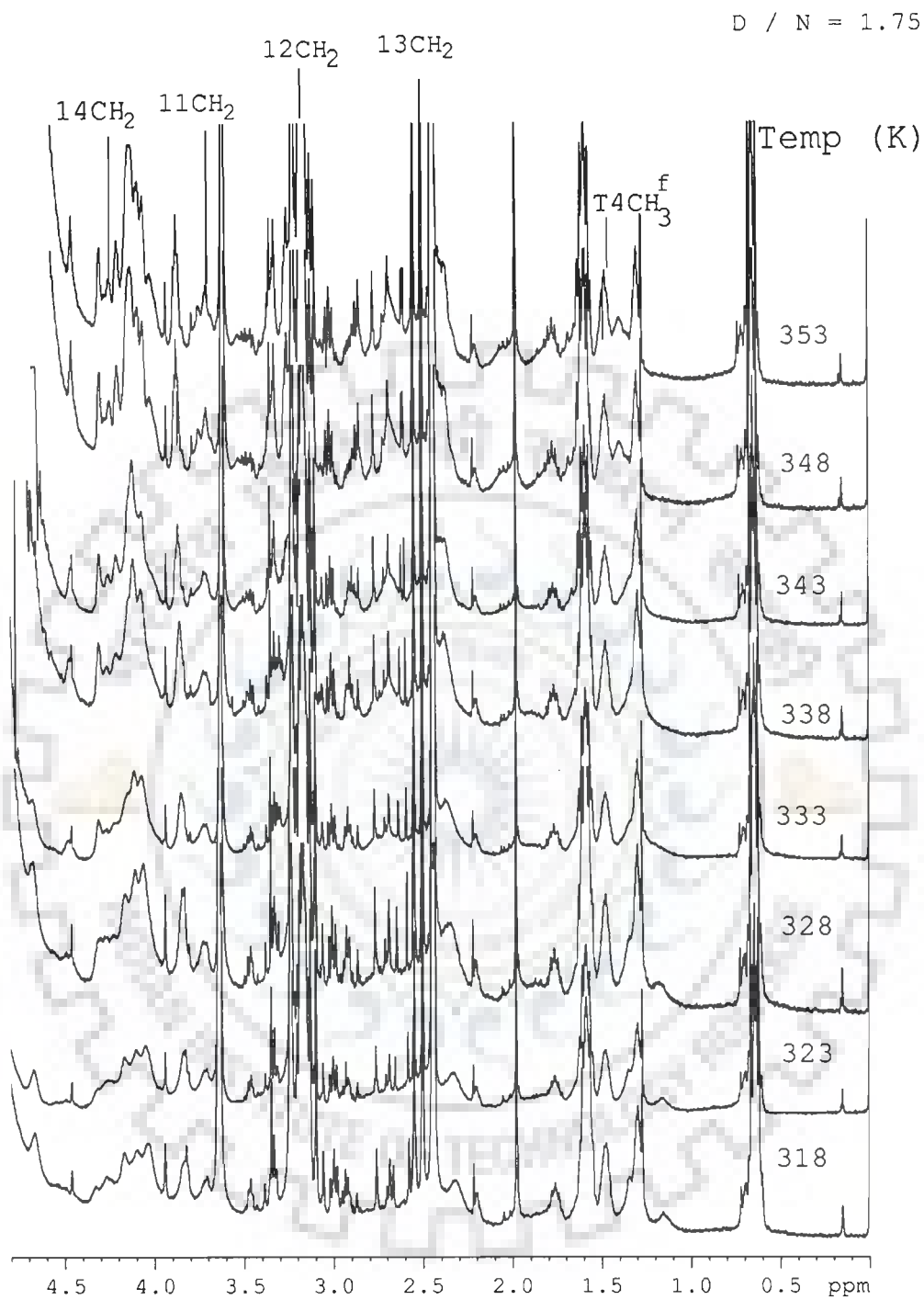


Fig. 6.3c(ii)

D / N = 1.75

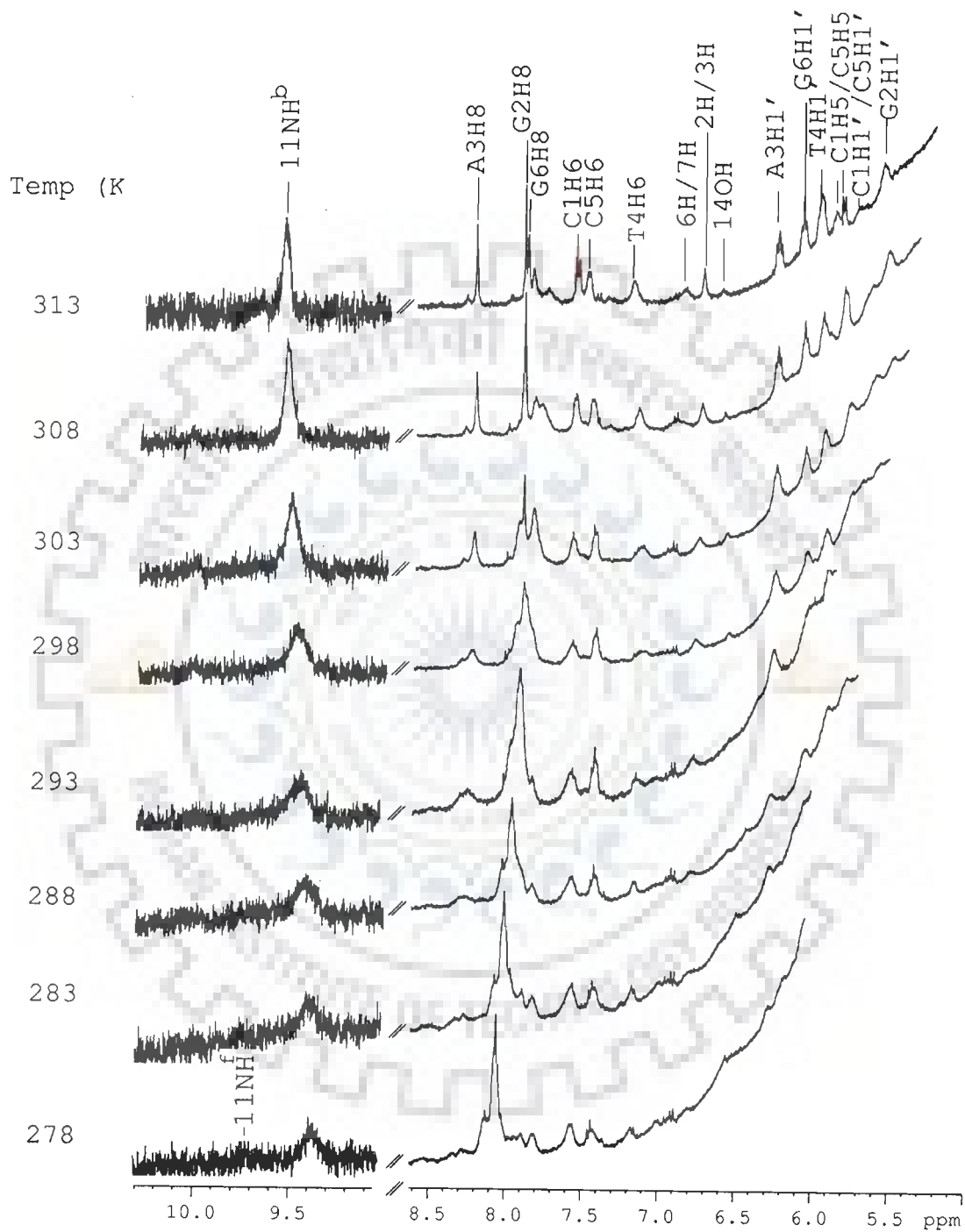


Fig. 6.3c(iii)

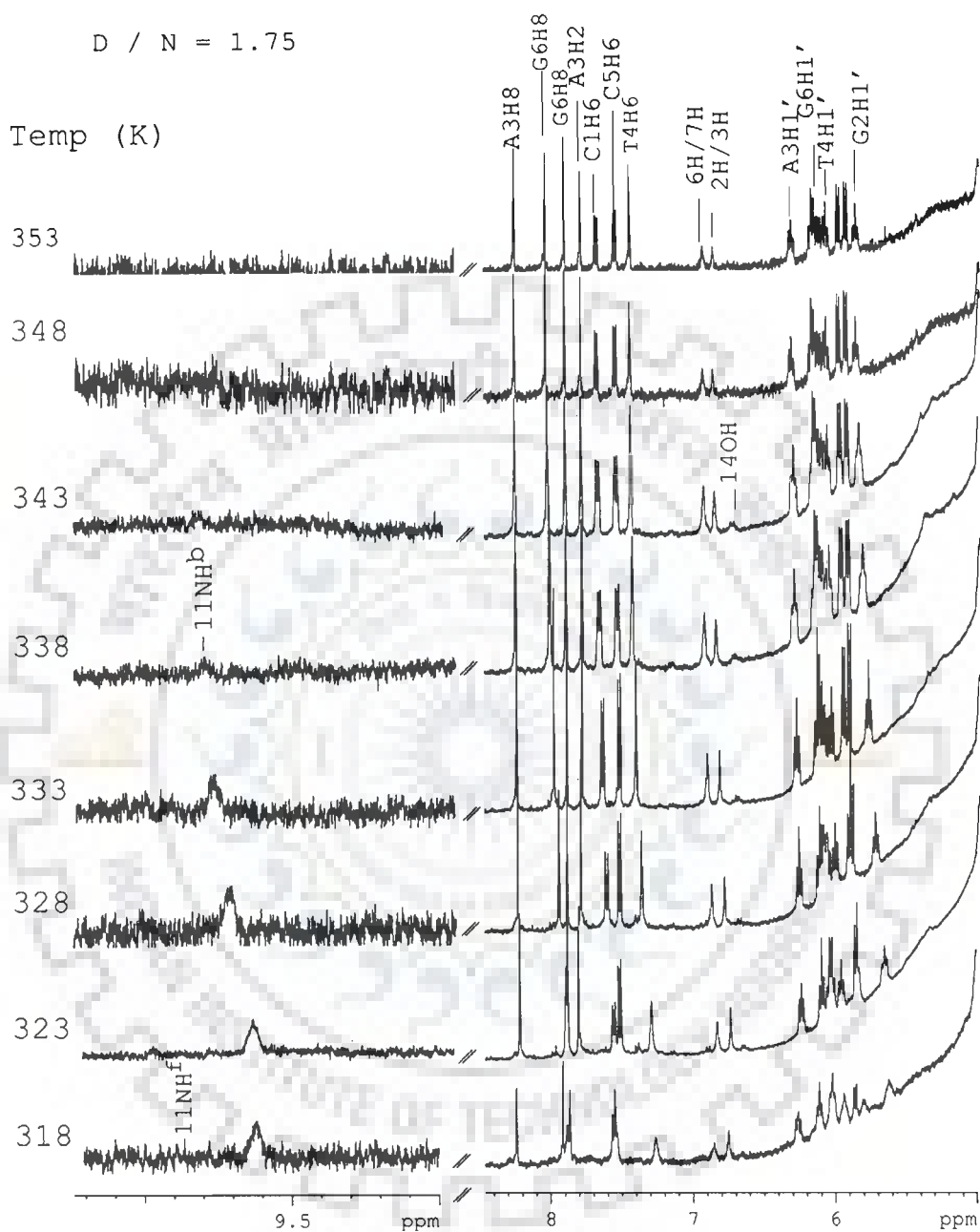


Fig. 6.3c(iv)

Fig 6.3c ¹H NMR spectra of mitoxantrone complexed with d-(CGATCG)₂ at D / N 1.75 function of temperature 278 K – 353K.

Table 6.3d Chemical shift (ppm) of nucleic acid protons in drug – DNA complex having D / N = 2.0 as a function of temperature. Also shown here is the net change in chemical shift with temperature,

that is, $\Delta\delta = \delta_{(353\text{ K})} - \delta_{(278\text{ K})}$

Temp(K)	C1H6	G2H8	A3H8	T4H6	C5H6	G6H8	A3H2	C1H5	C5H5
278	7.58	8.00	8.28	7.17	7.43	7.87	7.84	5.81	5.81
283	7.58	8.00	8.28	7.17	7.43	7.87	7.84	5.81	5.81
288	7.58	8.01	8.28	7.17	7.44	7.9	7.87	5.81	5.80
293	7.59	8.00	8.27	7.18	7.44	7.92	7.90	5.81	5.81
298	7.56	8.01	8.27	7.18	7.44	7.94	7.90	5.82	5.82
303	7.56	7.99	8.25	7.20	7.44	7.95	7.88	5.81	5.81
308	7.59	7.95	8.25	7.20	7.45	7.95	7.85	5.89	5.83
313	7.57	7.93	8.25	7.24	7.45	7.94	7.84	5.90	5.86
318	7.59	7.9	8.27	7.24	7.44	7.92	7.83	5.91	5.88
323	7.59	7.9	8.27	7.27	7.47	7.94	7.82	6.07	5.98
328	7.61	7.92	8.27	7.30u	7.48	7.94	7.81	6.08	6.02
333	7.64	7.94	8.3	7.34	7.51	7.92	7.81	6.10	6.05
338	7.67	7.97	8.28	7.37	7.52	7.9	7.81	6.12	6.06
343	7.68	8.04	8.28	7.4	7.54	7.87	7.81	6.12	6.07
348	7.69	8.05	8.28	7.41	7.56	7.85	7.81	6.12	6.08
353	7.7	8.06	8.28	7.44	7.57	7.84	7.82	6.13	6.08
$\Delta\delta$	+0.12	+0.06	0.00	+0.27	+0.14	-0.03	-0.02	+0.32	+0.27

Temp. (K)	C1H1'	G2H1'	A3H1'	T4H1'	C5H1'	G6H1'	T4CH ₃ ^f	T4CH ₃ ^b
278	5.67	5.58	6.29	5.93	5.60	6.06	1.35	1.17
283	5.67	5.54	6.29	5.93	5.62	6.07	1.36	1.17
288	5.68	5.54	6.29	5.93	5.62	6.08	1.36	1.18
293	5.69	5.53	6.28	5.94	5.61	6.08	1.36	1.18
298	5.69	5.52	6.28	5.94	5.61	6.08	1.37	1.20
303	5.75	5.52	6.27	5.95	5.64	6.09	1.38	–
308	5.69	5.53	6.27	5.97	5.69	6.10	1.38	–
313	5.74	5.58	6.27	5.99	5.66	6.11	1.38	–
318	5.80	5.61	6.27	6.01	5.69	6.12	1.38	–
323	5.90	5.68	6.29	6.07	5.68	6.13	1.38	–
328	5.97	5.72	6.29	6.11	5.92	6.15	1.38	–
333	5.96	5.77	6.30	6.13	5.93	6.17	1.39	–
338	5.98	5.80	6.31	6.14	5.95	6.17	1.39	–
343	5.98	5.84	6.32	6.15	5.95	6.18	1.39	–
348	6.00	5.84	6.33	6.16	5.95	6.19	1.39	–
353	6.00	5.86	6.33	6.17	5.95	6.19	1.39	–
$\Delta\delta$	+0.33	+0.28	+0.04	+0.24	+0.35	+0.13	+0.04	+0.03

-ve $\Delta\delta$ indicates upfield shift

+ve $\Delta\delta$ indicates downfield shift

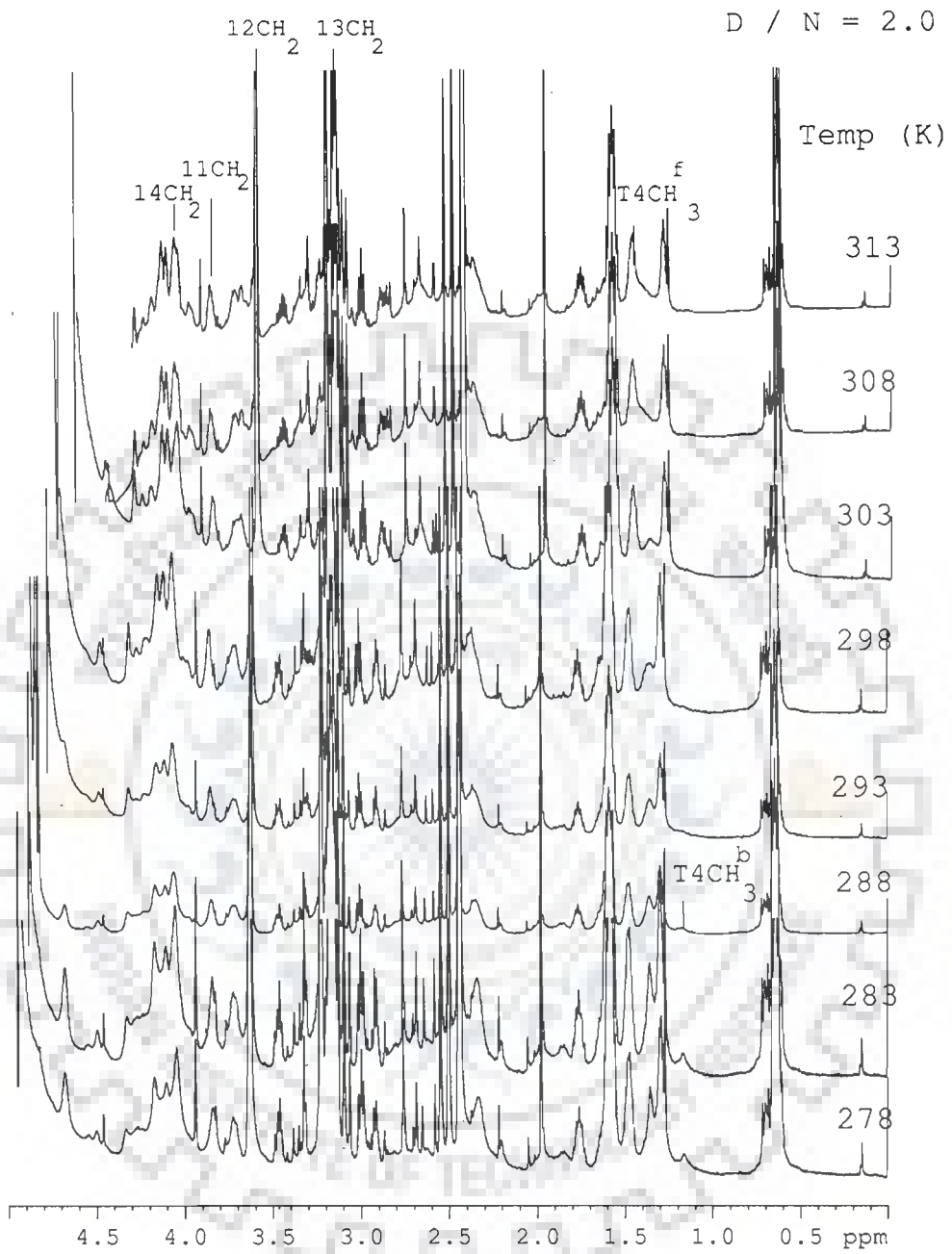


Fig. 6.3d(i)

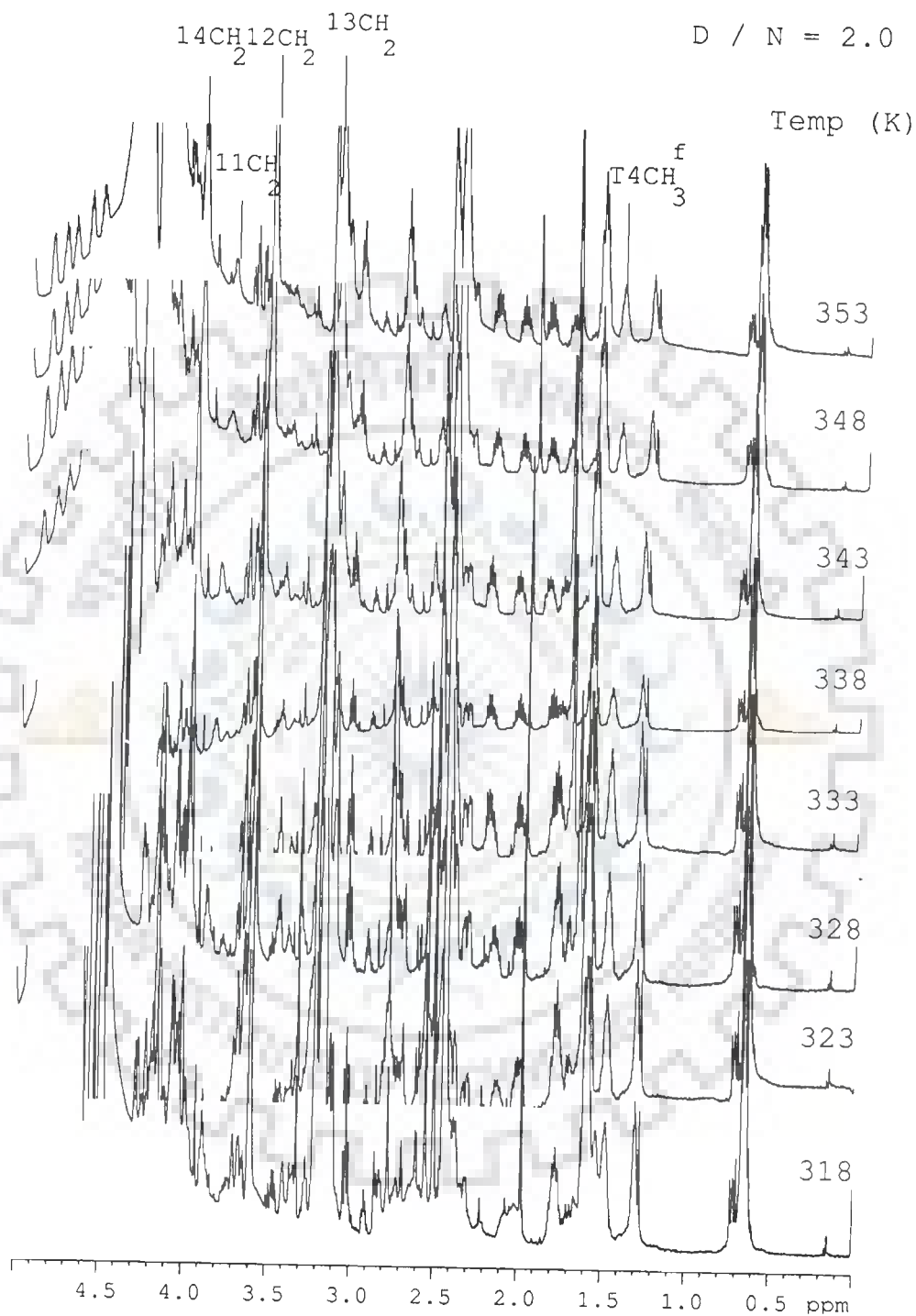


Fig. 6.3 d(ii)

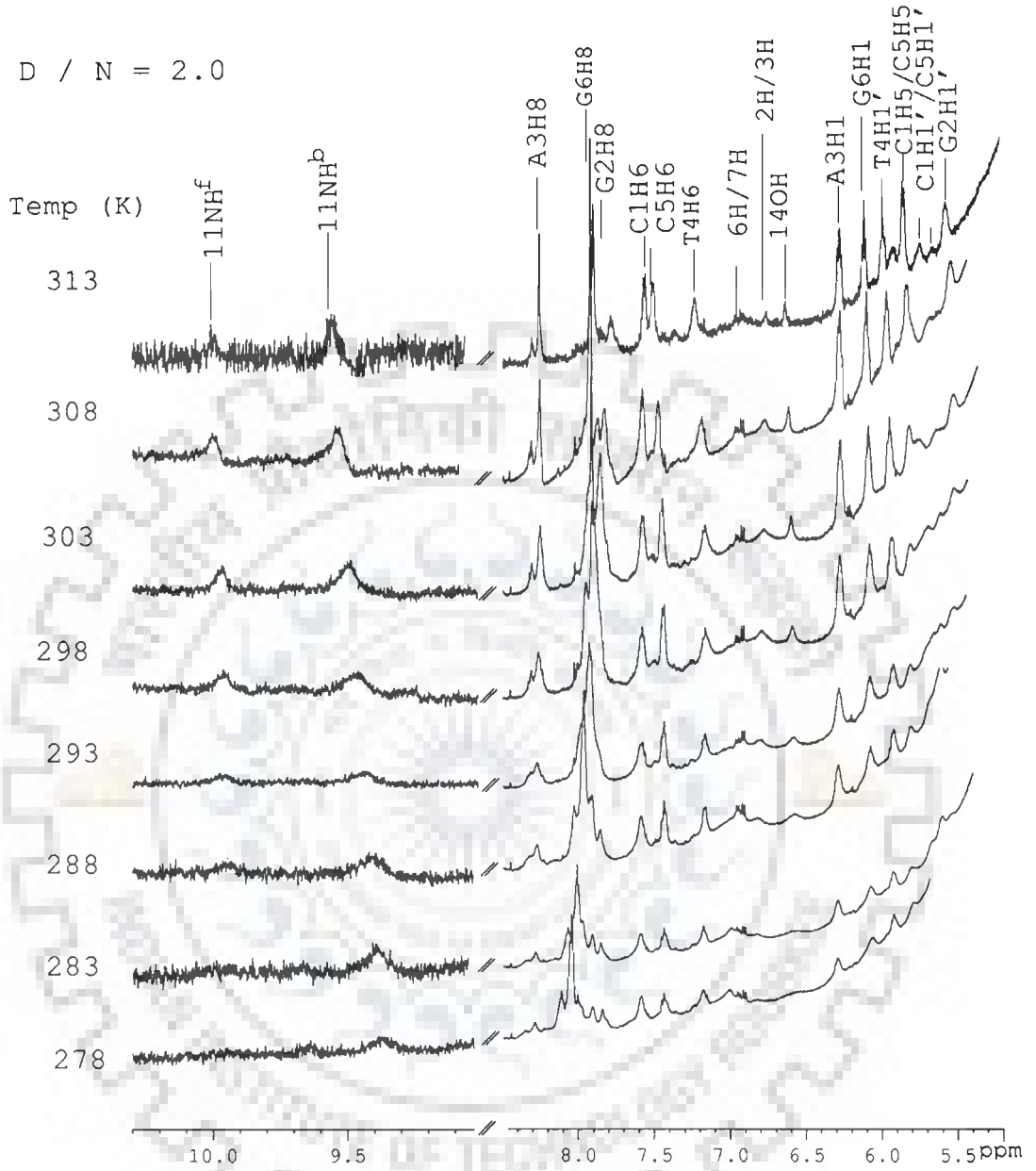


Fig. 6.3 d(iii)

D / N = 2.0

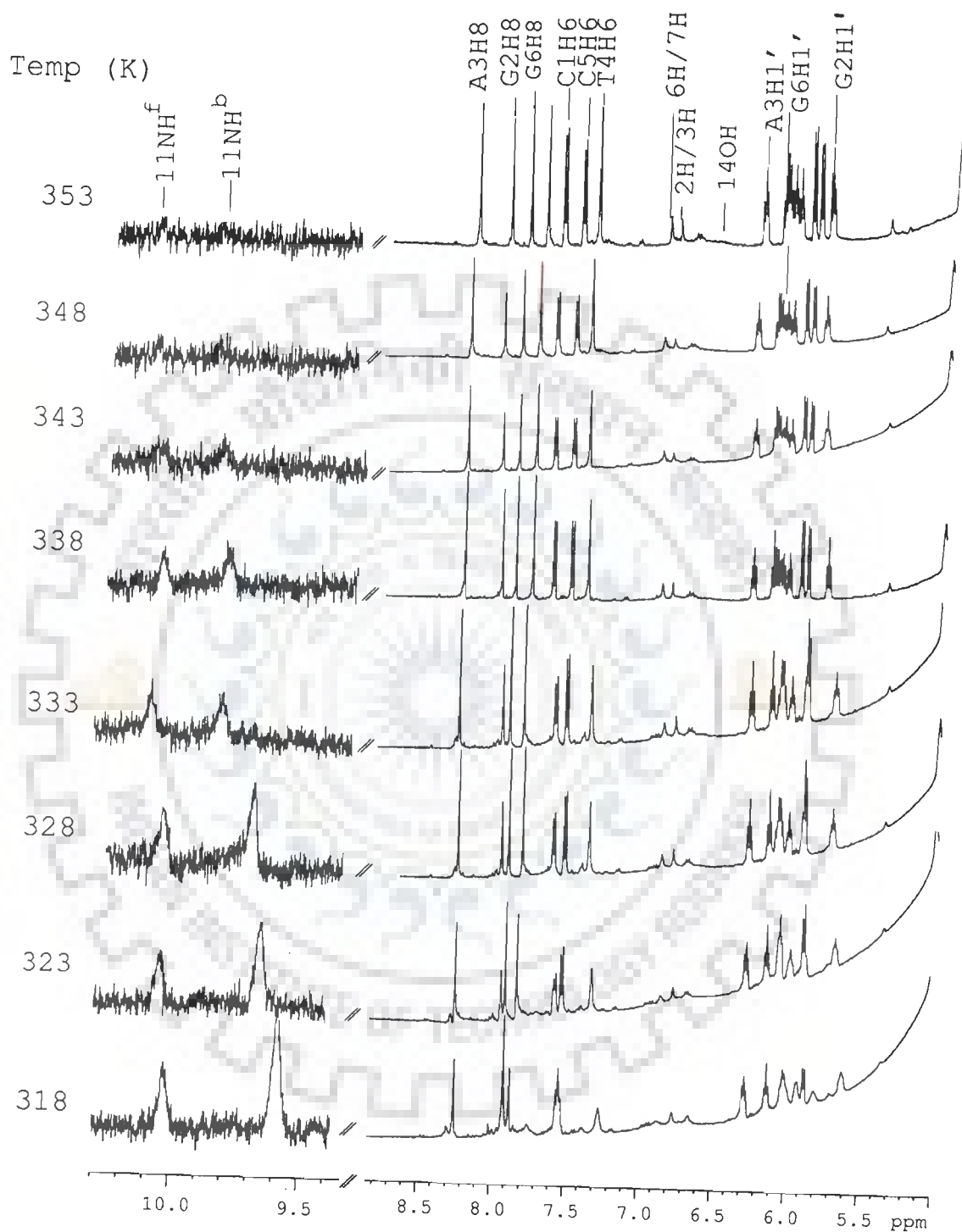


Fig. 6.3d(iv)

Fig 6.3 ^1H NMR spectra of mitoxantrone complexed with $d\text{-(CGATCG)}_2$ at various D/N ratios as a function of temperature (a) 1.0 (b) 1.50 (c) 1.75 (d) 2.0

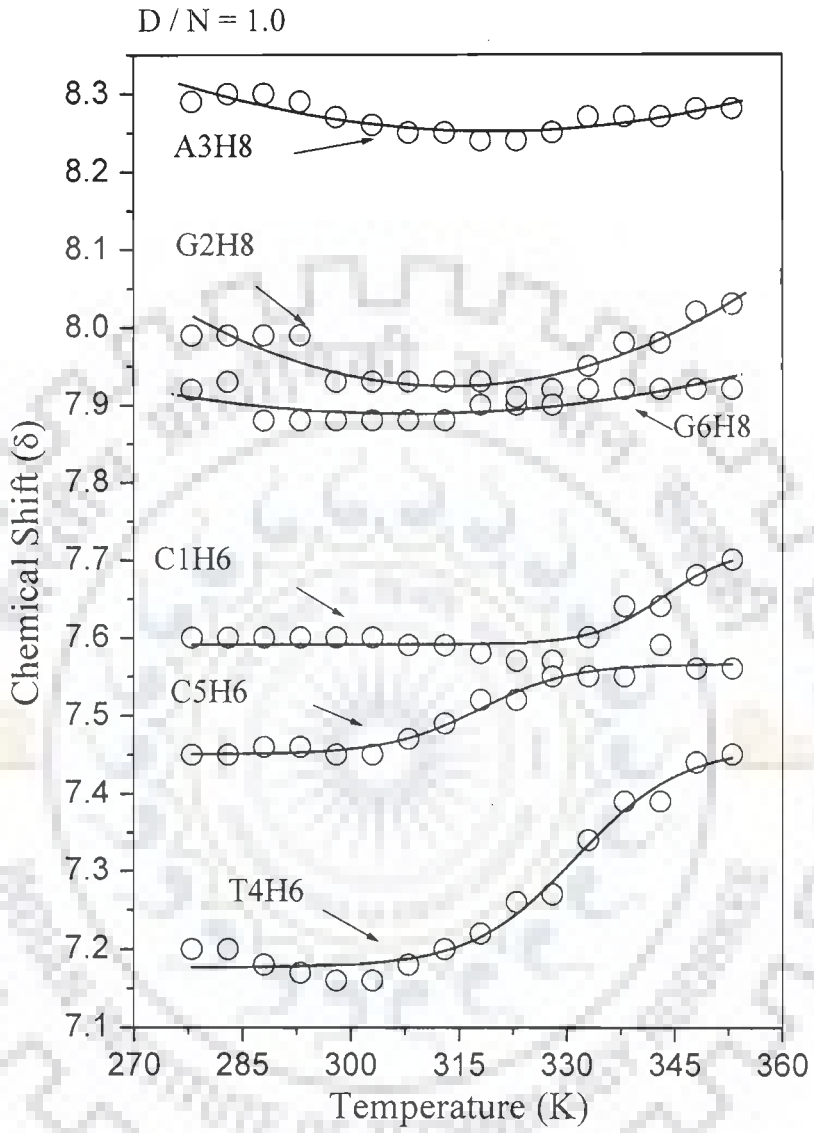


Fig. 6.4 a(i)

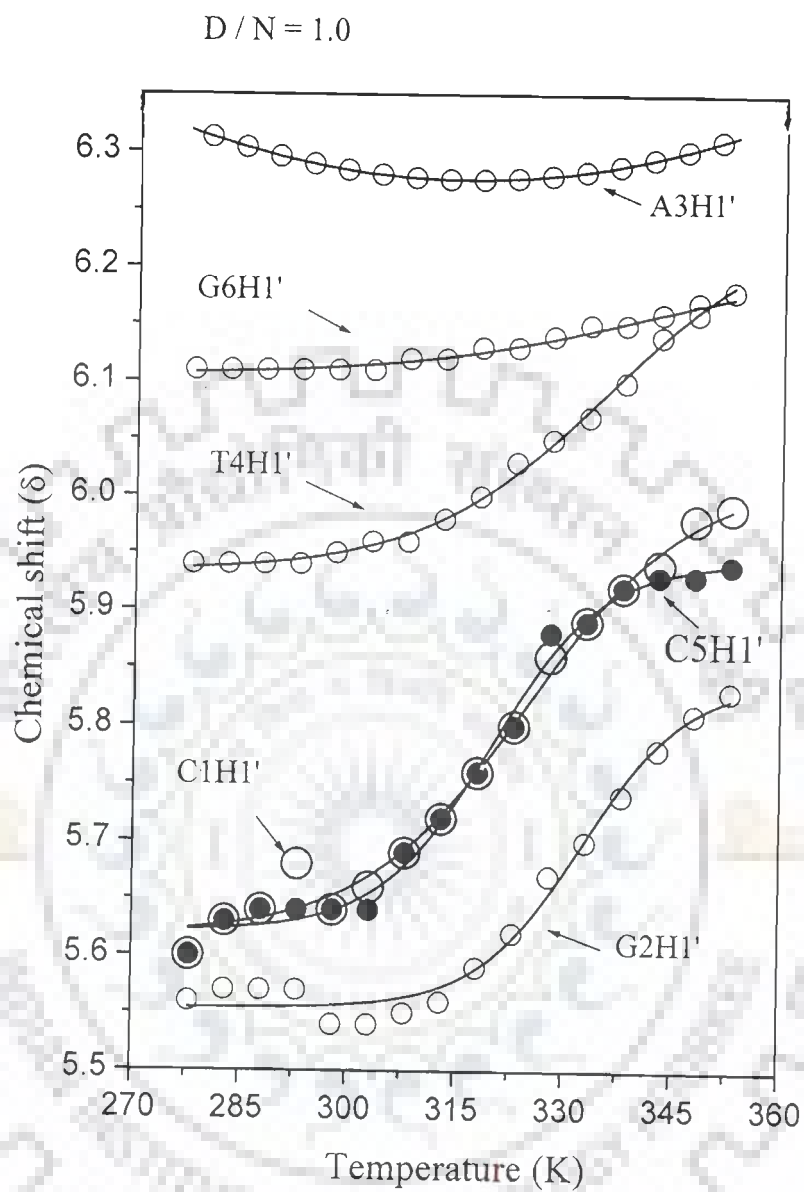


Fig. 6.4 a(ii)

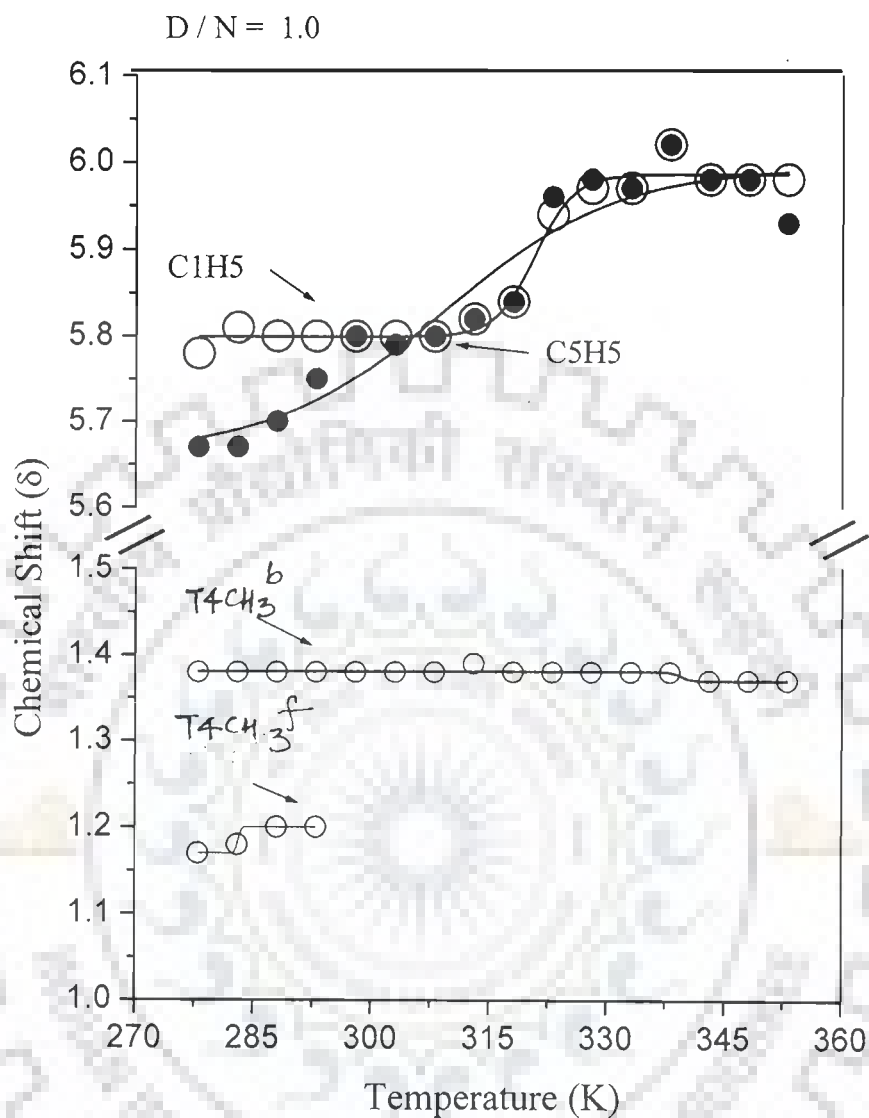


Fig. 6.4 a(iii)

Fig 6.4a ¹H chemical shift of mitoxantrone complexed with d-(CGATCG)₂ D / N = 1.0 at 278 K showing DNA protons. (i) Base region (ii) H1' region (iii) CH5 / TCH₃

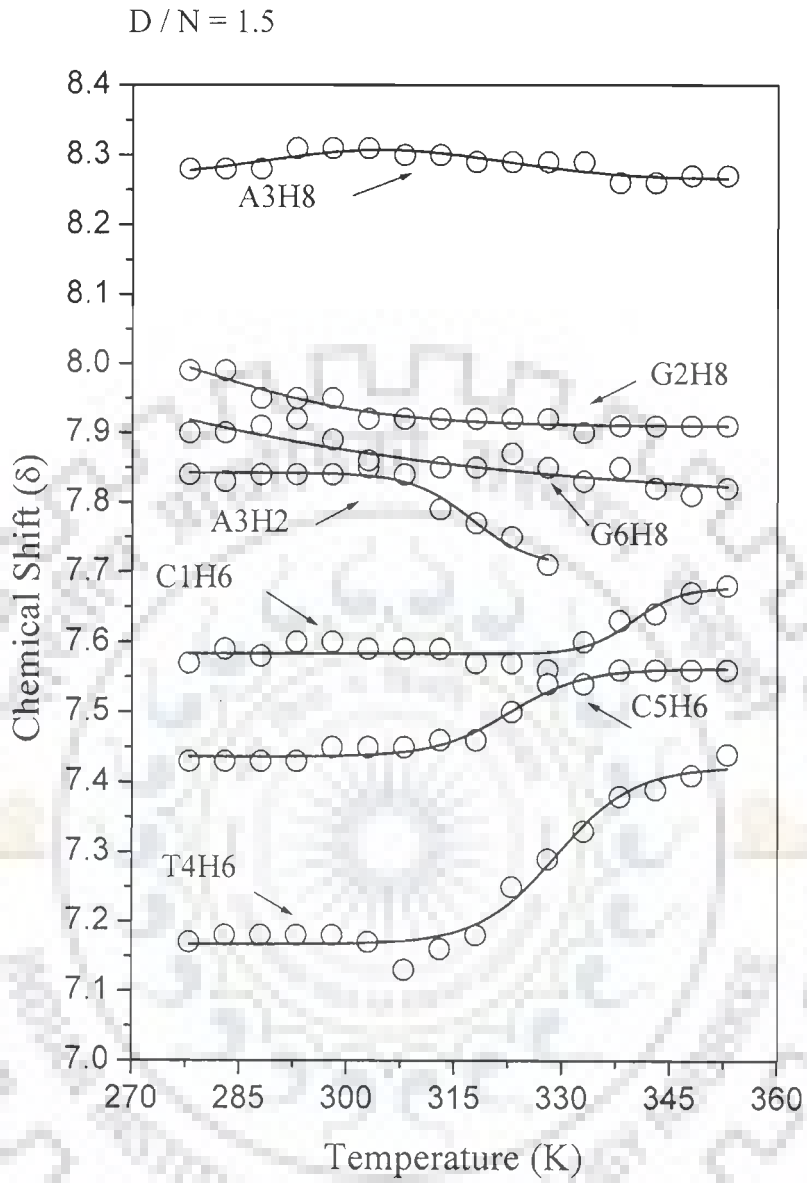


Fig. 6.4 b(i)

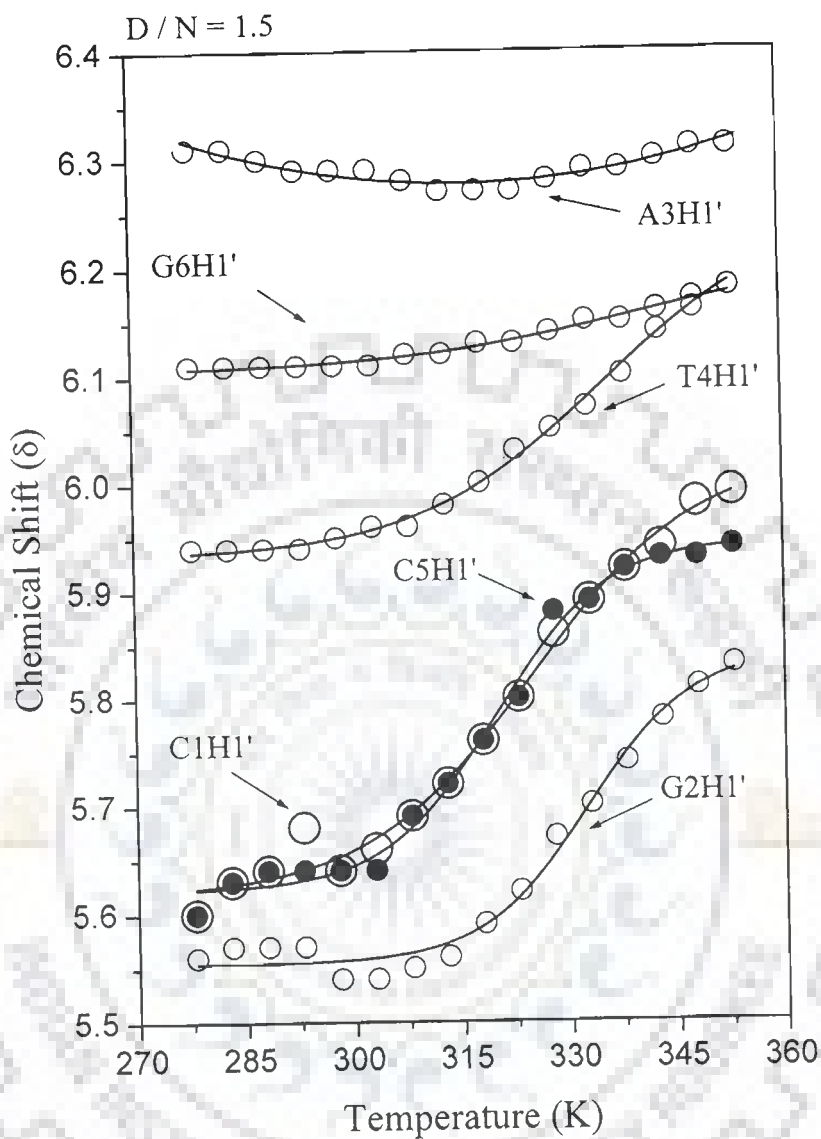


Fig. 6.4b(ii)

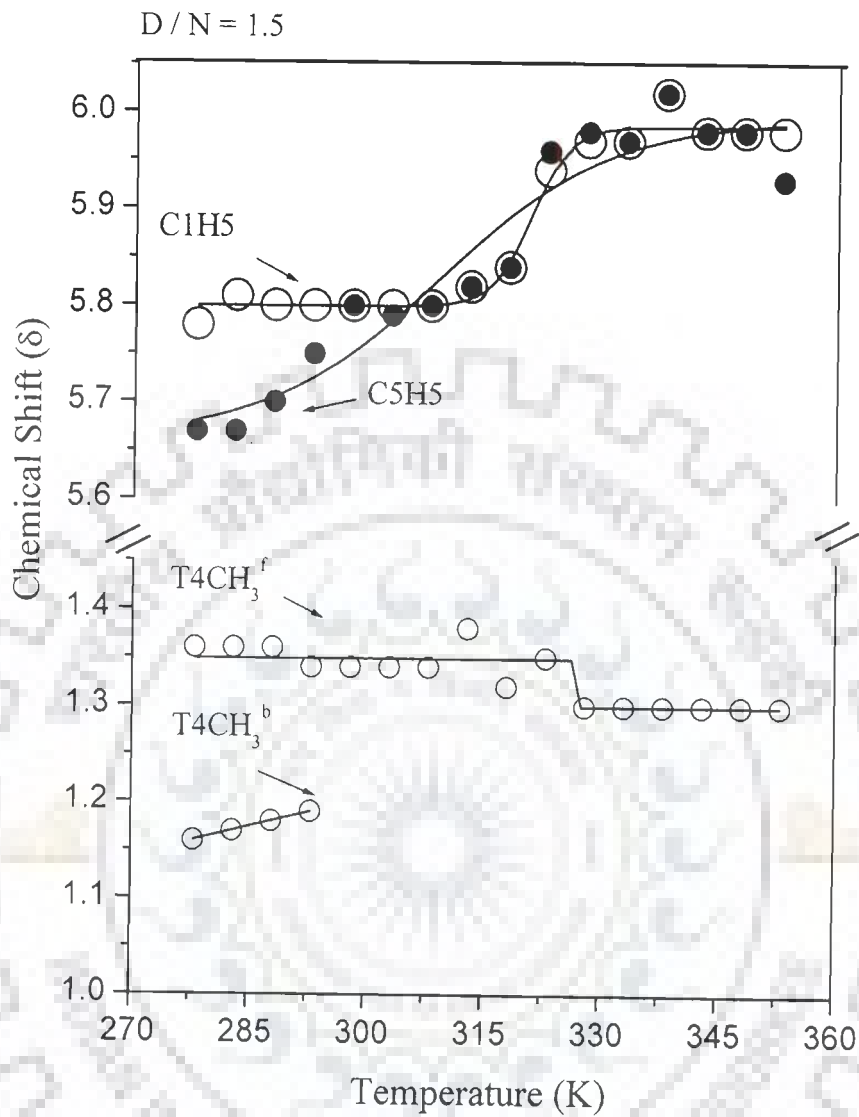


Fig. 6.4 b(iii)

Fig 6.4b ^1H chemical shift of mitoxantrone complexed with $d\text{-(CGATCG)}_2$ $D/N = 1.5$ at 278 K showing DNA protons. (i) Base region (ii) H1' region (iii) CH5 / TCH₃

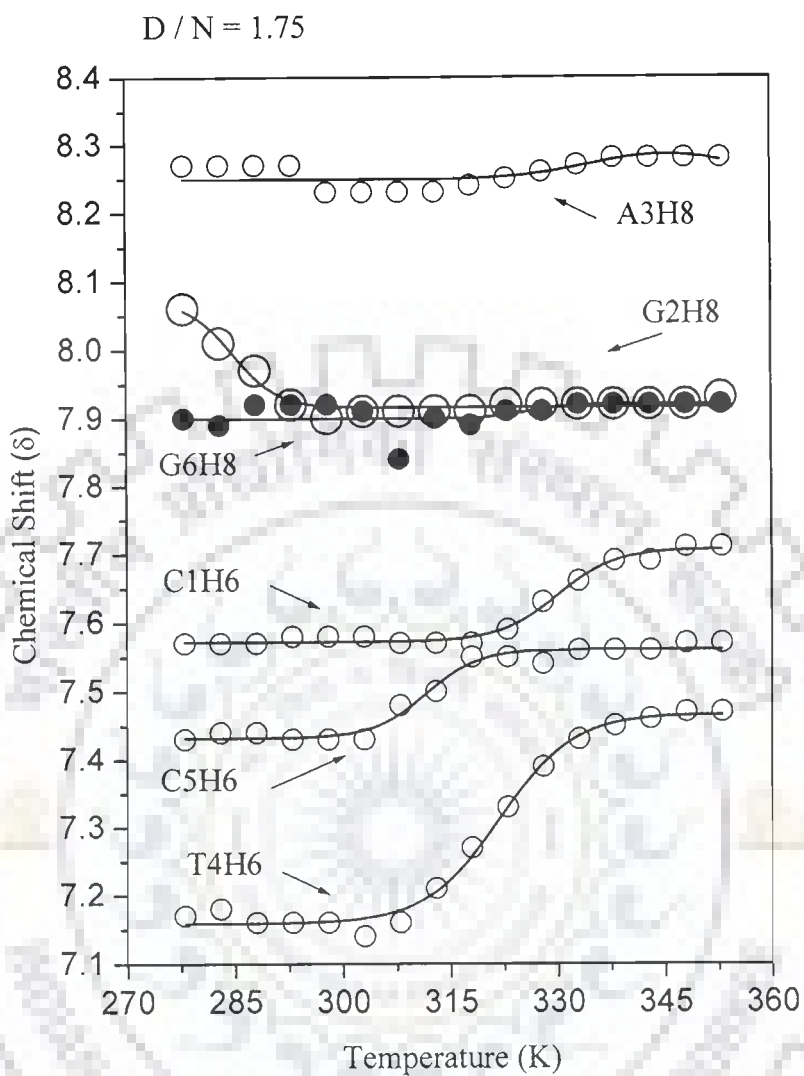


Fig. 6.4 c(i)

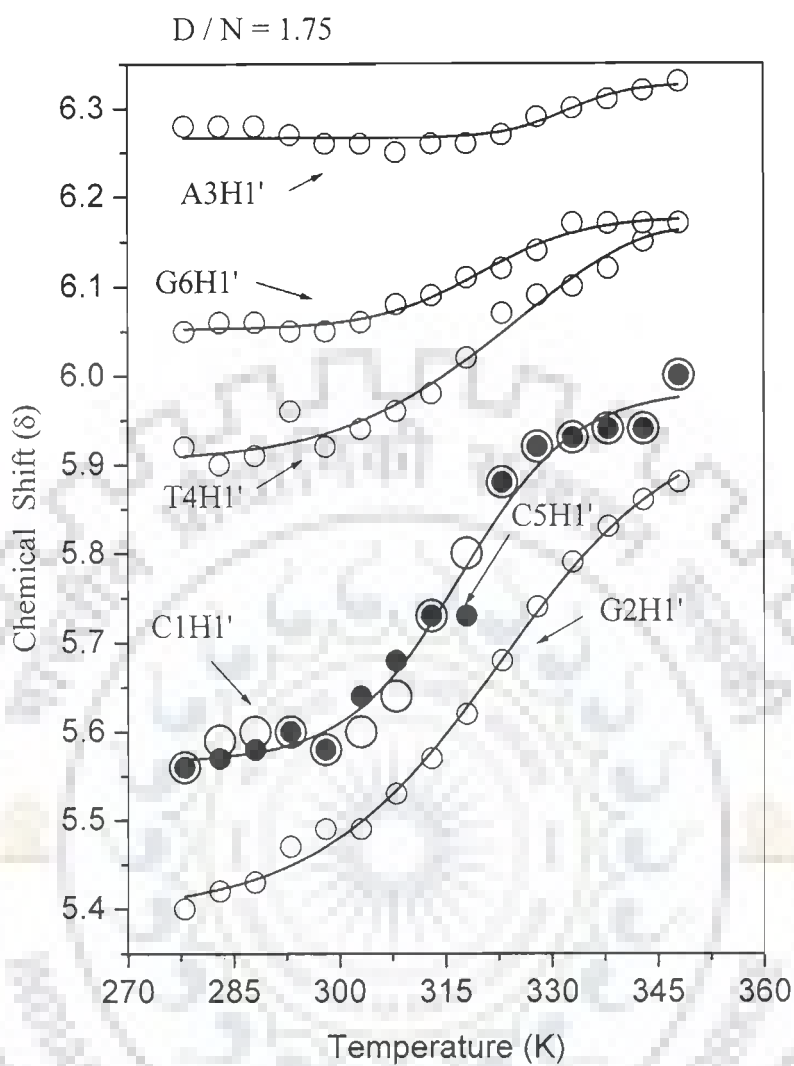


Fig. 6.4 c(ii)

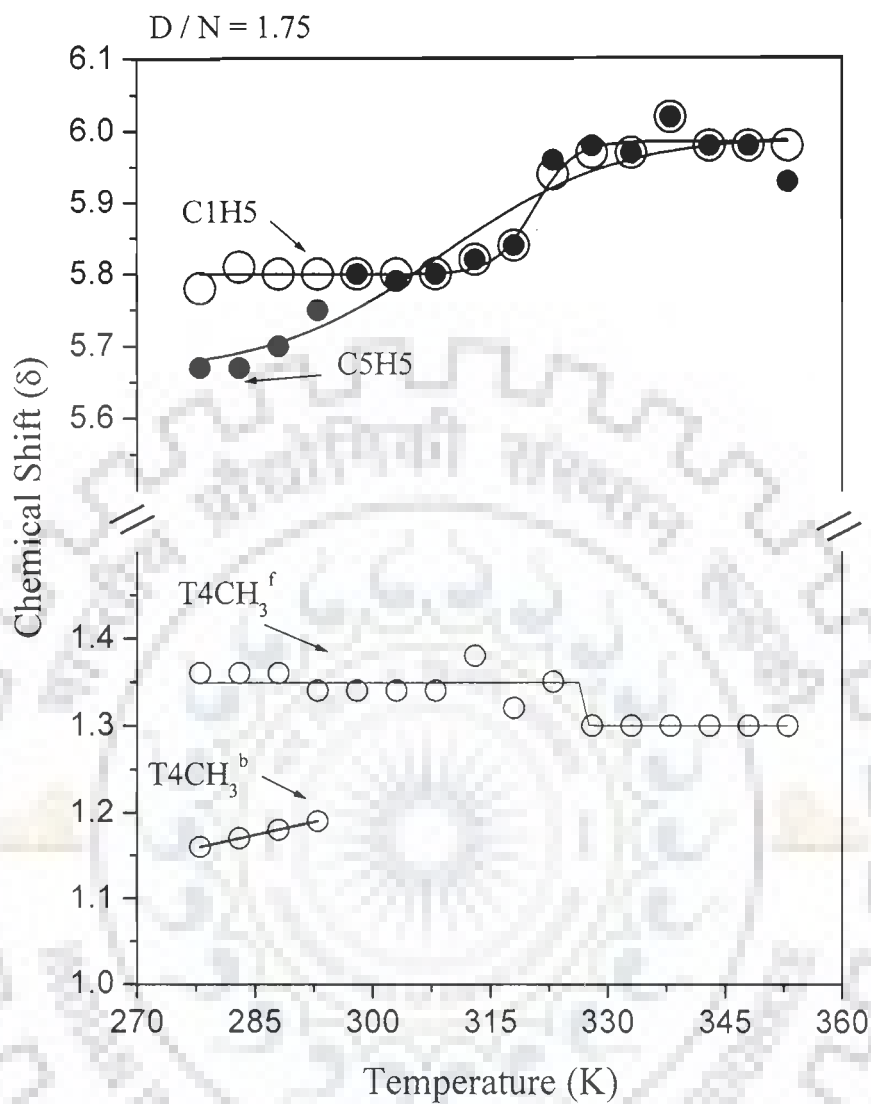


Fig. 6.4 c(iii)

Fig 6.4c ¹H chemical shift of mitoxantrone complexed with d-(CGATCG)₂ D / N = 1.75 at 278 K showing DNA protons. (i) Base region (ii) H1' region (iii) CH5 / TCH₃

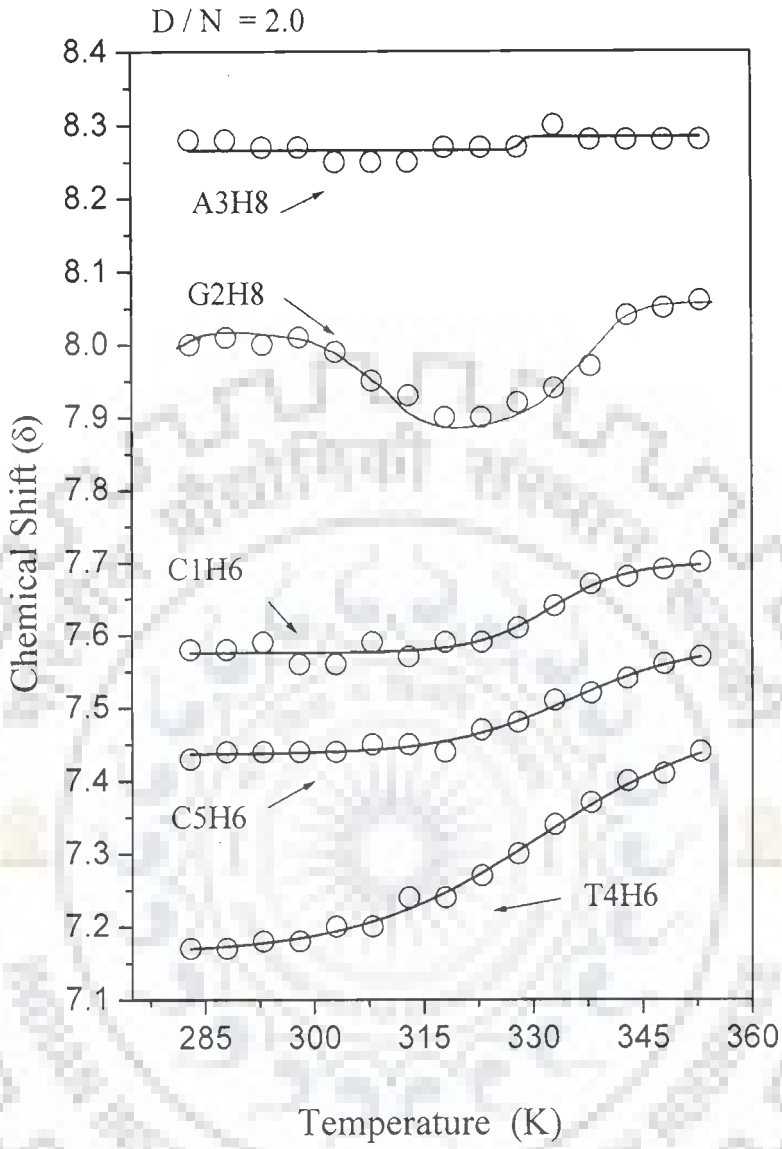


Fig. 6.4 d(i)

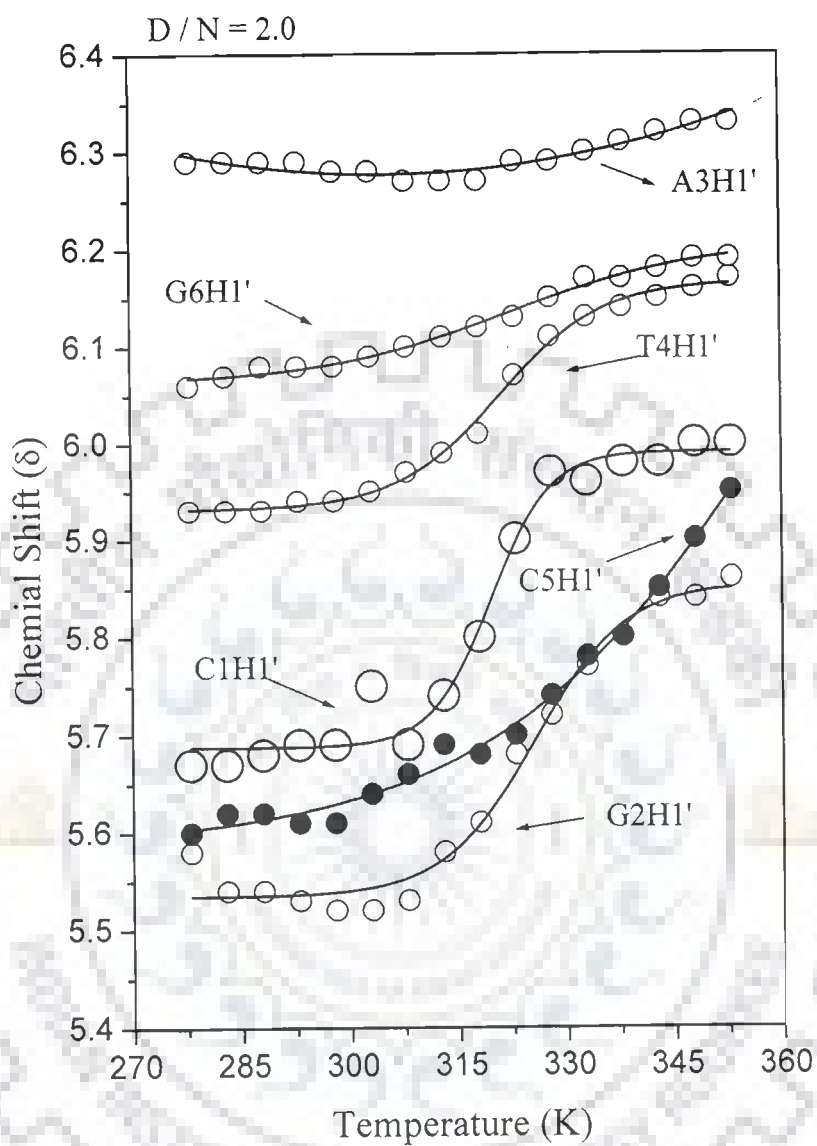


Fig. 6.4 d(ii)

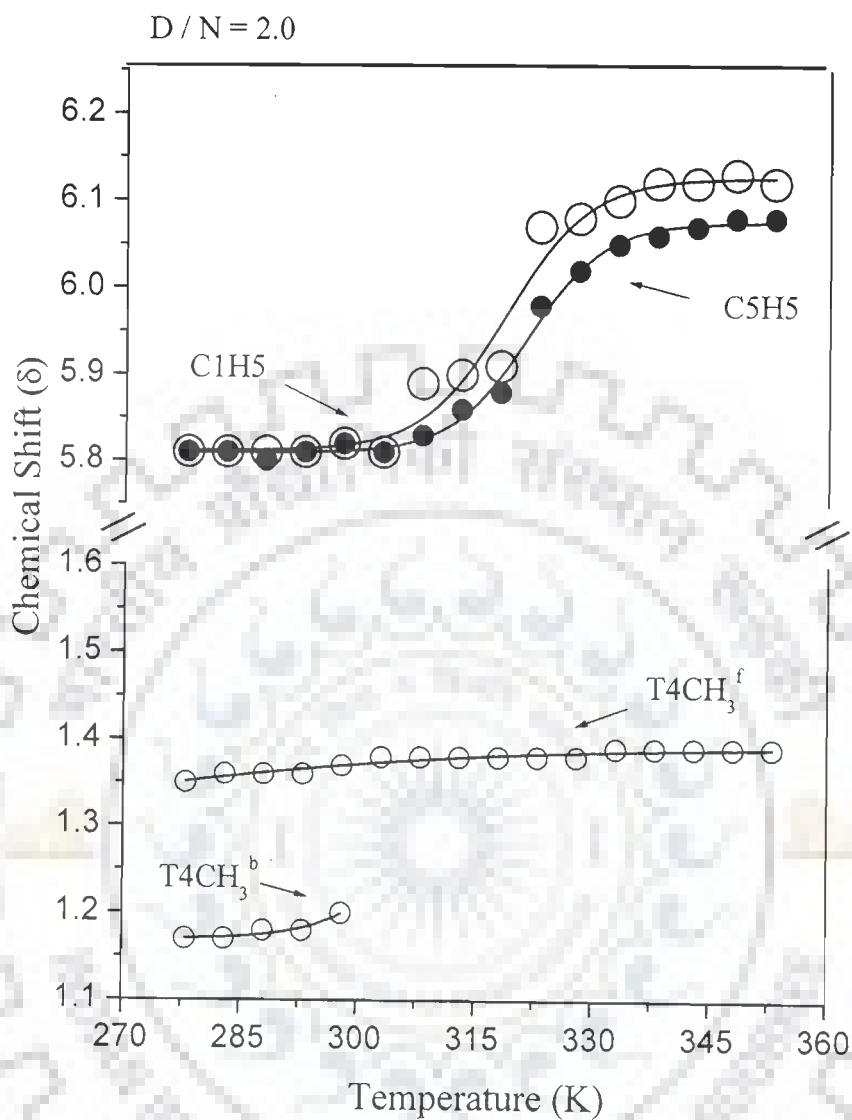


Fig 6.4d ^1H chemical shift of mitoxantrone complexed with $d\text{-(CGATCG)}_2$ D / N = 2.0 at 278 K showing DNA protons. (i) Base region (ii) H1' region (iii) CH5 / TCH₃

Table 6.4a Chemical shift (ppm) of some of the drug protons in drug –DNA complex having D / N = 1.00 as a function of temperature. Also shown here is the total change in chemical shift, $\Delta\delta$

$$(\text{D/N} = 1.0) = \delta_{353 \text{ K}} - \delta_{278 \text{ K}}$$

Temp. (K)	6H / 7H	2H / 3H	11NH ^b
278	6.92	6.82	9.39
283	6.92	6.82	9.43
288	6.92	6.81	9.44
293	6.92	6.81	9.46
298	6.92	6.81	9.50
303	6.92	6.79	9.50
308	6.91	6.78	9.50
313	6.91	6.77	9.55
318	6.91	6.77	9.58
323	6.89	6.77	9.64
328	6.89	6.77	9.68
333	6.91	6.79	9.71
338	6.94	6.82	9.82
343	6.97	6.86	9.87
348	7.00	6.88	9.91
353	7.02	6.90	9.93
$\Delta\delta_{(\text{D/N} = 1.0)}$	+ 0.10	+0.08	+0.54

-ve $\Delta\delta$ indicates upfield shift

+ve $\Delta\delta$ indicates downfield shift

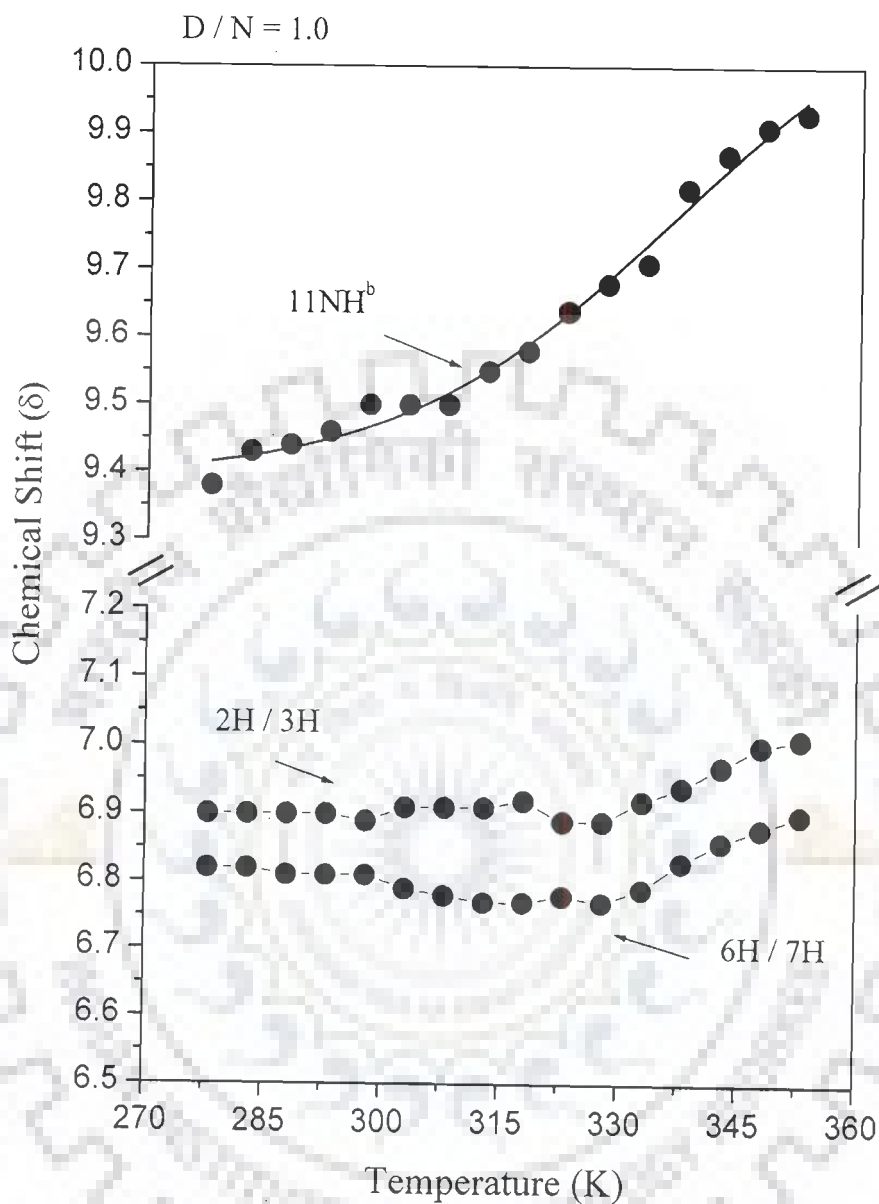


Fig. 6.5a

Fig.6.5a Chemical of drug protons shift of mitoxantrone complexed with d-(CGATCG)₂ at D / N = 1.0 in the temperature range 278K –353K.

Table 6.4b Chemical shift (ppm) of some of the drug protons in drug –DNA complex having D / N = 1.50 as a function of temperature. Also shown here is the total change in chemical shift, $\Delta\delta_{(D/N = 1.5)} = \delta_{353\text{ K}} - \delta_{278\text{ K}}$.

Temp. (K)	6H / 7H	2H / 3H	11NH ^b
278	6.92	6.82	9.38
283	6.91	6.80	9.40
288	6.92	6.80	9.42
293	6.90	6.80	9.43
298	6.90	6.79	9.47
303	6.90	6.77	9.49
308	6.91	6.76	9.52
313	6.92	6.76	9.55
318	6.91	6.75	9.57
323	6.88	6.75	9.59
328	6.88	6.75	9.63
333	6.88	6.76	9.67
338	6.88	6.78	9.72
343	6.91	6.81	9.78
348	6.94	6.83	9.83
353	6.96	6.85	9.85
$\Delta\delta_{(D/N = 1.5)}$	+0.04	+ 0.03	+ 0.47

-ve $\Delta\delta$ indicates upfield shift

+ve $\Delta\delta$ indicates downfield shift

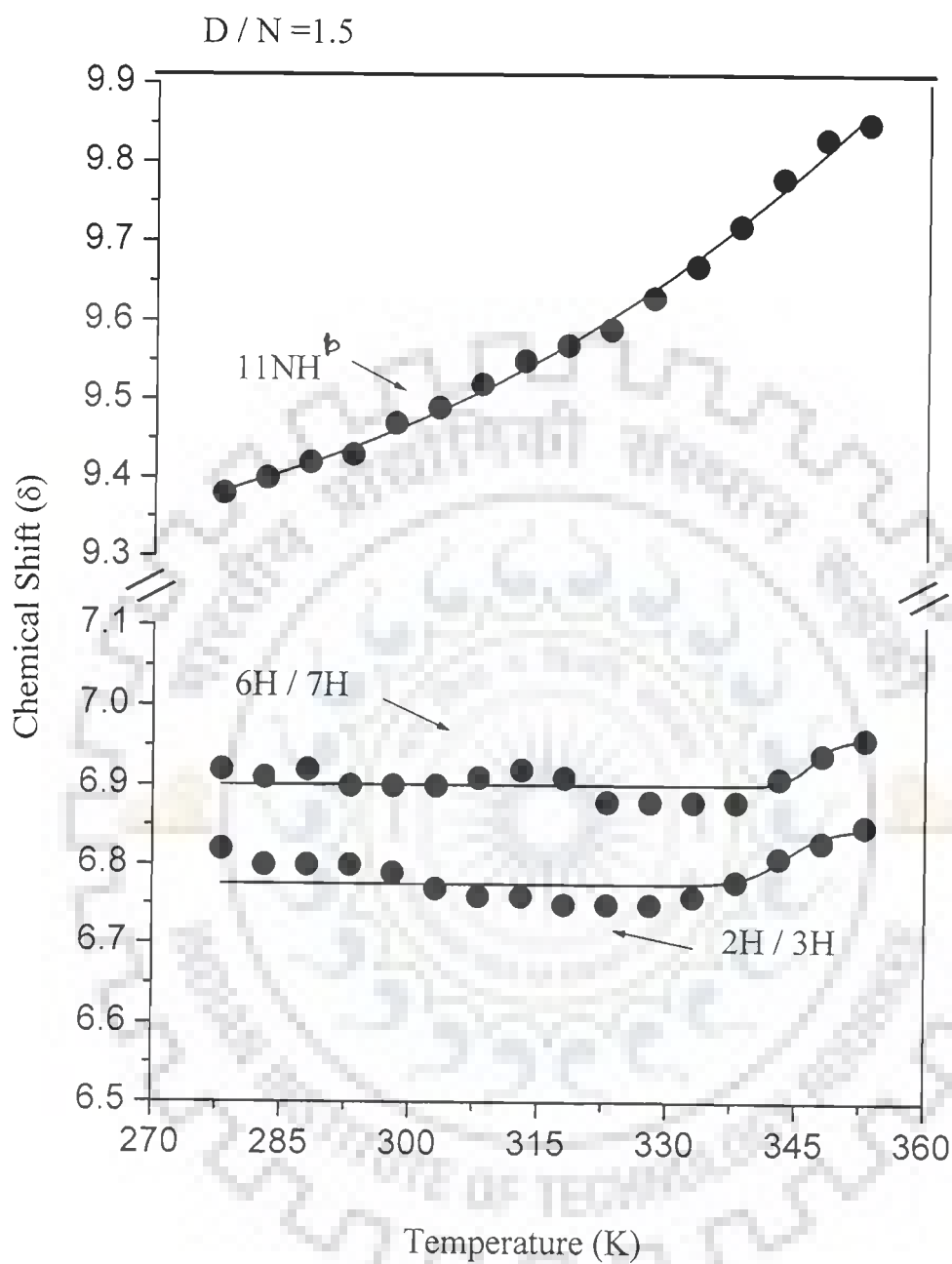


Fig. 6.5b

Fig.6.5b Chemical of drug protons shift of mitoxantrone complexed with d-(CGATCG)₂ at D / N = 1.5 in the temperature range 278K –353K.

Table 6.4c Chemical shift (ppm) of some of the drug protons in drug–DNA complex having $D/N = 1.75$ as a function of temperature. Also shown here is the total change in chemical shift, $\Delta\delta_{(D/N=1.75)} = \delta_{353\text{ K}} - \delta_{278\text{ K}}$.

Temp. (K)	6H / 7H	2H / 3H	11NH ^f	11NH ^b
278	6.89	6.82	9.72	9.38
283	6.89	6.82	10.00	9.40
288	6.90	6.80	10.00	9.41
293	6.90	6.78	10.00	9.45
298	6.90	6.78	9.99	9.46
303	6.90	6.76	10.02	9.51
308	6.91	6.75	10.02	9.53
313	6.87	6.75	10.07	9.57
318	6.85	6.75	10.06	9.62
323	6.86	6.76	10.05	9.68
328	6.90	6.80	10.05	9.77
333	6.93	6.84	10.06	9.81
338	6.94	6.86	10.06	9.86
343	6.95	6.87	–	9.87
348	6.95	6.88	–	–
353	6.95	6.88	–	–
$\Delta\delta_{(D/N=1.75)}$	+0.05	+0.04	+0.34	+0.49

-ve $\Delta\delta$ indicates upfield shift

+ve $\Delta\delta$ indicates downfield shift

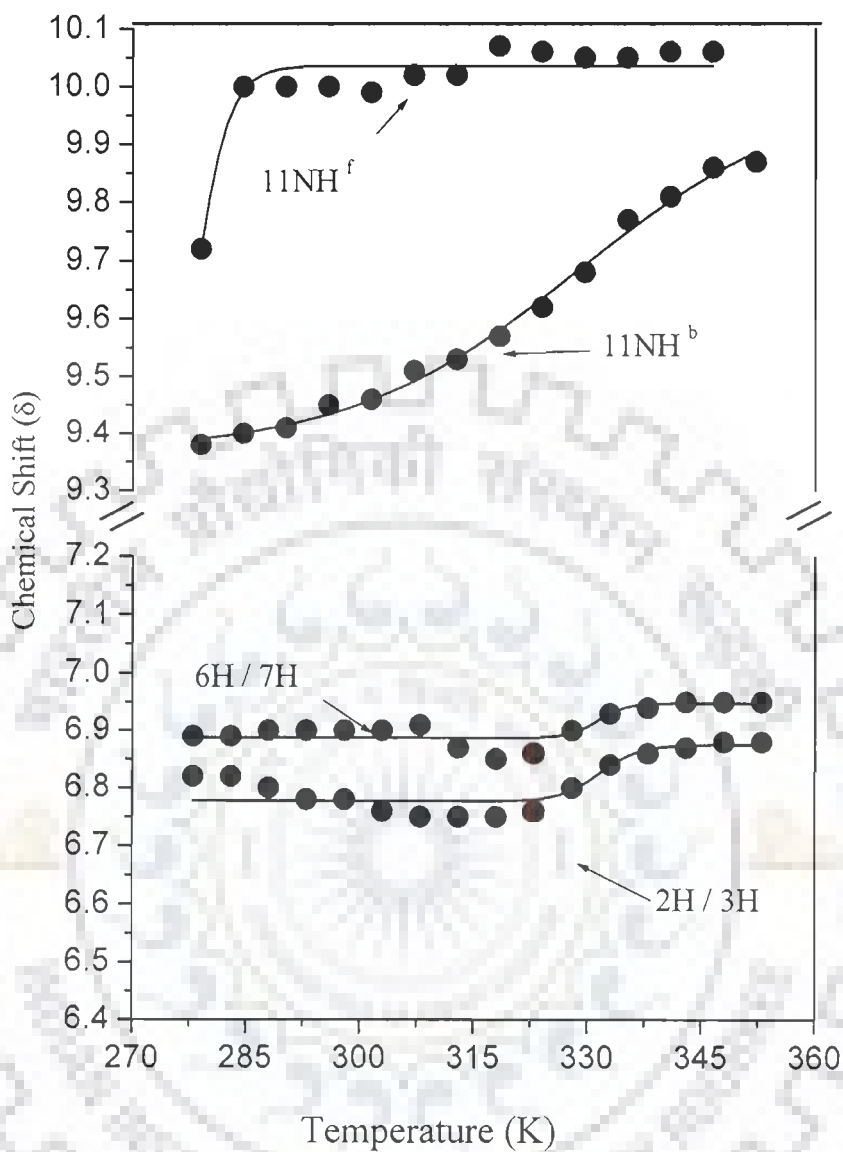


Fig. 6.5c

Fig.6.5c Chemical of drug protons shift of mitoxantrone complexed with d-(CGATCG)₂ at D / N = 1.75 in the temperature range 278K –353K.

Table 6.4d Chemical shift (ppm) of some of the drug protons in drug –DNA complex having D / N = 2.0 as a function of temperature. Also shown here is the total change in chemical shift, $\Delta\delta_{(D/N = 2.0)} - \delta_{353\text{ K}} - \delta_{278\text{ K}}$.

Temp (K)	6H / 7H	2H / 3H	11NH ^f	11NH ^b
278	6.93	6.81	10.03	9.38
283	6.93	6.82	10.00	9.40
288	6.92	6.82	9.96	9.41
293	6.92	6.82	9.95	9.44
298	6.92	6.79	9.96	9.46
303	6.90	6.78	9.98	9.50
308	6.96	6.77	10.03	9.54
313	6.91	6.76	10.03	9.58
318	6.91	6.86	10.03	9.59
323	6.96	6.88	10.05	9.67
328	6.96	6.86	10.07	9.72
333	6.95	6.85	10.08	9.80
338	6.94	6.93	10.09	9.83
343	6.93	6.88	10.15	9.86
348	6.97	6.84	10.15	9.89
353	6.97	6.85	10.15	9.89
$\Delta\delta_{(D/N = 2.0)}$	+0.04	+ 0.04	+ 0.12	+0.51

-ve $\Delta\delta$ indicates upfield shift

+ve $\Delta\delta$ indicates downfield shift

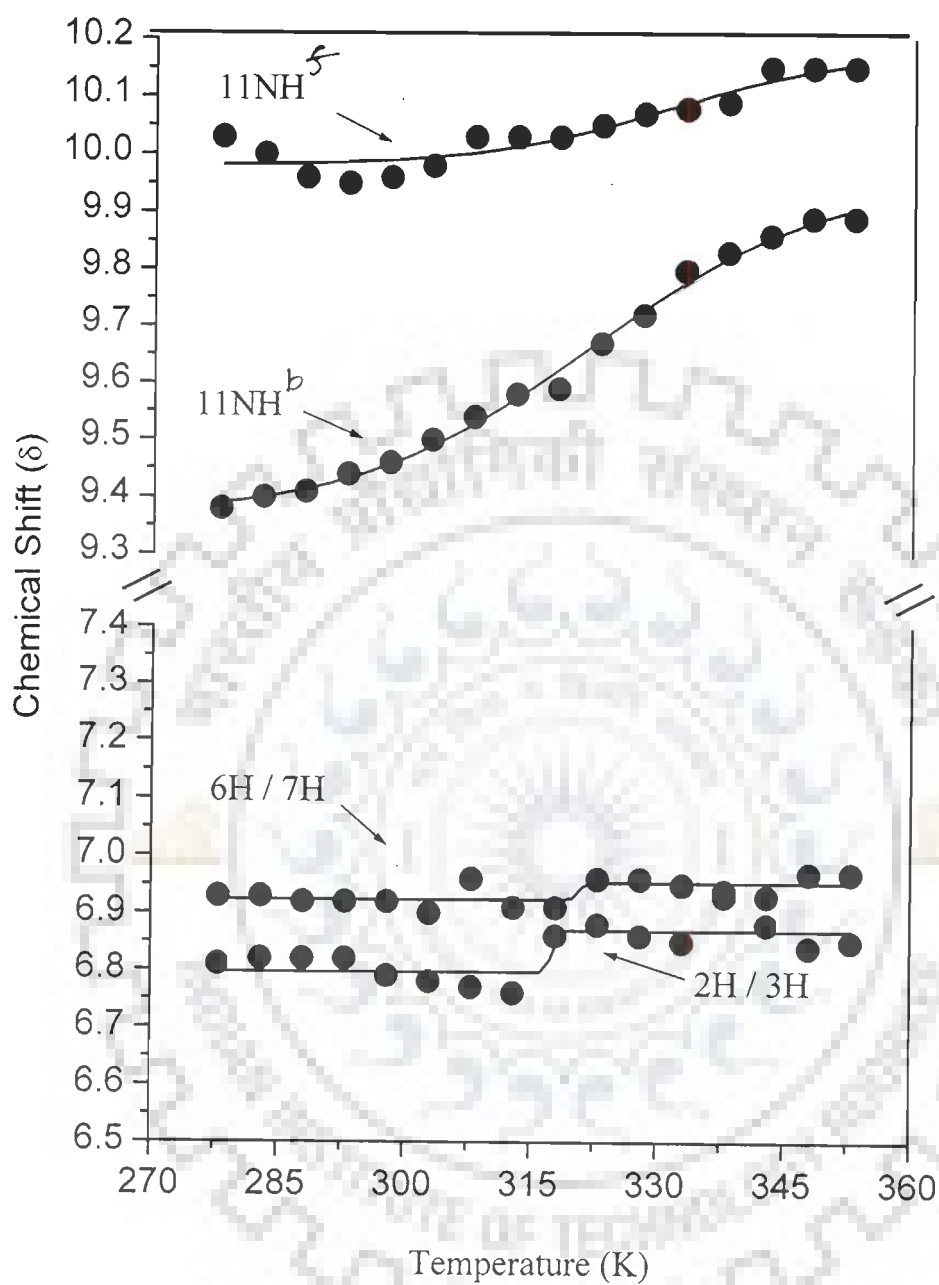


Fig. 6.5d

Fig.6.5d Chemical of drug protons shift of mitoxantrone complexed with $d\text{-(CGATCG)}_2$ at $D/N = 2.0$ in the temperature range 278K –353K.

D / N = 1.0

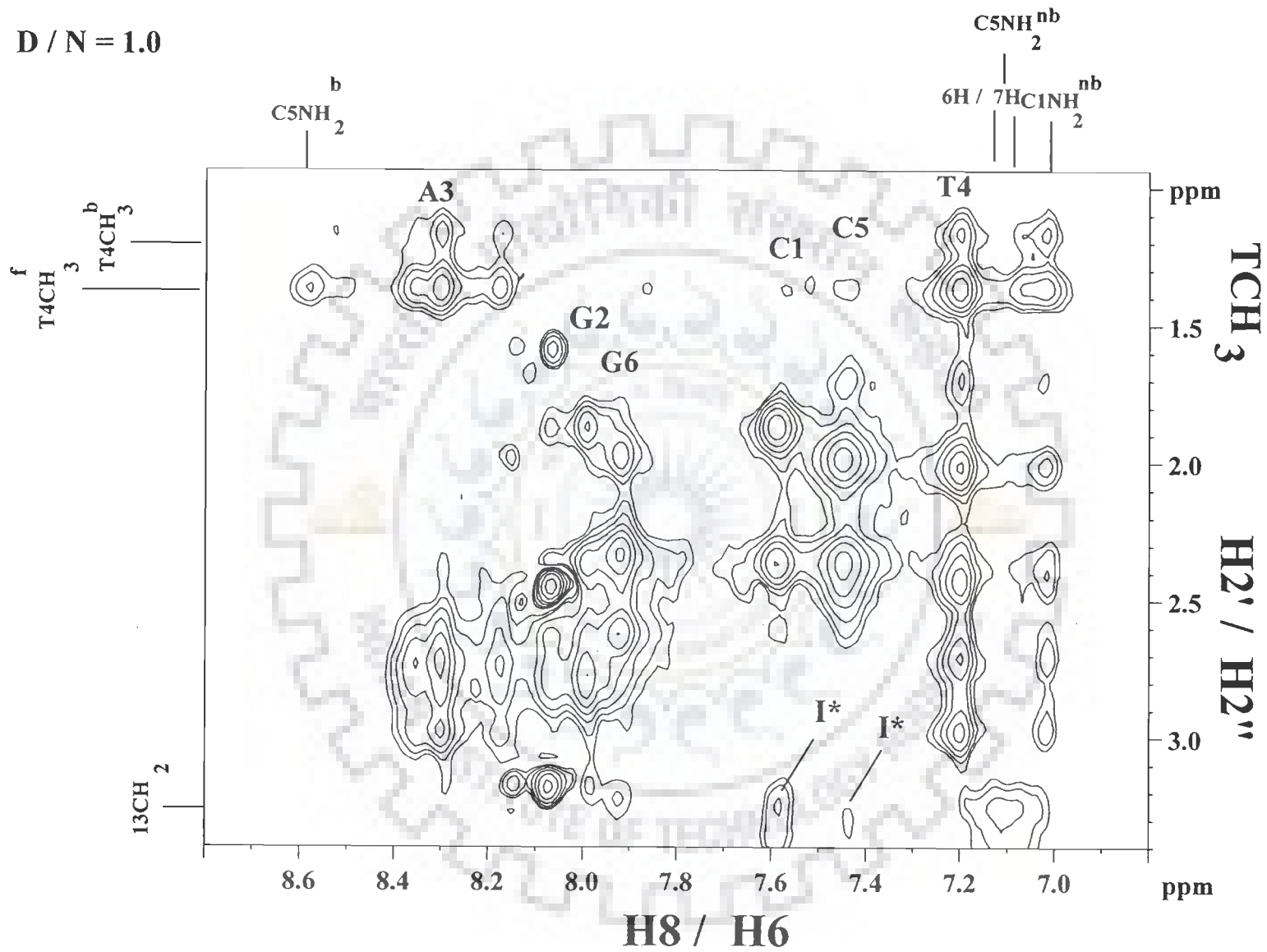
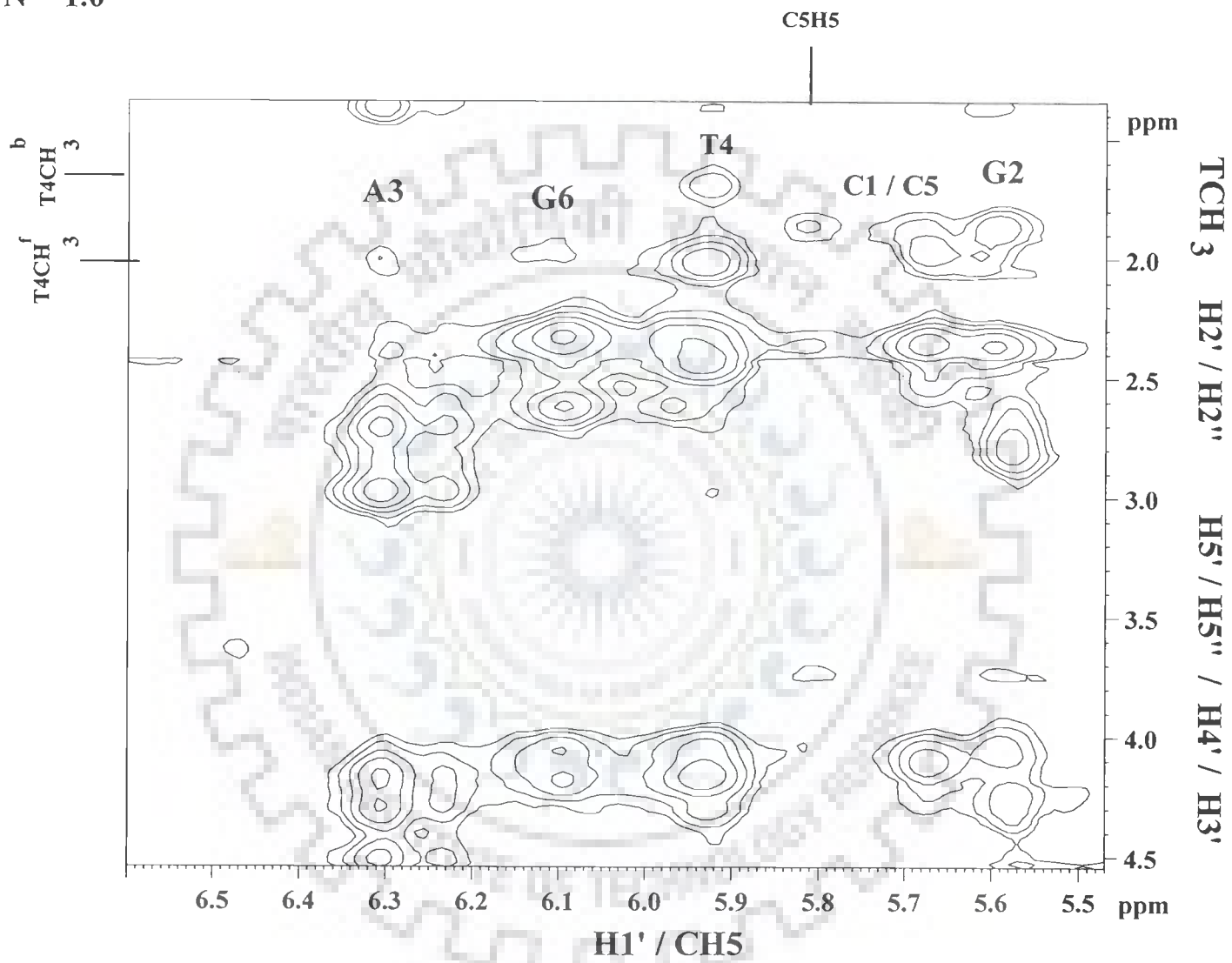


Fig. 6.6 (i)

$D/N = 1.0$ 

262b

Fig. 6.6 (ii)

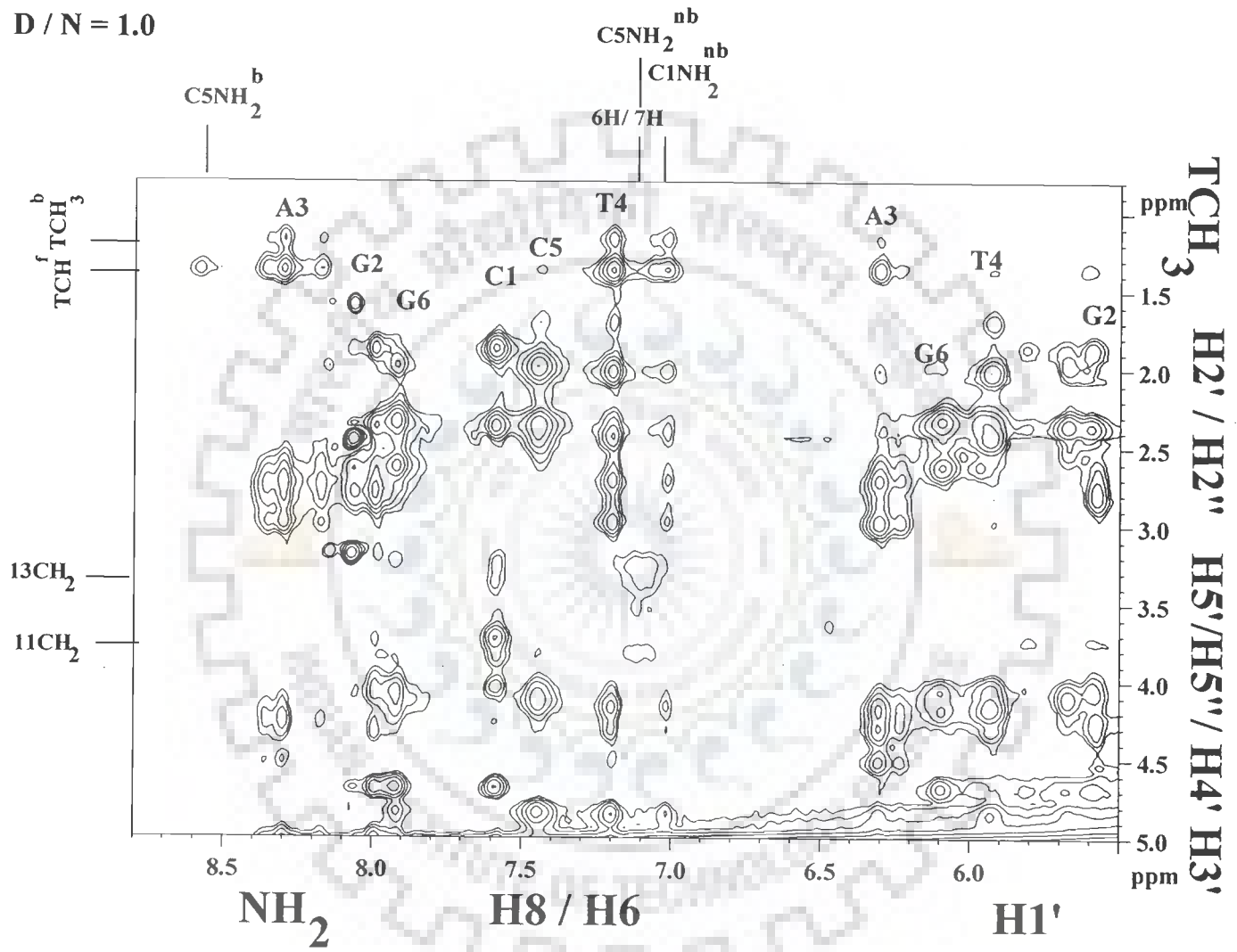


Fig. 6.6 (iii)

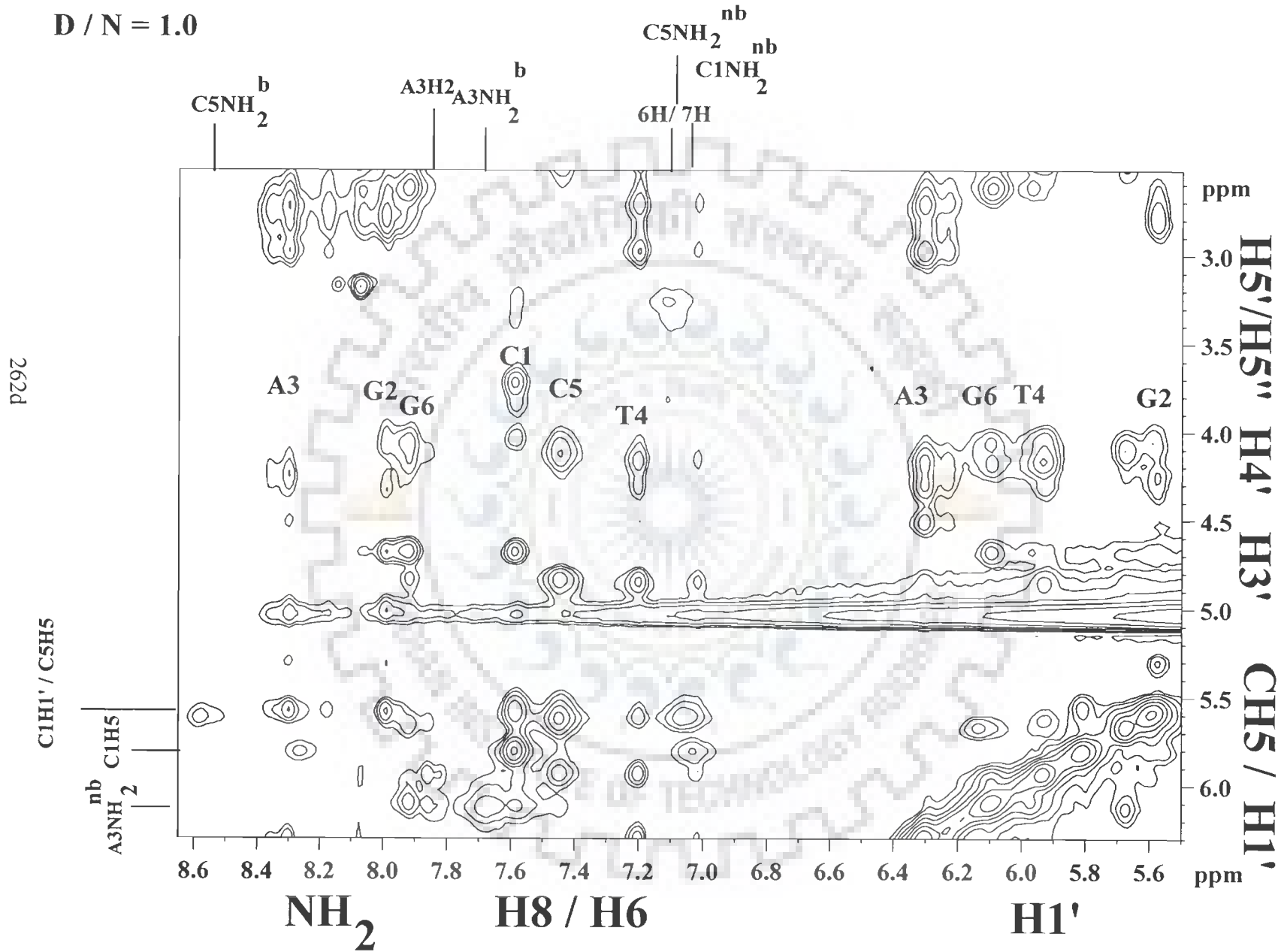


Fig. 6.6(iv)

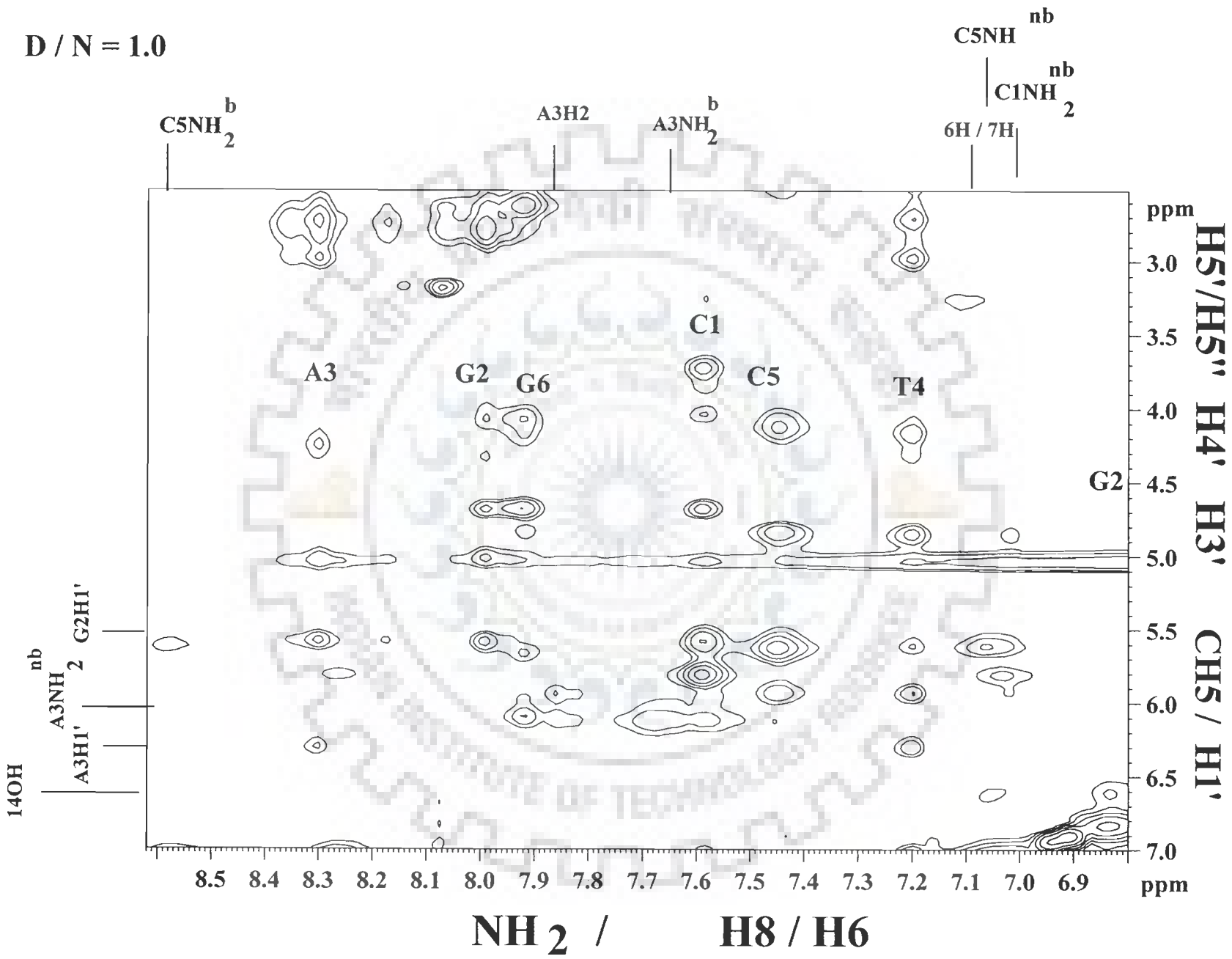


Fig. 6.6 (v)

262f

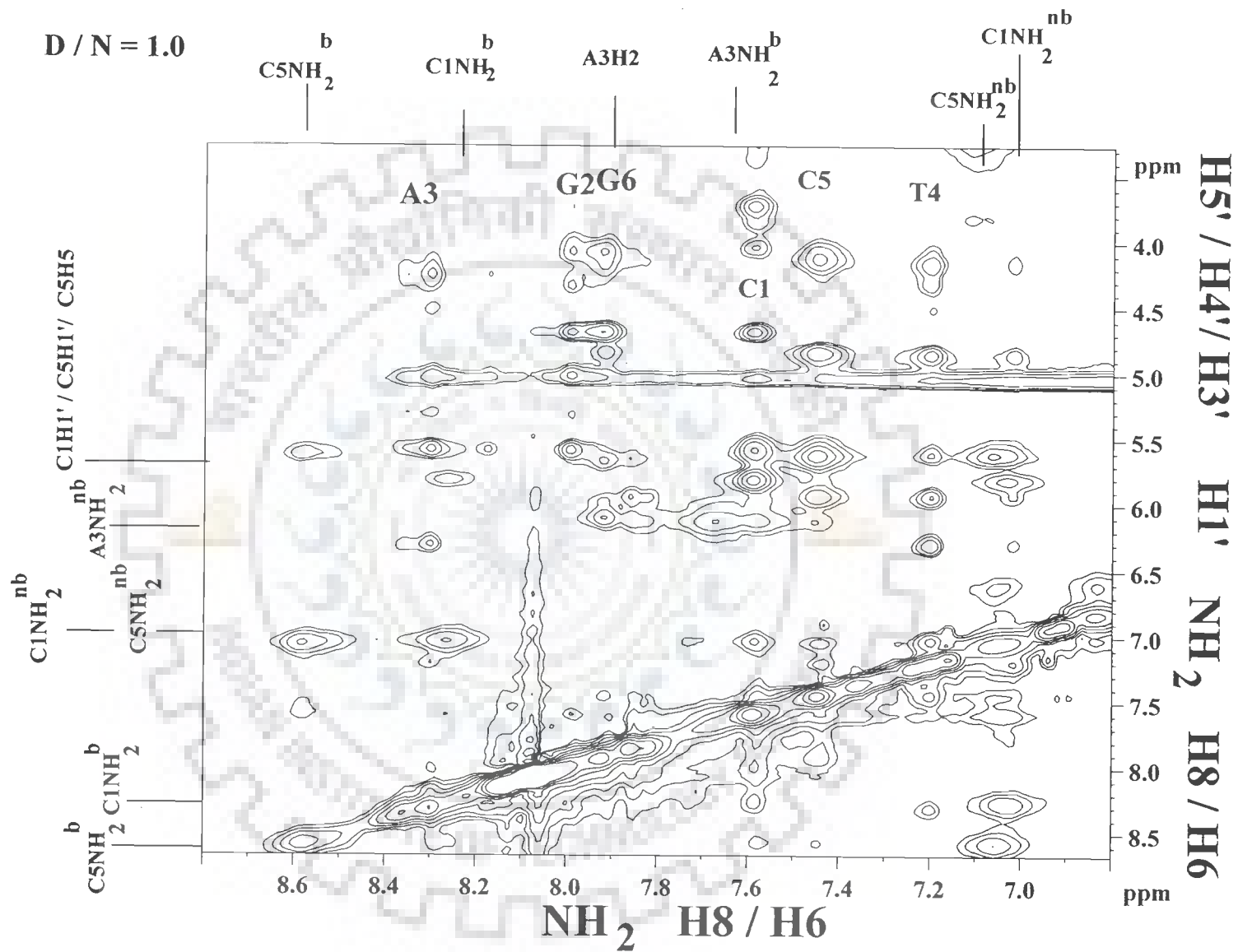


Fig. 6.6 (vi)

262g

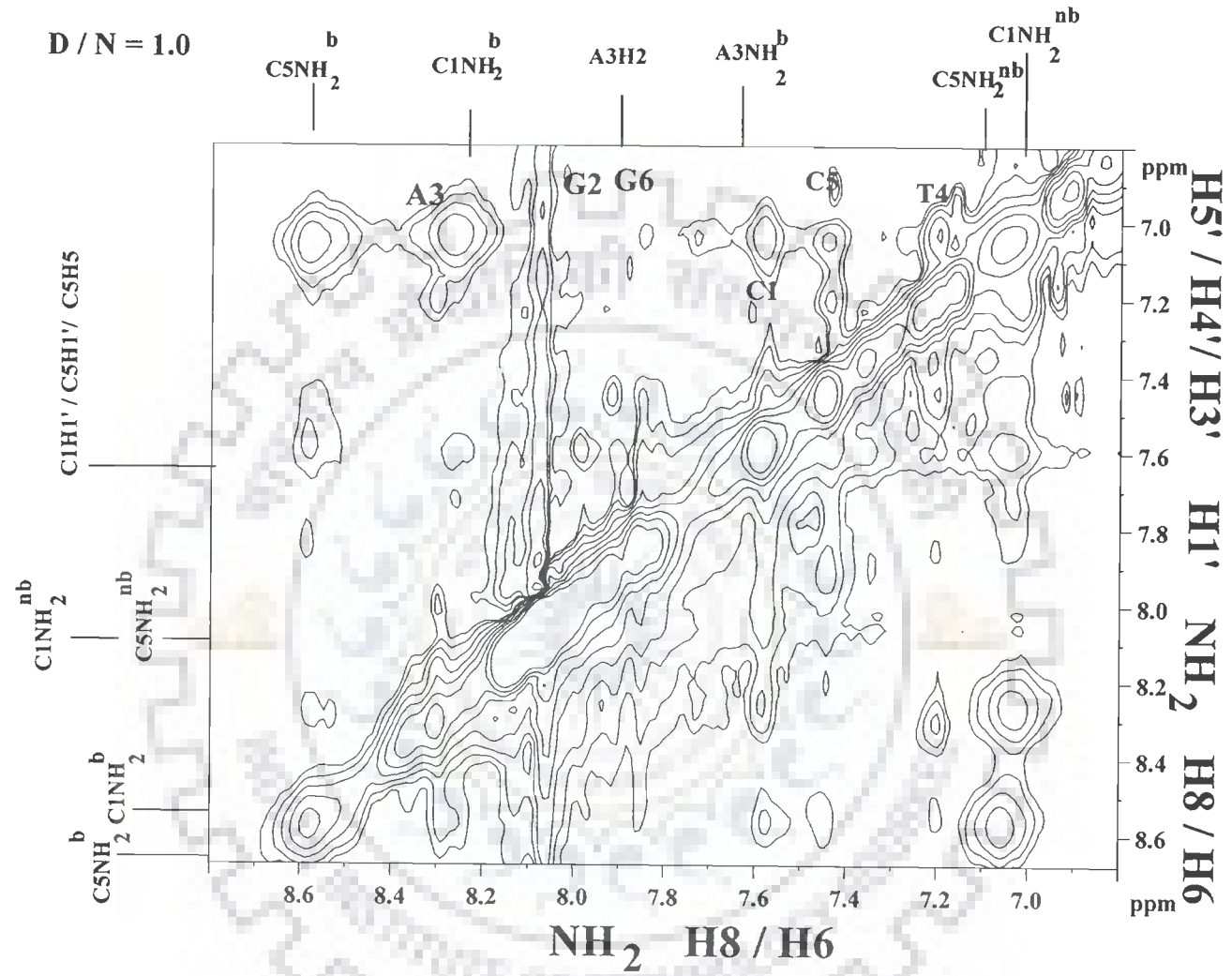


Fig. 6.6(vii)

Fig. 6.6(i-vii) Expansions of the specific region of the NOESY spectra of mitoxantrone complexed with d-(CGATCG)₂ to highlight connectivities at D / N = 1.0.

D / N = 1.0

262h

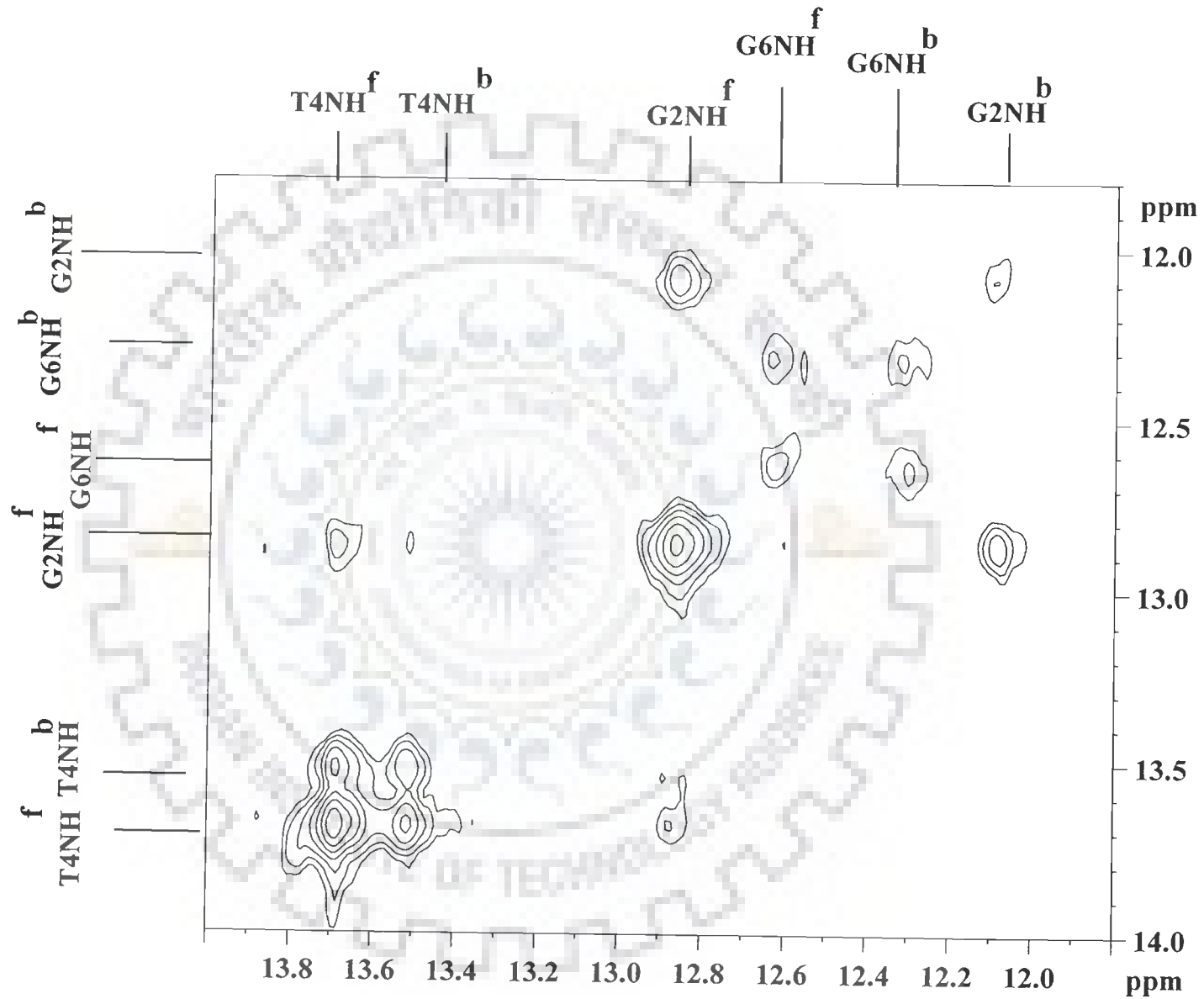


Fig. 6.6 (a)

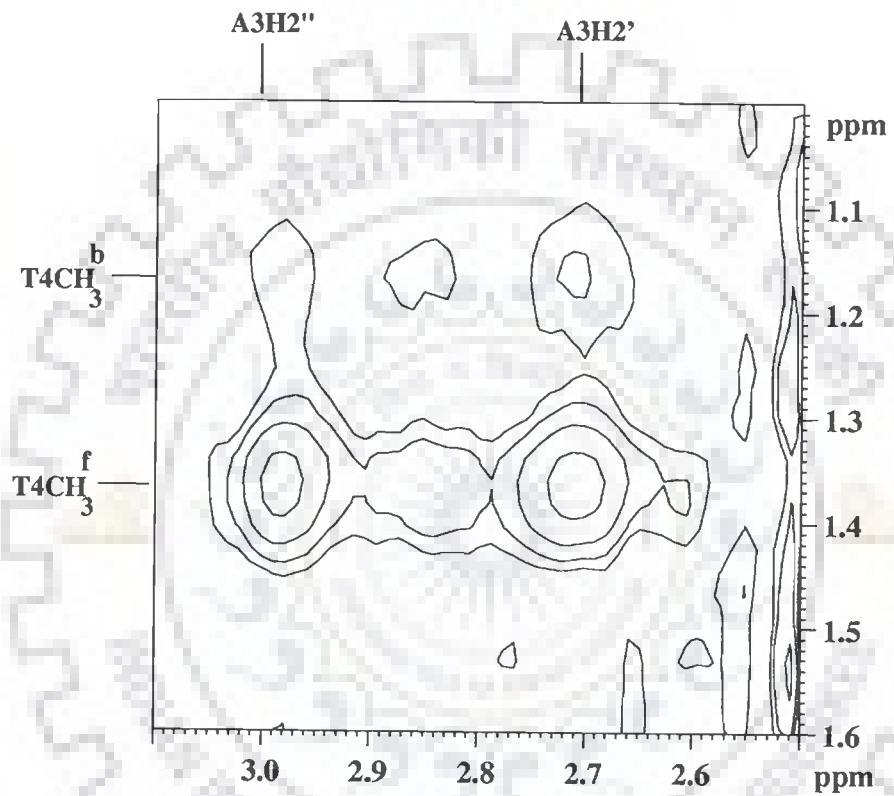


Fig. 6.6b

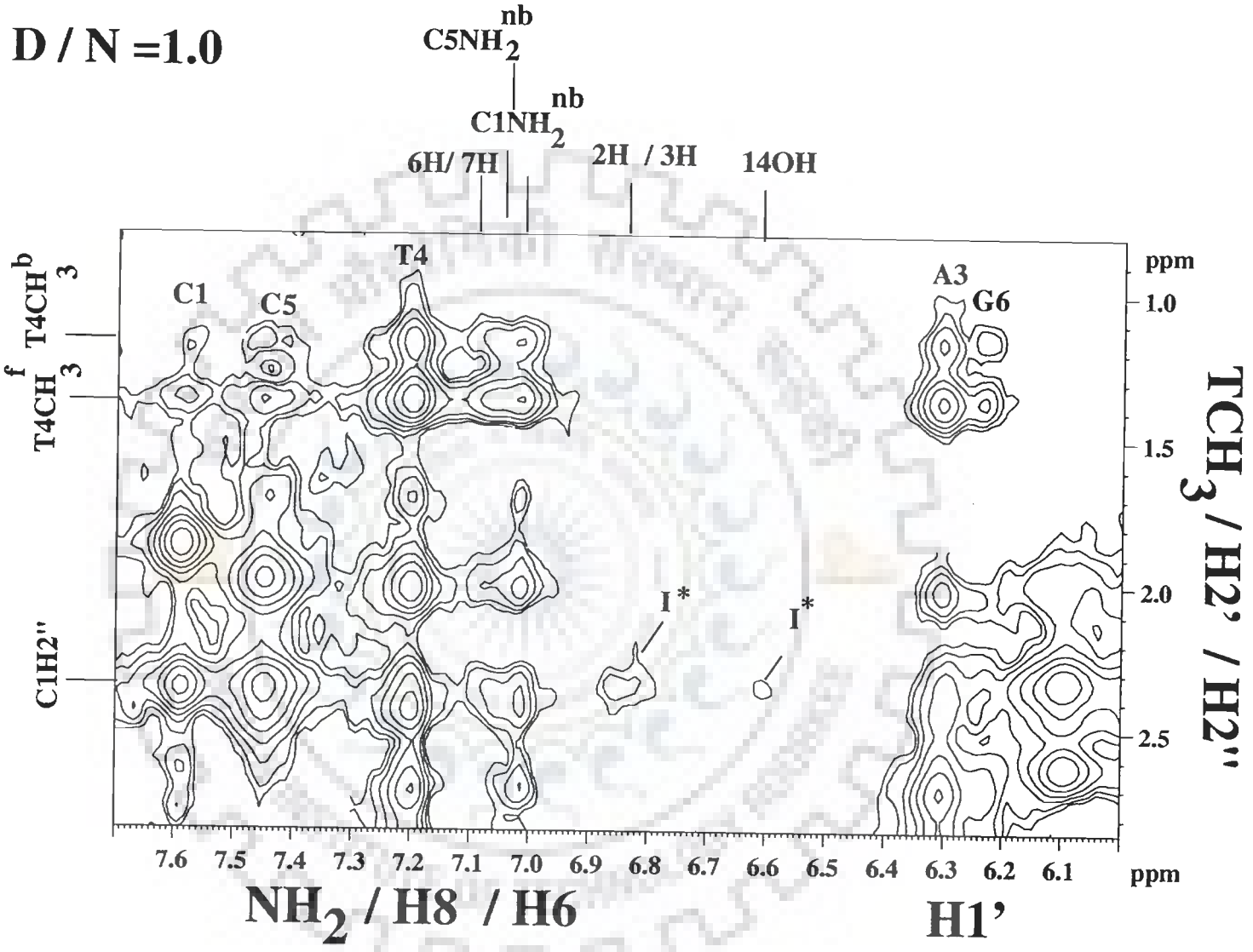
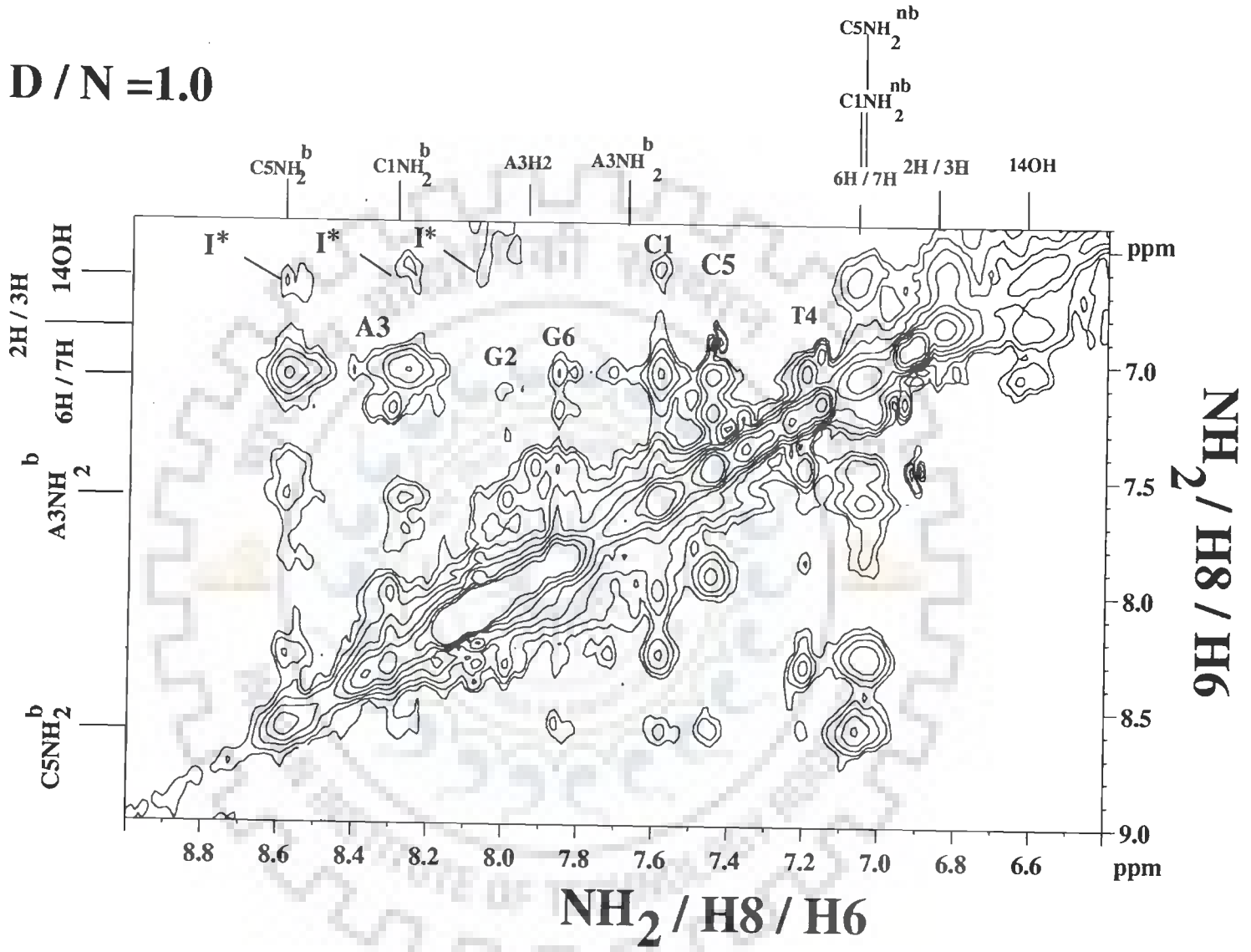


Fig. 6.6d

I* Intermolecular peaks

D / N = 1.0



266

Fig. 6.6e

I* Intermolecular peaks

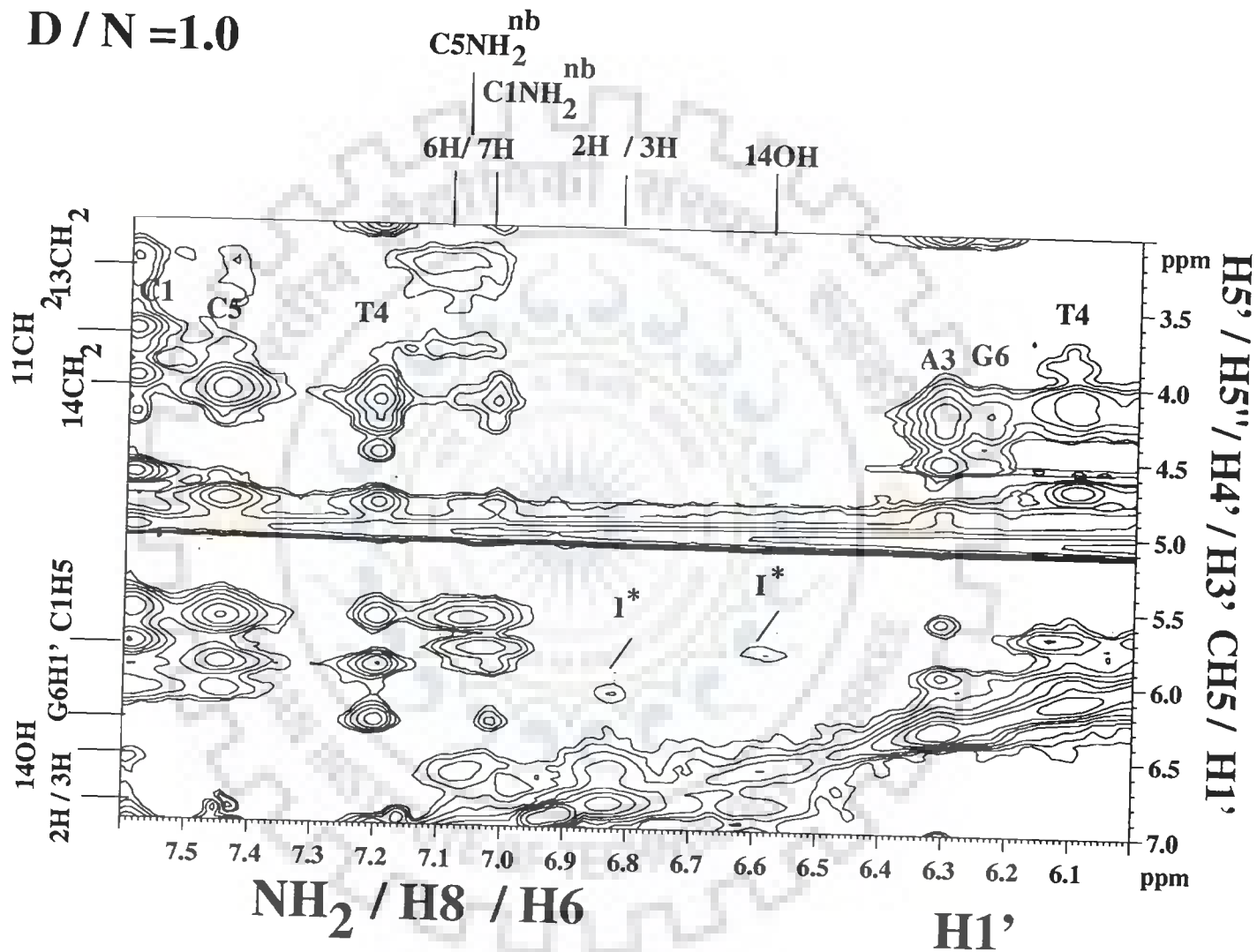


Fig. 6.6f

I* Intermolecular peaks

D / N = 1.0

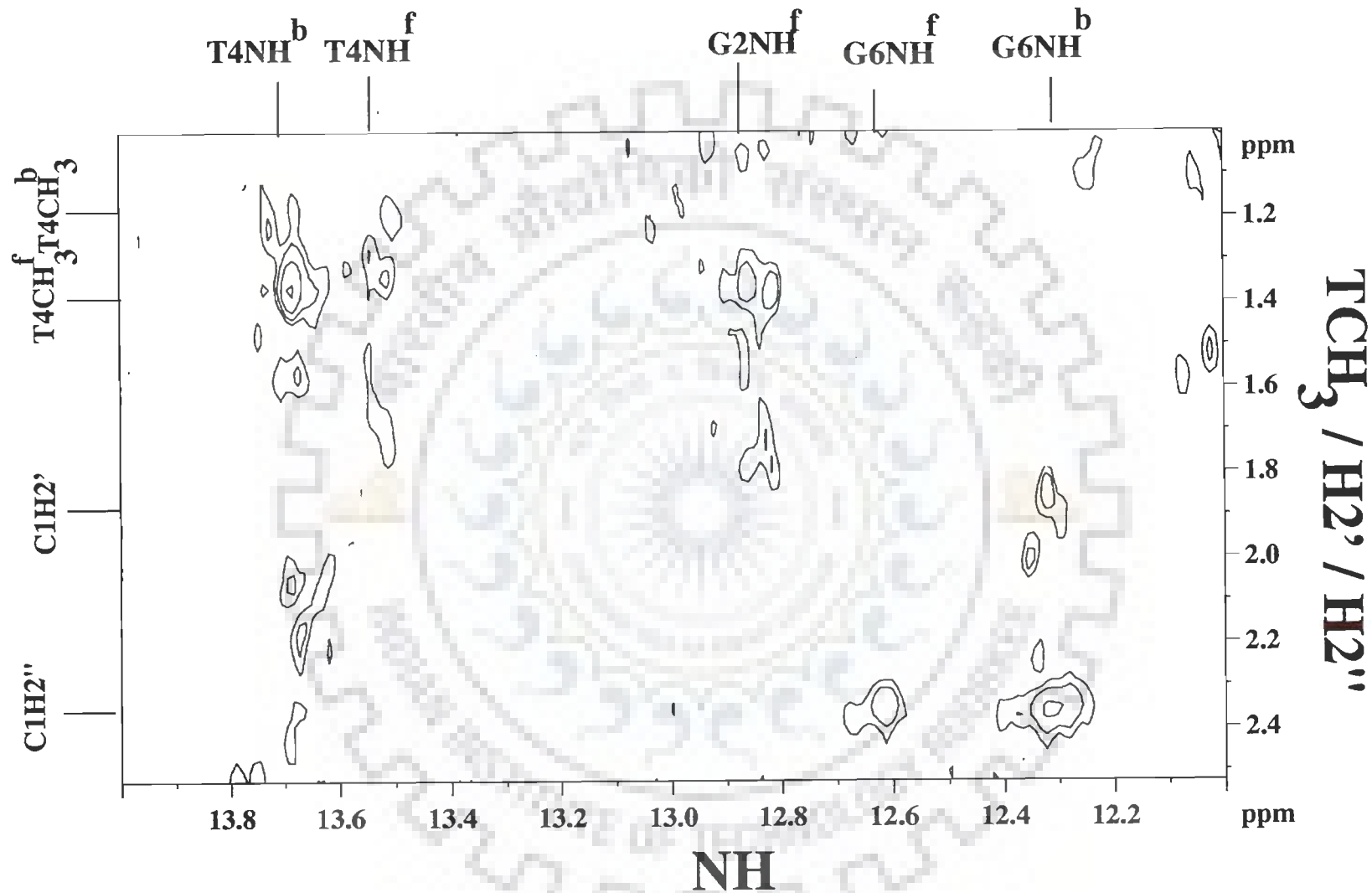


Fig. 6.6g

D / N = 1.0

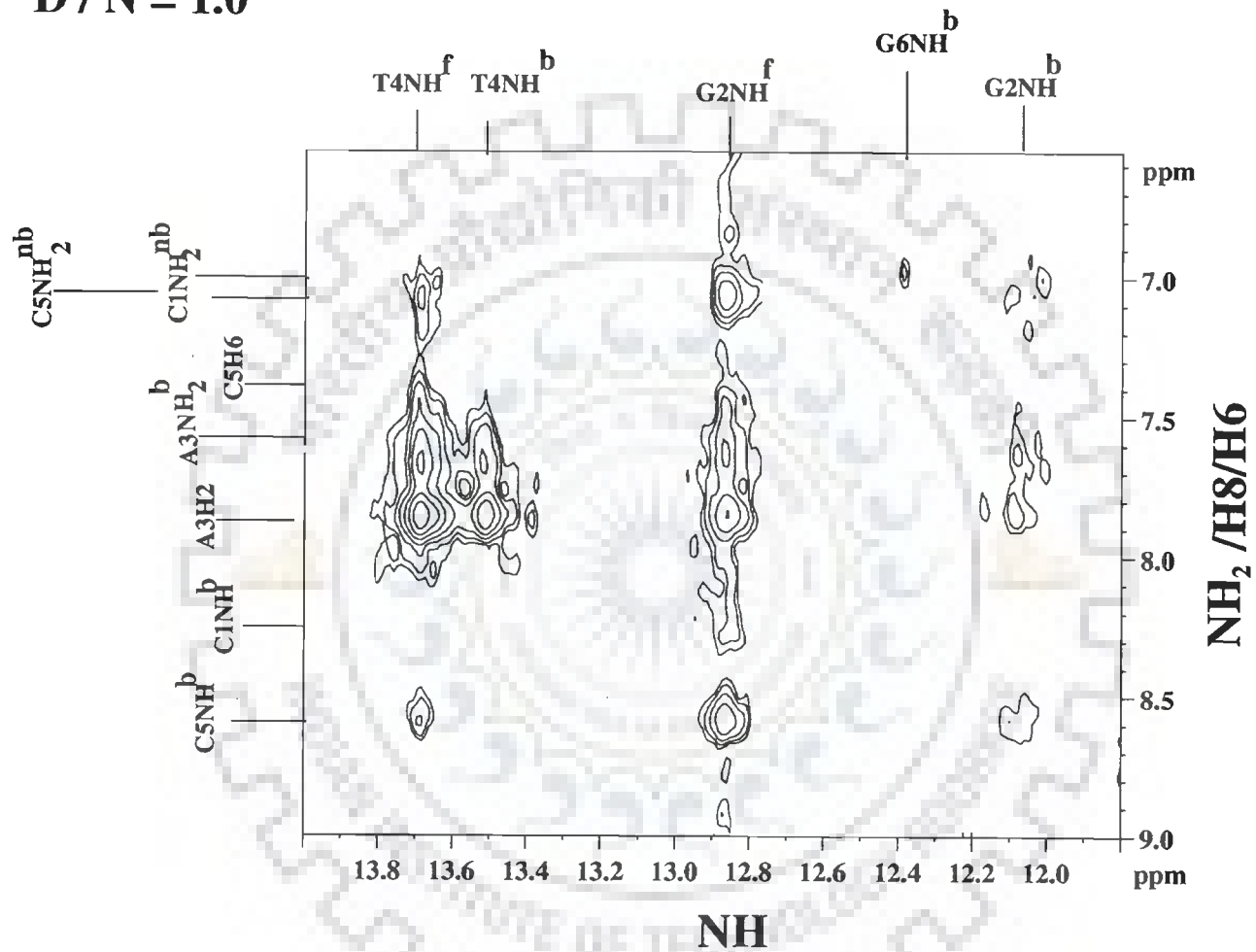


Fig. 6.6h

Fig. 6.6a-h Expansions of the specific region of the NOESY spectra of mitoxantrone complexed with $d\text{-(CGATCG)}_2$ to highlight connectivities as well as intermolecular peaks at $D / N = 1.0$

D / N = 1.5

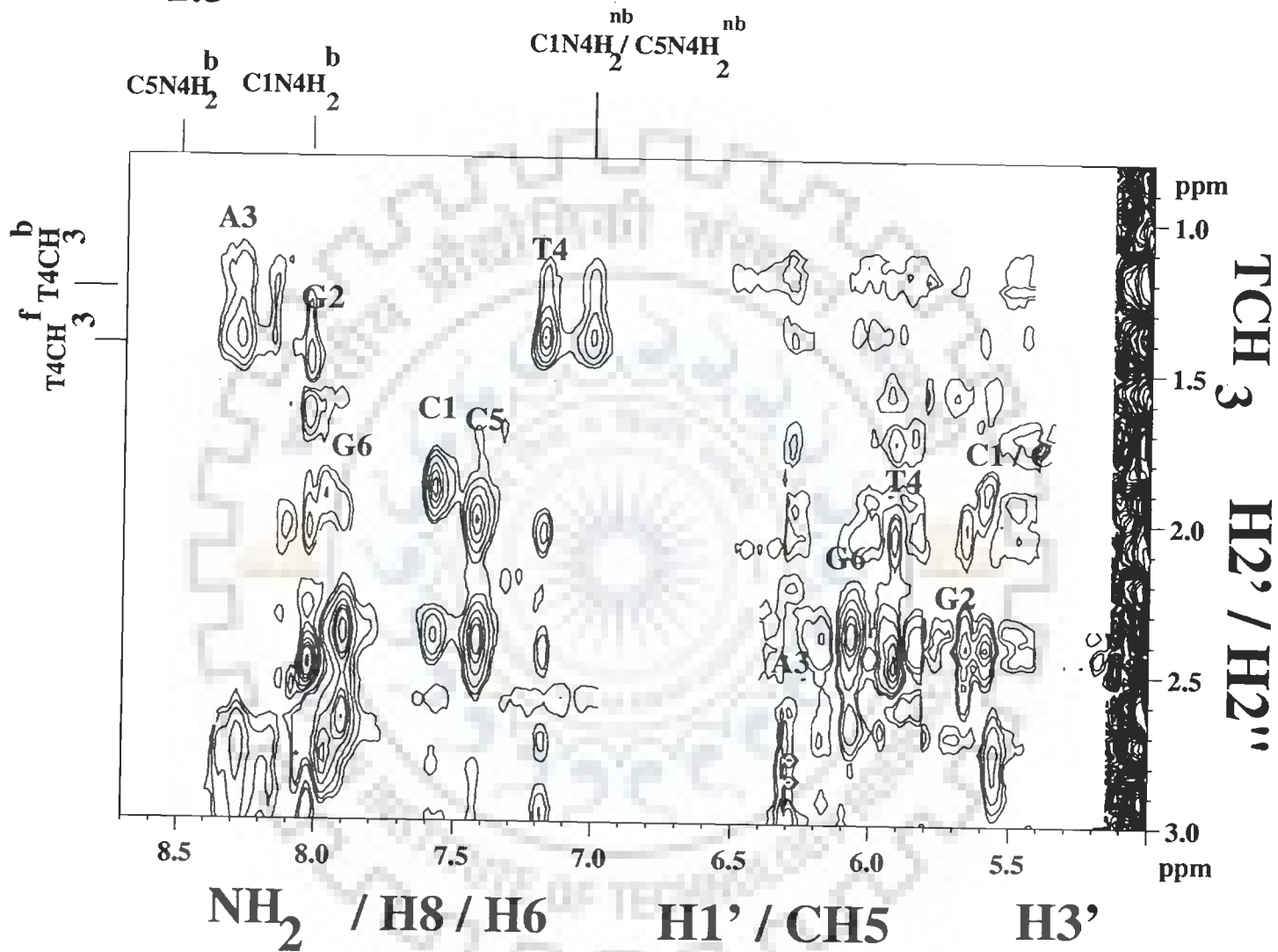


Fig. 6.7a

D / N = 1.5

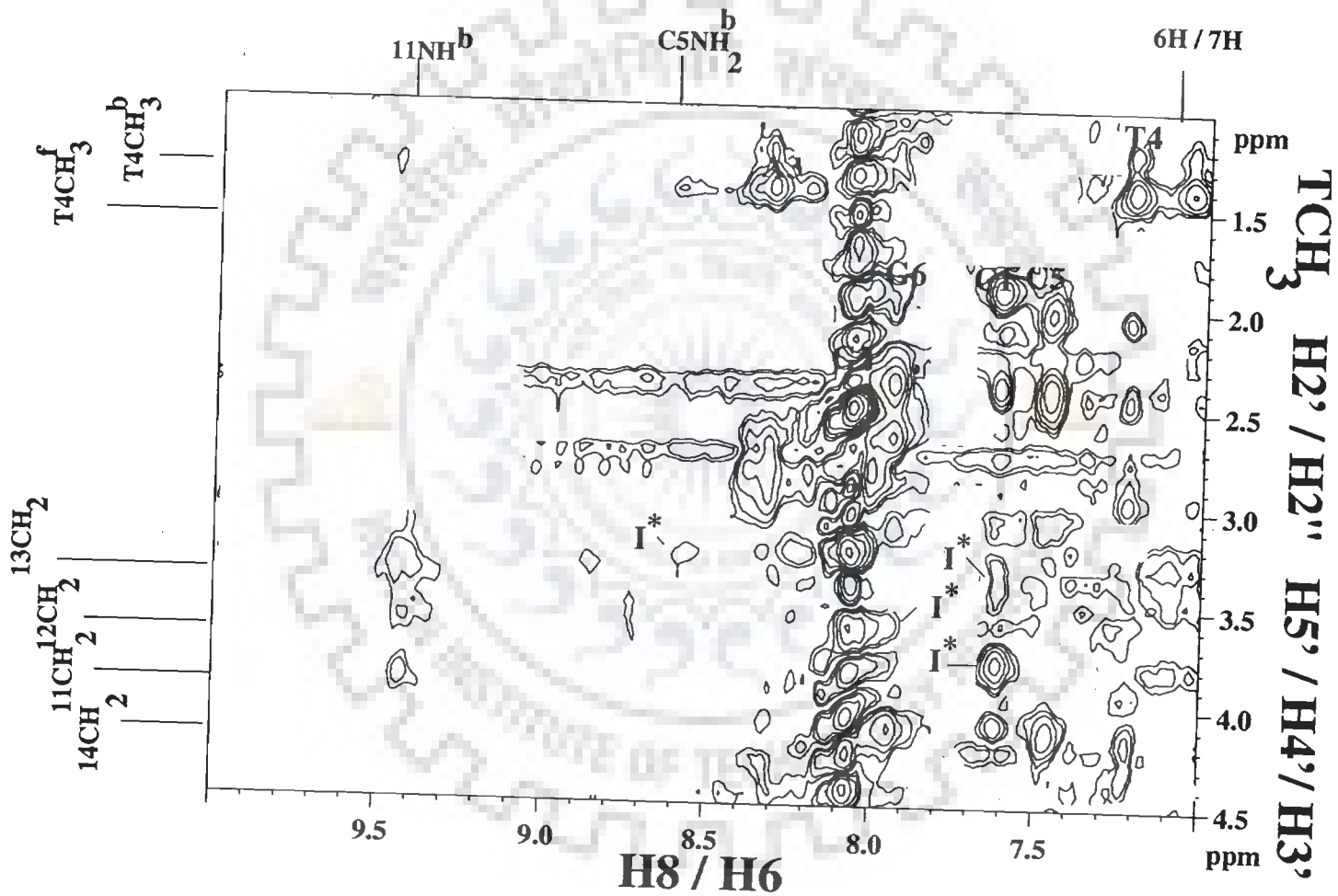


Fig. 6.7d

Proton NMR studies on binding of microxanthone with d-(CGATCG).

$D/N = 1.5$

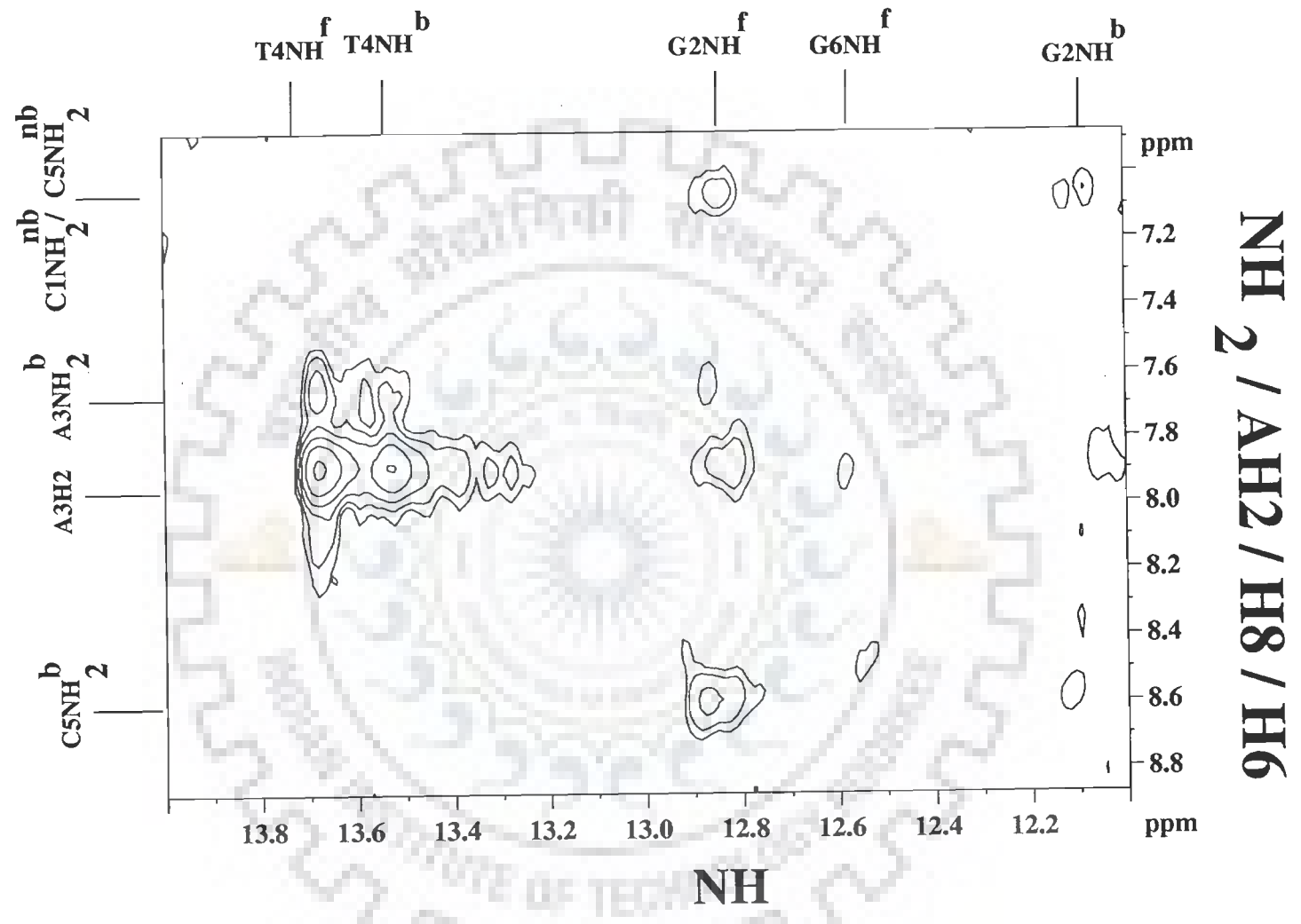


Fig. 6.7c

D / N = 1.5

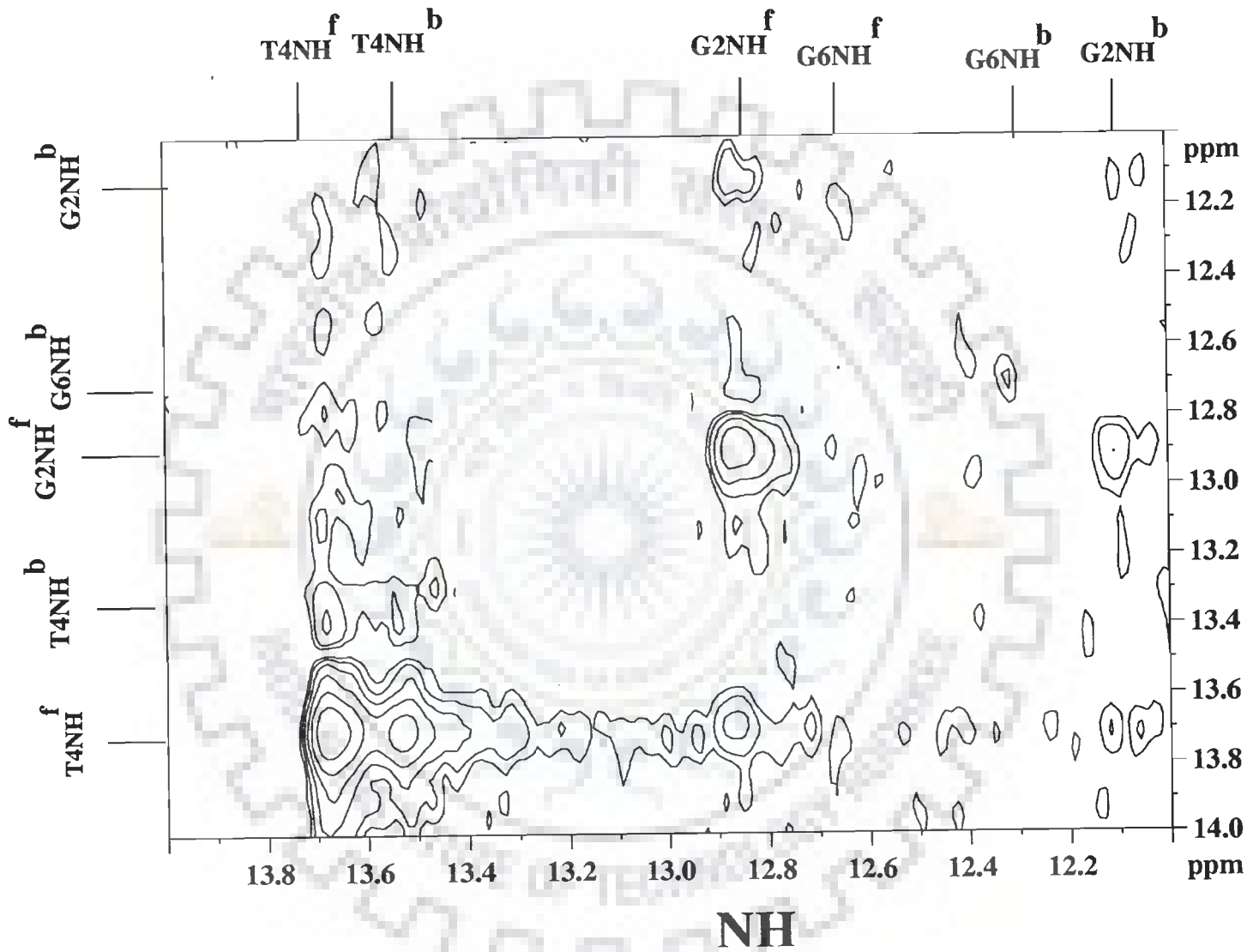


Fig. 6.7d

$D / N = 1.75$

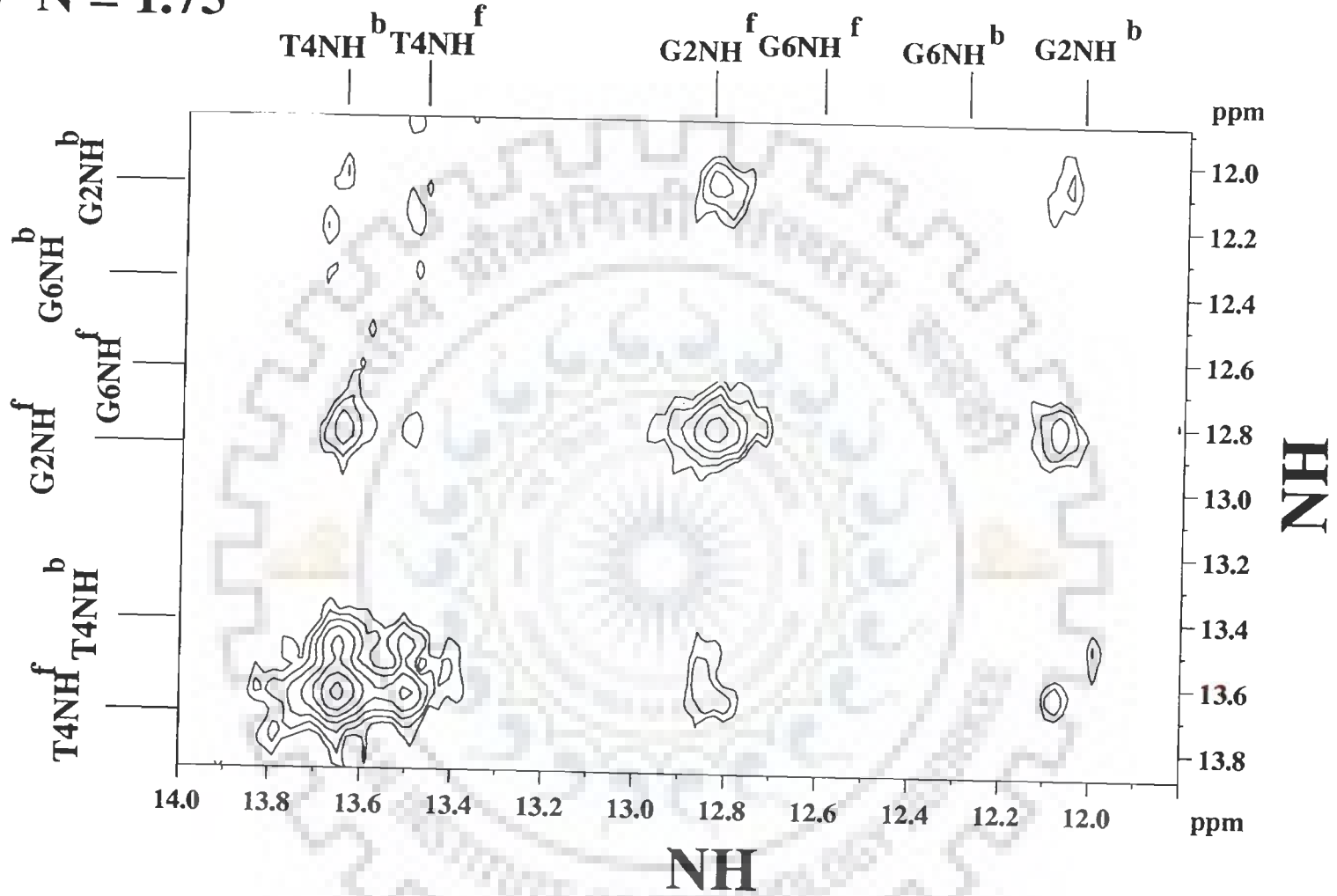


Fig. 6.8a

D / N = 1.75

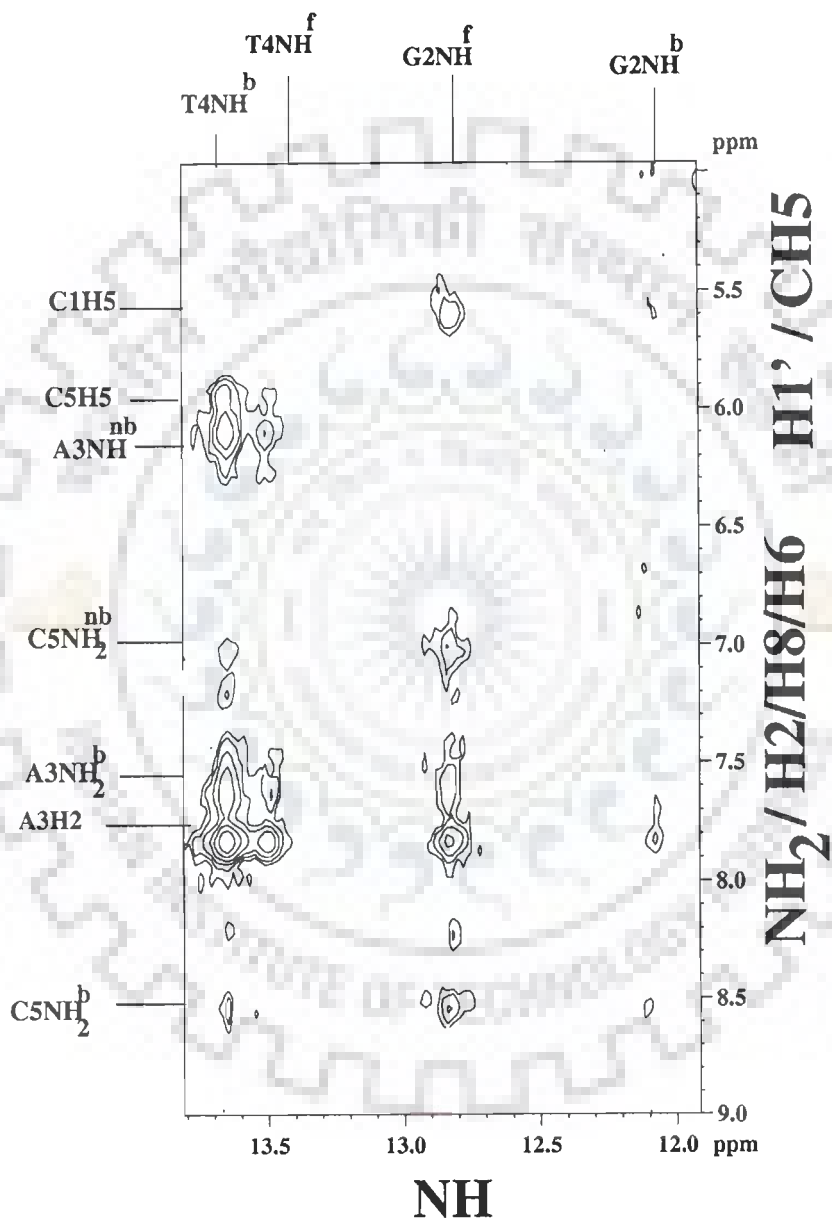


Fig. 6.8c

Fig.6.8a-c Expansions of the specific region of the NOESY spectra of mitoxantrone complexed with d-(CGATCG)₂ to highlight connectivities at D / N = 1.75

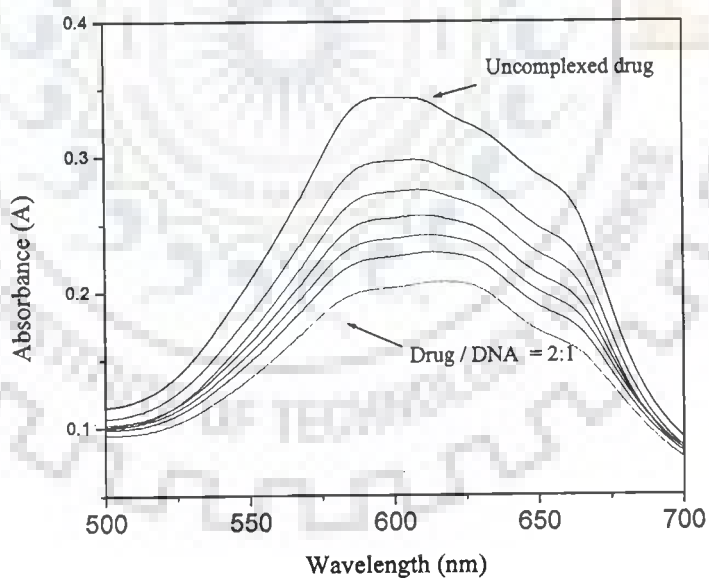
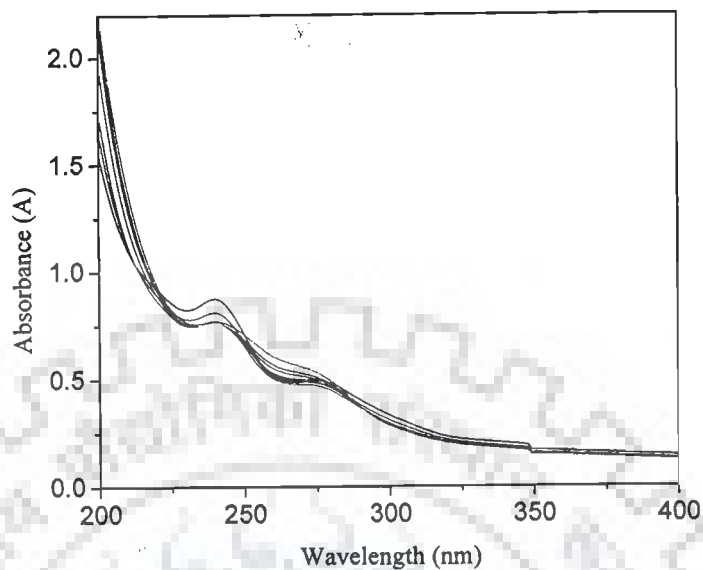


Fig. 6.9 Absorption Spectra of the mitoxantrone complexed with d-(CGATCG)₂

6.2.2 ABSORPTION STUDIES

We have also studied the binding of mitoxantrone with d-(CGATCG)₂ by titrating drug of known concentration with increasing aliquots of DNA till 2:1 drug / DNA ratio is achieved (Fig. 6.9) . Titrations were monitored from 200-700 nm. The overall molar absorption of drug is found to decrease with increasing in drug / DNA ratio. The total change in molar absorption was found to be 0.036 nm for the 600 nm peak. Red shift of ~ 5nm was observed for the 600 nm peak of the drug. Both bathochromic and hypochromic shift indicates that drug binds to DNA.

6.2.3 CONFORMATIONAL FEATURES OF DNA AND DRUG IN COMPLEX

The NOESY spectra of drug–DNA complex at stoichiometric D / N ratio of 1 (Fig. 6.6) have been investigated extensively at mixing time (τ_m) of 300 and 200 ms. The intensities of cross peak have been estimated qualitatively as strong intense (ss), strong (s) medium (ws) and weakly intense (w) and very weak (ww) for distances of the – 1.8 – 2.5, 2.5 – 3.0, 3.0 – 3.5, 3.5 – 4.0, and 4.0 – 5.0 Å, respectively from the spectra recorded at $\tau_m = 200$ ms. The inter–proton distances have also been evaluated by taking distance CH5–CH6 = 2.45 Å for $\tau_m = 200$ ms as an internal standard. The observed NOE for (a) sequential connectivities, (b) intranucleotide connectivities within sugar (c) intranucleotide base to sugar connectivities, and (d) connectivities involving amino and imino protons of base pairs are given in Table 6.5a–d. The connectivities within the drug molecules are given in Table 6.6. The intermolecular connectivities of drug protons to nucleic acid protons in the complex are given in Table 6.7, respectively. The sequential base (H6 / H8)_n to (H1')_{n-1}, (H2')_{n-1}, (H2'')_{n-1}, (H3')_{n-1}, base (H6 / H8)_{n-1} connectivities are observed at all base pair steps (Table 6.5a). The observation of NOEs between the imino protons of guanine bases and the amino protons of the hydrogen bonded partner cytosine bases in NOESY spectra (that is, pairs C1N4H₂^b 8.28 ppm, G6N1H^b 12.32 ppm;

C5N4H₂^b 8.58 ppm, G2N1H^b 12.12 ppm) (Fig.6.6h) establish Watson–Crick base pairing at all dG–dC base pair in the duplex. Similarly the observation of NOEs between imino proton of thymine and H2 and amino protons of adenine residues (that is, pairs T4NH^b 13.52 ppm, A3H2 7.85 ppm; T4NH^b 13.52 ppm, A3N6H₂^b 7.67 ppm) (Fig.6.6h) establish Watson and Crick pairing at all dA–dT base pairs. Thus practically all sequential connectivities among adjacent base pairs, expected for a typical B–DNA structure, are observed (Table 6.5d). This clearly demonstrates that DNA duplex is intact, apparently with no opening of base pairs to accommodate drug chromophore as expected on binding of typical intercalator to DNA molecule. The base sequence d–(CGATCG)₂ being self–complementary is responsible for a high symmetry in the NMR spectra, which remains unbroken in the presence of drug. Further, DNA hexamer predominantly adopts a B–DNA structure. The The NOE connectivity corresponding to H1'–H4' for A3 residue is weakly intense as compared to that of all other residues (Table 6.5b). This indicates that pseudorotation phase angle for A3 residue is ~162–180° while for all other residues it may be ≤ 162° [16]. The H2''–H4' distance serves as a marker for mole fraction of S–conformer, χ_s , since its value of 3.8 Å for P = 162° decreases to 2.3 Å as P decreases to 18°. This indicates that pseudorotation phase angle for A3 residue is ~162–180° while for all other residues it may be ≤ 162° [12]. The H2''–H4' distance serves as a marker for mole fraction of S–conformer, χ_s , since its value of 3.8 Å for P = 162° decreases to 2.3 Å as P decreases to 18°. The absence of the cross peak for A3 residue show that it has minimum fraction of N–conformer. The presence of intranucleotide base H6 / H8–H3' connectivity confirms further the presence of N–conformer [117]. The relatively weak intense base H6 / H8–H1' connectivity (Table 6.5) for A3 and T4 residues among purines and pyrimidines respectively show that A3 and T4 residue may be more close to anti conformation, while G2, G6, C1, C5 residue may be inclined somewhat towards high anti conformation.

Table 6.6 shows some of the intramolecular NOE connectivities observed within the drug molecule in the drug–DNA complex having D / N = 1. It is observed that 11NH is close to 6H / 7H, 11CH₂, 12CH₂ and 13CH₂ protons. Also the ring protons 6H / 7H are close to 11CH₂, 12CH₂, 13CH₂, 14CH₂ (overlap) and 14OH protons, as expected. However, the inter–molecular peaks observed in mitoxantrone dimer e.g. that is, 2H / 3H with 11CH₂, 12CH₂, 13CH₂, 14CH₂, 6H / 7H protons are clearly missing. The drug molecule, though present in high concentration, does not exist as a dimer and is bound as monomer molecule to the DNA.



Table 6.5a Intensity of sequential NOE cross peaks (d_s) of nucleotide protons in the drug-DNA complex at $D / N = 1.0$ at 278 K. The very strong (ss), strong (s), medium (ws) and weak (w) and very weak (ww), intensities correspond to distances in the range 1.8 – 2.5 Å, 2.5 – 3.0 Å, 3.0 – 3.5 Å, 3.5 – 4.0 Å, 4 – 5 Å, respectively in the NOESY spectra, Fig.6.6
Overlap of cross peaks is indicated as o.

Connectivity	Intensity	Connectivity	Intensity
C1pG2 step		T4pC5 step	
C1H1' - G2H5''	s	T4H1' - C5H5''	o
C1H2' - G2H5''	w	T4H2'' - C5H5''	o
C1H1' - G2H5''	ws	T4H4' - C5H5''	o
C1H2'' - G2H2'	ws	T4H2'' - C5H2'	s
C1H1' - G2H8	s	T4H1' - C5H6	s
C1H2' - G2H8	s	T4H2' - C5H6	s
C1H2'' - G2H8	s	T4H2'' - C5H6	s
C1H3' - G2H8	w	T4H3' - C5H6	w(o)
C1H6 - G2H8	s	T4H1' - C5H5	w(o)
G2pA3 step		T4H2' - C5H5	s
G2H1' - A3H5'	s	T4H2'' - C5H5	s
G2H2'' - A3H5''	s	T4H6 - C5H5	s
G2H4' - A3H5''	o	T4H6 - C5H6	ws
G2H2'' - A3H2'	s	C5pG6 step	
G2H1' - A3H8	s	C5H1' - G6H5''	o
G2H2' - A3H8	s	C5H2' - G6H5''	-
G2H2'' - A3H8	s	C5H4' - G6H5''	o
G2H3' - A3H8	-	C5H2'' - G6H2'	s
A3pT4 step		C5H1' - G6H8	ws
A3H1' - T4H5''	w	C5H2' - G6H8	s
A3H2'' - T4H5''	s	C5H2'' - G6H8	s
A3H4' - T4H5''	o	C5H3' - G6H8	w
A3H2'' - T4H2'	s	C5H6 - G6H8	w
A3H1' - T4H6	s		
A3H2' - T4H6	s		
A3H2'' - T4H6	s		
A3H2' - T4 CH ₃	s		
A3H3' - T4H6	w		
A3H8 - T4CH ₃	s		
A3H2'' - T4CH ₃	s		

Table 6.5b: Intensities of intra sugar NOE cross peaks (d_i) in the drug–DNA complex at D/N= 1.0 at 278 K. The very strong (ss), strong (s), medium (ws), weakly (w), and very weakly (ww) intense cross peaks refer to distances in the range 1.8–2.5 Å, 2.5–3.0 Å, 3.0–3.5 Å, 3.5–4.0 Å, and 4–5 Å, respectively from the NOESY spectra (Fig. 4). Overlap of peaks is indicated as o.

Connectivity	C1	G2	A3	T4	C5	G6
H1'–H2'	s	s	s	s	s	s
H1'–H2''	ss	ss	ss	ss	ss	ss
H1'–H3'	s	s	s	s	s	s
H1'–H4'	s	s	ws	s	s	s
H1'–H5'	s	w	o	s	o	o
H1'–H5''	s	o	o	s	o	o
H2'–H3'	ss	o	o	o	o	o
H2''–H3'	s	o	o	o	o	ss
H2'–H4'	s	s	–	s	s	s
H2''–H4'	s	s	–	s	s	s
H3'–H4'	ss	w	ss	w	ww	ss

Table 6.5c: Intensities of intra nucleotide NOE connectivities (d_i) of base to sugar protons of nucleic acid in drug–DNA complex at D/N= 1.0 at 278 K. The very strong (ss), strong (s), medium (ws), weakly (w), and very weakly (ww) intense cross peaks correspond to distances 1.8–2.5 Å, 2.5–3.0 Å, 3.0–3.5 Å, 3.5–4.0 Å, and 4–5 Å, respectively from the NOESY spectra (Fig. 4). Overlap of peaks is indicated as o.

Connectivity	C1	G2	A3	T4	C5	G6
H8/H6–H1'	ss	s	ws	w	ss	s
H8/H6–H2'	ss	o	ss	ss	ss	ss
H8/H6–H2''	s	o	s	s	s	s
H8/H6–H3'	s	s	s	ss	ss	s
H8/H6–H4'	ws	s	ws	s	s	s
H8/H6–H5'	s	s	s	s	o	s
H8/H6–H5''	s	s	s	s	o	o

Table 6.5d: Some of the interproton distances (\AA) within the hexanucleotide in drug–DNA complex at $D/N = 1.0$ estimated from NOESY spectra (Fig. 6.6) at 278 K using distance $\text{CH5–CH6} = 2.45 \text{ \AA}$ as a standard reference. The corresponding distances in standard B–DNA [117] are also shown here for reference. Overlap of peaks is indicated as o.

	Standard B–DNA	Drug–DNA Complex ($D/N = 1.0$)
d_{ps} peaks		
C1N4H ₂ ^b –G2N1H	4.0	4.12
G2N1H–A3N6H ₂	4.5	3.70
G2N1H–A3H2	3.7	3.37
G2N2H ₂ ^b –A3H2	3.5	2.92
A3N6H ₂ ^{nb} –T4N3H	4.5	o
T4N3H–C5N4H ₂ ^b	3.9	4.11
C5N4H ₂ ^b –G6N1H	4.0	3.38
A3H2–T4N3H	4.0	o
d_{ps} peaks		
G2N1H–G6N1H	3.4	3.26
G2N1H–G6N2H ₂	4.1 ^b	3.93
G2N2H ₂ –G6N1H	4.1 ^b	3.81
G2N2H ₂ –G6N2H ₂	4.1 ^b	4.00
A3N6H ₂ –C5N4H ₂	4.5 ^b	4.2
A3H2–A3H2	4.4	o
T4N3H–T4N3H	2.9	2.80 / 2.83
T4N3H–G2N1H	3.6	3.80
C5N4H ₂ –C1N4H ₂	2.9	3.5
d_{pi} peaks		
A3H2–T4N3H ^f	2.8	3.0
A3N6H ₂ –T4N3H ^f	2.5	2.5
G2N1H ^f –C5N4H ₂ ^b	2.5	3.21
G6N1H ^f –C1N4H ₂ ^b	2.5	–
d_i peaks		
C1N4H ₂ –C1H5	2.4 / 3.5	2.95/3.18
C1N4H ₂ –C1H6	4.6–5.3 ^b	3.14
G2N1H–G2N2H ₂	2.3–3.4	2.5
A3H2–A3N6H ₂ ^b	4.4–5.2	o
A3N6H ₂ ^b –A3N6H ₂ ^{nb}	1.7	1.75
A3N6H ₂ ^b –A3H8	4.8–6.10	o
T4N3H–T4CH ₃	4.9	3.87

	Standard B- DNA	Drug-DNA Complex (D/N = 1.0)
d_s peaks		
G2N1H ^b -G6H2''	-	2.65
G2N1H ^f -G6H2''	-	2.9
G2N1H ^b -C1H2'	-	3.0
G2N1H ^f -C1H2'	-	3.4
T4CH ₃ ^b -A3H2'	-	3.6
T4CH ₃ ^f -A3H8	3.8	4.0
T4CH ₃ ^b -A3H8	-	4.5
T4CH ₃ ^f -T4H6	2.9	3.05
T4CH ₃ ^b -T4H6	-	3.56
T4CH ₃ ^f -C5H6	3.8	4.25
T4CH ₃ ^b -C5H6	-	4.50
T4CH ₃ ^f -T4H2''	-	4.76
T4CH ₃ ^f -A3H2'	3.4	3.65
T4CH ₃ ^f -A3H2''	2.9	3.10
T4CH ₃ ^f -C5N4H ₂ ^{nb}	-	2.85
T4CH ₃ ^b -C5N4H ₂ ^{nb}	-	3.39
T4CH ₃ ^f -C5N4H ₂ ^b	-	3.54
T4CH ₃ ^b -C5N4H ₂ ^b	-	4.56
T4CH ₃ ^f -A3H1'	-	2.85
T4CH ₃ ^b -A3H1'	-	4.65

d_i –intranucleotide, d_s –sequential, d_{pi} – within base pair, d_{ps} – sequential among base pairs

Table 6.6: Relative intensities of intramolecular NOE cross peaks and the corresponding interproton distances (\AA) within the drug molecule in the drug– DNA complex at 278 K estimated from NOESY spectra, Fig. 6.6 using distance $\text{CH5–CH6} = 2.45 \text{ \AA}$ as a standard reference. Overlap of peaks is indicated as o

S. No.	Cross peak	Bound drug D/N=1.0	Uncomplexed drug
1.	11CH ₂ –2CH ₂	2.60	2.83
2.	13CH ₂ –14CH ₂	2.80	2.40
3.	11CH ₂ –13CH ₂	3.10	3.08
4.	12CH ₂ –13CH ₂	3.50	2.9–3.6
5.	12CH ₂ –14CH ₂	3.20	3.04
6.	11CH ₂ –6H/7H	3.62	2.15
7.	12CH ₂ –6H/7H	o	2.55
8.	13CH ₂ –6H/7H	3.28	–
9.	14CH ₂ –6H/7H	4.02	–
10.	11NH ^t –11CH ₂	–	2.69
11.	11NH ^b –11CH ₂	4.04	–
12.	11NH ^t –12CH ₂	3.77	3.32
13.	11NH ^b –12CH ₂	3.95	–
14.	11NH ^t –13CH ₂	3.80	–
15.	11NH ^b –13CH ₂	3.12	–
16.	11NH ^b –6H/7H	3.58	–
17.	11NH ^t –6H/7H	–	3.60–4.70
18.	11CH ₂ –2H/3H	–	3.38
19.	12CH ₂ –2H/3H	–	3.64
20.	13CH ₂ –2H/3H	–	5.43
21.	14CH ₂ –2H/3H	–	–
22.	6H/7H–14OH	o	–
23.	2H/3H–14OH	3.32	–

6.2.4 STRUCTURE OF COMPLEX

Table 6.7 gives a list of 19 some of the short intermolecular contacts observed between mitoxantrone and DNA hexamer (Fig. 6.6–6.8). Out of which several are close to C1.G6 base pair. Both $^{13}\text{CH}_2$ and ^{14}OH protons are close to C1H6 proton. Since $^{14}\text{CH}_2$ overlaps with some other DNA protons, its proximity to other protons cannot be ascertained unambiguously. ^{11}NH and ^{14}OH are in close proximity to C1 nucleotide protons and $^{13}\text{CH}_2$ is close to C1.G6 base pair. This is possible if $^{13}\text{CH}_2$ is located somewhere close to the middle of base pair. Also 2H / 3H proton on the ring of mitoxantrone is, simultaneously close to C1H2'' and G6H1' protons which are located on opposite sides of C1.G6 base pair. This is not possible if mitoxantrone aromatic chromophore intercalates between two base pairs of DNA like other normal intercalators [21] are having conjugated aromatic rings. Apparently drug is binding externally to the hexamer sequence in a specific orientation which gives rise to the observed NOEs.

The experimental results show that there is only one set of new resonance signals throughout the titration with mitoxantrone in both ^1H and ^{31}P NMR spectra. The addition of mitoxantrone in increasing amounts to DNA hexamer does not cause the ^1H as well as ^{31}P resonances to drift continuously, in particular the T4NH, G2NH, G6NH, T4CH₃ and all ^{31}P resonance lines. Instead it gives rise to new sets of broad signals at the expense of the intensities of the original ones, as evidenced by the integral plots of 1D NMR spectral lines giving area under the resonance peak and hence the intensity of signal. The direct proof of this comes from 2D ^{31}P NMR exchange spectra of the complex at stoichiometric ratio of 1, 1.5 as well as 1.75 (Chapter 5). The same is also clear in the NH region of ^1H NMR spectra (Fig. 6.6a) showing

Table 6.7: Relative intensities of intermolecular NOE connectivities between hexanucleotide and the drug molecule in the drug–DNA complex at drug to DNA ratio D/N = 1.0, D/N=1.5 and D/N = 1.75 from NOESY spectra at 278 K. The very strong (ss), strong (s), medium (ws) weakly (w) and very weakly (ww) intense cross peaks correspond to distance of ss 1.8–2.5 Å, s 2.5–3.0 Å, ws 3.0–3.5 Å, w 3.5–4.0 Å, ww 4–5 Å.

S. No.	Cross peak	Relative Intensity by visual inspection of NOESY spectra		
		D/N=1.0	D/N=1.50	D/N=1.75
I1	$^{13}\text{CH}_2\text{-C1H6}$	ss	ss	ss
I2	$^{13}\text{CH}_2\text{-G6H8}$	ss	ss	ss
I3	$^{14}\text{OH-C1H6}$	ws	ws	ws
I4	$^{14}\text{OH-C1N4H}_2^{\text{b}}$	s	s	s
I5	$^{14}\text{OH-C5N4H}_2^{\text{b}}$	s	s	s
I6	$^{11}\text{NH}^{\text{b}}\text{-C1H1}'$	o	o	o
I7	$^{11}\text{NH}^{\text{b}}\text{-C1H2}''$	w	w	w
I8	$^{2\text{H}/3\text{H-G6NH}}^{\text{b}}$	w	s	w
I9	$^{2\text{H}/3\text{H-C1H2}}''$	s	s	s
I10	$^{14}\text{OH-C1H2}''$	w	w	w
I11	$^{2\text{H}/3\text{H-G6H1}}'$	ww	ww	ww
I12	$^{11}\text{CH}_2\text{-G6H8}$	ws	ws	ws
I13	$^{13}\text{CH}_2\text{-C5H6}$	w	w	w
I14	$^{11}\text{NH}^{\text{b}}\text{-C1H2}'$	w	w	w
I15	$^{13}\text{CH}_2\text{-G6NH}^{\text{b}}$	w	w	w
I16	$^{13}\text{CH}_2\text{-G2H8}$	ss	ss	ss
I17	$^{12}\text{CH}_2\text{-G2H8}$	ww	ww	ww
I18	$^{11}\text{CH}_2\text{-C1H6}$	ws	ws	o
I19	$^{11}\text{CH}_2\text{-C5H6}$	ww	ww	o
I20	$^{13}\text{CH}_2\text{-G6NH}_2^{\text{b}}$	–	–	ww
I21	$^{13}\text{CH}_2\text{-C5NH}_2^{\text{nb}}$	–	–	ww
I22	$^{13}\text{CH}_2\text{-C1NH}_2^{\text{nb}}$	–	–	ws
I23	$^{13}\text{CH}_2\text{-G2NH}_2^{\text{b}}$	–	–	ws
I24	$^{\text{C1H5-14OH}}$	w	w	w

exchange of free and bound T4NH, G2NH and G6NH. There has been considerable evidence in literature [75] that mitoxantrone binds preferentially to CG sites [84]. It has slower dissociation rates for Poly dG-dC than for Poly dA-dT by an order of magnitude [63]. Since d-(CGATCG)₂ has two CpG binding sites, but only one set of new resonance signals are observed [64], the binding sites may be symmetrical and remote from each other giving ring current shifts of ~1 ppm in imino protons, as observed by us. The existence of intermolecular NOEs involving 11CH₂, 12CH₂, 13CH₂ and 14 CH₂ with C1H6, C1H5, C3H6, G4H8 protons in 1:1 complex of mitoxantrone with d-(CGCG)₂ duplex has been demonstrated [75]. Also 6H / 7H proton is close to C3H4' and G4H4' proton and G2H8 and C3H5 protons are significantly broadened in that complex [75]. Our detailed NMR analysis shows that all internucleotide sequential connectivities (Table 6.5a) exist. Further, the DNA hexamer in complexed state adopts a conformation close to that of canonical B-DNA structure with predominant S-conformation of deoxyribose and anti glycosidic bond. All the duplex pair peaks, including sequential intra and inter-strand peaks, exist. Thus it may be concluded that mitoxantrone binds externally to the DNA duplex, being in close proximity to C1.G6 base pair. All the spectral lines are somewhat uniformly broadened on binding except G6NH (as compared to G2NH and T4NH) and G6H8 as the internal motions are affected and the protons are getting immobilized. Notable among these are the G6NH which being easily accessible to solvent water exchange freely in uncomplexed d-(CGATCG)₂ and are broadened to the extent that they are not observable but are observable in both free and bound state in the 1:1 mitoxantrone d-(CGATCG)₂ complex. Also T4NH, G6NH, G2NH broaden with temperature considerably and are not observed at 293 K but 11NH is a distinct sharp peak even at a temperature of 348 K due to practically no exchange with solvent. This may also be so due to the reason that 11 NH is also expected to be hydrogen bonded with carbonyl of ring B. The

11NH proton of mitoxantrone shows substantial upfield shift ~ 0.86 ppm on binding while 6H / 7H and 2H / 3H shift by 0.45 ppm and 0.29 ppm, respectively (Table 6.2b). This is indicative of stacking of mitoxantrone chromophore with base pair of DNA, perhaps C1.G6 base pair. This may result in insignificant shift of 11CH₂, 12CH₂, 13CH₂ and 14CH₂ protons as observed. The shift in resonance peaks of DNA protons is not significant. In fact the change in chemical shift is not a sufficient indicator of the interaction as compensatory effect of anisotropic ring current, interaction with C=O / NH / OH groups etc., may exist. Instead the observed intermolecular short contacts (Table 6.7, Figs. 6.6– 6.8) are direct proof of the structure of a specific drug–DNA complex.

In chapter 7 we have attempted to make a model of the complex based on 19 intermolecular (Table 6.7) intramolecular (within drug and within DNA hexamer) NOEs (Tables 6.5–6.6). Distance restraints between atoms involved in the Watson–Crick hydrogen bonding pairs are imposed in the structure calculations based on experimental evidence by NOESY spectra. The structure obtained after restrained Energy Minimization followed by Restrained Molecular Dynamics is shown in Fig. 7.1.

Table 6.8 Relative intensities of intermolecular NOE connectivities between hexanucleotide and the drug molecule in the drug–DNA complex at drug to DNA ratio D / N =1.0, from NOESY spectra (Fig. 6.6) at 278 K. The very strong (ss), strong (s), medium (ws) and weakly (w) intense cross peaks correspond to distance of ss 1.8 – 2.5 Å, s 2.5 – 3.0 Å, ws 3.0 – 3.5 Å, w 3.5 – 4.0 Å, ww / ww 4 – 5 Å.

D / N =1.0			
S. No.	Cross peak	Relative Intensity by visual inspection of NOESY spectra	Distance in Model (Å)
1	¹³ CH ₂ –C1H6	s	2.68
2	¹³ CH ₂ –G6H8	w	2.39
3	14OH–C1H6	ws	2.77
4	14OH–C1N4H ₂ ^b	s	3.49
5	14OH–C5N4H ₂ ^b	s	3.12
6	11NH ^b –C1H1'	w	3.66
7	11NH ^b –C1H2''	w	4.0
8	2H / 3H–G6NH ^b	w	4.5
9	2H/3H–C1H2''	w	3.76
10	14OH–C1H2''	w	3.89
11	2H / 3H–G6H1'	w	3.73
12	11CH ₂ – G6H8	ws	3.05
13	¹³ CH ₂ –C5H6	w	3.72
14	11NH ^b –C1H2'	w	3.68
15	¹³ CH ₂ – G6NH ^b	w	4.0
16	¹³ CH ₂ – G2H8	ss	2.5
17	¹² CH ₂ –G2H8	ww	5.2
18	11CH ₂ –C1H6	s	3.0
19	¹³ CH ₂ – C5NH ₂ ^{nb}	ww	4.6
20	11CH ₂ –C5H6	ww	4.7

Chapter 7

Restrained Molecular Dynamics Study Of Mitoxantrone complexed d-(CGATCG)₂

7.1 INTRODUCTION

In this Chapter, we describe the conformational features of the structures obtained by the restrained molecular minimization followed by restrained molecular dynamics (rMD) using MOE software and analysed by CURVES software [66–67]. The starting structure is built using MOE software. Minimization has been carried in 10,000 steps each of Steepest Descent, Conjugate gradient and Newton Raphson methods.

In total 100 structures were saved at an interval of 1ps out of which 10 with minimum energy are superimposed. It was observed that they differ only marginally from each other in their overall feature. Further no significant drift in either potential energy or restraint deviations was observed during the final equilibration. It can therefore be concluded that the system reached a minimum energy conformation [82, 101]. This confirms that the structure is indeed defined by experimental restraints and not the refinement procedure or variables used. The root mean square deviation between any of the rMD structures and the starting structure is quite large but among various final structures was very low. This is generally acknowledged as an indication that convergence has been achieved.

7.2 RESULTS AND DISCUSSIONS

Table 7.1 indicates an assessment of refined structures in terms of energetics including root mean square derivative of energy with respect to atomic coordinates. The variation between the total potential energy of the 10 energy minimized structures is in the range 265-317 Kcal mol⁻¹.

7.2.1 Conformational features of rMD structures

The superimposition of 10 energy minimized structures is shown in Fig. 7.1. It is observed that aromatic base pairs are not exactly planar in this structure. Two different stereoviews of structure obtained after restrained molecular minimization is shown in Fig. 7.2. Stereoview of final rMD structure is shown in Fig. 7.3.

To gain more insight into structural details, all helical parameters, backbone torsional angles and sugar conformations of the resulting rMD structure (Fig. 7.4) of d-CGATCG complexed with mitoxantrone were thoroughly analyzed with program CURVES, version 5.1.

7.2.2 Helicoidal Parameters

The output from CURVES includes “global helical parameters” defined relative to a global helix axis and “local helical parameters” defined relative to local helix axis at each base pair. Unless a specified otherwise, we refer to the global helical parameters as calculated by CURVES. Plot of various helix axis parameters of d-(CGATCG)₂ in rMD structure as a function of residue position in the duplex is shown in Fig. 7.4a–b. The helicoidal parameters are classified into three categories: global base pair-axis parameters, intra-base pair or global base-base parameters and the inter-base pair or base pair-step parameters [14, 31]. Among the base pair-axis parameters, the average value of x-displacement is 1.17 Å close to -0.7 Å as seen in canonical B-DNA structures. The average y-axis displacement (dy) is -0.07 Å. The rMD structure display inclination values of $\pm 3.0^\circ$ average value being $+15^\circ$. The tip angle fluctuates within $\pm 7^\circ$ for most residues similar to canonical A-DNA and B-DNA forms. Among the intra base parameters, the shear (Sx) and stretch (Sy) values do not vary very much from their ideal values. The stagger (Sz) values lie within ± 0.7 Å

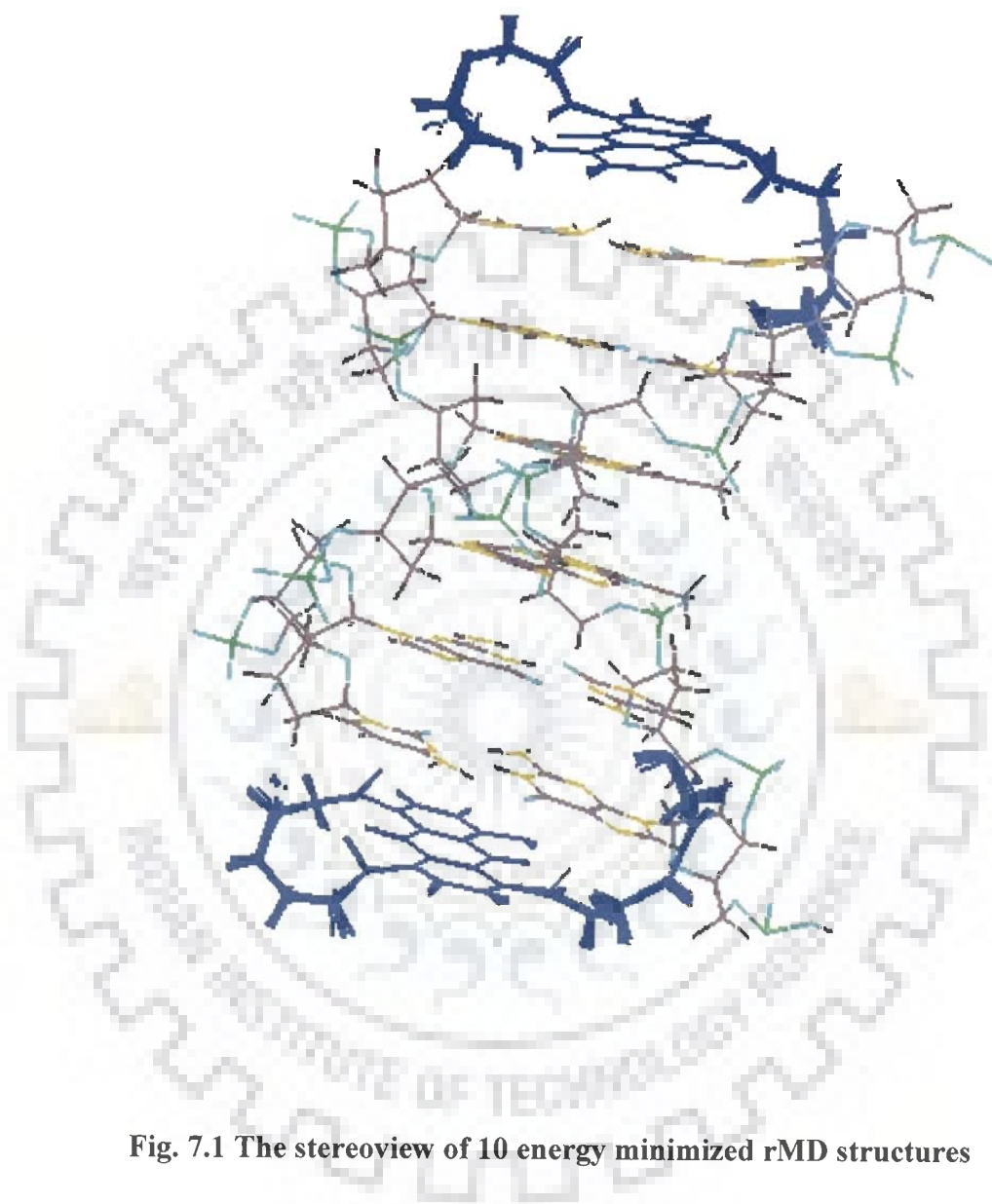


Fig. 7.1 The stereoview of 10 energy minimized rMD structures

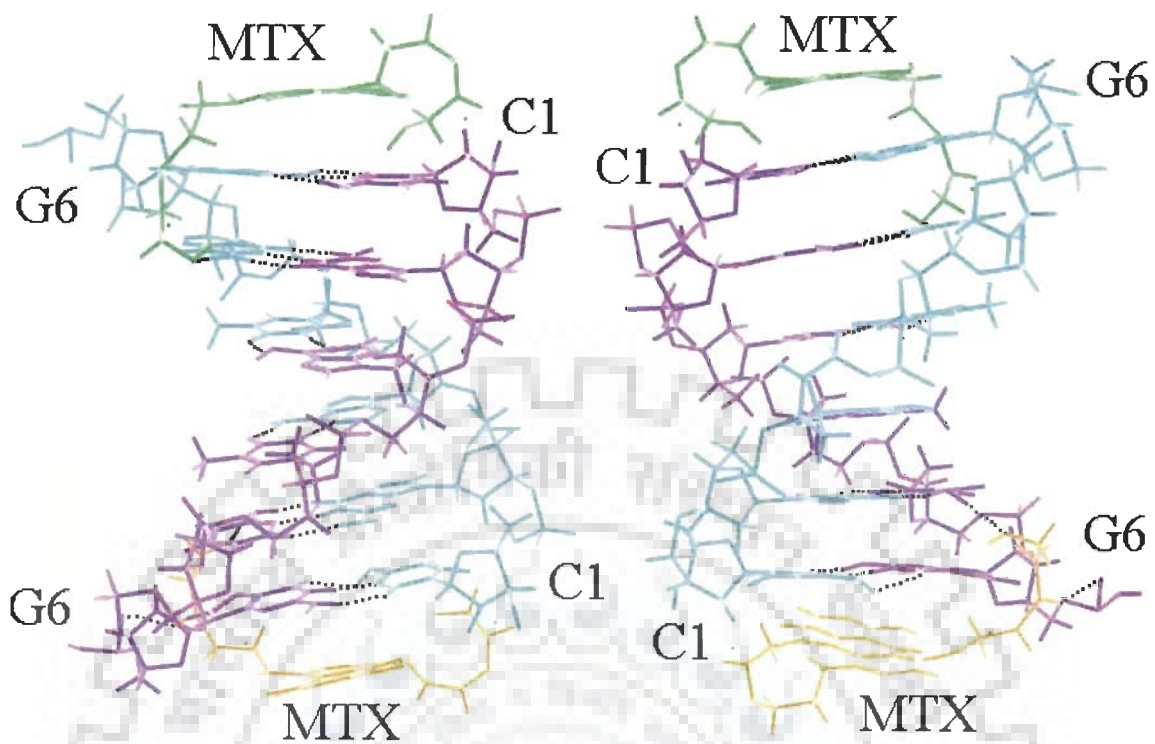


Fig. 7.2 Stereoviews of the energy minimized structure.

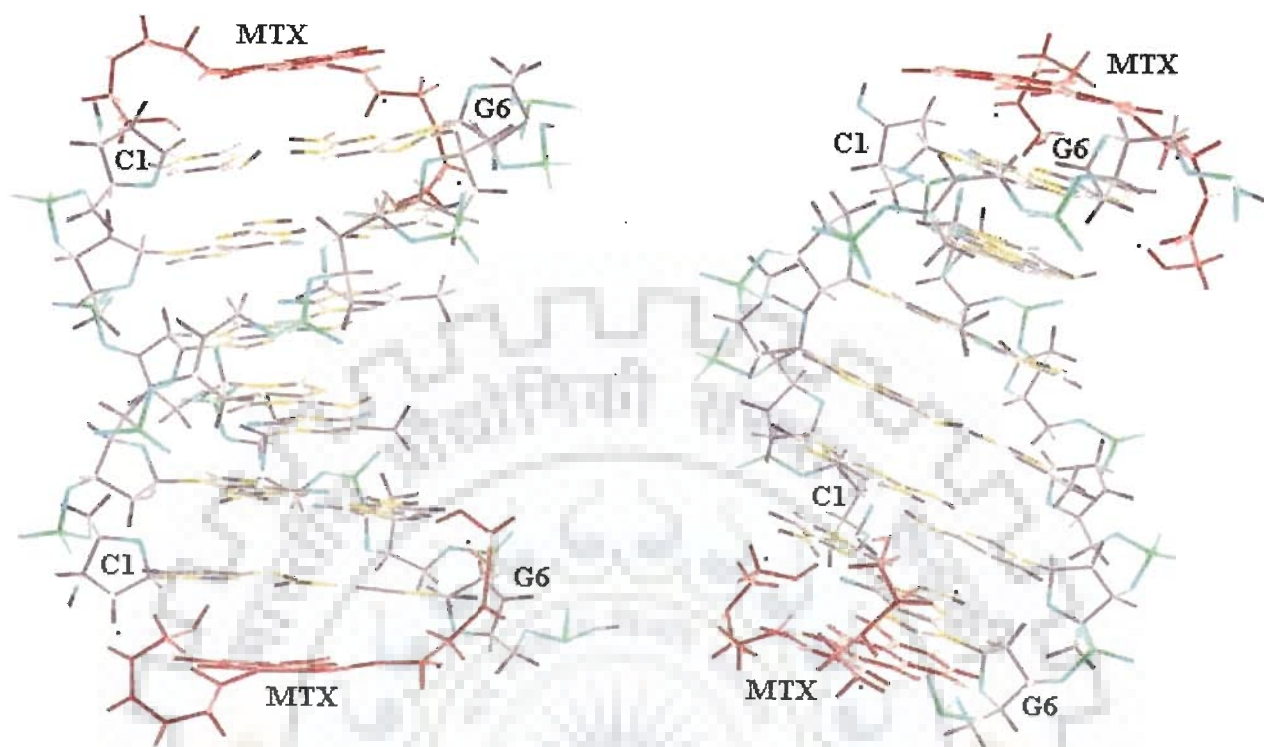


Fig. 7.3 Stereoviews of the final rMD structure.

The variations in the propeller twist are significantly large, for the non-terminal base pairs the large negative value in the range of 12° to 28° .

Negative values of propeller twist in A3T4 base pair have been reported in literature [32, 82, 101] and may possibly occur to avoid steric clashes between the $-\text{CH}_3$ group of thymine and 5' neighbouring sugar in AX / XT base pair step. The positive value of propeller twist for terminal base pair may be attributed to fraying effects at end of oligonucleotides. Base pair opening lies in the range 29 to 52 for all base pairs; it being smaller in magnitude for internal base pairs than the terminal base pairs in all rMD structures. In regular A-DNA and B-DNA geometries, global values of the inter base pair parameters - shift (Dx), slide (Dy), roll (ρ) and tilt (τ) are essentially zero. For rMD structures, the observed shift and slide values are small and do not show any significant variation with the base pair step. The rise per residue (Dz) approximately lies within the range 3.0-3.8 Å. The variation of tilt value is $\pm 12^\circ$ deviated from the ideal B-DNA value. The twist angle varies between 29° - 50° . The CURVES software reports both global and local helical parameters and therefore a correlation between them is expected [67]. The CURVES output for the rMD structure's pdb i.e. cgmtx.pdb is given as Appendix A.

7.2.3 GROOVE WIDTH

The groove widths of the double helix are defined using the coordinates of the phosphate atoms. The smallest separation between the phosphate atoms in 2 antiparallel strands reduced by the sum of the Van der Waal's radii of the two phosphate atoms (5.8 Å) is used to define the minor groove width in B-DNA and major groove width in A-DNA. The minor groove generally occurs between the i and $(i-4)'$ phosphates for B-DNA and between i and $(i-3)'$ for the A-DNA [14, 82]. In the hexanucleotide only one major and one minor groove exists in the middle of

helix. In the rMD structure the width and depth of the major groove $\sim 11 \text{ \AA}$ and $\sim 0.5 \text{ \AA}$ value. Thus there is no change in the major groove while the wider groove is narrower by 2.0 \AA .



Table 7.1 Energy terms (Kcal mol⁻¹) and root mean square of energy with respect to atomic coordinates Kcal mol⁻¹ Å⁻¹ for 10 energy minimized structure of d-(CGATCG)₂ complexed with mitoxantrone

Structures	Total_Energy	E _{ang}	E _{ele}	E _{nb}	E _{tor}	E _{vdw}	RMSD
1	310.2739	215.5183	-1438.13	-568.626	266.9703	864.5673	0.359487
2	317.8344	209.2684	-1452.06	-181.885	275.1109	1265.491	0.656454
3	309.6588	213.626	-1443.96	-606.966	277.1809	830.4013	0.524385
4	290.8663	216.4532	-1457.88	256.6717	251.5004	1708.954	0.471792
5	289.6663	210.2326	-1451.53	495.1538	269.9232	1940.908	0.589219
6	265.4588	213.1089	-1441.23	105.6991	248.5557	1542.926	0.613908
7	288.2208	230.7937	-1471.89	-15.5355	279.994	1448.848	0.558247
8	283.6129	221.7765	-1454.59	-52.5121	286.1808	1398.2	0.585787
9	300.74	208.4478	-1432.84	-300.984	257.6593	1125.884	0.698844
10	309.2782	213.3575	-1428.58	-415.65	263.7047	1008.157	0.507933

E_{ang} – Angular Energy

E_{ele} – Electrostatic Energy

E_{nb} – Nonbond Energy

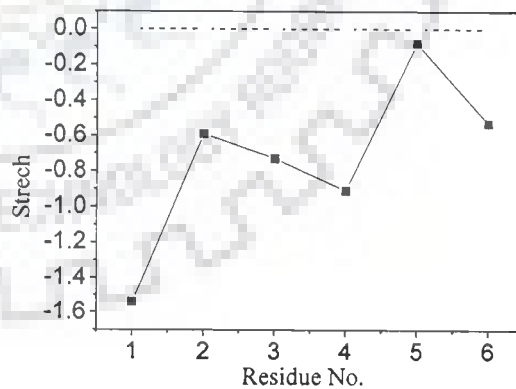
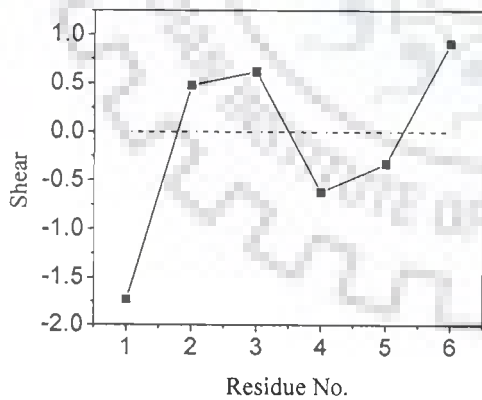
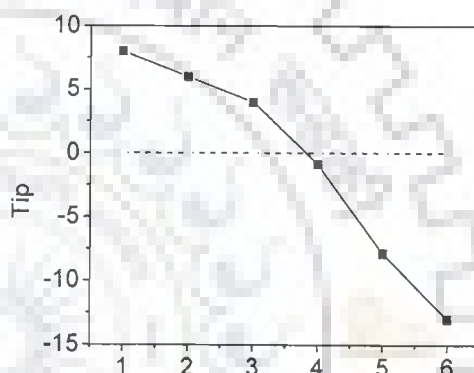
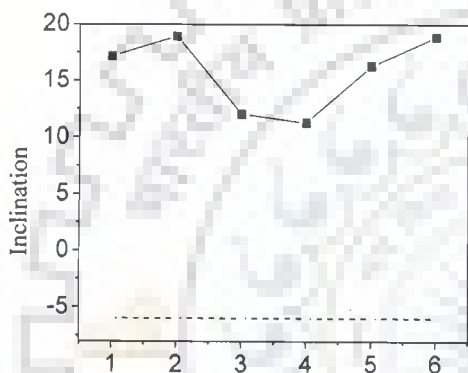
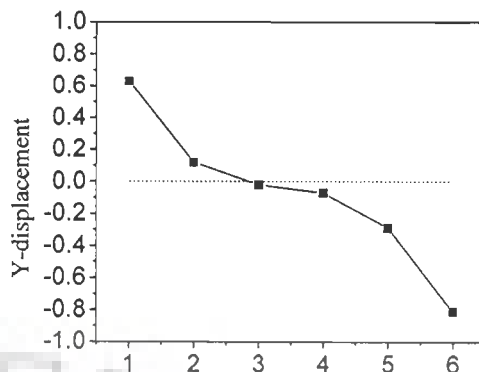
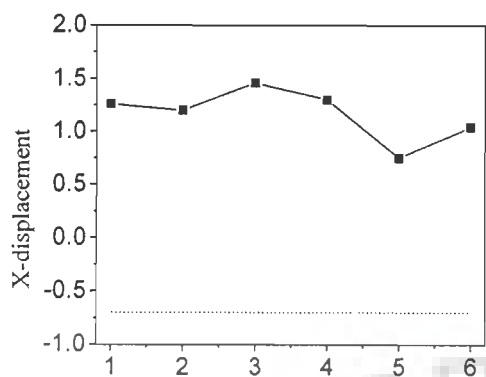
E_{tor} – Van der Waal Energy

RMSD – Root Mean square deviation.

Table 7.2 : Relative intensities of intermolecular NOE connectivities between hexanucleotide and the drug molecule in the drug–DNA complex at drug to DNA ratio D/N = 1.0 and D/N = 1.75 from NOESY spectra (Fig. 6.6-6.8) at 278 K. The very strong (ss), strong (s), medium (ws) weakly (w) and very weakly (ww) intense cross peaks correspond to distance of ss 1.8–2.5 Å, s 2.5–3.0 Å, ws 3.0–3.5 Å, w 3.5–4.0 Å, ww 4–5 Å. Distances obtained in rMD model are also shown.

S. No.	Cross peak	Relative Intensity by visual inspection of NOESY spectra		Distances in rMD Model (Å)
		D/N=1.0	D/N=1.75	
				2.49
I1	13CH ₂ –C1H6	ss	ss	2.01
I2	13CH ₂ –G6H8	ss	ss	2.84
I3	14OH–C1H6	ws	ws	–
I4	14OH–C1N4H ₂ ^b	s	s	–
I5	14OH–C5N4H ₂ ^b	s	s	–
I6	11NH ^b –C1H1'	o	o	–
I7	11NH ^b –C1H2''	w	w	4.44
I8	2H/3H–G6NH ^b	w	w	–
I9	2H/3H–C1H2''	s	s	–
I10	14OH–C1H2''	w	w	2.66
I11	2H/3H–G6H1'	ww	ww	5.30
I12	11CH ₂ –G6H8	ws	ws	–
I13	13CH ₂ –C5H6	w	w	–
I14	11NH ^b –C1H2'	w	w	3.93
I15	13CH ₂ –G6NH ^b	w	w	4.00
I16	13CH ₂ –G2H8	ss	ss	–
I17	12CH ₂ –G2H8	ww	ww	–
I18	11CH ₂ –C1H6	ws	o	3.30
I19	11CH ₂ –C5H6	ww	o	–
I20	13CH ₂ –G6NH ₂ ^b	–	ww	–
I21	13CH ₂ –C5NH ₂ ^{nb}	–	ww	–
I22	13CH ₂ –C1NH ₂ ^{nb}	–	ws	–
I23	13CH ₂ –G2NH ₂ ^b	–	ws	–
I24	C1H5–14OH	w	w	3.61

* Intermolecular NOEs used for rMD model



contd.

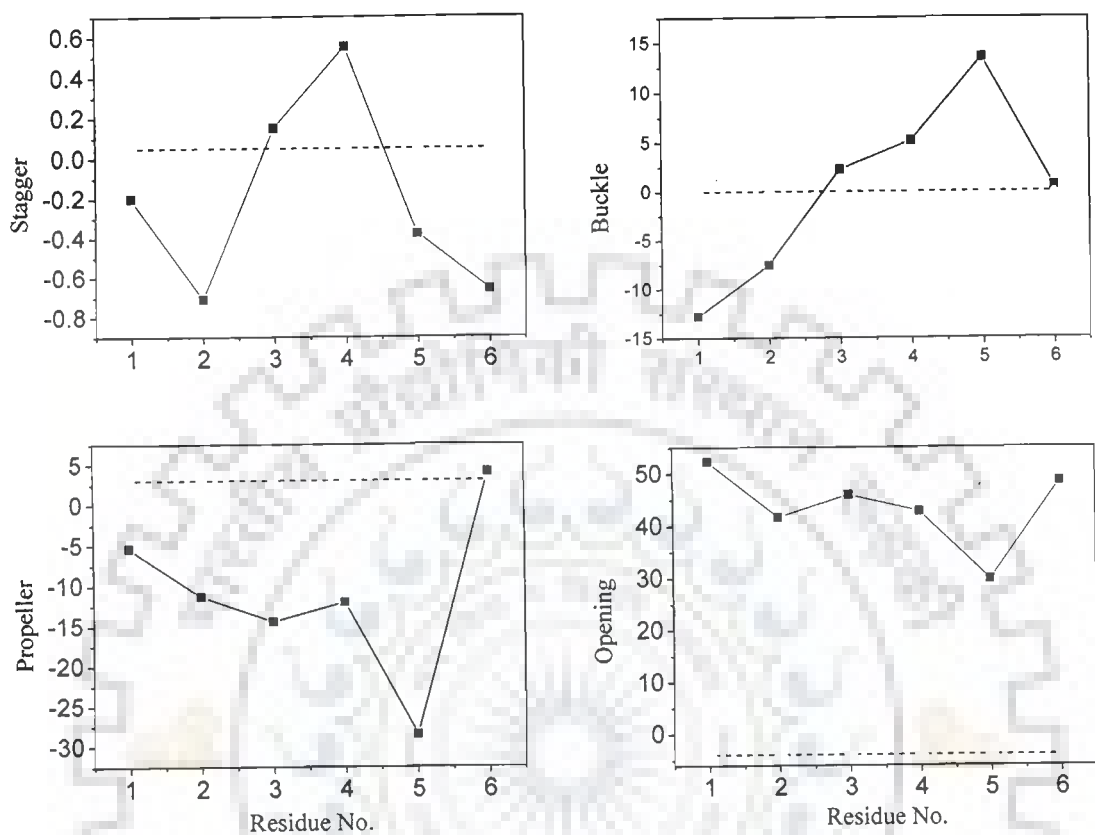


Figure 7.4a

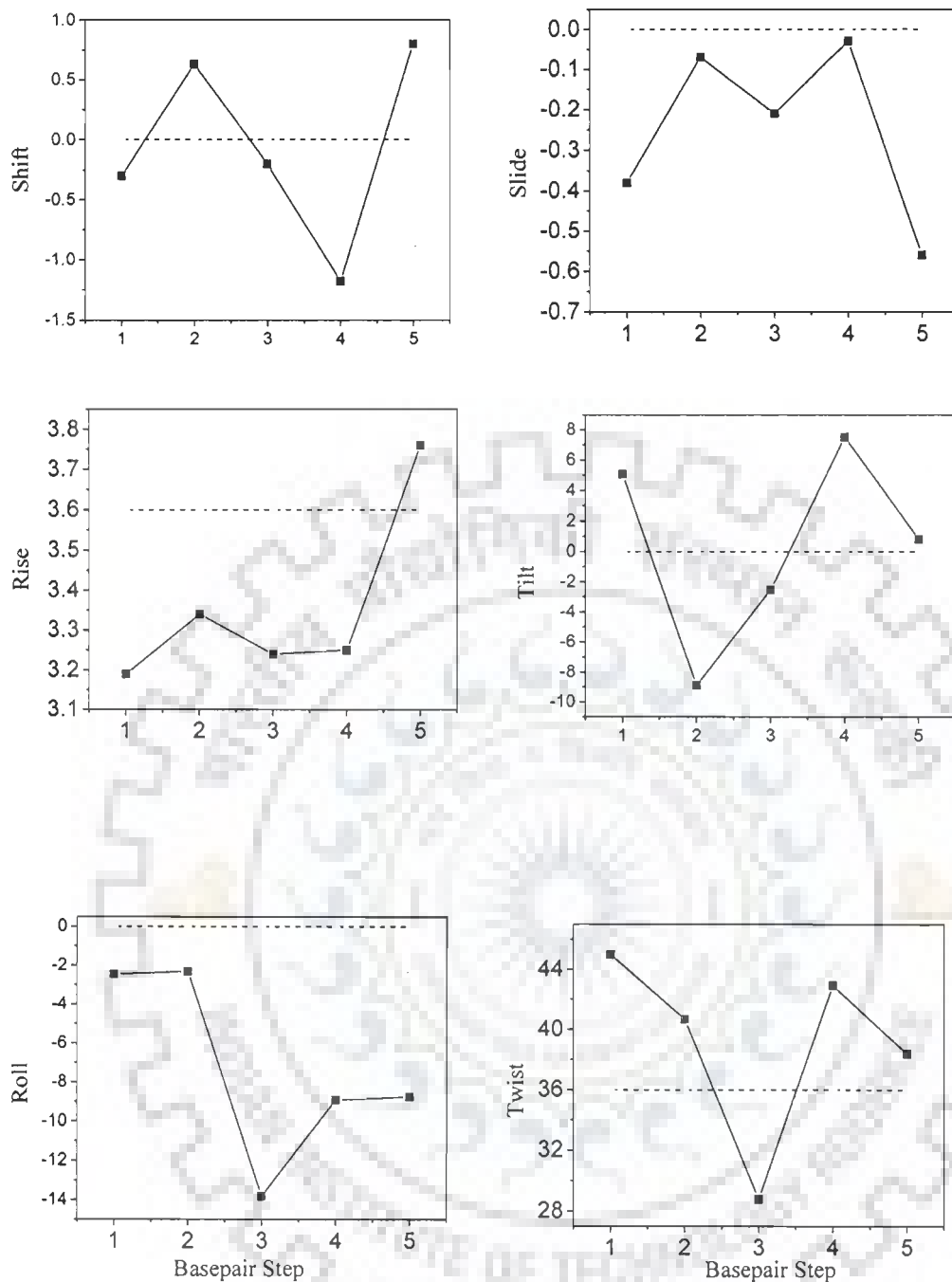


Figure 7.4b

Figure 7.4 Helical parameters for d-CGATCG complexed with Mitoxantrone calculated for structure obtained by restrained molecular dynamics simulations (●) and that for canonical B-DNA (-----) (a) Base pair axis and base base (b) Inter base pair

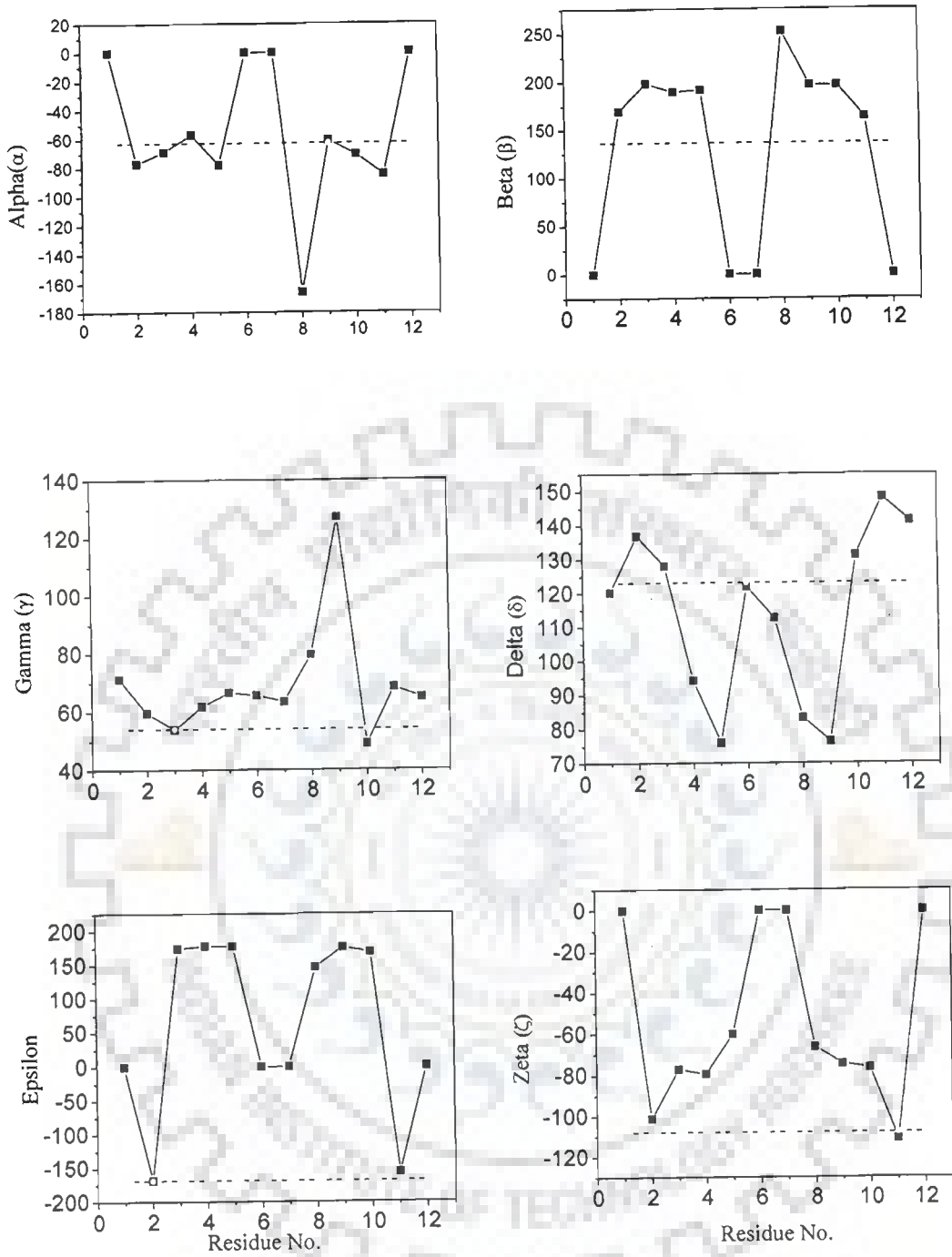


Figure 7.4c

Figure 7.4c Backbone torsional angles for complexed with Mitoxantrone calculated for structure obtained by restrained molecular dynamics simulations (●) and that for canonical B-DNA (-----)

Appendix A

```
*****
***** CURVES 5.3 R.L. 1998 *****
*****
```

```
FILE : cgmtx.pdb      LIS : cgmtx_res_final
dna :                axin :
axout:                DAF : cgmtx_res_final
PDB : cgmtx_res_finalout
```

```
acc : 0.000 wid : 0.750
```

```
maxn : 500 ior : 0 ibond: 0 splin: 3 break: -1
nleve: 3 nbac : 7
```

```
ends: F supp: T COMB: T dinu: F mini: T
rest: F line: F zaxe: F fit: F test: F
GRV : T old: T axonl: F
```

```
Strand: 1 Unit: 1 (CA 1) linkage from atom O3' ( 13) to P absent
Strand: 2 Unit: 6 (CB 1) linkage from atom O3' ( 205) to P absent
```

```
Strand= 2 Nucleo= 12 Atoms = 384 Units = 12
```

```
Input 1) Xdisp= 0.00 Ydisp= 0.00 Inclin= 0.00 Tip= 0.00
```

```
Combined strands have 6 levels ...
```

```
Strand 1 has 6 bases (5'-3'): CGATCG
Strand 2 has 6 bases (3'-5'): GCTAGC
```

```
FIRST SUM= 68.987 CPTS: 6.893 11.592 6.907 43.595
```

```
MINIMISATION: ACC = 0.100E-05 MAXN= 500 NVAR= 24
```

```
STEP 1 SUM= 68.987 DEL= 0.000E+00
STEP 2 SUM= 53.046 DEL= -0.159E+02
STEP 3 SUM= 47.486 DEL= -0.556E+01
STEP 4 SUM= 39.403 DEL= -0.808E+01
STEP 5 SUM= 38.868 DEL= -0.535E+00
STEP 6 SUM= 35.224 DEL= -0.364E+01
STEP 7 SUM= 30.338 DEL= -0.489E+01
STEP 8 SUM= 23.450 DEL= -0.689E+01
STEP 9 SUM= 101.371 DEL= 0.779E+02
STEP 10 SUM= 22.987 DEL= -0.784E+02
STEP 11 SUM= 22.139 DEL= -0.848E+00
STEP 12 SUM= 20.198 DEL= -0.194E+01
```

STEP 13 SUM= 17.498 DEL= -0.270E+01
 STEP 14 SUM= 27.894 DEL= 0.104E+02
 STEP 15 SUM= 17.036 DEL= -0.109E+02
 STEP 16 SUM= 17.053 DEL= 0.164E-01
 STEP 17 SUM= 16.809 DEL= -0.243E+00
 STEP 18 SUM= 16.709 DEL= -0.101E+00
 STEP 19 SUM= 16.526 DEL= -0.182E+00
 STEP 20 SUM= 16.189 DEL= -0.338E+00
 STEP 21 SUM= 15.549 DEL= -0.640E+00
 STEP 22 SUM= 14.931 DEL= -0.617E+00
 STEP 23 SUM= 14.588 DEL= -0.343E+00
 STEP 24 SUM= 14.454 DEL= -0.135E+00
 STEP 25 SUM= 14.377 DEL= -0.763E-01
 STEP 26 SUM= 14.330 DEL= -0.475E-01
 STEP 27 SUM= 14.326 DEL= -0.423E-02
 STEP 28 SUM= 14.322 DEL= -0.345E-02
 STEP 29 SUM= 14.322 DEL= -0.829E-04
 STEP 30 SUM= 14.322 DEL= -0.129E-03
 STEP 31 SUM= 14.322 DEL= -0.715E-04
 STEP 32 SUM= 14.322 DEL= -0.809E-05
 STEP 33 SUM= 14.322 DEL= -0.132E-04
 STEP 34 SUM= 14.322 DEL= -0.155E-04
 STEP 35 SUM= 14.322 DEL= -0.158E-05
 STEP 36 SUM= 14.322 DEL= -0.415E-06
 STEP 37 SUM= 14.322 DEL= -0.118E-06
 STEP 38 SUM= 14.322 DEL= -0.175E-07
 STEP 39 SUM= 14.322 DEL= -0.773E-09
 STEP 40 SUM= 14.322 DEL= -0.110E-10
 STEP 41 SUM= 14.322 DEL= -0.568E-13
 STEP 42 SUM= 14.322 DEL= 0.000E+00
 STEP 43 SUM= 14.322 DEL= 0.000E+00
 STEP 44 SUM= 14.322 DEL= 0.355E-14
 STEP 45 SUM= 14.322 DEL= -0.355E-14

FINAL SUM= 14.322 CPTS: 3.590 8.132 0.741 1.860

GRA=-0.81E-11-0.38E-11-0.18E-10 0.16E-10-0.54E-10 0.12E-09 0.19E-10 0.78E-11

GRA= 0.21E-09-0.20E-09 0.15E-10 0.17E-10-0.24E-09-0.16E-09-0.58E-11 0.86E-11

GRA=-0.52E-09 0.47E-09-0.85E-11 0.69E-11 0.35E-09 0.13E-11 0.91E-11-0.84E-11

 |A| Global axis parameters |

- 1) U: -0.129 -0.147 -0.981 P: -0.214 -1.284 0.433 D: 3.938
- 2) U: -0.072 -0.138 -0.988 P: 0.178 -0.566 3.523 D: 1.193
- 3) U: -0.082 -0.173 -0.982 P: 0.775 -0.196 6.808 D: 1.630
- 4) U: 0.072 -0.204 -0.976 P: 0.753 0.253 10.016 D: 3.480
- 5) U: 0.074 -0.150 -0.986 P: -0.100 0.612 13.193 D: 4.081

Chapter 7

6) U: 0.118 -0.098 -0.988 P: -0.307 1.562 16.862

 |B| Global Base-Axis Parameters |

1st strand		Xdisp (dx)	Ydisp (dy)	Inclin (eta)	Tip (theta)	Bc	Tc
1) CA	1	0.39	-0.14	10.77	-174.62	3	0
2) GA	2	1.44	-0.17	15.15	-179.96	1	10
3) AA	3	1.77	-0.39	13.19	176.89	2	22
4) TA	4	0.99	-0.53	13.84	173.10	4	-22
5) CA	5	0.59	-0.33	23.02	157.88	3	-10
6) GA	6	1.50	-1.07	19.13	168.90	1	0

2nd strand		Xdisp (dx)	Ydisp (dy)	Inclin (eta)	Tip (theta)	Bc	Tc
1) GB	6	2.12	-1.40	23.57	169.24	1	0
2) CB	5	0.96	-0.42	22.70	168.63	3	-10
3) TB	4	1.16	-0.34	10.86	168.67	4	-22
4) AB	3	1.62	-0.38	8.71	174.86	2	22
5) GB	2	0.91	0.25	9.55	173.58	1	10
6) CB	1	0.59	0.54	18.57	-164.87	3	0

 |C| Global Base pair-Axis Parameters |

Strand 1 with strand 2 ...

Duplex		Xdisp (dx)	Ydisp (dy)	Inclin (eta)	Tip (theta)	Bc	Tc
1) C 1-G	6	1.26	0.63	17.17	-171.93	3	0
2) G 2-C	5	1.20	0.12	18.93	-174.29	1	10
3) A 3-T	4	1.46	-0.02	12.02	-175.89	2	22
4) T 4-A	3	1.30	-0.07	11.28	179.12	4	-22
5) C 5-G	2	0.75	-0.29	16.28	172.15	3	-10
6) G 6-C	1	1.04	-0.81	18.85	166.88	1	0

Average: 1.17 -0.07 15.75 -0.66

 |D| Global Base-Base Parameters |

Strand 1 with strand 2 ...

Duplex	Shear (Sx)	Stretch (Sy)	Stagger (Sz)	Buckle (kappa)	Propel (omega)	Opening (sigma)	Bc	Tc
1) C 1-G 6	-1.73	-1.54	-0.20	-12.79	-5.38	52.34	3	0
2) G 2-C 5	0.48	-0.59	-0.71	-7.54	-11.32	41.58	1	10
3) A 3-T 4	0.62	-0.73	0.15	2.33	-14.44	45.90	2	22
4) T 4-A 3	-0.62	-0.91	0.55	5.12	-12.04	42.68	4	-22
5) C 5-G 2	-0.33	-0.08	-0.38	13.47	-28.54	29.72	3	-10
6) G 6-C 1	0.91	-0.53	-0.66	0.57	4.03	48.46	1	0
Average:	-0.11	-0.73	-0.21	0.19	-11.28	43.45		

 |E| Global Inter-Base Parameters |

1st strand	Shift (Dx)	Slide (Dy)	Rise (Dz)	Tilt (tau)	Roll (rho)	Twist (Omega)	Dc
2) C 1/G 2	0.80	0.09	2.93	7.70	-5.43	39.61	8
3) G 2/A 3	-0.70	-0.14	3.77	-3.95	-3.88	42.85	2
4) A 3/T 4	-0.82	-0.31	3.44	-1.13	-12.61	27.20	7
5) T 4/C 5	-1.03	0.39	2.78	11.69	-17.16	36.45	-2
6) C 5/G 6	1.42	-0.78	3.62	-5.63	7.53	47.77	8
2nd strand	Shift (Dx)	Slide (Dy)	Rise (Dz)	Tilt (tau)	Roll (rho)	Twist (Omega)	Dc
2) G 6/C 5	-1.41	0.86	3.44	2.45	-0.51	50.37	8
3) C 5/T 4	0.56	0.00	2.91	-13.82	0.76	38.53	-2
4) T 4/A 3	0.42	0.12	3.04	-3.92	15.01	30.42	7
5) A 3/G 2	-1.33	0.44	3.71	3.34	0.66	49.41	2
6) G 2/C 1	0.18	0.33	3.90	7.27	25.03	29.04	8

 |F| Global Inter-Base pair Parameters |

Strand 1 with strand 2 ...

Duplex	Shift (Dx)	Slide (Dy)	Rise (Dz)	Tilt (tau)	Roll (rho)	Twist (Omega)	Dc
2) C 1/G 2	-0.30	-0.38	3.19	5.07	-2.46	44.99	8
3) G 2/A 3	0.63	-0.07	3.34	-8.89	-2.32	40.69	2
4) A 3/T 4	-0.20	-0.21	3.24	-2.52	-13.81	28.81	7
5) T 4/C 5	-1.18	-0.03	3.25	7.52	-8.91	42.93	-2
6) C 5/G 6	0.80	-0.56	3.76	0.82	-8.75	38.40	8

Chapter 7

Average: -0.05 -0.25 3.36 0.40 -7.25 39.16

 |G| Local Inter-Base Parameters |

1st strand	Shift (Dx)	Slide (Dy)	Rise (Dz)	Tilt (tau)	Roll (rho)	Twist (Omega)	Dc
2) C 1/G 2	0.76	1.47	2.74	5.31	2.31	39.24	8
3) G 2/A 3	0.98	1.77	3.43	-2.87	7.37	41.66	2
4) A 3/T 4	-0.37	1.24	3.51	-1.88	-4.68	28.46	7
5) T 4/C 5	-0.17	1.94	2.41	19.00	-5.52	31.97	-2
6) C 5/G 6	2.78	1.05	2.96	6.87	24.26	46.57	8
2nd strand	Shift (Dx)	Slide (Dy)	Rise (Dz)	Tilt (tau)	Roll (rho)	Twist (Omega)	Dc
2) G 6/C 5	-2.58	1.64	2.69	-6.47	20.92	45.99	8
3) C 5/T 4	-0.17	1.60	2.64	-19.91	9.39	34.53	-2
4) T 4/A 3	-0.11	1.18	3.12	-4.85	-9.56	31.18	7
5) A 3/G 2	-1.68	0.99	3.49	-1.05	7.71	49.18	2
6) G 2/C 1	0.54	1.34	3.77	10.66	-17.50	28.84	8

 |H| Local Inter-Base pair Parameters |

Strand 1 with strand 2 ...

Duplex	Shift (Dx)	Slide (Dy)	Rise (Dz)	Tilt (tau)	Roll (rho)	Twist (Omega)	Dc
2) C 1/G 2	-0.82	2.06	2.67	-3.02	13.05	43.84	8
3) G 2/A 3	0.35	1.80	3.02	-10.25	10.90	38.34	2
4) A 3/T 4	-0.24	1.07	3.30	-4.03	-6.07	29.87	7
5) T 4/C 5	-0.99	1.67	2.95	10.55	4.08	40.15	-2
6) C 5/G 6	1.62	1.51	3.33	1.59	2.61	39.75	8
Average:	-0.01	1.62	3.05	0.18	4.91	38.39	

 |I| Global Axis Curvature |

Duplex	Ax	Ay	Ainc	Atip	Adis	Angle	Path	Dc
2) C 1/G 2	-0.25	0.13	3.32	-0.09	0.28	3.32	3.20	8

3) G 2/A 3	0.36	0.08	-1.98	-0.72	0.37	2.11	3.36	2
4) A 3/T 4	-0.04	-0.17	-1.78	-8.82	0.17	9.00	3.24	7
5) T 4/C 5	-0.63	0.19	2.51	-1.95	0.65	3.18	3.31	-2
6) C 5/G 6	0.51	-0.04	-1.74	-3.48	0.51	3.90	3.80	8

Overall axis bend ... UU= 14.45 PP= 10.28

Duplex Offset L.Dir ... wrt end-to-end vector

1) C 1	0.00	0.00
2) G 2	0.45	-121.51
3) A 3	1.03	171.04
4) T 4	1.03	137.83
5) C 5	0.36	49.11
6) G 6	0.00	0.00

Path length= 16.90 End-to-end= 16.67 Shortening= 1.34 %

 |J| Backbone Parameters |

Ist strand	C1'-C2'	C2'-C3'	Phase	Ampli	Pucker	C1'	C2'	C3'
1)CA 1	28.74	-22.81	145.79	28.47	C2'-endo	107.8	103.8	104.7
2)GA 2	38.09	-42.59	175.56	44.49	C2'-endo	110.1	95.7	104.5
3)AA 3	39.36	-40.38	166.12	42.72	C2'-endo	107.3	97.3	104.9
4)TA 4	33.71	-24.68	141.02	33.39	C1'-exo	110.0	99.9	105.9
5)CA 5	-8.32	31.15	44.10	44.28	C4'-exo	108.5	104.2	100.4
6)GA 6	41.00	-41.95	171.12	44.15	C2'-endo	104.8	103.9	97.6

Torsions Chi Gamma Delta Epsil Zeta Alpha Beta
 C1'-N C5'-C4' C4'-C3' C3'-O3' O3'-P P-O5' O5'-C5'

1)CA 1	-127.83	71.30	120.23
2)GA 2	-120.23	59.61	136.82	-168.00	-101.16	-77.41	168.79
3)AA 3	-120.11	53.82	128.04	173.91	-77.08	-69.42	-162.83
4)TA 4	-115.06	61.74	94.13	177.65	-79.42	-57.12	-171.77
5)CA 5	-158.30	66.46	75.89	177.39	-60.26	-78.12	-169.55
6)GA 6	-137.00	65.56	121.75

2nd strand C1'-C2' C2'-C3' Phase Ampli Pucker C1' C2' C3'

1)GB 6	43.13	-39.12	158.58	43.50	C2'-endo	104.7	101.7	99.7
2)CB 5	26.04	-16.28	129.05	26.49	C1'-exo	108.4	105.4	103.7
3)TB 4	33.13	-27.54	151.13	32.64	C2'-endo	107.8	103.5	102.7
4)AB 3	40.24	-41.58	167.46	43.98	C2'-endo	108.1	96.4	104.9

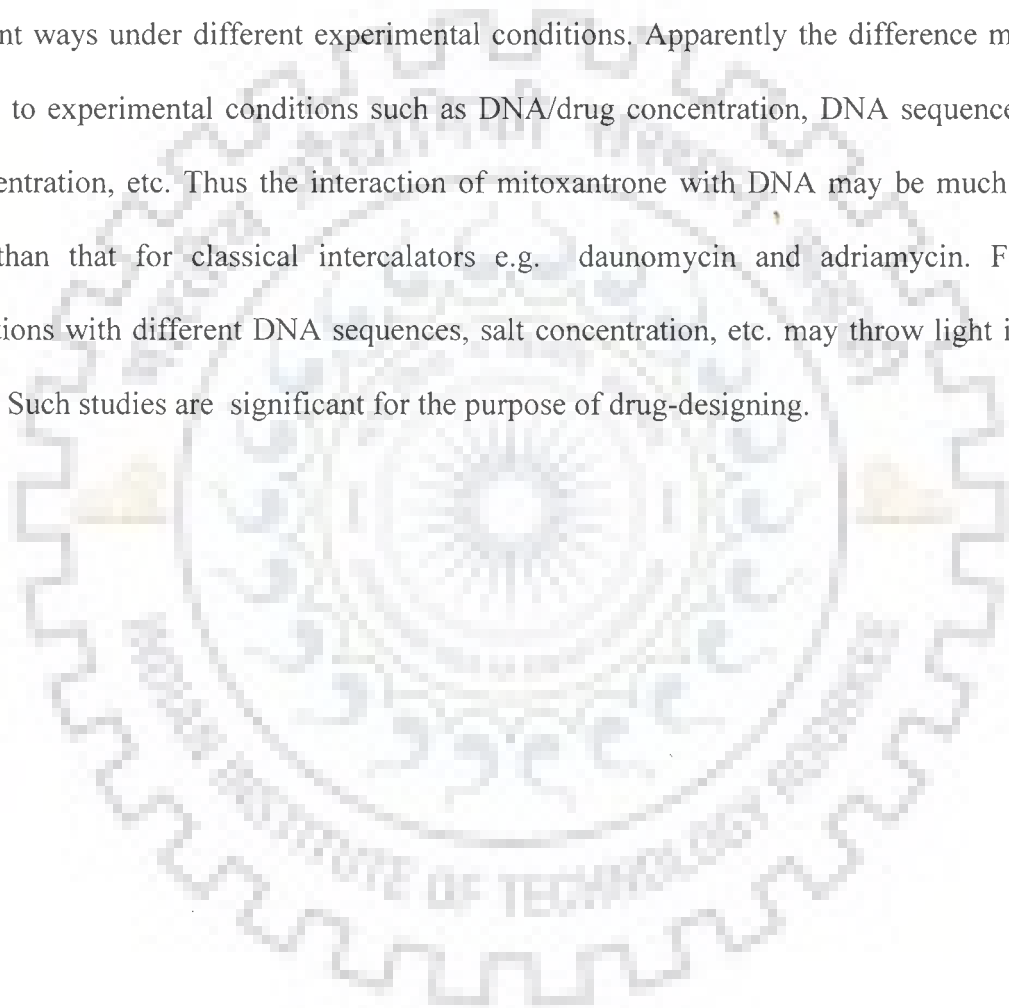
Chapter 8

Conclusions

The solution structure of the complex between mitoxantrone and DNA oligomer d-(CGATCG)₂ at 1:1, 1.5:1, 1.75:1 and 2:1 drug / duplex ratio has been characterized by combined use of protons and phosphorous-31 one- and two-dimensional NMR spectroscopy, molecular mechanics and molecular dynamics computations. Intermolecular nuclear Overhauser effects (NOEs), DNA structure perturbations, and resonance shifts induced by binding provide evidence that mitoxantrone binds to DNA. There is a slow exchange on NMR time scale between free and bound species as exhibited by 2 sets of peaks for the DNA protons – T4NH, G6NH, G2NH, T4CH₃ and drug protons, 11NH. The presence of intra base pair (d_{pi}) and sequential inter base pair (d_{ps}) NOE connectivities [117] show that all base pairs in DNA are intact.

The existence of all sequential intramolecular NOE cross peaks within DNA provides a clear evidence that DNA base pairs do not open to let the flat aromatic ring insert itself between them like a typical intercalative drug, such as ethidium bromide, daunomycin, adrimycin, actinomycin. Absence of large downfield shift (~ 1.5 ppm) in ³¹P NMR spectra which are characteristic of unwinding of the DNA helix and stretching of base pair separation to 6.8 Å with a change in backbone torsional angle ϵ , C4'–C3'–O3'–P, to permit intercalation of aromatic chromophore of the intercalative drugs further supports this argument. Also there are no significant distortions in B-type conformation of DNA as evidenced by intra sugar, base to sugar and sequential NOE cross peaks. The drug exists in monomeric form in the bound complex as NOE cross peaks, characteristic of self associated mitoxantrone (chapter 3) are absent. The drug thus binds externally to DNA with aromatic chromophore stacking with C1.G6 base pairs leading to large upfield shifts in 6H / 7H, 2H / 3H and particularly 11NH protons ($\Delta\delta \sim 0.85$ ppm upfield) and specific drug protons in close proximity of DNA protons (Figs. 6.6 – 6.8).

Stacking at ends of DNA sequence has earlier been observed in X-ray crystallographic study [118] of ametantrone (an analogue of mitoxantrone) with d-(CGTACG)₂. These findings are in contrast with transcriptional assay studies which show that mitoxantrone chromophore intercalates at 5' (A/T) CA and 5' (A/T) CG sites of DNA [84]. Since mitoxantrone has two long side chains having seven torsional angles hence large degrees of freedom, it may orient in different ways under different experimental conditions. Apparently the difference may be attributed to experimental conditions such as DNA/drug concentration, DNA sequence, pH, salt concentration, etc. Thus the interaction of mitoxantrone with DNA may be much more specific than that for classical intercalators e.g. daunomycin and adriamycin. Further investigations with different DNA sequences, salt concentration, etc. may throw light in this direction. Such studies are significant for the purpose of drug-designing.



REFERENCES

1. Adams, A., Guss, J. M., Denny, W. A. and Wakelin, L. P.G. Crystal structure of the topoisomerase-II poison 9-amino-[N-(2-dimethylamino)ethyl]acridine-4-carboxamide bound to the DNA hexanucleotide d(CGATCG)₂. Implications for structure-activity relationships of acridinecarboxamide topoisomerase poisons. *Nucleic Acids Research*, 2002, 30, 719-725.
2. Altona, C. and Sundaralingam, M. Conformational analysis of the sugar ring in nucleotides and nucleosides. A new description using pseudo-rotation. *J. Am. Chem. Soc.*, 1972, 94, 8205-8212.
3. Andreoni, A., Canti, G., Fabbrocini, G., Mastrocinque, M. and Quarto, E. B16 melanoma response in vivo to photochemotherapy with mitoxantrone and red light. *Cancer Letts.*, 1991, 61, 89-94.
4. Andreoni, A., Colasanti, A., Kissilinger, A., Malatesta, V. and Roberti, G. Phototoxicity of anthracyclines upon laser excitation in the long-wavelength absorption bands. *Radiation Research*, 1991, 127, 24-29.
5. Andreoni, A., Colasanti, A., Kissilinger, A., Malatesta, V. and Roberti, G. Enhancement of antitumor drug cytotoxicity via laser photoactivation. *Photochemistry and Photobiology*, 1991, 53, 797-805.
6. Andreoni, A., Colasanti, A., Malatesta, V., Mastrocinque, M., Roberti, G. and Vom Kisslingee A. Cell photosensitization by 5-iminodaunomycin activated with red light. *Biochim. Biophys. Acta*, 1989 1014, 8-13.
7. Arcamone, F. and Penco S. In "Anthracyclines and anthracediones based anticancer agents". (Eds. Lown J.W.), Elsevier, New York, 1988.

8. Arcamone, F. Doxorubicin: In "Anticancer Antibiotics". Academic Press, New York, 1981.
9. Babayan, Yu. S., Sngryan, A. E., Kazaayran, Avetisyan, M. G., Sogomonyan, L.R. and Garibyan, D. V. Interactions of antitumor drugs mitoxantrone and Ametantrone with DNA as Determined from the Changes in Circular Dichorism Spectra. *Molecular Biophysics* 1998, 43, 398–402.
10. Bailly, C., Rouier, S., Bernier, Jean-Luc. and Waring, M. J. DNA recognition by two mitoxantrone analogues: Influence of the hydroxyl groups. *FEBS letters*, 1986, 379, 269–272.
11. Balaji, V. N., Dixon, J. S., Smith, D. H., Venkataraghavan, R. and Murdock, K. C. Design of anticancer drugs using modeling techniques. *Annals of the New York Academy of Sciences*, 1985, 439, 140–161.
12. Barthwal, R., Monica., Awasthi, P., Srivastava, N., Sharma, U., Kaur, M. and Govil, G. Structure of DNA hexamer sequence d-CGATCG by two-dimensional Nuclear Magnetic Resonance Spectroscopy and Restrained Molecular Dynamics. *J. Biomol. Struct. Dyn.*, 2003, 21, 407– 423.
13. Bell, D. H. Characterization of fluorescence of the antitumor agent, mitoxantrone. *Biochemica et Biophysica.*, 1989, 949, 132–137.
14. Bhattacharya, D. and Bansal, M. Groove width and depth of B-DNA structure depend on local variations in slide. *J. Biomol. Struct. Dyn.*, 1992, 10, 213–216.
15. Birlirakis, N. and Perly, B. One and two-dimensional ^1H NMR investigations of the inclusion of the anti-cancer drug mitoxantrone in cyclomaltooligosaccharides. *Carbohydrate Research*, 1992, 235, C1–C4.
16. Bodenhausen, G., Freeman R. and Turner D.L. Suppression of artifacts in two-dimensional spectroscopy. *J. Magn. Reson.*, 1977, 27, 511–514.

17. Bodhenhausen, et al. *Phys. Rev. Lett.* 38, 1977, 1116–1119.
18. Bonnadonna, G. and Monfardini, S. Cardiac toxicity of daunorubicin. *Lancet.* 1969, 1, 837–854.
19. Chaires, J. B., Dattagupta, N. and Crothers, M. Self association of Daunomycin *Biochemistry*, 1982, 21, 3927–3932.
20. Chen, K. X. Gresh, N., and Pullman, B. A theoretical investigation on the sequence selective binding of mitoxantrone to double-stranded tetranucleotides. *J. Biomol. Struct. Dyn.* 1985, 3, 445–466.
21. Chen, T. K. Fico, R. and Canellakis, E. S. Diacridine, Bifunctional Intercalators. Chemistry and Antitumor Activity. *J. Med. Chem.* 1979, 21, 868–874.
22. Cheng, C. C. and Zee-Cheng, R. K. Y. The design synthesis and development of new class of potent antineoplastic anthraquinones. In “Progress in Medicinal Chemistry” (Eds. Ellis, G.P.; West, G. B.,) Elsevier, Amsterdam), 1983.
23. Clore, G. M. and Gronenborn, A. M. Probing the three-dimensional structures of DNA and RNA oligonucleotides in solution by nuclear Overhauser enhancement measurements. *FEBS Letts.*, 1985, 179, 187–198.
24. Collier, D. A. and Neidle, S. Synthesis, Molecular modeling, DNA binding and antitumor properties of some substituted amido anthraquinones. *J. Med. Chem.* 1988, 1, 847–857.
25. Davies D. B, Veselkov, D. A., Djimant, L. N. and Veselkov, A. N. Hetero-association of caeffine and aromatic drugs and their competitive binding with DNA oligomer. *Eur. Biophys. J.*, 2001, 30, 354–356.
26. Davies, D. B., Djimant, L. N. and Veselkov, A. N. ¹H NMR investigation of self-association of aromatic drug molecules in aqueous solutions. *J. Chem. Soc., Faraday Trans.*, 1996, 92, 383–390.

27. Davies, D. B., Pahomov, V. I. and Veselkov, A. N. NMR Determination of the conformational and drug binding properties of the DNA heptamer d-(GpCpGpApApGpC) in aqueous solution. *Nucleic Acids Research*, 1997, 25, 4523–4531.
28. Davies, D. B., Veselkov, D. A., Evstigneev, M. P. and Veselkov, A. N. Self-association of the antitumour agent novatrone (mitoxantrone) and its hetero-association with caffeine. *J. Chem. Soc., Perkin Trans 2*, 2001, 61–67.
29. Derome, A.E. In “Modern NMR techniques for Chemistry Research”. Volume 6, Pergamon Press, Oxford U.K. 1987.
30. Di Marco A., Arcamone, F. and Zunino, F. In “Antibiotics”. (Eds. Corcoran J.W. and Hahn I.E.) Springer-Verlag, Berlin, 1974. 101–108.
31. Dickerson R. E., Bansal, M., Calladine, C. R., Diekmann, S., Hunter W.N., Kennard O., Kitzing von E., Lavery R., Nelson H.C.M., Olson W. K., Saenger W., Shakked Z., Sklenar H., Soumpasis D.M, Tung C. S., Wang A. H. J. and Zhurkin V.B. Definitions and Nomenclature of Nucleic Acid Structure Parameters. *J. Mol. Biol.*, 1989, 208, 787–791.
32. Dronberger, U., Flemming, J. and Fritzsche, H. Structure determination and analysis of helix parameters in the DNA decamer d-(CATGGCCATG)₂ Comparison of results from NMR and crystallography. *J. Mol. Biol.* 1998, 284, 1453–1463.
33. Favier, A., Blackledge, M., Simmone, Jeanne-Pierre., Crouzy, S., Dabouis, V., Gueiffier, A., Dominique, M. and Debouzy, Jean-Claude. Solution structure of 2-(-(1, 2-e) purin-4-yl) amino-ethanol intercalated in the DNA duplex d-(CGATCG)₂ *Biochemistry*, 2001, 8717–8726.
34. Feigon J., Wright, J.M., Leupin, W., Denny, W. A. and Kearns, D.R. Use of two-dimensional NMR in the study of double-stranded decamer. *J. Amer. Soc.*, 1982, 104, 5540–5541.

35. Feofanov, A., Sharonov, S., Kudelina, I., Fleury, F., Nabiev, I. Localization and molecular interactions of mitoxantrone within living K562 cells as probed by confocal spectral imaging analysis. *Biophys J.* 1997, 73, 3317–3327
36. Feofanov, A., Sharonov, S., Kudelina, I., Fleury, F., Nabiev, I. Quantitative confocal spectral imaging analysis of mitoxantrone within living K562 cells: intracellular accumulation and distribution of monomers, aggregates, naphthoquinoline metabolite, and drug–target complexes. *Biophys J.* 1997, 73, 3328–3336
37. Foye, W.O., Vajragupta, O. and Sengupta, S. K. DNA–binding specificity and RNA polymerase inhibitory activity of bis(aminoaryl)anthraquinones and bis(methylthio)vinylquinolinium iodides. *J. Pharm. Sci.*, 1982, 71, 253–257.
38. Frederick, C. A., Williams, L. D., Ughetto, G., Van der Marel, G. A., Van Boom, J. H., Rich A. and Wang, A. H. J. Structural Comparison anticancer drug–DNA complex: Adriamycin and Daunomycin. *Biochemistry*, 1990, 29, 2538–2549.
39. Gabbay, E. J., Grier D., Fingerie, R. E., Reimer R., Levy R., Pearce S.W. and Wilson W. D. Interaction specificity of the anthracyclines with deoxyribonucleic acid. *Biochemistry*, 1976, 15, 2062–2070.
40. Gatto, B., Zagatto, G., Sissi, C., Cera, C., Uriate, E., Palu, G., Caparnici, G., and Palumbo, M. Peptidyl Anthraquinones as potential Antineoplastic Drugs: Synthesis, DNA Binding, Redox cycling and Biological activity. *J. Med. Chem.* 1996, 39, 3114–3122.
41. Giessner–Prettre C. and Pullman B. On the atomic or "local" contributions to proton chemical shifts due to the anisotropy of the diamagnetic susceptibility of the nucleic acid base. *Biochem. Biophys. Res. Commun.*, 1976, 578–581. , *Biopolymer*, 15, 2277. (1976)
42. Gorenstein, D.G. ³¹P NMR of DNA Spectroscopic methods for analysis of DNA. *Methods in Enzymology*, 1992, 211, 254–285.

43. Gorenstein, D.G. Conformation and dynamics of DNA and protein-DNA complexes by ^{31}P NMR. *Chem. Rev.* 1994, 94, 1315–1338.
44. Gresh, G. and Kahn, P. H. Theoretical design of Novel, 4 Base pair Selective derivatives of Mitoxantrone. *J. Biomol. Struct. Dyn.*, 1990, 7, 1141–1159.
45. Gresh, N. and Phillippe, H. K. Theoretical Design of a Bistrapeptide Derivative of Mitoxantrone targetted towards the double stranded hexanucleotide d-(GCCGGC)₂. *J. Biomol. Struct. Dyn.*, 1991, 8, 827–844.
46. Gresh, N., and Kahn, P. H. Theoretical design of novel, 4 base pair Selective derivatives of mitoxantrone. *J. Biomol. Struct. Dyn.*, 1985, 1141–1159.
47. Gronenborn, A. M. and Clore G. M. Investigation of the solution structure of short nucleic acid fragments by means of nuclear overhauser enhancements measurements. *Prog. NMR Spec.*, 1985, 17, 1–32.
48. Hilbers, C. W. and Patel, D. J. Proton Nuclear Magnetic resonance investigations of the Nucleation and Propagation Reactions associated with the helix-coil transition of d-ApTpGpCpApT in H₂O. *Biochemistry*, 1975, 12, 2656–2660.
49. Horn, D. E., Michael, S. L., Amy, J. F. and Gray, E. Synthesis of symmetrically substituted 1, 4- bis [(aminoalkyl) amino]-5, 8-Dimethylantracene-9,10-diones. *ARIKOV*, 2000, 1, 876–881.
50. Hosur, R. V., Ravikumar, M., Roy, K.B., Tan-Zu-Kunn and Miles, H. T. and Govil, G. In 'Magnetic resonance in Biology and medicine. (Eds. Govil, G. Khetrpal C. L. and Saran, A.) Tata Mc Graw Hill, New Delhi, 1985.
51. Hosur, R.V., Govil, G. and Miles, H.T. Application of two-dimensional NMR spectroscopy in the determination of solution conformation of nucleic acids. *Magn. Reson. Chem.*, 1988, 26, 927–944.

52. Isabella, P. D., Palumbo, M., Sissi, C., Carenini, N., Caparnicao, G., Menta, E., Oliva, A., Speneli, S., Krapcho, A.P., Guillani, F.C., and Zunino, F. Physicochemical properties, cytotoxic Activity and Topoisomerase Inhibition of 2, 3 Diaza–Anthracenediones. *Biochem. Pharmacology*, 1997, 53, 161–169.
53. Isabella, P. D., Palumbo, M., Sissi, C., Carenini, N., Caparnicao, G., Menta, E., Carenini, N., Oliva, A., Speneli, S., Krapcho, A.P., Guillani, F.C., and Zunino, F. Topoisomerase II DNA cleavage stimulation, DNA binding Activity, cytotoxicity, and physicochemical properties of 2–aza and 2–aza oxide– anthracene dione derivatives. *Molecular Pharmacology*, 1995, 30, 30–38.
54. Islam S.A., Neidle S., Gandecha B.M., Partridge M., Patterson L.H. and Brown J.R. Comparative computer graphics and solution studies of the DNA interaction of substituted anthraquinones based on doxorubicin and mitoxantrone. *J. Med. Chem.*, 1985, 28, 857–864.
55. Jeener, J. Paper presented at the AMPERE International summer school, Borsko, Polje, Yugoslavia, 1971.
56. Kapuscinski, J. and Darzynkiewicz, Z. Relationship between the pharmacological activity of antitumor drugs ametantrone and mitoxantrone (Novatrone) and their ability to condense nucleic acids. *Proc. Natl. Acad. Sci., USA*, 1986, 83, 6303–6306.
57. Kapuscinski, J. and Darzynkiewicz, Z. Interactions of antitumor agents ametantrone and mitoxantrone (novantrone) with double–stranded DNA. *Biochem. Pharmacol.*, 1985, 34, 4203–4213,
58. Kapuscinski, J., Darzynkiewicz, Z., Traganos, F. and Myron, R. Interactions of a new antitumor agent 1, 4–dihydroxy–5,8–bis [[2–[hydroxyethyl) amino]–ethyl] amino]–9,10 anthracenedione, with nucleic acids. *Biochem. Pharmacol.*, 1981, 30, 231–240.
59. Karplus, M. Vicinal protons coupling in nuclear magnetic resonance. *J. Am. Chem. Soc.*, 1963, 85, 2870–2871.

60. Karplus, M. Contact electron-spin coupling of nuclear magnetic moments. *J. Chem. Phys.*, 1959, 30, 11–15.
61. Keeler, J. and Neuhaus, D. Comparison and evaluation of methods for two-dimensional NMR spectra with absorption mode line shape. *J. Magn. Reson.*, 1985, 63, 454–472.
62. Kolodziejczyk, P. and Suillerot, A. G. Circular dichroism study of the interaction of mitoxantrone. Ametantrone and their Pd (II) complexes with deoxyribonucleic acid. *Biochimica et Biophysica Acta.*, 1987, 926, 249–257.
63. Kotovych, G., Lown, J.W., and Tong, P.K. High field ^1H and ^{31}P NMR studies on the binding of the anticancer agent mitoxantrone to d- [CpGpApTpCpG]₂. *J. Biomol. Struct. Dyn.*, 1986, 4, 111–125.
64. Krishnamoorthy, C. R., Yen, Shau-Fong., Smith J. C., William, J. W. and Wilson, W. D. Stopped flow kinetics analysis of the interaction of anthraquinone anticancer drugs with calf-thymus DNA, Poly[d(G–C).Poly[d–(G–C) and Poly[d(A–T). Poly[d–(A–T)]. *Biochemistry*, 1986, 25, 5933–5940.
65. Lavery, R. and Sklenar, H. CURVES 5.1. Helical analysis of irregular nucleic Acids. Laboratory of Theoretical Biology. CNRS, Paris, 1996.
66. Lavery, R. and Sklenar, H. The definition of generalized helicoidal parameters and of axis curvature for irregular nucleic acids. *J. Biomol. Struct. Dyn.*, 1988, 6, 63–91.
67. Lavery, R. and Sklenar, J. Defining the Structure of Irregular Nucleic Acids: Conventions and Principles. *J. Biomol. Struct. Dyn.*, 1989, 6, 655–667.
68. Lavery, R. Junctions and bends in nucleic acids: a new theoretical modelling approach. In *Structure and Expression 3* (Eds. Olson, W.K., Sarma, M.H., Sarma, R.H. & Sundaralingam, M.), Adenine Press, New York. 1988, 191– 211. Lavery, R., Sklenar, H., Zakrzewska, K. &

Pullman, B. The flexibility of the nucleic acids: (II). The calculation of internal energy and applications to mononucleotide repeat DNA. *J. Biomol. Struct. Dyn.* 1986, 3, 989–1014.

69. Lee, B.S. and Dutta, P. K. Optical Spectroscopic Studies of the Antitumor Drug 1, 4 – Dihydroxy,–5,8–bis[[2–[(2–hydroxyethyl)amino]ethyl] amino]–9,10– anthracenedione (Mitoxantrone). *J. Phy. Chem.*, 1989, 93, 5665–5672.

70. Leonard, G. A., Hambley, T. W., Mc Auley Hecht K., Brown T., and Hunter W. N. Anthracycline DNA interactions at unfavourable base pair triplet binding sites: Structures of d–(CGGCCG) / daunomycin and d–(TGGCCA) / adriamycin complexes. *Acta. Cryst.* 1993, D49, 458–467.

71. Lerman, L.S. Structural considerations in the interaction of DNA with acridines. *J. Mol. Biol.*, 1961, 3, 18–30.

72. Lown, J. W. Hanstock, C. C., Bleackley, R.C., Imbach, J. L. Rayner, B. and Vasseur, J. Synthesis and complete ¹H assignment and conformations of the self complementary hexanucleotide d–(CpGpApTpCpG)₂ and its fragment by high field NMR. *Nucleic Acids Research*, 1984, 12, 2519–2526.

73. Lown, J. W. Hanstock, C. C., Bradley, R. D. and Douglas G. S. Interactions of Antitumor agents Mitoxantrone and Deoxyribonucleic Acids studied by electron Microscopy. *Molecular Pharmacology*, 1983, 25, 178–184.

74. Lown, J. W., Morgan, A. R., Yen, Shau–Fong, Wang, Yueh–Hwa and Wilson, W.D. Characterization of binding of the anticancer agents mitoxantrone and ametantrone and related structures to deoxyribonucleic acids. *Biochemistry*, 1985, 24, 4028–4035.

75. Lown, J.W. and Hanstock C. C. High field ^1H -NMR analysis of the 1:1 intercalation complex of the antitumor agent mitoxantrone and the DNA duplex [d(CpGpCpG)]. *J. Biomol. Struc. Dyn* 1985, 2, 1097–1106.
76. Marion, D. and Wuthrich, K. Application of phase sensitive two-dimensional correlated spectroscopy (COSY) for measurement of ^1H - ^1H spin coupling constant in proteins. *Biochem. Biophys. Res. Comm.*, 1983, 113, 967–974.
77. Martin, R. B. Comparisons of Indefinite Self-Association Models. *Chem Rev.*, 1996, 96, 3043–3064.
78. Mazerski, J., Martelli, S. and Borowski, E. The geometry of intercalation complex of antitumor mitoxantrone and ametantrone with DNA: Molecular dynamics Simulations, *Acta Biochimica Polonica*, 1998, 45, 1–11.
79. Mazzini, S., Bellucci, M. C. and Mondelli, R. Mode of binding of cytotoxic alkaloid Berberine with the double Helix Oligonucleotide d-(AAGAATTCTT)₂. *Bioorganic and Medicinal Chemistry*, 2003, 505–514.
80. Mazzini, S., Mondelli, R. and Ragg, E., Structure and dynamics of intercalation complexes of Anthracyclines with d-(CGATCG)₂. 2D ^1H and ^{31}P NMR investigations. *J. Chem. Society, Perkin Trans, 2*, 1998, 1983–1991.
81. Moore, M. H., Hunter, W. N. and Langlois, d' Estaintot B. and Kennard, O. DNA–drug interactions. The crystal structure of d-CGATCG complexed with daunomycin. *J. Mol. Biol* , 1989, 206, 693–705.
82. Mujeeb, A., Kerwin, S. M., Kenyon, G. L. and James, T. L. Solution structure of conserved DNA sequence from the HIV-I genome: Restrained molecular dynamics simulations with distance and torsion angle restraints derived from the two-dimensional NMR spectra, *Biochemistry*, 1993, 32, 13419–13431.

83. Murdock, K. C., Child, R.G., Fabio, P.F., Angier, R.B., Wallace, T.E., Durr, F.E. and Citarella, R.V. Antitumor Agents. 1, 4 Bis-[aminoalkyl) amino]-9,10 anthracenedione J. Med. Chem, 1979, 22, 1024–1030.
84. Panousis, C. and Phillips D.R. DNA sequence specificity of Mitoxantrone. Nucleic Acids Research, 1994, 22, 1342–1345.
85. Panousis, C., Kettle, A. J. and Phillips, D. R. Oxidative metabolism of mitoxantrone by human neutrophil enzyme myeloperoxidase. Biochemical Pharmacology, 1994, 48, 2223–2226.
86. Panousis, C., Kettle, A.J. and Phillips, D. R. Myeloperoxidase oxidizes mitoxantrone to metabolites which bind covalently to DNA and RNA. Anti-Cancer Drug Design, 1995, 10, 593–605.
87. Parker, B. S., Buley, T., Evinson, B, Cutts, S. M., Neumann, G. M., Iskander, M. N., Phillips, D. R. Molecular understandings of mitoxantrone–DNA adduct formation: Effect of cytosine methylation and flanking sequences. J Biol. Chem., 2004, 279, 18814–18823.
88. Parker, B. S., Cullinane, C. and Phillips, D. R. Formation of DNA adducts by formaldehyde-activated mitoxantrone. Nucleic Acids Research, 1999, 27, 2918–2923.
89. Parker, B.S., Cutts, S.M., Cullinane, C. and Phillips, D.R. Formaldehyde activation of mitoxantrone yields CpG and CpA specific DNA adducts. Nucleic Acids Research, 2000, 28, 983–989.
90. Patel, D. J. d-CpGpGpC and d-GpGpCpC self-complementary duplexes: NMR studies of the Helix-coil transition. Biopolymers, 1977, 16 1635–1636.
91. Patel, D. J. Kolowski, S. A. and Rich, A. Right handed and left handed DNA: Studies of B- and Z-DNA by proton nuclear Overhauser effect and P-NMR. Proc. Natl. Acad. USA, 1982, 79, 1413–1417.

92. Patel, D. J. Kolowski, S.A. and Rice J. A. Hydrogen bonding, overlap geometry, and sequence specificity in anthracycline antitumor antibiotic: DNA complexes in solution. *Proc. Natl. Acad. USA.* 1981, 78, 3333–3337.
93. Paul Charlesworth (Chapter 3 thesis)
<http://chemistry.mtu.edu/~pcharles/RESEARCH/thesis/ch03/Homepage.html>)
94. Piantini, U., Sorensen, O.W. and Ernst R.R. Multiple quantum filters for elucidating NMR networks. *J. Am. Chem. Soc.*, 1982, 104, 6800–6801.
95. Ragg, E., Mondelli R., Battistini C., Garbesi A. and Colonna F.P. ³¹P NMR study of daunorubicin–d-(CGTACG) complex in solution: Evidence of the intercalation sites. *FEBS Letts.*, 1988, 236, 231–234.
96. Rao, M.V.R., Atreyi, M. and Kumar, A. Interaction of antitumor agent mitoxantrone with Poly[d (G–C)]– A Circular dichroic study. *Indian Journal of Biochemistry and Biophysics*, 1989, 26, 5–8
97. Redfield, A.G., Kunj, S. and Ralph, E. K. Dynamic range in Fourier transform proton magnetic resonance. *J. Magn. Reson.*, 1975, 19, 114–116.
98. Reid B.R., Banks K., Flynn P. and Nerdal W. NMR distance measurement in DNA duplex: Sugar and bases have the same correlation times. *Biochemistry*, 1989, 28, 10001–10007.
99. Reszka, K., Hartley, J.A., Kolodziejczyk P. and Lown, J. W. Interaction of the peroxidase derivative of mitoxantrone with nucleic acids. Evidence for covalent binding of ¹⁴C labeled drugs. *Biochem. Pharmacol.* 1989, 38, 4253–4260.
100. Roche, C. J. Berowitz, D., Sulkowski, G. A., Danishefsky, S. J. and Crothers, D. M. Binding affinity and site selectivity of daunomycin analogues. *Biochemistry*, 1994, 33, 926–935.
101. Schmitz, U., Sethson, I., Egan, W.M. and James, T. L. Solution structure of a DNA octamer containing the pribnov box via restrained molecular dynamics simulations with distance

- and torsion angles derived from two-dimensional nuclear magnetic resonance fitting. *J. Mol. Biol.*, 1992, 227, 510–531.
102. Searle, M. S., Hall, J. G., Denny, W. A. and Wakelin L. P. G. NMR studies of the interaction of the antibiotic nogalamycin with the hexadeoxyribonucleotide duplex d (5'-GCATGC)₂. *Biochemistry*, 1988, 27, 4340–4349.
103. Sissi, C., Moro, S., Zagatto, G., Ellis, M., Krapcho, A. P., Menta, E. and Palumbo, M. Binding of bis-substituted 2-aza-anthracenedione regioisomers to DNA: effects of the relative poisoning of the side chains. *Anti cancer Drug Design*, 1999, 14, 265–274.
104. Skladanowski, A. and Knopa, J. Relevance of the interstrand DNA crosslinking induced by the anthracyclines for their biological activity. *Biochem. Pharmacology*, 1994, 47, 2279–2287.
105. Sklandanowski, A. and Knoppa, J. Mitoxantrone and Ametantrone induce interstrand cross-links in DNA of tumour cells *British Journal of Chemistry*, 2000, 1300–1304.
106. Smith, I. E. Mitoxantrone (novantrone): A review of experimental and early clinical studies. *Cancer Treat Rev.*, 1983, 10, 103–115.
107. Smith, P. J., Morgan, S. A., Fox, M. E. and Watson, J.V. Mitoxantrone–DNA binding and the induction of topoisomerase II associated DNA damage in multi-drug resistant small cell lung cancer cells, *Biochem. Pharmacol.*, 1990, 40, 2069–2078.
108. States, D. J., Haberkorn, R.A. and Reuben, D. J. A two-dimensional nuclear overhauser experiment with pure absorption phase in four quadrants. *J. Magn. Reson.*, 1982, 48, 286.
109. Sundaralingam, M. Stereochemistry of nucleic acids and their constituents. Allowed and preferred conformations of nucleosides, nucleoside mono-, di-, tri-, tetraphosphates, nucleic acids and polynucleotides *Biopolymers*, 1969, 7, 821– 860.

110. Tanious, F.A., Jenkins, T.C., Neidle, S., and Wilson, W. D. Substituent position dictates the intercalative DNA–Binding mode for anthracene 9, 10–dione antitumor drugs, *Biochemistry*, 1992, 31, 11632–11640.
111. Tarasiuk, J., Tkaczyk–Gobis, K., Stefanska, B., Dzeieduszycka, M., Priebe, W., Martelli, S., Borowski, E. The role of structural factors of anthraquinone compounds and their quinone–modified analogues in NADH dehydrogenase–catalysed oxygen radical formation. *Anti–cancer Drug Design*, 1998, 13, 923–939.
112. Trotta, E., D’Ambrosio, E., Ravagnan, G. and Maurizio, P. Simulations and Different binding Mechanisms of 4’, 6–diamino–2–phenylindole to DNA hexamer d–(CGATCG)₂ A ¹H NMR study. *J. Biol. Chem.*, 1996, 271, 27608–27614.
113. Veselkov, A. N., Evstigneev, M. P. Vysotski., Veseklov, D. A., and Davies, D. B. Thermodynamic analysis of interaction of antibiotic mitoxantrone with tetranucleotide 5’–d(TpGpCpA) in aqueous solution based on ¹H NMR spectroscopy data. *Biofizika*, 2002, 47, 432–438.
114. Wang, A. H. J., Ughetto, G., Quigley, G. J. and Rich, A. Interaction between anthracycline antibiotic and DNA: Molecular structure of daunomycin complexed to d–CpGpTpApCpG at 1.2 Å resolution. *Biochemistry*, 1987, 26, 1152–1153.
115. Wang, H., Pin Yang, P., Tian, Y., Zhang, Z. and Zhao, C. Experimental antitumor activity of the Ce (IV)–Mitoxantrone complex and Its interaction with Deoxyribonucleic Acid. *J. Inorg. Chem.*, 1997, 68, 117–121.
116. Waring, M. J. Complex formation between ethidium bromide and nucleic acids. *Journal of Molecular Biology*, 1965, 13, 269–82.
117. Wüthrich, K. Resonance assignments and structure determination in nucleic acids. In “NMR of Proteins and Nucleic Acids”. Wiley Interscience, New York. 1986.

118. Yang, X. L., Robinson, H., Gao, Y. G. and Wang A. H. J. Binding of macrocyclic bisacridine and ametantrone to CGTACG involves similar unusual intercalation platforms. *Biochemistry*, 2000, 39, 10950–10957.
119. Yang, P., Wang, H., Gao, F. and Yang, B. Antitumour Activity of the Cu (II)–mitoxantrone and its interaction with deoxyribonucleic acid. *J. Inorg. Chem.*, 1996, 62, 137–145.
120. Zaggatto, G., Moro, S., Uriatte, E., Ferrazzi, E., Palu, G. and Palumbo, M. Amido analogues of mitoxantrone: Physico chemical properties, molecular modeling cellular effects and antineoplastic potential. *Anticancer Drug Design*, 1997, 12, 99–112.
121. Zaggatto, G., Supino, R., Favini, E. Moro, S. and Palumbo, M. New 1, 4 anthracence–9, 10 dione derivatives as potential anticancer agents. *IL Farmaco*, 2000, 55, 1–5.
122. Zee–Cheng, R. K.Y., Mathew, A. E., Northcutt, R. V. and Cheng, C. C. Structural Modification Study of Mitoxantrone (DHAQ). Chloro–Substituted Mono–and Bis[(aminoalkyl)amino]anthraquinones *J. Med. Chem.*, 1987, 30, 1682–1686.
123. Zhang, Y. Z., Patterson, Y. and Roder, H. Rapid amide proton exchange rates in peptides and proteins measured by solvent quenching and two dimensional methods. *Protein Sci.*, 1995, 4, 804–814.